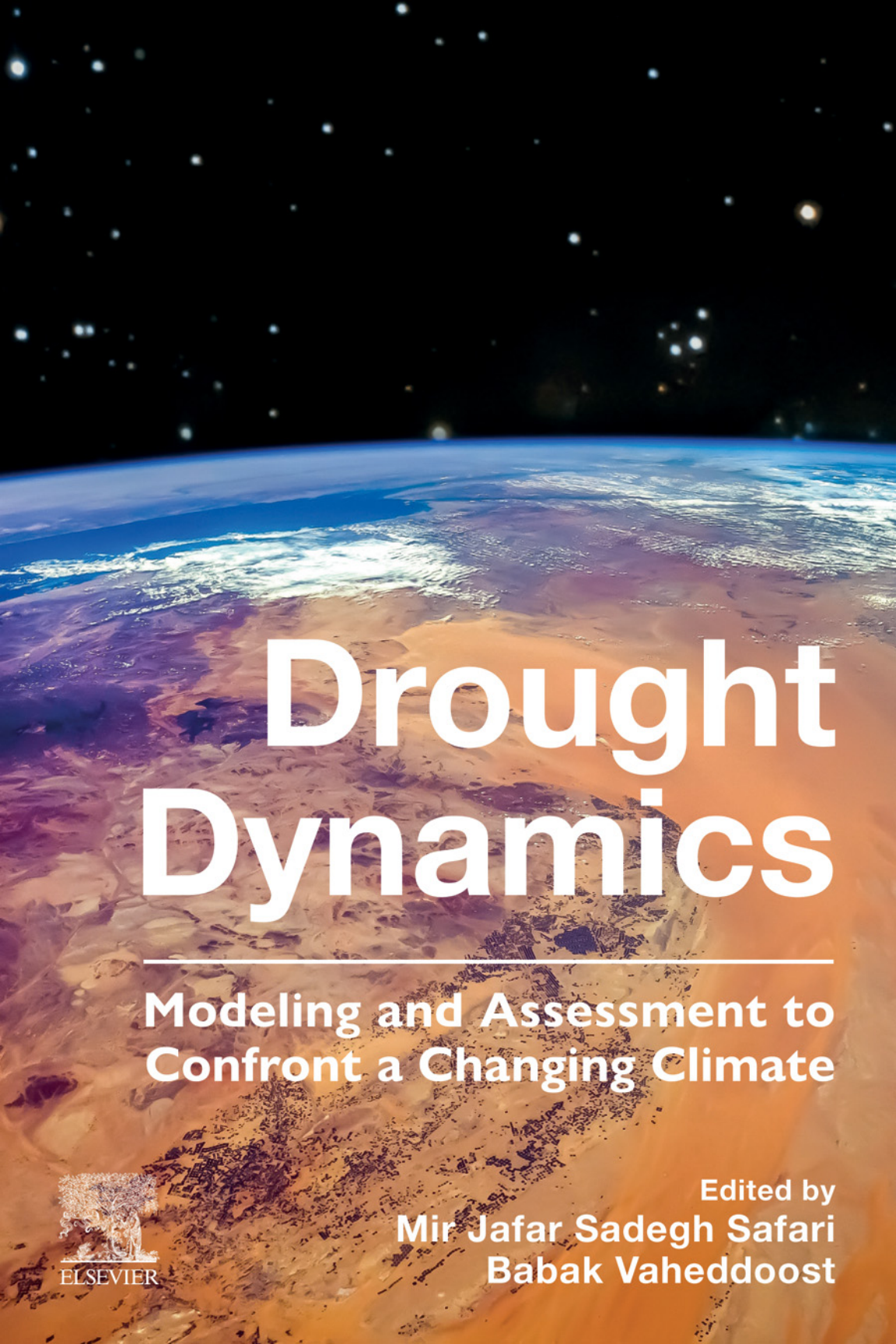

Drought Dynamics
Modeling and Assessment to Confront a Changing Climate
Edited by
Mir Jafar Sadegh Safari
Babak Vaheddoost
ELSEVIER



Drought Dynamics

This page intentionally left blank

Drought Dynamics

Modeling and Assessment to Confront a Changing Climate

Edited by

Mir Jafar Sadegh Safari
Department of Geography and Environmental Studies, Toronto Metropolitan University, Toronto, ON, Canada
Department of Civil Engineering, Yaşar University, Izmir, Türkiye

Babak Vaheddoost
Department of Civil Engineering, Bursa Technical University, Bursa, Türkiye



ELSEVIER

Elsevier
Radarweg 29, PO Box 211, 1000 AE Amsterdam, Netherlands
125 London Wall, London EC2Y 5AS, United Kingdom
50 Hampshire Street, 5th Floor, Cambridge, MA 02139, United States

Copyright © 2026 Elsevier Inc. All rights are reserved, including those for text and data mining, AI training, and similar technologies.

For accessibility purposes, images in electronic versions of this book are accompanied by alt text descriptions provided by Elsevier. For more information, see https://www.elsevier.com/about/accessibility.

Books and Journals published by Elsevier comply with applicable product safety requirements. For any product safety concerns or queries, please contact our authorised representative, Elsevier B.V., at productsafety@elsevier.com.

Publisher's note: Elsevier takes a neutral position with respect to territorial disputes or jurisdictional claims in its published content, including in maps and institutional affiliations.

No part of this publication may be reproduced or transmitted in any form or by any means, electronic or mechanical, including photocopying, recording, or any information storage and retrieval system, without permission in writing from the publisher. Details on how to seek permission, further information about the Publisher's permissions policies and our arrangements with organizations such as the Copyright Clearance Center and the Copyright Licensing Agency, can be found at our website: www.elsevier.com/permissions.

This book and the individual contributions contained in it are protected under copyright by the Publisher (other than as may be noted herein).

Notices

Knowledge and best practice in this field are constantly changing. As new research and experience broaden our understanding, changes in research methods, professional practices, or medical treatment may become necessary.

Practitioners and researchers must always rely on their own experience and knowledge in evaluating and using any information, methods, compounds, or experiments described herein. In using such information or methods they should be mindful of their own safety and the safety of others, including parties for whom they have a professional responsibility.

To the fullest extent of the law, neither the Publisher nor the authors, contributors, or editors, assume any liability for any injury and/or damage to persons or property as a matter of products liability, negligence or otherwise, or from any use or operation of any methods, products, instructions, or ideas contained in the material herein.

ISBN: 978-0-443-34205-9

For Information on all Elsevier publications
visit our website at https://www.elsevier.com/books-and-journals

Publisher: Peter Llewellyn
Acquisitions Editor: Jennette McClain
Editorial Project Manager: Ellie Barnett
Production Project Manager: Prem Kumar Kaliamoorthi
Cover Designer: Miles Hitchen

Typeset by MPS Limited, Chennai, India



Contents

List of contributors *xiii*

Section I Drought concept

1. Background and drought indices **3**

Gokmen Tayfur

1.1 Background 3
1.2 Drought assessment methods 4
1.3 Discussion and conclusions 11
References 11

2. Bibliometry and Review **15**

Mustafa Utku Yilmaz and Hulya Yilmaz

2.1 Introduction 15
2.2 Results of bibliometric analysis 18
2.3 Trending topics and emerging themes in drought-related research 28
2.4 The most commonly used datasets in drought-related research 31
2.5 The most commonly used methods and indices for drought prediction 33
2.6 Conclusion 35
AI disclosure 36
References 36

3. An overview of drought indices **41**

Ismail Dabanli, Furkan Sencer Kaçar, Abdullah Emin Demircioğlu, Cemre Erbil and Mehmet Şerif Kayaalp

3.1 Introduction 41
3.2 Characterization of drought 42
3.3 Drought indices 45
3.4 Conclusion 103
Acknowledgment 103
References 103

4. Application of General Circulation Models' outputs in the analysis of the extreme climatic events 109

Mustafa Nuri Balov, Farzad Rotbee and Maryam Khalilzadeh Poshtegal

4.1 Introduction 109
4.2 General Circulation Models—an overview 110
4.3 Emission scenarios 112
4.4 Downscaling 115
4.5 Uncertainty issue 116
4.6 Extreme climatic events 118
4.7 Case tudy: Drought A ssessment 122
4.8 Conclusion 125
References 125

5. Drought in arid and semiarid regions 133

Gokmen Tayfur

5.1 Learning and knowledge outcomes 133
5.2 Introduction 134
5.3 Methods 135
5.4 Application 137
5.5 Discussion 144
5.6 Conclusions 146
References 147

6. Drought propagation from meteorological to agricultural to hydrological 149

Gokmen Tayfur

6.1 Introduction 149
6.2 Drought types 150
6.3 Widely employed index for each drought 151
6.4 Drought propagation 154
6.5 Discussion and conclusions 155
References 155

7. Drought and architecture 161

Meysam Soleimani and Furkan Kavak

7.1 Introduction 161
7.2 The concept of climatic architecture 163
7.3 Traditional architecture in the hot and arid climate 165

7.4 Contemporary design inspired by traditional architecture 189
7.5 Conclusion 193
References 195

8. The psychological toll of drought in a changing climate 197
Mahsa Vaheddoost

8.1 Introduction 197
8.2 Methodology 198
8.3 Psychological effects of drought 199
8.4 Drought and eco-anxiety 204
8.5 The link between drought and eco-anxiety 206
8.6 Drought coping mechanisms 207
8.7 Conclusion 209
AI disclosure 211
References 211

Section II Drought management

9. Policy and governance in drought studies 217
Mustafa Utku Yilmaz and Hulya Yilmaz

9.1 Introduction 217
9.2 Developing a framework for effective drought governance 220
9.3 The Matrice d'Impacts Croisés Multiplication Appliquée à un Classement (MICMAC) method 222
9.4 Identifying factors influencing drought governance 225
9.5 Classification of factors using the Matrice d'Impacts Croisés Multiplication Appliquée à un Classement (MICMAC) method 230
9.6 Challenges and barriers to effective drought governance 235
9.7 Conclusion and policy recommendations 237
AI disclosure 240
References 240

10. Water demand management and behavior change in agriculture 245
Pelin Atakan and Cihat Günden

10.1 Introduction 245
10.2 What farmers are expected to do 246
10.3 How farmers are encouraged to do what they are expected to do 249
10.4 Understanding why farmers do what they do 252

10.5 Designing policies to promote behavior change in irrigation under water scarcity using behavioral insights 255
10.6 Conclusion 260
References 260

11. The state's efforts for effective water storage management to enhance resilience against droughts: case studies from the Bursa District 265

Murat Can

11.1 Introduction 265
11.2 Applications and Practices 268
11.3 Further Applications and Investments 272
11.4 Sum Up 275
11.5 Future Projections 277
References 278

Section III New trends in drought studies

12. Meteorological drought modeling using recurrent neural network and long short-term memory 281

Ali Danandeh Mehr, Hiba Alkubaisi and Rifat Tur

12.1 Introduction 281
12.2 Methods 283
12.3 Drought data gathering for central Iraq 285
12.4 Selection of the best predictors and model performance indices 287
12.5 Results 287
12.6 Conclusion 291
AI disclosure 292
References 292

13. Data assimilation technologies 295

Samira Sadat Soltani

13.1 Introduction 295
13.2 Emerging data assimilation methods for drought monitoring 297
13.3 Data assimilation in agricultural drought monitoring 298
13.4 Remote sensing in drought monitoring 299
13.5 Conclusions and future perspectives 318
References 323

Section IV Case studies

14. Models (linear, nonlinear, machine learning) 335
Babak Mohammadi

14.1 Introduction 335
14.2 Materials and methods 337
14.3 Results and discussion 341
14.4 Conclusions 348
AI disclosure 349
References 349

15. Climate and drought (climate variability, climate changes, future droughts) 353
Mohammad Jamali and Saeid Eslamian

15.1 Introduction 353
15.2 Climate variability 355
15.3 Climate change 357
15.4 Climate change models and scenarios 359
15.5 Drought 362
15.6 Future of drought and forecasting techniques 364
15.7 Conclusion 369
References 370

16. A regional case study of investigation of the meteorological drought trend using the SPI index and the Mann–Kendall test 375
Saeid Eslamian and Yaser Sabzevari

16.1 Introduction 375
16.2 Case study 383
16.3 Results and discussion 387
16.4 Conclusion 391
References 391

17. Spatiotemporal analysis of temperature rise impact on snow drought in Erzurum, Türkiye 395
Egemen Aras, Muhammet Savas, Babak Vaheddoost and Damla Yılmaz Çelik

17.1 Introduction 395
17.2 Materials and methods 398

17.3 Drought indices 399
17.4 Results 403
17.5 Discussion 408
17.6 Conclusions 412
Authorship contribution statement 412
Data availability 412
Declaration of competing interest 413
Acknowledgments 413
Statements and declarations 413
Artificial intelligence disclosure 413
References 413

18. A CMIP6-based frequency analysis of the extreme precipitation events in Virginia, USA 417

Sura Dhiyaa Hussein and Mustafa Nuri Balov

18.1 Introduction 417
18.2 Study area and data collection 420
18.3 Methodology 422
18.4 Results and discussions 426
18.5 Conclusion 433
References 436

19. Integrated modeling, prediction, and analysis of climate drought and groundwater quality: a comprehensive study of 609 sites in Iran 445

Soroosh Sharifi and Saeed Azimi

19.1 Introduction 445
19.2 Background 448
19.3 Materials and methods 450
19.4 Results and discussion 459
19.5 Conclusions 486
References 487
Further reading 489

20. Historical fluctuations of water storage in response to drought: a study of Iran 491

Behnam Khorrami

20.1 Introduction 491
20.2 Study area 493

20.3 Data preparation and analysis 494
20.4 GRACE and GRACE-FO data 494
20.5 Standardized precipitation index 494
20.6 Wetness percentile index 495
20.7 Reconstruction of the missing GRACE /GRACE-FO data 495
20.8 Seasonality assessment 496
20.9 Trend analysis 496
20.10 Results and discussion 497
20.11 Seasonal dynamics of water storage 499
20.12 Variations of standardized precipitation index 500
20.13 Associations between water storage variations and drought indices 502
20.14 Conclusion 506
References 507

Index *511*

This page intentionally left blank

List of contributors

Hiba Alkubaisi
Electrical and Computer Engineering Program, Institute of Postgraduate Education, Antalya Bilim University, Antalya, Türkiye

Egemen Aras
Department of Civil Engineering, Bursa Technical University, Bursa, Türkiye

Pelin Atakan
Department of Agricultural Economics, Graduate School of Natural and Applied Sciences, Ege University, İzmir, Türkiye

Saeed Azimi
Civil Engineering Department, Iran University of Science and Technology, Tehran, Iran

Murat Can
State Hydraulic Works of Turkey, 1st District, Bursa, Türkiye

Ismail Dabanli
Department of Civil Engineering, Faculty of Civil Engineering, Istanbul Technical University, Istanbul, Türkiye

Ali Danandeh Mehr
Civil Engineering Department, Antalya Bilim University, Antalya, Türkiye

Abdullah Emin Demircioğlu
Department of Civil Engineering, Faculty of Civil Engineering, Istanbul Technical University, Istanbul, Türkiye; Department of Civil Engineering, Faculty of Engineering, Marmara University, Istanbul, Türkiye

Cemre Erbil
Department of Civil Engineering, Faculty of Civil Engineering, Istanbul Technical University, Istanbul, Türkiye

Saeid Eslamian
Department of Water Science and Engineering, College of Agriculture, Isfahan University of Technology, Isfahan, Iran

Cihat Günden
Department of Agricultural Economics, Faculty of Agriculture, Ege University, İzmir, Türkiye

Sura Dhiyaa Hussein
Department of Civil Engineering, Istanbul Gelişim University, Istanbul, Türkiye

Mohammad Jamali
Department of Water Science and Engineering, College of Agriculture, Isfahan University of Technology, Isfahan, Iran

Furkan Sencer Kaçar
Department of Civil Engineering, Faculty of Civil Engineering, Istanbul Technical University, Istanbul, Türkiye; Department of Civil Engineering, Faculty of Engineering, Turkish-German University, Istanbul, Türkiye

Furkan Kavak
Department of Architecture, Bursa Technical University, Bursa, Türkiye

Mehmet Şerif Kayaalp
Department of Civil Engineering, Faculty of Civil Engineering, Istanbul Technical University, Istanbul, Türkiye

Behnam Khorrami
Department of Remote Sensing and GIS, University of Tabriz, Tabriz, Iran

Babak Mohammadi
Hydrology Research Unit, Swedish Meteorological and Hydrological Institute, Norrköping, Sweden

Mustafa Nuri Balov
Department of Civil Engineering, Istanbul Gelişim University, Istanbul, Türkiye

Maryam Khalilzadeh Poshtegal
Department of Environment, Culture, and Society, Thompson Rivers University, Kamloops, BC, Canada

Farzad Rotbee
Department of Civil Engineering, Istanbul Gelişim University, Istanbul, Türkiye

Yaser Sabzevari
Department of Water Science and Engineering, College of Agriculture, Isfahan University of Technology, Isfahan, Iran; Institute of Hydrology, Slovak Academy of Sciences, Bratislava, Slovakia

Muhammet Savas
Department of Civil Engineering, Bursa Technical University, Bursa, Türkiye

Soroosh Sharifi
Civil Engineering Department, University of Birmingham, Birmingham, United Kingdom

Meysam Soleimani
Department of Architecture, Bursa Technical University, Bursa, Türkiye

Samira Sadat Soltani
Institute of Bio- and Geosciences (IBG-3, Agrosphere), Forschungszentrum Jülich GmbH, Jülich, Germany

Gokmen Tayfur
Department of Civil Engineering, Izmir Institute of Technology, Gulbahce Campus, Urla, Izmir, Türkiye

Rifat Tur
Civil Engineering Department, Akdeniz University, Antalya, Türkiye

Babak Vaheddoost
Department of Civil Engineering, Bursa Technical University, Bursa, Türkiye

Mahsa Vaheddoost
Department of Psychology, Faculty of Arts and Social Sciences, Mudanya University, Bursa, Türkiye

Hulya Yilmaz
Quality and Accreditation Office, Kirklareli University, Kirklareli, Türkiye

Mustafa Utku Yilmaz
Department of Civil Engineering, Kirklareli University, Kirklareli, Türkiye

Damla Yılmaz Çelik
Department of Civil Engineering, Bursa Technical University, Bursa, Türkiye

This page intentionally left blank

SECTION I

Drought concept

This page intentionally left blank

CHAPTER ONE

Background and drought indices

Gokmen Tayfur
Department of Civil Engineering, Izmir Institute of Technology, Gulbahce Campus, Urla, Izmir, Türkiye

1.1 Background

Drought has been one of the natural disasters, more destructive than any other widely known ones such as earthquakes, floods, eruptions, etc. In a way, it is a stealth disaster that does not show its arrival (Vicente-Serrano et al., 2012). It can greatly challenge food production and cause widespread famine, consequently death of millions of people, animals, and force mass migration (Wilhite, 2000). For example, in sub-Saharan Africa, the droughts of the early to mid-1980s had adversely affected more than 40 million people, and the 1991–1992 droughts in Southern Africa affected 20 million people, resulting in a deficit of cereal supplies of more than 6.7 million tons (Wilhite, 1996, 2000). Although, historically human beings had experienced droughts, such as the one that occurred during the time of the Prophet Joseph, their frequency has increased in the last decades. Climate change, which started in the 20th century, due to the millions of tons of greenhouse gases, dumped into the atmosphere by the industrialized countries, has exacerbated drought conditions since the 1990s.

Drought is defined as a period of abnormally dry weather. It is an extreme event, showing different spatial and temporal characteristics (IPCC, 2014). It can occur in any region subjected to any climate, whether it has less or more rainfall (Wilhite et al., 2014). Drought may affect larger geographical areas and last significantly longer than other natural hazards. Due to climate change, they are expected to occur more frequently and at a greater intensity (Willby & Dessai, 2010). Although it can take place everywhere, the most severe consequences for humans occur in arid or semiarid regions. In such countries, the availability of water is

Drought Dynamics
DOI: https://doi.org/10.1016/B978-0-443-34205-9.00002-0
© 2026 Elsevier Inc. All rights are reserved, including those for text and data mining, AI training, and similar technologies.

already low, demand often is close or even exceeds natural availability, and society cannot often adapt to the drought hazard (Dai, 2011). Therefore, drought management is and will increasingly be crucial, especially in such regions. Knowledge of drought frequency and its severity plays a vital role not only in water resources management, but also in other social, economic, and environmental implications of a region as well.

It is impossible to avoid drought, but there are ways to mitigate its harmful effects (Morid et al., 2006). Drought occurs in almost all climatic systems as it stands for the climate's natural and recurring feature (Zarch et al., 2015), and it is rapidly emerging as one of the most serious natural hazards around the World. On one hand, drought is a long-term phenomenon, on the other hand, it allows a time frame for resistance against it and other mitigation preparations (Tsakiris, 2017). For this reason, a High-Level Meeting on National Drought Policy (HMNDP) was held in Switzerland in 2013, urging all countries to develop and implement national drought policies to survive (Zarch et al., 2015).

Recently, many researchers around the World have shown an increased interest in studies related to drought. Moreover, considerable attentions have been paid to effectively monitor and detect drought using various scientific formulations and techniques. Scientists concentrate on how to analyze, formulate, and determine these natural adverse events by using drought indices (Morid et al., 2006). Although drought analysis started in the late 1960s, it has become more common since the 2000s. One can see many scientific papers published concerning drought in almost all regions of the World. Drought analysis has been carried out using some drought indices. The following section briefly summarizes the most commonly employed drought indices.

1.2 Drought assessment methods

1.2.1 Standardized precipitation index

Standardized precipitation index (SPI) is the most widely employed drought index. It can be calculated for any location, based on the long-term precipitation records for a desired period. It forces records to fit the normal distribution such that the mean SPI becomes zero (McKee et al., 1993). Values greater than zero indicate wet periods, while the others stand for dry periods. Other than the classical normal distribution, some fit data to the log-normal or gamma distributions.

1.2.1.1 Normal-standardized precipitation index

The normal-standardized precipitation index (SPI-N) is computed as follows (Cacciamani et al., 2007):

$$SPI - N = z = \frac{x - \hat{\mu}}{\hat{\sigma}} \tag{1.1}$$

where z is the standardized value, and $\hat{\mu}$ and $\hat{\sigma}$ are the sample estimates of the population mean and standard deviation, respectively.

1.2.1.2 Log-normal standardized precipitation index

The log-normal SPI (SPI-L) can be calculated as follows (Lloyd-Hughes and Saunders, 2002):

$$SPI - L = z = \frac{\ln\,(x) - \hat{\mu}}{\hat{\sigma}} \tag{1.2}$$

1.2.1.3 Gamma-standardized precipitation index

In most cases, the gamma distribution of SPI is suggested for precipitation data. The density probability function for the gamma distribution is expressed as (Sonmez et al., 2005):

$$f\,(x,\,\alpha,\,\beta) = \frac{1}{\beta^{\alpha}\quad \Gamma\,(\alpha)} x^{\alpha-1} e^{x/\beta} \text{ for } x,\,\alpha,\,\beta > 0 \tag{1.3}$$

where α and β are the shape and scale parameters, respectively. x is the rainfall amount, and $\Gamma(\alpha)$ is the gamma function defined by the integral (Gasiorek & Musial, 2015):

$$\Gamma\,(x) = \lim_{n\to\infty} \prod_{v=0}^{n-1} \frac{n!\,n^{y-1}}{y+v} \equiv \int_0^{\infty} y^{\alpha-1} e^{-y} dy \tag{1.4}$$

The maximum likelihood method is used to estimate the optimal values of the parameters α and β by using Eqs. (1.5)–(1.6) (Barua et al., 2010) as:

$$\hat{\alpha} = \frac{1}{4A}\left(1 + \sqrt{1 + \frac{4A}{3}}\right) \tag{1.5}$$

$$\hat{\beta} = \frac{\overline{x}}{\hat{\alpha}} \tag{1.6}$$

where A is, for n number of observations, defined as (Barua et al., 2010):

$$A = \ln(\bar{x}) - \frac{\sum \ln(x)}{n} \tag{1.7}$$

and parameters are then used in the cumulative probability for non-zero rainfalls by using Eq. (1.8) as follows (Barua et al., 2010):

$$F(x) = \int_0^x f(x)\,dx = \frac{1}{\hat{\beta}^{\hat{\alpha}}\,\Gamma(\hat{\alpha})} \int_0^x x^{\hat{\alpha}-1} e^{-x/\hat{\beta}} dx \tag{1.8}$$

Eq. (1.8) can also be expressed as follows (Barua et al., 2010):

$$F(x) = \frac{1}{\Gamma(\hat{\alpha})} \int_0^x t^{\hat{\alpha}-1} e^{-t} dx \tag{1.9}$$

where $t = x/\hat{\beta}$. S is the gamma function is undefined for $x = 0$ and precipitation may contain zeros, the calculations of the probability of zero and non-zero become (Lloyd-Hughes et al., 2002)

$$H(x) = q + (1 - q)F(x) \tag{1.10}$$

Table 1 Standardized precipitation index (SPI) drought classification.

SPI value (z-score)	Category
2.00 or more	Extreme wet
1.50 to 1.99	Severe wet
1.00 to 1.49	Moderate wet
0.99 to -0.99	Near normal
-1.00 to -1.49	Moderate drought
-1.5 to -1.99	Severe drought
-2 or less	Extreme drought

Table 2 Percent of normal drought classification.

Threshold range	Drought classification
180% or more of normal rainfall	Extreme wet
161% to 180% of normal rainfall	Severe wet
121% to 160% of normal rainfall	Moderate wet
81% to 120% of normal rainfall	Near normal
41% to 80% of normal rainfall	Moderate drought
21% to 40% of normal rainfall	Severe drought
20% or less of normal rainfall	Extreme drought

where q is the probability of zero rainfall when m is the number of zeros in a precipitation time series, and q is estimated by m/n. The cumulative probability, $H(x)$, is then transformed to the standardized normal distribution so that the SPI mean (z) and the variance become 0 and 1, respectively. Using an approximation provided by Abramowitz and Stegun (1965);

$$SPI - G = z = -\left(k - \frac{c_0 + c_1 k + c_2 k^2}{1 + d_1 k + d_2 k^2 + d_3 k^3}\right) \tag{1.11}$$

when

$$k = \sqrt{\ln\left\{\frac{1}{[H(x)]^2}\right\}}$$

for $0 < H(x) \leq 0.5$

$$SPI - G = z = +\left(k - \frac{c_0 + c_1 k + c_2 k^2}{1 + d_1 k + d_2 k^2 + d_3 k^3}\right) \tag{1.12}$$

when $k = \sqrt{\ln\left\{\frac{1}{[1 - H(x)]^2}\right\}}$ for $0.5 < H(x) \leq 1$, where $c_0 = 2.515517$, $c_1 = 0.802853$, $c_2 = 0.010328$, $d_1 = 1.432788$, $d_2 = 0.189269$, and $d_3 = 0.001308$.

The z-ranges that are used to define the severity of the drought for SPI-N, SPI-L, and SPI-G are the same and presented in Table 1. (Barua et al., 2010)

1.2.2 Percent of Normal

The percent of normal (PN) can be calculated by dividing actual precipitation by normal precipitation, i.e., typically considered to be a

Table 3 Deciles drought classifications.

Threshold range	Drought classification
Deciles 1–2 (lowest 20%)	Much below normal
Deciles 3–4 (next lowest 20%)	Below normal
Deciles 5–6 (middle 20%)	Near normal
Deciles 7–8 (next highest 20%)	Above normal
Deciles 9–10 (highest 20%)	Much above normal

Table 4 Drought classification according to D-score values for wet and dry periods.

D-score (DPI value)	Category	Remark
0.25 or more	Extreme wet	about 75% or more less than the mean value
0.21—0.24	Severe wet	about 60–74% less than the mean value
0.14—0.20	Moderate wet	about 37–59% less than the mean value
0.13 to -0.19	Near normal	about 36% more or less than the mean value
-0.20 to - 0.39	Moderate drought	about 37–59% less than the mean value
-0.40 to - 0.59	Severe drought	about 60–74% less than the mean value
-0.60 or less	Extreme drought	about 75% or more less than the mean value

30-year mean, and multiplying the ratio by 100% (Hayes, 2006). The PN drought classification is presented in Table 2 (Barua et al., 2010).

1.2.3 Deciles

This method is based on dividing the distribution of monthly precipitation records into 10 parts (or deciles) (Tsakiris et al., 2007). It was developed by Gibbs and Maher (1967) to avoid some of the weaknesses within the "percent of normal" approach. In calculating deciles, long-term monthly rainfall records are first ranked from highest to lowest to construct a cumulative frequency distribution (Barua et al., 2010). The threshold ranges of deciles used to define drought conditions are presented in Table 3 (Gibbs & Maher, 1967).

1.2.3.1 China-Z index

The China-Z index (CZI) was introduced by the National Meteorological Center of China (NMCC) in the early 1990s. The CSI is calculated as (Ju et al., 1997):

$$z_i = \frac{6}{C_{si}}\left(\frac{C_{si}}{2}\varphi_i + 1\right)^{1/3} - \frac{6}{C_{si}} + \frac{C_{si}}{6} \tag{1.13}$$

$$C_{si} = \frac{\sum_{j=1}^{n}(x_{ij} - \overline{x}_i)}{n \star \sigma_i^{\,3}} \tag{1.14}$$

$$\varphi_i = \frac{x_i - \overline{x}_i}{\sigma_i} \tag{1.15}$$

where z_i is the CZI rate, i is the time scale interest, C_{si} is the coefficient of skewness, n is the total number of years in the record, φ_i is the standard

deviation, x_i is the precipitation, $\overline{x_i}$ is the average, and σ_i is the standard deviation. Note that the z-table given in Table 4 is used for the drought category.

1.2.3.2 Standardized precipitation evapotranspiration index

The standardized precipitation evapotranspiration index (SPEI) considers the variability of precipitation and temperature to predict drought conditions in a region. In calculating the SPEI, the initial step is to determine the monthly potential evapotranspiration (PET), determine the monthly deficit (D_i) as follows:

$$D_i = P_i - PET_i \tag{1.16}$$

where P_i is the total precipitation in the ith month, and PET_i is the monthly potential evapotranspiration in the ith month. Finally, the computed values are standardized and adapted to a log-logistics distribution function. The SPEI values for the ith month, which are the standardized values of the probability (p) of exceeding a given D_i, are calculated by (1.17) (Mehr et al., 2021).

$$SPEI_i = W_i - \frac{2.515517 + 0.802853W_i + 0.010328W_i^2}{1 + 1.432788W_i + 0.189269W_i^2 + 0.001308W_i^3} \tag{1.17}$$

$$W_i = \begin{cases} ifp < 0.5, \sqrt{-2lnp} \\ ifp > 0.5, \sqrt{-2\ln\ (1 - p)} \end{cases} \tag{1.18}$$

p is the exceedance probability of for calculated D_i values.

1.2.3.3 Reconnaissance drought index

The reconnaissance drought index (RDI) was first introduced by Tsakiris and Vangelis (2005) for assessing meteorological drought. The method employs precipitation and the evapotranspiration data, similar to the SPIE. It can be described in standardized (RDI_{st}), initial value (α_k), and normalized (RDI_n) forms (Zarch et al., 2015). The initial value (α_k) of RDI is usually calculated for the ith year in a time basis of k consecutive months as follows (Tsakiris & Vangelis, 2005):

$$\alpha_k^{(i)} = \frac{\sum_{j=1}^{k} P_{ij}}{\sum_{j=1}^{k} \mathrm{PET}_{ij}}, \quad i = 1(1)N \text{and} j = 1(1)k \tag{1.19}$$

where P_{ij} and PET_{ij} are the precipitation and potential evapotranspiration of the jth month of the ith year, and N is the total number of years of the available data. Further, Tigkas et al. (2015) and Tsakiris et al. (2007) showed that data can satisfactorily follow log-normal and/or gamma distributions for a wide range of locations and different reference periods. If log-normal distribution is applied, the following equation is used for the standardized RDI_{st} calculation (Tsakiris & Vangelis, 2005):

$$RDI_{st}^{(i)} = \frac{y^{(i)} - \overline{y}}{\hat{\sigma}_y} \tag{1.20}$$

where $y^{(i)}$ is the ln $(\alpha_k^{(i)})$, $\overline{y}$ is its arithmetic mean, and $\hat{\sigma}_y$ is its standard deviation. If the gamma distribution is used, then the RDI_{st} can be calculated as follows (Vangelis et al., 2013):

$$g(x) = \frac{1}{\beta^{\gamma}\Gamma(\gamma)} x^{\gamma-1} e^{-x/\beta}, \text{ for } x > 0 \tag{1.21}$$

For the computation of the normalized RDI_n, the following formula is used (Tsakiris & Vangelis, 2005):

$$RDI_{n(k)}^{(i)} = \frac{\alpha_k^{(i)}}{\overline{\alpha}_k} - 1 \tag{1.22}$$

where $\overline{\alpha}_k$ is the arithmetic mean of α_k values.

1.2.3.4 Discrepancy precipitation index

The proposed discrepancy precipitation index (DPI) is based on the discrepancy of precipitation data with respect to the mean value (Tayfur, 2021):

$$DPI = D_i = \log\left(\frac{P_i}{\overline{\boldsymbol{P}}}\right) \tag{1.23}$$

$$\overline{P} = \frac{1}{N}\sum_{i=1}^{N} P_i \tag{1.24}$$

where D_i is called the discrepancy value (D-score) for the ith precipitation, P_i is the ith precipitation of the data series, and $\overline{\boldsymbol{P}}$ is the mean value of the precipitation data series; typically considered to be a 30-year mean (Hayes, 2006; Willeke et al., 1994).

As to Eq. (1.5), $D = 0$ when P_i is equal to $\overline{P}$, and D is positive when $P_i > \overline{P}$ and D is negative when $P_i < \overline{P}$. The drought classification is categorized according to D-score values, as presented in Table 4.

The discrepancy measure (DM) can be employed for investigating the relation between the number of drought years and the precipitation received, and it is defined as follows (Tayfur, 2021):

$$DM = \frac{1}{N}\sum_{i=1}^{N}\left|\log\left(\frac{P_i}{\overline{P}}\right)\right| \tag{1.25}$$

1.3 Discussion and conclusions

Mishra and Singh (2010) have presented six different components of drought modeling: spatiotemporal drought analysis, probabilistic characterization of droughts, climate change impact on droughts, land data assimilation systems, drought forecasting, and drought management, which indicates that drought study is not a stand-alone effort. They have stated that "*even it is impossible to prevent the occurrence of a drought event, a preparedness and adoption of mitigation plans may smoothly convey the event to a risk rather than a disaster*".

The SPI is one of the most widely used indices in the World that is generally applied for meteorological drought monitoring. It has gained a lot of popularity and acceptance around the globe. Some other popular drought indices to quantify magnitude of meteorological drought are palmer drought severity index (PDSI), deciles index (DI), effective drought index (EDI), reconnaissance drought index (RDI), SPEI, and the DPI, which is gaining more attention in recent years. The SPI and DPI are preferable since they do require only the easily measurable precipitation data. However, it is worth noting that if a single drought index has to be suggested to be employed all over the World, such as the SPI or the DPI, the related score categories can be revised depending upon the climatic regions.

References

Abramowitz, M., & Stegun, I. A. (1965). Handbook of mathematical functions. In *NIBS applied mathematics series50*. New York: Cambridge University Press, 487.

Barua, S., Ng, A., & Perera, B. (2010). Comparative evaluation of drought indexes: Case study on the Yarra River catchment in Australia. *Journal of Water Resources Planning and Management, 137*, 215–226.

Cacciamani, C., Morgillo, A., Marchesi, S., & Pavan, V. (2007). Monitoring and forecasting drought on a regional scale: Emilia-Romagna region. In G. Rossi, (Ed.). *Methods and tools for drought analysis and management,* (pp. 29–48). Dordrecht: Springer Chapter 2.

Dai, A. (2011). Drought under global warming: A review. *Wiley Interdisciplinary Review Climate Change, 2*(1), 45–65.

Gasiorek, E., & Musial, E. (2015). Evaluation of the precision of standardized precipitation index (SPI) based on years 1954–1995 in Lodz. *Journal of Ecological Engineering, 16*, 49–53.

Gibbs, W. J., & Maher, J. V. (1967). Rainfall deciles as drought indicators. In *Bureau of meteorology bulletin No. 48*. Melbourne: Bureau of Meteorology.

Hayes, M. J. (2006). *Drought indices*. Wiley Online Library. Center. (Online) http://drought.unl.edu/whatis/indices.htm.

Ju, X., Yang, X., Chen, L.-J., & Wang, Y. (1997). Research on determination of station indexes and division of regional flood/drought grades in China. *Meteorological Applications, 8*, 26–32.

IPCC. (2014). *Synthesis Report. Contribution of working groups I, II and III to the fifth assessment report of the intergovernmental panel on climate change* (p. 151). IPCC.

Lloyd-Hughes, B., & Saunders, M. A. (2002). A drought climatology for Europe. *International Journal of Climatology, 22*, 1571–1592.

Mehr, A. D., Safari, M. J. S., & Nourani, V. (2021). Wavelet packet-genetic programming: A new model for meteorological drought hindcasting. *Teknik Dergi, 32*(4), 11029–11050.

Mishra, A. K., & Singh, V. P. (2010). A review of drought concepts. *Journal of Hydrology, 391*, 202–216.

Morid, S., Smakhtin, V., & Moghaddasi, M. (2006). Comparison of seven meteorological indices for drought monitoring in Iran. *International Journal of Climatology: A Journal of the Royal Meteorological Society, 26*(no. 7), 971–985.

Sonmez, F. K., Komuscu, A. U., Erkan, A., & Turgut, E. (2005). An analysis of spatial and temporal dimension of drought vulnerability in Turkey using the standardized precipitation index. *Natural Hazards, 35*, 243–264.

Tayfur, G. (2021). Discrepancy precipitation index for monitoring meteorological drought. *Journal of Hydrology, 597*, 126174. https://doi.org/10.1016/j.jhydrol.2021.126174.

Tigkas, D., Vangelis, H., & Tsakiris, G. (2015). DrinC: A software for drought analysis based on drought indices. *Earth Science Informatics, 8*(3), 697–709.

Tsakiris, G., & Vangelis, H. (2005). Establishing a drought index incorporating evapotranspiration. *European Water, 9*(10), 3–11.

Tsakiris, G., Pangalou, D., & Vangelis, H. (2007). Regional drought assessment based on the reconnaissance drought index (RDI). *Water Resources Management, 21*(5), 821–833.

Tsakiris, G. (2017). Drought risk assessment and management. *Water Resources Management, 31*(10), 3083–3095.

Vangelis, H., Tigkas, D., & Tsakiris, G. (2013). The effect of PET method on reconnaissance drought index (RDI) calculation. *Journal of Arid Environments, 88*(13), 130–140. https://doi.org/10.1016/j.jaridenv.2012.07.020.

Vicente-Serrano, S. M., Juan, I. L. M., Santiago, B., Jorge, L. L., Cesar, A. M., & Tejeda, E. M. (2012). Accurate computation of a streamflow drought index. *Journal of Hydrologic Engineering, 17*(2), 318–332.

Willby, R. L., & Dessai, S. (2010). Robust adaptation to climate change. *Weather, 65*(7), 180–185. https://doi.org/10.1002/wea.54Weather.

Wilhite, D. A. (1996). A methodology for drought preparedness. *Natural Hazards, 13*, 229–252.

Willeke, G., Hosking, J. R. M., Wallis, J., & Guttman, N. B. (1994). The National drought atlas. Institute for Water Resources Report 94-NDS-4, US Army Corps of Engineers.

Wilhite, D. A., Sivakumar, M. V. K., & Pulwarty, R. (2014). Managing drought risk in a changing climate: The role of national drought policy. *Weather and Climate Extremes, 3*, 4–13.

Zarch, M. A., Asadi, B., Sivakumar, & Sharma, A. (2015). Droughts in a warming climate: A global assessment of standardized precipitation index (SPI) and reconnaissance drought index (RDI). *Journal of Hydrology, 526*, 183–195.

This page intentionally left blank

CHAPTER TWO

Bibliometry and Review

Mustafa Utku Yilmaz[1], **and Hulya Yilmaz**[2]
[1]Department of Civil Engineering, Kirklareli University, Kirklareli, Türkiye,
[2]Quality and Accreditation Office, Kirklareli University, Kirklareli, Türkiye

2.1 Introduction

Drought is a significant natural disaster that can have widespread impacts on human populations, ecosystems, agricultural productivity, and economic stability (Yao et al., 2020). It can be defined as a prolonged imbalance between the supply and demand of water within a specified region over a designated period (Beran & Rodier, 1985). However, drought is not merely limited to water scarcity. It can also be characterized by long-term deviations from normal hydrological variables such as river flow, groundwater levels, and soil moisture. Due to its broad impacts across various sectors, drought can manifest in multiple forms, making it challenging to develop a universally accepted definition (Mishra & Singh, 2011; Parsons et al., 2019; Wilhite et al., 2014).

Drought has significant environmental, economical, and social consequences. Environmentally, drought reduces water availability (Tzanakakis et al., 2020), accelerates environmental degradation, and threatens biodiversity (Desbureaux & Damania, 2018). It also increases wildfire risks (Taufik et al., 2019), causes crop failures (Orimoloye et al., 2022), leads to the spread of diseases (Choudhary & Senthil-Kumar, 2024), and results in the loss of agricultural land (Musolino et al., 2018). As drought affects various sectors, its consequences extend beyond the environmental realm, significantly influencing economical and social dynamics. Economically, it leads to decreased production and rising prices (Fleming-Muñoz et al., 2023), increased poverty and unemployment (Ding et al., 2011), reduced income (Fleming-Muñoz et al., 2023), and increased transportation costs (Schweighofer, 2014). Socially, drought drives migration (Adaawen et al., 2019) and exacerbates poverty and unemployment (Orimoloye et al., 2022). It negatively affects living conditions, mental health, and public safety (Pribyl et al., 2019; Wutich et al., 2020).

Drought Dynamics
DOI: https://doi.org/10.1016/B978-0-443-34205-9.00001-9
© 2026 Elsevier Inc. All rights are reserved, including those for text and data mining, AI training, and similar technologies.

Additionally, it poses risks to both human and animal life (Ferreira et al., 2019), and leads to famine and reduced income (Pribyl et al., 2019; Samuel et al., 2024). These effects, interacti with one another, further increase the complexity of the system (Chen et al., 2022). Mitigating these effects and ensuring sustainable management require a strong stakeholder collaboration and an integrated approach (Yilmaz, 2025).

While drought is a temporary phenomenon with varying impacts, aridity is a more persistent climatic condition that requires long-term adaptation strategies. Aridity is defined as the natural decrease in rainfall over extended period of time. It is also influenced by other climatic factors, including but not limited to high temperatures, high winds, and low relative humidity (Wilhite, 2016). Aridity is primarily driven by large-scale atmospheric and oceanic circulation patterns as well as regional geographic and topographic factors. Unlike localized issues such as groundwater management, the root cause of aridity extends beyond local influence. Aridity represents a long-term hydrological and climatic condition characterized by water scarcity, necessitating adaptation by local communities regardless of its origin (Damian et al., 2023). To mitigate the impacts of drought, an interdisciplinary approach should be adopted for monitoring droughts, with events objectively defined and assessed (Yilmaz, 2023).

The rising global temperatures and extreme weather events increase both the frequency and severity of droughts (Ozcelik et al., 2024). Droughts can be categorized into four distinct types: meteorological, agricultural, hydrological, and socioeconomic drought, each characterized by unique outcomes (Gholinia & Abbaszadeh, 2024). As illustrated in Fig. 2.1, the interactions among these different types of droughts and their transitions are complex and non-linear; mutual interactions can further complicate the process. Drought typically begins as a meteorological drought, where a deficiency in precipitation leads to a reduction in soil moisture. This can subsequently result in either agricultural or hydrological drought. Agricultural drought emerges when soil moisture depletion adversely affects plant growth and crop yields, while hydrological drought occurs as declining precipitation reduces surface and groundwater availability, increasing pressure on water resources. The prolonged effects of hydrological drought create imbalances in water access, disrupting economic activities, food security, and societal well-being, which in turn give rise to socioeconomic drought. The socioeconomic drought can exacerbate the severity of other drought types by increasing pressure on water

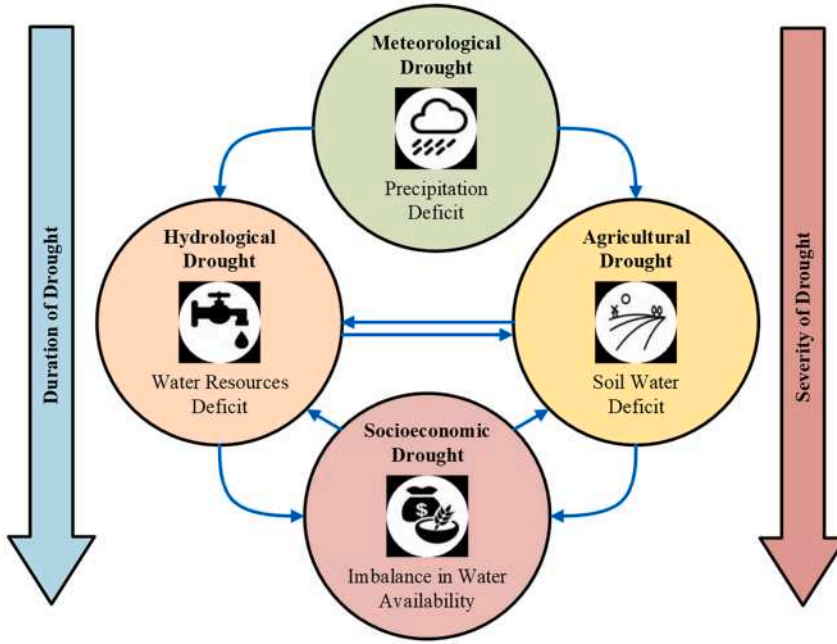


Figure 2.1 Flow diagram of drought types and drought development.

management and agricultural production (Mishra & Singh, 2011). This process does not necessarily follow a linear progression, as factors such as regional climate conditions, water management strategies, and human activities influence the pace and severity of drought cycles.

Given the increasing frequency and severity of drought, understanding the scientific landscape of drought research is essential for guiding future studies and informing policy decisions. Bibliometric analysis is an effective and widely used technique for gaining insight into a subject by observing the field of study as a whole. It is frequently used to understand how a discipline has evolved, define research questions, and contribute to the relevant field by identifying gaps in the literature (Ekundayo & Okoh, 2018; Yilmaz & Yilmaz, 2022; Yilmaz et al., 2025). To gain deeper insights into the evolution of this field, this chapter employs a bibliometric analysis, providing an assessment of key trends, emerging themes, methods, and research gaps. The maps generated in this analysis were obtained using VOSviewer software (van Eck & Waltman, 2010). To explain these issues, this chapter addresses the following research questions:

- **RQ1:** How has drought-related research evolved, and what are the temporal trends and changes?
- **RQ2:** What are the most cited drought-related studies in the literature? What topics were addressed in these studies?
- **RQ3:** Which countries and journals have published the most on the topic of drought?
- **RQ4:** How does the distribution of drought-related research vary according to different types of drought?
- **RQ5:** What are the key trends, prominent themes, and emerging developments in drought-related research?
- **RQ6:** What are the most commonly used datasets in drought-related research?
- **RQ7:** What are the most frequently applied methods and indices in drought prediction?
- **RQ8:** What gaps and underexplored areas exist in the current literature?

The structure of this chapter is as follows: Section 2.2 presents the bibliometric analysis results, including the trends in drought-related research over time, the countries and journals with the highest publication output, and the distribution according to drought types. Section 2.3 addresses thematic trends and emerging topics in drought-related research. Section 2.4 discusses the datasets commonly used in drought-related studies. Section 2.5 provides a detailed examination of the most frequently applied methods and indices for drought prediction. Finally, Section 2.6 summarizes the findings and offers recommendations for the future of drought research.

2.2 Results of bibliometric analysis

A well-defined search strategy is considered a fundamental prerequisite for conducting a bibliometric analysis, as it ensures the systematic retrieval of relevant literature. This process involves selecting appropriate keywords and specifying the fields in which these keywords are applied (e.g., title, abstract, keywords). In this context, the use of the wildcard character "*" in the term "drought" is considered crucial. The inclusion of "drought" enables the retrieval of various linguistic forms and derivatives (e.g., droughts, drought-related), thereby ensuring a more comprehensive dataset. Furthermore, bibliometric analyzes require a balanced approach to

avoid an excessively narrow or overly broad search scope (Donthu et al., 2021). To determine the optimal search criteria, various search queries using the term "drought*" are tested. The analysis, covering publications from 1980 to 2024, is conducted on January 10, 2025, using the Web of Science (WoS) database, focusing on English-language documents (including research articles, books, book chapters, and proceeding papers), yielding the following results:

- **Search 1** *(Title: 44567 results):* This search method retrieves publications in which "drought" is included in the title. Although it ensures a direct focus on the topic, it may lead to the exclusion of significant studies where the term is mentioned in the abstract or keywords but not in the title.
- **Search 2** *(Title OR Keywords: 61024 results):* By searching for "drought" in either the title or keywords, this approach captures a broader set of studies. However, this inclusivity may result in the inclusion of publications that mention drought only tangentially, thereby reducing the focus on research where drought is the central theme.
- **Search 3** *(Title AND Keywords: 25355 results):* Searching for "drought" in both the title and keywords yields a more focused set of studies. However, this approach may omit key publications where the abstract provides a substantial discussion of drought despite the absence of the term in the keywords. Therefore, while it ensures a narrower selection, it risks excluding important contributions.
- **Search 4** *(Title AND Abstract: 40783 results):* This approach retrieves publications that include "drought" in both the title and abstract. Such a criterion increases the likelihood that the retrieved articles focus primarily on drought, thereby filtering out works where drought is mentioned only peripherally.

Search 4 is selected for the bibliometric analysis due to its ability to retrieve a substantial number of publications, with a total of 40783 results. This approach is considered the most appropriate, as it ensures that the identified publications primarily focus on drought, enhancing the reliability and relevance of the analysis for policy development and future research. Among the retrieved documents, 38634 are classified as research articles, 1965 as proceeding papers, and 184 as book chapters. The subsequent subsections of this section present other findings obtained within this framework.

2.2.1 Trends of drought-related research

The trend of drought-related research has demonstrated a significant increase over time, as illustrated in Fig. 2.2. The publication trend is represented by a red line, with an R^2 value of 0.9779, indicating strong exponential growth in the field. The sharp increases in the number of publications are marked with green dashed lines in the years 2009, 2015, and 2020. Based on these changes, the publications are categorized into four distinct periods. The early period (1980–2009) is characterized by relatively low publication numbers, averaging 204 per year, reflecting limited attention to drought-related issues. The first growth period (2010–15) exhibits steady growth, with an average of 1182 publications per year. The period of rapid growth (2016–20) shows a more substantial increase, with an average of 2362 publications per year. Finally, the period of explosive growth (2021–24) represents the most pronounced surge, with an average of 3937 publications per year. This escalation can be attributed to the increasing concerns regarding the impacts of climate change on drought events.

2.2.2 Highly cited publications

Citation analysis is a method used to evaluate the academic and scientific impact of a document (such as an article, book, or conference paper) within

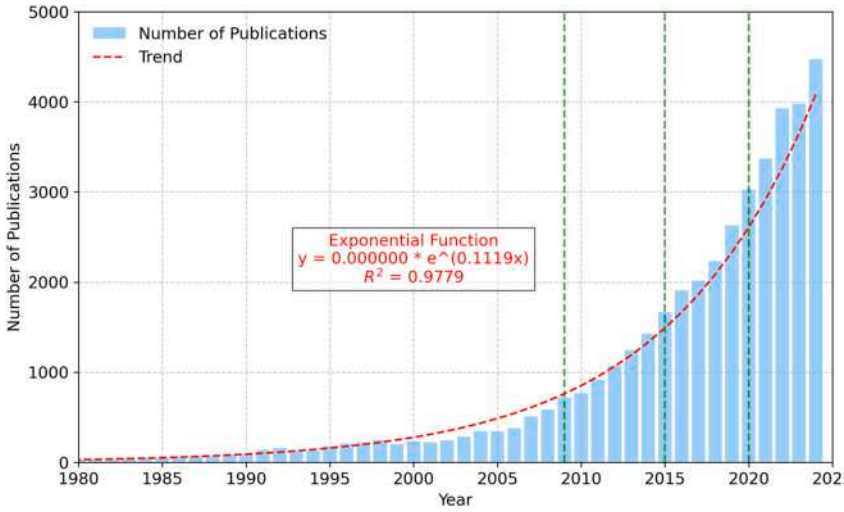


Figure 2.2 The trend of drought-related publication over time 1980–2024.

the scholarly literature. This analysis measures the frequency with which a document is cited and assesses the influence and contributions of specific studies or authors in the scientific domain. Citation analysis serves several purposes and offers various benefits. Highly cited publications provide valuable insights into influential research that has shaped the field of drought studies. The density visualization represents the citation levels of publications. Fig. 2.3 shows different citation levels using the colors red, yellow, green, and blue. Red represents the most cited studies. Yellow indicates publications with slightly fewer citations but still significant. Green corresponds to publications with moderate citation levels. Blue represents studies with lower citation counts, suggesting they have received less attention.

Additionally, Table 2.1 below presents the top 10 most cited drought-related studies, among which the Standardized Precipitation Evapotranspiration Index (SPEI) has become highly influential in drought research (Vicente-Serrano et al., 2010). This is followed by an exploration of the effects of climate stress on forests (Allen et al., 2010). Significant attention has also been given to studies on global aridity trends and crop yields (Ciais et al., 2005; Dai, 2013). Other highly cited works have addressed plant responses to drought stress (Farooq et al., 2009), molecular mechanisms underlying drought responses (Liu et al., 1998), and drought stress tolerance (Shinozaki & Yamaguchi-Shinozaki, 2007). In addition, the

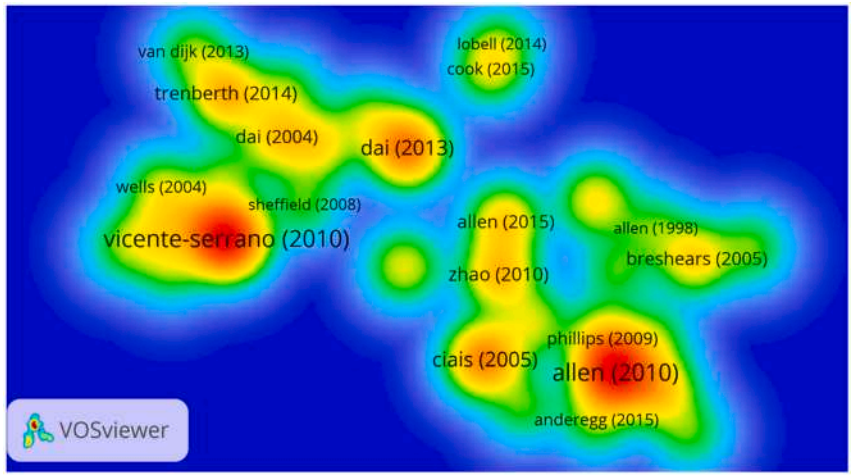


Figure 2.3 Citation analysis of highly cited publications.

Table 2.1 Top 10 most cited drought-related studies.

Author(s)	Year	TC	Focus
Vicente-Serrano, Beguería and López-Moreno (2010)	2010	5865	Proposed a new drought index
Allen *et al.* (2010)	2010	5462	Forests and climate stress
Dai (2013)	2013	3342	Global trends in aridity
Ciais *et al.* (2005)	2005	3074	Crop yields across Europe
Farooq *et al.* (2009)	2009	3070	Plant drought stress
Liu *et al.* (1998)	1998	2325	Molecular responses of plants to drought
Trenberth *et al.* (2014)	2014	2274	Global changes in drought patterns
Zhao and Running (2010)	2010	2047	Drought and carbon cycle
Choat *et al.*, (2012)	2012	1911	Forest mortality and hydraulic failure
Shinozaki and Yamaguchi-Shinozaki (2007)	2007	1816	Drought stress and tolerance mechanisms

TC, Total citations.

literature includes studies on global changes in drought patterns (Trenberth et al., 2014), the relationship between drought and the carbon cycle (Zhao & Running, 2010), and forest mortality associated with hydraulic failure (Choat et al., 2012). These studies cover a broad range of drought-related topics. The high citation counts indicate their significant impact on the field and widespread recognition in the scientific community. Their diverse focuses emphasize the importance of understanding drought from various perspectives, including ecological, agricultural, and climate-related aspects.

2.2.3 The most productive countries and international collaborations

The global distribution of countries with at least 100 drought-related publications is shown in Fig. 2.4. The number of publications is divided into categories and visualized with colors.

As can be seen from the world map, countries with more than 1000 drought-related publications are quite limited. The number of publications and citation effects for these countries are presented in Table 2.2 where China leads in total publications (12101), followed by the United States (8212) and India (2794). However, when considering research influence, measured by average citations per publication, France (60.49), the United

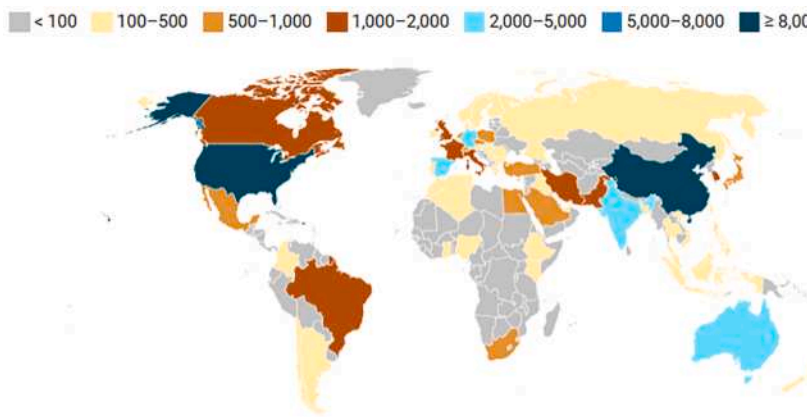


Figure 2.4 Global distribution of countries by drought-related publications. Map lines delineate study areas and do not necessarily depict accepted national boundaries.

Table 2.2 Countries with more than 1000 drought-related publications.

Country	NP	TC	API	Country	NP	TC	API
China	12,101	344,224	28.45	Iran	1991	42,117	21.15
United States	8212	421,591	51.34	Pakistan	1341	40,013	29.84
India	2794	74,247	26.57	Italy	1275	65,883	51.67
Germany	2336	105,242	45.05	France	1240	75,005	60.49
Australia	2033	97,120	47.77	Brazil	1223	41,049	33.56
Spain	2008	108,536	54.05	Canada	1186	54,338	45.82
United Kingdom	1992	112,834	56.64	South Korea	1070	39,260	36.69

NP, Number of publications; *TC,* total citations; *API,* average per item.

Kingdom (56.64), and Spain (54.05) have the highest citation averages. This suggests that publication quantity does not necessarily equate to research impact. Although China produces the largest volume of research, its average citation count (28.45) is lower than many European and North American countries. In contrast, European countries such as Germany, Spain, and the United Kingdom demonstrate both strong research productivity and high citation performance, underscoring their influence in the field. Notably, emerging contributors such as Iran (1991 publications), Pakistan (1336 publications), and Türkiye (891 publications) reflect

a growing engagement in drought-related studies, particularly in regions experiencing water stress. However, their relatively lower average citation counts suggest that while their research output is increasing, their global influence in the field remains in development.

Fig. 2.5 shows a co-authorship network map of the top 50 countries. This visualization highlights the scale and strength of international research collaborations. In the network, node size represents a country's publication output. Larger nodes indicate a stronger role in global scientific cooperation. The thickness of the connecting lines shows the strength of these collaborations, based on the frequency of joint publications.

The map reveals four distinct color clusters like blue, green, red, and yellow. The blue cluster includes countries such as the United States (8212 publications; API: 51.34), Brazil (1223 publications; API: 33.56), and Canada (1186 publications; API: 45.82), all of which have extensive international networks. Notably, the United States exhibits the largest node, reflecting both high productivity and citation impact. The green cluster features China (12101 publications; API: 28.45), India (2794 publications; API: 26.57), Australia (2033 publications; API: 47.77), Iran (1991 publications; API: 21.15), and Pakistan (1341 publications; API: 29.84), underscoring strong regional collaboration and increasing

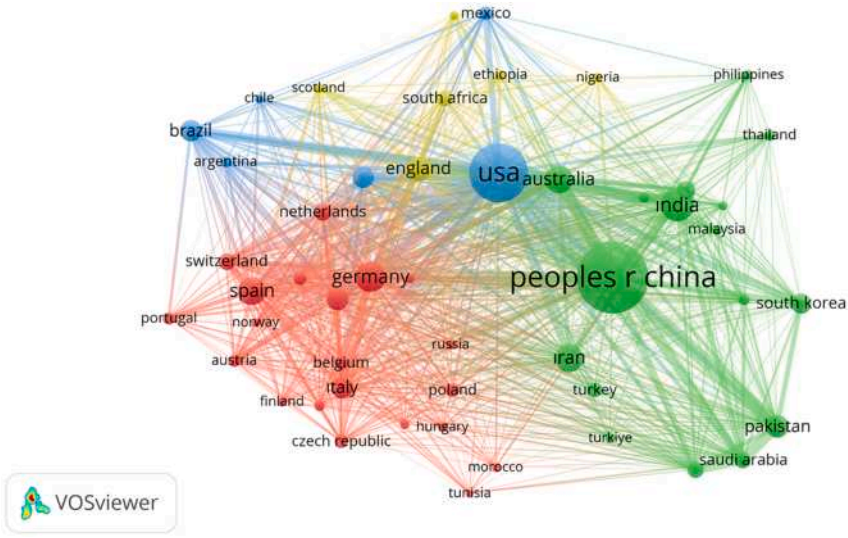


Figure 2.5 Co-authorship network map for the top 50 countries.

contribution. Türkiye, with 891 publications, and an API of 28.26 is also part of this cluster and maintains growing collaborations across both Asian and European research networks. The red cluster consists of European countries including Germany (2336 publications; API: 45.05), Spain (2008 publications; API: 54.05), Italy (1275 publications; API: 51.67), and France (1240 publications; API: 60.49), all characterized by dense internal connections and high citation averages, pointing to strong regional networks with high scientific quality. The yellow cluster groups countries like the United Kingdom (1992 publications; API: 56.64), South Africa (708 publications; API: 22.07), and Ethiopia (323 publications; API: 24.42), forming a unique network that also acts as a bridge between other clusters.

The co-authorship network demonstrates a rising level of international integration, with countries like the United States and China dominating both publication volume and partnerships, alongside the growing contribution of emerging economies. Notably, more than half of the top 10 countries listed in Table 2.2 belong to the green cluster, which includes many Asia-Pacific and developing nations, while European countries are predominantly concentrated in the red cluster. The generally higher average citation rates among European countries suggest strong regional collaboration networks and a focus on high-quality scientific output, underscoring the varied yet complementary roles of different clusters in global drought research.

2.2.4 Leading journals and citation analysis

Table 2.3 presents the top ten journals contributing to drought-related research, ranked based on the number of publications. The findings indicate that Frontiers in Plant Science is the most productive journal (1008 publications), followed by Plant Physiology and Biochemistry (574 publications) and the Journal of Hydrology (571 publications). These journals serve as key platforms for disseminating research on drought, particularly in the fields of plant sciences, hydrology, and environmental sciences. In terms of citation impact, the journals exhibit considerable variation. While PLOS One records the highest average citations per article (45.14), Scientific Reports (44.16) and the Journal of Hydrology (43.36) also demonstrate a high citation influence. These figures suggest that, although these journals publish fewer articles compared to the most productive outlets, the studies they disseminate tend to receive significant scholarly attention.

Table 2.3 The top 10 journals on drought-related research.

Rank	Journal	Category[a]	Impact[b]	NP	TC	API
1	*Frontiers in Plant Science*	Q1	4.8	1008	26,775	26.56
2	*Plant Physiology and Biochemistry*	Q1	5.7	574	20,476	35.67
3	*Journal of Hydrology*	Q1	6.3	571	24,761	43.36
4	*Plants-Basel*	Q1	4.1	560	7010	12.52
5	*Environmental and Experimental Botany*	Q1	4.7	538	19,037	35.38
6	*Science of The Total Environment*	Q1	8.0	530	16,857	31.81
7	*International Journal of Molecular Sciences*	Q1	4.9	525	9285	17.69
8	*Water*	Q2	3.0	498	6738	13.53
9	*Scientific Reports*	Q1	3.9	477	21,066	44.16
10	*PLOS One*	Q2	2.6	452	20,404	45.14

NP, Number of publications; *TC,* total citations; *API,* average per item.
[a] Quartile ranking from the 2024 Journal Citation Reports (JCR), Web of Science (WoS).
[b] Impact measured by the 2024 Journal Impact Factor (JIF), Web of Science (WoS).

The distribution of publications across journals reflects interdisciplinary research trends in drought studies. Plant-focused journals, including Environmental and Experimental Botany and International Journal of Molecular Sciences, contribute significantly, emphasizing the biological and physiological aspects of drought. Meanwhile, journals such as the Journal of Hydrology and Science of The Total Environment highlight the hydrological and environmental dimensions of drought research. Notably, multidisciplinary journals such as Scientific Reports and PLOS One rank among the most cited sources, demonstrating the broad relevance of drought research across different scientific domains. These journals provide platforms for studies integrating climatology, ecology, and policy-related aspects of drought. Overall, the analysis underscores that while Frontiers in Plant Science leads in research output, journals with higher citation rates such as PLOS One and Scientific Reports, play a crucial role in the dissemination of highly influential drought-related research.

2.2.5 Distribution of drought-related research by drought types

The analysis is then focused on understanding which drought types have been studied more extensively and how their interrelationships have been addressed in the literature. To examine the distribution of drought-related

research across different drought types, a new search was conducted in the WoS database, specifically within the title and abstract fields. This approach ensures the retrieval of only relevant publications, as titles typically provide summaries of a study's objectives. By limiting the search to these sections, the precision of the analysis is improved, and studies explicitly focused on the targeted drought types are captured. To identify relevant publications, specific keyword combinations are used. For individual drought types, searches are conducted using ("drought" AND "meteorological"), ("drought" AND "agricultural"), ("drought" AND "hydrologic*"), and ("drought" AND "socio-economic" OR "socioeconomic"). For studies covering multiple drought types, Boolean operators (i.e., AND, OR, NOT logical connectors used in search queries) are applied to the search. When two, three, or all four drought types are considered together, the relevant terms are combined, and unrelated categories are excluded using the "NOT" operator. For example, to find studies focusing only on meteorological and agricultural droughts, the query ("drought" AND "meteorological" AND "agricultural") NOT ("hydrologic*" OR "socio-economic" OR "socioeconomic") is used. This approach is consistently applied across all drought-type combinations. The term "hydrologic drought" is commonly used in the literature; therefore, the search uses "hydrologic*" to capture its variations. Similarly, since "socioeconomic" is more frequently preferred, the search includes both "socio-economic" OR "socioeconomic" to account for both variations. The search results, limited to articles, conference papers, and book chapters in English published up to the end of 2024, are obtained using the approach defined above and are presented in Table 2.4.

The high number of meteorological (1182), agricultural (1055), and hydrological (964) drought studies indicates a strong emphasis on the physical and environmental aspects of drought. In contrast, the lower number of socioeconomic drought studies (91) indicates that the social and economical dimensions of drought have not been sufficiently investigated. There are a limited number of studies that integrate socioeconomic impacts and examine multiple drought types simultaneously. Particularly, only two studies addressed all four drought types, highlighting a critical gap in holistic drought assessments. This suggests that the complex relationships between drought types have not been sufficiently explored. Both studies comprehensively assess drought vulnerability by considering all four drought types. The first study, uses statistical methods and Machine Learning (ML) and Deep Learning (DL) algorithms to evaluate the

Table 2.4 Results of drought types searched in the WoS database.

Drought type	Count
Meteorological	1182
Agricultural	1055
Hydrological	964
Socioeconomic	91
Meteorological and agricultural	95
Meteorological and hydrological	194
Meteorological and socioeconomic	5
Agricultural and hydrological	16
Agricultural and socioeconomic	8
Meteorological and agricultural and hydrological	36
Meteorological and agricultural and socioeconomic	1
Agricultural and hydrological and socioeconomic	-
Meteorological and agricultural and hydrological and socioeconomic	2

vulnerability of various drought types in India, highlighting the significant impacts of climate and economic factors on drought severity (Saha et al., 2023). Similarly, the second study, integrates multiple geospatial techniques and ML models to evaluate drought vulnerability in Northwestern Iran, emphasizing the importance of various geo-environmental factors, including all four drought types (Arabameri et al., 2022).

2.3 Trending topics and emerging themes in drought-related research

An overview of the top ten WoS categories and Citation Topics Meso in drought-related research is provided in Table 2.5. WoS categories classify publications based on their primary disciplinary fields, while Citation Topics Meso identify thematic clusters through citation patterns, revealing key research trends. Among WoS categories, Plant Sciences has the highest number of drought-related publications, followed by Environmental Sciences and Agronomy, underscoring the strong emphasis on agricultural and ecological aspects of drought. Other significant fields include Water Resources and Meteorology & Atmospheric Sciences, highlighting the hydrological and climatic dimensions of drought research. In Citation Topics Meso, Crop Science emerges as the most prominent theme, followed by Oceanography, Meteorology and Atmospheric

Table 2.5 The top 10 WoS categories and corresponding topics in drought-related research.

Rank	WoS Categories	Count	Citation Topics Meso	Count
1	Plant Sciences	11,930	Crop Science	14,628
2	Environmental Sciences	6946	Oceanography, Meteorology & Atmospheric Sciences	9483
3	Agronomy	4677	Forestry	4979
4	Water Resources	4580	Plant Pathology	1512
5	Meteorology Atmospheric Sciences	4289	Soil Science	1453
6	Geosciences Multidisciplinary	3495	Climate Change	1252
7	Ecology	2899	Remote Sensing	732
8	Forestry	2426	Marine Biology	539
9	Biochemistry Molecular Biology	1891	Photoproductivity	378
10	Multidisciplinary Sciences	1743	Entomology	324

Sciences, Forestry, and Soil Science, reflecting the diverse environmental and land-use implications of drought. This distribution underscores the interdisciplinary nature of drought research, with a strong presence in both biological and environmental sciences.

In addition to the disciplinary analysis presented earlier, drought-related studies engage with various Sustainable Development Goals (SDGs) (Dzhunushalieva & Teuber, 2024; Yumnam et al., 2024). The results indicate that the largest number of publications is associated with SDG 13 (Climate Action, 32236 records), followed by SDG 2 (Zero Hunger, 17438 records), SDG 14 (Life Below Water, 12088 records), SDG 15 (Life on Land, 10362 records), and SDG 6 (Clean Water and Sanitation, 9583 records). In contrast, fewer studies are linked to SDG 3 (Good Health and Well-Being, 2939 records), SDG 11 (Sustainable Cities and Communities, 1469 records), SDG 12 (Responsible Consumption and Production, 225 records), SDG 1 (No Poverty, 201 records), and SDG 7 (Affordable and Clean Energy, 144 records). It is important to note that a single study may address multiple SDGs, meaning that the total number of publications addressing SDGs exceeds the overall publication count. These findings suggest that while drought-related research predominantly focuses on

environmental and agricultural issues, socioeconomic and energy-related dimensions remain underexplored, highlighting promising areas for future research.

A more detailed analysis of emerging themes and research trends is carried out through keyword co-occurrence analysis. This co-occurrence analysis helps to reveal the conceptual structure of the field by identifying how key topics are interrelated and where research efforts have been concentrated. The clusters indicate thematic groupings based on their interconnections and frequency of co-occurrence in the literature in Fig. 2.6.

The green cluster keywords group is centered around the term "drought" and its connections with climate change, resilience, adaptation, precipitation, meteorological drought, agricultural drought, Standardized Precipitation Index (SPI), and SPEI. The presence of keywords such as machine learning, remote sensing, Normalized Difference Vegetation Index (NDVI), and Moderate Resolution Imaging Spectroradiometer (MODIS) suggests a strong focus on large-scale drought assessment and prediction, particularly on climate variability. These indicate the increasing integration of geospatial and computational methods in drought research.

The red cluster keywords group including drought stress, abiotic stress, transcription factor, transcriptome, and oxidative stress, focuses on plant physiological and genetic responses to drought conditions. The presence of crop-related terms such as rice, soybean, maize, wheat, and tomato

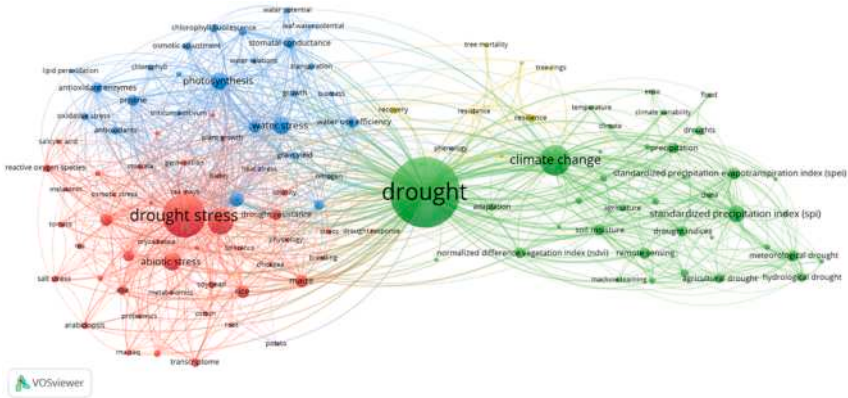


Figure 2.6 Visualization of co-occurring keywords in the drought-related studies.

highlights research in plant breeding and genetic engineering for drought resilience.

The blue cluster keywords group is linked to photosynthesis, water stress, stomatal conductance, transpiration, and water use efficiency, reflecting a strong emphasis on plant eco-physiological responses to drought. Keywords such as chlorophyll fluorescence and proline indicate research on biochemical markers used to assess plant stress responses, suggest the importance of drought mitigation strategies at the plant level.

The yellow cluster keyword group includes recovery, resilience, and resistance, which represent key ecological processes describing how ecosystems recover after drought and develop long-term resilience. Additionally, terms such as tree mortality and grassland indicate research focusing on the impacts of drought on forest ecosystems and natural vegetation.

The relationships between clusters reveal significant interdisciplinary connections in drought-related research. The green cluster and the blue cluster are frequently co-occurring, indicating that studies on plant physiological and molecular responses to drought often integrate both abiotic stress factors and water availability dynamics. This suggests that researchers tend to examine how plants physiologically cope with drought while simultaneously considering genetic and molecular adaptation mechanisms. Moreover, both the green and blue clusters are frequently linked to the red cluster, particularly through the climate change node. This reflects a broader trend in the literature where drought-related physiological and molecular studies are increasingly framed within the context of climate change impacts.

2.4 The most commonly used datasets in drought-related research

In this section, conclusions regarding datasets are drawn using the keywords obtained from the analysis in Section 2.2. The identified keywords were categorized based on the data types, and their frequencies were determined. The results are presented in Table 2.6

For meteorological data types, the most frequently used keywords are precipitation (520) and temperature (293). This indicates that most drought-related studies focus on precipitation and temperature data. This finding is supported by the widespread use of drought indices such as SPI

Table 2.6 Data types used in drought-related research.

Data Type	Keyword (Count)	Total Count
Meteorological	Precipitation (520), temperature (293), rainfall (196), potential evapotranspiration (52), humidity (12)	1021
Hydrological	Soil moisture (568), groundwater (156), streamflow (101), potential evapotranspiration (52), runoff (50), sea surface temperature (24), surface water (20), discharge (10)	981
Agricultural	Yield/crop yield (997), soil moisture (568), biomass (373), grow rate (75), harvest index (58), leaf temperature (31), soil temperature (16), crop growth (11)	2082
Socioeconomic	Migration (33), water consumption (18)	51
Satellite and Remote Sensing	Remote sensing (536), MODIS (228), Landsat (64), satellite/satellite imagery (43), spectral reflectance/imaging (38), sentinel-2 (29), sentinel-1 (13)	951

and SPEI. For hydrological data types, the most common keywords include soil moisture (568), groundwater (156), and streamflow (101). These data types play a crucial role in hydrological drought analysis. The importance of soil moisture and groundwater in monitoring water resources is highlighted by these results. Additionally, potential evapotranspiration is commonly used as it is a key component of the water cycle, representing the atmospheric demand for water and influencing drought severity assessments. For agricultural data types, the most frequently used keywords are yield or crop yield (997) and soil moisture (568). This highlights the relationship between drought and agricultural productivity, particularly the impact of soil moisture on crop yields. The studies have examined crop yields for various products, with grain yield (295) being the most frequently used keyword related to yield. Research on the socioeconomic impacts of drought is limited, resulting in the identification of only a small number (51) of keywords related to socioeconomic data types. However, keywords such as migration (33) and water consumption (18) indicate research on the effects of drought on communities, migration, and water consumption. These findings suggest the need for further studies on the socioeconomic impacts of drought. The most prominent keywords for Satellite and

Remote Sensing data types are remote sensing (536) and MODIS (228). Additionally, keywords related to specific satellite data, such as Landsat, Sentinel-1, and Sentinel-2, emphasize the use of high-resolution and precise analysis techniques in drought-related studies.

The most commonly used data types in drought-related research include meteorological data, with a focus on precipitation and temperature, hydrological data such as soil moisture and groundwater, and agricultural data, particularly yield and soil moisture. Research on the socioeconomic impacts of drought remains limited. Additionally, satellite data, particularly from MODIS and Landsat, are frequently utilized for high-resolution drought analysis.

2.5 The most commonly used methods and indices for drought prediction

This section aims to identify the methods used for drought prediction, the most commonly used drought indices, and the modeling approaches that have emerged in recent years. To ensure a broader perspective on drought prediction studies in the literature, a new search was conducted in the Title or Keywords fields using the keywords "drought" AND ("predict*" OR "estimate*" OR "forecast*") in the WoS database. The analysis includes only English-language research articles, books, book chapters, and conference proceedings. A total of 1923 documents met these criteria, including 15 book chapters, 185 conference papers, and 1723 research articles. The annual number of publications in this field remained below 50 until 2012, then exceeded 100 per year after 2017, peaking at 210 publications in 2024. These trends highlight a growing academic interest in drought prediction. When analyzed by subject area, Oceanography, Meteorology, and Atmospheric Sciences accounted for the largest share at 65.75%, followed by Forestry (7.57%), Crop Science (6.4%), and Climate Change (3.6%), respectively. This distribution suggests that drought prediction research is predominantly linked to climate and atmospheric processes. An analysis of contributions to drought prediction by country revealed that the United States (27.80%), China (19.72%), Iran (8.54%), India (7.01%), and Australia (6.81%) were the leading contributors. The high contributions from the United States and China may be associated with their advanced climate modeling infrastructures and large-scale research projects. Although Iran ranks 8th

globally in drought-related studies (see Table 2.2), it holds the 3rd position in studies specifically related to drought prediction. This may indicate that their research is primarily focused on drought prediction.

To provide deeper insights into the current trends in drought prediction studies, Fig. 2.7 illustrates a keyword co-occurrence map based on terms that appear at least 20 times in the selected literature. The analysis reveals the frequency and temporal distribution of these keywords, offering a visual representation of evolving research interests over time. The font size of the keywords on the map increases according to their frequency of usage in the literature. The color tones on the map represent the temporal distribution of these keywords: blue tones indicate earlier trends, while yellow tones reflect more recent trends. The analysis reveals that the SPI and SPEI are the most frequently used drought indices for drought prediction. In recent years, the use of data-driven methods such as ML and DL has significantly increased. Their ability to process large datasets has made these methods more attractive than traditional statistical approaches. Among them, Random Forest (RF) and Long Short-Term Memory (LSTM) have emerged as state-of-the-art methods. Meanwhile, Support Vector Machine (SVM) and Artificial Neural

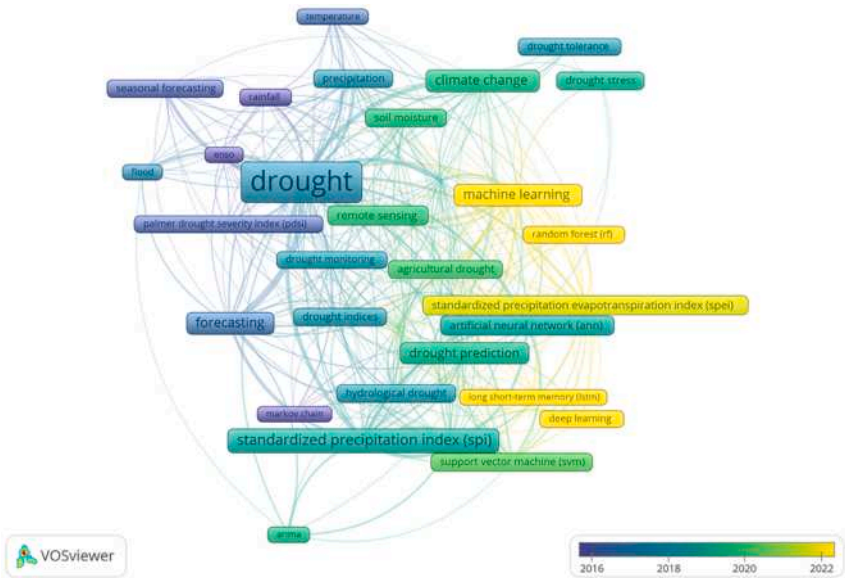


Figure 2.7 Temporal trends in keyword frequency for drought prediction research.

Networks (ANN) have gained popularity since the early 2020 s. This indicates a recent shift from traditional statistical models, such as ARIMA and Markov Chain, towards ML and DL methods.

2.6 Conclusion

This chapter presents a detailed bibliometric analysis of drought-related research from 1980 to 2024 based on the WoS database. It examines the development of the field, highlights common themes, and identifies areas where further research is needed. Since 2010, there has been a steady increase in publication volume. This trend became more pronounced after 2021, indicating growing academic interest in drought-related issues. Early studies focused mainly on meteorological and agricultural drought. In recent years, hydrological drought has received more attention. However, research on the social and economic aspects of drought remains relatively limited. Many highly cited studies address topics such as drought indices, plant stress responses, and ecological impacts. These findings show that the physical and environmental dimensions of drought are more frequently studied. In contrast, topics like water governance, community vulnerability, and long-term adaptation strategies are less often explored. Most of the research is carried out within natural sciences, with limited involvement from social sciences and humanities.

Geographical analysis shows that China has the highest number of publications. Countries like France, the United Kingdom, and Spain tend to have higher citation averages, which may reflect the visibility or impact of their research. The United States maintains strong output and international collaboration. Countries such as Iran and Türkiye are also contributing more in recent years. Türkiye, in particular, appears to connect research communities in both Asia and Europe. These observations suggest that both publication volume and international cooperation influence scientific visibility. Recent developments in machine learning and deep learning methods, especially RF and LSTM, offer useful tools for drought prediction and monitoring. Still, the use of these technologies in practical policy or management settings remains limited. In terms of alignment with the SDGs, most research relates to SDG 13 (Climate Action), SDG 2 (Zero Hunger), and SDG 14 (Life Below Water). However, links to SDG 1 (No Poverty) and SDG 12 (Responsible Consumption and Production) are relatively weak.

Despite the increase in research output, several gaps persist. Many studies are focused on climate and environmental aspects, while social, economic, and policy dimensions are often overlooked. Research activity also varies between regions. Developing countries, in particular, tend to have lower research output and impact. While new AI-based models offer potential, their practical applications are still in the early stages. To strengthen the impact of drought research, scientific findings should be more directly integrated into policy development and practical decision-making processes.

Overall, this chapter outlines how drought research has evolved and identifies the key challenges ahead. To better address the complex nature of drought, future studies should adopt more integrated approaches. Including social, economic, and governance perspectives will help improve understanding and support more effective and inclusive policies. Greater collaboration across disciplines and countries will also contribute to building more resilient societies.

AI disclosure

During the preparation of this work the author(s) used Grammarly and ChatGPT in order to improve the language, clarity, and readability. After using this tool/service, the author(s) reviewed and edited the content as needed and take(s) full responsibility for the content of the publication.

References

Adaawen, D., Rademacher-Schulz, C., Schraven, B., & Segadlo, N. (2019). Drought, migration, and conflict in sub-Saharan Africa: what are the links and policy options? *Current Directions in Water Scarcity Research, 2*, 15–31. https://doi.org/10.1016/B978-0-12-814820-4.00002-X.

Allen, C. D., Macalady, A. K., Chenchouni, H., Bachelet, D., McDowell, N., Vennetier, M., Kitzberger, T., Rigling, A., Breshears, D. D., Hogg, E. H., Gonzalez, P., Fensham, R., Zhang, Z., Castro, J., Demidova, N., Lim, J. H., Allard, G., Running, S. W., Semerci, A., & Cobb, N. (2010). A global overview of drought and heat-induced tree mortality reveals emerging climate change risks for forests. *Forest Ecology and Management, 259*(4), 660–684. https://doi.org/10.1016/j.foreco.2009.09.001.

Arabameri, A., Chandra Pal, S., Santosh, M., Chakrabortty, R., Roy, P., & Moayedi, H. (2021). Drought risk assessment: Integrating meteorological, hydrological, agricultural and socio-economic factors using ensemble models and geospatial techniques. *Geocarto International, 37*(21), 6087–6115. https://doi.org/10.1080/10106049.2021.1926558, http://www.tandfonline.com/toc/tgei20/current.

Beran, M. A., & Rodier, J. A. (1985). Hydrological aspects of drought: A contribution to the International Hydrological Programme. Studies and Reports in Hydrology, No. 39, UNESCO-WMO. https://unesdoc.unesco.org/ark:/48223/pf0000065181.

Chen, X., Tian, F., & Su, Y. (2022). How did the late 1920s drought affect northern Chinese society? *Weather and Climate Extremes, 36*, 100451. https://doi.org/10.1016/j.wace.2022.100451.

Choat, B., Jansen, S., Brodribb, T. J., Cochard, H., Delzon, S., Bhaskar, R., Bucci, S. J., Feild, T. S., Gleason, S. M., Hacke, U. G., Jacobsen, A. L., Lens, F., Maherali, H., Martínez-Vilalta, J., Mayr, S., Mencuccini, M., Mitchell, P. J., Nardini, A., Pittermann, J., Pratt, R. B., Sperry, J. S., Westoby, M., Wright, I. J., & Zanne, A. E. (2012). Global convergence in the vulnerability of forests to drought. *Nature, 491*(7426), 752–755. https://doi.org/10.1038/nature11688.

Choudhary, A., & Senthil-Kumar, M. (2024). Drought: A context-dependent damper and aggravator of plant diseases. *Plant, Cell & Environment, 47*(6), 2109–2126. https://doi.org/10.1111/pce.14863.

Ciais, P., Reichstein, M., Viovy, N., Granier, A., Ogée, J., Allard, V., Aubinet, M., Buchmann, N., Bernhofer, C., Carrara, A., Chevallier, F., De Noblet, N., Friend, A. D., Friedlingstein, P., Grünwald, T., Heinesch, B., Keronen, P., Knohl, A., Krinner, G., Loustau, D., Manca, G., Matteucci, G., Miglietta, F., Ourcival, J. M., Papale, D., Pilegaard, K., Rambal, S., Seufert, G., Soussana, J. F., Sanz, M. J., Schulze, E. D., Vesala, T., & Valentini, R. (2005). Europe-wide reduction in primary productivity caused by the heat and drought in 2003. *Nature, 437*(7058), 529–533. https://doi.org/10.1038/nature03972.

Dai, A. (2013). Increasing drought under global warming in observations and models. *Nature Climate Change, 3*(1), 52–58. https://doi.org/10.1038/nclimate1633.

Damian, N., Mitrică, B., Mocanu, I., Grigorescu, I., & Dumitraşcu, M. (2023). An index-based approach to assess the vulnerability of socio-ecological systems to aridity and drought in the Danube Delta, Romania. *Environmental Development, 45*, 100799. https://doi.org/10.1016/j.envdev.2022.100799.

Desbureaux, S., & Damania, R. (2018). Rain, forests and farmers: Evidence of drought induced deforestation in Madagascar and its consequences for biodiversity conservation. *Biological Conservation, 221*, 357–364. https://doi.org/10.1016/j.biocon.2018.03.005.

Ding, Y., Hayes, M. J., & Widhalm, M. (2011). Measuring economic impacts of drought: A review and discussion. *Disaster Prevention and Management, 20*(4), 434–446. https://doi.org/10.1108/09653561111161752.

Donthu, N., Kumar, S., Mukherjee, D., Pandey, N., & Lim, W. M. (2021). How to conduct a bibliometric analysis: An overview and guidelines. *Journal of Business Research, 133*, 285–296. https://doi.org/10.1016/j.jbusres.2021.04.070.

Dzhunushalieva, G., & Teuber, R. (2024). Roles of innovation in achieving the sustainable development goals: A bibliometric analysis. *Journal of Innovation & Knowledge, 9*(2), 100472. https://doi.org/10.1016/j.jik.2024.100472.

Ekundayo, T. C., & Okoh, A. I. (2018). A global bibliometric analysis of Plesiomonas-related research (1990–2017). *PLoS One, 13*(11), e0207655. https://doi.org/10.1371/journal.pone.0207655.

Farooq, M., Wahid, A., Kobayashi, N., Fujita, D., & Basra, S. M. A. (2009). Plant drought stress: Effects, mechanisms and management. In E. Lichtfouse, M. Navarrete, P. Debaeke, S. Véronique, & C. Alberola (Eds.), Sustainable agriculture (pp. 153–188). Dordrecht: Springer. https://doi.org/10.1007/978-90-481-2666-8_12.

Ferreira, S. M., le Roex, N., Greaver, C., & Cameron, E. Z. (2019). Species-specific drought impacts on black and white rhinoceroses. *PLoS One, 14*(1), e0209678. https://doi.org/10.1371/journal.pone.0209678.

Fleming-Muñoz, D. A., Whitten, S., & Bonnett, G. D. (2023). The economics of drought: A review of impacts and costs. *Australian Journal of Agricultural and Resource Economics, 67*(4), 501–523. https://doi.org/10.1111/1467-8489.12527.

Gholinia, A., & Abbaszadeh, P. (2024). Agricultural drought monitoring: A comparative review of conventional and satellite-based indices. *Atmosphere, 15*(9), 1129. https://doi.org/10.3390/atmos15091129.

Liu, Q., Kasuga, M., Sakuma, Y., Abe, H., Miura, S., Yamaguchi-Shinozaki, K., & Shinozaki, K. (1998). Two transcription factors, DREB1 and DREB2, with an EREBP/AP2 DNA binding domain separate two cellular signal transduction pathways in drought-and low-temperature-responsive gene expression, respectively, in Arabidopsis. *The Plant Cell, 10*(8), 1391–1406. https://doi.org/10.1105/tpc.10.8.1391.

Mishra, A. K., & Singh, V. P. (2011). Drought modeling—A review. *Journal of Hydrology, 403*(1–2), 157–175. https://doi.org/10.1016/j.jhydrol.2011.03.049.

Musolino, D. A., Massarutto, A., & de Carli, A. (2018). Does drought always cause economic losses in agriculture? An empirical investigation on the distributive effects of drought events in some areas of Southern Europe. *Science of the Total Environment, 633*, 1560–1570. https://doi.org/10.1016/j.scitotenv.2018.02.308 www.elsevier.com/locate/scitotenv.

Orimoloye, I. R., Belle, J. A., Orimoloye, Y. M., Olusola, A. O., & Ololade, O. O. (2022). Drought: A common environmental disaster. *Atmosphere, 13*(1), 111. https://doi.org/10.3390/atmos13010111.

Ozcelik, C., Yilmaz, M. U., & Benli, K. (2024). Assessing drought in Turkish basins through satellite observations. *International Journal of Climatology, 44*(10), 3613–3640. https://doi.org/10.1002/joc.8541.

Parsons, D. J., Rey, D., Tanguy, M., & Holman, I. P. (2019). Regional variations in the link between drought indices and reported agricultural impacts of drought. *Agricultural Systems, 173*, 119–129. https://doi.org/10.1016/j.agsy.2019.02.015 www.elsevier.com/inca/publications/store/4/0/5/8/5/1.

Pribyl, K., Nash, D. J., Klein, J., & Endfield, G. H. (2019). The role of drought in agrarian crisis and social change: the famine of the 1890s in south-eastern Africa. *Regional Environmental Change, 19*(8), 2683–2695. https://doi.org/10.1007/s10113-019-01563-y.

Saha, A., Pal, S. C., Chowdhuri, I., Roy, P., Chakrabortty, R., & Shit, M. (2023). Vulnerability assessment of drought in India: Insights from meteorological, hydrological, agricultural and socio-economic perspectives. *Gondwana Research, 123*, 68–88. https://doi.org/10.1016/j.gr.2022.11.006.

Samuel, J., Rama Rao, C. A., Pushpanjali, Anshida Beevi, C. N., Raju, B. M. K., Amarender Reddy, A., Kumar, R. N., Reddy, A. G. K., Singh, V. K., Prabhakar, M., Siva, G. S., Raju, G., & Teggelli (2024). Enhancing farm income resilience through climate smart agriculture in drought-prone regions of India. *Frontiers in Water, 6*, 1327651. https://doi.org/10.3389/frwa.2024.1327651.

Schweighofer, J. (2014). The impact of extreme weather and climate change on inland waterway transport. *Natural Hazards, 72*(1), 23–40. https://doi.org/10.1007/s11069-012-0541-6.

Shinozaki, K., & Yamaguchi-Shinozaki, K. (2007). Gene networks involved in drought stress response and tolerance. *Journal of Experimental Botany, 58*(2), 221–227. https://doi.org/10.1093/jxb/erl164 Japan.

Taufik, M., Veldhuizen, A. A., Wösten, J. H. M., & van Lanen, H. A. J. (2019). Exploration of the importance of physical properties of Indonesian peatlands to assess critical groundwater table depths, associated drought and fire hazard. *Geoderma, 347*, 160–169. https://doi.org/10.1016/j.geoderma.2019.04.001.

Trenberth, K. E., Dai, A., Van Der Schrier, G., Jones, P. D., Barichivich, J., Briffa, K. R., & Sheffield, J. (2014). Global warming and changes in drought. *Nature Climate Change, 4*(1), 17–22. https://doi.org/10.1038/nclimate2067.

Tzanakakis, V. A., Paranychianakis, N. V., & Angelakis, A. N. (2020). Water supply and water scarcity. *Water, 12*(9), 2347. https://doi.org/10.3390/w12092347, http://www.mdpi.com/journal/water.

van Eck, N. J., & Waltman, L. (2010). Software survey: VOSviewer, a computer program for bibliometric mapping. *Scientometrics, 84*(2), 523–538. https://doi.org/10.1007/s11192-009-0146-3.

Vicente-Serrano, S. M., Beguería, S., & López-Moreno, J. I. (2010). A multiscalar drought index sensitive to global warming: the standardized precipitation evapotranspiration index. *Journal of Climate, 23*(7), 1696–1718. https://doi.org/10.1175/2009JCLI2909.1.

Wilhite, D. A. (2016). Managing drought risk in a changing climate. *Climate Research, 70*(2–3), 99–102. https://doi.org/10.3354/cr01430, http://www.int-res.com/articles/theme/c070p099.pdf.

Wilhite, D. A., Sivakumar, M. V. K., & Pulwarty, R. (2014). Managing drought risk in a changing climate: The role of national drought policy. *Weather and Climate Extremes, 3*, 4–13. https://doi.org/10.1016/j.wace.2014.01.002.

Wutich, A., Brewis, A., & Tsai, A. (2020). Water and mental health. *Wiley Interdisciplinary Reviews: Water, 7*(5), e1461. https://doi.org/10.1002/wat2.1461.

Yao, N., Li, L., Feng, P., Feng, H., Li Liu, D., Liu, Y., Jiang, K., Hu, X., & Li, Y. (2020). Projections of drought characteristics in China based on a standardized precipitation and evapotranspiration index and multiple GCMs. *Science of The Total Environment, 704*, 135245. https://doi.org/10.1016/j.scitotenv.2019.135245.

Yilmaz, M. U. (2023). Keşif kuraklık indeksi ve standartlaştırılmış yağış indeksi kullanılarak Kırklareli ilinde kuraklığın eğilimi ve zamansal değişkenliği. *Doğal Afetler ve Çevre Dergisi, 9*(2), 341–364. https://doi.org/10.21324/dacd.1296428.

Yilmaz, M. U. (2025). Enhancing sustainable flood risk management through a novel fuzzy multi-stakeholder framework. *Water Resources Management, 39*(3), 1453–1480. https://doi.org/10.1007/s11269-024-04012-6.

Yilmaz, M. U., & Yilmaz, H. (2022). An investigation of meteorological drought studies on a global scale using a bibliometric analysis. *Journal of Innovative Science and Engineering (JISE), 6*(1), 76–93. https://doi.org/10.38088/jise.993473.

Yilmaz, D., Yilmaz, H., Erdem, E. A., Yilmaz, M. U., Vaheddoost, B., & Aras, E. (2025). Mapping the evolution of sea outfall research: Insights for marine environmental sustainability. *Journal of Polytechnic, 28*(3), 987–1001. https://doi.org/10.2339/politeknik.1543710.

Yumnam, G., Gyanendra, Y., & Singh, C. I. (2024). A systematic bibliometric review of the global research dynamics of United Nations Sustainable Development Goals 2030. *Sustainable Futures, 7*, 100192. https://doi.org/10.1016/j.sftr.2024.100192.

Zhao, M., & Running, S. W. (2010). Drought-induced reduction in global terrestrial net primary production from 2000 through 2009. *Science, 329*(5994), 940–943. https://doi.org/10.1126/science.1192666.

This page intentionally left blank

CHAPTER THREE

An overview of drought indices

Ismail Dabanli[1], Furkan Sencer Kaçar[1,2], Abdullah Emin Demircioğlu[1,3], Cemre Erbil[1], and Mehmet Şerif Kayaalp[1]

[1]Department of Civil Engineering, Faculty of Civil Engineering, Istanbul Technical University, Istanbul, Türkiye,
[2]Department of Civil Engineering, Faculty of Engineering, Turkish-German University, Istanbul, Türkiye,
[3]Department of Civil Engineering, Faculty of Engineering, Marmara University, Istanbul, Türkiye

3.1 Introduction

Drought is an insidious natural disaster rooted in water deficiency (Dabanlı & Şen, 2018). It is distinct from all other natural disasters due to its capacity to cause widespread damage and affect the lives of thousands of people. Proper determination and characterization are essential for managing and mitigating damage caused by drought. Through indicators and indices, drought characterization facilitates preemptive precautions and operations during drought events (Vicente-Serrano et al., 2010).

Drought indices are quantitative measures that enable the determination of drought types and severity levels (Dabanlı et al., 2017). These indices are derived from single or multiple indicators such as precipitation, surface flow, temperature, and remote sensing-derived vegetation indices. However, relying solely on direct indicators may not adequately characterize drought conditions. Therefore, indices have been developed to directly assess drought type and severity across different climatic conditions. A drought index simultaneously evaluates water deficit and surplus; however, since water surplus is beneficial, focusing on dry conditions is critical for drought characterization.

Numerous drought indices have been developed using multiple factors and methodologies (Zargar et al., 2011). Advancements in measurement and observation technologies, particularly remote sensing, have accelerated the development of new drought assessment methodologies (Vicente-Serrano et al., 2010). Additionally, hybrid drought indices have emerged following the proliferation of multiple drought assessment methodologies.

Drought Dynamics
DOI: https://doi.org/10.1016/B978-0-443-34205-9.00003-2
© 2026 Elsevier Inc. All rights are reserved, including those for text and data mining, AI training, and similar technologies.

The existence of over 100 drought indices can lead to inconsistencies when applied independently in research. Some indices use varying classification levels or probability density functions (PDFs) to define drought severity, while others apply different methodologies even when using the same index. These conflicts often originate from discrepancies in reference methodology. If foundational studies contain inconsistencies or minor variations, subsequent research may inadvertently perpetuate them. Therefore, a comprehensive review of methodologies is essential to minimize such conflicts and errors in future drought assessments. This work reviews 45 indices from the literature. Vegetation indices such as the Normalized Difference Vegetation Index (NDVI) (Huang et al., 2021) are not classified as standalone drought indices. NDVI measures vegetation health and density in a specific area; while it can reflect agricultural drought conditions via its 0–1 classification scale, it does not broadly represent drought dynamics. Where vegetation indices are incorporated into hybrid or comprehensive methodologies, they are addressed within the calculation workflow.

This chapter compiles a comprehensive list of drought indices for meteorological, agricultural, and hydrological droughts. It aims to equip researchers with mathematical formulations and step-by-step calculation workflows for widely used indices, eliminating the need for external references.

3.2 Characterization of drought

In general, water deficiency is the fundamental driver of drought. Dozens of drought indices have been used to illustrate drought variability in regional and global studies. First, the definition and characterization of drought should be grounded in established definitions. Subsequently, the classification and methodologies of drought indices can be effectively understood. Otherwise, misinterpretation or incomplete understanding of the drought concept may introduce methodological complexities in evaluating and classifying drought disasters.

3.2.1 Drought definition

The definition of drought is complex due to its stochastic nature. Many people consider drought to be a precipitation shortage; however, drought is influenced by a variety of parameters that vary based on its characteristics

and types. Drought is generally defined as the persistence of moderate, severe, or extreme water shortages under below-normal conditions in a specific region over a defined period (Zargar et al., 2011). The deficiency of precipitation marks the onset of a drought period; subsequently, deficiencies in other hydrometeorological and agricultural parameters extend drought impacts across various environmental and social domains (Tsakiris & Vangelis, 2005).

The primary types of drought are categorized into three main fields: meteorological, agricultural, and hydrological drought. The social impacts of these drought types have also led to the inclusion of a fourth type, known as socioeconomic drought (see Fig. 3.1). The initial deficiency of water begins with precipitation, which triggers meteorological drought. This is followed by agricultural drought, which affects soil moisture, and culminates in hydrological drought, impacting surface and groundwater flows.

The terminology used in drought studies has evolved since the emergence of early drought research. Although different terms have been used to describe the same physical processes, certain drought definitions are widely accepted and consistently applied in research. Therefore clearly defining key terminology is essential for any drought investigation to

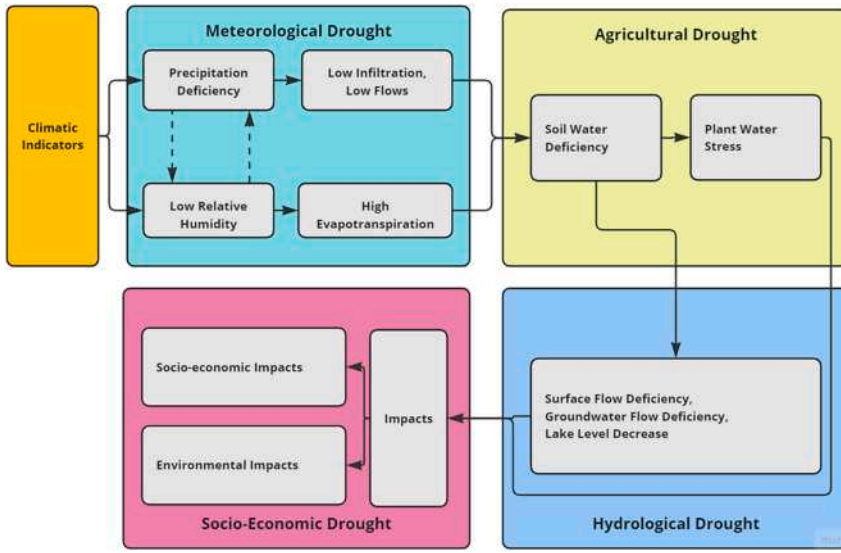


Figure 3.1 General development of drought types.

ensure clarity and prevent conflicts in terminology. The key terminologies related to drought are defined below to promote consistent usage in the literature:

Magnitude: The total accumulated deficiency of water relative to a designated threshold.

Duration: The time period between the onset and conclusion of water deficiency.

Severity: The degree of water deficiency.

Intensity: The ratio of magnitude to duration.

Frequency (Return Period):The average time interval between consecutive drought events.

Spatial (Geographic) Extent: The geographic area affected by drought.

Temporal Extent: The time period over which drought occurs.

3.2.2 Drought indicators

Precipitation is the primary indicator of meteorological drought. In addition to precipitation deficiency, other indicators such as potential and actual evapotranspiration, runoff, and soil moisture are also used to characterize drought events. Depending on the drought assessment model or framework, these indicators may be used individually or combined in various ways to generate a drought index. For example, precipitation and temperature are key indicators of meteorological drought. Similarly, surface flow, groundwater flow, groundwater level, and lake level are considered primary indicators of hydrological drought. Finally, the main indicators of agricultural drought include potential evapotranspiration and soil moisture. Additionally, vegetation cover is another critical parameter for evaluating agricultural drought.

3.2.3 Drought indices taxonomy

Generally, drought indices are classified based on the type of target field. Mostly, drought indices are categorized into meteorological, agricultural, and hydrological drought. Nowadays, a new drought concept has been added to these three types as socio-economic drought, which can be related to the post-impact of a drought period. Hydroclimatological, remote sensing-based, or combined indices have been used to evaluate drought conditions. The comprehensive approach can consist of single or multiple indicators or parameters. In this study, a comprehensive approach is followed to determine and evaluate all existing indices.

3.3 Drought indices

A comprehensive overview of all indices evaluated in this study, organized alphabetically, is presented in Table 3.1. The table provides detailed information on the parameters, advantages, limitations, and applications of each index for different drought characteristics.

3.3.1 Aggregate drought index

The aggregate drought index (ADI), proposed by Keyantash and Dracup (2004), is a comprehensive measure for evaluating hydrological, meteorological, and agricultural drought by integrating selected input parameters such as precipitation (P), evapotranspiration (ET), streamflow (SF), reservoir storage (ReS), soil moisture (SM), and snow water content (SWC). The inclusion or exclusion of these parameters is determined by the specific characteristics of the region being studied.

To compute ADI values, the P-mode principal component analysis (PCA) method is usually applied (Keyantash & Dracup, 2004). The computational process involves several steps:

- Construction of the Original Data Matrix (O) using the selected input variables.
- Formation of the *pxp* correlation matrix (R) for each month to derive principal components using Eq. (3.1):

$$R = \frac{1}{N-1} X^T X \tag{3.1}$$

where N is the hydrological years and X is the standardized data of the original data matrix.

Then, principal components are calculated for each correlation matrix by using Eq. (3.2):

$$Z = XE \tag{3.2}$$

where Z is the *nxp* principal components (PCs), n is the observation period, and E is the eigenvectors of PCA. Expressing the ADI as the first PC is normalized by its standard deviation using Eq. (3.3): $\mathrm{ADI}_{ik} = \frac{Z_{i1k}}{\sigma}$ (3.3)

where ADI_{ik} is the ADI value for month k in the year i, Z_{i1k} is the first PC for month k in the year i, and σ is the standard deviation of PC for month k over the observation period n (Keyantash & Dracup, 2004;Topçu et al., 2022). For a concise example of the computational procedures and additional details, readers are referred to (Keyantash & Dracup, 2004).

Table 3.1 An overview of drought indices (**Parameters:** *AET*, Actual Evapotranspiration; *BT*, Brightness Temperature; *ET*, Evapotranspiration; *EV*, Evaporation; *FC*, Field Capacity; *Gw*, Groundwater; *LST*, Land Surface Temperature; *NIR*, Near-Infrared; *P*, Precipitation; *PET*, Potential Evapotranspiration; *ReS*, Reservoir Storage; *RS*, Remote Sensing; *SF*, Streamflow/Runoff; *SM*, Soil Moisture; *SP*, Snowpack; *SNWC*, Snow Water Content; *T*, Temperature; *Tr*, Transpiration; *VWC*, Vegetation Water Content; *WP*, Wilting Point; **Drought Types:** *A*, Agricultural; *H*, Hydrological; *M*, Meteorological; **Drought Indices:** *NDVI*, Normalized Difference Vegetation Index).

No	Drought Indices	Parameters	Pros	Cons	References	Drought Type
1	Aggregate Drought Index (ADI)	*P*, *ET*, *SF*, *ReS*, *SM*, *SNWC*	• Meteorological, hydrological, and agricultural drought assessment • Rapid application to new data	• Noninclusion of temperature and groundwater	Keyantash and Dracup (2004)	A, H, M
2	Agricultural Drought Index (DTx)	*Tr*	• Sensitivity to drought when soil moisture is around wilting point • Use of a water balance model		Matera et al. (2007)	A
3	Agricultural Reference Index for Drought (ARID)	*P*, *PET*, *FC*, *WP*, *Tr*	• Simple to calculate • Physically and physiologically consistent	• Insufficient application in different regions	Woli et al. (2012)	A
4	Aridity Anomaly Index (AAI)	*AET*, *PET*	• Simple to calculate • Specific to agriculture	• Applicable to short-term period	India Meteorological Department	M
5	Aridity Index (AI)	*P*, *PET*	• Simple to calculate • Requires only two inputs	• Not suitable for specific applications	Thornthwaite (1948)	M

				• Unreliability in certain tropical regions		
6	China Z Index (CZI)	*P*	• Simple to calculate • Applicable to multiple time scales • Allow the incomplete data	• Sensitive to precipitation deficit • Limited representation of shorter timescales compared to SPI	China National Climate Center	M
7	Crop Water Stress Index (CWSI)	*RS, T*	• Straightforward calculations	• Irrigation-scheduling for some crops is not recommended	Idso et al. (1981)	A
8	De Martonne Aridity Index (I_{DM})	*P, T*	• Uses two inputs • Applicable to different time steps	• Ignore the effect of last time increment	De Martonne (1926)	M
9	Drought Area Index (DAI)	*P*	• Applicable for both drought and flood during Indian monsoons	• Insufficient amount of application in different climatic regions	Bhalme and Mooley (1980)	M
10	Drought Frequency Index (DFI)	*P, SF, SM*	• No effect of threshold and magnitude selection • Applicable to spatial analysis of drought due to the		González and Valdés (2006)	A, H, M

(*Continued*)

Table 3.1 (Continued)

No	Drought Indices	Parameters	Pros	Cons	References	Drought Type
			probabilistic nature of the index.			
11	Drought Severity Index (DSI)	*ET*, *PET*	• Uses relatively detailed scale maps		Mu et al. (2013a)	M
12	Effective Drought Index (EDI)	*P*	• Supported with detailed documentation • Powerful tool for drought monitoring and management	• May hinder operational use • Relies on solely precipitation data	Byun and Wilhite (1999)	M
13	Evaporative Stress Index (ESI)	*RS*, *ET*	• Shows areas in great detail and high resolution	• Data are not reliable on cloudy days	Anderson et al. (2011)	H, M
14	Evapotranspiration Deficit Index (ETDI)	*ET*, *SM*	• Considers two types of evapotranspiration	• Data can be problematic in summer	Narasimhan and Srinivasan (2005)	H, M
15	Groundwater Resource Index (GRI)	*Gw*	• Simple to use • More reliable results thanks to autocorrelation	• Being predictive creates several weaknesses	Mendicino et al. (2008)	H, M
16	Hybrid Drought Index (HDI)	*P, T, SWC, ReS*, *SF*, *SP*	• Calculation is made taking into account various factors	• Data accuracy and access to data is problematic	Kamruzzaman et al. (2019)	A, H, M
17	Hydro-thermal Coefficient of Selyaninov (HTC)	*P*, *T*	• Simple to calculate		Selyaninov, 1928	H

18	Keetch-Byram Drought Index (KBDI)	*P*, *T*	• Simple to calculate • Can be customized by location	• Does not take into account general assumptions	Keetch and Byram (1968)	M
19	Microwave Integrated Drought Index (MIDI)	*P*, *SM*, *S*	• Improve drought monitoring accuracy • Offers global and real-time observations	• May require expertize in data validation and computations	Zhang and Jia (2013)	A, H
20	Multivariate Standardized Drought Index (MSDI)	*P*, *SM*	• Simple to calculate • Monitor in dry and wet areas • Beneficial for specification of drought where precipitation and soil moisture are contributors	• Useful for certain areas	Hao and AghaKouchak (2013)	M
21	Palfai Aridity Index (PAI)	*P*, *T*, *Gw*		• Not easy to compute	Palfai (1990)	M
22	Palmer Moisture Anomaly Index or Palmer-Z Index (PZI)	*P*, *T*, *SF*, *SM*, *ET*	• Useful for comparing with different drought periods • Can be used to calculate the end of the drought	• Not useful for long term observations (more than 12 months) • May errors occur in heavy precipitation and frozen soils • Not easy to compute	Palmer (1965)	A, M

(*Continued*)

Table 3.1 (Continued)

No	Drought Indices	Parameters	Pros	Cons	References	Drought Type
23	Palmer Drought Severity Index (PDSI)	*P*, *T*, *SF*, *SM*, *ET*	• Offers global observations	• Not useful for short term observations • Not easy to compute	Palmer (1965)	M
24	Palmer Hydrological Drought Index (PHDI)	*P*, *T*, *SF*, *SM*, *ET*	• Compares meteorological and • hydrological drought across space and time	• Observations vary by region and time • Not easy to compute	Palmer (1965)	H, M
25	Percent of Normal Index (PNI)	*P*	• Simple and quick calculation • May be used for specifying impact of drought	• Not useful for comparing different clime regimes	Willeke et al. (1994)	H, M
26	Perpendicular Drought Index (PDI)	*P*	• Useful for drought assessment	• Not useful in different density type of soils	Ghulam et al. (2007)	M
27	Decile Index (DI)	*P*	• Meteorological, agricultural and hydrological drought assessment • Simple to calculate • Flexible for many situations	• Not useful for short-term observations	Alami and Tayfur (2022)	A, H, M
28		*P*	• Simple to calculate			A, M

	Rainfall Anomaly Index (RAI)		• Observation with one input for monthly, seasonal, annual duration	• Differences of data within a year must be small • Requires a dataset that is complete with estimations	Costa and Rodrigues (2017)	
29	Reconnaissance Drought Index (RDI)	*P*, *T*	• Simple to use	• Comparing for different climate regions may be cause error	Tsakiris and Vangelis (2005)	M
30	Regional Streamflow Deficiency Index (RDI)	*P*	• Simple to calculate	• Not useful for short-term observations	Stahl & Demuth, 2001	M
31	Scaled Drought Condition Index (SDCI)	*LST*, *NDVI*, *P*	• Drought assessment in both arid and humid regions		Rhee et al. (2010)	A
32	Soil Moisture Deficit Index (SMDI)	*SM*	• Thorough examination of the entire soil profile and different depths • Applicable for different crop types and growth periods	• Using all depth can raise problems about auto-correlation	Narasimhan and Srinivasan (2005)	A
33	Soil Water Deficit Index (SWDI)	*SM*, *FC*, *WP*	• Assessment of soil water deficiency	• Depends on unusual soil characteristics	Martínez-Fernández et al. (2015)	A
34	Standardized Anomaly Index (SAI)	*PET*	• Simple to calculate	• Solely relies on precipitation	Kraus (1977)	M, H

(*Continued*)

Table 3.1 (Continued)

No	Drought Indices	Parameters	Pros	Cons	References	Drought Type
			• Only one input is required • Calculate over any specified time frame			
35	Standardized Precipitation Evapotranspiration Index (SPEI)	*P*, *T*	• Includes two parameters • Applicable for many climate regimes	• Calculation steps are complex	Vicente-Serrano et al. (2010)	A, H
36	Standardized Precipitation Index (SPI)	*P*	• Simple to calculate • Only one input is required • Calculate over any specified time frame	• Solely relies on precipitation	McKee et al. (1993)	A, H
37	Standardized Runoff Index (SRI)	*P*, *SF*, *SM*	• Analyzes the spatial and temporal patterns of hydrological dryness.	• Not comprehensively depicts the spatial distribution of hydrological drought within a river basin	Shukla and Wood (2008)	H
38	Standardized Streamflow Index (SSI)	*P*, *PET*	• Observes and analyses water-related factors across various periods of time	• Disregards other possible factors	Modarres (2007)	A, H

39	Standardized Water Level Index (SWI)	*Gw*	• Categorizes and quantifies the severity of hydrological drought • Depicts the changing distribution of drought patterns over time	• Takes into account just water level anomalies	Bhuiyan (2004)	H
40	Streamflow Drought Index (SDI)	*SF*	• Accessible and user-friendly • Adaptable and resilient • Analyzes several timeframes	• Data quality of many variables making it challenging to use	Nalbantis and Tsakiris (2009)	H
41	Surface Water SupplyIndex (SWSI)	*ReS*, *SF*, *SP*, *P*	• Simple Calculation • Quantitative Assessment • Effective Communication	• Data Limitations • Assumption of Stationarity • Sensitivity to Inputs	Shafer and Dezman (1982)	H
42	Temperature–Vegetation Dryness Index (TVDI)	*T*, *NDVI*	• Integration of temperature and vegetation data • Sensitive to drought conditions • Remote sensing application • Timely and Spatially Explicit	• Sensitivity to input data quality • Interpretation challenge • Limited representation of hydrological conditions • Validation and calibration	Sandholt et al. (2002)	A
43	Thornthwaite Moisture Index (TMI)	*PET*, *P*, *T*	• Simple to calculate	• Requires statistically significant data of	Thornthwaite (1948)	A, H

(*Continued*)

Table 3.1 (Continued)

No	Drought Indices	Parameters	Pros	Cons	References	Drought Type
				temperature and rainfall		
44	Total Storage Deficit Index (TSDI)	*P*, *ET*, *SF*, *SM*, *Gw*	• Broad scope, remote sensing • Early detection	• Complexity of calculation • Data availability and quality • Spatial and temporal resolution	Yirdaw et al. (2008)	H
45	Vegetation Temperature Condition Index (VTCI)	*T*, *NDVI*	• Comprehensiveness • Spatial sensitivity • Early detection • Simple interpretation	• Site-specific and Time-specific • Data availability • Limited testing	Wang et al. (2001)	A
46	Water Balance Derived Drought Index (WBDDI)	*SF*	• Applicable in ungauged watersheds, • Easy to calculate and apply • Effective in specific regions	• Uncertainty propagation • Regional calibration limitations	Vasiliades et al. (2011)	H

Table 3.2 also provides the categorization of drought severity based on the ADI.

3.3.2 Agricultural drought index

The Agricultural Drought Index (DTx) was proposed by Matera et al. (2007) to express agricultural drought based on the summation of the difference between the daily maximum and effective transpiration computed by a water balance model. In comparison to other methods used to calculate agricultural drought, this approach is sensitive to drought when the soil moisture is close to the wilting point (Matera et al., 2007). DTx can be calculated for a range of periods (X=30, 60, and 180 days) as follows:

$$DT_x = \sum_{\text{today}-X}^{\text{today}} (\text{Tr}_m - \text{Tr}_e) \tag{3.4}$$

where Tr_m and Tr_e are the daily maximum and effective transpiration, respectively. Drought classes based on the DTx are given in Table 3.3

3.3.3 Agricultural reference index for drought

The Agricultural Reference Index for Drought (ARID) was developed by Woli et al. (2012) using a simple budget-based soil water balance approach. This approach requires fewer parameters, including precipitation (P), potential evapotranspiration (PET), field capacity (FC), and wilting point

Table 3.2 Drought severity based on the aggregate drought index (ADI).

ADI	Drought severity
≥ 1.50	Extremely wet
1.20 ~ 1.49	Very wet
0.90 ~ 1.19	Moderately wet
0.60 ~ 0.89	Slightly wet
0.30 ~ 0.59	Incipient wet
0.29 ~ −0.29	Near normal
− 0.30 ~ −0.59	Incipient drought
− 0.60 ~ −0.89	Mild drought
− 0.90 ~ −1.19	Moderate drought
− 1.20 ~ −1.49	Severe drought
≤ −1.50	Extreme drought

Source: From Wang, Sisi, Mo, Xingguo, Hu, Shi, Liu, Suxia Liu, Zhengjia. (2018). Assessment of droughts and wheat yield loss on the North China Plain with an aggregate drought index (ADI) approach. *Ecological Indicators*, 87, 107–116. https://doi.org/10.1016/j.ecolind.2017.12.047.

Table 3.3 Drought severity based on the agricultural drought index (DTx).

DTx	Drought severity
50%–75%	Normal
75%–90%	Moderate
90%–95%	Severe
95%–99%	Very severe
100%	Extreme

Source: From Matera, A., Fontana, G., Marletto, V., Zinoni, F., Botarelli, L., Tomei, F. (n.d.). Use of a new agricultural drought index within a regional drought observatory (Vol. 62, pp. 103–124). Springer Science and Business Media LLC. https://doi.org/10.1007/978-1-4020-5924-7_6.

(WP) of the soil. The grass is considered a reference crop to calculate ARID (Woli et al., 2012). When the grass is taken as the reference, transpiration is accepted to be nearly equal to evapotranspiration (Ritchie & Burnett, 1971; Woli et al., 2012). Therefore the daily ARID can be calculated by Eq. (3.5):

$$\mathrm{ARID}_i = 1 - \frac{\mathrm{Tr}_i}{\mathrm{PET}_{o,i}} \tag{3.5}$$

where daily transpiration and potential evapotranspiration are represented by Tr_i and $\mathrm{PET}_{o,i}$, respectively. In the case of no transpiration, ARID_i attains its maximum at 1, meaning the maximum water deficit. Conversely, when transpiration is at its maximum rate, ARID_i equals 0, denoting the absence of water deficit. Finally, the water deficit shows a linear increase with decreasing daily transpiration in the case of constant potential evapotranspiration (Woli et al., 2012).

3.3.4 Aridity anomaly index

According to Sarkar (2010), the Aridity Anomaly Index (AAI) was introduced by the India Meteorological Department (IMD) to observe agricultural drought during the summer crop season and rainfall patterns during the winter crop season. To calculate the AAI, the Aridity Index (AI), which is an index to monitor crop moisture stress, must first be calculated as (Sarkar, 2010):

$$\mathrm{IA} = \frac{\mathrm{PET} - \mathrm{AET}}{\mathrm{PET}} \tag{3.6}$$

where AET and PET are the actual and potential evapotranspiration, respectively. Then, the aridity anomalies can be calculated by using the actual and normal aridity indices for the same period as:

$$\mathrm{AAI} = \frac{\mathrm{IA} - \overline{\mathrm{IA}}}{\overline{\mathrm{IA}}} \times 100 \tag{3.7}$$

This index serves as a valuable tool for agricultural planning and enables timely warnings to authorities regarding severe drought conditions (Sarkar, 2010). The categorization of drought severity based on the AAI values is provided in Table 3.4.

3.3.5 Aridity index

The AI, proposed by Thornthwaite (1948), includes yearly P and PET to classify the aridity of a region. The AI can be calculated as:

$$\mathrm{AI} = \frac{\mathrm{P}}{\mathrm{PET}} \tag{3.8}$$

Five climatic classes are defined using the AI, which can be seen in Table 3.5.

3.3.6 China-Z index

The National Meteorological Center of China launched the China-Z Index (CZI) during the early 1990s to monitor drought and flood conditions in China (Wu et al., 2001). It is assumed that precipitation data follow a Pearson Type III distribution (Zeybekoğlu & Aktürk, 2021). The CZI can be expressed as:

$$Z_{ij} = \frac{6}{C_{si}}\left(\frac{C_{si}}{2}\varphi_{ij} + 1\right)^{1/3} + \left(\frac{C_{si}}{6} - \frac{6}{C_{si}}\right) \tag{3.9}$$

Table 3.4 Drought severity based on the aridity anomaly index (AAI).

AAI	Drought severity
AAI ≤ 25%	Mild drought
25% < AAI ≤ 50%f	Moderate drought
50% < AAI	Severe drought

Source: From Sarkar, J. (2010). Monitoring drought risks in India with emphasis on agricultural drought. In Agricultural drought indices. *Proceedings of the WMO/UNISDR Expert Group Meeting on Agricultural Drought Indices* (pp. 50–59). WMO.

Table 3.5 Drought severity based on the aridity index (AI).

AI	Drought severity
AI < 0.05	Hyper-arid, HA
0.05 ≤ AI < 0.20	Arid, A
0.20 ≤ AI < 0.50	Semi-arid, SA
0.50 ≤ AI < 0.65	Sub-humid, SH
0.65 ≤ AI	Humid, H

Source: From Proutsos, N. D., Tsiros, I. X., Nastos, P., Tsaousidis, A. (2021). A note on some uncertainties associated with Thornthwaite's aridity index introduced by using different potential evapotranspiration methods. *Atmospheric Research*, 260. https://doi.org/10.1016/j.atmosres.2021.105727.

where Z_{ij} is the CZI, i and j are the desired and current months, respectively. Wu et al. (2001) included i for computing the CZI for multiple time scales. Skewness (C_{si}) in Eq. (3.10) can be calculated as:

$$C_{si} = \frac{\sum_{j=1}^{n} (x_{ij} - \mu_i)^3}{n\sigma_i^3} \tag{3.10}$$

where n is the number of months in the record. The standardization of the P, also called the Z score, can be done as follows:

$$\varphi_{ij} = \frac{x_{ij} - \mu_i}{\sigma_i} \tag{3.11}$$

where x_{ij} is the precipitation of the j-th month for period i, μ_i is the average of the precipitation, and σ_i is the standard deviation of the precipitation. Drought severity based on the CZI is given in Table 3.6.

3.3.7 Crop water stress index

The crop water stress index (CWSI), empirically introduced by Idso et al. (1981) and theoretically proposed by Jackson et al. (1988), is a metric that combines canopy temperatures and water status to demonstrate the water stress of plants. The reexamined version of the CWSI (Jackson et al., 1988) is briefly summarized here. The CWSI is grounded in the energy balance equation at the surface:

$$R_n = G + H + \lambda E \tag{3.12}$$

where R_n is the net radiation (W m^{-2}), G, H, and λE are the heat fluxes into the surface, into the air above the surface, and latent heat fluxes (W m^{-2}), respectively. These terms can be expressed as:

Table 3.6 Drought severity based on the China-Z index (CZI).

CZI	Drought severity
≥ 2	Extremely wet
1.50–1.99	Very wet
1.00–1.49	Moderately wet
0.99 to − 0.99	Normal
− 1.00 to − 1.49	Moderately dry
− 1.50to − 1.99	Very dry
≤ −2	Extremely dry

Source: From Jain, V. K., Pandey, R. P., Jain, M. K. Byun, H. R. (2015). Comparison of drought indices for appraisal of drought characteristics in the Ken River Basin. *Weather and Climate Extremes*, 8, 1–11. https://doi.org/10.1016/j.wace.2015.05.002.

$$H = \frac{\rho C_p (T_c - T_a)}{r_a} \tag{3.13}$$

$$\lambda E = \frac{\rho C_p (e_c^{\star} - e_a)}{\gamma (r_a + r_c)} \tag{3.14}$$

where ρ is the density of air (kgm^{-3}), C_p is the heat capacity of air ($J\ kg^{-1}\ °C^{-1}$), T_c is the canopy temperature (°C), T_a is the air temperature (°C), $e_c^{\star}$ is the saturated vapor pressure of the air (Pa) at T_c, e_a is the vapor pressure of the air (Pa), γ is the psychrometric constant ($Pa\ °C^{-1}$), r_a is the aerodynamic resistance ($s\ m^{-1}$), and r_c is the canopy resistance to water loss ($s\ m^{-1}$). Equations (3.7.2) and (3.7.3) rely on several underlying assumptions, which can be found in Jackson et al. (1988). Errors produced by these equations and assumptions can be incorporated by taking G equal to $0.1R_n$ and defining an interception coefficient ($Ic = 0.9R_n$) and the slope of the saturated vapor pressure temperature ($\Delta = (e_c^{\star} - e_a^{\star})/(T_c - T_a)$). Thus the difference between the canopy and air temperature can be defined in terms of the aerodynamic and crop resistance, net radiation, and vapor pressure difference of air as in Eq. (3.15):

$$T_c - T_a = \frac{r_a I_c R_n}{\rho C_p} \frac{\gamma (1 + r_c/r_a)}{\Delta + \gamma (1 + r_c/r_a)} - \frac{e_a^{\star} - e_a}{\Delta + \gamma (1 + r_c/r_a)} \tag{3.15}$$

The upper and lower limits of the Eq. (3.15) can be found by considering that the canopy resistance goes to infinity and zero, respectively, as:

$$(T_c - T_a)_{ul} = r_a I_{cu} R_n / \rho C_p \tag{3.16}$$

$$(T_c - T_a)_{ll} = \left(\frac{r_a I_{cl} R_n}{\rho C_p}\right)\left(\frac{\gamma}{\Delta + \gamma}\right) - \left(\frac{e_a^{\star} - e_a}{\Delta + \gamma}\right) \tag{3.17}$$

where the lower limit means a nontranspiring crop and the upper limit means a wet canopy behaves like a free water surface (Jackson et al., 1988). By replacing γ with $\gamma^{\star}$

$\gamma^{\star} = \gamma(1 + r_{cp}/r_a)$, where denotes the canopy resistance at potential transpiration, because of the different resistance behavior of well-watered crops to water flow, the CWSI is obtained as:

$$CWSI = \frac{(T_c - T_a) - (T_c - T_a)_{ll}}{(T_c - T_a)_{ul} - (T_c - T_a)_{ll}} \tag{3.18}$$

where $(T_c - T_a)$ is the measured temperature difference (Jackson et al., 1988).

3.3.8 De Martonne aridity index

The De Martonne aridity index (I_{DM}) of a region can be calculated by using the equation proposed by De Martonne (1926) as

$$I_{DM} = \frac{P}{T + 10} \tag{3.19}$$

where P and T are the yearly average precipitation and temperature, respectively. This index can also be calculated using monthly averages with small differences in the equation.

$$I_m = \frac{12\mu_P}{\mu_T + 10} \tag{3.20}$$

μ_P and μ_T are the monthly mean precipitation and temperature, respectively. Drought severity based on the I_{DM} and P is given in Table 3.7.

3.3.9 Drought area index

The Drought Area Index (DAI) was developed by Bhalme and Mooley (1980) to characterize the drought/flood intensity during the four months of southwest monsoon from June to September in India. The DAI can be computed by considering zero drought intensity for the initial month (I_0=0) as:

$$I_k = 0.50I_{k-1} + (M_k/48.55) \tag{3.21}$$

where I_k is the drought intensity, M is the moisture anomaly index, and subscript k is the current month (Bhalme & Mooley, 1980). Since the monthly rainfall anomaly can be either positive or negative, drought intensity calculated using the DAI can also be positive or negative, where negative values indicate drought and positive values indicate flood. The classification of drought/flood based on the DAI are given in Table 3.8.

3.3.10 Drought frequency index

The drought frequency index (DFI) was proposed by González and Valdés (2006) as a drought indicator that can be used to assess different drought classes such as hydrological, meteorological, and agricultural by using a

Table 3.7 Drought severity based on the De Martonne aridity index (I_{DM}) and precipitation (P).

Climate	I_{DM}	P (mm)
Dry	IDM < 10	$P < 200$
Semi-dry	10 ≤ IDM < 20	$200 \le P < 400$
Mediterranean	20 ≤ IDM < 24	$400 \le P < 500$
Semi-humid	24 ≤ IDM < 28	$500 \le P < 600$
Humid	28 ≤ IDM < 35	$600 \le P < 700$
Very humid	a. 35 ≤ IDM ≤ 55	$700 \le P < 800$
	b. IDM > 55	$P > 800$

Source: From Baltas, E. A. (2008). Climatic conditions and availability of water resources in Greece. *International Journal of Water Resources Development*, 24(4), 635–649. https://doi.org/10.1080/07900620802230129.

Table 3.8 Drought severity based on the drought area index (DAI).

DAI	Drought severity
DAI ≥ 4.00	Extremely wet
3.00 ≤ DAI < 4.00	Very wet
2.00 ≤ DAI < 3.00	Moderately wet
1.00 ≤ DAI < 2.00	Slightly wet
− 1.00 < DAI < 1.00	Near normal
− 2.00 < DAI ≤ −1.00	Mild drought
− 3.00 < DAI ≤ −2.00	Moderate drought
− 4.00 < DAI ≤ −3.00	Severe drought
DAI ≤ −4.00	Extreme drought

Source: From Bhalme, H. N. Mooley, D. A. (1980). Large-scale droughts/floods and monsoon circulation. *Monthly Weather Review*, 108(8), 1197–1211. https://doi.org/10.1175/1520-0493(1980)108#60;1197:lsdamc#62;2.0.co;2.

related variable for each case (precipitation, streamflow, soil moisture) as a variable within the lower end of its probability function. The DFI provides a comprehensive assessment of both the severity and duration of a drought at each time increment relative to its probability of occurrence, expressed as a mean return period (Cañón et al., 2009). As droughts are not described as single events but as a series of low values in general, the algorithm seeks a sequence of length (w) that is concluded at the assessed time step and generates the most significant extreme persistent function (EPF). Depending on the selected criteria, this sequence denotes the most extreme drought until the assessment date (Cañón et al., 2009). The EPF can be calculated as:

$$\left(\begin{array}{c} \mathrm{EPF}(X_i,\ X_{i+1}, \ldots, X_{i+w-1}) \\ = P\left[F\left(x_i,\ x_{i+1}, \ldots, x_{i+w-1}\right)\right. \\ \left.\geq F\left(X_i,\ X_{i+1}, \ldots, X_{i+w-1}\right)\right] \\ F = P\left(x_i, \quad x_{i+1}, \ldots, \quad x_{i+w-1} \mid x_i \leq X_i,\ x_{i+1}\right. \\ \left.\leq X_{i+1}, \ldots, x_{i+w-1} \leq X_{i+w-1}\right. \end{array}\right) \tag{3.22}$$

where X_i is the time series of the selected variable. Numerical integration techniques should be applied to calculate the EPF. Once the sequence that gives the maximum EPF is identified, drought can be determined as the mean return period of sequences that have EPF values equal to or exceeding the current maximum, and with durations equal to or less than it (Cañón et al., 2009). This average return period denotes the DFI and can be calculated as:

$$\mathrm{DFI} \approx \frac{\tau\,(W-1)^k}{1 - F_w\left(F_c,\ W\right)} \tag{3.23}$$

where W is the extreme sequence, (τ, k) are parameters with maximum likelihood estimates of 1.13 and 0.20 for any random, independent processes, F_w is the cumulative extreme persistent probability function, ranging from 0 (brief) to 1 (highly persistent), depending on W and F_c. F_c is the upper limit of EPF for the onset of drought (Cañón et al., 2009).

3.3.11 Drought severity index

The drought severity index (DSI), developed by Mu et al. (2013), incorporates ET,PET, and the NDVI (Khan & Gilani, 2021).

The calculation method proceeds as follows:

- Determine the ratio between ET and PET.
- Standardize this ratio.
- Calculate the sum of both standardized values after the precalculated NDVI from MODIS is standardized.
- Standardize the sum of the obtained values in the previous step to obtain the DSI (Khan & Gilani, 2021). The calculation steps with formulas are as follows:

$$\text{Tran} = \frac{\text{ET}}{\text{PET}} \tag{3.24}$$

whereTran is the symbol for the ratio between the input variables.

$$Z_1 = \frac{\text{Tran}_i - \mu_{\text{Tran}}}{\sigma_{\text{Tran}}} \tag{3.25}$$

where Z_1 is the standardized Tran. Tran_i is the ET rate for the specified 8-day period, μ_{Tran} is the average ET, and σ_{Tran} is the standard deviation value for the ET ratio (Khan & Gilani, 2021). The calculation of NDVI is given in (3.26):

$$\text{NDVI} = \frac{\text{NIR} - \text{Red}}{\text{NIR} + \text{Red}} \tag{3.26}$$

where "*Red*" and "*NIR*" are spectral radiance (or reflectance) measurements obtained from sensors in the red (visible) and near-infrared regions, respectively (Huang et al., 2021). The NDVI obtained from Eq. (3.11.3) is standardized as given in (3.27):

$$Z_2 = \frac{\text{NDVI}_i - \mu_{\text{NDVI}}}{\sigma_{NDVI}} \tag{3.27}$$

where Z_2 is the standardized ratio for the NDVI values. NDVI_i is the NDVI value for the specified 8-day period, μ_{NDVI} symbolizes the mean, and σ_{NDVI} is the standard deviation of NDVI (Khan & Gilani, 2021). Z is the sum of the standardized values obtained from Eqs. (3.25) and (3.27) and is calculated as follows:

$$Z = Z_1 + Z_2 \tag{3.28}$$

DSI is then calculated by standardizing the sum of standardized Tran and NDVI as:

$$\mathrm{DSI} = \frac{Z_i - \mu_Z}{\sigma_Z} \tag{3.29}$$

where μ_Z is the mean, and σ_Z is the standard deviation of the Z value of the specified period. The categorization of drought severity based on the DSI is presented in Table 3.9.

3.3.12 Effective drought index

The effective drought index (EDI) was developed by Byun and Wilhite (1999). This index contains the effective precipitation (EP), where effective precipitation is defined as a function of the weighted precipitation from the previous period, defined by the current month's precipitation. This calculation is performed using a time-dependent decay function. The calculation of the EDI begins with the accumulation of stored water resulting from precipitation over a one-year period, while accounting for losses due to evaporation (Kamruzzaman et al., 2019). The calculation steps of EP are as follows:

$$\mathrm{EP}_i = \sum_{n=1}^{i} \left[\frac{\sum_{m=1}^{u} P_m}{n} \right] \tag{3.30}$$

where EP_i is the monthly cumulative effective precipitation; $\mathrm{P_m}$ is the precipitation for m months preceding the specific month, n is the duration of the preceding period, and i is the duration of aggregate rainfall, initially

Table 3.9 Drought severity based on the drought severity index (DSI).

DSI	Drought severity	Category
DSI ≥ 1.50	Extremely wet	W5
1.20 < DSI < 1.49	Very wet	W4
0.90 < DSI < 1.19	Moderately wet	W3
0.60 < DSI < 0.89	Slightly wet	W2
0.30 < DSI < 0.59	Incipient wet spell	W1
− 0.29 < DSI < 0.29	Near normal	WD
− 0.59 < DSI < − 0.30	Incipient drought	D1
− 0.89 < DSI < − 0.60	Mild drought	D2
− 1.19 < DSI < − 0.90	Moderate drought	D3
− 1.49 < DSI < − 1.20	Severe drought	D4
DSI < − 1.50	Extreme drought	D5

Source: From Mu, Q., Zhao, M., Kimball, J. S., McDowell, N. G., Running, S. W. (2013). A remotely sensed global terrestrial drought severity index. *Bulletin of the American Meteorological Society*, 94(1), 83–98. https://doi.org/10.1175/BAMS-D-11-00213.1.

set at 12 months (reflecting the overall precipitation duration). Consequently, the actual drought index is computed for one year starting from the onset date of precipitation (Kamruzzaman et al., 2019). The deviation of EP (DEP) is calculated as follows:

$$\mathrm{DEP} = \mathrm{EP} - \mathrm{MEP} \tag{3.31}$$

where mean effective precipitation (MEP) is determined for each calendar month. MEP is computed for each i-th value of every calendar month. Hence, the MEP for January is derived as the average of 30 values for January obtained over 30 years (Kamruzzaman et al., 2019). Finally, the calculation for EDI is as follows:

$$\mathrm{EDI} = \frac{\mathrm{DEP}}{\sigma_{\mathrm{DEP}}} \tag{3.32}$$

where σ_{DEP} is the standard deviation. The categorization of drought severity based on the EDI values is provided in Table 3.10.

3.3.13 Evaporative stress index

The evaporative stress index (ESI) was developed by Anderson et al. (2011). The computation of the ESI requires ET to capture available SM and PET to reflect the evaporative demand. PET is calculated based on Penman's (1948) equation, which integrates the effects of net radiation and the vapor pressure deficit, while ET represents the summation of evaporation and transpiration in the model. The ESI and its standardized change anomalies are computed as follows (Nguyen et al., 2019). The calculation of the ET fraction is as follows:

$$r_{\mathrm{ET}} = \frac{\mathrm{ET}}{\mathrm{PET}} \tag{3.33}$$

Table 3.10 Drought severity based on the effective drought index (EDI).

EDI	Drought severity
$-1.0 < \mathrm{EDI} \leq 1.0$	Near normal
$-1.5 < \mathrm{EDI} \leq -1.0$	Moderate drought
$-2 < \mathrm{EDI} \leq -1.5$	Severe drought
$\mathrm{EDI} \leq -2$	Extreme drought

Source: From Kim, D. W., Byun, H. R., Choi, K. S. (2009). Evaluation, modification, and application of the effective drought index to 200-year drought climatology of Seoul, Korea. *Journal of Hydrology*, 378(1–2), 1–12. https://doi.org/10.1016/j.jhydrol.2009.08.021.

The calculation of ESI is as in (3.34):

$$\mathrm{ESI} = \frac{r_{\mathrm{ET}} - \mu_{r_{\mathrm{ET}}}}{\sigma_{r_{\mathrm{ET}}}} \tag{3.34}$$

where $\mu_{r_{\mathrm{ET}}}$ is the ET fraction climatology, and $\sigma_{r_{\mathrm{ET}}}$ is the ET fraction standard deviation over a baseline period. The categorization of drought severity based on the ESI values is provided in Table 3.11.

3.3.14 Evapotranspiration deficit index

The evapotranspiration deficit index (ETDI), developed by Byun and Wilhit (1999), is based upon weekly soil moisture deficit and evapotranspiration deficit calculations starting with water stress (WS):

$$\mathrm{WS} = \frac{\mathrm{PET} - \mathrm{ET}}{\mathrm{PET}} \tag{3.35}$$

where WS is the weekly water stress ratio, PET is the weekly reference crop evapotranspiration, and ET is the weekly evapotranspiration. WS values range from 1 to 0, where 1 indicates no evapotranspiration and 0 indicates evapotranspiration occurring at the same rate as the reference crop ET (Narasimhan & Srinivasan, 2005).

$$if \begin{pmatrix} \mathrm{WS}_{i,j} = \mathrm{MWS}_j & \mathrm{WSA}_{i,j} = \frac{\mathrm{MWS}_j - \mathrm{WS}_{i,j}}{\mathrm{MWS}_j - \min WS_{i,j}} \times 100 \\ \mathrm{WS}_{i,j} > \mathrm{MWS}_j & \mathrm{WSA}_{i,j} = \frac{\mathrm{MWS}_j - \mathrm{WS}_{i,j}}{\max \mathrm{WS}_j - \mathrm{MWS}_{i,j}} \times 100 \end{pmatrix} \tag{3.36}$$

where $WSA_{i,j}$ is the water stress anomaly occurring in month i, week j over the years (j ranges from 1 to 12), MWS_j is the median level of water stress observed during month j, $\max \mathrm{WS}_j$ is the highest water stress recorded in

Table 3.11 Drought severity based on the evaporative stress index (ESI).

ESI	Drought severity
$2 < \mathrm{ESI}$	Extremely wet
$1.5 < \mathrm{ESI} < 1.99$	Very wet
$1.0 < \mathrm{ESI} < 1.49$	Moderately wet
$-0.99 < \mathrm{ESI} < 0.99$	Near normal
$-1.49 < \mathrm{ESI} < -1.0$	Moderate drought
$-1.99 < \mathrm{ESI} < -1.5$	Severe drought
$\mathrm{ESI} \leq -2.0$	Extreme drought

month j, while $\min WS_{i,j}$ is the lowest water stress recorded for the same period, $WS_{i,j}$ is the water stress ratio for the respective month (Narasimhan & Srinivasan, 2005). ETDI can be calculated as in (3.37) by taking 0 as the initial value ($ETDI_0 = 0$):

$$ETDI_j = 0.5ETDI_{j-1} + \frac{WSA_j}{50} \tag{3.37}$$

where $ETDI_{j-1}$ is the ETDI for the previous month, and WSA_j is the monthly water stress anomaly. The categorization of drought severity based on the ETDI values is provided in Table 3.12.

3.3.15 Groundwater resource index

The groundwater resource index (GRI) developed by Mendicino et al. (2008), is used for computing groundwater drought. The GRI was used and calculated using a normal distribution of groundwater storage. To calculate GRI, first calculate D as written below and then follow the next steps Fig. 3.2. To obtain D, when the total of P and snowmelt surpasses the sum of ET and snow accumulation, water replenishes the root zone reservoir. If this reservoir reaches full capacity, any excess water (S) is partitioned into surface runoff (αS) and groundwater recharge ((1 − α)S). The groundwater detention reservoir (D) generates a monthly groundwater runoff equivalent to β times D (Mendicino et al., 2008).

After calculating D as shown in Fig. 3.2, the GRI calculation is as in the following equation:

$$GRI_{y,m} = \frac{D_{y,m} - \mu_{D,M}}{\sigma_{D,m}} \tag{3.38}$$

Table 3.12 Drought severity based on the evapotranspiration deficit index (ETDI).

ETDI	Drought severity
2 < ETDI	Extremely wet
1.5 < ETDI < 1.99	Very wet
1.0 < ETDI < 1.49	Moderately wet
− 0.99 < ETDI < 0.99	Near normal
− 1.49 < ETDI < − 1.0	Moderate drought
− 1.99 < ETDI < − 1.5	Severe drought
ETDI ≤ −2.0	Extreme drought

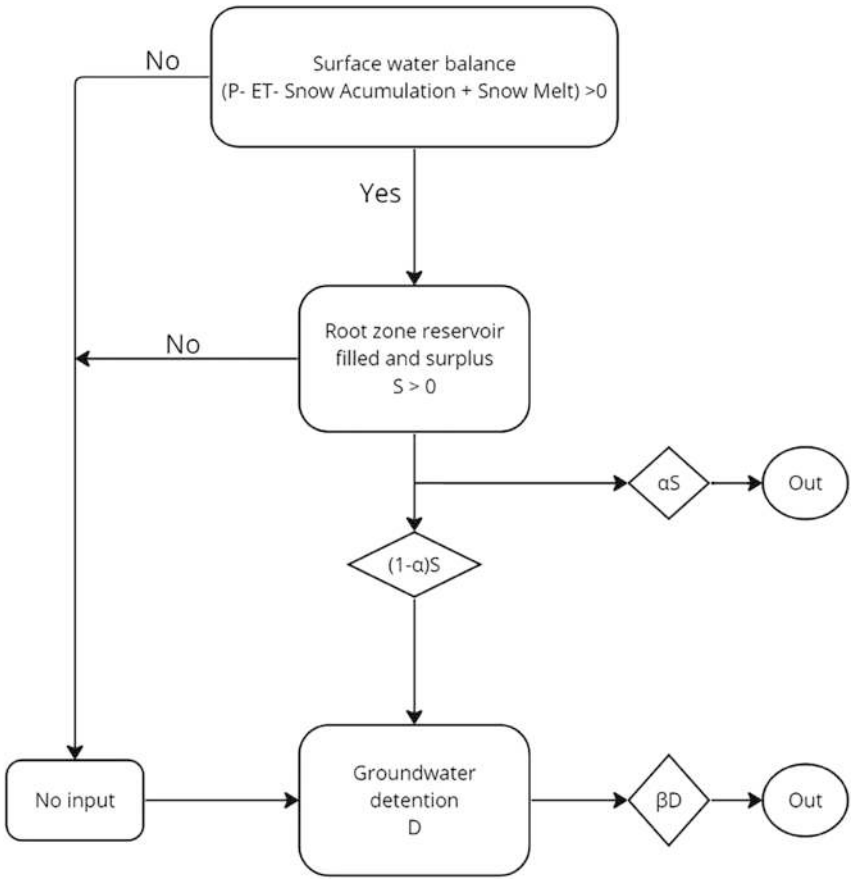


Figure 3.2 The groundwater detention reservoir calculation algorithm for groundwater resource index. From Mendicino, G., Senatore, A., & Versace, P. (2008).. A Groundwater Resource Index (GRI) for drought monitoring and forecasting in a mediterranean climate. *Journal of Hydrology*, 357(3–4), 282–302. https://doi.org/10.1016/j.jhydrol.2008.05.005.

where $D_{y,m}$ and $\mathrm{GRI}_{y,m}$ represent index values and groundwater retention time for year y and month m, respectively. In addition, $\mu_{D,M}$ and $\sigma_{D,m}$ represent the mean and standard deviation of simulated groundwater retention values for month m over a period of at least 30 years (Mendicino et al., 2008). The categorization of drought severity based on the GRI values is provided in Table 3.13.

Table 3.13 Drought severity based on the groundwater resource index (GRI).

GRI	Drought severity
2 < GRI	Extremely wet
1.5 < GRI < 1.99	Very wet
1.0 < GRI < 1.49	Moderately wet
− 0.99 < GRI < 0.99	Near normal
− 1.49 < GRI < − 1.0	Moderate drought
− 1.99 < GRI < − 1.5	Severe drought
GRI ≤ −2.0	Extreme drought

3.3.16 Hybrid drought index

The hybrid drought index (HDI), developed by Kamruzzaman et al., 2019, can capture the effects of various factors that influence drought severity. In this context, the Palmer drought severity index (PDSI), surface water supply index (SWSI), and standardized precipitation index (SPI) are combined through the assessment of drought damage as a new method to quantify drought impacts. Drought damage was chosen because it reflects all aspects of meteorological, hydrological, and agricultural drought. Consequently, a relationship for estimating drought damage can be considered as follows (Karamouz et al., 2009):

$$\text{Damage}_t = f\,(\text{SPI}_{t-1},\ \text{SWSI}_{t-1},\ \text{PDSI}_{t-1}) \tag{3.39}$$

Due to the difficulties in determining the function f in (3.39), artificial neural network (ANN) models are used (Karamouz et al., 2009). The HDI is formulated for damage estimation using SPI, SWSI, and PDSI. The framework of the adjusted SWSI index, first developed by Garen (1993), is adapted in the definition of the HDI as (Karamouz et al., 2009):

$$\text{HDI}_t = f\,(\text{Damage}_t) = \frac{P_t\,(\text{Damage}) - 100}{24} \tag{3.40}$$

where P_t signifies the cumulative probability of damage in month t. To estimate drought severity using the HDI with ANN, the following steps are followed (Karamouz et al., 2009):

1. Time series data should be calculated for SPI, SWSI, and PDSI as indicators that can show the meteorological, hydrological, and agricultural dimensions of drought.

2. There is a need to advance and enhance historical records by examining drought-related losses starting from the past and estimating monthly loss assessments.
3. Identify the most proper cumulative probability distribution that matches the historical monthly loss.
4. Derive HDI values from the cumulative possibility of damages using (3.40).
5. Categorize the HDI values into subgroups, where Class 1 refers to normal conditions and the last class refers to extremely severe drought conditions.
6. Predict HDI subgroups and consequently assess the extent of drought damage by training a computational system with calculated indices of various drought types.

The categorization of drought severity based on the HDI is proposed by Karamouz et al. (2009), as presented in Table 3.14.

3.3.17 Hydro-thermal coefficient of Selyaninov

The hydro-thermal coefficient of Selyaninov (HTC), developed by Selyaninov (1928), takes into account air temperatures in addition to precipitation. It can be calculated as:

Table 3.14 Drought severity based on the hybrid drought index (HDI).

HDI	Drought severity	Subclass
$-0.25 < HDI \leq 0$	Negligible severity	1
$-0.5 < HDI \leq 0.25$		2
$-0.75 < HDI \leq 0.5$		3
$-1 < HDI \leq 0.75$		4
$-1.25 < HDI \leq 1$	Mild	5
$-1.5 < HDI \leq 1.25$		6
$-1.75 < HDI \leq 1.5$		7
$-2 < HDI \leq 1.75$		8
$-2.25 < HDI \leq 2$	Moderate	9
$-2.5 < HDI \leq 2.25$		10
$-2.75 < HDI \leq 2.5$		11
$-3 < HDI \leq 2.75$		12
$-3.25 < HDI \leq 3$	Extreme severe	13
$-3.5 < HDI \leq 3.25$		14
$-3.75 < HDI \leq 3.5$		15
$-4 < HDI \leq 3.75$		16
$HDI \leq 4$		17

Source: From Karamouz, Mohammad, Rasouli, Kabir, Nazif, Sara. (2009). Development of a hybrid index for drought prediction: Case study. *Journal of Hydrologic Engineering*, 14(6), 617–627. https://doi.org/10.1061/(asce)he.1943-5584.0000022.

$$\mathrm{HTC} = \frac{P \quad x \quad 10}{\mu_T x \quad n} \tag{3.41}$$

where P is the total monthly precipitation, μ_T is the monthly average temperature, which should not exceed 10°C, and n is the number of days in a given month. The HTC can be determined between May and June, provided that the average daily temperature remains below 10°C. Drought severity based on the HTC can be categorized into five classes as given in Table 3.15.

3.3.18 Keetch-Byram drought index

Keetch and Byram (1968) proposed a drought index (KBDI) for monitoring drought and managing fire outbreaks. This index is calculated cumulatively using daily rainfall (inches) and maximum temperature (degree Fahrenheit), and average annual rainfall (inches) as its inputs. Its objective is to assess the dryness and, consequently, the flammability of organic material within the soil by considering the impacts of rainfall and evapotranspiration on moisture deficits in deep duff and upper soil layers (Keetch & Byram, 1968). KBDI calculation steps are as follows:

$$kf\,(t) = \frac{(800 - \mathrm{KBDI}_{t-1})((0.968e^{0.0875T\max_t} + 1.5552) - 8.30))}{1000(1 + 10.88e^{-0.0174R})} \tag{3.42}$$

where $kf\,(t)$ is the drought factor at time t, $T\max_t$ is the daily maximum temperature (°C), R is the annual average precipitation (cm), and $KBDI_{t-1}$

Table 3.15 Drought severity based on the hydro-thermal coefficient of Selyaninov (HTC).

HTC	Drought severity
3 < HTC	No drought
1.0 ≤ HTC < 1.3	Moderate dry
0.7 ≤ HTC < 1.0	Dry
0.4 ≤ HTC < 0.7	Very dry
0.0 ≤ HTC < 0.4	Extremely dry

Source: From Oleksiak, Tadeusz, Spyroglou, Ioannis, Pacoń, Darmara, Matysik, Przemysław, Pernisová, Markéta, Rybka, Krystyna. (2022). Effect of drought on wheat production in Poland between 1961 and 2019. *Crop Science*, 62(2), 728–743. https://doi.org/10.1002/csc2.20690.

is the KBDI for time $t-1$ (Keetch & Byram, 1968). As a general rule, DF calculations are based on temperature and precipitation thresholds. Keetch and Byram (1968) created lookup tables for DF for specific temperature ranges with a lower temperature limit of 10°C (50 °F). A swift inspection of Eq. (3.43) determines that 6.78°C is a limiting case; therefore, DF is zero when the daily maximum temperature is below 6.78°C. When the daily maximum temperature is higher than 6.78°C, DF increases exponentially (Janis et al., 2002). For KBDI calculation, the following conditions should be checked and processed:

$$if \begin{cases} P_t = 0 \ \ and \ \ T\max_t \leq 6.78°C & KBDI_t = KBDI_{t-1} \\ P_t = 0 \ \ and \ \ T\max_t > 6.78°C & KBDI_t = KBDI_{t-1} + kf(t) \\ P_t > 0 \ \ and \ \ \sum P_t \leq 0.51cm & KBDI_t = KBDI_{t-1} + kf(t) \\ P_t > 0 \ \ and \ \ \sum P_t > 0.51cm & KBDI_t = KBDI_{t-1} - 39.37 \sum P_t + kf(t) \end{cases} \quad (3.43)$$

where P_t is the daily precipitation. Fire hazard possibilities depending on the KBDI are classified as given in Table 3.16.

3.3.19 Microwave integrated drought index

The microwave integrated drought index (MIDI), developed by Zhang and Jia (2013), is calculated by integrating the precipitation condition index

Table 3.16 Drought severity based on the Keetch-Byram drought index (KBDI).

KBDI	Fire potential	Subclass
0 < KBDI < 99	No fire risk	0
100 < KBDI < 199	Low fire risk	1
200 < KBDI < 299	Medium fire risk	2
300 < KBDI < 399	High fire risk	3
400 < KBDI < 499	Very high fire risk	4
500 < KBDI < 599		5
600 < KBDI < 699	100% Certain fire risk	6
700 < KBDI < 800		7

Source: From Türkeş, M. Altan, G. (2012). Analysis of the year 2008 fires in the forest lands of the Muğla Regional Forest Service by using drought indices. *Journal of Human Sciences*, 9(1), 912–931.

(PCI) based on precipitation data, the soil moisture saturation index (SMSI) using SM data, and the TCI (Temperature Condition Index) using LST (Surface Temperature) data (Sur et al., 2019). In this respect, the PCI can be determined as

$$PCI = \frac{(P_i - P_{\min \backslash \text{funcapply})}}{(P_{\max} - P_{\min})} \tag{3.44}$$

where P_{max} and P_{min} are the maximum and minimum precipitation values, respectively, for the entire period of the pixel. To obtain SM:

$$SM = \frac{(1 - \alpha)}{(LST_{day} - LST_{night})} \tag{3.45}$$

where α is the land surface albedo, LST_{day} is the daytime average land surface temperature (LST), and LST_{night} is the nighttime average LST value. Finally, SMSI can be calculated by the following:

$$SMSI = \frac{(SM_i - SM_{\min})}{(SM_{\max} - SM_{\min})} \tag{3.46}$$

where SM_{max} and SM_{min} are the maximum and minimum values of the soil moisture, respectively. TCI calculation is required for MIDI calculation, so it can be calculated as follows:

$$TCI = \frac{(T_{\max} - T)}{T_{\max} - T_{\min}} x100 \tag{3.47}$$

where T_{max} and T_{min} refer to the highest and lowest values of the LST, respectively. After obtaining SMSI, PCI, and TCI, MIDI can be calculated by using below equation:

$$MIDI = 0.3xSMSI + 0.5xPCI + 0.2xTCI \tag{3.48}$$

Drought severity based on the MIDI is given in Table 3.17.

3.3.20 Multivariate standardized drought index

The multivariate standardized drought index (MSDI) was proposed by Hao and AghaKouchak (2013), which combines the SPI and the standardized soil moisture index (SSI) to take into consideration more than one drought index in some cases especially where heavy rainfall is observed.

In other words, the MSDI consolidates the agricultural and meteorological drought situations. In the methodology of MSDI, the Copula function is used to compose the distribution of two or more variables.

Table 3.17 Drought severity based on the microwave integrated drought index (MIDI).

MIDI	Drought severity
$0 < \text{MIDI} < 0.1$	Extreme drought
$0.1 < \text{MIDI} < 0.2$	Severe drought
$0.2 < \text{MIDI} < 0.3$	Moderate drought
$0.3 < \text{MIDI} < 0.4$	Mild drought
$0.4 < \text{MIDI} < 1$	No

Source: From Wei, W., Zhang, J., Zhou, L., Xie, B., Zhou, J., Li, C. (2021). Comparative evaluation of drought indices for monitoring drought based on remote sensing data. *Environmental Science and Pollution Research*, 28(16), 20408–20425. https://doi.org/10.1007/s11356-020-12120-0.

Considering precipitation and soil moisture as X and Y variables, respectively, the cumulative joint probability p can be stated with a Copula C as:

$$P(X \leq x, \quad Y \leq y) = C[F(X), G(Y)] = p \tag{3.49}$$

Also, there are other developed calculations for Copula. For example, Frank copula evaluates a symmetric dependence structure. On the other hand, Gumbel and Clayton copulas demonstrate an asymmetric structure. The Frank copula evaluates as:

$$C(u, v) = -\frac{1}{\theta}\ln\left[1 + \frac{(e^{-\theta u} - 1)(e^{-\theta v} - 1)}{e^{-\theta} - 1}\right] \tag{3.50}$$

where θ is a parameter, u and v are the marginal cumulative probabilities of precipitation and soil moisture, respectively. The θ can be evaluated from Kendall's rank collection τ:

$$\tau = 1 + \frac{4[D(\theta) - 1]}{\theta} \tag{3.51}$$

where $D(\theta)$ can be calculated as:

$$D(\theta) = \frac{1}{\theta}\int_0^{\theta} \frac{t}{\exp(t) - 1} dt \tag{3.52}$$

where t is the integration variable. From the joint probability p in Eq. (3.53), MSDI is defined as:

$$MSDI = \varphi^{-1}(p) \tag{3.53}$$

where φ is the standard normal distribution function. Drought severity based on the MSDI is given/can be seen in Table 3.18.

3.3.21 Palfai aridity index

The Palfai aridity index (PAI) is proposed by Palfai (1990) which measures the mean temperature of the vegetation and total precipitation during the vegetation period. The PAI is calculated using the formula:

$$PAI = (PAI_o)\,x\,(k_t)\,x\,(k_p)\,x\,(k_{gw}) \tag{3.54}$$

where PAI_o is the base value of the aridity index (°C/100 mm), k_t is the temperature (hot days) correction factor, k_p is the precipitation correction factor, and k_{gw} is the groundwater correction factor. Respectively, each correction factor can be calculated as:

$$k_t = \sqrt[6]{\frac{n+1}{\bar{n}+1}} \tag{3.55}$$

where n is the number of hot days ($t_{max} \geq 30$ °C), $\bar{n}$ is the long-term average of the n value,

$$k_p = \sqrt[4]{\frac{\tau_{max}}{\bar{\tau}_{max}}} \tag{3.56}$$

Table 3.18 Drought severity based on the multivariate standardized drought index (MSDI).

MSDI	Drought severity
MSDI ≥ 2.00	Exceptional wetness
1.60 ≤ MSDI < 1.99	Extreme wetness
1.29 ≤ MSDI < 1.59	Severe wetness
0.79 ≤ MSDI < 1.29	Moderate wetness
0.49 ≤ MSDI < 0.79	Abnormally wetness
0.00 ≤ MSDI < 0.49	Normal wetness
− 0.49 ≤ MSDI < 0.00	Normal drought
− 0.79 ≤ MSDI < − 0.49	Abnormally dry
− 1.29 ≤ MSDI < − 0.79	Moderate drought
− 1.59 ≤ MSDI < − 1.29	Severe drought
− 2.00 ≤ MSDI < − 1.599	Extreme drought
MSDI < 2.00	Exceptional drought

Source: From Hao, Zengchao, AghaKouchak, Amir. (2013). Multivariate standardized drought index: A parametric multi-index model. *Advances in Water Resources*, 57, 12–18. https://doi.org/10.1016/j.advwatres.2013.03.009.

where τ_{max} is the longest rainless period (d), and $\overline{\tau}_{max}$ is the long-term country-wide average. Groundwater correction factor is calculated as:

$$k_{gw} = \sqrt{\frac{\mu_H}{\overline{H}}} \tag{3.57}$$

where k_{gw} is the groundwater correction factor, μ_H is the mean depth of groundwater (m), $\overline{H}$ is the long-term value of H on the given area (m). The last step of the value of the AI, which is PAI_o is:

$$PAI_o = \frac{\mu_T}{P} x100 \tag{3.58}$$

where μ_T is the mean air temperature and P is precipitation amounts (mm). Drought severity based on the PAI is classified as in Table 3.19.

3.3.22 Palmer drought severity index

The Palmer-Z Index was developed by Palmer (1965), which focuses on short-term drought and moisture in soil on a monthly scale. This index was developed by Palmer as a solution to the palmer Drought Severity Index (PDSI), which is another Palmer index used for long-term drought observations, since it was not useful for short time calculations (Palmer, 1965). This index is also known as the standardized form of the PDSI. Palmer's method starts with water balancing, which is often done on a weekly or monthly basis using temperature and precipitation records from the past. By splitting the soil into two layers and presuming that the surface layer can hold 25 mm of water, soil moisture storage is accomplished. The usable capacity of the underlying layer varies based on the soil properties of the location under consideration. Until all available moisture is extracted (recharged) from the surface layer, moisture cannot be removed (refilled) from the underlying layer. The Thornthwaite method is typically used to

Table 3.19 Drought severity based on the Palfai aridity index (PAI).

PAI Values	Drought severity
$6 < PAI < 8$	Moderate drought
$8 < PAI < 10$	Medium drought
$10 < PAI < 12$	Heavy drought
$PAI > 12$	Extremely heavy drought

Source: From Savin, E., Cazacioc, L., Poenaru, V. (2010). Influence of the Atmospheric Circulation on the Droughts. *DAAAM International.* https://doi.org/10.2507/daaam.scibook.2010.29.

determine PET (Thornthwaite, 1948). If *PET* is greater than *P*, which is the monthly precipitation, then evapotranspiration losses from the soil occur. PET loss from the surface layer (L_s) is thought to happen at the potential rate. So, if $PET > P$:

$$\begin{pmatrix} \mathrm{L_S} = \min \mathrm{S_s}, & (\mathrm{PET} - \mathrm{P}) \\ L_U = \frac{[(PET - P) - L_S]S_U}{AWC}, & L_U \le S_U \end{pmatrix} \tag{3.59}$$

where P is precipitation and S_S and S_U are the available moisture stored at the beginning of the month in the surface and underlying layers, respectively. Additionally, potential recharge (PR), potential loss (PL), and potential runoff (PRO) can be calculated by using (Palmer, 1965) the method as:

$$\mathrm{PR} = \mathrm{AWC} - (\mathrm{S_s} + \mathrm{S_U}) \tag{3.60}$$

$$\mathrm{PL} = \mathrm{PL_s} + \mathrm{PL_U} \tag{3.61}$$

where:

$$\begin{pmatrix} \mathrm{PL_S} = \min(\mathrm{PET}, \mathrm{S_S}), \\ PL_U = \frac{[(PET - PL_S)]S_U}{AWC}, \quad L_U \le S_U \end{pmatrix} \tag{3.62}$$

lastly,

$$\mathrm{PRO} = \mathrm{AWC} - \mathrm{PR} = S_s + S_U \tag{3.63}$$

After these calculations, the PZI can be calculated by using the following steps. First, the coefficients for evapotranspiration (α), recharge (β), runoff (γ), and loss (δ) should be calculated.

The α coefficient of evapotranspiration can be calculated as:

$$\alpha = \mu_{\overline{ET}} / \mu_{\overline{PET}} \tag{3.64}$$

where $\mu_{\overline{ET}}$ is the long-term average ET for a month, and $\mu_{\overline{PET}}$ is the long-term average P for a month.

The β coefficient can be calculated as:

$$\beta = \mu_{\overline{R}} / \mu_{\overline{PR}} \tag{3.65}$$

$\mu_{\overline{R}}$ is the long-term average soil moisture for a month, and $\mu_{\overline{PR}}$ is the long-term average potential recharge for a month.

The γ coefficient can be calculated as:

$$\gamma = \mu_{\overline{RO}} / \mu_{\overline{PRO}} \tag{3.66}$$

$\mu_{\overline{RO}}$ is the long-term average runoff for a month, and $\mu_{\overline{PRO}}$ is the long-term potential runoff for a month.

The δ coefficient can be calculated as:

$$\delta = \mu_{\overline{L}} / \mu_{\overline{PL}} \tag{3.67}$$

where $\mu_{\overline{L}}$ is the long-term SM loss for a month, and $\mu_{\overline{PL}}$ is the long-term average potential loss of SM for a month.

The second step is finding climatically appropriate for existing conditions (CAFEC) values for every input in the calculation. The formulas for CAFEC quantities, which are ET, recharge, runoff, loss, and lastly precipitation, respectively, can be calculated as:

$$\begin{pmatrix} \widetilde{ET} = \alpha x PET\,(CAFEC\ Evapotranspiration) \\ \widetilde{R} = \beta x PR\,(CAFEC\ Recharge) \\ \widetilde{RO} = \gamma x PRO\,(CAFEC\ Runoff) \\ \widetilde{L} = \delta x PL\,(CAFEC\ Loss) \end{pmatrix} \tag{3.68}$$

with CAFEC inputs, finally CAFEC precipitation ($\widetilde{P}$) formula is the sum of all CAFEC inputs as:

$$\widetilde{P} = \widetilde{ET} + \widetilde{R} + \widetilde{RO} - \widetilde{L} \tag{3.69}$$

The third step is finding the difference between actual P and ($\widetilde{P}$) gives input d as follows:

$$d = P - \widetilde{P} \tag{3.70}$$

by using this difference, the Z is defined as:

$$Z = K_j d \tag{3.71}$$

where K_j is a weighting factor and given as:

$$K_j = \frac{17.67\hat{K}_j}{\sum_{i=1}^{12} \mu_{Dj} x \hat{K}_i}, j = 1, .,12 \tag{3.72}$$

where μ_{Dj} is the mean of absolute values of d for each month, and other parameters can be calculated by using the equations below:

$$\hat{K}_j = 1.5 \log_{10}\left[\left(\frac{\overline{PET_j} + \overline{R_j} + \overline{RO_j}}{\overline{P_j} + \overline{L_j}} + 2.8\right) \mu_{Dj} - 1\right] + 0.5 \tag{3.73}$$

The PDSI can be seen as a continuation of the Palmer-Z. This formula can be calculated as:

$$PDSI_i = 0897PDSI_{i-1} + \frac{1}{3}Z_i \tag{3.74}$$

Drought severity based on the PDSI is shown in Table 3.20

3.3.23 Palmer hydrological drought index

The Palmer hydrological drought index (PHDI) is a long-term drought index, developed to quantify hydrological effects. When circumstances change, the PHDI reacts more slowly than the PDSI. This hydrological drought index evaluates the cumulative moisture supply over an extended period of time. It is adapted from the original PDSI to account for longer-term dryness that may impact groundwater, streamflow, and water storage. PHDI uses a ratio of moisture received to moisture required to terminate a drought to determine when a drought will end based on the amount of precipitation needed. There are four types of droughts: near normal, which happens around 28%–50% of the time; mild to moderate, which happens about 11%–27% of the time; severe, which happens about 5%–10% of the time; and extreme, which happens about 4% of the time.

PHDI computation is similar to PDSI. Hence, the classification of PHDI (Table 3.21) is the same as that of other Palmer indices.

Table 3.20 Drought severity based on the Palmer drought severity index (PDSI).

PDSI	Drought severity
PDSI ≥ 4.00	Extremely wet
3.00 ≤ PDSI ≤ 3.99	Very wet
2.00 ≤ PDSI ≤ 2.99	Moderately wet
1.00 ≤ PDSI ≤ 1.99	Slightly wet
0.50 ≤ PDSI ≤ 0.99	Incipient wet spell
− 0.49 ≤ PDSI ≤ 0.49	Near normal
− 0.99 ≤ PDSI ≤ −0.50	Incipient drought
− 1.99 ≤ PDSI ≤ −1.00	Mild drought
− 2.99 ≤ PDSI ≤ −2.00	Moderate drought
− 3.99 ≤ PDSI ≤ −3.00	Severe drought
PDSI ≤ −4.00	Extreme drought

Source: From Palmer, W. C. (1965). USWB_Meteorological_Drought_1965. Office of Climatology U.S. Weayher Bureau, D.C.

Table 3.21 Drought severity based on Palmer hydrological drought index (PHDI).

PHDI	Drought severity
PHDI ≥ 4.00	Extremely wet
3.00 ≤ PHDI ≤ 3.99	Very wet
2.00 ≤ PHDI ≤ 2.99	Moderately wet
1.00 ≤ PHDI ≤ 1.99	Slightly wet
0.50 ≤ PHDI ≤ 0.99	Incipient wet spell
− 0.49 ≤ PHDI ≤ 0.49	Near normal
− 0.99 ≤ PHDI ≤ −0.50	Incipient drought
− 1.99 ≤ PHDI ≤ −1.00	Mild drought
− 2.99 ≤ PHDI ≤ −2.00	Moderate drought
− 3.99 ≤ PHDI ≤ −3.00	Severe drought
PHDI ≤ −4.00	Extreme drought

Source: From Palmer, W. C. (1965). USWB_Meteorological_Drought_1965. Office of Climatology U.S. Weayher Bureau, D.C.

3.3.24 Percent of normal index

The percent of normal index (PNI) was introduced by Willeke et al. (1994) as a meteorological drought index used to express the percentage of normal precipitation for different time scales (yearly, seasonal, and monthly). The calculation of PNI involves comparing the actual precipitation amount during a specified period with the long-term average (generally 30 years) or normal precipitation for that same period. The PNI can be calculated as:

$$PNI = \frac{P_i}{\mu_P} \quad x \quad 100 \tag{3.75}$$

where P_i is the P during the time increment labeled as "i" while μ_P is the mean normal precipitation for the duration of the study period. Drought severity based on the PNI is given in Table 3.22.

3.3.25 Perpendicular drought index

The perpendicular drought index (PDI) was developed by Ghulam et al. (2007). It is a spatially explicit, physically-based, and multiscale index that takes into account the vertical and horizontal components of the water balance equation. The PDI is based on the principle that during a drought, the soil moisture is depleted first, followed by a decrease in evapotranspiration, and eventually a reduction in runoff. The PDI is a line segment that

Table 3.22 Drought severity based on percent of normal index (PNI).

PNI	Drought severity
180% ≤ PNI	Extremely wet
160% < PNI < 180%	Very wet
120% < PNI < 160%	Moderately wet
80% < PNI < 120%	Near normal
40% < PNI ≤ 80%	Moderate drought
20% < PNI ≤ 40%	Severe drought
PNI ≤ 20%	Extreme drought

Source: From Barua, Shishutosh, Ng, A. W. M., Perera, B. J. C. (2011). Comparative evaluation of drought indexes: Case study on the Yarra River catchment in Australia. *Journal of Water Resources Planning and Management*, 137(2), 215–226. https://doi.org/10.1061/(asce)wr.1943–5452.0000105.

crosses the coordinate origin and is parallel to the soil line and perpendicular to the soil line's normal. The PDI can be calculated as:

$$PDI = \frac{R_{red} + MR_{NIR}}{\sqrt{M^2 + 1}} \tag{3.76}$$

where R_{Red} and R_{NIR} are the atmospherically corrected reflectance of the Red and NIR bands, M is the slope of the soil line. The graph shows the surface condition depending on the PDI in Fig. 3.3.

The range of PDI values is between 0.0 and 1.0. In comparison to a pixel with a smaller PDI value, which is located closer to the coordinate origin and represents less water stress or wet surface, a pixel with a bigger PDI value indicates more severe water stress and is farther away from the coordinate origin (Shahabfar et al., 2012).

3.3.26 Decile index

The decile index (DI) was developed by Gibbs and Maher (1967) to monitor monthly drought severity based on P. It is calculated by splitting long-term P data into ten deciles from lowest to highest. Using this approach, a cumulative frequency distribution is created by ranking long-term monthly P from highest to lowest. Based on equal probability, the distribution is divided into 10 segments, or deciles. The P value in a record that is not exceeded by the bottom 10% of all P values is known as the first decile. The lowest 10%, 20%, etc., are in the second decile (Alami & Tayfur, 2022). Drought severity is then categorized based on the DI as given in Table 3.23.

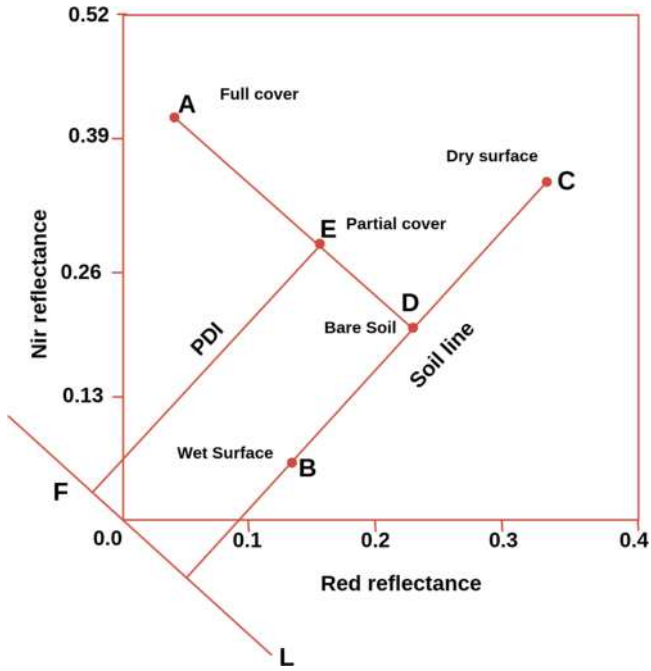


Figure 3.3 The simplified space of perpendicular drought index (*PDI*). From Qin, Q., Ghulam, A., Zhu, L., Wang, L., Li, J., & Nan, P. (2008). Evaluation of MODIS derived perpendicular drought index for estimation of surface dryness over northwestern China. *International Journal of Remote Sensing*, 29(7), 1983–1995. https://doi.org/10.1080/01431160701355264.

Table 3.23 Drought severity based on decile index (DI).

DI	Drought severity
10-9	Much above normal
8-7	Above normal
6-5	Near normal
4-3	Below normal
2-1	Much below normal

Source: From Alami, M. M. Tayfur, G. (2022). Meteorological drought analysis for Helmand River Basin, Afghanistan. *Teknik Dergi/Technical Journal of Turkish Chamber of Civil Engineers*, 33(4), 12223–12242. https://doi.org/10.18400/tekderg.868595.

3.3.27 Rainfall anomaly index

The rainfall anomaly index (RAI) was developed by Van-Rooy (1965) for categorizing the degrees of positive and negative intensities within rainfall anomalies (Costa & Rodrigues, 2017). The RAI is a statistical tool used to measure the deviation of P from its long-term average in a given region over a specific time period. It has a relatively simple structure, depending only on P, which is given for the positive and negative anomalies as follows.

For the positive anomaly:

$$\mathrm{RAI} = \mathrm{K}\left[\frac{\mathrm{N} - \mu_{\mathrm{N}}}{\mu_{\mathrm{M}} - \mu_{\mathrm{N}}}\right] if \begin{Bmatrix} Positve\ anamoly & K = 3 \\ Negative\ anamoly & K = -3 \end{Bmatrix} \tag{3.77}$$

where N is the observed P, μ_{N} is the mean P, and μ_{M} is the mean of the highest ten Ps. Drought severity is categorized based on the RAI as given in Table 3.24

3.3.28 Reconnaissance drought index

The reconnaissance drought index (RDI), developed by Tsakiris and Vangelis (2005), is used to assess water deficiency, incorporating PET by factoring in monthly maximum and minimum temperatures or mean temperatures at a specific observation point. It is a valuable tool for identifying drought conditions across diverse climatic regions (Thomas et al., 2015; Tsakiris et al., 2007). The equation below computes the initial value for the i^{th} year over a time span of k months (Qaisrani et al., 2024):

Table 3.24 Drought severity categorization based on the rainfall anomaly index (RAI).

RAI	Drought severity
RAI ≥ 4.00	Extremely humid
2.00 ≤ RAI < 4.00	Very humid
0 ≤ RAI < 2.00	Humid
− 2.00 ≤ RAI < 0	Dry
− 4.00 ≤ RAI < − 2.00	Very dry
RAI ≤ −4.00	Extremely dry

Source: From Araújo, Lincoln, Moraes Neto, João Sousa, Francisco. (2009). Classificação da precipitação anual e da quadra chuvosa da bacia do rio Paraíba utilizando índice de Anomalia de Chuva (IAC). *Ambiente e Agua - An Interdisciplinary Journal of Applied Science*, 4(3), 93–110. https://doi.org/10.4136/ambi-agua.105.

$$a_k^i = \frac{\sum_{j=1}^{k} P_{ij}}{\sum_{j=1}^{k} PET_{ij}} \tag{3.78}$$

where α_k is the start value of RDI, while P_{ij} and PET_{ij} are P and PET for the *j*-th month of the *i*-th year. The start value of RDI fits either a gamma or lognormal distribution, contingent upon the time scale and geographical location (Tigkas et al., 2015). If the distribution is lognormal, the Standardized RDI can be computed as (Qaisrani et al., 2024):

$$y^{(i)} = \ln(a_k^{(i)}) \quad RDI_{st}^{(i)} = \frac{y^{(i)} - \mu_y}{\sigma_y} \tag{3.79}$$

where μ_y is the mean, and σ_y is the standard deviation of $y^{(i)}$. With the assumed gamma distribution, the gamma probability function is fitted for the frequency distribution of the initial value of α_k. In short periods, accumulated precipitation is assumed to be zero. In such cases, the RDI_{st} is calculated using the combined cumulative distribution, the gamma probability function, and the probability of zero precipitation (Qaisrani et al., 2024). The categorization of drought severity based on the RDI is presented in Table 3.25

3.3.29 Regional streamflow deficiency index

The regional streamflow deficiency index (RSDI) was developed by Stahl & Demuth, 2001 to quantify the severity of streamflow deficiency in a particular region and assess the impact of drought on water resources. The natural variability of streamflow is taken into account in the RSDI

Table 3.25 Drought severity classification based on reconnaissance drought index (RDI).

RDI	Drought Severity
2.0 ≤ RDI	Extremely wet
1.5 ≤ RDI ≤ 1.99	Very wet
1.0 ≤ RDI ≤ 1.49	Moderately wet
− 0.99 ≤ RDI ≤ 0.99	Near normal
− 1.0 ≤ RDI ≤ 1.49	Moderate drought
− 1.5 ≤ RDI ≤ 1.99	Severe drought
RDI ≤ −2.0	Extreme drought

Source: From Tigkas, Dimitris, Vangelis, Harris, Tsakiris, George. (2015). DrinC: A software for drought analysis based on drought indices. *Earth Science Informatics*, 8(3), 697–709. https://doi.org/10.1007/s12145-014-0178-y.

calculation. The RSDI is calculated by taking the difference between the observed streamflow and a long-term average streamflow. The long-term average streamflow is calculated using historical data, usually spanning over 30 years. A positive RSDI value indicates above-average streamflow, while a negative value indicates below-average streamflow. The formula of the RSDI is given as:

$$RSDI = \frac{1}{n}\sum_{i=1}^{n} DI_G(t) \tag{3.80}$$

where DI is the daily deficiency of all the individual stations G in a cluster, and n is the number of stations. The distribution of RSDI values of a cluster is a measure of the homogeneity of the group of catchments that make up a cluster. By definition, the optimal concurrent behavior of cluster members will be represented by an RSDI value distribution of 90% of zero (threshold percentile p) and 10% of one. The homogeneity of a cluster may be determined by measuring the area between this optimum and the cumulative distribution F(x) of the real RSDI values of the cluster.

3.3.30 Scaled drought condition index

The scaled drought condition index (SDCI), developed by Rhee et al. (2010), is a widely used drought index for evaluating agricultural drought in both arid and humid regions. Three separate indices obtained from remote sensing data are weighted to calculate the SDCI as follows (Zhao & Wang, 2021):

$$SDCI = 0.25TCI + 0.5PCI + 0.25VCI \tag{3.81}$$

where TCI, PCI, and VCI are the condition indices for temperature, precipitation, and vegetation, respectively. According to Zhao and Wang (2021), it is necessary to do more research on the usability of the weights of each condition index in different regions. The SDCI values can be divided into six categories to characterize the agricultural drought severity, as shown in Table 3.26

3.3.31 Soil moisture deficit index

The Soil Moisture Deficit Index (SMDI), developed by Narasimhan and Srinivasan (2005), is a drought index computed weekly by using the soil moisture simulated by the SWAT hydrological model. Due to the different water extraction potentials of different crop types and crops at their different growth periods, the SMDI is computed at four different soil levels, considering the entire soil profile, at the top 2 ft. (SMDI-2), 4 ft.

Table 3.26 Drought severity based on the scaled drought condition index (SDCI).

SDCI	Drought severity
$0.0 \le SDCI < 0.1$	Exceptional drought
$0.1 \le SDCI < 0.2$	Extreme drought
$0.2 \le SDCI < 0.3$	Severe drought
$0.3 \le SDCI < 0.4$	Moderate drought
$0.4 \le SDCI < 0.5$	Abnormal dry
$SDCI > 0.5$	No drought

Source: From Rhee, J., Im, J., Carbone, G.J. (2010). Monitoring agricultural drought for arid and humid regions using multi-sensor remote sensing data. *Remote Sensing of Environment*, 114(12), 2875–2887. https://doi.org/10.1016/j.rse.2010.07.005.

(SMDI-4), and 6 ft. (SMDI-6) (Narasimhan & Srinivasan, 2005). The index can be simply computed as (Yao et al., 2022):

$$SD_{i,j} = \begin{cases} SW_{i,j} \le MSW_j & \frac{SW_{i,j} - MSW_j}{MSW_j - \min SW_j} \times 100 \\ SW_{i,j} > MSW_j & \frac{SW_{i,j} - MSW_j}{\max SW_j - MSW_j} \times 100 \end{cases} \tag{3.82}$$

$$SMD_{i,j} = \begin{cases} j > 1 & 0.5 SMDI_{i,j-1} + \frac{SD_{i,j}}{50} \\ j = 1 & \frac{SD_{i,j}}{50} \end{cases} \tag{3.83}$$

where $SD_{i,j}$ is the soil water deficit of j-th month in the i-th year, $SW_{i,j}$ is the weekly-average soil water content (mm) of the soil profile, MSW_j is the long-term median available soil water (mm) of the soil profile, and $\max SW_j$ and $\min SW_j$ are the long-term maximum and minimum available soil water (mm) of the soil profile, respectively. According to the SMDI values, drought severities can be classified as given in Table 3.27.

3.3.32 Soil water deficit index

The Soil Water Deficit Index (SWDI), developed by Martínez-Fernández et al. (2015) as a soil-water-based agricultural drought index, is an extension of the WDI introduced by Martínez-Fernández et al. (2005). The SWDI can be calculated as:

$$SWDI = 10\left(\frac{\theta - \theta_{AWC}}{\theta_{FC}}\right) \tag{3.84}$$

Table 3.27 Drought severity based on the soil moisture deficit index (SMDI).

SMDI	Drought severity
$2.00 \leq \text{SMDI} < 4.00$	Extremely wet
$1.50 \leq \text{SMDI} < 2.00$	Severely wet
$1.00 \leq \text{SMDI} < 1.50$	Moderate wet
$0.50 \leq \text{SMDI} < 1.00$	Slightly wet
$-0.50 < \text{SMDI} < 0.50$	Normal
$-1.00 < \text{SMDI} \leq -0.50$	Slightly dry
$-1.50 < \text{SMDI} \leq -1.00$	Moderate dry
$-2.00 < \text{SMDI} \leq -1.50$	Severely dry
$4.00 < \text{SMDI} \leq -2.00$	Extremely dry

Source: From Yao, Ning, Li, Yi, Liu, Qingzhu, Zhang, Siyuan, Chen, Xinguo, Ji, Yadong, Liu, Fenggui, Pulatov, Alim, Feng, Puyu. (2022). Response of wheat and maize growth-yields to meteorological and agricultural droughts based on standardized precipitation evapotranspiration indexes and soil moisture deficit indexes. *Agricultural Water Management*, 266. https://doi.org/10.1016/j.agwat.2022.107566.

where θ is the soil moisture, θ_{AWC} is the available water content, which is the difference between the field capacity and wilting point of the soil, and θ_{FC} is the field capacity of the soil. Here, the soil moisture is multiplied by 10 to obtain a meaningful range in terms of agricultural drought (Martínez-Fernández et al., 2015). Daily calculations of the SWDI are averaged over weeks due to the weekly irrigation schedules of farmers (Martínez-Fernández et al., 2015). Agricultural drought severity is classified by using the SWDI as given in Table 3.28.

3.3.33 Standardized anomaly index

The standardized anomaly index (SAI), developed by Kraus (1977), is widely used to assess rainfall variability in various regions (Bayable et al., 2021; Koudahe et al., 2017). By calculating the annual P events that deviate from the annual average precipitation during the study period, the frequency of dry and wet events is clarified. Positive and negative SAI values indicate that there is more or less rainfall than normal and that this poses a risk for flooddrought conditions (Sittichok & Thepprasit, 2022). It can be calculated as:

$$\text{SAI}_i = \frac{(x_i - \mu_i)}{\sigma_i} \tag{3.85}$$

where x_i is the annual P of year *i*, μ_i long-term period means, and σ_i standard deviation of the long-term *i*-th year. Drought severity based on the SAI is given in Table 3.29.

3.3.34 Standardized precipitation evapotranspiration index

The standardized precipitation evapotranspiration index (SPEI), developed by Vicente-Serrano et al. (2010), is relatively new and detailed. The SPEI incorporates both P and temperature data and is used to estimate PET. The SPEI is typically determined by standardizing the differences between P and PET through a log-logistic probability distribution function (Hussain et al., 2023). SPEI is calculated with the following calculation steps:

Table 3.28 Drought severity based on the soil water deficit index (SWDI).

SWDI	Drought severity
SWDI > 0	No drought
0 > SWDI > − 2	Mild drought
− 2 > SWDI > − 5	Moderate drought
− 5 > SWDI > − 10	Severe drought
− 10.00 > SWDI	Extreme drought

Source: From Martínez-Fernández, J., González-Zamora, A., Sánchez, N., Gumuzzio, A. (2015). A soil water based index as a suitable agricultural drought indicator. *Journal of Hydrology*, 522, 265–273. https://doi.org/10.1016/j.jhydrol.2014.12.051.

Table 3.29 Drought severity based on standardized anomaly index (SAI).

SAI	Drought severity
SAI > 2.00	Extremely wet
1.50 < SAI < 1.99	Very wet
1.00 < SAI < 1.49	Moderately wet
-0.99 < SAI < 0.99	Near normal
-1.49 < SAI < -1.00	Moderately dry
-1.99 < SAI < -1.50	Severely dry
SAI < -2.00	Extremely dry

Source: From Sittichok, K. Thepprasit, C. (2022). The differences of precipitation characteristics among GCMs over Southeast Asia under AR6 climate change scenarios. *ASEAN Journal of Scientific and Technological Reports*, 25(1), 11–23. https://doi.org/10.55164/ajstr.v25i1.244632.

$$D_n^k = \sum_{i-1}^{k-1} P_{n-1} - PET_{n-1} \tag{3.86}$$

where D is the values at different timescales, k is the number of months over which the sum is calculated, and n is the specific month for which the sum is being evaluated. The variables n and a log-logisti c PDF can be specified using Eqs. (3.87) and (3.88):

$$f(x) = \left[1 + \left(\frac{\alpha}{x} - y\right)^{\beta}\right]^{1} \tag{3.87}$$

$$f(x) = \frac{\beta}{\alpha}\left(\frac{x-\gamma}{\alpha}\right)^{\beta-1}\left[1 + \left(\frac{x-\gamma}{\alpha}\right)^{\beta}\right]^{-2} \tag{3.88}$$

where α, β, and γ are the scale, shape, and origin parameters, respectively, with $\gamma > 0$ and $D < \infty$. The computed f(x) is then converted into a Z-standardized value. The formula for the SPEI can be expressed as follows:

$$SPEI = W - \frac{C_0 + C_1 W + C_1 W^2}{1 + d_1 W + d_2 W^2 + d_3 W^3} \tag{3.89}$$

where W is calculated as given below:

$$\text{for } P \le 0.5 \text{ and } W = \sqrt{-2\ln(P)} \tag{3.90}$$

The probability of exceeding a specific D_i value is given by P = 1 - f(x). Constants in Eq. (3.89) are defined as follows (Tirivarombo et al., 2018):

$$\begin{aligned} C_0 = 2.515517,\ C_1 = 0.802853,\ C_2 = 0.010328 \quad d_1 \\ = 1.432788,\ d_2 = 0.189269,\ d_3 = 0.001308 \end{aligned} \tag{3.91}$$

The drought severity based on the SPEI is given in Table 3.30.

3.3.35 Standardized precipitation index

The standardized precipitation index (SPI), developed by McKee et al. (1993), is a method widely used in many studies for its computational simplicity and in drought analysis studies utilizing precipitation data. Due to its widespread use, the SPI is among the main drought indices recommended by the World Meteorological Organization (WMO) (Isia et al., 2023). In the SPI method, initially, assuming that the data follows a normal distribution, time series are standardized using the formula shown in Eq. (3.92) to create standardized time series.

Table 3.30 Drought classification based on severity standardized precipitation evapotranspiration index (SPEI) (Hussain et al., 2023).

SPEI	Drought severity
SPEI > 2.00	Extremely wet
1.50 < SPEI < 1.99	Severely wet
1.00 < SPEI < 1.49	Moderately wet
−0.99 < SPEI < 0.99	Nearly normal
−1.49 < SPEI < −1.00	Moderately drought
−1.99 < SPEI < −1.50	Severely drought
SPEI < −2.00	Normal
−1.49 < SPEI < −1.00	Moderately drought
−1.99 < SPEI < −1.50	Severely drought
SPEI < −2.00	Extremely drought

Source: From Hussain, A., Jadoon, K. Z., Rahman, K. U., Shang, S., Shahid, M., Ejaz, N., Khan, H. (2023). Analyzing the impact of drought on agriculture: Evidence from Pakistan using standardized precipitation evapotranspiration index. *Natural Hazards*, 115(1), 389–408. https://doi.org/10.1007/s11069-022-05559-6.

$$SPI = \frac{x - \mu_x}{\sigma_x} \tag{3.92}$$

where x is precipitation, μ_x is the mean of the precipitation, and σ_x is its standard deviation. The PDF that generally fits the standardized precipitation data has emerged as the Gamma distribution. The Gamma PDF distribution is shown in Eq. (3.93)

$$p(x) = \frac{1}{\beta^{\alpha}\Gamma(\alpha)} x^{\alpha-1} e^{-\frac{x}{\beta}} \tag{3.93}$$

In this equation, with the condition that α, β *and*$x > 0$;
α: represents the shape parameter,
β: represents the scale parameter,
x: represents the monthly precipitation amount,
$\Gamma(\alpha)$: represents the Gamma PDF, and
$p(x)$: represents the probability value.

The α parameter given in Eq. (3.93) is obtained by substituting the μ value obtained in Eq. (3.94) into Eq. (3.95).

$$\mu = \ln(x_{mean}) - \frac{\sum \ln(x)}{n} \tag{3.94}$$

$$\alpha = \frac{1}{4\mu}\left(1 + \sqrt{1 + \frac{4\mu}{3}}\right) \tag{3.95}$$

β parameter is calculated by dividing the mean values by α Eq. (3.96).

$$\beta = \frac{x_{mean}}{\alpha} \tag{3.96}$$

Once the shape and scale parameters are obtained, the PDF can be calculated using the formula given in Eq. (3.97).

$$P(x) = \int_0^x p(x)\,dx = \frac{1}{\beta^{\alpha}\Gamma(\alpha)} \int_0^x x^{\alpha-1} e^{-\frac{x}{\beta}} dx \tag{3.97}$$

The fact that the Gamma function is not defined at 0 poses a problem for calculations during dry periods with no precipitation. In this case, it is necessary to perform a separate probability calculation for data where $x = 0$. Different probability calculation methods can be used for data that are 0, but in the most general sense, it can be calculated using Eq. (3.98).

$$G(x) = \frac{n}{t} + \left(1 - \frac{n}{t}\right) P(x) \tag{3.98}$$

where

n is the number of data points with a total precipitation amount of 0, and

t is the total length of the time series.

Ultimately, all the obtained probability values are transformed into z values with a mean of 0 and a variance of 1. Based on the obtained z values, the data are categorized into sub-classes according to the SPI drought classes shown in Table 3.31.

3.3.36 Standardized runoff index

Shukla and Wood (2008) developed a hydrological drought index that considers the hydrological processes responsible for the decrease in streamflow during different seasons. The standardized runoff index (SRI) is a widely used metric for evaluating hydrological drought. The computation procedure is as follows:

Runoff *(x)* at a specific time period is assumed to follow the probability density function *(x)* of the Gamma (Γ) distribution, and Eq. (3.99) is used to calculate $f(x)$.

$$f(x) = \frac{1}{\gamma^{\beta}\Gamma(\beta)} x^{\beta-1} e^{\left(-\frac{x}{\gamma}\right)} \tag{3.99}$$

Table 3.31 Drought severity classification based on standardized precipitation index (SPI).

SPI	Drought severity
2.0 ≤ SPI	Extremely wet
1.5 ≤ SPI ≤ 1.99	Very wet
1.0 ≤ SPI ≤ 1.49	Moderately wet
− 0.99 ≤ SPI ≤ 0.99	Near normal
− 1.0 ≤ SPI ≤ 1.49	Moderate drought
− 1.5 ≤ SPI ≤ 1.99	Severe drought
SPI ≤ −2.0	Extreme drought

Source: From McKee, T. B., Nolan, J., Kleist, J. (1993). The relationship of drought frequency and duration to time scales. In *Eighth Conf. on Applied Climatology* (pp. 179–184). Amer. Meteor, Soc.

where γ and β can be calculated using the maximum likelihood method. The cumulative probability function of runoff at a specific time scale can be calculated using Eq. (3.100):

$$\begin{aligned} F(x) = & \int_0^x f(x)\,dx = \int_0^x \frac{1}{\gamma^{\beta}\Gamma(\beta)} x^{\beta-1} e^{\left(-\frac{x}{\gamma}\right)} dx, \quad x \\ & > 0 \quad t = \sqrt{2\ln(F)} \quad F > 0.5, \quad S \\ & = 1 \quad F < 0.5, \quad S = -1 \end{aligned} \tag{3.100}$$

where F is the cumulative probability distribution of runoff that is associated with the Γ, and S shows the probability density coefficient. The SRI values obtained in this way are used to categorize drought. Drought severity classification based on the SRI is given in Table 3.32.

3.3.37 Standardized streamflow index

The standardized streamflow index (SSI) quantifies variations in streamflow over a specific period in terms of standard deviations from the mean. This index assists in identifying long-term trends and unusual events in streamflow. Monthly streamflow data are typically used for calculating SSI. First, the accumulated probability F(x) is determined for each month. This represents the percentage of streamflow values observed up to that period within the distribution. Subsequently, this accumulated probability value is normalized into standard units. This normalization process is carried out using various statistical distributions. The calculation of SSI results in a standardized streamflow value for each month. This value indicates how much deviation the streamflow amount for that period shows from the

Table 3.32 Drought severity based on the standardized runoff index (SRI).

SRI	Drought severity
$SRI \geq 2$	Extremely wet
$1.50 < SRI < 1.99$	Moderately wet
$1.00 < SRI < 1.49$	Slightly wet wet
$-0.99 < SRI < 0.99$	Near normal
$-1.49 < SRI < -1.00$	Moderate drought
$-1.99 < SRI < -1.5$	Severe drought
$SRI < -2.00$	Extremely dry

Source: From Shukla, S., Wood, A. W. (2008). Use of a standardized runoff index for characterizing hydrologic drought. *Geophysical Research Letters*, 35(2). https://doi.org/10.1029/2007GL032487.

mean value. These deviations can be used to identify unusual changes or long-term trends in streamflow.

$$SSI = \frac{F_i - \overline{F}}{\sigma} \tag{3.101}$$

where F_i is the flow rate in time interval I, $\overline{F}$ is the mean of the series, and σ is the standard deviation of the series. For the monthly series, the SSI is written as follows (Modarres, 2007):

$$SSI_\tau = \frac{F_{\nu\tau} - \overline{F_\tau}}{\sigma_\tau} \tag{3.102}$$

$$\overline{F_\tau} = \frac{1}{n}\sum_{\nu=1}^{N} F_{\nu\tau},\ \tau = 1, \ldots\ldots, \omega \tag{3.103}$$

$$\sigma_\tau = \sqrt{\frac{1}{n-1}\sum_{\nu=1}^{n}(F_{\nu,\tau} - \overline{F_\tau})} \tag{3.104}$$

where ν is the year and τ is the interval within a year, and $\overline{F_\tau}$ and σ_τ are the mean and standard deviation of the month τ and $\omega = 12$. Drought severity classification based on the SSI can be seen in Table 3.33.

3.3.38 Standardized water level index

The standardized water-level index (SWI), developed at the Indian Institute of Technology by Bhuiyan (2004), which evaluates deficiencies in groundwater recharge. This index uses hydrology and well data to estimate the impact of drought on groundwater levels. The SWI is

particularly useful in regions experiencing seasonal flow reductions in river and stream flow, as it measures the effects of drought on groundwater, which is critical for agriculture and urban water supplies. The SWI algorithm calculates the standard deviation of water levels from the mean using a specific equation, with positive values indicating moist conditions and negative values indicating aridity. The SWI can be calculated using Eq. (3.105):

$$SWI = \frac{W_{ij} - \mu}{\sigma} \tag{3.105}$$

where W_{ij} is the seasonal water level for the i-th well and j-th observation, μ is the seasonal mean, and σ is the standard deviation. Drought severity classification based on the SWI can be seen in Table 3.34.

Table 3.33 Drought severity based on the standardized streamflow index (SSI) (Modarres, 2007).

SSI	Drought severity
$-1.0 < SSI < -0.50$	Light drought
$-1.5 < SSI < -1.00$	Middle drought
$-2.0 < SSI < -1.50$	Severe drought
$SSI < -2.00$	Extreme drought

Source: From Modarres, Reza. (2007). Streamflow drought time series forecasting. *Stochastic Environmental Research and Risk Assessment*, 21(3), 223–233. https://doi.org/10.1007/s00477-006-0058-1.

Table 3.34 Drought severity based on the standardized water-level index (SWI).

SWI	Drought severity
$SWI > 4.00$	Extreme
$4.00 > SWI > 2.50$	Severe
$2.50 > SWI > 1.00$	Moderate
$1.00 > SWI > 0.00$	Mild
$SWI < 0.00$	No Drought

Source: From Bhuiyan, C. (2004). Various drought indices for monitoring drought condition in Aravalli Terrain of India. In *International Archives of the Photogrammetry, Remote Sensing and Spatial Information Sciences - ISPRS Archives* (Vol. 35, pp. 1283–1288). International Society for Photogrammetry and Remote Sensing. http://www.isprs.org/proceedings/XXXVIII/4-W15/.

3.3.39 Streamflow drought index

The streamflow drought index (SDI) was proposed by Nalbantis and Tsakiris (2009). The SDI is used for the estimation of the frequency and severity of hydrological drought (Gulmez et al., 2023). In this method for the calculation of SDI, it is supposed that a time series of monthly streamflow $Q_{i,j}$ is available, where *i* is the hydrological year and j is the month in the same hydrological year. In this way, it is evaluated that the time series of monthly streamflow volumes ($Q_{i,j}$) are continuous, and are accumulated according to the time length of k. The cumulative streamflow volume can be obtained as:

$$V_{i,k} = \sum_{j=1}^{3k} Q_{i,j} \quad (i = 1, \quad 2, . \quad ; \quad j = 1, \quad 2, .,12 \quad ; \quad k = 1, \quad 2, \quad 3, \quad 4) \tag{3.106}$$

where $V_{i,k}$ is the cumulative streamflow for the *i*-th hydrological year with a period duration of k. At that point, the SDI for the *i*-th hydrological year with period term *k* is characterized by computing the cumulative streamflow volumes $V_{i,k}$ as follows:

$$SDI_{i,k} = \frac{V_{i,k} - \mu_{Vk}}{\sigma_{Vk}} \quad (i = 1, \quad 2, . \quad ; \quad k = 1, \quad 2, \quad 3, \quad 4) \tag{3.107}$$

where μ_{Vk} is the long-term mean of cumulative streamflow volumes, and σ_{Vk} is the standard deviation for the cumulative streamflow volumes. Nalbantis and Tsakiris (2009), employed the two-parameter log-normal distribution, where normalization can be done by taking the natural logarithm of streamflow. Five drought severity classes are defined using the SDI, which can be seen in Table 3.35.

3.3.40 Surface water supply index

The surface water supply index (SWSI) was developed by Shafer and Dezman (1982). The SWSI evaluates the total volume of water in a basin or subbasin by comparing it with the volume available in the same month of historical years. This comparison allows for the analysis of how the current water situation has changed compared to past periods and the stability of the water supply. The approximate frequency of mild drought occurrence is identified by the SWSI at 26%–50%, moderate drought occurrence at 14%–26%, and severe drought occurrence at 2%–14%.

Extreme drought is experienced approximately less than 2% of the time. The SWSI can be calculated as

$$\mathrm{SWSI} = \frac{[(a \times \mathrm{PN_{SP}}) + (b \times \mathrm{PN_P}) + (c \times \mathrm{PN_{RP}}) - 50]}{12} \quad (3.108)$$

where *a*, *b*, and *c* correspond to the probability of non-exceedance PN(%), snowpack (SP), and precipitation (P), respectively. Each basin has unique values of *a*, *b*, and *c*, which represent the weights for each component and must satisfy the condition $a+ b+ c=1$. Drought severity based on the SWSI is given in Table 3.36

Table 3.35 Drought severity classification based on streamflow drought index (SDI).

SDI	Drought severity
SDI > 2.00	Extremely wet
1.50 < SDI < 1.99	Very wet
1.00 < SDI < 1.49	Moderately wet
-0.99 < SDI < 0.99	Near normal
-1.49 < SDI < -1.00	Moderately dry
-1.99 < SDI < -1.50	Severely dry
SDI < -2.00	Extremely dry

Source: From Gulmez, Ayse, Mersin, Denizhan, Vaheddoost, Babak, Safari, Mir Jafar Sadegh, Tayfur, Gokmen. (2023). A joint evaluation of streamflow drought and standard precipitation indices in Aegean region, Türkiye *Pure and Applied Geophysics*, 180(12), 4319–4337. https://doi.org/10.1007/s00024-023-03378-9.

Table 3.36 Drought severity based on the surface water supply index (SWSI).

SWSI	Drought severity
4 > SWSI	Abundant supply
2 < SWSI < 4	Near normal
− 1 < SWSI < –2	The Water Availability Task Force (WAFT) activated
− 2 < SWSI < − 3	Moderate drought - other task forces activated
− 3 < SWSI < − 4	Severe drought - agency sought programs activated
SWSI < − 4	Extreme drought

Source: From Shafer, B. A. Dezman, L. E. (1982). Development of a Surface Water Supply Index (SWSI) to assess the severity of drought conditions in snowpack runoff areas (Colorado). *Proceedings: Eastern Snow Conference, 39th Annual Meeting*, 164–175.

3.3.41 Temperature vegetation drought index

The temperature vegetation drought index (TVDI) was developed by Sandholt et al. (2002). The TVDI utilizes the correlation between surface temperature and soil moisture (relative soil moisture) to indicate the severity of drought. The TVDI comprehensively considers the relationship and changes between the NDVI and LST. The temperature method is a technique that uses surface temperature data to monitor soil moisture. Temperature serves as a time-sensitive indicator of water stress, but it tends to be influenced by vegetation cover when employing the temperature method to monitor soil moisture. TVDI integrates vegetation indices and surface temperature to monitor soil moisture, thereby possessing a wider range of applicability. Fig. 3.4 illustrates the simplified feature space of NDVI. The TVDI can be calculated as (Du et al., 2017):

$$\mathrm{TVDI} = \frac{T_s - T_{s-\min}}{T_{s-\max} - T_{s-\min}} \tag{3.109}$$

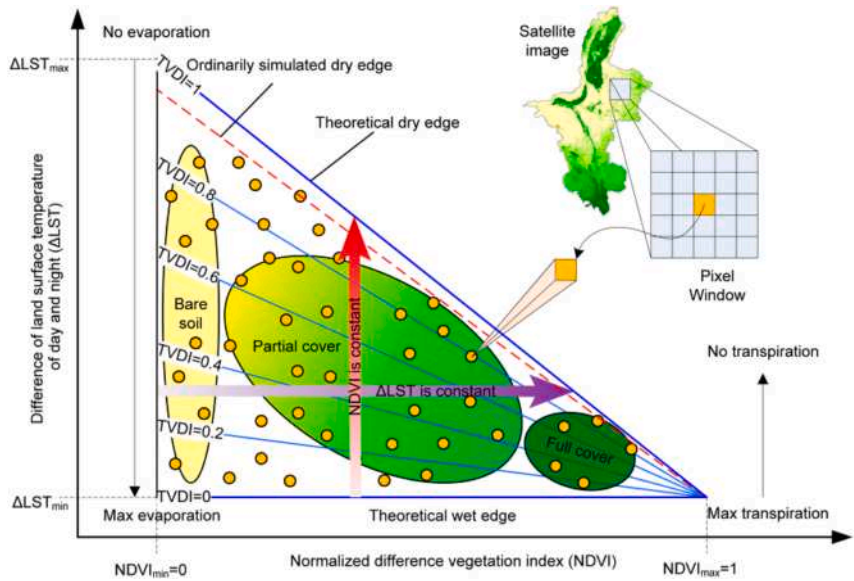


Figure 3.4 The simplified featue space of normalized difference vegetation index (*NDVI*). Map lines delineate study areas and do not necessarily depict accepted national boundaries. *LST*, Land surface temperature; *TVDI*, Temperature–vegetation dryness index. From Du, L., Song, N., Liu, K., Hou, J., Hu, Y., Zhu, Y., Wang, X., Wang, L., & Guo, Y. (2017). Comparison of two simulation methods of the temperature vegetation dryness index (TVDI) for drought monitoring in semi-arid regions of China. *Remote Sensing*, 9(2). https://doi.org/10.3390/rs9020177.

where T_{s-min} and T_{s-max} are the minimum and maximum of LST, respectively, when the NDVI is equal to a particular value.

The NDVI-Ts feature space can be simplified into a triangular form, with T and Ts being linearly fitted simultaneously, yielding the following result:

$$T_{s-max} = a + b\,(\mathrm{NDVI}) \tag{3.110}$$

$$T_{s-min} = a' + b'\,(\mathrm{NDVI}) \tag{3.111}$$

$$\mathrm{TDVI} = \frac{[T_s - (a' + b'\,(\mathrm{NDVI}))]}{(a + b\,(\mathrm{NDVI})) - (a' + b'\,(\mathrm{NDVI}))} \tag{3.112}$$

a, a', b',and b are the coefficients of the fitting equation for the dry side and wet side, respectively. The TVDI ranges from 0 to 1, where a TVDI value of 1 indicates dry conditions and a value of 0 indicates wet conditions. Higher TVDI values correspond to lower soil moisture levels and increased drought severity.

3.3.42 Thornthwaite moisture index

The Thornthwaite moisture index (TMI) was developed by Thornthwaite (1948). This index was introduced as a new climate categorization tool. The main usage of TMI was to map the climate zones in the United States and other areas of the World. The other usage of the index was defining water balance and hydrological functioning owing to its numerical base. TMI can also be identified as one of the indices that form the basis of the Palmer Drought Index. According to the hypothesis of Thornthwaite, drought could not be defined through only one input, which is precipitation. After his observation in northern Europe and Africa, he found out that potential evapotranspiration should be considered to obtain a moisture index. Thornthwaite formulated his calculations in two ways:

$$\mathrm{M} = \mathrm{I_h} - 0.6\mathrm{I_a} = \frac{100\alpha - 60\beta}{\gamma} \tag{3.113}$$

where a is water surplus, β is water deficiency, and γ is water need potential evapotranspiration. I_h is the humidity index that can be calculated by the formula as:

$$\mathrm{I_h} = 100\left(\frac{\mathrm{R}}{\mathrm{PET}}\right) \tag{3.114}$$

where R is moisture runoff, and PET is potential evapotranspiration. I_a is the aridity index that can be calculated as:

$$I_a = 100\frac{D}{PET} \tag{3.115}$$

where D is moisture deficit and PET is potential evapotranspiration. Thornthwaite, presented the potential evapotranspiration equation PET as shown below:

$$PET = Pet_i\left(\frac{D_i N_i}{30}\right) \tag{3.116}$$

where D_i is the day length correction factor for month i, N_i is the number of days in month i; Pet_i is the nonadjusted potential evapotranspiration for month i, and the formula for Pet_i is:

$$Pet_i = 1.6\left(\frac{10\mu_T}{H_y}\right)^a \tag{3.117}$$

where μ_T is the mean monthly temperature in °C for a given month i, and the calculation for the average of the minimum and maximum temperature. H_y is the yearly heat index, and the calculation of it:

$$H_y = \sum_{i=1}^{12} (0.2t_i)^{1.54} \tag{3.118}$$

where y is the given year. The power term a is a coefficient that ranges between 0 and 4.25 and can be calculated like:

$$\begin{aligned} a = {} & (6.75xH_y{}^3x10^{-7}) - (7.71xH_y{}^2x10^{-5}) \\ & + (0.01792xH_y) + 0.49239 \end{aligned} \tag{3.119}$$

The results of the calculation show that the positive value of TMI is humid or wet with high soil moisture. On the other hand, a negative output indicates an arid climate with low moisture. Drought severity based on the SWSI is given in Table 3.37

3.3.43 Total storage deficit index

The total storage deficit index (TSDI) was developed by Yirdaw et al. (2008). The TSDI is widely recognized as a drought measure derived from GRACE satellite data. However, its effectiveness diminishes in basins with

Table 3.37 Drought severity based on the Thornthwaite moisture index (TMI).

TMI	Drought severity	Climatic type
TMI > 100	Perhumid	A
80 ≤ TMI ≤ 100	Humid	B4
60 < TMI ≤ 80	Humid	B3
40 < TMI ≤ 60	Humid	B2
20 < TMI ≤ 40	Humid	B1
0 < TMI ≤ 20	Moist subhumid	C2
− 20 < TMI ≤ 0	Dry subhumid	C1
− 40 < TMI ≤ −20	Semi-arid	D
TMI ≤ −40	Arid	E

Source: From Thornthwaite, C. W. (1948). An approach toward a rational classification of climate. *Geographical Review*, 38(1). https://doi.org/10.2307/210739.

high water usage due to the influence of water harvesting activities, which can alter the GRACE signal. The TSD can be calculated as

$$TSD_{i,j} = \frac{TSA_{i,j} - \mu_{TSA_j}}{TSA_{j_{max}} - TSA_{j_{min}}} \tag{3.120}$$

The percentage of total storage deficit ($TSD_{i,j}$) and the monthly total storage anomaly ($TSA_{i,j}$) obtained from GRACE are utilized to calculate the TSDI.

$$\begin{aligned} TSDI_i &= p(TSDI_{i-1}) + q(TSD_i) \quad p = 1 - \frac{m}{m+b} \quad q \\ &= \frac{C}{m+b} \end{aligned} \tag{3.121}$$

where C is the TSDI value derived from the best-fit line (drought monograph) during the dry period, m is the slope, and b is the intercept of the cumulative TSD curve. The determination of the p and q parameters relies on the cumulative TSD. Drought severity based on the TSDI is given in Table 3.38.

3.3.44 Vegetation temperature condition index

The vegetation temperature condition index (VTCI) was developed by Wang et al. (2001) to monitor drought events on a regional scale over specific time periods within a year. It can also be utilized to analyze the spatial distribution of drought across the region. LST can be calculated by using the following formula:

Table 3.38 Drought severity based on the total storage deficit index (TSDI).

TSDI	Drought severity
TSDI ≥ 4.0	Extreme wet
3.0 ≤ TSDI ≤ 3.99	Very wet
2.0 ≤ TSDI ≤ 2.99	Moderately wet
1.99 ≤ TSDI ≤ −1.99	Normal
− 2.0 ≤ TSDI ≤ −2.99	Moderate drought
− 3.0 ≤ TSDI ≤ −3.99	Severe drought
− 4.0 ≤ TSDI	Extreme drought

Source: From Yirdaw, S. Z., Snelgrove, K. R., Agboma, C. O. (2008). GRACE satellite observations of terrestrial moisture changes for drought characterization in the Canadian Prairie. *Journal of Hydrology*, 356(1–2), 84–92. https://doi.org/10.1016/j.jhydrol.2008.04.004.

$$LST = T_4 + 3.63(T_4 - T_5) + 0.87 \tag{3.122}$$

where T_4 and T_5 are the brightness temperatures of AVHRR channels 4 and 5, respectively. The VTCI can be calculated by using the following equation:

$$VTCI = \frac{LST_{NDVI_{i_{max}}} - LST_{NDVI_i}}{LST_{NDVI_{i_{max}}} - LST_{NDVI_{i_{min}}}} \tag{3.123}$$

VTCI is not solely influenced by changes in NDVI within a region but is also affected by variations in land surface temperature among pixels with identical NDVI values. The VTCI value falls within the range of 0 to 1, where lower values typically indicate more severe drought occurrences. Drought severity based on the VTCI is given in Table 3.39.

3.3.45 Water balance derived drought index

The water balance derived drought index (WBDDI) was developed by Vasiliades et al. (2011). The WBDDI is a measure used to assess drought conditions in a basin. This index evaluates drought conditions by considering the water balance of a basin. Water balance is a concept that accounts for the inputs and outputs of water in a specific area over a certain period. It typically quantifies precipitation, evaporation, runoff, and changes in storage (such as groundwater replenishment or depletion). Using this water balance information, the WBDDI calculates an index that reflects water deficit or surplus in the basin compared to normal conditions. It comprehensively evaluates the drought situation by taking into account

Table 3.39 Drought severity based on the vegetation temperature condition index (VTCI).

VTCI	Drought severity
VTCI > 0.55	Normal or wet
0.46 < VTCI ≤ 0.55	Mid drought
0.37 < VTCI ≤ 0.46	Moderate drought
VTCI ≤ 0.37	Severe drought

Source: From Tian, Miao, Wang, Pengxin, Khan, Jahangir. (2016). Drought forecasting with vegetation temperature condition index using ARIMA models in the Guanzhong plain. *Remote Sensing*, 8(9). https://doi.org/10.3390/rs8090690.

Table 3.40 Drought severity based on the water balance derived drought index (WBDDI).

WBDDI	Drought severity
WBDDI ≥ 2.0	Extremely wet
1.50 ≤ WBDDI ≤ 1.99	Severely wet
1.0 ≤ WBDDI ≤ 1.49	Moderately wet
0.99 ≤ WBDDI ≤ −0.99	Near normal
− 1.0 ≤ WBDDI ≤ −1.49	Moderately dry
− 1.50 ≤ WBDDI ≤ −1.99	Severely dry
− 2.0 ≤ WBDDI	Extremely dry

Source: From Vasiliades, Lampros, Loukas, Athanasios, Liberis, Nikos. (2011). A water balance derived drought index for Pinios river basin, Greece. *Water Resources Management*, 25(4), 1087–1101. https://doi.org/10.1007/s11269-010-9665-1.

both natural hydrological processes and human impacts on water usage. The WBDDI can be calculated as:

$$Y = \begin{cases} \lambda \neq 0 & \frac{(X^{\lambda} - 1)}{\lambda} \\ \lambda = 0 & \ln(X) \end{cases} \tag{3.124}$$

$$Z_{WBI} = \frac{Y - \mu}{\sigma_y} \tag{3.125}$$

where, X is the original time series of surface runoff, Y is the values of the transformed time series, and λ is a parameter determining this transformation. The standardized time series values are represented by Z_{WBI}. The mean value of the transformed time series is denoted by μ, and the standard deviation of the transformed time series is σ_y. Drought severity based on the WBDDI is given in Table 3.40

3.4 Conclusion

Drought is an inevitable consequence of water scarcity in a region. It directly affects not only the agricultural economy but also society, causing a wide range of problems. Drought can generally be classified as agricultural, meteorological, or hydrological, depending on the parameters and indicators used. To anticipate the problems caused by drought and propose solutions—such as the effective use and development of water resources—before these issues escalate, it is essential to use drought indices that incorporate different parameters. These indices classify drought into agricultural, meteorological, and hydrological types and determine its severity.

Although over 100 drought indices exist in the literature, there are relatively few studies that explain the parameters included in the most commonly used indices, their calculation methods, their advantages and limitations, and the types of droughts they measure. In this essence, vegetation-based indices are excluded from this study due to their role as a sub-process in drought assessment. However, vegetation indices are often used as a parameter in drought assessment.

Instead, in this study, 46 indices were selected based on their popularity and ability to cover different drought types. These indices are summarized with their mathematical formulations and applications for drought categorization. Future studies aim to identify and develop indices that best determine and predict drought severity by applying and comparing indices representing different drought types across various regions.

Acknowledgment

This study was conducted under the guidance of Associate Professor Ismail Dabanli at Istanbul Technical University, within the Master's/PhD program in Hydraulic and Water Resources Engineering.

References

Alami, M. M., & Tayfur, G. (2022). Meteorological drought analysis for helmand river basin, Afghanistan. *Teknik Dergi/Technical Journal of Turkish Chamber of Civil Engineers, 33*(4), 12223–12242. https://doi.org/10.18400/tekderg.868595, https://dergipark.org.tr/en/download/article-file/1534434.

Anderson, M. C., Hain, C., Wardlow, B., Pimstein, A., Mecikalski, J. R., & Kustas, W. P. (2011). Evaluation of drought indices based on Thermal remote sensing of evapotranspiration over the continental United States. *Journal of Climate, 24*(8), 2025–2044. https://doi.org/10.1175/2010JCLI3812.1, http://journals.ametsoc.org/doi/pdf/10.1175/2010JCLI3812.1 United States.

Bayable, G., Amare, G., Alemu, G., & Gashaw, T. (2021). Spatiotemporal variability and trends of rainfall and its association with Pacific Ocean Sea surface temperature in West Harerge Zone, Eastern Ethiopia. *Environmental Systems Research, 10*(1). https://doi.org/10.1186/s40068-020-00216-y, https://www.springer.com/journal/40068.

Bhalme, H. N., & Mooley, D. A. (1980). Large-scale droughts/floods and monsoon circulation. *Monthly Weather Review, 108*(8), 1197–1211. 10.1175/1520-0493(1980)108<1197:lsdamc>2.0.co;2.

Bhuiyan, C. (2004). Various drought indices for monitoring drought condition in Aravalli Terrain of India. In *International archives of the photogrammetry, remote sensing and spatial information sciences—ISPRS archives* (Vol. 35, pp. 1283–1288). http://www.isprs.org/proceedings/XXXVIII/4-W15/.

Byun, H. R., & Wilhite, D. A. (1999). Objective quantification of drought severity and duration. *Journal of Climate, 12*(9), 2747–2756. http://journals.ametsoc.org/loi/clim.

Cañón, J., González, J., & Valdés, J. (2009). Reservoir operation and water allocation to mitigate drought effects in crops: A multilevel optimization using the drought frequency index. *Journal of Water Resources Planning and Management, 135*(6), 458–465. https://doi.org/10.1061/(asce)0733-9496(2009)135:6(458).

Costa, J. A., & Rodrigues, G. P. (2017). Space-time distribution of rainfall anomaly index (RAI) for the salgado basin, Ceará state—Brazil. *Ciência e Natura, 39*(3), 627. https://doi.org/10.5902/2179460X26080.

Dabanlı, İ., Mishra, A. K., & Şen, Z. (2017). Long-term spatio-temporal drought variability in Turkey. *Journal of Hydrology, 552*, 779–792. https://doi.org/10.1016/j.jhydrol.2017.07.038, www.elsevier.com/inca/publications/store/5/0/3/3/4/3.

Dabanlı, İ., & Şen, Z. (2018). Precipitation projections under GCMs perspective and Turkish Water Foundation (TWF) statistical downscaling model procedures. *Theoretical and Applied Climatology, 132*(1–2), 153–166. https://doi.org/10.1007/s00704-017-2070-4, http://link.springer.de/link/service/journals/00704/.

Du, L., Song, N., Liu, K., Hou, J., Hu, Y., Zhu, Y., Wang, X., Wang, L., & Guo, Y. (2017). Comparison of two simulation methods of the temperature vegetation dryness index (TVDI) for drought monitoring in semi-arid regions of China. *Remote Sensing, 9*(2), 177. https://doi.org/10.3390/rs9020177.

Garen, D. C. (1993). Revised surface-water supply index for western United States. *Journal of Water Resources Planning and Management, 119*(4), 437–454. https://doi.org/10.1061/(ASCE)0733-9496(1993)119:4(437).

Ghulam, A., Qin, Q., & Zhan, Z. (2007). Designing of the perpendicular drought index. *Environmental Geology, 52*(6), 1045–1052. https://doi.org/10.1007/s00254-006-0544-2.

Gibbs, W. J., & Maher, J. V. (1967). *Rainfall deciles as drought indicators. Bureau of Meteorology Bulletin No 48*. Bureau of Meteorology.

González, J., & Valdés, J. B. (2006). New drought frequency index: Definition and comparative performance analysis. *Water Resources Research, 42*(11). https://doi.org/10.1029/2005WR004308.

Gulmez, A., Mersin, D., Vaheddoost, B., Safari, M. J. S., & Tayfur, G. (2023). A joint evaluation of streamflow drought and standard precipitation indices in aegean region, Turkey. *Pure and Applied Geophysics, 180*(12), 4319–4337. https://doi.org/10.1007/s00024-023-03378-9.

Hao, Z., & AghaKouchak, A. (2013). Multivariate standardized drought index: A parametric multi-index model. *Advances in Water Resources, 57*, 12–18. https://doi.org/10.1016/j.advwatres.2013.03.009.

Huang, S., Tang, L., Hupy, J. P., Wang, Y., & Shao, G. (2021). A commentary review on the use of normalized difference vegetation index (NDVI) in the era of popular remote

sensing. *Journal of Forestry Research, 32*(1), Available from https://doi.org/10.1007/s11676-020-01155-1, https://www.springer.com/journal/11676.

Hussain, A., Jadoon, K. Z., Rahman, K. U., Shang, S., Shahid, M., Ejaz, N., & Khan, H. (2023). Analyzing the impact of drought on agriculture: Evidence from Pakistan using standardized precipitation evapotranspiration index. *Natural Hazards, 115*(1), 389–408. https://doi.org/10.1007/s11069-022-05559-6, https://www.springer.com/journal/11069.

Idso, S. B., Jackson, R. D., Pinter, P. J., Reginato, R. J., & Hatfield, J. L. (1981). Normalizing the stress-degree-day parameter for environmental variability. *Agricultural Meteorology, 24*, 45–55. https://doi.org/10.1016/0002-1571(81)90032-7.

Isia, I., Hadibarata, T., Jusoh, M. N. H., Bhattacharjya, R. K., Shahedan, N. F., Bouaissi, A., Fitriyani, N. L., & Syafrudin, M. (2023). Drought analysis based on standardized precipitation evapotranspiration index and standardized precipitation index in Sarawak, Malaysia. *Sustainability (Switzerland), 15*(1). https://doi.org/10.3390/su15010734, http://www.mdpi.com/journal/sustainability/.

Jackson, R. D., Kustas, W. P., & Choudhury, B. J. (1988). A reexamination of the crop water stress index. *Irrigation Science, 9*(4), 309–317. https://doi.org/10.1007/BF00296705.

Kamruzzaman, M., Hwang, S., Cho, J., Jang, M. W., & Jeong, H. (2019). Evaluating the spatiotemporal characteristics of agricultural drought in bangladesh using effective drought index. *Water (Switzerland), 11*(12). https://doi.org/10.3390/W11122437, https://www.mdpi.com/2073-4441/11/12/2437.

Karamouz, M., Rasouli, K., & Nazif, S. (2009). Development of a hybrid index for drought prediction: Case study. *Journal of Hydrologic Engineering, 14*(6), 617–627. https://doi.org/10.1061/(asce)he.1943-5584.0000022.

Keetch, J. J., & Byram, G. M. (1968). A drought index for forest fire control. U.S.D.A. Forest Service Research Paper SE-38..

Keyantash, J. A., & Dracup, J. A. (2004). An aggregate drought index: Assessing drought severity based on fluctuations in the hydrologic cycle and surface water storage. *Water Resources Research, 40*(9), W0930401. https://doi.org/10.1029/2003WR002610.

Khan, R., & Gilani, H. (2021). Global drought monitoring with drought severity index (DSI) using Google Earth Engine. *Theoretical and Applied Climatology, 146*(1–2), 411–427. https://doi.org/10.1007/s00704-021-03715-9.

Koudahe, K., Kayode, A. J., Samson, A. O., Adebola, A. A., & Djaman, K. (2017). Trend analysis in standardized precipitation index and standardized anomaly index in the context of climate change in Southern Togo. *Atmospheric and Climate Sciences, 7*(4), 401–423. https://doi.org/10.4236/acs.2017.74030.

Kraus, E. B. (1977). Subtropical droughts and cross-equatorial energy transports. *Monthly Weather Review, 105*(8), 1009–1018. https://doi.org/10.1175/1520-0493(1977)105<1009:sdacee>2.0.co;2.

Martonne, E. D. (1926). Une nouvelle function climatologique: L'indice d'aridité. *Meteorologie, 2*, 449–459.

Martínez-Fernández, J., González-Zamora, A., Sánchez, N., & Gumuzzio, A. (2015). A soil water based index as a suitable agricultural drought indicator. *Journal of Hydrology, 522*, 265–273. https://doi.org/10.1016/j.jhydrol.2014.12.051.

Martínez-Fernández, J., Ceballos, A., Casado, S., Morán, C., & Hernández ,V. (2005). *Runoff and soil moisture relationships in a small forested basin in the Sistema Central Ranges (Spain)* (pp. 31–36). IAHS-AISH Publication Spain..

Matera, A., Fontana, G., Marletto, V., Zinoni, F., Botarelli, L., & Tomei, F. (2007). *Use of a new agricultural drought index within a regional drought observatory*. Springer, 103–124. 10.1007/978-1-4020-5924-7_6.

McKee, T. B., Nolan, J., & Kleist, J. (1993). The relationship of drought frequency and duration to time scales. In *Eighth Conference on Applied Climatology, Anaheim*179–184.

Mendicino, G., Senatore, A., & Versace, P. (2008). A Groundwater Resource Index (GRI) for drought monitoring and forecasting in a mediterranean climate. *Journal of Hydrology, 357*(3–4), 282–302. https://doi.org/10.1016/j.jhydrol.2008.05.005.

Modarres, R. (2007). Streamflow drought time series forecasting. *Stochastic Environmental Research and Risk Assessment, 21*(3), 223–233. https://doi.org/10.1007/s00477-006-0058-1.

Mu, Q., Zhao, M., Kimball, J. S., McDowell, N. G., & Running, S. W. (2013). A remotely sensed global terrestrial drought severity index. *Bulletin of the American Meteorological Society, 94*(1), 83–98. https://doi.org/10.1175/BAMS-D-11-00213.1, http://journals.ametsoc.org/doi/pdf/10.1175/BAMS-D-11-00213.1.

Nalbantis, I., & Tsakiris, G. (2009). Assessment of hydrological drought revisited. *Water Resources Management, 23*(5), 881–897. https://doi.org/10.1007/s11269-008-9305-1.

Narasimhan, B., & Srinivasan, R. (2005). Development and evaluation of soil moisture deficit index (SMDI) and Evapotranspiration Deficit Index (ETDI) for agricultural drought monitoring. *Agricultural and Forest Meteorology, 133*(1–4), 69–88. https://doi.org/10.1016/j.agrformet.2005.07.012.

Nguyen, H., Wheeler, M. C., Otkin, J. A., Cowan, T., Frost, A., & Stone, R. (2019). Using the evaporative stress index to monitor flash drought in Australia. *Environmental Research Letters, 14*(6). https://doi.org/10.1088/1748-9326/ab2103, https://iopscience.iop.org/article/10.1088/1748-9326/ab2103/pdf.

Palfai, I. (1990). Description and forecasting of droughts in Hungary. In Proc. of 14th Congress on Irrigation and Drainage, Rio de Janeiro (Vol. 1, pp. 151–158), .ICID ..

Palmer, W. C. (1965). USWB_meteorological_drought. Office of Climatology U.S. Weayher Bureau, D.C.

Qaisrani, Z. N., Nuthammachot, N., Techato, K., Asadullah, Jatoi, G. H., Mahmood, B., & Ahmed, R. (2024). Drought variability assessment using standardized precipitation index, reconnaissance drought index and precipitation deciles across Balochistan, Pakistan. *Brazilian Journal of Biology, 84*. https://doi.org/10.1590/1519-6984.261001.

Rhee, J., Im, J., & Carbone, G. J. (2010). Monitoring agricultural drought for arid and humid regions using multi-sensor remote sensing data. *Remote Sensing of Environment, 114*(12), 2875–2887. https://doi.org/10.1016/j.rse.2010.07.005.

Ritchie, J. T., & Burnett, E. (1971). Dryland evaporative flux in a subhumid climate: II. plant influences 1. *Agronomy Journal, 63*(1), 56–62. https://doi.org/10.2134/agronj1971.00021962006300010019x.

Sandholt, I., Rasmussen, K., & Andersen, J. (2002). A simple interpretation of the surface temperature/vegetation index space for assessment of surface moisture status. *Remote Sensing of Environment, 79*(2–3), 213–224. https://doi.org/10.1016/s0034-4257(01)00274-7.

Sarkar, J. (2010). Monitoring drought risks in India with emphasis on agricultural drought agricultural drought indices. In *Proceedings of the WMO/UNISDR expert group meeting on agricultural drought indices* (pp. 50–59). WMO..

Shafer, B.A., & Dezman, L.E. (1982). Development of a Surface Water Supply Index (SWSI) to assess the severity of drought conditions in snowpack runoff areas (Colorado). In *Proceedings: Eastern snow conference, 39th annual meeting* (164–175). Colorado State University, Fort Collins..

Selyaninov, G. T. (1928). About climate agricultural estimation. In *Proceedings on Agricultural Meteorology 20*. 165–177.

Shahabfar, A., Ghulam, A., & Eitzinger, J. (2012). Drought monitoring in Iran using the perpendicular drought indices. *International Journal of Applied Earth Observation and Geoinformation, 18*(1), 119–127. https://doi.org/10.1016/j.jag.2012.01.011.

Shukla, S., & Wood, A. W. (2008). Use of a standardized runoff index for characterizing hydrologic drought. *Geophysical Research Letters, 35*(2). https://doi.org/10.1029/2007GL032487.

Sittichok, K., & Thepprasit, C. (2022). The differences of precipitation characteristics among GCMs over Southeast Asia under AR6 climate change scenarios. *ASEAN Journal of Scientific and Technological Reports, 25*(1), 11–23. https://doi.org/10.55164/ajstr.v25i1.244632, https://ph02.tci-thaijo.org/index.php/tsujournal/index.

Sur, C., Park, S. Y., Kim, T. W., & Lee, J. H. (2019). Remote sensing-based agricultural drought monitoring using hydrometeorological variables. *KSCE Journal of Civil Engineering, 23*(12), 5244–5256. https://doi.org/10.1007/s12205-019-2242-0, http://www.springer.com/engineering/journal/12205.

Thomas, T., Gunthe, S. S., Ghosh, N. C., & Sudheer, K. P. (2015). Analysis of monsoon rainfall variability over Narmada basin in central India: Implication of climate change. *Journal of Water and Climate Change, 6*(3), 615–627. https://doi.org/10.2166/wcc.2014.041.

Thornthwaite, C. W. (1948). An approach toward a rational classification of climate. *Geographical Review, 38*(1), 55. https://doi.org/10.2307/210739.

Tigkas, D., Vangelis, H., & Tsakiris, G. (2015). DrinC: A software for drought analysis based on drought indices. *Earth Science Informatics, 8*(3), 697–709. https://doi.org/10.1007/s12145-014-0178-y.

Tirivarombo, S., Osupile, D., & Eliasson, P. (2018). Drought monitoring and analysis: Standardised precipitation evapotranspiration index (SPEI) and standardised precipitation index (SPI). *Physics and Chemistry of the Earth, 106*, 1–10. https://doi.org/10.1016/j.pce.2018.07.001, http://www.journals.elsevier.com/physics-and-chemistry-of-the-earth/.

Topçu, E., Seçkin, N., & Haktanır, N. A. (2022). Drought analyses of Eastern Mediterranean, Seyhan, Ceyhan, and Asi Basins by using aggregate drought index (ADI). *Theoretical and Applied Climatology, 147*(3–4), 909–924. https://doi.org/10.1007/s00704-021-03873-w, https://rd.springer.com/journal/volumesAndIssues/704.

Tsakiris, G., Pangalou, D., & Vangelis, H. (2007). Regional drought assessment based on the reconnaissance drought index (RDI). *Water Resources Management, 21*(5), 821–833. https://doi.org/10.1007/s11269-006-9105-4.

Tsakiris, G., & Vangelis, H. (2005). Establishing a drought index incorporating evapotranspiration. *European Water, 9*(10), 3–11.

Van-Rooy, M. P. (1965). A rainfall anomaly index (RAI), independent of the time and space. *Notos, 14*, 43–48.

Vasiliades, L., Loukas, A., & Liberis, N. (2011). A water balance derived drought index for pinios river basin, Greece. *Water Resources Management, 25*(4), 1087–1101. https://doi.org/10.1007/s11269-010-9665-1.

Vicente-Serrano, S. M., Beguería, S., & López-Moreno, J. I. (2010). A multiscalar drought index sensitive to global warming: The standardized precipitation evapotranspiration index. *Journal of Climate, 23*(7), 1696–1718. https://doi.org/10.1175/2009JCLI2909.1Spain, http://journals.ametsoc.org/doi/pdf/10.1175/2009JCLI2909.1.

Stahl, K. & Demuth, S. (2001) Atmospheric Circulation and Drought. In: Demuth, S. & Stahl, K. (eds) (2001) ARIDE - Final Report to the European Union. Institute of Hydrology. Freiburg. Germany.

Wang, P. X., Li, X. W., Gong, J. Y., & Song, C. (2001). Vegetation temperature condition index and its application for drought monitoring. In *International geoscience and remote sensing symposium (IGARSS)*, (pp. 141–143), IEEE..

Willeke, G. E., Guttman, N. B., Hosking, J. R. M., & Wallis, J. R. (1994). National drought atlas developed. *Eos, Transactions American Geophysical Union, 75*(8), 89–90. https://doi.org/10.1029/94eo00706.

Woli, P., Jones, J. W., Ingram, K. T., & Fraisse, C. W. (2012). Agricultural reference index for drought (ARID). *Agronomy Journal, 104*(2), 287–300. https://doi.org/10.2134/agronj2011.0286, https://www.agronomy.org/publications/aj/pdfs/104/2/287.

Wu, H., Hayes, M. J., Weiss, A., & Hu, Q. (2001). An evolution of the standardized precipitation index, the China-Z index and the statistical Z-score. *International Journal of Climatology, 21*(6), 745–758. https://doi.org/10.1002/joc.658.

Yao, N., Li, Y., Liu, Q., Zhang, S., Chen, X., Ji, Y., Liu, F., Pulatov, A., & Feng, P. (2022). Response of wheat and maize growth-yields to meteorological and agricultural droughts based on standardized precipitation evapotranspiration indexes and soil moisture deficit indexes. *Agricultural Water Management, 266*, 107566. https://doi.org/10.1016/j.agwat.2022.107566.

Yirdaw, S. Z., Snelgrove, K. R., & Agboma, C. O. (2008). GRACE satellite observations of terrestrial moisture changes for drought characterization in the Canadian Prairie. *Journal of Hydrology, 356*(1–2), 84–92. https://doi.org/10.1016/j.jhydrol.2008.04.004.

Zargar, A., Sadiq, R., Naser, B., & Khan, F. I. (2011). A review of drought indices. *Environmental Reviews, 19*(1), 333–349. https://doi.org/10.1139/a11-013, http://pubs.nrc-cnrc.gc.ca/cgi-bin/rp/rp2_desc_e?er.

Zeybekoğlu, U., & Aktürk, G. (2021). A comparison of the China-Z Index (CZI) and the standardized precipitation index (SPI) for drought assessment in the Hirfanli Dam basin in central Turkey. *Arabian Journal of Geosciences, 14*(24). https://doi.org/10.1007/s12517-021-09095-8.

Zhang, A., & Jia, G. (2013). Monitoring meteorological drought in semiarid regions using multi-sensor microwave remote sensing data. *Remote Sensing of Environment, 134*, 12–23. https://doi.org/10.1016/j.rse.2013.02.023.

Zhao, Z., & Wang, K. (2021). Capability of existing drought indices in reflecting agricultural drought in China. *Journal of Geophysical Research: Biogeosciences, 126*(8). https://doi.org/10.1029/2020jg006064.

CHAPTER FOUR

Application of General Circulation Models' outputs in the analysis of the extreme climatic events

Mustafa Nuri Balov[1], **Farzad Rotbee**[1], **and Maryam Khalilzadeh Poshtegal**[2]
[1]Department of Civil Engineering, Istanbul Gelişim University, Istanbul, Türkiye,
[2]Department of Environment, Culture, and Society, Thompson Rivers University, Kamloops, BC, Canada

4.1 Introduction

Extreme climatic events can be defined as abnormalities in the normal climate conditions. These abnormalities, usually, are observed in the form of high deviation from the average such as heavy rainfall events, droughts, etc. The increasing frequency and intensity of extreme climatic events can be considered as indicators of climate change, mainly due to the global warming. According to the Intergovernmental Panel on Climate Change (IPCC), it was projected that the severity and frequency of extreme events would increase during the coming years (IPCC, 2013). A rise in water-holding capacity of the atmosphere as a result of temperature rise has changed the rainfall pattern globally. In this way, a comprehensive study of the possible changes in the number and intensity of extreme events can shed light on the future planning in various fields including infrastructure, water, food safety, etc. One of the most common ways to project the future conditions of the climate in a region is to use the outputs of a group of mathematical models called General Circulation Models (GCMs). These models include the historical simulations of the climate and future projections under a number of emission scenarios. These models have been developed at different organizations all around the world as Coupled Model Intercomparison Project (CMIP). The last released assessment report by IPCC (AR6)

Drought Dynamics
DOI: https://doi.org/10.1016/B978-0-443-34205-9.00006-8
© 2026 Elsevier Inc. All rights are reserved, including those for text and data mining, AI training, and similar technologies.

includes phase 6 of CMIP models, the outputs of which have been used in many studies to investigate future variations in extreme climatic events. All GCM outputs include a level of uncertainty due to various sources such as the complexity of the climate system and the lack of appropriate data (IPCC, 2006). Therefore, a number of studies focused on the performance of various GCMs in terms of precipitation and temperature projections for different regions (Akinsanola et al., 2020; Ali et al., 2023; Chatterjee et al., 2023; Chen et al., 2020; Hemanandhini & Vignesh Rajkumar, 2023; Kim et al., 2020; Nguyen-Duy et al., 2023; Shiru & Chung, 2021) evaluated the level of uncertainties in the outputs of GCMs in India. They concluded that the agreement between observations and simulations during the historical period is within an acceptable range. A similar study was conducted for Nigeria and ranked 13 CMIP6 models based on temperature and precipitation modeling.

On the other hand, various studies have focused on the future of extreme climatic events based on the outputs of GCMs. Those studies can be categorized in projecting drought (Araujo et al., 2025; Tadase & Tekile, 2025; Wang et al., 2021; Wang et al., 2025; Xu et al., 2024; Zhao & Dai, 2022), and extreme rainfall events (Das et al., 2022; Klutse et al., 2021; Saha & Sateesh, 2022; Suthinkumar et al., 2024; Varghese et al., 2025). In recently published research article, the authors generated drought indices by using the outputs of GCMs under four emission scenarios for different parts of the world including the United States, Europe, China, Brazil, South Africa, and Australia. They provided a dataset of drought indices for the above-mentioned areas. In a study conducted by Kurniadi et al. (2024) the authors used the outputs of 24 GCMs from CMIP6 to project extreme rainfalls in Indonesia. They found that during the 21st century, dry and wet extreme rainfall conditions will be observed more frequently and intensely.

This chapter aims to provide a scientific background in the study of future climatic extremes. The methodology, limitations, and concerns in the application of the GCMs, are investigated.

4.2 General Circulation Models—an overview

GCMs are complex numerical models used to simulate the Earth's climate system. They help scientists understand past, present, and future

climatic conditions by representing physical processes in the atmosphere, ocean, land surface, and ice. GCMs are essential tools for climate change research, policy-making, and weather forecasting (Intergovernmental Panel on Climate Change, 2022). Key Components of GCMs consist of multiple interlinked components, including:

- Atmospheric Models to simulate atmospheric circulation, temperature, humidity, and wind patterns (Peixoto & Oort, 1992)
- Ocean Models which represent ocean currents, temperature distribution, and interactions with the atmosphere (Griffies, 2018)
- Land Surface Models that account for vegetation, soil moisture, and heat exchange between land and atmosphere (Bonan, 2019)
- Sea Ice and Cryosphere Models to simulate polar ice changes and their effects on climate (Holland et al., 2006).

GCMs originated from early numerical weather prediction models developed in the mid-20th century. Early models focused primarily on atmospheric dynamics but they have since evolved into Earth System Models (ESMs) that incorporate biogeochemical cycles (IPCC, 2007). Today, organizations such as the IPCC and NASA Goddard Institute for Space Studies (GISS) use GCMs to assess climate change and its impacts (Intergovernmental Panel on Climate Change, 2022).

GCMs use mathematical equations based on physical laws (e.g., conservation of mass, energy, and momentum) to simulate atmospheric and oceanic circulation. These models divide the Earth's surface into a grid system, where climate variables (temperature, precipitation, wind, etc.) are calculated at each grid point over time (Washington & Parkinson, 1988).

GCMs are significant because they are used in climate projections to predict future climate conditions based on different greenhouse gas (GHG) emission scenarios (Intergovernmental Panel on Climate Change, 2022), policy planning to support decision-making for climate adaptation and mitigation strategies (van Vuuren et al., 2011), and weather seasonal forecasting to improve understanding of atmospheric dynamics for better forecasting (Palmer, 2019).

However, some challenges and considerations should be taken into account while using GCMs because of some limitations including resolution and computational limitations, which need higher-resolution models that require significant computational resources (Schneider et al., 2017), or parameterization, because some small-scale processes (e.g., cloud

formation) must be approximated rather than directly simulated (Stevens & Bony, 2013), and some uncertainties because of variability in model projections due to different assumptions, initial conditions, and emissions scenarios. The ongoing developments recently are:

- Coupled Earth System Models (ESMs): For more comprehensive climate projections, biogeochemical cycles have been integrated in coupled Earth system models.
- Higher Spatial Resolution: To capture regional climate details more accurately, grid resolution is now improving.
- Machine Learning and Artificial Intelligence (AI) Integration: To enhance model efficiency and prediction accuracy using data-driven approaches, AI is now in use.

4.3 Emission scenarios

Emission scenarios are critical frameworks used to project the future climate conditions based on varying levels of GHG emissions with consideration to different assumptions about human activities, economic development, technological progress, population growth, and policy decisions. Emission scenarios are not projections but "what-if" projections based on different policy, economic, and technological choices. They are crucial for understanding future climate risks, mitigation strategies, and adaptation planning. These scenarios, particularly the Representative Concentration Pathways (RCPs), help understand potential temperature increases and the implications for climate policy and sustainability efforts (Xue, 2024).

4.3.1 Representative Concentration Pathways

RCPs are GHG concentration trajectories developed for climate modeling by the IIPCC. Introduced in the IPCC Fifth Assessment Report (AR5), they describe possible future levels of radiative forcing (measured in watts per square meter, W/m^2) by 2100. These pathways help estimate future climate change based on different emission trajectories and are widely used in GCMs to project warming and associated impacts (Intergovernmental Panel on Climate Change, 2014). The four RCPs are shown below:

- RCP 2.6 – Strong mitigation, peak emissions around 2020, then decline (warming ~1.5°C relative to pre-industrial levels)
- RCP 4.5 – Moderate mitigation (warming ~2.4°C relative to pre-industrial levels)

- RCP 6.0 – Stabilization scenario, delayed action (warming ~3°C relative to pre-industrial levels)
- RCP 8.5 – Business-as-usual (BAU), high fossil fuel use (warming ~4–5°C relative to pre-industrial levels).

4.3.2 Shared Socioeconomic Pathways

SSPs (2017-present) are frameworks designed to explore various future scenarios related to climate change, focusing on socioeconomic factors and their implications for sustainability. Initially developed for global climate modeling, the SSPs consist of five distinct narratives that represent different levels of challenges in climate mitigation and adaptation. These pathways serve as a basis for scenario analysis in climate research, policy-making, and sustainability assessments, allowing for a structured examination of potential futures and their impacts on both society and the environment.

4.3.2.1 SSP1 ("Sustainability")—Green growth, low inequality

The world shifts gradually but pervasively toward a more sustainable path, emphasizing more inclusive development that respects perceived environmental boundaries. Management of the global commons slowly improves, educational and health investments accelerate the demographic transition, and the emphasis on economic growth shifts toward a broader emphasis on human well-being. Driven by an increasing commitment to achieving development goals, inequality is reduced both across and within countries. Consumption is oriented toward low material growth and lower resource and energy intensity (Nolan & Mckinstry, 2020).

4.3.2.2 SSP2 ("Middle of the Road")—moderate growth, medium population

The world follows a path in which social, economical, and technological trends do not shift markedly from historical patterns. Development and income growth proceed unevenly, with some countries making relatively good progress while others fall short of expectations. Global and national institutions work toward but make slow progress in achieving sustainable development goals. Environmental systems experience degradation, although there are some improvements, and overall, the intensity of resource and energy use declines. Global population growth is moderate

and levels off in the second half of the century. Income inequality persists or improves only slowly, and challenges to reducing vulnerability to societal and environmental changes remain (Nolan & Mckinstry, 2020).

4.3.2.3 SSP3 ("Regional Rivalry")—nationalism, weak global cooperation, high emissions

A resurgent nationalism, concerns about competitiveness and security, and regional conflicts push countries to increasingly focus on domestic or, at most, regional issues. Policies shift over time to become increasingly oriented toward national and regional security issues. Countries focus on achieving energy and food security goals within their regions at the expense of broader-based development. Investments in education and technological development decline. Economic development is slow, consumption is material-intensive, and inequalities persist or worsen over time. Population growth is low in industrialized and high in developing countries. A low international priority for addressing environmental concerns leads to strong environmental degradation in some regions (Nolan & Mckinstry, 2020).

4.3.2.4 SSP4 ("Inequality")—strong division between rich and poor, regional disparities

Highly unequal investments in human capital, combined with increasing disparities in economic opportunity and political power, lead to increasing inequalities and stratification both across and within countries. Over time, a gap widens between an internationally-connected society that contributes to knowledge- and capital-intensive sectors of the global economy, and a fragmented collection of lower-income, poorly educated societies that work in a labor-intensive, low-tech economy. Social cohesion degrades, and conflict and unrest become increasingly common. Technology development is high in the high-tech economy and sectors. The globally connected energy sector diversifies, with investments in both carbon-intensive fuels like coal and unconventional oil, and low-carbon energy sources. Environmental policies focus on local issues around middle and high-income areas (Nolan & Mckinstry, 2020).

4.3.2.5 SSP5 ("Fossil-Fueled Development")—high fossil fuel use

In this scenario, it is assumed that the world places increasing faith in competitive markets, innovations, and participatory societies to produce

rapid technological progress and development of human capital as the path to sustainable development. Global markets are increasingly integrated. There are also strong investments in health, education, and institutions to enhance human and social capital. At the same time, the push for economic and social development is coupled with the exploitation of abundant fossil fuel resources and the adoption of resource and energy-intensive lifestyles around the world. All these factors lead to rapid growth of the global economy, while the global population peaks and declines in the 21st century. Local environmental problems like air pollution are successfully managed. There is faith in the ability to effectively manage social and ecological systems, including by geo-engineering if necessary (Nolan & Mckinstry, 2020).

Each SSP can be paired with an RCP, as follows (Intergovernmental Panel on Climate Change, 2022):

- SSP1–1.9 → Strong climate action, net-zero emissions before 2100 (~1.5°C)
- SSP2–4.5 → Moderate mitigation (~2.4°C)
- SSP5–8.5 → High emissions, fossil-fuel-driven economy (~4–5°C).

4.4 Downscaling

GCMs are numerical models that have been developed to simulate the global climate conditions by including all components of the climate system. Therefore, the spatial and temporal resolution of these models has shortcomings for climate change impact studies on regional scales (Di Virgilio et al., 2022). To increase the quality and resolution of GCMs' outputs, researchers use various downscaling techniques. Those techniques can be classified into two main groups as statistical and dynamical downscaling (Wilby & Wigley, 1997). Both approaches can be used for improving the outputs of GCMs, however, available data, and computing capacities can affect the selection (Keller et al., 2022). Nevertheless, there are no specific criteria to evaluate which approach is better for a particular purpose and region (Keller et al., 2022). Accordingly, both techniques have been widely used by researchers for various cases (Ashfaq et al., 2022; Fan et al., 2021; Ferrarin et al., 2024; Goldenson et al., 2023; Lima et al., 2021; Liu et al., 2024; Qiu et al., 2022; Tabari et al., 2021).

4.5 Uncertainty issue

GCMs, like all numerical models, include a level of uncertainty (Vetter et al., 2017). Those uncertainties are rooted in the structure of the models and the complicated nature of the climate system (IPCC, 2006). One approach to deal with uncertainty is to use the ensemble of many GCMs, as each GCM has a different structure (Gholami et al., 2023). Another approach is to apply an appropriate bias-correction method (Nuri Balov & Altunkaynak, 2019). However, according to IPCC, the outputs of GCM can be evaluated considering the level of confidence and likelihood scale presented in Tables 4.1 and 4.2

4.5.1 Bias correction

All GCMs' outputs consist of a level of biases, and the application of an appropriate bias-correction method is kind of imperative (Maraun, 2016). Bias-correction methods are roughly divided into two groups of statistical and distribution-based methods (Watanabe et al., 2012). Table 4.3 presents a list of various bias-correction methods which are widely used by researchers.

Table 4.1 The level of confidence (IPCC, 2006).

Level of confidence	Correctness probability
Very high	At least 9 in 10
High	About 8 in 10
Medium	About 5 in 10
Low	About 2 in 10
Very low	Less than 1 in 10

Table 4.2 Degree of likelihood (IPCC, 2006).

Degree of likelihood	Probability of occurrence
Virtually certain	More than 99%
Very likely	More than 90%
Likely	More than 66%
About as likely as not	33%–66%
Unlikely	Less than 33%
Very unlikely	Less than 10%
Exceptionally unlikely	Less than 1%

Table 4.3 Bias-correction methods.

Method	Parameters that applied	Type	References
Linear scaling	Temperature precipitation	Statistical	Berg et al. (2012); Fang et al. (2015); Lafon et al. (2013); Teutschbein and Seibert (2012)
Local intensity scaling	Precipitation	Statistical	Fang et al. (2015); Teutschbein and Seibert (2012)
Power transformation	Precipitation	Statistical	Fang et al. (2015); Teutschbein and Seibert (2012)
Variance scaling	Temperature	Statistical	Fang et al. (2015); Teutschbein and Seibert (2012)
Distribution mapping	Temperature precipitation	Distribution-based	Fang et al. (2015)
Quantile mapping	Precipitation	Distribution-based	Fang et al. (2015); Hashino et al. (2007)
Nonlinear correction	Temperature precipitation	Statistical	Lafon et al. (2013)
Gamma distribution correction	Temperature precipitation	Distribution-based	Lafon et al. (2013)
Empirical distribution correction	Temperature precipitation	Distribution-based	Lafon et al. (2013)
Event bias correction	Temperature precipitation	Statistical	Hashino et al. (2007)
Regression	Temperature precipitation	Statistical	Hashino et al. (2007)
Additive correction	Temperature	Statistical	Berg et al. (2012)
Histogram equalization correction	Temperature precipitation	Distribution-based	Berg et al. (2012)
Multiplicative correction	Precipitation	Statistical	Berg et al. (2012)

4.6 Extreme climatic events

Extreme climate events are unusual and severe weather phenomena that significantly disrupt natural and human systems. These events, which include floods, droughts, heatwaves, and storms, are increasingly influenced by climate change, leading to more frequent and intense occurrences. These events deviate significantly from historical averages and can be short-lived (such as hurricanes and heatwaves) or long-lasting (such as prolonged droughts). They often have significant environmental, social, and economical impacts.

4.6.1 Types of extreme climate events

Meteorological Events: Heavy rainfall, snowstorms, and tropical cyclones can lead to flooding and landslides (Meyer et al., 2022).

Thermal Events: Heatwaves and cold spells affect ecosystems and human health, with heatwaves becoming more common due to rising global temperatures (Extreme events, 2023).

Hydrological Events: Droughts and storm surges impact water availability and coastal communities, exacerbated by climate change (Meyer et al., 2022; Extreme weather & climate events, 2024).

Examples of extreme climate events include:

- Heatwaves: Prolonged periods of excessively high temperatures
- Droughts: Extended periods of significantly reduced rainfall
- Heavy rainfall and floods: Intense precipitation leads to overflowing rivers or urban flooding
- Tropical cyclones (hurricanes, typhoons): Powerful storms with strong winds and heavy rainfall
- Wildfires: Large, uncontrolled fires fueled by dry conditions and high temperatures.

4.6.2 Drought

Drought is a prolonged period of deficient precipitation that results in water shortages, affecting ecosystems, agriculture, and human societies. Unlike other natural disasters that have immediate impacts, droughts develop gradually, making them difficult to predict and manage effectively. They can occur in any climate but are more frequent and severe in arid and semi-arid regions. The significance of studying drought has increased in recent years due to climate change, which is intensifying its frequency and severity.

4.6.2.1 Types of droughts

Depend on the effects of the dryness, drought can be catagorized in the different types. If the weather pattern of a region has changed the drought is known as meteorological drought (Adapa & Venkatareddy, 2024). On the other hand, if there is a scarcity in the available water resources the drought is hydrological (Adapa & Venkatareddy, 2024). Simillarly, the damage in agricultural crops and economical activities can be the results of agricultural (Panda et al., 2020) and socioeconomic (Adapa & Venkatareddy, 2024) drought, respectively.

4.6.2.2 Impacts of drought

Droughts are among the most devastating natural disasters, with far-reaching consequences on the environment, economy, and society. These impacts are multifaceted and can vary depending on the severity, duration, and geographic location of the drought.

Droughts significantly affect ecosystems and natural resources. Reduced water availability leads to the depletion of surface water and groundwater reserves, which can disrupt aquatic ecosystems and reduce biodiversity (Mishra & Singh, 2010). Prolonged droughts also contribute to soil degradation, including erosion and desertification, making land less fertile and productive (Berdugo et al., 2020). Additionally, dry conditions increase the risk of wildfires, which can destroy forests and wildlife habitats (Abatzoglou et al., 2019).

Droughts exacerbate social challenges, including food insecurity, health risks, and displacement. Reduced agricultural output can lead to food shortages and malnutrition, particularly in vulnerable communities (Hasegawa et al., 2018). Long-lasting drought would cause water quality to be poor, and in consequence, the risk of waterborne diseases would increase. Additionally, as a result of severe drought conditions, people are forced to migrate, which is one of the reasons for social and economic disruption.

4.6.2.3 Drought indices

Drought indices are essential tools for monitoring, assessing, and predicting drought conditions. They provide a quantitative measure of drought severity, duration, and spatial extent, helping policymakers, researchers, and stakeholders make informed decisions. Those indices have been introduced to study various impacts of droughts and can be

catagorized in meteorological, hydrological, agricultural, and socioeconomic droughts (Wilhite & Glantz, 1985). The application of those indices also depends on the data used to calculate the value of the index. For instance, one needs to use only monthly precipitation data to calculate the Standardized Precipitation Index (SPI) (Mishra & Singh, 2010), whereas monthly temperature is needed for Standardized Precipitation Evapotranspiration Index (SPEI) (Beguería et al., 2014). Drought indices can be used to monitor the impacts of droughts on various activities such as agricultural or other economic activities. On the other hand, other climatic phenomena e.g. Northern Atlantic Oscillation (NAO), can be investigated in parallel to the drought by using an appropriate drought index (Tosunoglu et al., 2018). Palmer Drought Severity Index (PDSI) (Dai, 2013), Soil Moisture Anomaly Index (SMAI) (AghaKouchak et al., 2021), Standardized Runoff Index (SRI) (Shukla & Wood, 2008), Composite Drought Index (CDI) (Zargar et al., 2011), and Vegetation Health Index (VHI) (Park et al., 2016) are some of widely used drought indices.

4.6.3 Extreme rainfall indices

Extreme rainfall indices are quantitative measures used to assess the frequency, intensity, and duration of extreme rainfall events. These indices are crucial for understanding the impacts of climate variability and change on hydrological systems and agriculture. They help in identifying trends and patterns in rainfall data, which can inform climate resilience and adaptation strategies. The indices are often derived from long-term precipitation data and are used to evaluate the potential consequences of extreme weather events on various sectors, including agriculture and disaster management. Below are some key aspects of extreme rainfall indices. The extreme weather index was initially calculated using the extreme rainfall index developed by the Expert Team on Climate Change Detection and Index (ETCCDI), as shown in Table 4.4 (Yanfatriani et al., 2024).

4.6.3.1 Key extreme rainfall indices

- **PRCPTOT (Total Precipitation):** Measures the total amount of precipitation over a specific period. It is used to assess overall rainfall trends and has shown significant positive trends in some regions, indicating increased rainfall events (Yanfatriani et al., 2024).

Table 4.4 Extreme precipitation index from Expert Team on Climate Change Detection and Index.

Index	Indicator
PRCPTOT (mm)	The total amount of rainfall during a specific period
R85P (mm)	The number of days with rainfall above the 85th percentile of the rainfall distribution
R95P (mm)	The number of days with rainfall above the 95th percentile of the rainfall distribution
R99P (mm)	The number of days with rainfall above the 99th percentile of the rainfall distribution
CDD (day)	Maximum number of consecutive days with less than a certain threshold of precipitation
CWD (day)	Maximum number of consecutive days with precipitation above a certain threshold
R1mm (day)	The number of days with rainfall equal to or exceeding 1 mm
R10mm (day)	The number of days with rainfall equal to or exceeding 10 mm
R20mm (day)	The number of days with rainfall equal to or exceeding 20 mm
R50mm (day)	The number of days with rainfall equal to or exceeding 50 mm
Rx1day (mm)	The maximum amount of rainfall in a single day
Rx5day (mm)	The maximum amount of rainfall over five consecutive days
SDII (mm/day)	The average daily intensity of rainfall during a specific period

- **R95P and R99P (Very Wet and Extremely Wet Days):** These indices represent the amount of precipitation from days exceeding the 95th and 99th percentiles, respectively. They are crucial for understanding the intensity of extreme rainfall events and have shown decreasing trends in some areas (Yanfatriani et al., 2024).
- **CWD and CDD (Consecutive Wet and Dry Days):** CWD measures the maximum number of consecutive days with significant rainfall, while CDD measures the maximum number of consecutive dry days. These indices help in understanding the duration of wet and dry spells, with CWD showing increasing trends in some regions (Yanfatriani et al., 2024).
- **RX1Day and RX5Day (Maximum 1-day and 5-day Precipitation):** These indices capture the highest amount of rainfall recorded in a single day or over five consecutive days, providing

insights into the potential for flooding and other hydrometeorological disasters (Yanfatriani et al., 2024).

4.6.3.2 Applications of extreme rainfall indices

Agricultural Impact: Extreme rainfall indices significantly affect crop calendars, influencing land preparation, sowing, and harvesting times. Variations in these indices can lead to adjustments in agricultural practices to mitigate adverse impacts (Meharie et al., 2023).

Disaster Management: Understanding extreme rainfall indices is vital for predicting and managing hydrometeorological disasters such as floods and landslides. Positive correlations between these indices and disaster occurrences highlight the need for effective risk-reduction strategies (Yanfatriani et al., 2024).

While extreme rainfall indices provide valuable insights into climate variability, it is essential to consider their limitations. These indices often rely on historical data, which may not fully capture future climate scenarios. Additionally, regional variations in climate patterns necessitate localized studies to develop effective adaptation and mitigation strategies. Understanding these indices in conjunction with large-scale atmospheric teleconnections can enhance predictive capabilities and inform policy decisions (Früh et al., 2024; Vinod & Mahesha, 2024).

4.7 Case tudy: Drought A ssessment

As an example for the application of the outputs of GCMs in future projection of extreme climatic events, we perform a GCM-based drought analysis for a meteorological station in the United States. We used monthly precipitation data to generate SPI for further drought assessment.

4.7.1 Study Area and Data

In this chapter, we used the monthly precipitation data from a meteorological station called Camp Angelus, California, United States (Fig. 4.1). The station is located at 34.1491°N and 116.9802°W. The altitude of the location is 1758.7 m. The historical precipitation values measured between 1985 and 2014 were downloaded from the National Oceanic and Atmospheric Administration website.

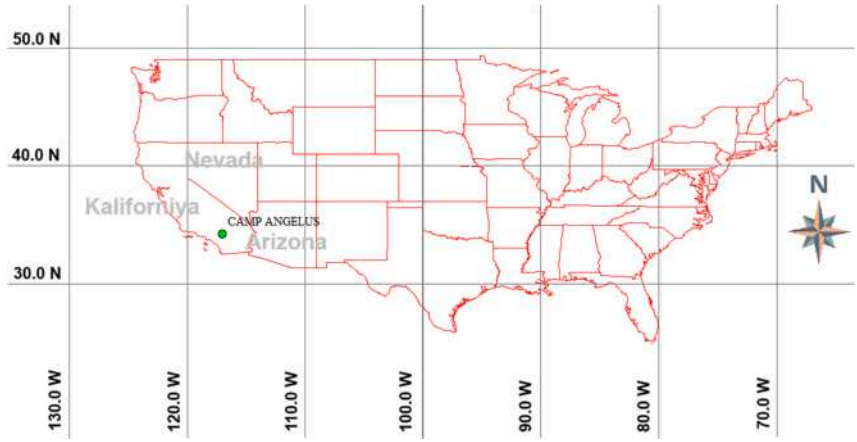


Figure 4.1 The study area. Map lines delineate study areas and do not necessarily depict accepted national boundaries.

In order to investigate the future of the drought in the study area, the monthly precipitation values from the outputs of a GCM developed based on CMIP6, called GFDL-ESM4, under SSP2–4.5 and SSP5–8.5 emission scenarios are used. These data were downloaded from the website of Copernicus project supported by Europian Union.

4.7.2 Application

The outputs of the GCM were corrected by using the linear scaling method. Later, the monthly time series from observed values and GCM's outputs under two scenarios were used to generate the SPI index with various time steps, including 1, 3, 6, 9, and 12 months moving averages using a software called DrinC (Tigkas et al., 2015). The values of SPI can be used to categorize the drought condition so that for the values between 0 and -0.99, between -1.00 and -1.49, between -1.5 and -1.99, and less than -2.00 the drought is mild, moderate, severe, and extreme, respectively (Naresh Kumar et al., 2009).

Accordingly, the number of months with a kind of drought is presented in Table 4.5.

Table 4.5 The number of months with any type of drought.

Dataset	Period	Time step	# of months			Dataset	Period	Time step	# of months		
			ExD	SeD	MoD				ExD	SeD	MoD
ref	1985–2014	1	13	24	33	ref	1985–2014	9	18	17	20
SSP2–4.5	2015–40	1	12	16	23	SSP2–4.5	2015–40	9	9	16	34
SSP2–4.5	2041–70	1	6	17	35	SSP2–4.5	2041–70	9	15	15	24
SSP2–4.5	2071–2100	1	13	19	35	SSP2–4.5	2071–2100	9	3	15	39
SSP5–8.5	2015–40	1	9	10	29	SSP5–8.5	2015–40	9	10	11	31
SSP5–8.5	2041–70	1	12	22	31	SSP5–8.5	2041–70	9	20	23	22
SSP5–8.5	2071–2100	1	13	23	33	SSP5–8.5	2071–2100	9	6	15	21
ref	1985–2014	3	11	24	34	ref	1985–2014	12	23	6	17
SSP2–4.5	2015–40	3	7	16	24	SSP2–4.5	2015–40	12	9	23	36
SSP2–4.5	2041–70	3	13	20	29	SSP2–4.5	2041–70	12	17	9	29
SSP2–4.5	2071–2100	3	15	18	32	SSP2–4.5	2071–2100	12	3	10	33
SSP5–8.5	2015–40	3	9	12	21	SSP5–8.5	2015–40	12	9	11	44
SSP5–8.5	2041–70	3	20	12	27	SSP5–8.5	2041–70	12	19	23	24
SSP5–8.5	2071–2100	3	12	14	34	SSP5–8.5	2071–2100	12	2	12	24
ref	1985–2014	6	11	25	28						
SSP2–4.5	2015–40	6	9	14	31						
SSP2–4.5	2041–70	6	18	12	16						
SSP2–4.5	2071–2100	6	9	16	36						
SSP5–8.5	2015–40	6	5	12	23						
SSP5–8.5	2041–70	6	19	18	33						
SSP5–8.5	2071–2100	6	12	13	28						

ExD, Extreme drought; *SeD*, severe drought; *MoD*, moderate drought.

4.8 Conclusion

In this chapter, the main aspects of the application of the outputs of GCMs for analyzing the future of extreme climatic events were discussed. Additionally, a small example was presented about drought projection by using GCM's outputs. However, notwithstanding that the outputs of GCMs include a level of uncertainties which show low agreement with observations, especially for precipitation projections, the application can shed a light on the future condition of the climate in terms of extreme events, which are the point of concern for various organizations. Therefore, new opportunities that have been born by implementing AI for bias correction and other modeling activities, more reliable results with a high level of confidence can be presented.

References

Abatzoglou, J. T., Williams, A. P., & Barbero, R. (2019). Global emergence of anthropogenic climate change in fire weather indices. *Geophysical Research Letters, 46*(1), 326–336. Available from https://doi.org/10.1029/2018GL080959, http://agupubs.onlinelibrary.wiley.com/hub/journal/10.1002/(ISSN)1944-8007/.

Adapa, J. D., & Venkatareddy, K. (2024). Drought analysis of an area using Google Earth Engine. In *Lecture notes in civil engineering, vol. 450*. Springer, 123–141. https://www.springer.com/series/15087 10.1007/978-981-99-8568-5_10.

AghaKouchak, A., Mirchi, A., Madani, K., Di Baldassarre, G., Nazemi, A., Alborzi, A., Anjileli, H., Azarderakhsh, M., Chiang, F., Hassanzadeh, E., Huning, L. S., Mallakpour, I., Martinez, A., Mazdiyasni, O., Moftakhari, H., Norouzi, H., Sadegh, M., Sadeqi, D., Van Loon, A. F., & Wanders, N. (2021). Anthropogenic drought: Definition, challenges, and opportunities. *Reviews of Geophysics, 59*(2). https://doi.org/10.1029/2019RG000683, http://agupubs.onlinelibrary.wiley.com/agu/journal/10.1002/(ISSN)1944-9208/.

Akinsanola, A., Kooperman, K., Pendergrass, P., Hannah, H., & Reed, R. (2020). Seasonal representation of extreme precipitation indices over the United States in CMIP6 present-day simulations. *Environmental Research Letters, 15*(9), Available from https://doi.org/10.1088/1748-9326/ab92c1, https://iopscience.iop.org/article/10.1088/1748-9326/ab92c1.

Ali, Z., Hamed, M. M., Muhammad, M. K. I., Iqbal, Z., & Shahid, S. (2023). Performance evaluation of CMIP6 GCMs for the projections of precipitation extremes in Pakistan. *Climate Dynamics, 61*(9–10), 4717–4732. https://doi.org/10.1007/s00382-023-06831-6, https://www.springer.com/journal/382.

Araujo, D. S. A., Enquist, B. J., Frazier, A. E., Merow, C., Roehrdanz, P. R., Moulatlet, G. M., Zvoleff, A., Song, L., Maitner, B., & Nikolopoulos, E. I. (2025). Global future drought layers based on downscaled CMIP6 models and multiple socioeconomic pathways. *Scientific Data, 12*(1). https://doi.org/10.1038/s41597-025-04612-w.

Ashfaq, M., Rastogi, D., Kitson, J., Abid, M. A., & Kao, S. C. (2022). Evaluation of CMIP6 GCMs Over the CONUS for downscaling studies. *Journal of Geophysical Research: Atmospheres, 127*(21). https://doi.org/10.1029/2022JD036659, http://agupubs.onlinelibrary.wiley.com/hub/jgr/journal/10.1002/(ISSN)2169-8996/.

Beguería, S., Vicente-Serrano, S. M., Reig, F., & Latorre, B. (2014). Standardized precipitation evapotranspiration index (SPEI) revisited: Parameter fitting, evapotranspiration models, tools, datasets and drought monitoring. *International Journal of Climatology, 34*(10), 3001–3023. Available from https://doi.org/10.1002/joc.3887, http://onlinelibrary.wiley.com/journal/10.1002/(ISSN)1097-0088.

Berdugo, M., Delgado-Baquerizo, M., Soliveres, S., Hernández-Clemente, R., Zhao, Y., Gaitán, J. J., Gross, N., Saiz, H., Maire, V., Lehman, A., Rillig, M. C., Solé, R. V., & Maestre, F. T. (2020). Global ecosystem thresholds driven by aridity. *Science (New York, N.Y.), 367*(6479), 787–790. https://doi.org/10.1126/science.aay5958, https://science.sciencemag.org/content/367/6479/787/tab-pdf.

Berg, P., Feldmann, H., & Panitz, H.-J. (2012). Bias correction of high resolution regional climate model data. *Journal of Hydrology, 448–449*, 80–92. https://doi.org/10.1016/j.jhydrol.2012.04.026.

Bonan, G. (2019). *Climate change and terrestrial ecosystem modeling climate change and terrestrial ecosystem modeling*. Cambridge University Press, 1–438. http://doi.org/10.1017/9781107339217 http://doi.org/10.1017/9781107339217.

Chatterjee, D., Singh, D., Singh, P. K., Fohrer, N., & Singh, B. B. (2023). Performance evaluation of different gridded precipitation and CMIP6 model products with gauge observations for assessing rainfall variability under the historical and future climate change scenario over a semi-arid catchment, India. *Physics and Chemistry of the Earth, Parts A/B/C, 131*, 103433. https://doi.org/10.1016/j.pce.2023.103433.

Chen, Z., Zhou, T., Zhang, L., Chen, X., Zhang, W., & Jiang, J. (2020). Global land monsoon precipitation changes in CMIP6 projections. *Geophysical Research Letters, 47*(14). https://doi.org/10.1029/2019gl086902.

Dai, A. (2013). Increasing drought under global warming in observations and models. *Nature Climate Change, 3*(1), 52–58. https://doi.org/10.1038/nclimate1633.

Das, S., Kamruzzaman, M., & Islam, A. R. M. T. (2022). Assessment of characteristic changes of regional estimation of extreme rainfall under climate change: A case study in a tropical monsoon region with the climate projections from CMIP6 model. *Journal of Hydrology, 610*. https://doi.org/10.1016/j.jhydrol.2022.128002 www.elsevier.com/inca/publications/store/5/0/3/3/4/3.

World Meteorological Organization. (2023). *Extreme events*. *State of the global climate 2022. United Nations*. World Meteorological Organization. http://doi.org/10.18356/9789263113160C004.

World Meteorological Organization. (2024). *Extreme weather and climate events*. State of the Global Climate 2023. United Nations. World Meteorological Organization. doi: 10.18356/9789263113474C005..

Fan, X., Jiang, L., & Gou, J. (2021). Statistical downscaling and projection of future temperatures across the Loess Plateau, China. *Weather and Climate Extremes, 32*, 100328. https://doi.org/10.1016/j.wace.2021.100328.

Fang, G. H., Yang, J., Chen, Y. N., & Zammit, C. (2015). Comparing bias correction methods in downscaling meteorological variables for a hydrologic impact study in an arid area in China. *Hydrology and Earth System Sciences, 19*(6), 2547–2559. https://doi.org/10.5194/hess-19-2547-2015.

Ferrarin, L., Stucchi, L., & Bocchiola, D. (2024). Statistical downscaling of GCMs wind speed data for trend analysis of future scenarios: A case study in the Lombardy region. *Theoretical and Applied Climatology, 155*(6), 4875–4890. https://doi.org/10.1007/s00704-024-04921-x.

Früh, D., Strnad, F., Goswami, B., Früh, D., Strnad, F., & Goswami, B. (2024). *Climate indices of extreme rainfall in the South Asian Monsoon domain using a Bayesian hierarchical model*. EGUGA. https://doi.org/10.5194/EGUSPHERE-EGU24-17701.

Gholami, H., Lotfirad, M., Ashrafi, S. M., Biazar, S. M., & Singh, V. P. (2023). Multi-GCM ensemble model for reduction of uncertainty in runoff projections. *Stochastic Environmental Research and Risk Assessment, 37*(3), 953–964. https://doi.org/10.1007/s00477-022-02311-1, https://www.springer.com/journal/477.

Goldenson, N., Leung, L. R., Mearns, L. O., Pierce, D. W., Reed, K. A., Simpson, I. R., Ullrich, P., Krantz, W., Hall, A., Jones, A., & Rahimi, S. (2023). Use-inspired, process-oriented GCM selection prioritizing models for regional dynamical downscaling. *Bulletin of the American Meteorological Society, 104*(9), E1619. https://doi.org/10.1175/BAMS-D-23-0100.1, https://journals.ametsoc.org/view/journals/bams/104/9/BAMS-D-23-0100.1.xml.

Griffies, S. (2018). *Fundamentals of ocean climate models*. Princeton University Press. http://doi.org/10.1515/9780691187129.

Hasegawa, T., Fujimori, S., Havlík, P., Valin, H., Bodirsky, B. L., Doelman, J. C., Fellmann, T., Kyle, P., Koopman, J. F. L., Lotze-Campen, H., Mason-D'Croz, D., Ochi, Y., Pérez Domínguez, I., Stehfest, E., Sulser, T. B., Tabeau, A., Takahashi, K., Takakura, J., van Meijl, H., ... Witzke, P. (2018). Risk of increased food insecurity under stringent global climate change mitigation policy. *Nature Climate Change, 8*(8), 699–703. https://doi.org/10.1038/s41558-018-0230-x, http://www.nature.com/nclimate/index.html.

Hashino, T., Bradley, A. A., & Schwartz, S. S. (2007). Evaluation of bias-correction methods for ensemble streamflow volume forecasts. *Hydrology and Earth System Sciences, 11*(2), 939–950. https://doi.org/10.5194/hess-11-939-2007.

Hemanandhini, S., & Vignesh Rajkumar, L. (2023). Performance evaluation of CMIP6 climate models for selecting a suitable GCM for future precipitation at different places of Tamil Nadu. *Environmental Monitoring and Assessment, 195*(8). https://doi.org/10.1007/s10661-023-11454-9.

Holland, M. M., Bitz, C. M., & Tremblay, B. (2006). Future abrupt reductions in the summer Arctic sea ice. *Geophysical Research Letters, 33*(23). https://doi.org/10.1029/2006GL028024.

Intergovernmental Panel on Climate Change. (2014). Climate change 2014: Synthesis report. In (R. K. Pachauri, & L. A. Meyer (Eds.). *Contribution of Working Groups I, II and III to the Fifth Assessment Report of the Intergovernmental Panel on Climate Change*. IPCC.

Intergovernmental Panel on Climate Change. (2022). *Climate change 2022: Mitigation of climate change. Contribution of Working Group III to the Sixth Assessment Report of the Intergovernmental Panel on Climate Change*. Cambridge University Press. https://doi.org/10.1017/9781009157926.001.

IPCC. (2006). *Guidance notes for lead authors of the IPCC fourth assessment report on addressing uncertainties*. IPCC.

IPCC. (2007). *Climate Change 2007—The physical science basis contribution of working Group I to the fourth assessment report of the IPCC*. Cambridge University Press.

IPCC. (2013). *Climate Change 2013: The physical sciences basis*. Cambridge University Press.

Keller, A. A., Garner, K. L., Rao, N., Knipping, E., & Thomas, J. (2022). Downscaling approaches of climate change projections for watershed modeling: Review of theoretical and practical considerations. *PLOS Water, 1*(9). https://doi.org/10.1371/journal.pwat.0000046, https://journals.plos.org/water/article?id=10.1371/journal.pwat.0000046.

Kim, Y. H., Min, S. K., Zhang, X., Sillmann, J., & Sandstad, M. (2020). Evaluation of the CMIP6 multi-model ensemble for climate extreme indices. *Weather and Climate Extremes, 29*. https://doi.org/10.1016/j.wace.2020.100269, http://www.journals.elsevier.com/weather-and-climate-extremes/.

Klutse, N. A. B., Quagraine, K. A., Nkrumah, F., Quagraine, K. T., Berkoh-Oforiwaa, R., Dzrobi, J. F., & Sylla, M. B. (2021). The climatic analysis of summer monsoon extreme precipitation events over West Africa in CMIP6 simulations. *Earth Systems and Environment, 5*(1), 25–41. https://doi.org/10.1007/s41748-021-00203-y, https://link.springer.com/journal/41748.

Kurniadi, A., Weller, E., Salmond, J., & Aldrian, E. (2024). Future projections of extreme rainfall events in Indonesia. *International Journal of Climatology, 44*(1), 160–182. https://doi.org/10.1002/joc.8321.

Lafon, T., Dadson, S., Buys, G., & Prudhomme, C. (2013). Bias correction of daily precipitation simulated by a regional climate model: A comparison of methods. *International Journal of Climatology, 33*(6), 1367–1381. https://doi.org/10.1002/joc.3518.

Lima, C. H. R., Kwon, H. H., & Kim, Y. T. (2021). A Bayesian Kriging model applied for spatial downscaling of daily rainfall from GCMs. *Journal of Hydrology, 597*. https://doi.org/10.1016/j.jhydrol.2021.126095 www.elsevier.com/inca/publications/store/5/0/3/3/4/3.

Liu, S., Zeman, C., & Schär, C. (2024). Dynamical downscaling of climate simulations in the tropics. *Geophysical Research Letters, 51*(5). https://doi.org/10.1029/2023gl105733.

Maraun, D. (2016). Bias correcting climate change simulations—A critical review. *Current Climate Change Reports, 2*(4), 211–220. https://doi.org/10.1007/s40641-016-0050-x.

Meharie, E. A., Taye, M. A., Lema, A. T., & Alemu, M. M. (2023). Extreme rainfall indices and their consequences on the local farming crop calendar: An agro-climatic zone based study. *Advances in Modern Agriculture, 4*(2), 2312. https://doi.org/10.54517/ama.v4i2.2312.

Meyer, A., Bresson, H., Gorodetskaya, I. V., Harris, R. M. B., & Perkins-Kirkpatrick, S. E. (2022). Earth and its resources extreme climate and weather events in a warmer world. *Frontiers for Young Minds, 10*, 1–10.

Mishra, A. K., & Singh, V. P. (2010). A review of drought concepts. *Journal of Hydrology, 391*(1–2), 202–216. https://doi.org/10.1016/j.jhydrol.2010.07.012.

Naresh Kumar, M., Murthy, C. S., Sesha Sai, M. V. R., & Roy, P. S. (2009). On the use of Standardized Precipitation Index (SPI) for drought intensity assessment. *Meteorological Applications, 16*(3), 381–389. https://doi.org/10.1002/met.136.

Nguyen-Duy, T., Ngo-Duc, T., & Desmet, Q. (2023). Performance evaluation and ranking of CMIP6 global climate models over Vietnam. *Journal of Water and Climate Change, 14*(6), 1831–1846. https://doi.org/10.2166/wcc.2023.454.

Nolan, P., & Mckinstry, A. (2020). *EC-Earth global climate simulations: Ireland's contributions to CMIP6*. Environmental Protection Agency (EPA). https://doi.org/10.31223/OSF.IO/Y8SFK.

Nuri Balov, M., & Altunkaynak, A. (2019). Frequency analyses of extreme precipitation events in Western Black Sea Basin (Turkey) based on climate change projections. *Meteorological Applications, 26*(3), 468–482. https://doi.org/10.1002/met.1776.

Palmer, T. (2019). The ECMWF ensemble prediction system: Looking back (more than) 25 years and projecting forward 25 years. *Quarterly Journal of the Royal Meteorological Society, 145*(S1), 12–24. https://doi.org/10.1002/qj.3383.

Panda, A., Sahoo, N., Panigrahi, B., & Das, D. M. (2020). Drought assessment using standardized precipitation index and normalized difference vegetation index. *International Journal of Current Microbiology and Applied Sciences, 9*(7), 1125–1136. https://doi.org/10.20546/ijcmas.2020.907.132.

Park, S., Im, J., Jang, E., & Rhee, J. (2016). Drought assessment and monitoring through blending of multi-sensor indices using machine learning approaches for different climate regions. *Agricultural and Forest Meteorology, 216*, 157–169. https://doi.org/10.1016/j.agrformet.2015.10.011.

Peixoto, J. P., & Oort, A. H. (1992). *Physics of climate*. American Institute of Physics.

Qiu, Y., Feng, J., Yan, Z., Wang, J., & Li, Z. (2022). High-resolution dynamical downscaling for regional climate projection in Central Asia based on bias-corrected multiple GCMs. *Climate Dynamics, 58*(3–4), 777–791. https://doi.org/10.1007/s00382-021-05934-2.

Saha, U., & Sateesh, M. (2022). Rainfall extremes on the rise: Observations during 1951–2020 and bias-corrected CMIP6 projections for near- and late 21st century over Indian landmass. *Journal of Hydrology, 608*, 127682. https://doi.org/10.1016/j.jhydrol.2022.127682.

Schneider, T., Lan, S., Stuart, A., & Teixeira, J. (2017). Earth system modeling 2.0: A blueprint for models that learn from observations and targeted high-resolution simulations. *Geophysical Research Letters, 44*(24), 12–417. https://doi.org/10.1002/2017GL076101, http://onlinelibrary.wiley.com/journal/10.1002/(ISSN)1944-8007/issues?year=2012.

Shiru, M. S., & Chung, E. S. (2021). Performance evaluation of CMIP6 global climate models for selecting models for climate projection over Nigeria. *Theoretical and Applied Climatology, 146*(1–2), 599–615. Available from https://doi.org/10.1007/s00704-021-03746-2, https://rd.springer.com/journal/volumesAndIssues/704.

Shukla, S., & Wood, A. W. (2008). Use of a standardized runoff index for characterizing hydrologic drought. *Geophysical Research Letters, 35*(2). https://doi.org/10.1029/2007GL032487.

Stevens, B., & Bony, S. (2013). Water in the atmosphere. *Physics Today, 66*(6), 29–34. https://doi.org/10.1063/PT.3.2009.

Suthinkumar, P. S., Varikoden, H., & Babu, C. A. (2024). Assessment of extreme rainfall events over the Indian subcontinent during the historical and future projection periods based on CMIP6 simulations. *International Journal of Climatology, 44*(1), 39–58. https://doi.org/10.1002/joc.8314.

Tabari, H., Paz, S. M., Buekenhout, D., & Willems, P. (2021). Comparison of statistical downscaling methods for climate change impact analysis on precipitation-driven drought. *Hydrology and Earth System Sciences, 25*(6), 3493–3517. Available from https://doi.org/10.5194/hess-25-3493-2021, http://www.hydrol-earth-syst-sci.net/volumes_and_issues.html.

Tadase, A. T., & Tekile, A. K. (2025). Future projections of climate variables and meteorological drought: Insight from CMIP6 models in Southeast Ethiopia. *Dynamics of Atmospheres and Oceans, 110*. https://doi.org/10.1016/j.dynatmoce.2025.101538, https://www.sciencedirect.com/science/journal/03770265.

Teutschbein, C., & Seibert, J. (2012). Bias correction of regional climate model simulations for hydrological climate-change impact studies: Review and evaluation of different methods. *Journal of Hydrology, 456–457*, 12–29. https://doi.org/10.1016/j.jhydrol.2012.05.052.

Tigkas, D., Vangelis, H., & Tsakiris, G. (2015). DrinC: A software for drought analysis based on drought indices. *Earth Science Informatics, 8*(3), 697–709. https://doi.org/10.1007/s12145-014-0178-y.

Tosunoglu, F., Can, I., & Kahya, E. (2018). Evaluation of spatial and temporal relationships between large-scale atmospheric oscillations and meteorological drought indexes in Turkey. *International Journal of Climatology, 38*(12), 4579–4596. https://doi.org/10.1002/joc.5698.

Varghese, S. J., Pentakota, S., Thadivalasa, P., Podapati, G., & Ashok, K. (2025). Changes in physical characteristics of extreme rainfall events during the Indian summer monsoon based on downscaled and bias-corrected CMIP6 models. *Scientific Reports, 15*(1). https://doi.org/10.1038/s41598-025-87949-x, https://www.nature.com/srep/.

Vetter, T., Reinhardt, J., Flörke, M., van Griensven, A., Hattermann, F., Huang, S., Koch, H., Pechlivanidis, I. G., Plötner, S., Seidou, O., Su, B., Vervoort, R. W., & Krysanova, V. (2017). Evaluation of sources of uncertainty in projected hydrological changes under climate change in 12 large-scale river basins. *Climatic Change, 141*(3), 419–433. https://doi.org/10.1007/s10584-016-1794-y www.wkap.nl/journalhome.htm/0165-0009.

Vinod, D., & Mahesha, A. (2024). Large-scale atmospheric teleconnections and spatiotemporal variability of extreme rainfall indices across India. *Journal of Hydrology, 628*, 130584. https: //doi.org/10.1016/j.jhydrol.2023.130584.

Di Virgilio, G., Ji, F., Tam, E., Nishant, N., Evans, J. P., Thomas, C., Riley, M. L., Beyer, K., Grose, M. R., Narsey, S., & Delage, F. (2022). Selecting CMIP6 GCMs for CORDEX dynamical downscaling: Model Performance, independence, and climate change signals. *Earth's Future, 10*(4), 23284277. https://doi.org/10.1029/2021EF002625, http://onlinelibrary.wiley.com/journal/10.1002/(ISSN)2328-4277.

van Vuuren, D. P., Edmonds, J., Kainuma, M., Riahi, K., Thomson, A., Hibbard, K., Hurtt, G. C., Kram, T., Krey, V., Lamarque, J. F., Masui, T., Meinshausen, M., Nakicenovic, N., Smith, S. J., & Rose, S. K. (2011). The representative concentration pathways: An overview. *Climatic Change, 109*(1), 5–31. https://doi.org/10.1007/s10584-011-0148-z.

Wang, S., Huang, S., Wang, C., Zhang, X., Wu, J., Gulakhmadov, A., Niyogi, D., & Chen, N. (2025). Global anthropogenic effects on meteorological—hydrological—soil moisture drought propagation: Historical analysis and future projection. *Journal of Hydrology, 653*, 132755. https://doi.org/10.1016/j.jhydrol.2025.132755.

Wang, T., Tu, X., Singh, V. P., Chen, X., & Lin, K. (2021). Global data assessment and analysis of drought characteristics based on CMIP6. *Journal of Hydrology, 596*, 126091. https://doi.org/10.1016/j.jhydrol.2021.126091.

Washington, W. M., & Parkinson, C. L. (1988). An introduction to three-dimensional climate modeling. *Transactions American Geophysical Union, 69*(2). https://doi.org/10.1029/88EO00016 27–27.

Watanabe, S., Kanae, S., Seto, S., Yeh, P. J. F., Hirabayashi, Y., & Oki, T. (2012). Intercomparison of bias-correction methods for monthly temperature and precipitation simulated by multiple climate models. *Journal of Geophysical Research Atmospheres, 117*(23). https://doi.org/10.1029/2012JD018192, http://onlinelibrary.wiley.com/journal/10.1002/(ISSN)2169-8996.

Wilby, R. L., & Wigley, T. M. L. (1997). Downscaling general circulation model output: A review of methods and limitations. *Progress in Physical Geography: Earth and Environment, 21*(4), 530–548. https://doi.org/10.1177/030913339702100403.

Wilhite, D. A., & Glantz, M. H. (1985). Understanding: The drought phenomenon: The role of definitions. *Water International, 10*(3), 111–120. https://doi.org/10.1080/02508068508686328.

Xu, F., Qu, Y., Bento, V. A., Song, H., Qiu, J., Qi, J., Wan, L., Zhang, R., Miao, L., Zhang, X., & Wang, Q. (2024). Understanding climate change impacts on drought in China over the 21st century: A multi-model assessment from CMIP6. *npj Climate and Atmospheric Science,* 7(1). https://doi.org/10.1038/s41612-024-00578-5, https://www.nature.com/npjclimatsci/.

Xue, L. (2024). Historical and future global warming under different RCP emission scenarios. *Applied and Computational Engineering, 63*(1), 34–44. https://doi.org/10.54254/2755-2721/63/20240991.

Yanfatriani, E., Marzuki, M., Vonnisa, M., Razi, P., Hapsoro, C. A., Ramadhan, R., & Yusnaini, H. (2024). Extreme rainfall trends and hydrometeorological disasters in tropical regions: Implications for climate resilience. *Emerging Science Journal, 8*(5), 1860–1874. https://doi.org/10.28991/ESJ-2024-08-05-012, https://ijournalse.org/index.php/ESJ/article/download/2361/pdf.

Zargar, A., Sadiq, R., Naser, B., & Khan, F. I. (2011). A review of drought indices. *Environmental Reviews, 19*(1), 333–349. https://doi.org/10.1139/a11-013 http://pubs.nrc-cnrc.gc.ca/cgi-bin/rp/rp2_desc_e?er.

Zhao, T., & Dai, A. (2022). CMIP6 model-projected hydroclimatic and drought changes and their causes in the twenty-first century. *Journal of Climate, 35*(3), 897–921. https://doi.org/10.1175/JCLI-D-21-0442.1, https://journals.ametsoc.org/view/journals/clim/35/3/JCLI-D-21-0442.1.xml.

This page intentionally left blank

CHAPTER FIVE

Drought in arid and semiarid regions

Gokmen Tayfur
Department of Civil Engineering, Izmir Institute of Technology, Gulbahce Campus, Urla, Izmir, Türkiye

5.1 Learning and knowledge outcomes

The objective of this study is to analyze the historical droughts in arid and semiarid regions and show which drought index is more suitable for capturing such extreme events.

The limitation would be that this chapter is not able to present all the drought studies in all the countries, subjected to arid and semiarid climate conditions, rather it exemplifies by using selective studies.

The audience would be those who are interested in research in drought and those who are supposed to mitigate drought effects such as governmental technocrats.

Drought is a very important natural disaster and it became common in recent decades due to the climate change. Hence, its investigation is vital, especially in arid regions.

The analysis of the historical droughts and confirmation of suitable drought index would be beneficial for the related technocrats to predict and develop drought mitigation measures.

They should be aware of the results and their implications.

Case studies were chosen from regions subjected to the arid and semiarid climatic conditions. A comparative study was performed.

No challenges were encountered. It is uncovered that the SPI, is not suitable for drought assessment in arid regions.

The outcome is that rather than the SPI, the DPI is more suitable drought index for assessing drought in arid regions.

It is learnt that may be it is better to revise z-scores (or D-scores) for drought categories, depending upon different climatic conditions.

Drought Dynamics
DOI: https://doi.org/10.1016/B978-0-443-34205-9.00007-X
© 2026 Elsevier Inc. All rights are reserved, including those for text and data mining, AI training, and similar technologies.

5.2 Introduction

Drought is one of the important natural extreme events that has different spatial and temporal characteristics. It can occur in any region with any climate, whether it has less or more rainfall (Wilhite et al., 2014). Therefore, understanding and monitoring drought is quite difficult (Mersin et al., 2022).

As well known, especially the Western World has dumped tons of greenhouses gases into atmosphere since late 1800s, which in time, caused the climate change (Haji et al.,2023, Wang et al., 2021). This has, in turn, resulted in extreme drought and wet conditions in most parts of the World (Kew et al., 2019). Although wet conditions can cause floods resulting in human suffering, these events happen in very short periods. Droughts on the other hand, can last longer than the wet periods, even for years, and result in severe human suffering, economical, life, livelihood losses, and even migration.

The most severe consequences of drought occur in arid, e.g., East and North Africa, and semiarid regions, e.g., Central Asia, where the availability of water is already low under normal conditions, the demand is often close to or even exceeds the natural availability, and society cannot often adapt to the drought hazard (Dai, 2011). Since late 1960s, the Sahel, a semiarid region in West Africa between the Sahara Desert and the Guinea Coast rainforest, had experienced a drought of unprecedented severity in recorded history (Mishra & Singh, 2010). For example, in sub-Saharan Africa, the Office of Foreign Disaster Assistance (OFDA) reported that the droughts of the early to mid-1980s had adversely affected more than 40 million people (Wilhite, 1996). The 1991–1992 droughts in southern Africa affected 20 million people and resulted in a deficit of more than 6.7 million tons of cereal supplies in (Wilhite, 2000). One of the worst droughts hit the East African region in July 2011, causing extensive destruction; a catastrophic food crisis that threatened the lives and health of 9.5 million people in Djibouti, Somalia, Kenya, and Ethiopia. The year 2024 is also accepted as a severe drought year in this region, especially for Somalia (BBC News).

Droughts in Somalia, especially in semiarid Puntland state, have resulted in death of thousands of people and livestock and had significant economic consequences for the agricultural sector due to the uneven temporal and spatial distribution of rainfall. Mauritania, which is one of the Sahelian countries, was the worst-affected country. In 1983–84, Mauritania was

afflicted with its worst drought since the beginning of the 1970s when it experienced an extended severe drought (Spinage, 2012). Afghanistan, with its semiarid climate, has faced more drought events since the late 1990s. Hence, droughts are expected to be the norm, resulting in desertification, land degradation, and severe soil erosion in Afghanistan (Ansari & Tayfur, 2023).

Drought management is increasingly crucial, especially in such regions. Knowledge on drought frequency and severity plays a vital role not only in water resource management but also in other social, economical, and environmental implications for a region. Drought assessment is performed by using drought indices. There are several indices such as standard precipitation index (SPI), percent normal (PN), Chinese *Z*-index (CZI), standard precipitation evapotranspiration index (SPEI), reconnaissance drought index (RDI), deciles, discrepancy precipitation index (DPI), etc. One or more of these tools have been employed in the literature for drought analysis in different parts of the World, including the above mentioned countries (e.g., Mersin et al., 2022; Muse et al., 2023; Mustafa & Rahman, 2018; Tayfur, 2021; Yacoub & Tayfur,2017; Hayat and Tayfur 2023, Simsek & Turhan, 2024).

The objective of this chapter is to carry out a comparative analysis of drought using the most commonly employed SPI against the most recently introduced DPI, to define the most appropriate one for the studied basins in each country, located in arid and semiarid regions.

5.3 Methods

5.3.1 Standard precipitation index

This index may be sometimes more effective, at the computational level, to standardize the data directly from a fitted normal distribution when possible. The normal-SPI is computed as follows (Cacciamani et al., 2007):

$$SPI = z = \frac{x - \hat{\mu}}{\hat{\sigma}} \tag{5.1}$$

where z is the standardized value, and $\hat{\mu}$ and $\hat{\sigma}$ are the sample estimates of the population mean and standard deviation, respectively.

There is also a commonly employed and supposedly more accurate index, the gamma-SPI (SPI-G), which fits the given precipitation data to a gamma distribution (Sonmez et al., 2005):

$$f(x, \alpha, \beta) = \frac{1}{\beta^{\alpha}\ \Gamma(\alpha)} x^{\alpha-1} e^{x/\beta} \text{for x, } \alpha, \beta > 0 \tag{5.2}$$

where α and β are the shape and scale parameters, respectively, x is the rainfall amount, and $\Gamma(\alpha)$ is the gamma function (Gasiorek & Musial, 2015). The maximum likelihood method is used to estimate the optimal values of the parameters α and β (Barua et al., 2010). Using an approximation provided by Abramowitz and Stegun (1965), which converts cumulative probability into the standard normal random variable, called z and can be determined as:

$$SPI = z = -\left(k - \frac{c_0 + c_1 k + c_2 k^2}{1 + d_1 k + d_2 k^2 + d_3 k^3}\right) \tag{5.3}$$

when $k = \sqrt{\ln\left\{\frac{1}{[H(x)]^2}\right\}}$ for $0 < H(x) \leq 0.5$

$$SPI = z = +\left(k - \frac{c_0 + c_1 k + c_2 k^2}{1 + d_1 k + d_2 k^2 + d_3 k^3}\right) \tag{5.4}$$

when $k = \sqrt{\ln\left\{\frac{1}{[1 - H(x)]^2}\right\}}$ for $5.5 < H(x) \leq 1$

where $c_0 = 2.515517$, $c_1 = 0.802853$, $c_2 = 0.010328$, $d_1 = 1.432788$, $d_2 = 0.189269$, and $d_3 = 0.001308$. The details of the SPI-G can be obtained from Yacoub and Tayfur (2017).

Therefore, Table 5.1 presents the category of a drought, based on the z-score computed either by Eq. (5.1) (the normal-SPI), Eq. (5.3), or Eq. (5.4) (the SPI-G).

Table 5.1 Standard precipitation index (SPI) based drought classification. (*Source:* Comparative evaluation of drought indexes: case study on the yarra river catchment in Australia. Journal of Water Resources Planning and Management, 137, 215–226).

SPI value (*z*-score)	Category
2.00 or more	Extreme wet
1.50 to 1.99	Severe wet
1.00 to 1.49	Moderate wet
0.99 to -0.99	Near normal
-1.00 to -1.49	Moderate drought
-1.5 to -1.99	Severe drought
-2 or less	Extreme drought

5.3.2 Discrepancy precipitation index

The proposed drought index is based on the discrepancy of precipitation data with respect to the mean value (Tayfur, 2021):

$$DPI = D_i = \log\left(\frac{P_i}{\overline{\boldsymbol{P}}}\right) \tag{5.5}$$

$$\overline{P} = \frac{1}{N}\sum_{i=1}^{N} P_i \tag{5.6}$$

where D_i is called the discrepancy value (D-score) for the ith precipitation, P_i is the ith precipitation of the data series, and $\overline{\boldsymbol{P}}$ is the mean value of the precipitation data series; typically considered to be a 30-year mean (Hayes, 2006, Willeke et al., 1994).

As to Eq. (5.5), $D = 0$ when P_i is equal to $\overline{P}$ and D is positive when $P_i > \overline{P}$ and D is negative when $P_i < \overline{P}$. The drought classification is categorized according to D-score values, as presented in Table 5.2

The discrepancy measure (DM) can be employed for investigating the relation between the number of drought years and the precipitation received and it is defined as follows (Tayfur, 2021):

$$DM = \frac{1}{N}\sum_{i=1}^{N}\left|\log\left(\frac{P_i}{\overline{P}}\right)\right| \tag{5.7}$$

5.4 Application

Application of SPI-G and DPI is carried out at stations in Puntlan, Trarza, Kabul, and Aegean regions of Somalia, Mauritania, Afghanistan,

Table 5.2 Drought classification according to ***D***-score values for wet and dry periods.

***D*-score (DPI value)**	**Category**	**Remark**
0.25 or more	Extreme wet	about 75% or more less than the mean value
0.21—0.24	Severe wet	about 60–74% less than the mean value
0.14—0.20	Moderate wet	about 37–59% less than the mean value
0.13—-0.19	Near normal	about 36% more or less than the mean value
-0.20— -0.39	Moderate drought	about 37–59% less than the mean value
-0.40— -0.59	Severe drought	about 60–74% less than the mean value
-0.60 or less	Extreme drought	about 75% or more less than the mean value

and Türkiye, respectively. It is noteworthy that since the normal-SPI cannot perform as good as the SPI-G, its application is not presented herein.

5.4.1 Puntland region of Somalia

The study area and the locations of the meteorological stations are presented in Fig. 5.1. Puntland region has a population of about 2.4 million people and covers about one-third of the country's geographical area. The state's climate is described as semiarid with a warm climate, with a poor rainfall distribution pattern of 27–250 mm annually. Most of Puntland territory is arid rangelands, and it is best suited for livestock grazing and not for crop production due to the general scarcity of water and the saline soils with high content of salt deposits. Long-term precipitation records (monthly for 41 years, from 1980 to 2020) are used to investigate annual drought characteristics and trend analysis in Somalia's northern region.

Table 5.3 presents the drought years captured by each index. As seen, the DPI captured the 2014 drought at S1; 1980, 1981, and 2002 at S2; and 1982 at S3. Also, it predicted some moderate droughts of the SPI as severe, e.g., 2009 at S1; 1988 at S2; and 1996, 2001 at S3.

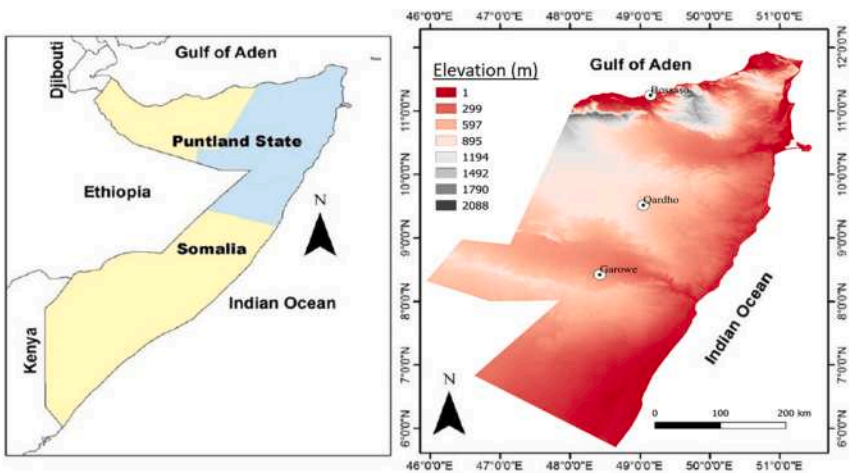


Figure 5.1 Puntland region of Somalia and the employed meteorological stations. Map lines delineate study areas and do not necessarily depict accepted national boundaries.

Table 5.3 Historical droughts, captured by standard precipitation index-gamma (SPI-G) and discrepancy precipitation index (DPI), at Putland region of Somalia.

Methods	Drought intensity	Bossaso (S1)	Qardho (S2)	Garowe (S3)
SPI-G	Extreme	2011	20082011	20112012
	Severe	19881989	2000 2015	20152016
	Moderate	19811986198720022009	19871988	19861987199519962001
DPI	Extreme	2011	20082011	20112012
	Severe	198819892009	19882000 2015	1996200120152016
	Moderate	19811986198720022014	1980198119872002	19821986198719951996 2001

5.4.2 Trarza region of Mauritania

Mauritania is located in western Africa and it is generally composed of the Sahara desert (arid zone) in the north and the Sahel (semiarid zone) in the south (Fig. 5.2). The rainy season lasts only 3 months (July–September) with average annual rainfall being 99 mm, but this varies from less than 20 mm in the north to more than 500 mm in the southeast. Trarza is a region in southwest Mauritania, it borders the regions of Inchiri and Adrar to the north, Brakna to the east, and the country of Senegal to the south, as is shown in Fig. 5.2, which also shows the locations of the employed meteorological stations. Long-term precipitation records (monthly recorded for 44 years) in three stations of Boutilimit (station 1), Nouakchott (station 2), and Rosso (station 3) are employed to investigate the drought characteristics in the Trarza region, Mauritania.

Table 5.4 presents the drought years captured by the SPI and DPI. As it can be summarized, the DPI captured four more moderate drought years (1971, 1990, 1997, 2004) at S1, two more extreme drought years (1971, 2007) and three more moderate (1970, 1980, 1992) at S2, and two more moderate (1991 and 1993) at S3.

5.4.3 Kabul river basin in Afghanistan

Kabul river basin (KRB) is located in the eastern part of Afghanistan (Fig. 5.3) with a total area of 108,392.00 km^2. Meteorological data from four stations, almost covering the whole basin, namely Asmar, Gulbahar, Pul-i-Surkh, and Pul-i-Kama, are shown in Fig. 5.3.

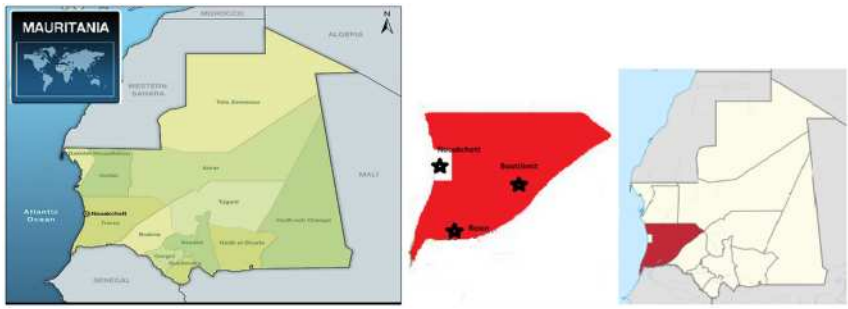


Figure 5.2 Trarza region of Mauritania and the employed meteorological stations. Map lines delineate study areas and do not necessarily depict accepted national boundaries.

Table 5.4 Historical droughts, detected by the discrepancy precipitation index (DPI) and standard precipitation index-gamma (SPI-G), at Trarza region in Mauritania.

Stations	DPI			SPI-G		
Boutilimit (S1)	Extreme 1987	Severe 1972197319771-9842011	Moderate 19711981198-319901997-2004	Extreme 1987	Severe 19721973197-719842011	Moderate 19811983
Nouakchott (S2)	19711977198-319842007	197419922004	19701978198-019821985-199420022-0032008	197719831984	197120042007	19741978198-219851992-1994
Rosso (S3)	1983	19721984	19711974197-719911998	19831972	1984	197119741977

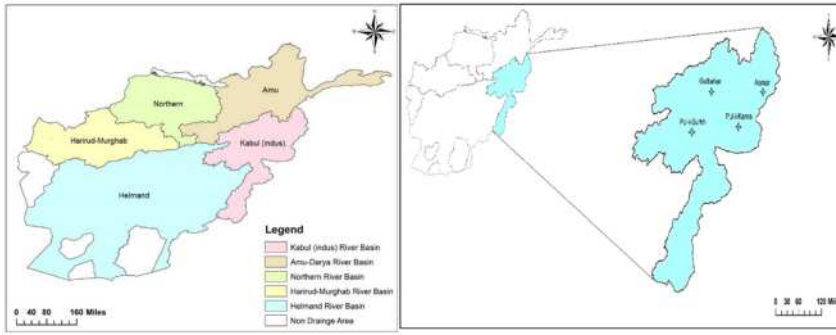


Figure 5.3 Kabul river basin of Afghanistan and the employed meteorological stations. Map lines delineate study areas and do not necessarily depict accepted national boundaries.

The employed data included 38 years (1979–2016) of recorded precipitation data, where the annual mean precipitations in Asmar, Gulbahar, Pul-i-Surkh, and Pul-i-Kama are, respectively, 525.9, 381.3, 321.3, and 212.8 mm. Table 5.5 presents the drought years captured by the SPI and DPI. As it can be summarized, the DPI did not capture any extreme drought at any station, but only at the S3 station. On the other hand, the SPI-G predicted the extreme drought of 2001 at each station. The DPI predicted the 2000 and 2001 droughts as severe at the other three stations of S1, S2, and S4. Table 5.5 indicates that droughts mostly occurred after year 1999, and both methods showed comparable results for the KRB by capturing all the nine different drought years (1993, 2000–2005, 2010, and 2013).

5.4.4 Aegean region of Türkiye

The indices are applied to capture the historical droughts at three meteorological stations (Cesme, Kusadasi, ve Nazilli) in the Aegean region of Türkiye (Fig. 5.4). The data contains the annual precipitation recorded from 1960 to 2020. The mean annual rainfall in the Aegean Region is about 625 mm (Bahadir 2011), while it is about 585 mm for the three stations.

Table 5.6 presents the drought years captured by the SPI and DPI. As it can be summarized, the DPI was unable to capture 1963 and 1989 as extreme, and 1990 and 1992 as severe drought years, as it is the case for the SPI-G, which also predicted four more drought events at the Cesme

Table 5.5 Historical droughts, detected by the discrepancy precipitation index (DPI) and the standard precipitation index-gamma (SPI-G), at Kabul river basin in Afghanistan.

Stations	DPI			SPI-G		
Asmar (S1)	Extreme	Severe	Moderate	Extreme	Severe	Moderate
	–	20002001	20022004	20002001	20022004	20052010
Gulbahar (S2)	–	2001	20002002	2001	20002002	20042013
Pul-i-Surkh (S3)	2001	–	2000200220102013	2001	2000	200220102013
Pul-i-Kama (S4)	–	20002001	19932002200320042005 2010	–	–	19932002200320042010

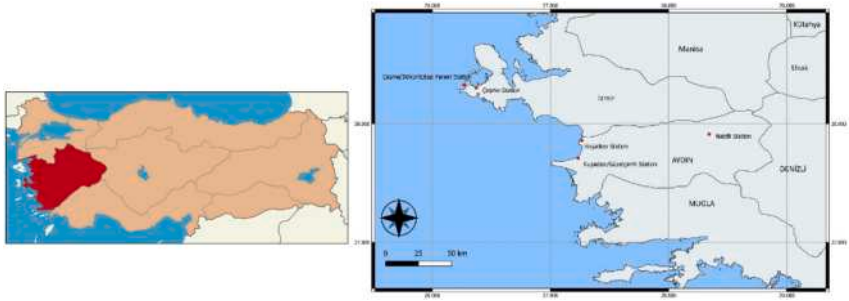


Figure 5.4 Aegean region of Türkiye and the employed meteorological stations. Map lines delineate study areas and do not necessarily depict accepted national boundaries.

station. On the other hand, while the DPI captured four moderate drought events at Kusadasi station, the SPI-G could not predict any drought at this station. Lastly, the DPI captured 2008 and 2020 as moderate ones, rather than the severe ones by the SPI-G at Nazilli station, which also captured three more moderate drought years. (Table 5.7).

5.5 Discussion

The DPI method does not impose any transformation or any other probability distribution function. It does not require the normal or gamma distribution of the data. It requires only the long-term precipitation data, as it is also required by the SPI-G, which can be easily available in most parts of the World. Its computation is easy as given by Eqs. (5.5) – (5.6). The categories and the related ranges of the DPI are straightforward, as the z-values of the SPI method. Therefore, from a practical point of view, its use and application, and the communication with the public, become quite easy and favorable.

The DPI method, as opposed to the SPI-G, captured the dry spell in 1980–1981 at Quardho Station. This result is supported by the findings of Musei et al., (2021). Uhe et al., (2018) studied drought conditions in Kenya, located in the southwest of Somalia, utilizing precipitation data through two global climate models and reported that a severe drought in Kenya occurred in 2016, which is also observed at Garowe station, the nearest one to Kenya.

Table 5.6 Historical droughts, detected by the discrepancy precipitation index (DPI) and the standard precipitation index-gamma (SPI-G), in the Aegean region of Türkiye.

Stations	**DPI**			**SPI-G**		
Cesme(S1)	**Extreme**	**Severe**	**Moderate**	**Extreme**	**Severe**	**Moderate**
	-	**19631989**	**1977199019922006**	**19631989**	**19901992**	**196719721977200020062008**
Kusadası(S2)	–	–	1963198519891992	–	–	–
Nazilli(S3)	1971	–	20082020	1971	20082020	197219922006

Table 5.7 Number of captured droughts and the average discrepancy measure (DM) values for each region.

Regions	DPI	SPI-G	DM
Puntland (Somalia)	**30**	**23**	**0.22**
Trarza (Mauritania)	**37**	**26**	**0.23**
Kabul (Afghanistan)	20	23	0.12
Aegean (Türkiye)	13	16	0.09

The drought years of 1970, 1980, 1990, 1991, 1997, 1998, and 2002 were not captured at the Trarza region by the SPI-G, as opposed to the DPI. According to the studies, these years, in fact, experienced the drought (Masih et al., 2014; Nouaceur, 1995; Trape, 2009). According to the UN-Water Activity Information System and Ba and Mughal (2020), 2002–2003, and 2008 were also classified as drought periods. The DPI captured these years, as opposed to the SPI-G.

The studies summarizes the number of drought events, irrespective of their category, captured by each index for each region. As seen, the DPI outperformed the SPI-G in arid regions of Mauritania and Somalia, while it performed comparatively in a semiarid region of Afghanistan. It may be stated that the SPI-G has slightly better performance than that of the DPI in the Mediterranean region. Also as given in are the computed average DM values (i.e., average of computed DM values for each station) for each region. As seen, when DM is greater than 0.2, its performance becomes highly remarkable.

5.6 Conclusions

The computation and application of the DPI is easy, user-friendly, and practical. It also does not require any parameter estimation and/or fitting of any probability density function to data. Its effectiveness is shown when applied to arid climatic region precipitation data having a high rate of discrepancy. Hence, the DPI is quite suitable for the drought assessment at arid climatic regions such as Somalia, Mauritania, and/or any other country subjected to a similar climate and sporadic/discrepant rainfall pattern. The higher the DM value, the better is the performance of the DPI in capturing historical events. It can be stated that when DM is equal to or greater than 0.12, it can outperform the SPI-G method. The DPI can produce

comparable results to the SPI-G for assessing the drought in regions subjected to semiarid conditions such as Afghanistan. The DPI can be applied to capture historical droughts, with caution, in regions, subjected to the Mediterranean climate.

References

Abramowitz, M., & Stegun, I. A. (1965). Handbook of mathematical functions. In *NBS applied mathematics series 50*. USA: Department of Commerce, 487.

Ansari, A., & Tayfur, G. (2023). Comparative analysis of estimation of slope-length gradient (LS) factor for entire Afghanistan. *Geomatics Natural Hazards and Risk, 14*(1).

Barua, S., Ng, A., & Perera, B. (2010). Comparative evaluation of drought indexes: Case study on the yarra river catchment in Australia. *Journal of Water Resources Planning and Management, 137*, 215–226.

Cacciamani, C., Morgillo, A., Marchesi, S., & Pavan, V. (2007). Monitoring and forecasting drought on a regional scale: Emilia-Romagna region. In G. Rossi, (Ed.). *Methods and tools for drought analysis and management,* (pp. 29–48). Springer Chapter 2.

Dai, A. (2011). Drought under global warming: A review. *Wiley Interdisciplinary Review Climate Change, 2*(1), 45–65.

Gasiorek, E., & Musial, E. (2015). Evaluation of the precision of standardized precipitation index (SPI) based on years 1954–1995 in Lodz. *Journal of Ecological Engineering, 16*, 49–53.

Haji, A. S., Amerian, Y., & Amiri, S. A. (2023). Impact of climate change parameters on groundwater level: Implications for two subsidence regions in iran using geodetic observations and artificial neural networks (ANN). *Remote Sensing, 15*(6), 1555.

Hayat, E., & Tayfur, G. (2023). Meteorological drought and trend effects on transboundary river basins in Afghanistan. *Theoretical and Applied Climatology, 154*, 1253–1275.

Hayes, M. J. (2006). *Drought indices*. Wiley Online Library. Center. (Online. http://drought.unl.edu/whatis/indices.htm.

Kew, S. F., Philip, S. Y., Hauser, M., Hobbins, M., et al. (2019). Impact of precipitation and increasing temperatures on drought in eastern Africa. *Earth System Dynamics,* 1–29.

Masih, I., Maskey, S. F., Mussa, E. F., & Trambauer, P. (2014). A review of droughts on the African continent: A geospatial and long-term perspective. *Hydrological Earth System Sciences, 18*(9), 3635–3649.

Mersin, D., Gulmez, A., Safari, M. J. S., & Tayfur, G. (2022). Drought assessment in the Aegean Region of Turkey. *Pure and Applied Geophysics, 179*(8), 3035–3053.

Mishra, A. K., & Singh, V. P. (2010). A review of drought concepts. *Journal of Hydrology, 391*, 202–216.

Muse, N. M., Tayfur, G., & Safari, M. J. S. (2023). Meteorological drought assessment and trend analysis in Puntland Region of Somalia. *Sustainability, 15*, 10652. https://doi.org/10.3390/su151310652.

Musei, S. K., Nyaga, J. M., & Dubow, A. Z. (2021). SPEI-based spatial and temporal evaluation of drought in Somalia. *Journal of Arid Environments, 184*, 104296.

Mustafa, A., & Rahman, G. (2018). Assessing the spatio-temporal variability of meteorological drought in Jordan. *Earth Systems and Environment, Volume 2*, 247–264. https://doi.org/10.1007/s41748-018-0071-9.

Nouaceur, Z. (1995). Rainfall disparities, drought and modification of the environmental equilibrium in Mauritania. *Revue de géographie de Lyon, 70*(3–4), 239–245 (in French).

Simsek, S. D., & Turhan, E. (2024). An evaluation of spatiotemporal changes of meteorological drought in the Mediterranean sub-basins in Türkiye using discrepancy

precipitation and standardized precipitation index. *Natural Hazards*. https://doi.org/10.1007/s11069-024-06906-5.

Sonmez, F. K., Komuscu, A. U., Erkan, A., & Turgut, E. (2005). An analysis of spatial and temporal dimension of drought vulnerability in Turkey using the standardized precipitation index. *Natural Hazards, 35*, 243–264.

Spinage, C. (2012). *African ecology: Benchmarks and historical perspectives*. Springer Science & Business Media.

Tayfur, G. (2021). Discrepancy precipitation index for monitoring meteorological drought. *Journal of Hydrology, 597*, 126174. https://doi.org/10.1016/j.jhydrol.2021.126174.

Trape, S. (2009). Impact of climate change on the Relict Tropical Fish Fauna of Central Sahara: Threat for the survival of Adrar Mountains Fishes, Mauritania. *PLoS One, 4*(2), e4400. https://doi.org/10.1371/journal.pone.0004400.

Uhe, P., Philip, S., Kew, S., Shah, K., Kimutai, J., Mwangi, E., et al. (2018). Attributing drivers of the 2016 Kenyan drought. *International Journal of Climatology, 38*, e554–e568.

Wang, S., Zhang, Q., Wang, J., Liu, Y., & Zhang, Y. (2021). Relationship between drought and precipitation heterogeneity: An analysis across rain-fed agricultural regions in eastern Gansu China. *Atmosphere, 12*(10), 1274.

Wilhite, D. A. (1996). A methodology for drought preparedness. *Natural Hazards, 13*, 229–252.

Wilhite, D. A. (2000). In D. Wilhite (Vol. Ed.), *Drought: A Global Assessment: Vol. 1*, (pp. 3–18). London, UK: Routledge Publisher.

Wilhite, D. A., Sivakumar, M. V. K., & Pulwarty, R. (2014). Managing drought risk in a changing climate: The role of national drought policy. *Weather Climate Extremes, 3*, 4–13.

Willeke, G., Hosking, J. R. M., Wallis, J., & Guttman, N. B. (1994). The national drought atlas. In *Institute for Water Resources Report 94-NDS-4*. US Army Corps of Engineers.

Yacoub, E., & Tayfur, G. (2017). Evaluation and assessment of meteorological drought by different methods in Trarza Region, Mauritania. *Water Resources Management, 31*(3), 825–845. https://doi.org/10.1007/s11269-016-1510-8.

CHAPTER SIX

Drought propagation from meteorological to agricultural to hydrological

Gokmen Tayfur
Department of Civil Engineering, Izmir Institute of Technology, Gulbahce Campus, Urla, Izmir, Türkiye

6.1 Introduction

It is commonly accepted that droughts are among the most severe natural disasters that can inflict on social life, economical life, and human survival. they can lead to mass starvation and migration (Wilhite, 1996). Drought typically start with the lack of precipitation over a region for prolonged period (meteorological drought). If the time is too prolonged in the order of consecutive years, it can easily result in lack of surface and subsurface flows (hydrological drought), and eventually it can result in lack of soil moisture, intense evaporation, lack of water for irrigation, and thus significant decline cause in crop production (agricultural drought). All these eventually result in mass malnutrition, starvation, loss of lives, economical fallout, and migration (social and economic drought). Such disastrous events had been experienced in sub-Saharan Africa, where the droughts of the early to mid-1980s had adversely affected more than 40 million people, and droughts in 1991–1992 affected 20 million people (Wilhite, 2000). According to U.S. weather and climate disaster (2016), droughts have cost about $10 billion per event in the United States. The World's history has experienced droughts in the past due to natural effects. However, in this last half century, it has become more frequent because of the greenhouse gas release effects; billions of tons of CO_2 have been dumped into the atmosphere, especially by the industrialized countries since the late 1800s (Wilby & Dessai, 2010).

Short-period meteorological events, especially following a wet season, may not propagate to hydrological or agricultural droughts. Some may propagate to the hydrological one, but not necessarily to the agricultural drought.

Drought Dynamics
DOI: https://doi.org/10.1016/B978-0-443-34205-9.00005-6
© 2026 Elsevier Inc. All rights are reserved, including those for text and data mining, AI training, and similar technologies.

All may occur consecutively; if in a short period of time, it may not result in the socio-economic drought. Therefore, it is important to investigate the drought propagation and the interrelations among the different forms of drought. Since the 2000s, many studies have been devoted to this area, and this chapter is trying to briefly summarize and give a basic background in this regard.

6.2 Drought types

There are basically three types of droughts: meteorological, agricultural, and hydrological (Mishra & Singh, 2010). Precipitation amount is the basic variable in the case of meteorological drought analysis (Eltahir, 1992), whereas streamflow rate and soil moisture amount are the basic variables when quantifying both the hydrological and agricultural droughts (Clausen & Pearson, 1995). Meteorological drought is defined as the lack of precipitation (way less than the mean value) over a region for prolonged period (e.g., month, 3-months, 6-months, 9-months, and generally and commonly a year). Similarly, hydrological drought is defined as a lack of flow rate in a particular basin, and agricultural drought is defined as the lack of soil moisture over a basin. Note that prolonged meteorological drought can trigger the other droughts. Lastly, when all these droughts occur consecutively, the socio-economic drought can take place, which is the failure of the water resources system for meeting the water demands of the public and industry (AMS 2004). Socio-economic drought occurs when the demand for an economic good exceeds supply as a result of a weather-related shortfall in water supply (Mishra & Singh, 2010).

There have been many studies to understand relations among different types of droughts (Keyantash & Dracup, 2002; Vasiliades & Loukas, 2009; Vicente-Serrano et al., 2012). Some tried to have a single drought index for representing all the droughts (Mo & Lettenmaier, 2014; Brown et al., 2008; Karamouz et al., 2009; Rajsekhar et al., 2015). Some studied propagation from meteorological to agricultural and hydrological droughts using correlation (Huang et al., 2017; Leng et al., 2015). Such studies may be useful for applicability assessments but may be inadequate for a thorough understanding of propagation (Bae et al., 2019). Hence, drought propagation, which is important for establishing a viable drought monitoring system, may require further study.

6.3 Widely employed index for each drought

6.3.1 Standardized precipitation index

Standardized precipitation index (SPI) is one of the widely employed index (McKee et al., 1993), which is regarded as a good and easy tool for drought monitoring. Wu et al., (2007) used it for arid and humid regions in China, Surendran et al., 2017 applied it for a semiarid region in India, Onusluel et al., (2022) investigated drought behavior in the Aegean region in Türkiye, and Zerouali et al., (2021) applied it to examine spatial and temporal drought pattern in the Oued Sebaou basin in Algeria. It is used by Wossenyeleh et al., (2022) in Ethiopia, Rahmani & Fattahi, 2021, 2024 in the United Kingdom, Fahimirad & Shahkarami, 2021 in Iran, Waseem et al., (2021) in Pakistan, and Yildirim & Rahman, 2021 in Australia. The World Meteorological Organization (WMO) has recommended the SPI as a suitable drought monitoring index for all regions with different climatic conditions. *SPI* is defined as follows, McKee et al., (1993)

$$SPI = z - \text{score} = \frac{x_{ij} - x_{im}}{\sigma} \tag{6.1}$$

where x_{ij} is the monthly, seasonal, or annual precipitation at the ith rain gauge station and jth observation, x_{im} is the long-term precipitation mean and is σ its standard deviation of the related data. The method basically enforces data to fit the normal distribution and make drought categories depending upon the z-scores values given in Table 6.1

Table 6.1 Standardized precipitation index and soil moisture anomaly index-based drought classifications.

Description of State	Criterion
Extremely wet	z-score ≥ 2.0
Very wet	1.5 ≤ z-score < 2.0
Moderately wet	1.0 ≤ z-score < 1.5
Near normal	− 1.0 ≤ z-score < 1.0
Moderately dry	− 1.5 ≤ z-score ≤ 1.0
Severely dry	− 2.0 ≤ z-score ≤ 1.5
Extremely dry	z-score ≤ −2

Note that there are variants of the SPI, such as the log-SPI (when data is first fit to the log-normal distribution), and the gamma-SPI (when data is fit to gamma-distribution) (Tayfur, 2021; Yacoub & Tayfur, 2020).

6.3.2 Agricultural drought index

For the agricultural drought, most of the indices are derived from soil moisture (SM) deficiency based on precipitation and air temperature (Mishra & Singh, 2010; Palmer, 1965). However, the SM in irrigated areas relies not only on local precipitation but also on the withdrawal of water from reservoirs when available. Hence, another simple way of assessing the agricultural drought would be the assessment of the agricultural reservoir levels. Agricultural drought might occur if the agricultural reservoir storage level falls below 75% of average storage levels (Lee, 2016).

Drought indices based on different parameters such as SM and soil water deficit, were proposed to quantify agricultural drought (AghaKouchak, 2014). The SM is the key component of water transport in this approach, thus making it a fundamental indicator for agricultural drought monitoring (Brocca et al., 2011; Liu et al., 2019). The soil moisture anomaly index (*SMAI*) is a common index to monitor agricultural drought conditions, which can be calculated as follows (Pan et al., 2023; Shahzaman et al., 2021):

$$SMAI = z - score = \frac{sm_i - \mu}{\sigma} \tag{6.2}$$

where sm_i is the monthly SMin the *i*th month, and μ and σ are the mean and standard deviations of the monthly SM data, respectively. Table 6.1 presents the SMAI agricultural drought classifications.

6.3.3 Streamflow drought index

Hydrological drought is defined as a lack of water in surface flows (Nalbantis & Tsakiris, 2009). Several indices, such as the standardized streamflow index (SSI), the standardized runoff index (SRI), and the streamflow drought index (SDI), were developed in the literature for this purpose (Vicente-Serrano et al., 2012; Shukla & Wood, 2008). The SDI index is accepted as an effective hydrological drought index (Gumus & Algin, 2017). It was applied for hydrological drought analysis in several

basins in Türkiye, Romania, Pakistan, the United Kingdom, and Iran (Abbas & Kousar, 2021; Minea et al., 2022).

The SDI, which is defined according to the cumulative streamflow volumes $V_{i,k}$ for each reference period of the ith hydrological year, is expressed as follows (Nalbantis & Tsakiris, 2009):

$$\text{SDIi, k} = z - score = \frac{V_{i,k} - \overline{V_k}}{s_k} \quad i = 1, 2, \ldots, \quad k = 1, 2, 3, 4 \tag{6.3}$$

where $V_{i,k}$ is the cumulative streamflow volume for the ith hydrological year and the kth reference period (i.e., $k = 1$ for October–December, $k = 2$ for January–March, $k = 3$ for April–June, and $k = 4$ for July–September). $\overline{V_k}$ is the mean, and s_k is the standard deviation of the cumulative streamflow volumes of the reference period k, as these are calculated over a long period of time.

A monthly series of streamflow volumes ($Q_{i,j}$) (with i implying the hydrological year and j being the rank of the month in that hydrological year (i.e., $j = 1$ for October and $j = 12$ for September) over a given period can be expressed as (Nalbantis & Tsakiris, 2009):

$$V_{i,k} = \sum_{j=1}^{3k} Q_{i,j} \quad i = 1, 2, \ldots \quad j = 1, 2, \ldots, 12 \quad k = 1, 2, 3, 4 \tag{6.4}$$

Table 6.2 presents the z-score values and the related drought categories for the SDI (Nalbantis & Tsakiris, 2009).

Note that Bae et al., 2019 used water levels in dams for the hydrological drought when assessing drought propagation in South Korea. When the

Table 6.2 Streamflow drought index-based hydrological drought classifications.

State	Description	Criterion	Probability (%)
0	Non-drought	z-score ≥ 0.0	50
1	Mild drought	−1.0 ≤ z-score < 0.0	34.1
2	Moderate drought	−1.5 ≤ z-score ≤ 1.0	9.2
3	Severe drought	− 2.0 ≤ z-score ≤ 1.5	4.4
4	Extreme drought	z-score ≤ 2.0	2.3

dam storage level falls below 75% of the average storage level, then hydrological drought occurs.

6.4 Drought propagation

Drought propagation does generally occur from meteorological to agricultural to hydrological (Bae et al., 2019). Numerous factors such as climatic conditions, seasonality, precipitation, low temperatures in dry seasons, and catchment characteristics (landcover, size, topography, aquifer, drainage network, and soil properties) can influence the drought propagation (Huang et al., 2023; van Xu et al., 2019). Leng et al., (2015) and Huang et al., (2017) studied the propagation from meteorological drought to agricultural and hydrological droughts in China using the correlation analysis and comparison among each type of drought index, similar to those of Bae et al., 2019 used for South Korea. Such studies have proved useful for applicability assessments and understanding the relationships between each drought index. There are basically two methods to assess the propagation: (1) Finding the Pearson's correlation coefficients between the respected drought indices, e.g., SDI-1 and SPI-*n*; SMI-1 and SPI-*n*; SDI-1 and SMI-*n*, where the *n* is the highest SPI-*n* correlation indicates the drought propagation period. Likewise, (2) the comparison of the time difference between the drought events (Bevacqua et al., 2021) can be used as the alternative method.

Therefore, drought propagation period can change from region to region or even within the same region, depending upon climatic and watershed conditions. According to Bhardwaj et al., 2020 the drought propagation period (from meteorological to hydrological) in India is about 2 to 4 months in most of the river basins. This period is about 6–9 months in the densely forest region in Slovakia (Kubiak-Wojcicka et al., 2021), 7 months in the Awash river basin in Ethiopia (arid region) (Edossa et al., 2010), and 2 months in the humid sub-tropical region of the Poyang lake catchment in China (Ye et al., 2016). Nevertheless, it is widely accepted that the propagation of meteorological drought to agricultural drought and/or hydrological drought takes about 3–6 months (Forootan et al., 2019) and therefore SPI3 and SPI6 are suggested for agricultural drought or hydrological drought studies (Gebrehiwot et al., 2011). For instance, the SPI3 is employed for evaluating the propagation of meteorological drought to agricultural drought to hydrological drought in India.

6.5 Discussion and conclusions

Although it is impossible to avoid drought, there are ways to mitigate its harmful effects (Smakhtin & Schipper, 2008). Drought occurs in almost all climatic systems as it stands for climate's natural and recurring feature. It is becoming one of serious natural hazard around the World. On one hand, drought is a long-term phenomenon, on the other hand, it allows a time frame for resistance against it and other mitigation preparations (Tsakiris, 2017). For this reason, a High-Level Meeting on National Drought Policy (HMNDP) was held in Switzerland in 2013 which was organized by the WMO, Food and Agriculture Organization of the United Nations (FAO), and the Secretariat of the United Nations Convention to Combat Desertification (UNCCD), urging all countries to develop and implement national drought policies to survive. Recently, many researchers around the World have shown an increased interest in studies related to drought and trends in both precipitation and temperature, especially in arid and semiarid regions. Also, attentions have been paid on how to properly monitor and detect drought and trends using various scientific formulations and techniques. Scientists concentrate on how to analyze, formulate, and determine these natural adverse events. Policy makers try to construct efficient frameworks to confront droughts so as to persist. Then, drought indices supply information to decision makers on drought severity and are helpful to be used to trigger drought contingency plans in case of their availability (Morid et al., 2006).

Understanding the relationship between meteorological, agricultural, and hydrological droughts might provide a foundation for establishing a comprehensive drought monitoring system, especially in drought-prone regions (Bae et al., 2019). This also necessitates the establishment of well-distributed network of monitoring and data collection systems in including gauging stations, to retrieve field data on SM, precipitation, and streamflow. Also, utilizing the remote sensing, radar, and satellite technology to retrieve meteorological, hydrological and geomorphological, etc, data for regions lacking a monitoring system and/or for completing missing data gaps would be strongly recommended.

References

Abbas, S., & Kousar, S. (2021). Spatial analysis of drought severity and magnitude using the standardized precipitation index and streamflow drought index over the Upper Indus Basin, Pakistan. *Environment, Development and Sustainability, 23*(10), 15314–15340. https://doi.org/10.1007/s10668-021-01299-y, www.wkap.nl/journalhome.htm/1387-585X.

AghaKouchak, A. (2014). A baseline probabilistic drought forecasting framework using standardized soil moisture index: Application to the 2012 United States drought. *Hydrology and Earth System Sciences, 18*(7), 2485–2492. https://doi.org/10.5194/hess-18-2485-2014.

AMS (American Meteorological Society). (2004). Meteorological Drought. In *Bulletin of American Meteorological Society, 85*. https://www.ametsoc.org/AMS/about-ams/ams-statements/archive-statements-of-the-ams/meteorological-drought/.

Bae, H., Ji, H., Lim, Y. J., Ryu, Y., Kim, M. H., & Kim, B. J. (2019). Characteristics of drought propagation in South Korea: Relationship between meteorological, agricultural, and hydrological droughts. *Natural Hazards, 99*(1), 1–16. https://doi.org/10.1007/s11069-019-03676-3, www.wkap.nl/journalhome.htm/0921-030X.

Bevacqua, A. G., Chaffe, P. L. B., Chagas, V. B. P., & AghaKouchak, A. (2021). Spatial and temporal patterns of propagation from meteorological to hydrological droughts in Brazil. *Journal of Hydrology, 603*. https://doi.org/10.1016/j.jhydrol.2021.126902, www.elsevier.com/inca/publications/store/5/0/3/3/4/3.

Bhardwaj, K., Shah, D., Aadhar, S., & Mishra, V. (2020). Propagation of meteorological to hydrological droughts in India. *Journal of Geophysical Research: Atmospheres, 125*(22). https://doi.org/10.1029/2020jd033455.

Brocca, L., Hasenauer, S., Lacava, T., Melone, F., Moramarco, T., Wagner, W., Dorigo, W., Matgen, P., Martínez-Fern´andez, J., Llorens, P., Latron, J., Martin, C., & Bittelli, M. (2011). Soil moisture estimation through ASCAT and AMSR-E sensors: an intercomparison and validation study across Europe. *Remote Sensing Environment, 115*(12), 3390–3408. https://doi.org/10.1016/j.rse.2011.08.003.

Brown, J. F., Wardlow, B. D., Tadesse, T., Hayes, M. J., & Reed, B. C. (2008). 'The vegetation drought response index (VegDRI): a new integrated approach for monitoring drought stress in vegetation. *GIScience Remote Sensing, 45*, 16–46. https://doi.org/10.2747/1548-1603.45.1.16.

Clausen, B., & Pearson, C. P. (1995). Regional frequency analysis of annual maximum streamflow drought. *Journal of Hydrology, 173*(1–4), 111–130. https://doi.org/10.1016/0022-1694(95)02713-y.

Edossa, D. C., Babel, M. S., & Das Gupta, A. (2010). Drought Analysis in the Awash River Basin. Ethiopia. *Water Resources Management, 24*(7), 1441–1460. https://doi.org/10.1007/s11269-009-9508-0.

Eltahir, E. A. B. (1992). Drought frequency analysis in Central and Western Sudan. *Hydrological Sciences Journal, 37*(3), 185–199.

Fahimirad, Z., & Shahkarami, N. (2021). The impact of climate change on hydro-meteorological droughts using copula functions. *Water Resources Management, 35*(12), 3969–3993. https://doi.org/10.1007/s11269-021-02918-z, www.wkap.nl/journalhome.htm/0920-4741.

Forootan, E., Khaki, M., Schumacher, M., Wulfmeyer, V., Mehrnegar, N., van Dijk, A. I. J. M., Brocca, L., Farzaneh, S., Akinluyi, F., Ramillien, G., Shum, C. K., Awange, J., & Mostafaie, A. (2019). Understanding the global hydrological droughts of 2003–2016 and their relationships with teleconnections. *Science of the Total Environment, 650*(Pt 2), 2587–2604. https://doi.org/10.1016/j.scitotenv.2018.09.231.

Gebrehiwot, T., van der Veen, A., & Maathuis, B. (2011). Spatial and temporal assessment of drought in the Northern highlands of Ethiopia. *International Journal of Applied Earth Observation Geoinformation, 13*(3), 309–321. https://doi.org/10.1016/j.jag.2010.12.002.

Gumus, V., & Algin, H. M. (2017). Meteorological and hydrological drought analysis of the Seyhan−Ceyhan River Basins, Turkey. *Meteorological Applications, 24*(1), 62–73. https://doi.org/10.1002/met.1605, http://onlinelibrary.wiley.com/journal/10.1002/(ISSN)1469-8080.

Huang, S., Li, P., Huang, Q., Leng, G., Hou, B., & Ma, L. (2017). The propagation from meteorological to hydrological drought and its potential influence factors. *Journal of Hydrology, 547*, 184–195. https://doi.org/10.1016/j.jhydrol.2017.01.041.

Huang, S., Gan, Y., Zhang, X., Chen, N., Wang, C., Gu, X., Ma, J., & Niyogi, D. (2023). Urbanization amplified asymmetrical changes of rainfall and exacerbated drought: Analysis over five urban agglomerations in the Yangtze River Basin, China. *Earth's Future, 11*(2). https://doi.org/10.1029/2022EF003117, http://onlinelibrary.wiley.com/journal/10.1002/(ISSN)2328-4277.

Karamouz, M., Rasouli, K., & Nazif, S. (2009). 'Development of a hybrid index for drought prediction: a case Study. *Journal of Hydrologic Engineering, 14*, 617–627. https://doi.org/10.1061/(ASCE)HE.1943-5584.0000022.

Keyantash, J., & Dracup, J. A. (2002). The quantification of drought: An evaluation of drought indices. *Bulletin of the American Meteorological Society, 83*(8), 1167–1180. https://doi.org/10.1175/1520-0477(2002)083<1191:TQODAE>2.3.CO;2, http://ams.allenpress.com.

Kubiak-Wojcicka, K., Nagy, P., Zelenakova, M., Hlavata, H., & Abd-Elhamid, H. F. (2021). Identification of Extreme Weather Events Using Meteorological and Hydrological Indicators in the Laborec River Catchment. Slovakia. *Water, 13*(10), 1413. https://doi.org/10.3390/w13101413.

Lee, J.-W. (2016). Evaluation of the relationship between meteorological, agricultural and in-situ big data droughts. *Journal of the Korean Association of Geographic Information Studies, 19*(1), 64–79. https://doi.org/10.11108/kagis.2016.19.1.064.

Leng, G., Tang, Q., & Rayburg, S. (2015). 'Climate change impacts on meteorological, agricultural and hydrological droughts in China. *Global Planet Change, 126*, 23–34. https://doi.org/10.1016/j.gloplacha.2015.01.003.

Liu, S. Y., Huang, S. Z., Xie, Y. Y., Huang, Q., Wang, H., & Leng, G. Y. (2019). 'Assessing the non-stationarity of low flows and their scale-dependent relationships with climate and human forcing. *Science of Total Environment, 687*, 244–256. https://doi.org/10.1016/j scitotenv.2019.06.025.

Mckee, T. B., Doesken, N. J., & Kleist, J. (1993). 'The relationship of drought frequency and duration to time scales. *In: 8th Conference on Applied Climatology, 17*, 179–183.

Minea, I., Iosub, M., & Boicu, D. (2022). Multi-scale approach for different type of drought in temperate climatic conditions. *Natural Hazards, 110*(2), 1153–1177. https://doi.org/10.1007/s11069-021-04985-2.

Mishra, A. K., & Singh, V. P. (2010). A review of drought concepts. *Journal of Hydrology, 391*(1–2), 202–216. https://doi.org/10.1016/j.jhydrol.2010.07.012.

Mo, K. C., & Lettenmaier, D. P. (2014). Objective drought classification using multiple land surface models. *Journal of Hydrometeorology, 15*(3), 990–1010. https://doi.org/10.1175/JHM-D-13-071.1, http://journals.ametsoc.org/doi/pdf/10.1175/JHM-D-13-071.1.

Morid, S., Smakhtin, V., & Moghaddasi, M. (2006). Comparison of seven meteorological indices for drought monitoring in Iran. *International Journal of Climatology, 26*, 971–985.

Nalbantis, I., & Tsakiris, G. (2009). Assessment of hydrological drought revisited. *Water Resources Management, 23*(5), 881–897. https://doi.org/10.1007/s11269-008-9305-1.

Onusluel, G. G., Gül, A., & Najar, M. (2022). Historical evidence of climate change impact on drought outlook in river basins: analysis of annual maximum drought severities through daily SPI definitions. *Natural Hazards, 110*, 1389–1404. https://doi.org/10.1007/s11069-021-04995-0.

Palmer, W. C. (1965). *Meteorological drought (Vol. 30)*. U.S. Department of Commerce, Weather Bureau.

Pan, Y., Zhu, Y., Lü, H., Yagci, A. L., Fu, X., Liu, E., Xu, H., Ding, Z., & Liu, R. (2023). Accuracy of agricultural drought indices and analysis of agricultural drought

characteristics in China between 2000 and 2019. *Agricultural Water Management, 283*. https://doi.org/10.1016/j.agwat.2023.108305, http://www.journals.elsevier.com/agricultural-water-management/.

Rahmani, F., & Fattahi, M. H. (2021). A multifractal cross-correlation investigation into sensitivity and dependence of meteorological and hydrological droughts on precipitation and temperature. *Natural Hazards, 109*(3), 2197–2219. https://doi.org/10.1007/s11069-021-04916-1, www.wkap.nl/journalhome.htm/0921-030X.

Rajsekhar, D., Singh, V. P., & Mishra, A. K. (2015). Multivariate drought index: an information theory based approach for integrated drought assessment. *Journal of Hydrology, 526*, 164–182. https://doi.org/10.1016/j.jhydrol.2014.11.031.

Shahzaman, M., Zhu, W., Ullah, I., Mustafa, F., Bilal, M., Ishfaq, S., Nisar, S., Arshad, M., Iqbal, R., & Aslam, R. W. (2021). Comparison of multi-year reanalysis, models, and satellite remote sensing products for agricultural drought monitoring over south asian countries. *Remote Sensing, 13*(16). https://doi.org/10.3390/rs13163294, https://www.mdpi.com/2072-4292/13/16/3294/pdf.

Smakhtin, V. U., & Schipper, E. L. F. (2008). Droughts: The impact of semantics and perceptions. *Water Policy, 10*(2), 131–143. https://doi.org/10.2166/wp.2008.036.

Surendran, U., Kumar, V., Ramasubramoniam, S., & Raja, P. (2017). Development of drought indices for semi-arid region using drought indices calculator (DrinC)—A Case study from Madurai district, a semi-arid Region in India. *Water Resources Management, 31*(11), 3593–3605. https://doi.org/10.1007/s11269-017-1687-5.

Tayfur, G. (2021). Discrepancy precipitation index for monitoring meteorological drought. *Journal of Hydrology, 597*, 126174. https://doi.org/10.1016/j.jhydrol.2021.126174.

Tsakiris, G. (2017). Drought risk assessment and management. *Water Resources Management, 31*(10), 3083–3095. https://doi.org/10.1007/s11269-017-1698-2.

U.S. weather and climate disaster (2016). '2016: A historic year for billion-dollar weather and climate disasters in U.S.' https://www.climate.gov/news-features/blogs/beyond-data/2016-historic-year-billion-dollar-weather-and-climate-disasters-us.

Vasiliades, L., & Loukas, A. (2009). Hydrological response to meteorological drought using the Palmer drought indices in Thessaly, Greece. *Desalination, 237*(1-3), 3–21. https://doi.org/10.1016/j.desal.2007.12.019.

Vicente-Serrano, S. M., López-Moreno, J. I., Beguería, S., Lorenzo-Lacruz, J., Azorin-Molina, C., & Morán-Tejeda, E. (2012). Accurate computation of a streamflow drought index. *Journal of Hydrologic Engineering, 17*(2), 318–332. https://doi.org/10.1061/(asce)he.1943-5584.0000433.

Waseem, M., Khurshid, T., Abbas, A., Ahmad, I., & Javed, Z. (2021). Impact of meteorological drought on agriculture production at different scales in Punjab, Pakistan. *Journal of Water & Climate Change, 13*(1), 113–124. https://doi.org/10.2166/wcc.2021.244.

Wilby, R. L., & Dessai, S. (2010). Robust adaptation to climate change. *Weather,* 180–185. https://doi.org/10.1002/wea.543 RMS.

Wilhite, D. A. (1996). A methodology for drought preparedness. *Natural Hazards, 13*(3), 229–252. https://doi.org/10.1007/BF00215817, www.wkap.nl/journalhome.htm/0921-030X.

Wilhite, D. A. (2000). 'Drought as a natural hazard: concepts and definitions. In D. A. Wilhite (Vol. Ed.), *Drought: A Global Assessment: Vol. 1*, (pp. 1–18). New York, USA: Routledge.

Wossenyeleh, B. K., Worku, K. A., Verbeiren, B., & Huysmana, M. (2022). Drought propagation and its impact on groundwater hydrology of wetlands: a case study on the Doode Bemde nature reserve (Belgium). *Natural Hazards and Earth System Sciences, 21*(1). https://doi.org/10.5194/nhess-21-39-2021.

Wu, H., Svoboda, M. D., Hayes, M. J., Wilhite, D. A., & Wen, F. (2007). Appropriate application of the standardized precipitation index in arid locations and dry seasons. *International Journal of Climatology, 27*(1), 65–79. https://doi.org/10.1002/joc.1371.

Xu, Y., Zhang, X., Wang, X., Hao, Z. C., Singh, V. P., & Hao, F. H. (2019). 'Propagation from meteorological drought to hydrological drought under the impact of human activities: A case study in northern China. *Journal of Hydrology, 579*, 124147. https://doi.org/10.1016/j.jhydrol.2019.124147.

Yacoub, E., & Tayfur, G. (2020). Spatial and temporal of variation of meteorological drought and precipitation trend analysis over whole Mauritania. *Journal of African Earth Sciences, 163*, 103761. https://doi.org/10.1016/j.jafrearsci.2020.103761.

Ye, X., Li, X., Xu, C.-Y., & Zhang, Q. (2016). Similarity, difference and correlation of meteorological and hydrological drought indices in a humid climate region—the Poyang Lake catchment in China. *Hydrology Research, 47*(6), 1211–1223. https://doi.org/10.2166/nh.2016.214.

Yildirim, G., & Rahman, A. (2021). Spatiotemporal meteorological drought assessment: A case study in south-east Australia. *Natural Hazards,* 1–28.

Zerouali, B., Santos, C. A. G., Nascimento, T. V. M., & Silvia, R. M. (2021). A cloud-integrated GIS for forest cover loss and land use change monitoring using statistical methods and geospatial technology over northern Algeria. *Journal of Environmental Management, 341*, 17. https://doi.org/10.1016/j.jenvman.2023.118029.

This page intentionally left blank

CHAPTER SEVEN

Drought and architecture

Meysam Soleimani, and Furkan Kavak
Department of Architecture, Bursa Technical University, Bursa, Türkiye

7.1 Introduction

Water is known as one of the most sacred natural elements in many ancient civilizations. The four elements of Greek philosophy on which the Universe is based are Fire, Water, Earth, and Air. This is a theory which explains the building blocks of all substances are derived from the four elements. In ancient Iran, water was considered a messenger of light and purity. Due to Iran's water scarcity, this essential resource had significant value among its populace. Water served not just to fulfill Iranian necessities but also significantly impacted spiritual and psychological dimensions. Water, embodying attributes such as vitality, clarity, brightness, abundance, illumination, serenity, and dynamism, has evoked diverse emotions within the human psyche. According to the Iranian mythological beliefs, water was created in the second stage of the six stages of creation. Anahita, meaning pure and clean, is the patron deity of the water element and is recorded in various ways in Persian literature. Accordingly, Anahita is the main source of all water resources on Earth and the cause of all productivity. The beliefs and traditions regarding the sacredness of water have existed among the Iranian nation since ancient times, and some of these beliefs and traditions still maintain their place as before.

Drought has historically been a significant issue for humanity, particularly in hot and arid regions. Climatic conditions of a region are influenced by the angle of solar radiation, latitude, proximity to the equator, ocean current intensity and direction, seasonal winds, water presence, humidity, vegetation, altitude above sea level, and topographical variations. Arid and high-temperature climates are prevalent in Africa, certain regions of Asia, and the Middle East, particularly Iran. The attributes of a hot and arid environment encompass elevated summer temperatures, severe winter cold, minimal humidity, scant precipitation, and occurrences of sandstorms. This climate necessitates distinctive architectural methods and

Drought Dynamics
DOI: https://doi.org/10.1016/B978-0-443-34205-9.00004-4
© 2026 Elsevier Inc. All rights are reserved, including those for text and data mining, AI training, and similar technologies.

tactics due to its specific qualities. In arid settings, the management of water scarcity is crucial for sustaining the lives of inhabitants. Architects and urban planners were required to ensure healthy living circumstances for individuals with limited amenities.

To locate and maintain water, traditional architects used many innovative ways. Traditional architecture is referred to as premodern architecture, occurring during an era when advanced technologies for water transportation, infrastructure development, and urban planning were not feasible at contemporary speeds. Addressing the issue of contemporary drought necessitates examining historical architecture and leveraging prior experiences as potential solutions. This chapter examines the experiences of traditional architecture in Iran and other nations historically situated in arid and hot climates, characterized by severe environmental conditions.

Nowadays, human beings have rapidly harvested and exploited natural resources using advanced technologies. The neglect of effective natural resource utilization has resulted in their waste over the last decades. Buildings (residential, commercial, and public) have consumed more than 30% of World's total primary energy supply (Chen et al., 2015). It is predicted that a day will arrive when countries will even fight for water resources. The global paucity of water resources and their mismanagement will result in a significant water shortage in the near future. Humans are now aware that resources will eventually be reduced and will fail to satisfy human needs. What solutions can architecture provide to address these issues? The high potential of constructing buildings towards energy efficiency has drawn special attention to the passive design parameters, that is, building envelope characteristics and passive strategies such as natural ventilation, shading devices, overhangs, and daylighting. The efficient utilization of fossil fuels and water resources will facilitate sustainable development in the future. Certain treatments are remarkably simple yet efficacious. To understand these, we must examine historical experiences. Addressing the issue of contemporary drought necessitates an examination of historical architecture and the application of its insights as a potential solution. This chapter examines the traditional architecture of Iran and other nations in arid and hot climates, characterized by severe weather and unstable situations. Traditional architecture has devised efficient strategies to mitigate drought. As these solutions function passively without fossil fuels, they are being utilized and regarded in the concepts of sustainable and green building.

7.2 The concept of climatic architecture

Climatic architecture is the art and science of designing and constructing buildings and spaces that are designed to optimally utilize resources and create comfort for residents, taking into account climatic conditions, natural resources, and local culture. The significance of climate is evident. All living things are wholly reliant on the climate for their survival and adjust to this environmental factor. Most organisms are confined to habitats with a restricted climate range. Certain species, such as humans, may create a conducive microclimate that meets their needs. Humankind does this through several methods. Humans can modify their microclimate by altering their attire, constructing a suitable dwelling, combusting fuel, planting trees, excavating artificial lakes, and employing machinery to heat, chill, humidify, or desiccate the surrounding air. A primary objective of the construction is to alter the microclimate.

Climate, specifically, generates distinct and observable impacts on architectural designs. Primitive humans constructed shelters to protect themselves from the elements, such as rain, wind, sunlight, and snow. Their objective was to create an atmosphere conducive to their comfort and survival. The microclimate at each construction site is transformed into multiple distinct microclimates due to the house's construction. Prior to the onset of the industrial period and mechanization, humans relied on natural energy sources and locally accessible materials to construct their habitats in accordance with their physiological requirements. Throughout many millennia, individuals globally seem to have acquired the ability to engage with their climate. The climate influences the cadence of their existence as well as their environment and attire. Consequently, they construct residences that are somewhat adequate in supplying the requisite microclimate. In the warm, humid regions of East Asia, the indigenous population resides in huts with fragile, loosely woven walls that permit even the slightest wind to circulate. Inhabitants of the desert, exposed to intense sunlight, build residences with thick walls for thermal insulation and minimal openings to exclude hot air and sunlight glare. The ratio of window area to wall area diminishes as one approaches the equator. In warm regions, individuals avoid the sun's glare and heat, evidenced by the diminishing size of windows. In subtropical and tropical regions, more pronounced alterations in architectural design arise to address the challenges posed by extreme heat. In Egypt, Iraq, India, and Pakistan, extensive loggias, protruding balconies, and overhangs create elongated shadows on

building walls. Wooden or marble lattices occupy expansive openings to mitigate sunlight glare while allowing airflow. These patterns define the architecture of hot zones, eliciting both comfort and esthetic pleasure from humanity's obvious efforts to shield itself from extreme heat. In Northern Europe and regions experiencing significant snowfall, gables are steep; however, in the sunnier southern areas, the pitch gradually diminishes. In the arid regions of the North African coast, roofs are predominantly flat, offering a decent sleeping surface in certain locales. Further south, in the tropical rainfall zone, the roofs are steeply pitched to safeguard against the region's regular torrential downpours (Fathi & Abd al-Rahman, 1986) (Fig. 7.1).

The contemporary architects are liberated from almost all material limitations due to their accessible skills and tools. The modern ideas claimed to free the architect and architecture from the constraints and limitations resulting from climatic considerations. Individuals have access to millennia of styles and may select their designs from every nation globally. However, obligations towards the surrounding environment should not be forgotten. If architects neglect this duty and harm the ecosystem by constructing without consideration, they are perpetrating an offense against both the architecture and civilization (Fathi & Abd al-Rahman, 1986). Global warming is anticipated to adversely affect global precipitation, evaporation, and evapotranspiration rates. Recent publications detailing climate change events at global, regional, and local levels highlight the urgent need for the international community to respond and implement policies to mitigate greenhouse gas emissions.



Figure 7.1 Two typical building prototypes from distinct climates; the left pertains to a humid coastal climate, while the right illustrates a hot and arid region (Ghobadian, 2015). From Ghobadian, V. (2015). Shape of sustainable houses in Iran: A climatic analysis. European Online Journal of Natural and Social Sciences: Proceedings, 4, 110–120.

To effectively diminish energy emissions, there is a necessity for worldwide implementation of innovative low-carbon technologies that facilitate the decarbonization of energy usage byproducts (Osman & Sevinc, 2019). The built environment generates changes in the microclimate. The organization, orientation, and configuration of buildings establish a distinct microclimate for each location. Additionally, the construction materials, surface textures, and colors of the structures' exposed surfaces, as well as the design of open spaces, including streets, courtyards, gardens, and squares. These man-made aspects engage with the natural microclimate to influence the determinants of comfort in the constructed environment: illumination, temperature, airflow, and moisture. Any savings in fossil fuel consumption can have a positive impact on climate change and prevent widespread droughts. Savings in electricity consumption can also lead to the expansion of equipment related to the purification of useless water and transformation into water suitable for sanitary and drinking purposes.

7.3 Traditional architecture in the hot and arid climate

In hot and dry regions, the climatic architecture become very important as its principles can adapt with extreme conditions. The climate has been a significant factor influencing the development of Iranian architecture, urban landscape, and human existence. Climatic factors such as sunlight and wind have influenced the spatial configuration of buildings, dictating the placement of structures and thoroughfares, as well as the organization of mass and space in urban environment (Ghobadian, 1998). Taking into account the appropriate wind directions and movement of the sun, can significantly enhance spatial quality to offer improved environmental comfort for users (Tavassoli, 2016).

The attributes of a hot and arid climate are as follows:

- Temperature and heat: In a hot and arid climate, temperatures typically surpass 30°C. Summers are exceedingly hot and arid, with temperatures in certain regions exceeding 40°C. Consequently, energy usage is crucial for maintaining comfortable temperatures in buildings within this environment.
- Precipitation and water scarcity: A significant characteristic of arid and hot regions is the scarcity of water. Precipitation in this environment is minimal and erratic, typically manifesting as unexpected heavy rains

and floods. Consequently, water storage and resource management in buildings situated in arid and hot regions are essential.

- Wind and Dust: The occurrence of vigorous winds and dust constitutes another characteristic of the arid climate. Intense winds can adversely affect edifices and constructions. Consequently, protective measures against wind and dust must be incorporated into building design.
- Direct solar radiation: In arid and warm settings, the intensity of direct sunlight is significantly elevated. These rays can result in an elevation of the building's warmth and heat. Consequently, the implementation of awnings, appropriate lighting, and construction materials with superior insulating characteristics can enhance the internal conditions of the structure.

The general strategies applied by architects to mitigate climatic challenges, heat, and water scarcity in arid and high-temperature environments are as follows:

- Typically, structures in these areas are constructed using materials like brick and mud, which possess significant thermal capacity (Fathi & Abd al-Rahman, 1986).
- The architectural design of the buildings is optimized for density and compactness, with a focus on minimizing the external surface area relative to their volume.
- Structures are typically constructed in dense configurations and compact complexes, hence maximizing shadow on external surfaces.
- In many parts of these regions, the scarcity of rainfall and, consequently, timber has resulted in roofs constructed as trusses, arches, or domes, devoid of any framework, and composed of raw brick and mud.
- To minimize heat accumulation in the walls caused by solar radiation, the exterior surfaces are typically whitewashed.
- The quantity and surface area of windows in buildings in these regions have been minimized, with windows positioned in the higher sections of the walls.
- In arid and high-temperature settings, the installation of blinds and the infiltration of external air through windows or apertures are restricted. The incorporation of wooden inner courtyards and the alignment of living areas towards these courtyards constitute primary architectural characteristics in hot and dry regions.
- The orientation of the structures in these regions is south or southeast. This orientation is optimal for regulating and reducing solar heat ingress into the structure throughout the afternoon.

7.3.1 Characteristics of urban fabric

Climate significantly influences traditional town planning, resulting in notable homogeneity in urbanization throughout all hot desert regions. The configurations of nearly all conventional cities in the region are distinguished by two characteristics: small, serpentine streets and expansive open courtyards and indoor gardens. Large courtyards, functioning as reservoirs of cool, fresh air, typically dominate urban planning, as exemplified by Marrakech, Morocco, Tunis, and Iran. The narrow, winding streets with obstructed views serve the same purpose as a courtyard. They preserve any cool air that may settle overnight from being displaced by the initial gust of wind, as would happen in a gridiron layout with broad boulevards (see Figs. 7.2 and 7.3).

The adaptability of urban and rural environments and the modification of living conditions in response to natural causes, particularly in extremely severe weather conditions, are noteworthy. It can be confidently asserted that a significant accomplishment of traditional architecture lies in its adaptability to create a suitable living environment in arid and water-scarce regions.

The overarching framework of urban and rural morphology is as follows:

- Highly concentrated urban and rural fabric.
- Fully enclosed urban area.



Figure 7.2 The urban fabric of Marrakech with narrow and winding streets (Google Earth).



Figure 7.3 The urban structure of Tun is. From Fathi, H., & Abd al-Rahman, S. (1986). Natural energy and vernacular architecture: Principles and examples with reference to hot arid climates.



Figure 7.4 A bird view of urban structure of Yazd, Iran (https://whc.unesco.org).

- Constricted and uneven passageways, occasionally adorned with arches.
- Integrated structures.
- Orientation of buildings and settings according to solar and wind patterns (see Figs. 7.4 and 7.5).



Figure 7.5 Aerial photo of Yazd (https://earth.google.com/).

The urban fabric in these regions is dense, with buildings interconnected. The lanes are constricted, featuring relatively tall walls and extending in a fragmented manner. Essentially, there are no unenclosed urban spaces in these regions, as it is impractical to shield such locations from unfavorable environmental conditions. The narrowness of the lanes, often accommodating only two individuals side by side, is intended to enhance climatic convenience within the passageway. The existence of tall walls adjacent to the corridors substantially contributes to providing shade from sunlight and shielding the passages from desert winds. The convoluted layout of the alleyways is advantageous in hot, arid, and desert regions, as straight and broad pathways allow desert winds to move rapidly, disrupting daily life.

7.3.2 Spatial orientation regarding the sunlight

In hot and arid climates, the sun serves as the primary source of heat. To design any site, it is essential to ascertain the sun's position for every hour of the day throughout all seasons, along with the direction of prevailing winds, particularly during the warm season (Fathi & Abd al-Rahman, 1986). Traditional architecture has consistently considered passive solutions to confront the harsh regional climate. A building's placement has been determined by the angle and orientation of the sun's rays. Positioning the majority of substantial openings and windows on the southern front of the structure while shielding them from the summer sun with a canopy or

veranda, is a hallmark of traditional Iranian architecture. As depicted in Fig. 7.6 Pirnia (1991) consistently underscored the impact of light direction on traditional architecture. The primary objective in selecting the appropriate orientation in this area is to mitigate solar impact and lower indoor temperatures during summer, while enhancing solar exposure in winter (Sharami, 2023). In the northern hemisphere, the sun ascends in the northeast and descends in the northwest during summer. However, during winter, it ascends in the southeast and descends in the southwest (see Fig. 7.7. In Iran, the optimal orientation for evading sunlight is from northeast to west, while the ideal orientation for solar absorption is from southeast to south (Kasmai, 1984).

Architects have underlined the need to focus on the southern wall of the building and utilize solar energy to supply heat, particularly during winter. Consequently, the structure was partitioned into two sections: winter and summer. Modern architecture has also taken into account the optimization of solar utilization during winter for interior heating.

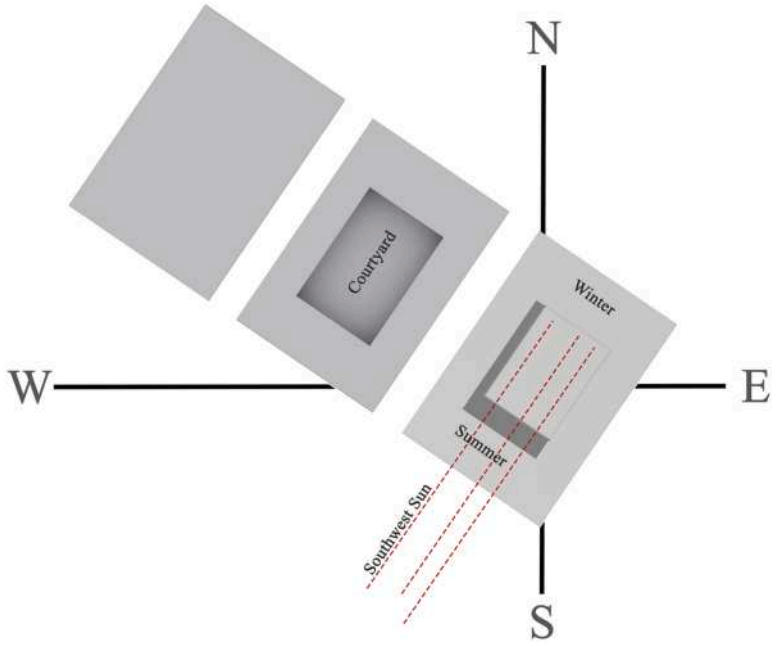


Figure 7.6 The positioning of a traditional house regarding the sun. From Jafari Sharami, Hatef. (2023). Investigation of Pirnia's orientation theory (Roon) in Yazd Qajar houses. Frontiers of Architectural Research, 12(5), 906–922. https://doi.org/10.1016/j.foar.2023.06.002.

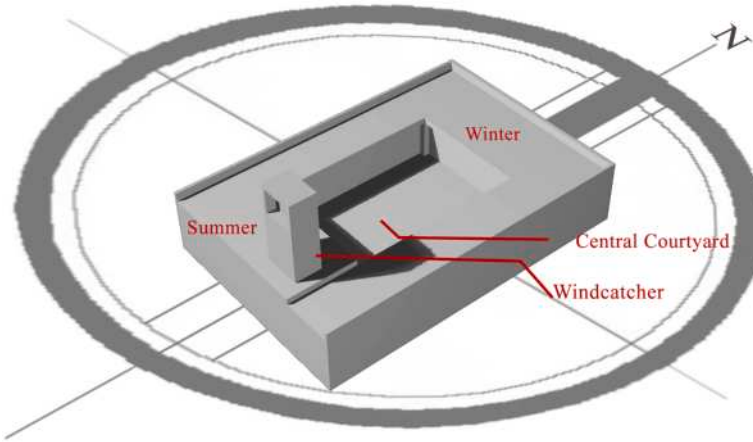


Figure 7.7 Different parts of a house with courtyard to maximize sunshine exposure in winter and to ensure a shielded façade during summer. From Jafari Sharami, Hatef. (2023). Investigation of Pirnia's orientation theory (Roon) in Yazd Qajar houses. Frontiers of Architectural Research, 12(5), 906–922. https://doi.org/10.1016/j.foar.2023.06.002.

The incorporation of walls in solar structures that accumulate solar thermal energy during the day exemplifies one of these strategies. This energy is retained in materials or liquids, such as water, that possess a high capacity for heat absorption and release it gradually. Heat is typically stored using either water barrels or the building materials employed in the construction of the edifice. During the night, when the ambient temperature declines, these materials persist in retaining the day's heat and progressively transport this warmth to the interior of the building. At daybreak, nearly all accumulated heat dissipates, and solar heat gathering resumes (see Fig. 7.8).

7.3.3 Architectural features of buildings

Similar to urban areas that are shielded from unfavorable natural elements, buildings and their courtyards are likewise surrounded by barriers and maintain a regulated climate. This pertains to all structures in regions with hot and arid climates, encompassing commercial, religious, service, and residential buildings.

The typical architectural features of buildings in arid regions of Iran are as follows:

- All structures are entirely introverted and enclosed.
- All structures, with the exception of restrooms, include a central courtyard, and the majority possess a basement, veranda, and wind catcher.

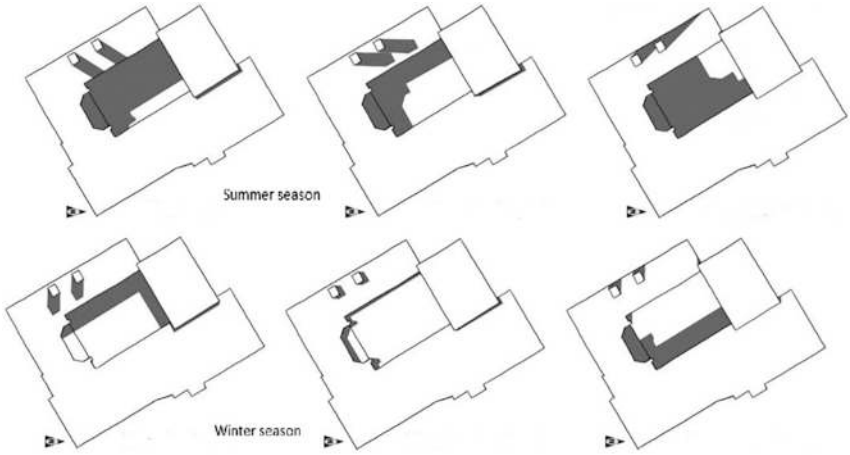


Figure 7.8 The orientation of Iranian traditional house regarding the sun. From Tavassoli, M. (2016). Urban structure in hot arid environments. In Strategies for sustainable development. Springer Nature.

- The floors of the structures, particularly the courtyard, are situated below the level of the passages, while the height of the living area is comparatively elevated. The vaults are frequently arched and domed.
- The walls are rather thick packed with thermally resistive materials.

The temperature variations in the region are significant, and the humidity level is below the comfort threshold. The sun's rays and heat provide a sweltering climate throughout summer, while the dusty desert winds that prevail on numerous days annually compromise comfort. Consequently, the establishment of a central courtyard within the building, complemented by a water basin and garden, enhances humidity levels in the living space. The relatively thick adobe and brick walls, designed to support the substantial weight of the arched and dome vaults, function as thermal capacitors, mitigating temperature variations throughout the day (see Fig. 7.9 Ultimately, by orienting all openings towards the comparatively humid and temperate courtyard and obstructing the exterior wall of the building (aside from the entrance), the linkage between the indoor living area and the outdoor environment is minimized, thereby establishing a microclimate conducive to human comfort in the region's hot and arid climate.

The buildings surrounding the courtyard are used in accordance with the particular season. The northern side of the courtyard, which receives winter sunlight and is warmer, serves as the wintering area, where most

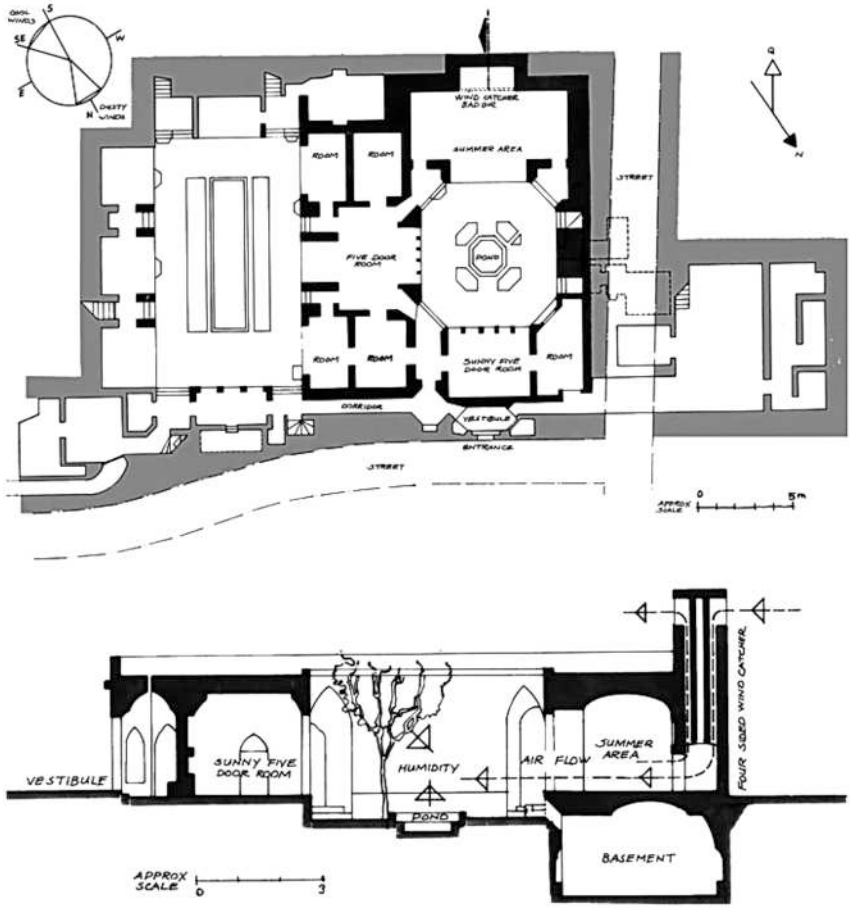


Figure 7.9 The plan and section of a traditional house in Yazd illustrating the orientation of the building regarding the sun and the direction of the winds. From Tavassoli, M. (2016). Urban structure in hot arid environments. In Strategies for sustainable development. Springer Nature.

household activities are conducted. During the summer, the converse applies; the rooms on the southern side of the courtyard, which are covered and cooler, serve as the family's dwellings. This region is referred to as the Nissar (providing shade and coolness), and the cellar (basement) is typically situated beneath this area. During warm seasons, the cellar's temperature is lower than that of other areas due to its subterranean location. During elevated temperatures, the household would retreat to the cellar to utilize its cooler air. In certain residences where the Qanat system (a traditional

drainage system) traversed under, a passage existed from the cellar to the Qanat for access. Occasionally, the Qanat water would flow into a tiny pond on one side and escape on the opposite side, referred to as the cistern room. The water pond and the inflow ducts of the wind catcher enhanced the dampness and coolness in this area.

The elevation of the summer home in these houses is typically substantial, causing hot air to ascend while cooler air occupies the lower portion of the space. Wind catchers and ventilators are frequently positioned on the southern front of the structure to enhance ventilation. The octagonal wind catchers of the Borujerdi house connect the main hall on the ground floor to the cellar beneath it in the summer residence. The apertures in the dome of the hall serve as wind catchers on the windward side and as ventilators on the leeward side, thereby enhancing the comfort of the inhabitants during the hot seasons in Kashan (see Fig. 7.10).

The existence of the pond and the vegetation in the courtyard mitigates the deficiency of humidity and, while offering shade, enhances the air's softness. All openings and entrances to the rooms lead to the courtyard or the adjoining area, with the courtyard functioning as a connective space among all sections of the home. Virtually no windows provide access to the exterior of the home, with the sole opening being the entrance that links to the courtyard via a somewhat lengthy vestibule and corridor. In the

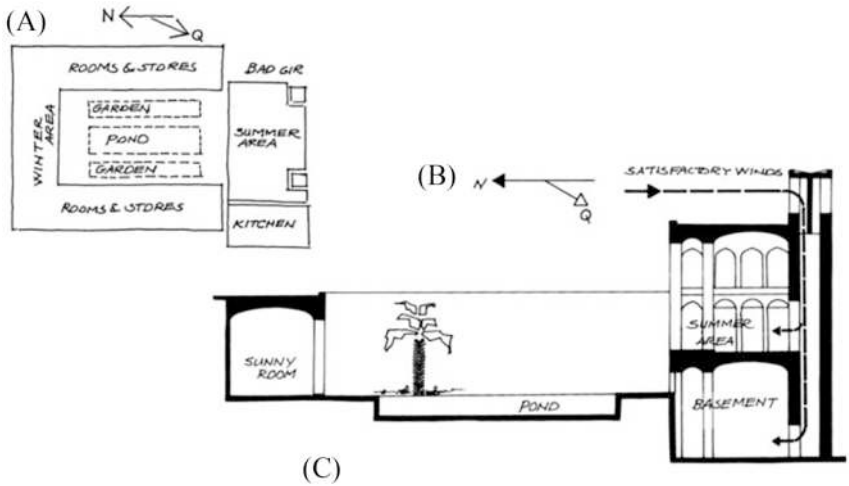


Figure 7.10 A large house in Zaware; (A) the spatial organization of the house. (B) the pattern of wind flow. From Tavassoli, M. (2016). Urban structure in hot arid environments. In Strategies for sustainable development. Springer Nature.

majority of residences, a substantial wooden bed was situated in the courtyard. During the summer, the family would irrigate the gardens and moisten the courtyard in the evening and at night, engaging in various activities such as gathering, dining, and other tasks on this bed. During this period, the family frequently occupied the courtyard, enjoying its temperate and refreshing ambiance. At night, they would also rest on the bed in the courtyard. Occasionally, they slept on the roof, which is more temperate than other areas at night, particularly at dawn.

7.3.4 The wind catcher

When the skin is wet with perspiration and exposed to air with a dew point lower than the skin temperature, the perspiration evaporates. The skin temperature decreases as energy is required to transform perspiration into water vapor. Nonetheless, the air in contact with the skin rapidly becomes saturated, halting evaporation. To sustain the evaporation process, the air must be eliminated either mechanically, using a fan, or naturally via air movement and drafts. The architectural design can facilitate natural air movement through two concepts. Initially, variations in wind velocity create a pressure differential that causes air to move from areas of greater pressure to those of lower pressure. In the second instance, air is heated, resulting in convection, where the warm air ascends and is supplanted by cooler air. A draft is generated in the space between the warm region and the cool-air intake aperture. The airflow rate due to convection in buildings is dictated by the disparity in the elevation of openings, with more airflow corresponding to a larger height difference between the openings. It is crucial when external air is stagnant and the interior necessitates ventilation for comfort. Both ideas have been applied in architectural design and urban planning through various developments.

In countries like Egypt and Pakistan, a malqaf or windcatcher was used to satisfy the need for ventilation alone. This device is a shaft rising high above the building with an opening facing the prevailing wind. It traps the wind from high above the building, where it is cooler and stronger, and channels it down into the interior of the building. The malqaf thus dispenses with the need for ordinary windows to ensure ventilation and air movement (see Fig. 7.11). The malqaf is also useful in reducing the sand and dust so prevalent in the winds of hot arid regions. The wind it captures above the building contains less solid material than the wind at lower heights, and much of the sand that does enter is dumped at the bottom of the shaft.

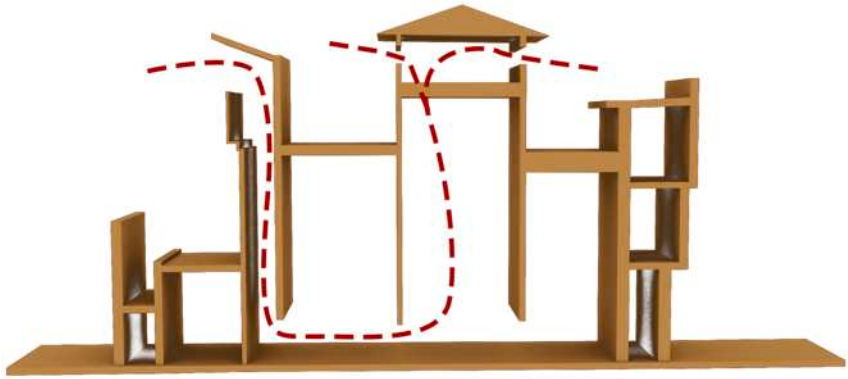


Figure 7.11 An example of a Malqaf in Cairo and the diagram illustrating the direction and power of airflow. From Fathi, H., & Abd al-Rahman, S. (1986). Natural energy and vernacular architecture: Principles and examples with reference to hot arid climates. University of Chicago.

Differences in temperature and air pressure, along with the Earth's rotation, induce air movement, resulting in wind. Wind transports rain clouds and precipitation, which are vital for life; without wind, human existence on Earth would be untenable. In Iran, precipitation originates from the Mediterranean Sea and the Indian Ocean. A separate wind stream originates from the north, delivering severe cold. In southern Iran, arid winds originating from Arabia inhibit the formation of rain clouds in this area. Each region experiences local breezes that originate from various directions. Certain winds are characterized as humid and cool, while others are hot and arid. Wind catchers are structures constructed on the rooftops of residences for ventilation purposes. They are also constructed above water tanks and mine shafts to facilitate ventilation. Furthermore, the wind catchers were often constructed using brick and mud, and reinforced with wooden beams to enhance their resistance to wind (see Fig. 7.12).

Wind catchers have been utilized in Iran since antiquity. They have been constructed in several configurations in central and southern Iranian cities, each tailored to the height and direction of prevailing winds. The wind catchers often consist of diminutive towers shaped as quadrilaterals or regular polygons, with the triangular framework entirely concealed and these towers nearly exceed the height of the house's roof. Furthermore, the wind catchers were typically constructed in an area of desert dwellings referred to as pond. The pond was a diminutive terrace situated at the terminus of the summer quarters of each edifice. The summer rooms comprised spacious areas,

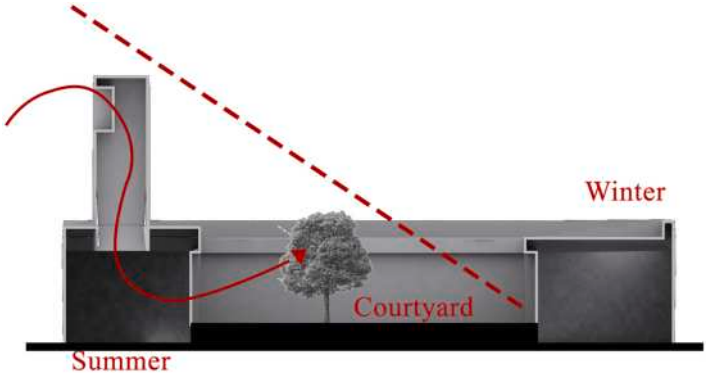


Figure 7.12 The sections of a unidirectional wind catcher in a house. From Ghobadian, V. (1998). Climatic analysis of the traditional Iranian buildings. Tehran University.

including many doors—occasionally as many as five—facilitating air circulation, with a pond located at their terminus. The water pond served as a link between the house's courtyard and the summer rooms. The wind catchers are positioned directly above the pond, directing airflow onto the water through their holes. In this regard, the operation of wind catchers was similar to contemporary water coolers. The electrical cooler allows air to enter through a similar wind catcher aperture. It directs the air concentrically onto the water basin, resulting in evaporation upon contact with the water. Evaporation is a thermodynamic process that absorbs heat, resulting in the cooling of air entering through the wind catcher aperture, which then cools the air within the summer rooms. In many historic mansions owned by affluent individuals, the pond functioned as an enclosed area, while the summer rooms included openings and passageways resembling air conditioning ducts, allowing cool breezes to circulate throughout the residence, particularly when multiple summer rooms were present. Wind catchers were also utilized to cool cellar spaces for food storage and to maintain the temperature of water in tanks (see Fig. 7.13).

To improve the cooling efficiency of the wind catcher and implement evaporative cooling, additional techniques have been employed, for instance, in the city of Bam (located in southern Iran), a wind catcher located approximately 50 m from the building is linked to it via an underground conduit. A garden is situated above this channel. Subsequent to irrigating the garden, the moisture infiltrates the walls of the communication channel, thereby cooling the air that travels from the wind catcher

to the building. In certain instances, they positioned mats, sofas, or thorn bushes at the entrance of the wind catcher and applied water to it, therefore enhancing the dampness and coolness of the incoming air.

7.3.5 Underground architecture

Weather factors and temperature variations exert minimal influence on underground structures, as the Earth's crust acts as a barrier, protecting the building from such changes. Storms and winds cannot infiltrate the ground, and the Earth's crust, functioning as a dense thermal insulator, obstructs heat transfer into the substrate. As the depth of a building increases, temperature fluctuations diminish due to the greater soil thickness; above a depth of 1.6 m, ground temperature is nearly constant, approximating the average annual temperature of the surrounding environment. The elevation of the central courtyard in Iranian buildings is inferior to the natural height code of the surrounding ground and lane. The courtyard's lower elevation relative to the alley presents four advantages:

- The water from the aqueduct or stream, which flows at the same elevation as the alley, naturally enters the garden and orchard within the courtyard, and if the water reservoir is located in the basement, it flows into the reservoir.
- The excavated soil, provided it is of adequate quality, is utilized to manufacture bricks for building construction.
- By situating a portion of the structure subterraneously, the thermal exchange between the interior and exterior is diminished, hence reducing temperature fluctuations.
- The building's foundations, and hence the entire structure, exhibit enhanced resilience to seismic forces.

To facilitate access to the aqueduct water that flowed beneath them for the irrigation of gardens and orchards, the designers constructed certain courtyards deeper than standard. These courtyards were referred to as garden pits. The residences of the aristocracy and affluent individuals contained over two courtyards, ultimately increasing to six, each designated for a certain use. The remaining four courtyards comprised the stables, servants', eunuchs', and orange groves' courtyards.

The ground not only supplies thermal energy but also serves as an appropriate medium for energy storage. Positioning the structure on the ground addresses various climatic needs and challenges. In Iranian urban and rural areas, several structures have been constructed underground to harness geothermal energy in response to climatic challenges. Examples of



Figure 7.13 Three methods of designing a subterranean building. From Hashemi (2019). The architecture of underground dwellings in Iran (pp. 72–79). Informa UK Limited. https://doi.org/10.1201/9780429424441-8.

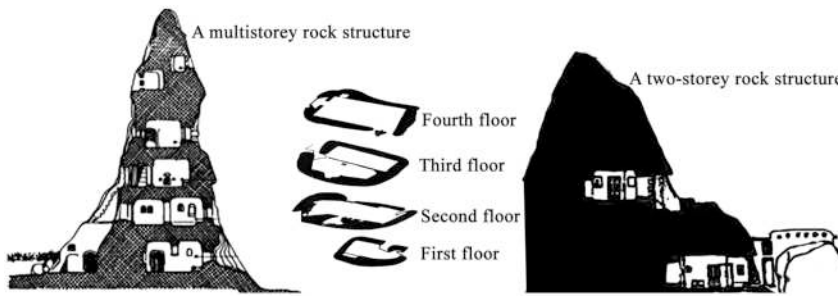


Figure 7.14 Meymand underground settlement. (en.mehrnews.com/news/143255/).

the structures, which include bathrooms, mosques, water tanks, and refrigerators, are even seen in subterranean villages. Traditional Iranian architecture exemplifies the effective and valuable utilization of geothermal energy, achieving sustainability through various methods. Notable patterns of geothermal energy application in this architectural style include Sezan, Sardab (Shabestan), Shodan, Hozkhaneh, Zamhrir, and Goodal Bagh, among others (see Fig. 7.14).



Figure 7.15 The plan of a home in Meymand underground settlement. From Hashemi, S. (2019). The architecture of underground dwellings in Iran (pp. 72–79). Informa UK Limited. https://doi.org/10.1201/9780429424441-8.

Meymand is known for its underground settlement. This village is situated in the western region of Kerman province, adjacent to the city of Babak, and is distinctive within Iran. All the structures in this community have been excavated into the mountain throughout the ages, resembling a series of expansive caves, with the sole connection between the interior and exterior of these subterranean edifices being the entrance. This serves as both the entrance and exit of the house, facilitating light and ventilation. These edifices exhibit remarkable stability due to their construction from solid stone and their subterranean positioning, which accounts for their enduring habitation by the local populace for numerous ages. The temperature variation within the building throughout day and night is minimal, and it is impervious to wind and rain, exhibiting fire resistance. The ventilation within the residences is inadequate, and the natural illumination is insufficient. This issue can be partially resolved by excavating the Earth to incorporate windows or skylights (see Figs. 7.15 and 7.16).

Earth-sheltered structures have additional advantages including:

- Reduced building maintenance expenses (diminished surface area of exposed building envelopes).
- Enhanced attenuation of noise and vibration (soil effectively mitigates the amplitude of acoustic waves).
- Protection against severe weather phenomena including strong winds, hailstorms, hurricanes, tornadoes, and earthquakes; diminished



Figure 7.16 Matmata's subterranean habitats adapted for harsh climatic conditions. (http://www.pangea-project.org/).

vulnerability to fire; decreased insurance costs; reduced maintenance requirements; inherent soundproofing; and judicious utilization of land and natural resources.

- Offering optimal protection against man-made disasters, including explosions, nuclear incidents, thievery, and burglaries.

The historic community of Matmata, situated between the eastern coastline and the desert in southern Tunisia, features residential structures excavated into the clay-gypsum strata of the terrain. The chronology of the initial settlements is ambiguous. These structures have vaulted chambers, typically round or square, encircling a central pit or courtyard with a diameter of 5 to 10 m and a depth not exceeding 9 m. The interiors are longitudinally divided between two levels; the lower level comprises bedrooms (kamour), a kitchen (matbakh), and stables, and the upper level is allocated for storage (makhzen). The submerged courtyard provides illumination and ventilation while accommodating communal activities. The courtyard is accessible from the exterior ground level by a tiny staircase embedded in the wall or by using a ladder. A stepped tunnel may help facilitate access to the courtyard (see Fig. 7.17).

Some of the most intricate residences comprise many courtyards, interlinking subterranean corridors, and rooms over various levels. The region is marked by prolonged heat waves, hence the cave-like residences assist in regulating temperature and humidity while providing shade for the residents. During summer, the temperature disparity between the exterior and interior of cave houses can attain 15°C, due to the about 7 m high soil cover from floor to ceiling, which offers efficient thermal insulation.

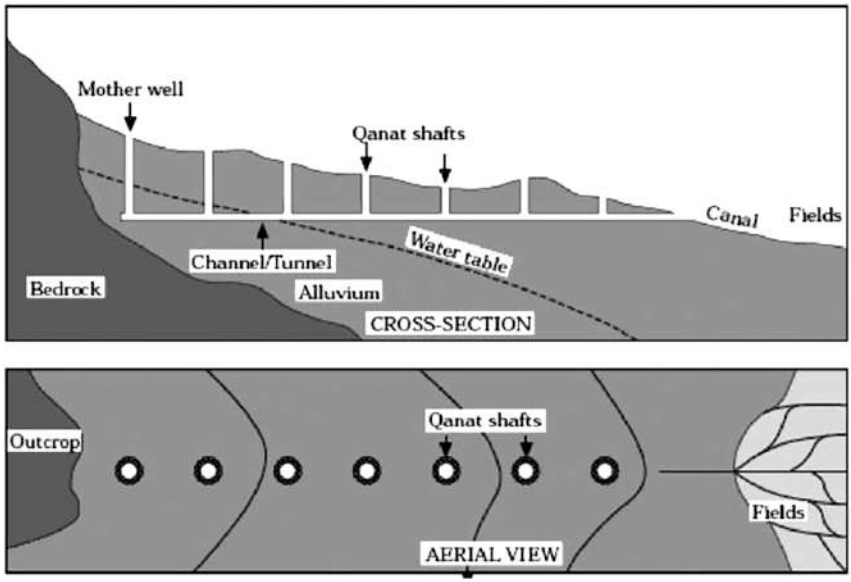


Figure 7.17 Plan and schematic section of a typical Qanat (Reza Balali et al., 2009). From Reza Balali, M., Keulartz, J., & Korthals, M. (2009). Reflexive water management in arid regions: The case of Iran. Environmental Values, 18(1), 91–112. https://doi.org/10.3197/096327109x404807.

7.3.5.1 Qanat

Water is a fundamental necessity for human existence, without which life on Earth would be unfeasible. Currently, water scarcity is a significant issue in numerous areas globally. The rapid increase in global population, particularly in emerging nations, coupled with unregulated water extraction and excessive use, threatens human communities globally. Each nation strives to address the issue of water scarcity according to its specific climatic circumstances. Several thousand years ago, the ancient Iranians applied Qanat (or Kahriz in local language) technology, successfully extracting subterranean water supplies. Situated in a semi-arid region, Iran has consistently faced a persistent threat of water scarcity. Consequently, for an extended period, many strategies have been employed to maximize water resource utilization and address the issue of water scarcity. The increased urbanization, characterized by population growth and excessive urban development, has led to the degradation of Qanats, a vital water supply.

In Qanat's system, the water resources such as natural springs have emerged from the Earth without the use of equipment. This invention also

familiarized the technologies of the water clock and water mill, and despite the passage of several millennia since its inception, it is still utilized in agricultural and animal husbandry in rural regions and communities. In central Iran, the subterranean fluids are saline and unsuitable for usage; they have utilized the Qanat system for water extraction. The Qanat consists of vertical shafts connected at their bottom with an underground tunnel through which water flows (Hosseini et al., 2010). This tunnel links a network of wells originating from the primary underground channel, transfers water for agricultural and other purposes. It extracts water from aquifers and conveys it from hills to the surface of the Earth through gravity alone (Abedi et al., 2023). The wells, referred to as rods during excavation, facilitate the extraction of materials to the surface, provide ventilation within the subterranean channel, and are employed in the cleaning, repairing, and maintenance of the horizontal tunnel. This tunnel may need to extend thousands of meters till it reaches the surface. The subterranean tunnel linking these wells ultimately emerges at the surface, referred to as the mouth, head, or mezhar of the Qanat. Since the Qanats are fed by underground water sources that are not very deep and the sources are not very rich, they are very sensitive to changes in underground water sources. For example, in hot seasons, plants need more water, and again in dry years and seasons, the water in the Qanats decreases. They are also very vulnerable to floods, earthquakes, and similar natural disasters; while sometimes the damage they suffer cannot be repaired, and thus the Qanat becomes unusable (see Figs. 7.18 and 7.19).

The Qanat system has shaped the location and growth patterns, as well as the physical configuration and spatial organization of neighborhoods, communal areas, residences, public edifices, agricultural fields, gardens, green corridors, and recreational places. Prominent structures, including mosques, educational institutions, noble residences, and caravanserais, were constructed along the principal pathway of the Qanat. The building and installation of water infrastructure, including wells, residences, streams, ponds, reservoirs, Qanats, refrigeration units, restrooms, fountains, dams, and pools, have been impacted by the Qanat system. Moreover, the urban road network was established in accordance with the hierarchy of the water distribution system, with routes typically aligning with the course of underground channels, streams, and surface channels of the Qanat. The social order and land values in urban and rural regions were influenced by their proximity to the Qanat. The upper social classes resided upstream,

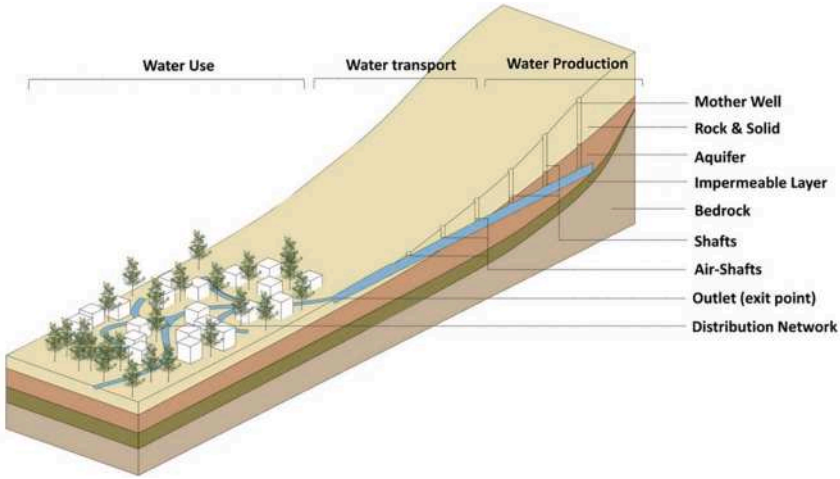


Figure 7.18 The diagram of a Qanat with its components. From Abedi, S., Ansari, M., Haghighatbin, M. & Mansouri, S.A. (2023). Comprehensive classification and categorization of Qanat features: An interdisciplinary exploration using landscape infrastructure concept and semi-systematic review. Environmental Systems Research, 12(1). https://doi.org/10.1186/s40068-023-00318-3.

whereas the lesser ones inhabited downstream. Regions with access to Qanat water often saw an increase in property and land values.

The construction technology of Qanat gained prevalence in the hilly and dry areas of Iran during the first millennium BC (e.g., Meymand Qanats date back to 10,000 BCE). This invention enabled farmers to participate in agriculture in places afflicted by prolonged drought and lacking adequate water resources for farming. It has gained global recognition and subsequently spread from Iran to other nations. The Qanats meet the water needs of populations in various countries including China, Morocco, and the United States. The subterranean structure of Qanat inhibits water evaporation or infiltration into the soil. It is also a multilayered water distribution system that carries significant environmental, social, and cultural values (Abedi et al., 2023).

The substantial water consumption in outdoor spaces like parks and gardens has prompted the creation of innovative landscaping designs that minimize water usage. New landscaping concepts including "Water-Wise, Water-Smart," "Low-Water," and "Natural Landscaping," have emerged

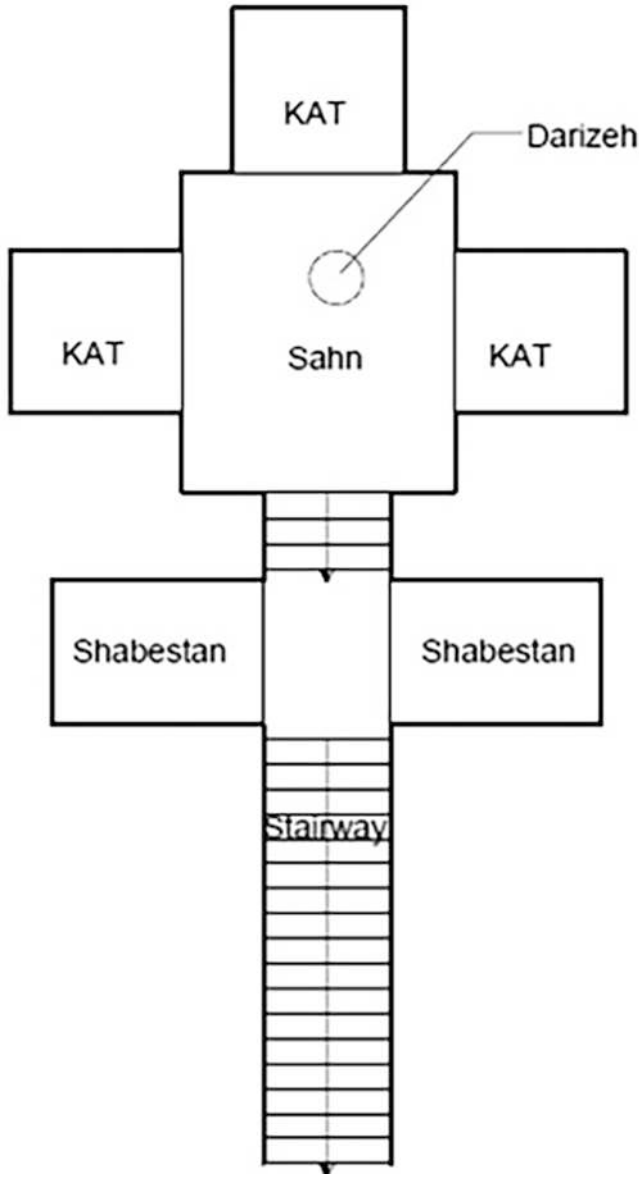


Figure 7.19 Different parts of a Shovadan. From Hazbei, M., Nematollahi, O., Behnia, M., & Adib, Z. (2015). Reduction of energy consumption using passive architecture in hot and humid climates. Tunneling and Underground Space Technology, 47, 16–27. https://doi.org/10.1016/j.tust.2014.12.001.

under the overarching term "Water-Efficient Landscaping," distinguishing them from traditional landscaping paradigms. Despite the distinctions in their philosophies and methodologies, these notions fundamentally adhere to the same principles and are typically employed interchangeably to convey identical meanings. The initial conceptual approach, established by articulating these fundamental concepts, is "Xeriscape." Xeriscape, recognized globally, can be succinctly defined as a specialized landscape design that adheres to the philosophy of conserving water resources and the environment by utilizing less water. Colorado , USA, implemented Xeriscape in 1978. The etymology of the term derives from the Greek word xeros, signifying dry. Xeriscape refers to innovative landscaping practices that optimize water and energy usage. Xeriscape is defined as an effective landscaping method that saves the environment and reduces water usage. The applications are founded on the fundamental premise of developing landscape projects to reduce water consumption. The objective is to use landscape strategies that harmonize with nature, particularly in dry or semi-arid regions. Given the significance of water for human existence, the value of Xeriscape becomes more apparent as it offers landscaping solutions that safeguard the environment and optimize water usage.

7.3.5.2 Shovadan

Shovadan is an underground structure excavated beneath the edifices in the historic areas of Dezful and Shooshtar (located in southern Iran). The depth ranges from 5 to 12 m, accessible by several staircases. Shovadan has been utilized for heating and cooling applications, with ambient temperatures of 7°C in January and 47°C in July, whereas the average temperatures for Shovadan are 17°C and 23°C, respectively (Hazbei et al., 2015). The appropriate temperature range for Shovadan demonstrates the capacity of this location to conserve energy. Shovadan represents one of the most innovative forms of sustainable architecture in Iran. It is utilized in both summer and winter seasons, maintaining an average air temperature in both hot and cold climates and ensuring human comfort (see Figs. 7.20 and 7.21).

The components of Shovadan include:

- Entrance: The entrance and staircase are located in the courtyard.
- Shabestan: Different levels may exist in Shovadan with the first level called Shabestan.
- Sahn: It is the main and deepest area that could be more than one.
- Kats: These are rooms connected to Sahn that could have different levels and heights.

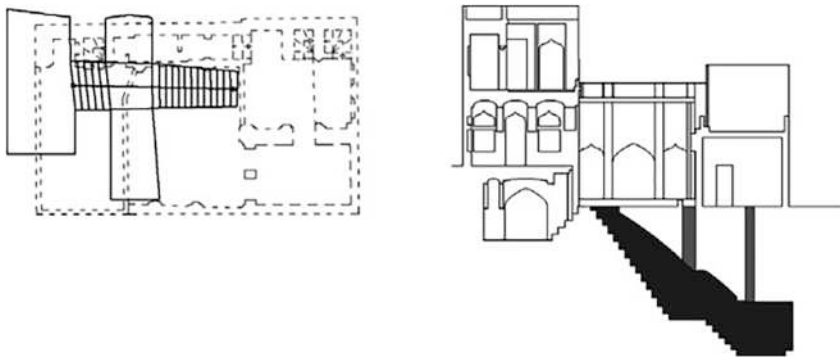


Figure 7.20 The section and spatial organization of a Shovadan. From Hazbei, M., Nematollahi, O., Behnia, M., & Adib, Z. (2015). Reduction of energy consumption using passive architecture in hot and humid climates. Tunneling and Underground Space Technology, 47, 16–27. https://doi.org/10.1016/j.tust.2014.12.001.



Figure 7.21 The underground space of Shovadan in a traditional house. From Ghobadian, V. (1998). Climatic analysis of the traditional Iranian buildings. Tehran University.

- Tal: Tunnels that connect one Shovadan to a neighbor's and Qanat channels.
- Darize: Vertical ducts that were significant for air conditioning and humidity reduction.

The rooms (Kats) were utilized throughout the summer or in hot weather when the temperature of the nightstand became unbearable for living and working. A hard ground, typically characterized by conglomerate soil, is required to construct Shovadan to eliminate the need for

supporting columns in the excavated underground chambers. Access to Shovadan was achieved via a staircase at a depth of 8–12 m. Sometimes, Shovadan was interconnected through tunnels, establishing an underground network (see Fig. 7.22).

With the exception of the regions near coastlines, the majority of traditional residences in Iran featured basements, where inhabitants would retreat during hot seasons. As Shovadan is connected to the water supply system (Qanat), it could act as a shelter to stay for a long time. Since some people could not afford the building of Shovadan, they went to their neighbors' houses to rest in the 50°C summer heat. Sometimes the Shovadan extended into the underground to parcel boundaries of neighbors. By Tals (tunnels), houses were connected to each other, and then to a mosque or a castle in some cases. The close neighborhoods' relationships in the streets and public spaces were transferred to the underground areas. A network of private, semi-public, and public spaces is formed that resembles an underground city. The archeological excavation has still continued to discover the complexities of these relations in the cities of Dezful and Shushtar. The underground city of Noushabad has been recently discovered at a 350 km distance with a more complex spatial organization including meeting rooms, wind catchers, and storage rooms. These underground living areas are successful examples of confronting extreme climatic conditions (Soleimani, 2024).

In recent years, the design and construction of contemporary subterranean residences in frigid locations such as North America and Europe has significantly increased. The technique of execution involves situating

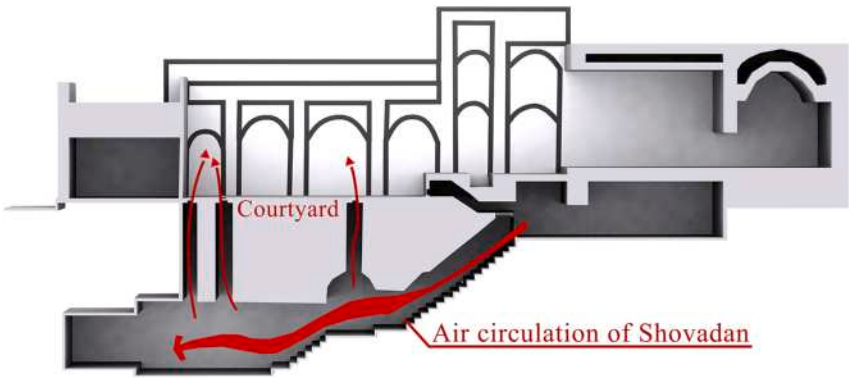


Figure 7.22 A section depicting the interconnected network of Shovadans and Qanats. (https://civilica.com/note/11000).

the entire structure underground, with the roof around 1 m beneath the surface. This elevation is then covered with agricultural soil, upon which grass and shrubs are cultivated. If the site is inclined, the structure is constructed on the southern aspect of the slope, with the southern elevation of the building elevated above the ground.

7.4 Contemporary design inspired by traditional architecture

Like the traditional architecture, passive systems are employed in contemporary times. Solar and wind energies are the primary sources in these systems. Passive solar systems supply heating, cooling, ventilation, and lighting, while passive wind systems deliver cooling and ventilation. Passive solar system applications facilitate heat recovery during winter and enable natural ventilation and cooling in summer. When passive systems are evaluated within the scope of solar energy, there are three elements in the applications. These elements can be classified as "collectors, storage, and distributors." Solar walls (trombe walls), water walls, metal walls, roof pools, sunrooms, thermosyphon systems, solar chimneys, and double-layered facades serve as collectors to collect solar energy and convert it into heat.

7.4.1 Tadjourah SOS Children's Village in Djibouti

The SOS Children's Village project was initiated by Urko Sanchez Architects for SOS Kinderdorf, an international NGO (standing for Non-Governmental Organization) focused on supporting orphaned or disadvantaged children by offering them a stable home and family environment (Sanchez, 2022). The project was executed in Tadjourah, a city situated in Djibouti with arid climate conditions. It has 15 residences featuring 1400 m^2 of internal space and 266 m^2 of open inner garden/courtyard, culminating in a total area of 2600 m^2. The architectural team sought to construct a compact hamlet featuring residences very similar to the traditional urban fabric of a hot and arid climate. The residential units are oriented inward and sealed off from the exterior in extreme weather circumstances. The compact and inward structure ensured seclusion and safeguarding from external influences. Every communal component of the residences, including the kitchen and living room, features an open courtyard (see Fig. 7.23). The architects



Figure 7.23 A view from an alley showing the congested arrangement of the houses around public and private open spaces. (https://arquitecturaviva.com/works/social-dwellings-in-tadjourah).

aim to satisfy the desires of the village residents by creating a shaded and cool inner courtyard, conducive to their traditional lifestyle activities such as cooking with firewood, raising pets, and sleeping under the stars (Ramku, 2019).

The proximity of Tadjoura, a city plagued by persistent droughts and acute famines, to the Horn of Africa, known for its record-high temperatures and hot-arid climate, significantly influenced the architectural solution. All residences adhere to a uniform design to ensure adequate shade and cross ventilation, hence mitigating negative climatic impacts. Nonetheless, their distribution and positioning on the site vary, occasionally resulting in two overlapping structures, wherein the roof may serve as a terrace. A biological digester system was implemented to replenish the soil with clean water due to insufficient rainfall. Furthermore, due to the scarcity of native plant species in arid regions, the architects conserved all existing trees and included new vegetation in the building. Consequently, the plants would mature within a few years, offering the requisite shade in the vicinity. Constricted alleys emerge between closely situated residences, which cast shade upon one another and the streets. These narrow alleys were designed to facilitate passive ventilation, and ventilation corridors were established. In instances where airflow proved unfeasible, elevated ventilation chimneys were constructed to capture wind. These chimneys facilitate the capture and conveyance of wind into interior spaces (see Fig. 7.24).

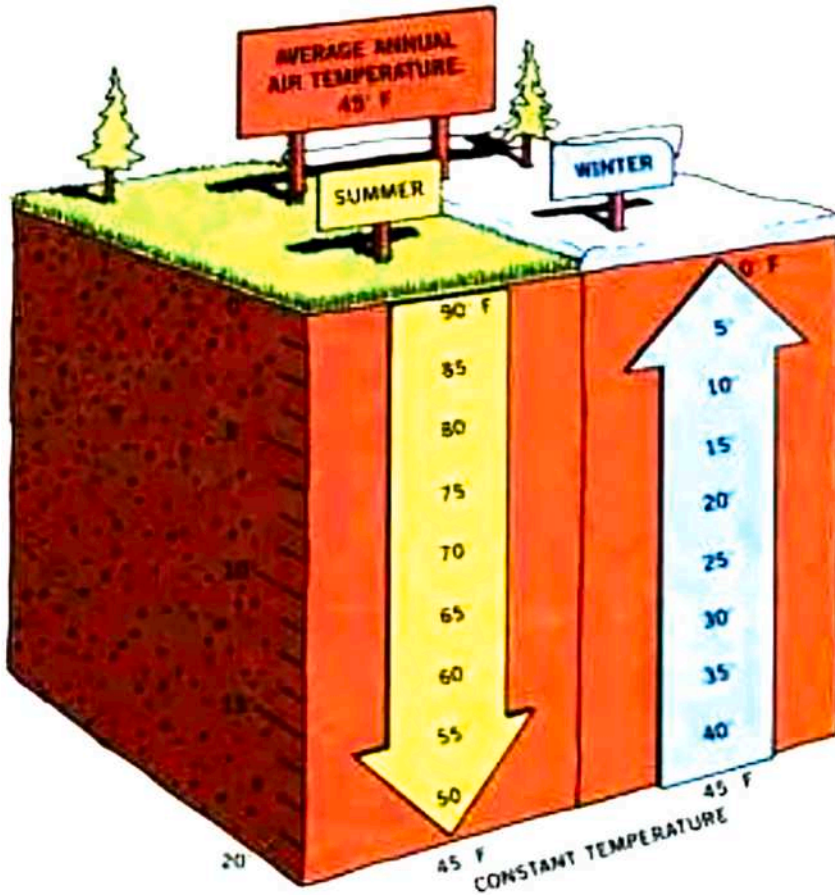


Figure 7.24 A diagram depicting the underground constant temperature. From Anselm, A.J. (2008). Passive annual heat storage principles in earth sheltered housing, a supplementary energy saving system in residential housing. Energy and Buildings, 40(7), 1214–1219. https://doi.org/10.1016/j.enbuild.2007.11.002.

7.4.2 Earthscrapers

The strategy for the innovative development of subterranean urban spaces constitutes the scientific field of underground urban planning. Underground urbanism is a discipline within architecture and urban planning that focuses on the cohesive utilization of subterranean spaces in cities and other settlements, adhering to the principles of urban esthetics, social cleanliness, and technical and economic viability (Praslova & Riabets, 2023).

The benefits of urban underground space development for sustainable progress encompass climatic stability, noise and vibration isolation, radioactivity and gas mitigation, seismic resilience, and the efficient utilization of groundwater, geomaterials, and geothermal energy. Underground constructions can be found throughout the city, exerting minimal influence on the natural terrain and surroundings. They are consistently shielded from the direct impact of climatic elements. Subterranean structures provide significant vibration resistance and acoustic insulation properties. And safeguarded against the impacts of seismic waves and penetrating radiation, which guarantees their immunity to mass destruction (Praslova & Riabets, 2023).

Earthscrapers are the antithesis of skyscrapers. They commence at the surface and expand beneath, analogous to how a skyscraper ascends upward. It was proposed as an alternative building method for the future, as it requires less surface area and lower operating costs than an equivalent aboveground structure (Tahmasebinia et al., 2020). The primary considerations when examining the design of earthscrapers versus skyscrapers include spatial limitations, structural stability, and energy efficiency. Earthscrapers can diminish energy consumption by utilizing the substantial soil surrounding the structure as insulation, in addition to leveraging the advantageous constant temperatures of the Earth (Van Dronkelaar et al., 2014). Despite the variability of elements influencing loads, such as solar radiant heat, based on the surrounding climate, overall energy reduction is attainable across all climates and functions (Anselm, 2008). When comparing the best case (lowest energy demand) of the aboveground building with the worst case (highest energy demand) of the underground building, at their higher probability, the difference is significant.

Although earthscrapers appear to be a contemporary innovation prompted by increasing urban populations and diminishing urban space, such concepts have historical precedents. The notion of earthscrapers was initially presented in 1931. Japan has consistently been susceptible to catastrophic earthquakes. A depthscraper was suggested as a remedy for catastrophic earthquakes and a novel habitat for life.

The United Nations has forecasted that the global population would attain 9.7 billion by 2050, reflecting an increase of 2.5 billion from the current figure. The heightened demand for housing options to support the expanding population while minimizing the carbon footprint has prompted BNKR Arquitectura, located in Mexico City, to design an earthscraper. This 65-storey deep structure is an inverted pyramid designed to house

100,000 individuals while occupying minimal surface area, facilitating its integration into urban environments (Tahmasebinia et al., 2020). Furthermore, its embedding in the soil mitigates wind loading and maintains a consistent warm temperature from the surrounding earth, hence decreasing energy consumption for heating and cooling. Mexico City enforces height rules that limit new constructions in its central square. The elevated demand for centrally situated properties provides an opportunity to suggest a deep earthscraper beneath the surface. The proposed earthscraper extends 1000 feet underground, featuring 35 levels of office space at the base, with 10 levels each designated for residential apartments, retail spaces, and a museum. The concept suggests that the 65-storey structure be organized around a central, cylindrical void featuring a glass roof to provide light and ventilation within the earthscraper. The glazed ceiling would further serve as a flooring surface in the upper square (see Fig. 7.35).

Thermal energy transmission occurs through two distinct thermal pathways. The Perlucor ceiling collects solar radiation at the ambient surface temperature, conducting heat within and heating the internal air by convection. Moreover, the walls of the building, at the ambient temperature of the surrounding soil, transmit this energy via the wall system and dissipate it by convection within the structure. An ambient temperature of 22.1°C was established at the upper surface, while a linearly increasing ambient temperature was implemented along the sidewalls of the soil (Tahmasebinia et al., 2020).

7.5 Conclusion

To address the issue of contemporary drought, it is essential to examine historical architecture and leverage prior experiences as potential solutions. Traditional architecture in Iran and other nations historically situated in arid and hot climates has devised efficient strategies to mitigate drought, which are now being considered in sustainable and green building concepts. The climatic conditions of these regions are influenced by factors such as solar radiation, latitude, ocean current intensity, seasonal winds, water presence, humidity, vegetation, altitude above sea level, and topographical variations. By focusing on passive design parameters and strategies like natural ventilation, architecture can mitigate fossil energy consumption and provide sustainable solutions to the global paucity of water resources and their mismanagement. By examining historical

experiences, we can better understand the potential solutions to the issue of drought and develop sustainable and green building practices.

Climate, particularly in hot and dry regions, has generated distinct and observable impacts on architectural designs, with primitive humans creating shelters to protect themselves from high temperatures, direct solar radiation, water scarcity, and dusty winds. Climatic architecture is the art and science of designing and constructing buildings and spaces that optimize resource utilization and create comfort for residents. The spatial configuration and designed strategies, by taking into account wind direction and intensity, along with sunlight intensity and direction, can significantly enhance life quality and offer improved environmental comfort for users. To minimize heat accumulation caused by solar radiation, other strategies were used, including materials like brick and mud, optimizing density and compactness, and constructing structures in dense configurations to maximize shadow on external surfaces. Climate significantly influences urban planning, leading to a highly concentrated urban and rural fabric and fully enclosed urban areas throughout hot desert regions.

Underground structures, as a design technique in hot and arid climates, are less influenced by climatic conditions and temperature fluctuations, since the Earth's crust serves as a barrier, shielding the building from alterations. The ground provides thermal energy and serves as an appropriate medium for energy storage, addressing various climatic needs and challenges. The lower elevation of the central courtyard in traditional Iranian buildings offers several advantages such as supplying natural water to the garden and orchard, using excavated soil for brick manufacturing, reducing thermal exchange between interior and exterior, and enhancing seismic resilience. Earth-sheltered structures like Shovadan offered protection against severe weather phenomena, diminished vulnerability to fire, and provided accessibility to subterranean water supplies by the Qanat system.

The design strategies of traditional architecture serve as a resource for addressing contemporary water scarcity and drought challenges. This chapter discusses that passive approach of traditional buildings can be improved with modern techniques to meet the new needs and requirements. Enhancing building self-sufficiency by reducing reliance on fossil fuels can directly or indirectly impact the preservation of water resources. This is also one of the main goals of sustainable development in urban environments.

References

Abedi, S., Ansari, M., Haghighatbin, M., & Mansouri, S. A. (2023). Comprehensive classification and categorization of Qanat features: An interdisciplinary exploration using landscape infrastructure concept and semi-systematic review. *Environmental Systems Research, 12*(1), 35.

Anselm, A. J. (2008). Passive annual heat storage principles in earth sheltered housing, a supplementary energy saving system in residential housing. *Energy and Buildings, 40*(7), 1214–1219.

Ashrafian, T., Ferdos, N. M., & Haghlesan, M. (2011). Human comfort in underground buildings. In *5th SASTech*. Mashhad.

Chen, X., Yang, H., & Lu, L. (2015). A comprehensive review on passive design approaches in green building rating tools. *Renewable and Sustainable Energy Reviews, 50*, 1425–1436.

Fathi, H., & Abd al-Rahman, S. (1986). *Natural energy and vernacular architecture: Principles and examples with reference to hot arid climates*. University of Chicago.

Ghobadian, V. (1998). *Climatic analysis of the traditional Iranian buildings*. Tehran University.

Ghobadian, V. (2015). Shape of sustainable houses in Iran: A climatic analysis. *European Online Journal of Natural and Social Sciences: Proceedings, 4*(3), 110–120.

Hashemi, S. (2019). The architecture of underground dwellings in Iran. In *Tunnels and underground cities. Engineering and innovation meet archaeology, architecture and art*. CRC Press, 72–79.

Hazbei, M., Nematollahi, O., Behnia, M., & Adib, Z. (2015). Reduction of energy consumption using passive architecture in hot and humid climates. *Tunnelling and Underground Space Technology, 47*, 16–27.

Hoseini, T., & Hajizadeh Javaran, M. (2023). The study and investigation of Pirnia's theory of Kermani Roon through examining the optimal orientation in architecture and urban planning of Kerman. *Karafan Journal, 19*(4), 67–90.

Hosseini, S. A., Shahraki, S. Z., Farhudi, R., Hosseini, S. M., Salari, M., & Pourahmad, A. (2010). Effect of urban sprawl on a traditional water system (Qanat) in the City of Mashhad, NE Iran. *Urban Water Journal, 7*(5), 309–320.

Kasmai, M. (1984). *Climate and architecture*. Iran Housing Construction Company.

Osman, M. M., & Sevinc, H. (2019). Adaptation of climate-responsive building design strategies and resilience to climate change in the hot/arid region of Khartoum, Sudan. *Sustainable Cities and Society, 47*, 101429.

Pirnia, M. K. (1991). About traditional urban planning and architecture of Iran. Abadi. *Quarterly Journal on Architecture & Urbanism, 1*(1), 4e15.

Praslova, V., & Riabets, Y. (2023). Modern trends of organization of the underground urban space. *Architecture, Civil Engineering, Environment, 16*(2), 45–51.

Ramku, B. (2019). *Tadjourah SOS children's village on-site review report*. AKDN (Aga Khan Development Network).

Reza Balali, M., Keulartz, J., & Korthals, M. (2009). Reflexive water management in arid regions: The case of Iran. *Environmental Values, 18*(1), 91–112.

Sanchez, U. (2022). Design for fragility+ children. *Design for fragility* (pp. 3–10). Routledge.

Sharami, H. J. (2023). Investigation of Pirnia's orientation theory (Roon) in Yazd Qajar houses. *Frontiers of Architectural Research, 12*(5), 906–922.

Soleimani, M. (2024). Shovadan; A network of underground private and public spaces. In *2nd international congress on sustainable development in the human environment & current and future challenges*, Antalya, Türkiye.

Tahmasebinia, F., Yu, K., Bao, J., Chammoun, G., Chang, E., Sepasgozar, S., & Marroquin, F. A. (2020). *Earthscraper: A smart solution for developing future underground cities*. IntechOpen, 17.

Tavassoli, M. (2016). Urban structure in hot arid environments. In *Strategies for sustainable development*. Springer Nature.

Van Dronkelaar, C., Cóstola, D., Mangkuto, R. A., & Hensen, J. L. (2014). Heating and cooling energy demand in underground buildings: Potential for saving in various climates and functions. *Energy and Buildings, 71*, 129–136.

CHAPTER EIGHT

The psychological toll of drought in a changing climate

Mahsa Vaheddoost
Department of Psychology, Faculty of Arts and Social Sciences, Mudanya University, Bursa, Türkiye

8.1 Introduction

Water has always been the most vital resource for the survival of civilizations throughout history. Societies that formed around water sources thrived when they controlled these resources, but declined due to drought and famine when they lost access to them. Today, it is clear that the water crisis has not only persisted but has also worsened significantly.

According to the World Economic Forum's Global Risk Report (WEF, 2021), access to water and food ranks among the top five global risks, posing a significant threat to many countries worldwide. Studies reported that drought causes maladaptation and negativity in mental health. In a study conducted with male farmers in Australia, prolonged drought events were found to pose a risk for suicide (Hanigan et al., 2012). Similar results were also observed among Indian farmers, where high temperatures and low agricultural yields were found to increase the risk of suicide (Carleton, 2017). Other studies in the psychology literature report that drought causes stress or acute stress on mental health (e.g., Barreau et al., 2017; O'Brien et al., 2014), high rates of mental health problems and low levels of well-being (e.g., Edwards et al., 2015), and higher anxiety and emotional problems (e.g., Coêlho et al., 2004). This information describes the emotional damage caused by drought on mental health.

Although various studies have been conducted in many countries around the world, focusing on the socioeconomic and environmental impacts of drought, and the effects of drought on mental health have not been adequately covered. The "*water crisis*", depicting drought, is a hybrid disaster that threatens human existence. With this scope, it poses a threat to the continuity of life in all living things, confronts the danger of extinction,

Drought Dynamics
DOI: https://doi.org/10.1016/B978-0-443-34205-9.00008-1
© 2026 Elsevier Inc. All rights are reserved, including those for text and data mining, AI training, and similar technologies.

and causes loss of hope by creating anxiety for the future. In this regard, when the statement of the art is examined, many studies have been conducted on the environment and human health from the past to the present. Fisher (2016) conceptualized the link between climate change and psychology, introducing the term eco-melancholia to describe the psychological states created by environmental problems in human life, building upon earlier studies on ecological crises and their impact on mental health.

Hence, in the growing research the literature on climate change and mental health, it has been revealed that the changing climate conditions increase posttraumatic stress disorder (PTSD), major depressive disorders (MDD), anxiety, depression, complex grief, guilt, conscientious trauma, maladaptive recovery, substance abuse, and suicidal ideation (Berry, 2009; Doherty & Clayton, 2011; Kevin et al., 2012). Drought, as one of the most prominent indicators of climate change, has profound impacts on both natural ecosystems and human communities. Prolonged water scarcity can negatively affect agriculture, livestock, and other livelihoods, creating economic uncertainties as well as social unrest. This process can have serious psychological consequences, such as stress, anxiety, depression, and even increased suicide rates, especially for individuals living in rural areas.

8.2 Methodology

This study was carried out by reviewing and analyzing existing literature on the psychological effects of drought on individuals and society.

Within the scope of the study, initially, national and international academic sources focusing on the relationship between drought and psychology, were reviewed. In this regard, studies published in the fields of psychology, sociology, environmental sciences, and public health, were systematically analyzed.

In the review process, studies addressing the psychological effects of drought in different dimensions were categorized. In particular, individual psychological effects such as stress, anxiety, depression, PTSD, and psychosocial consequences at the societal level (e.g., migration, social unrest, and effects of economic uncertainties on mental health), were examined. In addition, regional differences and common trends were identified by evaluating research conducted in different geographies.

8.3 Psychological effects of drought

The concept of ecological grief, which emerged about the environmental losses caused by drought, explains the deep grief and despair that individuals feel as a result of the severing of their ties with their natural environment. Fritze et al. (2008) draw attention to the devastating effects of drought on the overall resilience of societies by addressing the fine balance between hope and despair created by climate change. Research shows that uncertainty and constant adaptation efforts during droughts deplete individuals' psychological resources, which increases the importance of resilience strategies at the societal level. Cunsolo and Ellis (2018) defined ecological grief as an expression of emotional trauma caused by lost cultural and identity elements in communities facing the loss of the natural environment. This is particularly observed in communities that depend on agriculture-based lifestyles during prolonged periods of drought. Furthermore, the causal pathway framework developed by Berry et al. (2010) systematizes how environmental stressors lead to chronic psychological problems in individuals. This model shows that prolonged environmental crises such as droughts create a complex interaction between economic uncertainty, social disconnection, and psychological stress. This interaction sets the stage for individuals to develop not only immediate stress reactions but also persistent mental health problems over time (Berry et al., 2010).

8.3.1 Ecological grief and loss of identity

The increasing frequency and intensity of extreme heat events can have serious consequences for human health. Elderly individuals, those with chronic conditions, and outdoor workers are particularly vulnerable to these effects. During periods of extreme heat, problems such as fatigue, sleep disturbances, dehydration, and other health complications may arise, and if appropriate preventive measures are not taken, these issues can reach life-threatening levels. Therefore, heat waves should not be viewed merely as climatic phenomena but also as significant public health concerns that require careful consideration.

In addition to physical health effects, heat waves may also trigger psychological issues and associated psychosomatic disorders. The psychological impacts of climate change can range from ordinary stress to chronic stress and other mental health conditions. Heat waves act as significant stressors that affect human health, contributing to a wide array of problems,

from heart attacks to temporary loss of consciousness and even traffic accidents. More profound consequences often arise following extreme weather events such as floods, wildfires, and hurricanes, which can result in large-scale community trauma. Individuals who lose their loved ones, homes, jobs, and social environments are often confronted with various psychological challenges. These may include trauma-related disorders such as PTSD, excessive anxiety, impaired concentration, social withdrawal, profound sadness, sleep disorders, sexual dysfunction, and irritability. In some cases, these psychological conditions may lead to increased substance use including alcohol and drugs (Atay et al., 2012).

The concept of ecological grief has been introduced to emphasize that environmental losses can lead to profound feelings of sadness and despair. In communities with a strong connection to nature, environmental degradation caused by drought can significantly contribute to psychological distress and depression by disrupting cultural identity and a sense of belonging. In light of these challenges, it is essential not only to implement strategies to mitigate climate change but also to strengthen mental health services and develop programs that foster social resilience (Cunsolo & Ellis, 2018).

8.3.2 The effects of drought on mental health disorders

Water scarcity is increasingly recognized as a critical environmental issue with wide-ranging effects on communities. In many parts of the world, limited access to safe and sufficient water disrupts daily life and places additional strain on already vulnerable populations. This problem is particularly visible in regions where rainfall is low, infrastructure is underdeveloped, and resources are not managed effectively. Communities living in rural and economically disadvantaged areas often face the greatest difficulties, as water shortages not only affect physical health and living conditions but also create additional burdens on emotional well-being. Feelings of stress, uncertainty, and insecurity about the future are frequently heightened in such contexts. Moreover, inequalities in access to water can give rise to social tensions and compel people to relocate in search of more stable conditions. While many responses to water scarcity have focused on physical needs, the broader psychological and social dimensions of the problem deserve greater attention.

In the Türkiye Climate Change Report published by the Ministry of Environment, Urbanization, and Climate Change (2019), it is emphasized that environmental crises, particularly those associated with droughts,

engender a persistent sense of economic uncertainty and psychological distress among individuals. The report underscores that such adversities not only exacerbate financial insecurities but also contribute significantly to the deterioration of mental well-being. Specifically, the prolonged exposure to these environmental stressors is identified as a crucial determinant in the rising prevalence of chronic stress, generalized anxiety disorders, and depressive symptomatology. The link between environmental degradation and mental health is thus highlighted as a pressing societal concern, necessitating comprehensive policy interventions and adaptive strategies to mitigate the psychological burden imposed by climate change.

8.3.3 Economic uncertainty and chronic stress

A severe and prolonged decline in the amount of water available can lead to life-changing decisions that have stressful impacts on individuals, families, and communities (Vins et al., 2015). Although suicide occurs through the complex interaction of many factors, prolonged drought is recognized as one of the main factors that increase suicide rates in at-risk groups, particularly among farmers in India and communities in rural Australia and South Africa (Carleton, 2017; Hanigan et al., 2012; Vins et al., 2015).

Uncertainty is also a source of stress and can be a risk factor for psychological stress. Climate-induced disasters represent a significant source of stress that not only jeopardizes physical health but also profoundly affects psychological well-being. In turn, the deterioration of mental health can further exacerbate physical health conditions by disrupting essential physiological and behavioral functions, such as sleep patterns, dietary habits, and physical activity levels, ultimately compromising immune system efficacy (Clayton et al., 2017). The complex interaction between environmental stressors and mental health outcomes underscores the multifaceted consequences of climate change on human well-being. Environmental crises driven by climate change foster a pervasive sense of stress, anxiety, and hopelessness among individuals, which, if sustained over time, can contribute to the development of severe mental health disorders. One particularly acute manifestation of these challenges is observed in the agricultural sector, where prolonged droughts and other climate-related adversities lead to a decline in crop yields and a corresponding reduction in household income. The economic strain experienced during such periods places substantial financial pressure on families, exacerbating psychological distress and increasing the prevalence of chronic stress and depressive symptoms. Moreover, the uncertainty associated with future

environmental conditions amplifies these effects, as individuals and communities struggle to adapt to unpredictable economic and ecological circumstances. Given the far-reaching implications of climate-induced stress on both mental and physical health, policymakers must integrate psychological resilience strategies into climate adaptation frameworks to mitigate the adverse effects of environmental crises on human well-being (Clayton et al., 2017).

8.3.4 Drought and depression

Depression constitutes a multifaceted mental health condition that may arise from the interplay of prolonged stress, persistent feelings of hopelessness, and adverse environmental circumstances. The condition is particularly salient in communities whose subsistence relies heavily on climate-dependent sectors such as agriculture and livestock production. In such contexts, environmental challenges like drought extend beyond financial losses, fostering heightened uncertainty and insecurity regarding future stability. The continued difficulty in securing reliable income and resources intensifies psychological strain, thereby reinforcing the deterioration of mental well-being over time.

Berry et al. (2010) introduced a causal framework elucidating how climate-induced environmental stressors disrupt economic and social structures, thereby increasing vulnerability to depressive disorders. Prolonged drought events, in particular, act as a catalyst for significant socioeconomic disruptions, including widespread job losses, forced displacement, and the erosion of established social support systems. These factors, when combined, create conditions conducive to the emergence and persistence of chronic depression among affected individuals. The weakening of community cohesion and the breakdown of traditional coping mechanisms further compound the psychological burden, making it increasingly difficult for individuals to adapt to environmental adversities. Additionally, the cumulative effects of recurrent climate-related crises contribute to a sense of learned helplessness, wherein individuals perceive their circumstances as insurmountable, leading to long-term declines in mental health. Given the profound implications of these environmental and socioeconomic stressors, it is imperative to implement targeted intervention strategies that address both the immediate psychological impacts and the broader structural vulnerabilities that exacerbate depression in climate-affected communities.

8.3.5 Drought and anxiety

Anxiety is a mental health condition characterized by excessive worry and stress, often linked to uncertainty about the future. In communities where livelihoods depend on water and agriculture, drought creates ongoing economic insecurity and uncertainty, leading to heightened anxiety levels.

According to the *Mental Health and Our Changing Climate* report, environmental disasters significantly contribute to increased anxiety and stress-related disorders. Since drought is largely beyond individual control, prolonged exposure to water scarcity fosters a sense of helplessness and intensifies fears about the future (Clayton et al., 2017). Individuals living in rural areas experience significant economic hardship during periods of drought, and this financial pressure plays a key role in the development of anxiety disorders. The study also found that women and elderly individuals were particularly vulnerable, reporting more intense symptoms of anxiety (O'Brien et al., 2014).

8.3.6 Drought and posttraumatic stress disorder

Post-traumatic stress disorder (PTSD) is a psychological condition that may develop following exposure to uncontrollable and highly distressing events. Situations such as drought-induced displacement, economic decline, or social instability can create conditions under which individuals are more likely to exhibit trauma-related symptoms and experience post-traumatic stress responses.

PTSD is a severe psychological condition that is intricately linked to a wide range of co-occurring mental health challenges including substance use disorders, major depressive episodes, generalized anxiety disorders, increased propensity for violence and aggression, interpersonal dysfunction, and significant occupational difficulties (Simpson et al., 2011). The complex nature of PTSD underscores its far-reaching implications, as individuals suffering from this disorder often experience persistent emotional dysregulation, heightened reactivity to stressors, and diminished capacity for adaptive coping mechanisms. These psychological disturbances not only impair individual well-being but also contribute to broader societal challenges such as decreased workforce productivity, social withdrawal, and elevated healthcare burdens.

Empirical evidence further highlights the profound impact of environmental stressors on PTSD prevalence and severity. For instance, research conducted by Kolassa et al. (2010) demonstrated that climate refugees who

have been exposed to multiple traumatic events exhibit significantly higher lifetime rates of P TSD and poorer recovery trajectories than those who have encountered fewer traumatic stressors. This finding suggests that cumulative exposure to environmental adversities exacerbates psychological vulnerability, prolonging the duration and intensity of PTSD symptoms. Similarly, Cianconi et al. (2020) established a direct correlation between environmental disasters and heightened PTSD risk, indicating that individuals affected by such crises are particularly susceptible to developing trauma-related psychopathologies.

Prolonged or recurrent natural hazards, particularly severe droughts, can exert sustained psychological pressure on individuals, leading to the gradual accumulation of traumatic experiences. Unlike sudden-onset disasters, slow-developing crises create a persistent sense of uncertainty that intensifies the mental burden on affected populations. In these contexts, economic instability, forced migration, and the weakening of social support networks further increase the risk of adverse psychological outcomes. Consequently, addressing the mental health implications of climate-related trauma requires a comprehensive approach that not only provides individual support but also strengthens community resilience and implements policies aimed at mitigating the detrimental effects of environmental crises on human well-being.

8.4 Drought and eco-anxiety

Eco-anxiety is defined by the American Psychological Association (APA) (Clayton et al., 2017) as the intense fear, worry, and stress that individuals experience in the face of climate change and environmental destruction. This is particularly prevalent in communities that experience the direct impacts of climate change.

Although eco-anxiety is not recognized as a medical condition, the APA defines it as "a chronic fear of environmental doom". Because eco-anxiety is a kind of belief in a poor quality of life in the future, psychologically, some people experience daily periods of grief and despair or exhibit sudden panic attacks. Some people may even decide not to have children (Arcanjo, 2019). With the increase in such studies and a greater understanding of the effects of climate change on well-being, the concept of eco-anxiety was included in the Intergovernmental Panel on Climate Change (IPCC) in 2018 (Gustafson et al., 2019).

Alternatively, climate change exerts profound and multifaceted effects on human psychology, primarily by intensifying the frequency, severity, and unpredictability of environmental disasters. The escalating occurrence of extreme weather events, prolonged droughts, and shifting climate patterns has given rise to significant psychological distress among individuals and communities. In recent years, the term eco-anxiety has been introduced to conceptualize the heightened levels of stress, worry, and emotional turmoil associated with the anticipation and reality of climate-related adversities (Clayton et al., 2017). Unlike conventional anxiety disorders, eco-anxiety is distinguished by its persistent, existential nature, as it stems from the recognition of large-scale environmental degradation and the perceived inadequacy of institutional responses to mitigate climate change.

One of the most immediate and tangible manifestations of climate change-induced psychological distress arises from prolonged droughts, which not only disrupt essential ecological and economic systems but also induce chronic uncertainty regarding future sustainability. Droughts contribute to severe resource scarcity, reductions in agricultural productivity, and the exacerbation of socioeconomic instability, all of which intensify psychological distress among affected populations. Beyond these direct consequences, droughts foster a pervasive sense of helplessness, as individuals feel powerless in the face of an unpredictable and worsening environmental crisis. Pihkala (2020) argues that this state of uncertainty and loss of control plays a pivotal role in the spread of eco-anxiety, reinforcing a continuous cycle of psychological distress that extends beyond directly impacted communities to the broader population.

The mental health impacts of climate change extend beyond immediate material or economic losses, shaping individuals' long-term sense of safety and overall well-being. As environmental disruptions linked to climate variability become increasingly frequent and intense, people may experience a diminishing trust in institutional responses, scientific solutions, and the capacity of their communities to adapt. This erosion of confidence can contribute to feelings of uncertainty, helplessness, and reduced motivation for future planning. Addressing these psychological challenges requires the incorporation of mental health considerations into broader climate adaptation efforts. Initiatives such as local resilience-building programs, accessible mental health resources, and public education campaigns play a critical role in supporting emotional coping strategies, fostering adaptive capacities, and promoting societal well-being amid ongoing environmental change.

8.5 The link between drought and eco-anxiety

8.5.1 Future anxiety and uncertainty

Drought gives rise to significant psychological strain by evoking fears that fundamental human needs—such as access to clean water and food—may become increasingly unattainable. One of the central mechanisms underlying eco-anxiety is the uncertainty surrounding the future, which is exacerbated by ongoing and unpredictable environmental degradation (Hickman et al., 2021). This phenomenon is especially pronounced among youth and children, who may internalize a sense of hopelessness when contemplating the long-term implications of climate-induced events such as drought. Empirical findings suggest that eco-anxiety is frequently associated with direct or anticipated experiences of environmental disruption. In particular, drought conditions appear to heighten this form of distress by eroding individuals' emotional connection to nature and fostering a perceived loss of control over their environment.

8.5.2 Economic anxieties and social collapse

Drought has a significant impact on the financial security of communities, especially in areas where people rely heavily on climate-sensitive activities such as farming and animal husbandry. Reductions in crop production and the scarcity of water needed for livestock create notable economic strain for individuals and families involved in these sectors. The drop in productivity can ripple through local economies, contributing to rising food costs, fluctuations in employment opportunities, and an increased need for external support or government assistance. These interconnected economic effects intensify overall community vulnerability and create additional challenges for maintaining stability in affected regions.

As a consequence, prolonged drought-induced economic instability manifests in multiple socioeconomic stressors, including widespread job losses, declining household incomes, and, in severe cases, forced migration due to the inability to sustain livelihoods in affected regions. The persistent uncertainty surrounding financial security fosters heightened psychological distress, as individuals struggle with mounting debts, an inability to meet basic needs, and the erosion of long-term economic prospects (O'Brien et al., 2014). The financial pressures caused by drought can place a considerable mental burden on affected individuals, often leading to increased anxiety, prolonged stress, and in some cases, symptoms associated with depression. The interplay between resource scarcity and economic

instability emphasizes the importance of interventions that address both material hardships and psychological well-being. Developing targeted economic support programs, promoting community resilience, and providing accessible mental health resources are key strategies for mitigating the lasting social, economic, and emotional consequences of drought.

8.5.3 Strategies to mitigate drought-induced eco-anxiety

To enhance the psychological resilience of individuals and communities in the face of drought and eco-anxiety, several strategies can be implemented as follows:

- *Psychosocial Support Programs*: Expanding mental health services and providing psychological support in drought-affected communities can help individuals cope with environmental stressors.
- *Education and Awareness*: Teaching individuals how to manage climate-related challenges can reduce feelings of helplessness and foster proactive coping strategies (Pihkala, 2020).
- *Community Solidarity and Collective Action*: Strengthening social support networks and encouraging collective efforts to address environmental concerns can provide individuals with a sense of agency and belonging (Hickman et al., 2021).
- *Enhancing Climate Policies*: Developing sustainable water management and agricultural policies can help alleviate long-term economic and environmental concerns associated with drought (O'Brien et al., 2014).

8.6 Drought coping mechanisms

Psychosocial support plays a crucial role in increasing individual resilience during times of crisis (Berry et al., 2010). This is particularly important in rural communities, where strengthening social support networks can help mitigate the psychological effects of drought. Research conducted in rural Australia by O'Brien et al. (2014) found that individuals who had access to social support mechanisms during drought periods experienced lower levels of anxiety.

8.6.1 Cognitive and emotional coping strategies

Cognitive restructuring, which involves replacing negative thoughts with more constructive and realistic perspectives, is an effective strategy for

coping with the stress of drought (Clayton et al., 2017). In this respect, the following strategies can be recommended for further implementation:

- *Cognitive Restructuring*: Individuals are encouraged to shift their perceptions of uncontrollable environmental stressors, such as drought, and focus instead on making the best use of available resources (Reser & Swim, 2011).
- *Emotional Support*: Self-help groups and professional psychological support services can help reduce anxiety and stress, allowing individuals to manage the emotional burden of environmental crises more effectively.
- *Mindfulness and Stress Management Techniques*: Mindfulness is a valuable technique that helps individuals manage stress more healthily (Pihkala, 2020). Mindfulness-based interventions are particularly effective in addressing drought-related stress in communities that depend heavily on nature for their livelihoods (Hickman et al., 2021). In this regard, meditation, breathing exercises, and mindfulness-based cognitive therapy (MBCT) can be suggested for practical applications.

8.6.2 Policies and educational programs to enhance resilience

At the societal level, education and climate change adaptation strategies are essential tools for mitigating the far-reaching consequences of drought and enhancing community resilience. Education plays a dual role in this regard: first, it equips individuals with effective coping mechanisms to manage the psychological distress associated with environmental crises, thereby reducing the prevalence of anxiety, depression, and other stress-related disorders; and second, it fosters awareness and knowledge about sustainable agricultural practices, efficient water resource management, and climate-resilient farming techniques (Berry et al., 2010). By integrating climate change education into formal curricula and community outreach programs, societies can cultivate a proactive approach to environmental challenges, enabling individuals and communities to make informed decisions that enhance long-term sustainability.

A notable example of such an initiative is the Farm and Ranch Stress Assistance Network in the United States, which provides targeted stress management training to agricultural communities, helping them navigate the psychological and economic burdens associated with drought and other climate-related adversities (Wilner, 2024). Similar programs, when systematically implemented, not only offer crucial psychological support to individuals facing economic and environmental uncertainties but also

reinforce adaptive capacities by promoting innovative solutions to climate-induced disruptions. These initiatives serve to strengthen social cohesion, foster resilience, and enhance overall community well-being by addressing both the immediate mental health impacts of climate stressors and the structural challenges that exacerbate vulnerability.

Incorporating mental health initiatives into broader climate adaptation efforts is essential for fostering comprehensive resilience within communities. Programs that provide psychological support, facilitate peer networks, and ensure access to mental health services can help reduce the emotional strain associated with drought and prevent enduring psychological impacts. When combined with awareness and educational initiatives, such approaches promote the development of a mentally resilient and environmentally informed population, better equipped to respond to the growing challenges posed by climate variability.

8.7 Conclusion

Drought should not be viewed solely as an environmental issue but also as a significant mental health crisis. Individuals affected by drought need access to psychological support mechanisms, as prolonged exposure to environmental stressors can contribute to eco-anxiety, depression, and a sense of ecological grief. The uncertainty surrounding the future, economic insecurity, and disruptions in individuals' connection to nature weaken psychological resilience. Therefore, fostering mental health support systems, enhancing community resilience, and implementing sustainable policies are essential steps in mitigating the impact of environmental crises.

Drought is a complex crisis that must be addressed through ecological, economic, and psychosocial dimensions. Given the psychological toll of drought and climate change, it is imperative to restructure both environmental policies and mental health services to develop more effective interventions. Existing scientific research underscores the need for holistic approaches aimed at strengthening the psychological resilience of individuals and communities in response to these crises. Accordingly, drought-related policies should not be limited to environmental and economic measures but should also incorporate mental health support initiatives. In this regard, to promote effective coping mechanisms and resilience in response to drought, the following measures should be implemented:

- *Psychosocial support programs*: By expanding mental health services to assist individuals affected by drought.
- *Community-based interventions*: Strengthen social support networks to enhance community resilience.
- *Mindfulness programs*: Integrate mindfulness and stress management techniques into public health initiatives.
- *Education and awareness campaigns*: Provide training on water conservation, sustainable agriculture, and psychological resilience, particularly for farmers and rural populations.
- *Community resilience initiatives*: For developing training programs and social support mechanisms to help individuals adapt to environmental changes.
- *Early intervention strategies*: For incorporating mental health services into emergency response plans for environmental crises, to prevent the development of disorders such as depression and anxiety.

Addressing the psychological consequences of drought requires a multidimensional approach that combines mental health support, education, policy reforms, and community engagement. By adopting comprehensive strategies, societies can better prepare for and mitigate the long-term mental health effects of environmental crises.

As a result, the following are suggested for action:

- *Monitoring the Long-Term Psychological Effect*s: While most studies focus on the short-term impacts of drought,such as stress and anxiety, there is limited systematic monitoring of its long-term psychological consequences including chronic stress, depression, and PTSD. Future longitudinal research is essential to better understand the enduring mental health outcomes associated with prolonged exposure to drought.
- *Examining Cultural and Regional Differences*: The psychological effects of drought and climate-related stress can vary significantly across cultures and regions. Comparative research is needed to investigate the resilience mechanisms, coping strategies, and psychosocial support systems employed by individuals in diverse cultural contexts.
- *Investigating Technology-Based Psychological Support Tools*: The effectiveness of mobile health applications and telepsychology tools in providing support to drought-affected populations—particularly in rural and hard-to-reach areas—should be systematically examined. These technology-based interventions may offer scalable and accessible solutions to address mental health needs in regions with limited resources.

The limitation of this study is mostly due to the limited number of studies available in the statement of the art for implementation, and not performing field sampling and observations. The reviewed studies also showed some insufficiencies related to the following topics:

- *Sampling Limitations and Representativeness*: Many studies are based on small, homogenous, or region-specific samples, limiting the ability to generalize findings to broader populations or culturally diverse groups.
- *Cross-Sectional Research Designs*: Research on the psychological impacts of drought often relies on cross-sectional data, which limits the capacity to establish causal inferences and fails to capture long-term mental health outcomes.
- *Neglect of Cultural and Contextual Factors*: Cultural beliefs, coping styles, and social norms influence how individuals respond to environmental stressors. However, many studies fail to consider these contextual variables, limiting the depth of interpretation.
- *Overlooking Complex Contributing Factors*: Multiple cooccurring factors such as economic hardship, migration, agricultural losses, and lack of social support often accompany drought conditions. However, many studies fail to adequately control for these variables, making it difficult to isolate and clarify the specific psychological impacts of drought.
- *Time and Resource Constraints*: The investigation of long-term environmental issues such as drought often requires substantial time, financial resources, and institutional support. A lack of these elements can limit the depth, scope, and continuity of research efforts in this field.

AI disclosure

During the preparation of this work, the author(s) used ChatGPT to enhance the quality of the grammar and proofreading. After using this tool/service, the author(s) reviewed and edited the content as needed and take(s) full responsibility for the content of the publication.

References

Arcanjo, M. (2019). *Eco-anxiety: Mental health impacts of environmental disasters and climate change*. A Climate Institute Publication.

Atay, H., Tüvan, A., Demir, Ö., & Balta, İ. (2012). *The impacts of climate change on health: An overview of the relationship between climate and health—Diseases, vulnerable groups, adaptation, and recommendations*. Republic of Turkey Ministry of Forestry and Water Affairs, General Directorate of Meteorology, Research Department, Climatology Division.

Barreau, T., Conway, D., Haught, K., Jackson, R., Kreutzer, R., Lockman, A., & Wilken, J. A. (2017). Physical, mental, and financial impacts from drought in two California counties, 2015. *American Journal of Public Health, 107*(5).

Berry, H. L. (2009). Social capital and mental health among indigenous Australians, new Australians and other Australians living in a coastal region. *Advances in Mental Health, 8*.

Berry, H. L., Bowen, K., & Kjellstrom, T. (2010). Climate change and mental health: A causal pathways framework. *International Journal of Public Health, 55*(2).

Carleton, T. A. (2017). Crop-damaging temperatures increase suicide rates in India. *Proceedings of the National Academy of Sciences, 114*(33), 8746–8751. https://doi.org/10.1073/pnas.1701354114.

Cianconi, P., Betrò, S., & Janiri, L. (2020). The impact of climate change on mental health: A systematic descriptive review. *Frontiers in Psychiatry, 11*, 74.

Clayton, S., Manning, C. M., Krygsman, K., & Speiser, M. (2017). *Mental health and our changing climate: Impacts, implications, and guidance*. American Psychological Association & ecoAmerica.

Coêlho, A. E., Adair, J. G., & Mocellin, J. S. (2004). Psychological responses to drought in northeastern Brazil. *Revista Interamericana de Psicologia/Interamerican Journal of Psychology, 38*(1). https://doi.org/10.30849/rip/ijp.v38i1.845.

Cunsolo, A., & Ellis, N. R. (2018). Ecological grief as a mental health response to climate change-related loss. *Nature Climate Change, 8*(4), 275–281. http://www.nature.com/nclimate/index.html https://doi.org/10.1038/s41558-018-0092-2, http://www.nature.com/nclimate/index.html.

Doherty, T. J., & Clayton, S. (2011). The psychological impacts of global climate change. *American Psychologist, 66*(4), 265–276. https://doi.org/10.1037/a0023141.

Edwards, B., Gray, M., & Hunter, B. (2015). The impact of drought on mental health in rural and regional Australia. *Social Indicators Research, 121*(1). https://doi.org/10.1007/s11205-014-0638-2.

Fisher, A. (2016). Going deep: a review of environmental melancholia: psychoanalytic dimensions of engagement by Renee Lertzman. *Ecopsychology, 8*(3), 133–138. https://doi.org/10.1089/eco.2016.0021.

Fritze, J. C., Blashki, G. A., Burke, S., & Wiseman, J. (2008). Hope, despair and transformation: Climate change and the promotion of mental health and wellbeing. *International Journal of Mental Health Systems, 2*. https://doi.org/10.1186/1752-4458-2-13.

Gustafson, A., Leiserowitz, A., & Maibach, E. (2019). *Americans are increasingly 'Alarmed' about global warming*. Yale Program on Climate Change Communication.

Hanigan, I. C., Butler, C. D., Kokic, P. N., & Hutchinson, M. F. (2012). Suicide and drought in New South Wales, Australia, 1970–2007. *Proceedings of the National Academy of Sciences, 109*(35), 13950–13955. https://doi.org/10.1073/pnas.1112965109.

Hickman, C., Marks, E., Pihkala, P., Clayton, S., Lewandowski, R. E., Mayall, E. E., Wray, B., Mellor, C., & van Susteren, L. (2021). Climate anxiety in children and young people and their beliefs about government responses to climate change: A global survey. *The Lancet Planetary Health, 5*(12), e863. https://www.journals.elsevier.com/the-lancet-planetary-health https://doi.org/10.1016/S2542-5196(21)00278-3, https://www.journals.elsevier.com/the-lancet-planetary-health.

Kevin, J., Coyle, J. D., & Susteren, M. D. (2012). *The psychological effects of global warming on The United States: And why the US mental health care system is not adequately prepared*. National Wildlife Federation.

Kolassa, I. T., Ertl, V., Eckart, C., Kolassa, S., Onyut, L. P., & Elbert, T. (2010). Spontaneous remission from PTSD depends on the number of traumatic event types experienced. *Psychological Trauma: Theory, Research, Practice, and Policy, 2*(3), 169–174. https://doi.org/10.1037/a0019362.

O'Brien, L. V., Berry, H. L., Coleman, C., & Hanigan, I. C. (2014). Drought as a mental health exposure. *Environmental Research, 131*. https://doi.org/10.1016/j.envres.2014.03.014.

Pihkala, P. (2020). Eco-anxiety and environmental education. *Sustainability, 12*(23), 10149. https://doi.org/10.3390/su122310149.

Republic of Turkey, Ministry of Environment, Urbanization and Climate Change. (2019). *Turkey climate change Report 2019*. Republic of Turkey, Ministry of Environment, Urbanization and Climate Change.

Reser, J. P., & Swim, J. K. (2011). Adapting to and coping with the threat and impacts of climate change. *American Psychologist, 66*(4), 277–289. https://doi.org/10.1037/a0023412.

Simpson, D. M., Weissbecker, I., & Sephton, S. E. (2011). Extreme weather-related events: Implications for mental health and well-being. In I. Weissbecker (Ed.). *Climate change and human well-being: Global challenges and opportunities*. Springer, Verlag.

Vins, H., Bell, J., Saha, S., & Hess, J. J. (2015). The mental health outcomes of drought: A systematic review and causal process diagram. *International Journal of Environmental Research and Public Health, 12*(10), 13251–13275. http://www.mdpi.com/1660-4601/12/10/13251/pdf https://doi.org/10.3390/ijerph121013251, http://www.mdpi.com/1660-4601/12/10/13251/pdf.

Wilner, S. (2024). *NH farm and ranch stress assistance network impact report: Addressing the root causes of stress, mental health, and suicide in the farming community*. University of New Hampshire Cooperative.

World Economic Forum (WEF). (2021). The global risk report 2021. accessible through https://www.weforum.org/reports/the-global-risks-report-2021.

This page intentionally left blank

SECTION II

Drought management

This page intentionally left blank

CHAPTER NINE

Policy and governance in drought studies

Mustafa Utku Yilmaz[1], **and Hulya Yilmaz**[2]
[1]Department of Civil Engineering, Kirklareli University, Kirklareli, Türkiye,
[2]Quality and Accreditation Office, Kirklareli University, Kirklareli, Türkiye

9.1 Introduction

The intensity and severity of droughts are expected to increase significantly due to the impacts of climate change (Liu et al., 2018; Ozcelik et al., 2024). Drought refers to a prolonged water shortage that develops in stages. It often begins as a meteorological drought, where a region experiences an extended period of below-average rainfall. This reduces soil moisture, leading to agricultural drought and lower crop yields. As the drought continues, surface and groundwater levels decline, resulting in hydrological drought. In its final stage, socioeconomic drought emerges, affecting human activities, economies, and regional development (Mishra & Singh, 2011; Wilhite & Glantz, 1985; Yilmaz, 2023). The impacts of drought result from various climatic factors and levels of societal resilience, and they are felt at local, national, regional, and global scales. Therefore, the increasing impact of drought on various sectors has attracted considerable research attention (Wilhite et al., 2007; Yilmaz & Yilmaz, 2022).

Drought governance and risk management are highly complex, as they involve an interconnected system affecting various fields such as agriculture, industry, ecology, energy, food, and health (Gharehbaghi et al., 2025; Mersin et al., 2022). The presence of multiple stakeholders, each with varied priorities, further increases this complexity (Yilmaz, 2025). However, due to the nature of governance, it is essential to involve various stakeholders in the system. Beyond stakeholder participation, governance refers to the set of strategies and policies developed to effectively manage drought risks and reduce their negative impacts. Typically, drought management strategies can be divided into reactive and proactive approaches. While responding to crises is a necessary component of any risk management system, shifting towards proactive drought management

Drought Dynamics
DOI: https://doi.org/10.1016/B978-0-443-34205-9.00011-1
© 2026 Elsevier Inc. All rights are reserved, including those for text and data mining, AI training, and similar technologies.

(including public education, legislation, reliable drought forecasting, public participation in water conservation, and risk-sharing systems) is crucial for enhancing overall resilience. Proactive drought management not only mitigates the immediate impacts of drought but also fosters long-term adaptation and sustainability. As droughts become more frequent, coordination will increasingly be essential (Zhang et al., 2016). In conclusion, drought risk governance should involve decision-making processes at multiple levels to reduce the potential impacts of water scarcity on people, nature, and resources. It must also incorporate various stakeholders and ensure the establishment of solid and reliable agreements (Jalink & Dieperink, 2024).

The concept of governance includes elements such as the blending of public and private resources (Peters & Pierre, 1998). This implies that both resources and responsibilities should be considered in governance. In contrast to traditional governance models that rely on single-stakeholder initiatives, contemporary governance is characterized by multi-stakeholder collaboration across various scales and levels. Centralized, hierarchical governance approaches and reliance on a single scale can increase vulnerabilities related to climate change (Motsumi et al., 2023). Therefore, to address the complex issues created by climate change, there is a need for more inclusive, multi-level, and adaptable governance approaches. In this context, the Benefit of Governance in Drought Adaptation (DROP) project aimed to enhance drought preparedness and resilience in the Northwest European region. In this project, drought situations in six regions from Germany, Belgium, France, the United Kingdom, and the Netherlands were examined, evaluating the measures taken and the role of governance in their implementation (Bressers et al., 2016). The project developed a Governance Assessment Tool (GAT) that examines governance across five dimensions: levels and scales, problem perceptions and goal aspirations, actors and networks, responsibilities and resources, and strategies and tools. Additionally, it incorporates four key criteria: scope, consistency, flexibility, and intensity. Further, key principles for climate adaptation governance were evaluated using five governance principles and 17 indicators (de Bruijn & Dieperink, 2022). Their proposed framework can be employed to determine the strengths and weaknesses of governance and is useful for determining areas for improvement.

Previous studies on drought governance have generally focused on planning, legislation, and governance dimensions. However, drought is

not solely a concern for water managers; it also directly affects sectors that rely on water, including agriculture, tourism, industry, energy, and transportation. Additionally, considerable research exists on the psychological and social impacts of drought (Abunyewah et al., 2024). The interplay among these factors further complicates the inherently complex nature of drought, thereby posing substantial challenges to effective governance and policy development. Nevertheless, a significant gap remains in systematically identifying and classifying the various factors that influence effective drought governance, particularly regarding their implications for policymaking and practical implementation. This chapter aims to identify and classify these factors, with a special focus on their policy-related implications.

The chapter highlights the complex interdependencies among governance factors and demonstrates how these insights can inform the development of more effective and resilient policy frameworks by applying the Matrice d'Impacts Croisés Multiplication Appliquée à un Classement (MICMAC) method (Duperrin & Godet, 1973). This analysis offers a clearer understanding of how various factors interact to shape governance outcomes, generating valuable insights that inform the development of more effective policy and governance strategies. To explore these issues, this chapter addresses the following research questions:

- **RQ1:** What are the key principles of effective drought governance?
- **RQ2:** How does stakeholder engagement impact the effectiveness of drought governance?
- **RQ3:** What are the factors influencing drought governance?
- **RQ4:** How can these factors be classified, and how do they contribute to policymaking?
- **RQ5:** What are the key challenges and barriers in drought governance and policymaking?

To address these questions, this chapter is structured as follows: Section 2 presents a conceptual framework outlining the fundamental principles of effective drought governance. Section 3 introduces the MICMAC method and explains its steps. Section 4 identifies the important factors influencing drought governance. Section 5 classifies these factors using the MICMAC method and emphasizes their interrelationships. Section 6 explores the challenges and barriers in drought governance. Finally, Section 7 synthesizes the key findings of the analysis and offers policy recommendations for drought governance.

9.2 Developing a framework for effective drought governance

This section explores the principles for effective governance presented in the literature. Eight key principles for effective governance in natural resource management were identified: accountability, adaptability, capability, fairness, inclusiveness, integration, legitimacy, and transparency (Lockwood, 2010). These principles aim to guide the management of natural resources by ensuring that governance processes are fair, transparent, and capable of adapting to changing conditions. Similarly, five core principles for climate adaptation governance namely transparency, accountability, inclusiveness, connectivity, and government effectiveness (de Bruijn & Dieperink, 2022). Notably, transparency, accountability, and inclusiveness are common to both studies. Connectivity and integration are closely related, with connectivity representing a broader concept. While connectivity and integration are closely linked, connectivity reflects a broader systemic perspective. Government effectiveness parallels capability, highlighting the importance of sufficient resources and skills in governance systems. Another contribution outlined seven governance principles including resilience, which introduces an adaptive dimension to the framework (Lockwood, 2010). In the context of drought risk governance, coordinated multi-level approaches have been emphasized, identifying five key dimensions for effective governance: administration, policy, information, capacity, and funding (Jalink & Dieperink, 2024). These dimensions highlight the need for an integrated approach to drought management, while also acknowledging the differences between international and national governance levels in addressing drought risks. To ensure that drought governance is effective in practice, these principles must be operationalized in ways that enhance institutional performance, policy implementation, and adaptive capacity. After reviewing related studies, a comprehensive framework of principles is proposed in Fig. 9.1.

Each of the principles plays a crucial role in ensuring that drought governance is effective, inclusive, and resilient in the face of increasing climate variability. For example, legitimacy requires governance authority to be established through democratic processes or stakeholder acceptance, and with integrity. Transparency ensures that decision-making processes in drought governance are open, with clear justifications and readily accessible information (de Bruijn & Dieperink, 2022). Accountability involves clearly defined roles and responsibilities, with mechanisms to ensure compliance

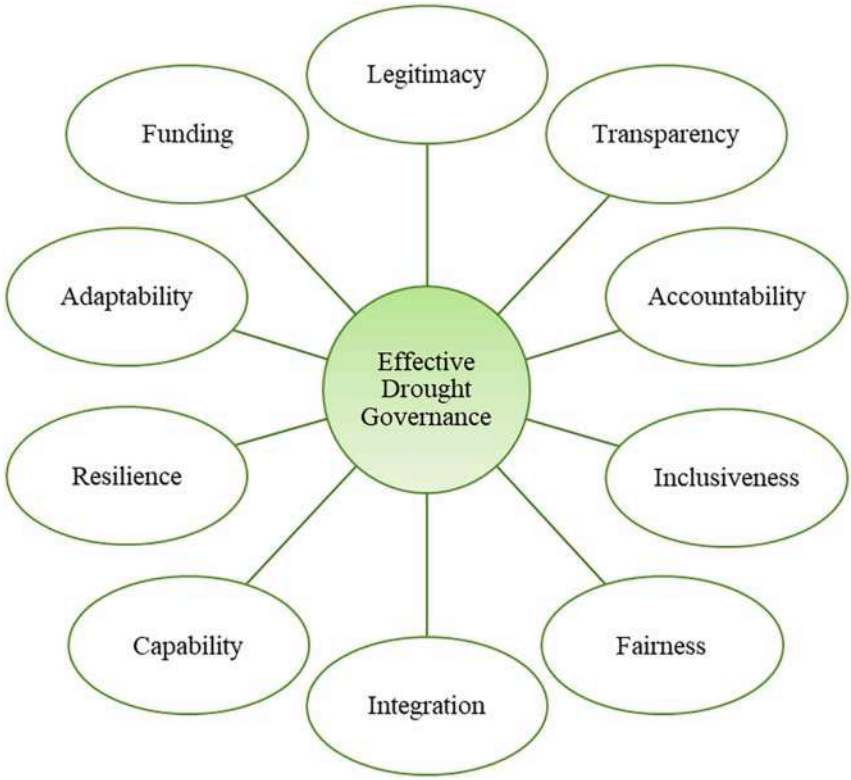


Figure 9.1 Principles for strengthening drought governance effectiveness color.

and effective implementation of drought management strategies. Stakeholder engagement plays a critical role in enhancing the effectiveness of governance (Yilmaz, 2025). Inclusiveness guarantees that all stakeholders, including local communities, policymakers, and scientists, have equal opportunities to participate, thereby fostering diversity and collaboration in developing drought adaptation and mitigation measures. Fairness demands that decisions are impartial, with a balanced distribution of costs and benefits. Integration promotes coordination among different levels and institutions to support sustainable resource management. Capability refers to the knowledge, skills, and resources necessary for governance bodies to carry out their duties. Adaptability ensures that governance systems remain flexible, can incorporate new scientific knowledge, and adjust to evolving drought conditions and socioeconomic challenges. Resilience underscores the need for systems that can reorganize and adapt without compromising

essential processes (Lockwood, Davidson, et al., 2010). Finally, adequate funding is essential for implementing drought policies and ensuring long-term water sustainability (Jalink & Dieperink, 2024).

These principles are interdependent and interact synergistically. For example, transparency and accountability reinforce one another, thereby enhancing legitimacy and building trust among stakeholders. Similarly, inclusiveness improves governance by integrating diverse perspectives into fair decision-making processes. In particular, inclusive governance structures that actively engage stakeholders not only enhance legitimacy but also contribute to more effective policy design and implementation, ensuring that governance frameworks address the specific challenges of different regions and communities. In addition, integration and connectivity promote coordination across governance levels, while adaptability and resilience enable systems to respond effectively to evolving environmental and social conditions. Thus, stakeholder engagement drives more responsive, equitable, and effective drought governance. To conclude, these principles form the basis for a robust and flexible governance framework capable of addressing the complex challenges posed by drought.

9.3 The Matrice d'Impacts Croisés Multiplication Appliquée à un Classement (MICMAC) method

The MICMAC method is a strategic management tool used to analyze and address complex problems. It also analyzes the interactions in the system and reveals the influence and dependence of one factor on others. This method examines the relationships among factors and classifies them (Godet, 1994). The steps of the method are as follows:

Step 1 - Identification of factors: Identify the factors that play an important role in the relevant field. To identify the factors, a detailed literature review can be conducted, industry reports can be analyzed, or expert opinions can be gathered.

Step 2 - Analyzing direct relationships: The relationships among factors and the degree of these relationships are evaluated by experts. Experts can be selected from key stakeholders, industry professionals, or academics in the relevant field. To evaluate the direct relationships among factors, the scale is given in Table 9.1(Bagherian et al., 2024). Further, Fig. 9.2 shows an example structural diagram for factor direct relationships.

Table 9.1 Linguistic variables scale.

Linguistic variable	Value
No influence	0
Very low influence	1
Low influence	2
High influence	3
Very high influence	4

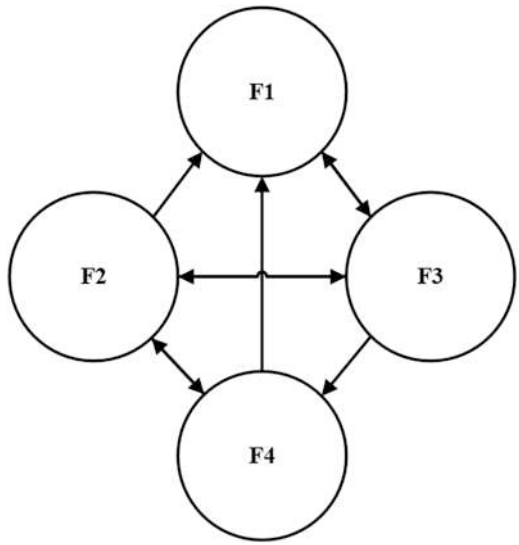


Figure 9.2 An example of a structured diagram not color.

The data collected from the experts is kept in the form of an $n \times n$ matrix (where n is the number of factors). Here, n x ($n-1$) evaluations are required for n factors.

Step 3 - Analyzing indirect relationships: When determining the relationships between two factors, indirect relationships should be analyzed in addition to direct relationships. Because considering only direct relationships may not be sufficient to represent the complex structure. Indirect relationships, which are very difficult to evaluate by experts, are determined by taking the powers of the direct relationship matrix. This powering process continues until the order of the row and column sums of

two consecutive powers is the same. In general, this process stabilizes after a multiplication degree of three, four, or five (Godet, 1994).

Step 4 - Drawing influence-dependence charts and interpreting the results: Both the direct relationships obtained in the second step and the indirect relationships obtained in the third step are used to create influence-dependency charts. An influence-dependency chart developed using the relationships is shown in Fig. 9.3 as an example (Godet, 1994). In this chart, the *x*-axis shows the degree of dependency of the factor, and the *y*-axis shows the degree of influence of the factor.

Factors are categorized into four groups: influential factors, linkage factors, dependent factors, and autonomous factors. The thresholds dividing the four regions are usually taken as average values. The influential factors have a high influence and low dependency level, and these factors are the most important. Because they have a significant influence on other factors and are little influenced by others. Linkage factors have a high influence and a high dependence level, and these factors affect other factors. Similarly, changes in other factors affect the factors in this cluster. Factors in this category are not stable because any influence or feedback on them can affect the system. Dependent factors display influence and high

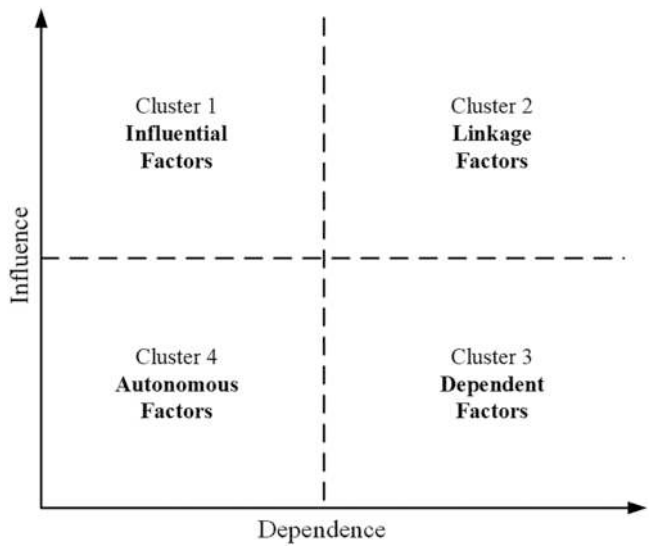


Figure 9.3 Influence-dependence chart of Matrice d'Impacts Croisés Multiplication Appliquée à un Classement analysis not color.

dependence levels and are highly dependent on other factors in the system. Autonomous factors have a low level of influence and a low level of dependence and thus lack a significant connection with the whole system.

The MICMAC method has been used in different fields such as agriculture (Barati et al., 2019), construction (Jung et al., 2021), digital services (Favoretto et al., 2024), education (Yilmaz & Yanik, 2025), energy (Bagherian et al., 2024), supply chain (Sharma et al., 2021), sustainable food management (Ashrafi & Maoua, 2024), and wastewater management (Nazlabadi et al., 2023). However, the classification of factors has not yet been addressed in the context of drought governance. Therefore, in this chapter, the effective factors in drought governance will be classified using the MICMAC method. The factors discussed in the next section are defined and detailed.

9.4 Identifying factors influencing drought governance

Water scarcity is the primary cause of drought, but many other factors exacerbate and intensify its impacts (Bokal et al., 2014). These interconnected factors form a complex network of interactions, making drought management more challenging. Understanding these interactions is crucial for developing effective governance strategies and facilitating the formulation of appropriate drought policies (Motsumi et al., 2023). Below are the key factors influencing drought governance.

9.4.1 Climatic and meteorological factors

Drought is typically caused by a temporary change in the usual precipitation patterns; however, other climatic factors, including high levels of temperature and low levels of relative humidity, can significantly increase the intensity of the event (Naumann et al., 2021). This situation leads to destructive impacts not only on water resources but also on agriculture and ecosystems. Climate change is expected to further complicate these processes, with predictions indicating that droughts will become more severe in the forthcoming years (Dobler-Morales & Bocco, 2021). The accuracy of meteorological data plays a critical role in determining the capacity of drought prediction systems and ultimately contributes to policy processes. Improving data quality will allow for the development of more effective strategies to combat drought. Moreover, the impacts of drought and climate change vary regionally, making it essential to understand how

policies implemented in different climatic regions diverge and how these differences are reflected in policymaking processes. This diversity highlights the need for solutions tailored to local needs.

9.4.2 Economic factors

Drought causes a complex network of impacts across various sectors of the economy including agriculture, livestock, energy, tourism, and transportation services (Naumann et al., 2021). Agriculture is particularly vulnerable because it directly depends on soil moisture (Dobler-Morales & Bocco, 2021). The most obvious and immediate effect of drought is the reduction in crop yields, which extends far beyond farmers to affect communities that rely on agriculture for their livelihoods (Bokal et al., 2014). Additionally, drought can increase food prices, disrupt trade, and strain local economies, particularly in regions heavily dependent on agriculture. It can lead to shortages in food production, disrupting both local and international trade (Gil et al., 2013). The economic impact of disrupted supply chains can result in higher food and water prices, affecting consumers, businesses, and governments. Governments and businesses must adapt to these economic challenges by investing in drought-resistant crops and water-efficient technologies, thereby mitigating financial impacts. Furthermore, economic resources are required to fund long-term drought adaptation measures including research into drought-resistant crops, the construction of reservoirs, and investments in water-efficient technologies. While these investments can be costly, they are crucial for long-term economic sustainability in drought-prone regions.

9.4.3 Technological factors

The integration of new technologies, including artificial intelligence, remote sensing, and data analytics, into policy processes is crucial for effective drought management and adaptation. The importance of developing appropriate technologies and facilitating technology transfer to reduce drought recurrence and enhance adaptive capacity has been underscored. Moreover, the need to establish community-centered early warning and information management systems to monitor drought variability was also emphasized (Kamara et al., 2020). These technological advancements improve the accuracy of drought risk prediction and enable policymakers to make more informed decisions. Moreover, the adoption of information and communication technologies in drought governance has been shown to enhance stakeholder coordination and streamline data sharing, contributing to more dynamic and efficient policy responses.

9.4.4 Environmental factors

Drought impacts natural resources in a variety of ways including adverse effects on water resources, biodiversity, water quality, forest fire risk, and soil structure (Bokal et al., 2014). The environmental changes caused by drought, such as deforestation, the deterioration of water and soil systems, and alterations in ecosystems, pose serious threats to community living conditions and the economy (Kamara et al., 2020). The pressure on water resources necessitates the restructuring of water management policies and the development of strategies for efficient water use and distribution (Bokal et al., 2014). Therefore, drought mitigation policies must not be confined solely to water management but should also encompass soil conservation, forest management, and ecosystem restoration (Kamara et al., 2020). Furthermore, these environmental factors compel national and local policymakers in drought management to integrate agriculture, water, and energy policies.

9.4.5 Social factors

Social factors influencing drought governance include community participation, community resilience, social capital, and socioeconomic inequalities. These factors play a crucial role in the formulation and implementation of drought policies. Community participation is essential for balancing supply- and demand-driven drought management by promoting sustainable practices. Additionally, it enhances public engagement in decision-making processes and strengthens collaboration between local governments and policymakers (Lindsay et al., 2017). The recurring impacts of drought lead to the development of varying coping and adaptation capacities, which manifest through shared values, experiences, commitment, and the ability to acquire and exchange knowledge (Kamara et al., 2020). Social capital influences migration decisions in response to the drought, which in turn shapes policy development (Haeffner et al., 2018). Urban and rural communities experience drought differently, with rural populations, particularly farmers, being more vulnerable due to their dependence on land and water resources (Lindsay et al., 2017). Moreover, socioeconomic disparities exacerbate drought vulnerability, as low-income communities often lack access to critical resources and infrastructure. This situation underscores the need for equitable resource allocation and effective planning of social assistance programs in governance processes.

Additionally, cultural perceptions of drought shape public awareness and influence water governance policies. A comprehensive understanding of these social dimensions is essential for formulating inclusive, adaptive, and effective drought policies.

9.4.6 Institutional factors

This factor encompasses organizational culture, the integration of information among relevant institutions and stakeholders, the implementation of early warning systems, and the provision of public and institutional education. The literature emphasizes the importance of integrating information both top-down and bottom-up in the context of drought (Bretan & Engle, 2017). For example, public awareness of early warnings, the use of early-maturing seeds, and traditional practices such as intercropping have contributed to community adaptation to drought conditions (Kamara et al., 2018). Furthermore, local data on weather and drought forecasts can be shared through official channels to support early warning systems. These systems enhance preparedness by evaluating the impact of drought forecasts and enabling informed decision-making (Wittrock et al., 2011). Drought-related education is another critical factor that influences vulnerability and resilience. The importance of educational initiatives in both public and private sectors for effective drought preparedness was emphasized, noting that inadequate education may hinder institutional management (Zaidi & Pelling, 2014). Another key aspect of institutional factors is the governance structure, which delineates the responsibilities of local, national, and international institutions (Herrfahrdt-Pähle et al., 2020). Once established, coherent policies must be developed across sectors such as water resources, agriculture, and energy. The level of stakeholder participation in these policy processes is crucial, as each stakeholder can affect the system differently or be influenced by others. This topic is discussed in detail in the following section.

9.4.7 Collaboration among stakeholders

A fundamental pillar of drought governance is collaboration among stakeholders. Identifying interactions among actors from different decision-making levels and sectors is crucial in this process (Motsumi et al., 2023). Involving diverse stakeholders not only increases the integrative nature of the governance process but also strengthens management efforts by incorporating multiple perspectives (Yilmaz, 2025). Therefore, improving the effectiveness of drought governance requires not only

national level engagement but also the active participation of local actors, non-governmental organizations, relevant experts, and the public in decision-making processes (Motsumi et al., 2023). More specifically, facilitating the continuous sharing of information, data, and knowledge among stakeholders facilitates overcoming challenges in drought management (Bretan & Engle, 2017). Within this regard, the development of international cooperation models for transboundary water resources is essential for effective drought risk management (Bokal et al., 2014). Indeed, a proper understanding of transboundary drought risks is an integral part of risk reduction strategies (Krishna Prabhakar, 2022). Furthermore, ensuring the financial sustainability of the governance process requires mechanisms such as participating in international agreements, establishing bilateral relations with foreign governments, and fostering cooperation with donors (Motsumi et al., 2023).

9.4.8 Preparedness planning and risk management

Risk management through preparedness and mitigation measures is a core principle of drought governance. These measures must be ready for deployment as drought conditions arise, and they should be adaptable to different sectors, regions, and population groups. Key actions include integrated monitoring, early warning systems, the development of preparedness plans at various government levels, the adoption of mitigation programs, and the establishment of emergency response networks (Wilhite, 2009). A critical aspect of addressing drought risk is understanding vulnerability. Assessing drought vulnerability involves identifying key factors and evaluating the levels of vulnerability, which is essential for developing effective mitigation and adaptation strategies (Kukuntod & Wijitkosum, 2024).

9.4.9 Mitigation planning and crisis management

Governments often view drought as a rare and unpredictable event, leading to limited or no preparedness planning until the next occurrence. However, since drought is a normal part of the climate, strategies for mitigating its effects and responding to emergencies should be clearly defined in advance (Bokal et al., 2014). Effective drought management can be supported by developing preparedness plans at various government levels, adopting mitigation actions and programs, establishing emergency response networks that provide timely and targeted aid, and fostering an organizational structure that enhances coordination among government

levels and stakeholders (Wilhite, 2009). Furthermore, long-term strategies should be designed even in non-drought periods, while community engagement and stakeholder involvement are crucial to ensure an inclusive and effective response (Yilmaz, 2025).

9.4.10 Legal regulations

Legal regulations are essential for effective drought governance and policy as they provide clear guidelines for managing the agriculture, energy, and environmental sectors. Robust legal frameworks are emphasized as crucial for coordinating efforts across various levels and for ensuring that policies remain enforceable and adaptable to changing conditions (Bokal et al., 2014). Moreover, given that many river basins span national borders, regional integration of drought monitoring and early warning systems is often insufficient. This shortfall calls for internationally integrated legal approaches and harmonized standards at both national and local levels. Establishing financial incentives and support mechanisms to promote technology transfer and investment in drought management infrastructure is essential for enhancing policy outcomes. Together, these components form a comprehensive legal framework that supports effective, coordinated, and adaptive responses to drought challenges.

9.5 Classification of factors using the Matrice d'Impacts Croisés Multiplication Appliquée à un Classement (MICMAC) method

This section presents the classification of factors influencing drought governance. These factors, which are described in detail in Section 4, are summarized in Table 9.2. The MICMAC analysis used the Delphi method to identify direct relationships among factors. This method, which involves the systematic collection and evaluation of expert opinions, facilitates consensus among decision-makers (Linstone & Turoff, 1975).

Table 9.3 presents the direct relationships among the factors, as identified by experts using the Delphi method. The Delphi assessment process involved multiple iterative rounds, where experts independently assessed the degree of direct influence each factor exerts on the others. The evaluations were based on the linguistic scale defined in Table 9.1, ranging from No influence (0) to Very high influence (4). After each round, anonymized group feedback was provided to the experts to refine

Table 9.2 Factors influencing drought governance.

Code	Factors	References
F1	Climatic and meteorological	Dobler-Morales and Bocco (2021), Naumann et al. (2021)
F2	Economic	Gil et al. (2013), Naumann et al. (2021)
F3	Technological	Kamara et al. (2020)
F4	Environmental	Bokal et al. (2014), Kamara et al. (2020)
F5	Social	Lindsay et al. (2017), Haeffner et al. (2018)
F6	Institutional	Wittrock et al. (2011), Zaidi and Pelling (2014), Herrfahrdt-Pähle et al. (2020)
F7	Collaboration among stakeholders	Yilmaz (2025), Bretan and Engle (2017), Krishna Prabhakar (2022), Motsumi et al., 2023
F8	Preparedness planning and risk management	Wilhite et al. (2007), Kukuntod and Wijitkosum (2024)
F9	Mitigation planning and crisis management	Yilmaz (2025), Wilhite et al. (2007), Bokal et al. (2014)
F10	Legal regulations	Bokal et al. (2014)

Table 9.3 Direct relationships among factors.

Factors	F1	F2	F3	F4	F5	F6	F7	F8	F9	F10
F1	-	3	1	4	2	1	1	3	3	1
F2	0	-	1	0	2	3	1	1	1	1
F3	0	2	-	0	1	2	2	3	2	1
F4	0	1	2	-	3	2	2	1	2	1
F5	0	0	1	2	-	2	2	2	2	1
F6	0	3	2	2	3	-	3	4	3	3
F7	0	2	3	2	3	2	-	4	3	2
F8	0	3	0	3	2	3	3	-	3	0
F9	0	1	0	2	1	2	1	2	-	0
F10	0	2	2	1	2	3	3	3	2	-

individual judgments and facilitate convergence toward consensus. The final influence matrix in Table 9.3 reflects the aggregated expert assessments, representing the direct relationships between factors. Fig. 9.4 shows the graphical representation of these direct relationships. F1 (climatic and meteorological), F6 (institutional), F7 (collaboration among stakeholders), and F8 (preparedness planning and risk management) emerge as factors with strong relationships. On the other hand, F2 (economic), F5 (social),

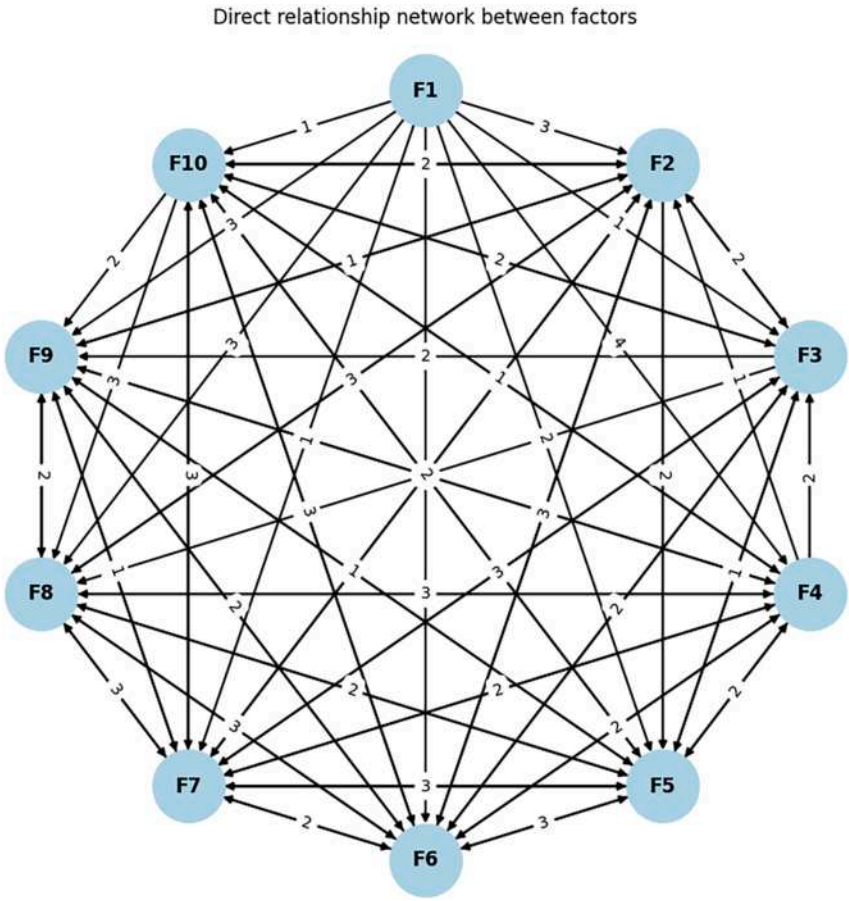


Figure 9.4 Direct relationship network among factors color.

and F9 (mitigation planning and crisis management) show weaker relationships, with more bounded interactions. This suggests that these factors have less direct impact and their interactions are more limited in scope.

After identifying the direct relationships among the factors, the analysis proceeds to evaluate indirect relationships, as outlined in Step 3 of the MICMAC Method. Indirect relationships among factors were calculated through successive matrix multiplications, following the MICMAC analysis framework (Godet, 1994). Specifically, starting from the direct influence matrix (first matrix), matrix exponentiation was performed by multiplying the matrix by itself iteratively. This process captures higher-order (indirect)

influences by considering paths of length two or more between factors. In the first iteration, the direct influence matrix is squared to obtain the second matrix, which incorporates first-degree indirect relationships through two-step interactions. The sums of each row and column in this matrix represent preliminary influence and dependency values for each factor. In the second iteration, the resulting second matrix is multiplied again by the original direct influence matrix to produce the third matrix, accounting for indirect relationships of a higher degree. Impact and dependency values are recalculated based on this updated matrix. This iterative process continues until the influence and dependence values converge that is, when two consecutive matrix powers yield stable results within a predefined tolerance. At this point, the final matrix effectively summarizes both direct and indirect relationships among factors. In this chapter, indirect relationships were identified after the second iteration, as convergence criteria were sufficiently met.

Table 9.4 shows the influence and dependence rankings for direct and indirect relationships. The rankings are largely similar, except for a few factors. The F1 (climatic and meteorological) shows a high dependence in both types of relationships but experiences a decrease in its influence ranking in indirect relationships. This indicates that the direct effects of the F1 are stronger, while their indirect effects are weaker. In addition, its position at the lowest rank for dependence indicates that it is less influenced by other factors. The dependence ranking of the F6 (institutional) factor places third in indirect relationships and second in indirect relationships,

Table 9.4 Influence and dependency rankings for direct and indirect relationships.

Factors	Direct relationship		Indirect relationship	
	Influence	**Dependence**	**Influence**	**Dependence**
F1	3	10	4	10
F2	9	6	9	6
F3	7	8	7	8
F4	6	7	6	7
F5	8	4	8	4
F6	1	3	1	2
F7	2	5	2	5
F8	5	1	5	1
F9	10	2	10	3
F10	4	9	3	9

indicating that the F6 exhibits reduced dependence in indirect relationships. The influence of F10 (legal regulations) is more significant in indirect relationships, suggesting that legal regulations exert more influence indirectly than directly. In conclusion, these findings demonstrate that the influence and dependence levels of various factors vary depending on their type and nature. The observed variability in dependence levels in indirect relationships underscores the necessity for a distinct evaluation of the direct and indirect effects of factors in complex systems, such as drought. Experts need to consider the role of factors in both relationship types to enhance comprehension of their dynamics and to adapt strategies accordingly.

Following the determination of direct and indirect relationships, the influence-dependence chart was created, utilizing the influence levels and dependency levels. The chart based on direct relationships is presented in Fig. 9.5. As all factors align within the same categories for indirect relationships, they were not incorporated separately. The influential factors area is the first category, containing two factors, followed by three factors in the linkage factors area, and four in the dependent factors area. F1 (climatic and meteorological) and F10 (legal regulations) are categorized as influential factors due to their significant role in drought governance, where they strongly influence the system while being minimally affected by

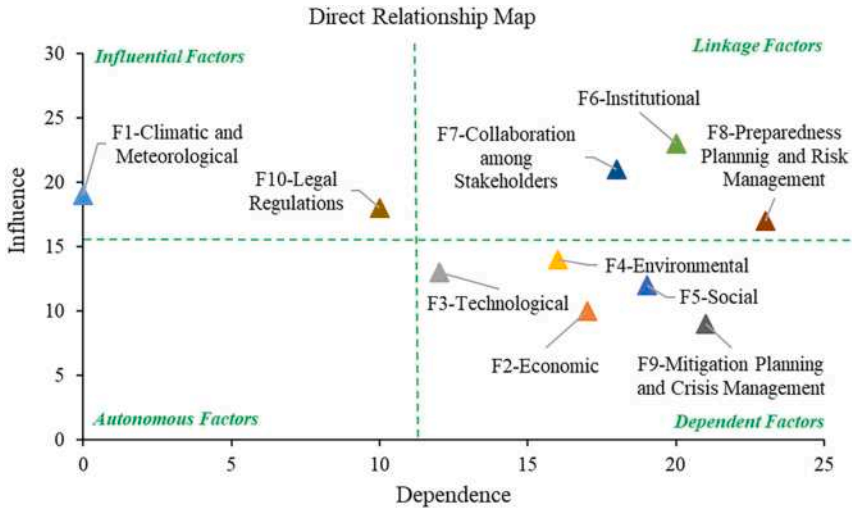


Figure 9.5 Influence and dependency chart according to direct relationships color.

other factors. The crucial role of climatic and meteorological factors in drought governance has been emphasized in previous studies (Naumann et al., 2021). These factors can directly trigger drought events or exacerbate their impact. F6 (institutional), F7 (collaboration among stakeholders), and F8 (preparedness planning and risk management) are identified as linkage factors. These factors significantly influence other factors in the system and are continuously engaged in interaction with feedback from them. F6 ensures the effective functioning of institutional structures, while F7 facilitates information and resource sharing through interactions with the external environment. Additionally, F8 fosters cooperation among stakeholders to improve preparedness for risks. F2 (economic), F3 (technological), F4 (environmental), F5 (social), and F9 (mitigation planning and crisis management) are categorized as dependent factors. These factors emerge as outcome-oriented elements influenced by other factors. Autonomous factors refer to independent elements that demonstrate a weak connection with the system in terms of both impact and dependency. However, according to expert opinions, no factors were defined in this category. This classification is based on expert views aimed at understanding the dynamics of drought governance, and it should be noted that some details may vary depending on the application and local context. Finally, the interaction among these factors highlights the fact that no single factor provides a solution on its own; rather, all factors must act together. Therefore, the interactions of such factors should be studied and evaluated for the formulation and development of appropriate policies in drought governance.

9.6 Challenges and barriers to effective drought governance

Effective drought governance requires addressing challenges that hinder the implementation of policies and strategies aimed at risk reduction and resilience building. These challenges include limited institutional and technical capacity, insufficient coordination, climate change, lack of financing, data gaps, low public awareness, and limited stakeholder engagement. Mitigating the impacts of drought requires strong political will; however, weak governance structures can significantly hinder policy implementation (Petersen-Perlman et al., 2022). Local, regional, and national agencies must be committed to executing comprehensive drought

strategies; however, a lack of political commitment can undermine long-term planning and the enactment of preventive measures (Haigh et al., 2023; Mullin & Rubado, 2017). Local authorities face considerable constraints, including financial, technical, and human resource limitations, which undermine their capacity to develop and enforce effective drought management policies (Haigh et al., 2023; Measham et al., 2011). Enhancing local capacities, especially in institutional strengthening and stakeholder collaboration, is essential for overcoming these challenges (Yilmaz, 2025). Moreover, the escalating effects of climate change exacerbate the risks posed by drought. Therefore, drought policies must integrate climate adaptation strategies to build community resilience (Herrfahrdt-Pähle et al., 2020; Wilhite, 2009). Addressing climatic and meteorological factors, as outlined in Fig. 9.5, is crucial for developing adaptive governance strategies that account for these heightened risks.

Another major barrier to effective drought governance is insufficient financial resources. Adequate funding is indispensable for the development of drought monitoring systems, the activation of early warning systems, and the strengthening of crisis management infrastructures. Financial constraints limit proactive interventions and hinder effective risk management (Haigh et al., 2023; Vargas & Paneque, 2017). In low-income regions, the scarcity and poor quality of drought-related data further hinder the establishment of reliable, real-time early warning systems (Vargas & Paneque, 2017). Moreover, methodological discrepancies across different disciplines complicate information sharing and coordination, exacerbating governance inefficiencies (Nohrstedt et al., 2021).

Beyond institutional and financial constraints, human behavior also significantly influences drought outcomes, particularly through traditional water management practices and public attitudes. Traditional water usage practices and insufficient public awareness can obstruct the implementation of modern, sustainable drought management strategies (Wilhite et al., 2014). Thus, public education and awareness campaigns are essential for increasing the effectiveness of drought policies. Additionally, social and cultural factors must be accounted for to ensure the widespread adoption of effective drought policies (Haigh et al., 2023). Furthermore, poor coordination among stakeholders significantly undermines the effectiveness of drought governance. Given that drought impacts multiple sectors and spans various administrative levels, successful drought management requires collaborative efforts from government agencies, industry representatives, non-governmental organizations, and local stakeholders. However,

conflicting interests, information gaps, and coordination failures can obstruct integrated management efforts.

Another complexity arises when droughts cross national borders, necessitating regional collaboration and careful identification of stakeholders. At the national level, drought management is typically the responsibility of local authorities, who collaborate with stakeholders that share a significant role in risk management and governance. However, for transboundary droughts, identifying the cross-border effects of droughts is often more complex. Therefore, it is imperative that cross-border impacts are closely analyzed, and appropriate stakeholders are identified and engaged (Krishna Prabhakar, 2022). As emphasized in Section 5, stakeholder involvement is critical in addressing the complexities inherent in drought governance.

In conclusion, drought governance is a complex, multidimensional challenge. While the obstacles outlined above limit the success of drought policies, they also present opportunities for systemic reform and improvement. Strong institutional cooperation, political commitment, adequate financing, and heightened public awareness are crucial for achieving effective drought governance. Success relies not only on technical and financial resources but also on the development of robust social, institutional, and stakeholder relationships. The factors discussed in Section 5 should be integrated to formulate effective drought policies. Without holistic, sustainable approaches, the risks associated with future droughts are likely to escalate. Hence, adopting an integrated approach that considers both direct and indirect relationships among factors, is essential for crafting effective and sustainable drought governance policies.

9.7 Conclusion and policy recommendations

Drought governance is a complex and multifaceted challenge that requires an integrated approach involving multiple stakeholders, institutions, and governance levels. This chapter has explored the fundamental aspects of drought governance by responding to the research questions introduced in the introduction.

First, effective drought governance is grounded in several key principles, including accountability, adaptability, capability, fairness, integration, inclusiveness, transparency, resilience, legitimacy, and adequate funding. These principles are crucial for ensuring that governance structures are

robust and responsive to evolving climatic and socioeconomic conditions. Transparency and accountability build trust and reinforce legitimacy, while inclusiveness fosters broader stakeholder participation. The ability to integrate different governance levels and adapt to emerging challenges enhances resilience against drought-induced disruptions. Without these principles, governance frameworks risk becoming ineffective, fragmented, or exclusionary.

Second, stakeholder engagement plays a central role in the success of drought governance. Inclusive governance structures that actively involve local communities, policymakers, scientists, and private sector actors enhance both legitimacy and policy effectiveness. Participation ensures that policies are tailored to regional and local needs, improving their feasibility and social acceptance. Moreover, collaboration among stakeholders facilitates knowledge exchange, resource sharing, and coordinated action, reducing inefficiencies and bridging governance gaps. However, barriers such as power imbalances, conflicting interests, and inadequate coordination mechanisms must be addressed to optimize stakeholder engagement.

Third, drought governance is influenced by various interrelated factors. These include climatic and meteorological, economic, technological, environmental, social, institutional, collaboration among stakeholders, preparedness planning and risk management, mitigation planning and crisis management, and legal regulations, as identified in Table 9.2. The interplay of these factors emphasizes the need for a systemic approach to drought governance, as no single factor is sufficient on its own for effective policy implementation.

Fourth, these factors can be classified based on an influence–dependence analysis. Influential factors (e.g., climatic and meteorological, legal regulations) shape the overall governance framework and are only slightly influenced by other factors. Linkage factors (e.g., institutional, collaboration among stakeholders, preparedness planning) serve as critical intermediaries that influence other components of governance while also being shaped by them. Dependent factors (e.g., economic, technological, environmental, social, and crisis management) are outcome-oriented elements that rely on other governance mechanisms for their development. This classification enables policymakers to prioritize interventions, ensuring that influential and linkage factors receive adequate attention to strengthen the overall governance framework. By addressing these factors, drought governance can become more responsive and resilient.

Finally, drought governance faces several key challenges and barriers, such as weak institutional and technical capacity, insufficient coordination, the impacts of climate change, lack of financing, data gaps, and limited stakeholder engagement. Governance failures often arise from fragmented responsibilities, weak enforcement mechanisms, and inadequate integration of scientific knowledge into decision-making. Additionally, financial constraints impede the development of effective monitoring systems and proactive risk management strategies. Strengthening governance structures, increasing financial resources, improving coordination across sectors, and investing in public awareness campaigns are essential to overcoming these barriers.

Building on the findings of this chapter, the following policy recommendations are suggested:

- *Development of an Integrated Drought Database*: A centralized, publicly accessible database should be established to enhance data sharing, improve drought preparedness, and facilate response coordination. This database should integrate meteorological, hydrological, and socioeconomic data, enabling real-time monitoring and predictive modeling.
- *Strengthening Institutional and Stakeholder Capacities*: Institutional frameworks should be reinforced by providing capacity-building programs for policymakers, local authorities, and water resource managers. Collaborative governance structures should be established to improve communication and knowledge exchange among stakeholders.
- *Alignment of National and Local Drought Management Plans:* Drought management plans should be aligned with national policies and include clear performance indicators to assess effectiveness. These plans should define thresholds for drought declarations and include mechanisms to prevent misuse of emergency resources.
- *Integration of Climate Adaptation into Drought Governance*: As climate change increasingly influences drought frequency and intensity, governance frameworks should integrate robust, long-term adaptation strategies to enhance resilience and sustainability. This includes promoting nature-based solutions, sustainable land management practices, and investments in climate-resilient infrastructure.
- *Improved Financial Mechanisms for Drought Resilience*: Sustainable financing mechanisms should be developed to support proactive risk management and crisis response. Investments should focus on early warning systems, water-saving technologies, and community-based resilience programs.

- *Enhancing Public Awareness and Behavioral Change*: Public awareness campaigns should be designed to educate communities on sustainable water use practices and the importance of drought preparedness.
- *Strengthening Cross-Border and Regional Cooperation*: Transboundary droughts require regional collaboration to ensure effective water management and policy coordination.

Drought governance requires an adaptive, comprehensive, and proactive approach. Classifying governance factors provides a structured understanding of underlying dynamics, helping policymakers identify and prioritize key intervention areas.

AI disclosure

During the preparation of this work the author(s) used Grammarly and ChatGPT in order to improve the language, clarity, and readability. After using this tool/service, the author(s) reviewed and edited the content as needed and take(s) full responsibility for the content of the publication.

References

Abunyewah, M., Okyere, S. A., Opoku Mensah, S., Erdiaw-Kwasie, M., Gajendran, T., & Byrne, M. K. (2024). Drought impact on peri-urban farmers' mental health in semi-arid Ghana: The moderating role of personal social capital. *Environmental Development, 49*, 100960. https://doi.org/10.1016/j.envdev.2023.100960.

Ashrafi, D. M., & Maoua, J. (2024). Harvest to basket: Understanding drivers of organic food purchase behaviour through interpretive structural modelling and MICMAC approach. *Journal of Modelling in Management, 19*(5), 1617–1643. https://doi.org/10.1108/JM2-12-2023-0299.

Bagherian, A., Gershon, M., Kumar, S., & Kumar Mishra, M. (2024). Analyzing the relationship between digitalization and energy sustainability: A comprehensive ISM-MICMAC and DEMATEL approach. *Expert Systems with Applications, 236*, 121193. https://doi.org/10.1016/j.eswa.2023.121193.

Barati, A. A., Azadi, H., Dehghani Pour, M., Lebailly, P., & Qafori, M. (2019). Determining key agricultural strategic factors using AHP-MICMAC. *Sustainability, 11*(14), 3947. https://doi.org/10.3390/su11143947.

Bokal, S., Grobicki, A., Kindler, J., & Thalmeinerova, D. (2014). From national to regional plans—the integrated drought management programme of the global water partnership for central and Eastern Europe. *Weather and Climate Extremes, 3*, 37–46. https://doi.org/10.1016/j.wace.2014.03.006.

Bressers, H., Bressers, N., & Larrue, C. (2016). *Governance for drought resilience: Land and water drought management in Europe*. Cham: Springer, 1–256. http://doi.org/10.1007/978-3-319-29671-5.

Bretan, E., & Engle, N. L. (2017). Drought preparedness policies and climate change adaptation and resilience measures in Brazil: An institutional change assessment. In

Evaluating climate change action for sustainable development. Cham: Springer, 305–326. https://doi.org/10.1007/978-3-319-43702-6_17.

de Bruijn, E., & Dieperink, C. (2022). A framework for assessing climate adaptation governance on the Caribbean Island of Curaçao. *Sustainability, 14*(22), 15092. https://doi.org/10.3390/su142215092.

Dobler-Morales, C., & Bocco, G. (2021). Social and environmental dimensions of drought in Mexico: An integrative review. *International Journal of Disaster Risk Reduction, 55*, 102067. https://doi.org/10.1016/j.ijdrr.2021.102067.

Duperrin, J.-C., & Godet, M. (1973). *Méthode de hiérarchisation des éléments d'un système: Essai de prospective du système de l'énergie nucléaire dans son contexte sociétal*. Centre national de l'entrepreneuriat (CNE).

Favoretto, C., Mendes, G. H. D. S., Mota, R. D. O., Filho, M. G., Osiro, L., & Ganga, G. M. D. M. D. (2024). An integrated ISM fuzzy MICMAC approach for unfolding the digital servitization implementation. *Journal of Business and Industrial Marketing, 39*(9), 2038–2054. https://doi.org/10.1108/JBIM-06-2022-0254.

Gharehbaghi, A., Ghasemlounia, R., Vaheddoost, B., & Ahmadi, F. (2025). Development of deep learning approaches for drought forecasting: A comparative study in a cold and semi-arid region. *Earth Science Informatics, 18*, 78. https://doi.org/10.1007/s12145-024-01650-7.

Gil, M., Garrido, A., & Hernández-Mora, N. (2013). Direct and indirect economic impacts of drought in the agri-food sector in the Ebro River basin (Spain). *Natural Hazards and Earth System Sciences, 13*(10), 2679–2694. https://doi.org/10.5194/nhess-13-2679-2013.

Godet, M. (1994). *From anticipation to action: A handbook of strategic prospective*. UNESCO Publishing.

Haeffner, M., Baggio, J. A., & Galvin, K. (2018). Investigating environmental migration and other rural drought adaptation strategies in Baja California Sur, Mexico. *Regional Environmental Change, 18*, 1495–1507. https://doi.org/10.1007/s10113-018-1281-2.

Haigh, T., Wickham, E., Hamlin, S., & Knutson, C. (2023). Planning strategies and barriers to achieving local drought preparedness. *Journal of the American Planning Association, 89*(3), 348–362. https://doi.org/10.1080/01944363.2022.2071324.

Herrfahrdt-Pähle, E., Schlüter, M., Olsson, P., Folke, C., Gelcich, S., & Pahl-Wostl, C. (2020). Sustainability transformations: Socio-political shocks as opportunities for governance transitions. *Global Environmental Change, 63*, 102097. https://doi.org/10.1016/j.gloenvcha.2020.102097.

Jalink, H., & Dieperink, C. (2024). Towards design principles for good multi-level drought risk governance: Some lessons from the Rhine basin. *Water, 16*(6), 879. https://doi.org/10.3390/w16060879.

Jung, S., Lee, S., & Yu, J. (2021). Identification and prioritization of critical success factors for off-site construction using ISM and MICMAC analysis. *Sustainability, 13*(16), 8911. https://doi.org/10.3390/su13168911.

Kamara, J. K., Akombi, B. J., Agho, K., & Renzaho, A. M. N. (2018). Resilience to climate-induced disasters and its overall relationship to well-being in southern africa: A mixed-methods systematic review. *International Journal of Environmental Research and Public Health, 15*(11), 2375. https://doi.org/10.3390/ijerph15112375.

Kamara, J. K., Sahle, B. W., Agho, K. E., & Renzaho, A. M. N. (2020). Governments' policy response to drought in Eswatini and Lesotho: A systematic review of the characteristics, comprehensiveness, and quality of existing policies to improve community resilience to drought hazards. *Discrete Dynamics in Nature and Society, 2020*(1), 3294614. https://doi.org/10.1155/2020/3294614.

Krishna Prabhakar, S. V. R. (2022). Implications of regional droughts and transboundary drought risks on drought monitoring and early warning: A review. *Climate, 10*(9), 124. https://doi.org/10.3390/cli10090124.

Kukuntod, N., & Wijitkosum, S. (2024). Interaction of drought-influencing factors for drought mitigation strategies in Lam Ta Kong Watershed, Khorat Plateau. *Heliyon, 10*(11), e32347. https://doi.org/10.1016/j.heliyon.2024.e32347.

Lindsay, J., Dean, A. J., & Supski, S. (2017). Responding to the Millennium drought: Comparing domestic water cultures in three Australian cities. *Regional Environmental Change, 17*, 565–577. https://doi.org/10.1007/s10113-016-1048-6.

Linstone, H. A., & Turoff, M. (Eds.). (1975). The Delphi method: Techniques and applications. Addison-Wesley.

Liu, W., Sun, F., Lim, W. H., Zhang, J., Wang, H., Shiogama, H., & Zhang, Y. (2018). Global drought and severe drought-Affected populations in 1.5 and 2°C warmer worlds. *Earth System Dynamics, 9*(1), 267–283. https://doi.org/10.5194/esd-9-267-2018.

Lockwood, M. (2010). Good governance for terrestrial protected areas: A framework, principles and performance outcomes. *Journal of Environmental Management, 91*(3), 754–766. https://doi.org/10.1016/j.jenvman.2009.10.005.

Lockwood, M., Davidson, J., Curtis, A., Stratford, E., & Griffith, R. (2010). Governance principles for natural resource management. *Society and Natural Resources, 23*(10), 986–1001. https://doi.org/10.1080/08941920802178214.

Measham, T. G., Preston, B. L., Smith, T. F., Brooke, C., Gorddard, R., Withycombe, G., & Morrison, C. (2011). Adapting to climate change through local municipal planning: Barriers and challenges. *Mitigation and Adaptation Strategies for Global Change, 16*, 889–909. https://doi.org/10.1007/s11027-011-9301-2.

Mersin, D., Gulmez, A., Safari, M. J. S., Vaheddoost, B., & Tayfur, G. (2022). Drought assessment in the Aegean region of Turkey. *Pure and Applied Geophysics, 179*(8), 3035–3053. https://doi.org/10.1007/s00024-022-03089-7.

Mishra, A. K., & Singh, V. P. (2011). Drought modeling—A review. *Journal of Hydrology, 403*(1–2), 157–175. https://doi.org/10.1016/j.jhydrol.2011.03.049.

Motsumi, K. O., Ziervogel, G., & New, M. (2023). Drought governance: A cross-level governance analysis in Botswana. *Climate Risk Management, 42*, 100557. https://doi.org/10.1016/j.crm.2023.100557.

Mullin, M., & Rubado, M. E. (2017). Local response to water crisis: Explaining variation in usage restrictions during a texas drought. *Urban Affairs Review, 53*(4), 752–774. https://doi.org/10.1177/1078087416657199.

Naumann, G., Cammalleri, C., Mentaschi, L., & Feyen, L. (2021). Increased economic drought impacts in Europe with anthropogenic warming. *Nature Climate Change, 11*(6), 485–491. https://doi.org/10.1038/s41558-021-01044-3.

Nazlabadi, E., Maknoon, R., Moghaddam, M. R. A., & Daigger, G. T. (2023). A novel MICMAC approach for cross impact analysis with application to urban water/wastewater management. *Expert Systems with Applications, 230*, 120667. https://doi.org/10.1016/j.eswa.2023.120667.

Nohrstedt, D., Mazzoleni, M., Parker, C. F., & Di Baldassarre, G. (2021). Exposure to natural hazard events unassociated with policy change for improved disaster risk reduction. *Nature Communications, 12*, 193. https://doi.org/10.1038/s41467-020-20435-2.

Ozcelik, C., Yilmaz, M. U., & Benli, K. (2024). Assessing drought in Turkish basins through satellite observations. *International Journal of Climatology, 44*(10), 3613–3640. https://doi.org/10.1002/joc.8541.

Peters, B. G., & Pierre, J. (1998). Governance without government? Rethinking public administration. *Journal of Public Administration Research and Theory, 8*(2), 223–243. https://doi.org/10.1093/oxfordjournals.jpart.a024379.

Petersen-Perlman, J. D., Aguilar-Barajas, I., & Megdal, S. B. (2022). Drought and groundwater management: Interconnections, challenges, and policyresponses. *Current*

Opinion in Environmental Science and Health, 28, 100364. https://doi.org/10.1016/j.coesh.2022.100364.

Sharma, A., Abbas, H., & Siddiqui, M. Q. (2021). Modelling the inhibitors of cold supply chain using fuzzy interpretive structural modeling and fuzzy MICMAC analysis. *PLoS One, 16*(4), e0249046. https://doi.org/10.1371/journal.pone.0249046.

Vargas, J., & Paneque, P. (2017). Methodology for the analysis of causes of drought vulnerability on the River Basin scale. *Natural Hazards, 89*(2), 609–621. https://doi.org/10.1007/s11069-017-2982-4.

Wilhite, D. A. (2009). Drought monitoring as a component of drought preparedness planning. In *Coping with drought risk in agriculture and water supply systems. Advances in natural and technological hazards research, vol 26*. Dordrecht: Springer, 3–19. https://doi.org/10.1007/978-1-4020-9045-5_1.

Wilhite, D. A., & Glantz, M. H. (1985). Understanding: The drought phenomenon: The role of definitions. *Water International, 10*(3), 111–120. https://doi.org/10.1080/02508068508686328.

Wilhite, D. A., Sivakumar, M. V. K., & Pulwarty, R. (2014). Managing drought risk in a changing climate: The role of national drought policy. *Weather and Climate Extremes, 3*, 4–13. https://doi.org/10.1016/j.wace.2014.01.002.

Wilhite, D. A., Svoboda, M. D., & Hayes, M. J. (2007). Understanding the complex impacts of drought: A key to enhancing drought mitigation and preparedness. *Water Resources Management, 21*(5), 763–774. https://doi.org/10.1007/s11269-006-9076-5.

Wittrock, V., Kulshreshtha, S. N., & Wheaton, E. (2011). Canadian prairie rural communities: Their vulnerabilities and adaptive capacities to drought. *Mitigation and Adaptation Strategies for Global Change, 16*, 267–290. https://doi.org/10.1007/s11027-010-9262-x.

Yilmaz, H., & Yanik, S. (2025). Exploring factors influencing the structure of micro-credentials in distance learning from multiple stakeholders' perspectives. In G. Durak, & S. Çankaya (Eds.). *Integrating micro-credentials with AI in open education* (pp. 89–114). IGI Global. http://doi.org/10.4018/979-8-3693-5488-9.ch005.

Yilmaz, M. U. (2023). Keşif kuraklık indeksi ve standartlaştırılmış yağış indeksi kullanılarak Kırklareli ilinde kuraklığın eğilimi ve zamansal değişkenliği. *Doğal Afetler ve Çevre Dergisi, 9*(2), 341–364. https://doi.org/10.21324/dacd.1296428.

Yilmaz, M. U. (2025). Enhancing sustainable flood risk management through a novel fuzzy multi-stakeholder framework. *Water Resources Management, 39*(3), 1453–1480. https://doi.org/10.1007/s11269-024-04012-6.

Yilmaz, M. U., & Yilmaz, H. (2022). An investigation of meteorological drought studies on a global scale using a bibliometric analysis. *Journal of Innovative Science and Engineering (JISE), 6*(1), 76–93. https://doi.org/10.38088/jise.993473.

Zaidi, Z., & Pelling, M. (2014). Chapter 6 - Vulnerability to drought and heatwave in London: Revealing institutionally configured risk. In *Assessment of vulnerability to natural hazards: A European perspective*. Elsevier Inc., 125–148. https://doi.org/10.1016/B978-0-12-410528-7.00006-0.

Zhang, Q., Han, L., Jia, J., Song, L., & Wang, J. (2016). Management of drought risk under global warming. *Theoretical and Applied Climatology, 125*, 187–196. https://doi.org/10.1007/s00704-015-1503-1.

This page intentionally left blank

CHAPTER TEN

Water demand management and behavior change in agriculture*

Pelin Atakan[1], and Cihat Günden[2]
[1]Department of Agricultural Economics, Graduate School of Natural and Applied Sciences, Ege University, İzmir, Türkiye,
[2]Department of Agricultural Economics, Faculty of Agriculture, Ege University, İzmir, Türkiye

10.1 Introduction

Water is a finite resource that plays a vital role in agricultural production. Water availability directly affects agricultural yields and is therefore linked to food security. Over the years, the increasing global food demand has led to higher agricultural production, resulting in greater water demand and putting additional pressure on freshwater resources (FAO, 2020). Concurrently, climate change and intensive irrigation practices negatively impact both the availability and quality of freshwater (Attou et al., 2025). This growing scarcity highlights the critical need for efficient agricultural water management (AWM). AWM aims to meet the water needs of plants and animals to enhance productivity while conserving natural resources for the benefit of downstream users and ecosystem services (USAID, 2015). Since late 1990s, AWM's focus has shifted from expanding water supply for irrigated agriculture to managing water demand (FAO, 2020; Thivet and Fernandez, 2012). This shift has been driven by growing water scarcity caused by climate change, population growth, water misuse, and unequal access to water resources (FAO, 1993, 2020). Demand management encompasses a range of strategies aimed at minimizing water losses within urban and irrigation distribution networks. It includes measures to lower user demand such as the implementation of drip irrigation systems and conducting awareness-raising campaigns.

* This chapter is part of the Pelin Atakan's doctoral research conducted at Ege University, under the supervision of Prof. Dr. Cihat Günden.

Drought Dynamics
DOI: https://doi.org/10.1016/B978-0-443-34205-9.00013-5
© 2026 Elsevier Inc. All rights are reserved, including those for text and data mining, AI training, and similar technologies.

Additionally, it involves the effective reallocation of water resources to optimize usage (Molle & Sanchis-Ibor, 2019). Despite widespread acknowledgment of the significance of demand management policies, their effective implementation remains inadequate (Molle and Sanchis-Ibor, 2019; Thivet and Fernandez, 2012). This can be attributed to several economic, organizational, and technical challenges; however, a particularly critical factor is the necessity of fostering behavioral change among stakeholders. To understand how behavior change happens, it is essential to consider various factors, including individual motivations, the abilities of different stakeholders, and the contextual influences on behavior. By examining these elements, policymakers can gain valuable insights that inform the design of bottom-up policies—often leading to higher adoption rates (Wuepper et al., 2023).

This chapter focuses on using behavioral insights as a tool for designing policies related to agricultural water demand management, particularly in on-farm irrigation practices. The first section introduces several practices for on-farm irrigation, outlining what farmers are expected to accomplish within the framework of water demand management. The next section describes several available demand management policies that aim to encourage farmers to meet these expectations. Next, the gap between the expectations and the available incentive instruments is explored, focusing on how behavior occurs. Finally, the last section discusses how these behavioral factors can be addressed or leveraged through policy interventions to promote better water use practices, with the aim of adapting to climate change.

10.2 What farmers are expected to do

In the context of agricultural water demand management (AWDM), policies are typically designed to address technical, financial, or institutional challenges in order to optimize plant water, improve irrigation system performance, and reallocate water (Molle & Sanchis-Ibor, 2019; Pereira, 2003). Irrigation system performance is typically assessed using efficiency ratios for each of the irrigation subsystems: storage, conveyance, off-farm and on-farm distribution, and on-farm application (Pereira, 2003).

The policies related to on-farm practices typically call on farmers to adopt practices (often voluntarily) that reduce water demand by increasing irrigation efficiency. Increasing irrigation efficiency is generally expected to

result in higher farm revenues due to increasing productivity and decreasing marginal cost of water (Lawell, 2016). On-farm irrigation efficiency is expressed as a percentage and calculated by the proportion of the amount of water applied that is beneficially used by the crop (Burt et al., 1997; Pfeiffer & Lin, 2014). As known by practitioners, the thumb rule generally suggests that efficiency tends to increase when the focus is placed on minimizing the amount of water that plants do not consume. However, nonconsumed water should not always be considered "lost." For instance, nonconsumed water can serve beneficial purposes such as leaching salts from the soil to prevent salinization (Pereira, 2003). The approach should be expanded to include (Perry et al., 2017):

- Consumptive use (conversion of water into water vapor), comprising beneficial consumption (crop transpiration; evaporation from wetlands; cooling towers) and nonbeneficial consumption (evaporation from free water surfaces and wet soil; transpiration by weeds)
- Nonconsumptive use (water that remains in liquid state), comprising recoverable flows (returning to a river or aquifer for potential reuse) and nonrecoverable flows (flowing to the sea or other economically unviable sink)
- Change in storage

Two interrelated measurements used to manage on-farm nonconsumptive water use are distribution uniformity and application efficiency (Pereira, 2003; Rogers et al., 1997). When other system variables are constant and appropriate, an on-farm irrigation system with high uniformity typically demonstrates greater application efficiency (Pereira, 2003). Distribution uniformity largely depends on the irrigation method employed. Irrigation method concerns how water is distributed in the field. In surface irrigation systems, water is directed over the soil surface by gravity, often using small and shallow channels (furrows) or artificial slopes. It is very difficult to control how much water is supplied to plants. Surface irrigation methods often face challenges with uneven water distribution, resulting in dry spots and oversaturated areas. Distribution uniformity and application efficiency are often observed to be low compared to pressurized irrigation systems. Pressurized irrigation methods are based on delivering water to plants using a network of pipes, pumps, and emitters that operate under pressure. On-farm nonconsumptive water use is more controllable, as the specific area and amount of water each plant receives can be planned with greater accuracy, leading to higher uniformity in water distribution. Drip irrigation (surface and subsurface) and sprinkler irrigation are two common pressurized

irrigation methods. Decision-making in irrigation methods is constrained by water supply system limitations, agronomic requirements, and economic factors (Pereira, 2003).

Irrigation scheduling plays a vital role in enhancing water use efficiency. It refers to how much and when water is supplied to plants. The aim is to maximize crop yields while minimizing water and nutrient loss to groundwater (Sammis et al., 2012). Decision-making in irrigation scheduling is constrained by factors such as irrigation method and equipment limitations, climatic conditions, system delivery schedule policies, and crop–water–soil interactions (Pereira, 2003). The most common scheduling methods are visually observing plants or soil, using past experience, and following peer practices (Hazneci & Kızılaslan, 2017; Kebede et al., 2014). The strong influence of visual observation and personal experience on the decision-making process is evident even in the presence of alternative and more objective tools such as soil moisture sensors and scheduling tools based on scientific models (Kebede et al., 2014). Another scheduling strategy is deficit irrigation, which intentionally allows crops to endure some level of water deficit, leading to minor yield reductions while significantly decreasing the irrigation water use (Pereira, 2003). It does not require a significant change in the existing irrigation method, but necessitates careful irrigation planning, considering crop water requirements, critical growth periods, and farmers' revenues (Fereres & Soriano, 2007; Peake et al., 2016; Pereira, 2003). However, the research on its long-term impacts on plants is still very limited (Fereres & Soriano, 2007). Nighttime irrigation is another effective strategy that reduces wind drift and evaporation, particularly with sprinkler methods (Cavero et al., 2008; Yacoubi et al., 2010), while careful planning is crucial for this scheduling strategy. It is important to evaluate if nighttime irrigation benefits overshadow daytime implementation, considering the drought tolerance levels of plants that will not be watered during the day and the managerial costs associated with watering at night (Al-Oqaili et al., 2020; Cavero et al., 2008; Yacoubi et al., 2010).

Irrigation methods and scheduling improvements can be enhanced by incorporating agronomic measures when applicable. Techniques for soil and water conservation, such as slope stabilization, bunds, and terraces, enhance water infiltration into the soil (USAID, 2015). Additionally, increasing soil organic content helps to improve soil water retention (Ankenbauer & Loheide, 2017). Employing diversified agricultural systems, such as agroforestry, transitioning to less water-intensive plant species, minimum tillage, and mulching can help decrease water demand (Pereira, 2003; USAID, 2015).

However, there are several common challenges the adoption of these methods. These include the need for acquiring new skills, making significant changes to current fieldwork practices, upfront investment expenses, and potential marketing uncertainties (Atış et al., 2018; USAID, 2015). Moreover, positive outcomes such as stable or increased profits and enhanced water-retaining soil may not be immediately apparent.

Policy interventions in numerous regions have predominantly concentrated on enhancing on-farm irrigation performance, typically promoting pressurized irrigation systems (Venot et al., 2017; Thivet and Fernandez, 2012). This widespread focus is rooted from the common, yet often flawed, belief that efficiencies demonstrated at the plot level will translate perfectly to larger scales (Molle & Sanchis-Ibor, 2019). In practice, however, such direct scaling is problematic, as a multitude of interacting factors, such as diverse soil characteristics, varying climatic conditions, human behaviors, infrastructural limitations, and economic realities, are present at broader scales and are not accounted by simple extrapolation (Molle & Sanchis-Ibor, 2019).

10.3 How farmers are encouraged to do what they are expected to do

Governments often encourage farmers to adopt improved irrigation practices by providing financial incentives such as grants, subsidies and low-interest loans. These programs aim to reduce overall water consumption by facilitating investment in more efficient irrigation technologies (Molle & Sanchis-Ibor, 2019). However, the effectiveness of voluntary, incentive-based cost-sharing programs is debated, particularly given two factors: the exclusive focus on improving irrigation efficiency and the neglect of irrigators' behavioral responses to these initiatives (Lawell, 2016; Whittlesey & Huffaker, 1995).

While improving on-farm irrigation efficiency is often pursued as a water-saving strategy, such efforts rarely lead to reduced water consumption at the basin or catchment level (Grafton et al., 2018; Wang, 2019; Whittlesey & Huffaker, 1995). Paradoxically, higher irrigation efficiency can result in increased (or constant) water use, primarily due to two underlying reasons (Pfeiffer & Lin, 2014; Scheierling et al., 2006): first, farmers may increase their water use on the intensive margin, meaning that they may shift to a different crop pattern that is more water-intensive and

more valuable. Second, they may irrigate more land, are less likely to leave the fields fallow, or prefer nonirrigated crops, increasing water use on an extensive margin. This situation can be regarded as an example of Jevon's Paradox, which claims that increasing efficiency in resource use tends to increase consumption and demand for that resource (Jevons, 2018). In parallel, water management also represents a classic common pool resource problem, producing cost externality and stock or strategic externality (Lawell, 2016). When one user's withdrawal decreases available water, it raises the pumping costs for everyone, resulting in a cost externality. Additionally, water that a farmer does not withdraw today will be withdrawn by other farmers. Consequently, farmers who do not withdraw water today risk losing it to others (Lawell, 2016).

Another consequence of increased irrigation efficiency is the potential reduction in the ability of water sources to recharge through runoff or deep percolation, which constitutes a nonconsumptive but beneficial portion of water (Grafton et al., 2018; Ward & Pulido-Velazquez, 2008). For example, Attou et al. (2025) challenge the assumption that drip irrigation always saves water. Their study highlights that deep percolation from flood irrigation can play a vital role in groundwater recharge and overall water management, potentially making it more beneficial than drip systems in certain contexts (Attou et al., 2025). This indicates that demand management efforts should prioritize in reducing water extraction instead of solely focusing on enhancing irrigation efficiency (Wang, 2019). Achieving genuine reductions in water consumption requires a balanced approach that combines improvements in irrigation efficiency with the clear definition and effective enforcement of water rights, while also addressing broader agricultural, socioeconomic, and policy priorities. The first challenge is that policies that enforce reductions in the amount of water a user is permitted to withdraw, using tools such as water rights, taxes, and crop pattern limitations, are very difficult (therefore costly) to design and implement (Pfeiffer & Lin, 2014). Another key challenge is that unrestrictive policies are often politically more popular and preferred by states, as a strong reaction is typically expected from irrigators otherwise. It is often politically easier to spend money on increasing water supply than to encourage or force farmers to reduce their water use, which can lead to public anger and economic hardship (Molle & Sanchis-Ibor, 2019). Environmental costs are frequently externalized or postponed. Moreover, when enforcement is overly strict, these restrictive policies could lead to

increased overdrafts of water supplies or a proliferation of unauthorized wells (Molle & Sanchis-Ibor, 2019).

From the behavioral point of view, such restrictive policies, despite their benefits, are often associated with the widespread cognitive barriers resulting from loss aversion, the endowment effect, and the tendency to maintain the status quo that emerges when individuals are presented with an alternative to their usual ways of doing things. The following section of this chapter discusses these barriers in detail.

The policies examined so far have been developed in a Western context, where water prices are dominantly determined by nonmarket authorities. Several studies argued that water markets, where the price of water is determined by market factors, can be the potential tool to create more efficient water allocations (Zilberman & Schoengold, 2005). However, attention must be paid to a variety of factors. First of all, water markets are very difficult to design because nonmarket functions, such as public interest in water distribution, need to be monitored and maintained by institutional frameworks (Whittlesey & Huffaker, 1995). Second, to ensure the proper functioning of a water market, it is essential to take into account some critical and difficult-to-measure factors in the pricing of water. These factors include the provision costs of the water, the cost of dynamic adjustment associated with water supply, conveyance costs, and environmental costs. It is important to acknowledge that accurately assessing these costs presents significant challenges due to real-life uncertainties (Zilberman & Schoengold, 2005). On the other hand, increasing water prices almost never encourage reduction in water use because water's production value is higher than its cost (Molle & Sanchis-Ibor, 2019). Similar to restrictive policies, this often leads to social unrest and drives farmers to utilize cheaper, likely unauthorized, groundwater (Dinar & Mody, 2004).

As briefly discussed above, even when policies are adopted, they can lead to unintended consequences, particularly if postadoption behavioral responses are not adequately considered. Conversely, some policies fail to achieve the desired level of adoption in the first place. Research shows that in some cases, financial incentives and extension services have failed to promote the adoption of more efficient irrigation technologies (Molle & Sanchis-Ibor, 2019). One reason for this is that the differing characteristics of farmers in terms of their financial and social capital, risk assessments, and perceptions are critically disconnected from what these policies offer (Özerol & Bressers, 2017). Understanding the context in which farmers' behaviors develop and identifying the adaptation practices they are likely to adopt in response to climate change, along with the barriers to those practices, will assist policymakers in

creating effective adaptation strategies (Atis et al., 2024). The following section discusses these factors in shaping behavior.

10.4 Understanding why farmers do what they do

Behavior is a highly complex process. The main theory of the neoclassical approach, the "Theory of Rational Choice," assumes that individuals are goal-oriented and rational, have full information and cognitive capacity, and make decisions in a way that maximizes utility by making the best use of these (Robbins, 2007; Bentham, 1970). However, this theory fails to explain an important part of the decision-making mechanism. For example, individuals may not have sufficient information and resources to make rational decisions (Simon, 1955). Moreover, they may perceive information asymmetrically, associating it with losses or gains based on a subjective and contextual reference point (Kahneman & Tversky, 1979). Evaluating all options in the decision-making process is usually either impossible or cognitively very costly. Therefore, individuals develop some cognitive shortcuts. These include (Kahneman et al., 1991; Moffitt et al., 2023): evaluating potential outcomes compared to a specific reference point, with a tendency to avoid loss relative to that point, particularly in situations involving risk or uncertainty (loss aversion-endowment effect), taking the default option (default effect), opting for the middle ground, when faced with various alternatives (decoy effect), paying less attention to or ignoring future payoffs compared to more recent ones (present bias, i.e., myopia or short-sightedness), the inclination to maintain existing conditions (status-quo effect, i.e., inertia) and taking the readily available option (availability effect).

These shortcuts can reduce cognitive costs and enable quick decision-making. Although they often lead to beneficial outcomes for the individual, they can sometimes lead to cognitive biases that result in decisions that are less beneficial for the individual or society (Tversky & Kahneman, 1974).

On the other hand, not all decisions translate into behavior (Georgantzis Garcia et al., 2021). First, behaviors can be influenced by cues or stimuli in the environment. Second, most behaviors are unconscious and may result from habits (Hallsworth & Kirkman, 2020). Finally, behavior sometimes occurs under the influence of social norms and sometimes under the influence of external facilitating factors or barriers (Kizos et al., 2011; Pakmehr et al., 2020).

Fogg Behavior Model (FBM) synthesizes various behavioral analysis models and produces a very simple understanding of how a behavior occurs. FBM claims that any behavior is a product of three elements: motivation, ability, and trigger (i.e., prompt) (Fogg, 2009). All of these elements must converge for a behavior to take place. Motivation refers to an individual's desire to perform a behavior, while ability is the capacity to carry out that behavior. A trigger serves as a cue to engage in behavior. There are three main sources of motivation toward the behavior: sensation (pleasure or pain), anticipation (hope or fear), and belonging (social acceptance or rejection) toward the behavior. Enhancing motivation is often targeted by policymakers through awareness-raising campaigns about climate change, environmental stewardship, or water scarcity. Motivation has been studied widely by researchers in many different contexts. It is often used interchangeably with intention in other behavioral models and is considered one of the major explanators of any behavior (Ajzen, 1991). Although consistently reported as important, intention only explains behavior to a limited extent (Georgantzis Garcia et al., 2021). The ability to perform a behavior is another crucial factor in determining whether that the behavior will actually take place, according to the FBM. It implies that if a behavior is too complex for an individual, motivation alone will not be sufficient to initiate that behavior, regardless of how strong that motivation might be. Ability to perform a behavior encompasses more than just the necessary skills to perform a behavior. FBM argues that it relies on six key factors that indicate simplicity of behavior: time, money, physical effort, brain cycles (mental effort), social deviance, and nonroutine. The likelihood of a behavior occurring increases as its simplicity increases. If a behavior requires too much time, money, physical and mental effort and if it includes breaking social norms and routines, then it is not simple to (and therefore unlikely) perform. If the simplicity of a behavior is low, high motivation is necessary for it to occur. Conversely, high simplicity may be sufficient for behavior to occur when motivation is low. In other words, motivation and ability exist in a compensatory relationship; if one is lacking, it can be compensated by the other (Fogg, 2009). These two elements are partially addressed by existing demand management policy interventions: financial incentives primarily target farmers' financial capacity, while extension services aim to influence their motivation and help to reduce the mental effort involved in adoption, depending on their content. The possible insufficient targeting of these two factors as well as the factors

that remain entirely unaddressed, may help explain why the intended behavioral changes are not being realized.

A trigger (i.e., prompt) is the third essential element required for a behavior to occur, alongside motivation and ability (Fogg, 2009). The trigger serves as a prompt, cue, or signal that drives individuals to take action at a specific moment. Even when a person has sufficient motivation and ability, the behavior is unlikely to happen unless they are prompted by an effective trigger that tells them "do this now." FBM identifies three types of triggers based on their functions: sparks, facilitators, and signals. A spark leverages motivation and is effective when the target behavior is simple enough to perform. It might include highlighting one or more motivational elements such as sensation, anticipation, and belonging related to the outcomes of the target behavior. A facilitator helps make behavior easier and results in execution of the behavior when the person has high motivation. The facilitator trigger simplifies the behavior by reducing frictions associated with the six factors of ability (money, physical effort, mental effort, social norms, and nonroutine). An example of this is when a person is highly motivated to invest in drip irrigation instead of continuing with surface irrigation. Although drip irrigation may be the preferred choice, surface irrigation is much easier because it has become a habitual practice of the farmer and it requires less mental effort (because, it is predictable and demands less attention or decision-making). As a result, when a triggering event such as watering time occurs, the desired behavior change (shifting to drip irrigation) does not take place. The third trigger type is signal. A signal indicates or serves as a reminder, and it works best when ability and motivation are high enough (Fogg, 2009).

Water use behavior can be seen as a response to the actual or expected threat of water scarcity. Understanding the underlying mechanism of how this behavior occurs requires a deeper understanding of the decision-making environment in which farmers operate. Developed based on Protection Motivation Theory (PMT) by Grothmann and Patt (2005), Model of Private Proactive Adaptation to Climate Change (MPPACC) allows us to take a closer look at the underlying factors that contribute to both the motivational and ability aspects of irrigation behavior. MPPACC focuses on the effects of individual cognition on climate change-related threats and uncertainties, and individual responses. This model studies individual responses to climate change as "adaptation" and "maladaptation" that are primarily driven by two building blocks of individual cognition: individual risk appraisal and adaptation appraisal

(Grothmann & Patt, 2005). Individual risk appraisal consists of the perceived severity and perceived probability of the threat. Adaptation appraisal is shaped by perceived adaptation efficacy, perceived self-efficacy, and perceived adaptation costs. These two building blocks are influenced by biases, mental shortcuts, risk experience appraisal, reliance on public adaptation, social discourse, and objective adaptation capacity which are noncognitive elements such as resources, knowledge, social or institutional support (Grothmann & Patt, 2005). The main idea of the MPPACC is that high risk appraisal and low adaptation appraisal lead to maladaptation, which in turn constitutes a barrier to adaptation. When a maladaptive response successfully addresses a threat, it can lead to repeated reactions when similar threats arise. As this response becomes more frequent, it turns into a habit (i.e., part of the status quo), making it increasingly difficult to change (Fogg, 2020). Furthermore, if this maladaptive response involves a prior investment, behavioral change becomes even more complicated due to the sunk cost fallacy, where individuals continue to invest in failing strategies, even when new information advising otherwise is available. For example, in groundwater contexts, this means that even when early wells fail or water tables decline, farmers may still invest in deeper extractions to compensate their initial expense, even when policy interventions discourage such practices (Maréchal, 2010).

In sum, human behavior is deeply impacted by factors such as loss aversion, various cognitive shortcuts, social norms, and environmental stimuli. While intention (or motivation) partially explains observed actions, behavior ultimately occurs when elements of motivation, ability, and trigger are all present at a specific time, as suggested by FBM (Fogg, 2009). As MPPACC suggests, behaviors that emerge in response to threats such as water use in the context of water scarcity can be conceptualized as a function of an individual's risk appraisal and adaptation appraisal (Grothmann and Patt, 2005). Drawing from the behavioral mechanisms underlying water use behavior that are presented in this section, the following section discusses approaches for policy design using insights from the behavioral perspective to improve the effectiveness of drought-targeting policies.

10.5 Designing policies to promote behavior change in irrigation under water scarcity using behavioral insights

What prevents individuals from adopting behaviors that lead to desirable personal or social outcomes? The answer to this question usually

involves a combination of factors: a lack of intent, inadequate skills or knowledge needed to change the behavior, and insufficient environmental cues, as discussed earlier in this chapter. Conversely, the decision-making environment may promote undesirable behaviors to such an extent that it hinders the possibility of alternative, more favorable behaviors. This includes what were previously described as maladaptive responses.

The behavioral insights approach is an inductive method of policy-making that focuses on understanding the factors that influence human behavior. By leveraging this understanding, it aims to address common challenges encountered in daily life (Hallsworth & Kirkman, 2020). Given the complexities of behavior change, it is crucial to determine which aspects of the behavior formation process need to be addressed, the tools for policy intervention design, and the potential outcomes of these behavioral changes. Mapping the behavior from the intention to the action stage often provides discernment to determine where to intervene (Mullainathan & Thaler, 2000). A key tool within behavioral insights approach, "choice architecture" refers to the design of the decision-making environment in which individuals make choices. This concept is rooted in the understanding that much of human behavior is influenced by the contextual features of the surrounding environment. Consequently, it is proposed that intentionally shaping this environment can lead to behavior change (Thaler & Sunstein, 2008). A specific aspect of choice architecture that influences people's behavior predictably (without restricting any options or significantly altering their economic incentives) is known as a "nudge." This perspective is rooted in libertarian paternalism, which aims to guide people's choices for their benefit while maintaining their freedom to decide (Thaler & Sunstein, 2008). Nudges can be designed in various policy design frameworks. This includes MINDSPACE Framework, developed by Dolan et al. (2012). The MINDSPACE categorizes the nine elements influencing human behavior to guide nudge design (Dolan et al., 2012):

- **Messenger:** We are heavily influenced by who communicates information to us
- **Incentives:** Our responses to incentives are shaped by predictable mental shortcuts such as strongly avoiding losses
- **Norms:** We are strongly influenced by what others do
- **Defaults:** We "go with the flow" of preset options
- **Salience:** Our attention is drawn to what is novel and seems relevant to us

- **Priming:** Our acts are often influenced by subconscious cues
- **Affect:** Our emotional associations can powerfully shape our actions
- **Commitments:** We seek to be consistent with our public promises, and reciprocate acts
- **Ego:** We act in ways that make us feel better about ourselves

Drawing on their thorough analysis of behavioral and experimental economics research that focuses on policy intervention design in agri-environmental settings, Palm-Forster et al. (2019) argue that agri-environmental behavioral contexts, including water use behavior, are distinguished from other behavioral domains by two defining characteristics. First, agri-environmental programs are designed to influence the long-term, voluntary behaviors of agricultural producers. Unlike regulatory approaches that mandate specific actions, these programs rely on farmers choosing to adopt certain practices within competitive markets over extended periods. Often, benefits are uncertain or delayed. Second, achieving the desired behavioral change often entails a collective action problem, as agricultural production frequently relies on one or more common pool resources such as water, soil, and shared grazing lands (Palm-Forster et al., 2019). These resources are susceptible to overuse and degradation, making the establishment of effective governance mechanisms particularly challenging. Often, the result is inefficient mechanisms that produce unintended outcomes such as overextraction of water (Molle & Sanchis-Ibor, 2019).

Based on the MINDSPACE and FBMs described in the previous section, along with insights gained from behavioral analysis, a practical approach to policy design can be formulated as follows[1]:

- Select a set of nine behavioral components, focusing on the barriers that prevent the desired behavior and/or the factors that facilitate undesired behavior.
- Aim for a balance in their functions within the design, considering how much they enhance ability versus how much they boost motivation.
- Design the policy intervention incorporating a relevant trigger element.

Consider a typical scenario where farmers are generally aware of the significant negative impacts of water scarcity on their agricultural production, recognizing the need to switch to more efficient irrigation technologies. In this context, the policy goal is to promote the adoption of high-efficiency irrigation methods, such as drip systems, through the provision of low-interest loans or grants.. However, despite having access

[1] For a similar approach, see Atakan et al. (2025).

to this public financial support, many farmers tend to refrain from utilizing it. In this typical scenario, policy tool or the "trigger" formed as financial incentives did not take into account that farmers may be unsure of where or when to begin and cannot envision the entire process step by step. Moreover, changing their irrigation practices constitutes a hassle factor as the switch will change many things that they have been doing so far (i.e., routines) and require adapting to new practices, which may even involve acquiring new skills. Therefore, they tend to perceive the adoption as a sacrifice of present convenience for uncertain benefits in the future (i.e., present bias). Additionally, they may believe that their effort to invest in a drip irrigation method will not significantly impact their profits or increase their ability to cope with the water scarcity threat due to other adverse factors that they cannot interfere such as local water management or future precipitation.

From the FBM perspective, the trigger in this scenario addresses only one of the six elements of ability (i.e., money) while the target behavior remains difficult due to physical and mental effort, routine disruption, social deviance, and time investment required to adopt drip irrigation. Although farmers are moderately motivated (they express an intention to adopt new practices and acknowledge the threat of water scarcity), the perceived benefits of the target behavior are delayed and uncertain, which weakens their motivation for immediate action. As a result, the trigger, designed as a facilitating prompt in the form of financial support, fails to produce the successful adoption of the drip irrigation.

Similarly, from the MPPACC's point of view, there is a clear imbalance between farmers' risk appraisal and adaptation appraisal in evaluating drip irrigation as a means to respond to water scarcity. In this scenario, farmers demonstrate a high level of risk appraisal, which contributes to their motivation to change water use behavior. However, their adaptation appraisal remains low, primarily influenced by cognitive biases such as status quo bias and present bias, that is, a preference for maintaining current practices rather than sacrificing immediate convenience for uncertain future benefits (Moffitt et al., 2023; O'Donoghue & Rabin, 1999). Furthermore, the perceived financial and social risks associated with adopting drip irrigation (such as, the fear of reputational loss or marginalization) are weighted more heavily than the potential benefits, reflecting loss aversion (Kahneman & Tversky, 1979). While the policy intervention in the form of financial support enhances adaptive capacity to some extent, it does not adequately address these behavioral barriers. Consequently, this

mismatch may lead to maladaptive responses such as wishful thinking, behavioral inertia, or even the unauthorized use of water resources, particularly when perceived risks are extremely high (Grothmann & Patt, 2005; Molle & Sanchis-Ibor, 2019).

Given the dominance of *loss aversion, status quo bias* and *present bias* in the above scenario, *framing* appears to be one of the effective nudges (Palm-Forster et al., 2019). Framing involves changing how information about the outcomes of a behavior is presented, aiming to increase the likelihood that the behavior will be adopted (Kahneman, 2011). This technique often targets the tendency of loss aversion and present bias concurrently. For example, the presentation of the incentive in the previously described scenario (i.e., a low-rate loan) could be coupled with information that is framed to effectively underline and communicate what nonadopters will lose as a result of not adopting drip irrigation (such as excessive water use degradation their soil or gradually lowering water levels in their watershed) rather than what they gain in the future. Thus, they will be more motivated to take the required financial or social risks and change their current behavior (i.e., status quo). Reflecting the scenario presented above using MINDSPACE tool, the nudge design incorporating loss-framed information can be further enhanced by taking into account the following considerations:

- Framed information should be as *salient* as possible, possibly including a *default option* that encompasses preset, small steps for adoption.
- Framed information could attach the adoption of drip irrigation to being a successful and respectful farmer, targeting *ego and priming*
- Framed information could involve a description of the typical practices implemented by successful farmers who have adopted drip irrigation, targeting *(descriptive) norms*.
- Framed information be coupled with a social accountability boost mechanism that allows farmers to make public *commitments*, such as signing a public pledge on their water reduction target.

The effectiveness of nudge design can be further supported by prioritizing the most relevant MINDSPACE tool in relation to the elements of FBM, motivation, ability and trigger. The primary focus should be on strengthening the weakest element. In our case, ability appears to be the weakest. Ability is determined not only by the financial capacity to adopt the behavior but also by the mental effort required and the disruption to existing routines. Minimizing these barriers using a trigger could be the central aim of the nudge design.

10.6 Conclusion

Designing a policy intervention to promote adaptive behavior among farmers facing water scarcity should begin with designing a clear roadmap. This roadmap must include forecasts of the macroscale outcomes expected once the desired target behaviors are adopted, as well as the behavioral response of the target farmers. Focusing solely on technology adoption as a policy goal often leads to unintended negative consequences. In this chapter, we discussed the disparity between the expectations placed on farmers in terms of drought adaptation and the outcomes of typical policies intended to encourage them. We focused on individual behavior, however, tackling water scarcity requires policy measures beyond that. For example, while promoting efficient irrigation technologies is important, it must be accompanied by fundamental institutional changes such as implementing quotas and establishing water management that does not perpetuate existing social inequalities (Perry et al., 2017). Additionally, complementary agronomic strategies, like encouraging the cultivation of less water-intensive plant species, and addressing market uncertainties, are also necessary (Salalı et al., 2019). Policymakers should first examine the needs and capacities of the primary implementers (i.e., farmers) and the context in which undesirable behaviors occur. This foundational understanding will enable the development of a step-by-step strategy to achieve the desired policy objectives effectively.

References

Ajzen, I. (1991). The theory of planned behavior. *Organizational Behavior and Human Decision Processes, 50*(2), 179–211. https://doi.org/10.1016/0749-5978(91)90020-t.

Al-Oqaili, F., Good, S. P., Frost, K., & Higgins, C. W. (2020). Differences in soil evaporation between row and interrow positions in furrowed agricultural fields. *Vadose Zone Journal, 19*(1). https://doi.org/10.1002/vzj2.20086, https://acsess.onlinelibrary.wiley.com/journal/15391663.

Ankenbauer, K. J., & Loheide, S. P. (2017). The effects of soil organic matter on soil water retention and plant water use in a meadow of the Sierra Nevada, CA. *Hydrological Processes, 31*(4), 891–901. https://doi.org/10.1002/hyp.11070, http://onlinelibrary.wiley.com/journal/10.1002/(ISSN)1099-1085.

Atakan, P., Günden, C., Yercan, M., Mattas, M., & Knez, M. (2025). Behavioral barriers in the inclusion of neglected and underutilized species into mainstream diets. *Frontiers in Sustainable Food Systems, 9*, 1623138. In this issue https://doi.org/10.3389/fsufs.2025.1623138.

Atis, E., Gunden, C., & Atakan, P. (2024). *Behavioral economics to tackle climate change in agriculture*. Nobel Tip Kitabevleri, 35–60. http://doi.org/10.69860/nobel.9786053359432.3.

Attou, T., Kuppel, S., Kharrou, M. H., Ezzahar, J., Bouchaou, L., Ait Brahim, Y., Demarez, V., & Chehbouni, A. (2025). A process-based modelling of groundwater

recharge under contrasting irrigation methods in semi-arid crops. *Agricultural Water Management, 316*. https://doi.org/10.1016/J.AGWAT.2025.109584.

Atış, E., Salalı, H. E., Akyüz, Y., Ceyhan, V., Türkten, H., Yıldırım, Ç., Hasdemir, M., & Güngör, F. U. (2018). Çiftçilere göre gelecekte uygulanacak politikalarda çevrenin önceliği. *Uluslararası Tarım, Çevre ve Sağlık Kongresi*. Aydın, Turkey .

Bentham, J. (1970). *An introduction to the principles of morals and legislation*. Athlone Publishers.

Burt, C. M., Clemmens, A. J., Strelkoff, T. S., Solomon, K. H., Bliesner, R. D., Hardy, L. A., Howell, T. A., & Eisenhauer, D. E. (1997). Irrigation performance measures: Efficiency and uniformity. *Journal of Irrigation and Drainage Engineering, 123*(6), 423–442. https://doi.org/10.1061/(ASCE)0733-9437(1997)123:6(423).

Cavero, J., Jiménez, L., Puig, M., Faci, J. M., & Martínez-Cob, A. (2008). Maize growth and yield under daytime and nighttime solid-set sprinkler irrigation. *Agronomy Journal, 100*(6), 1573–1579. https://doi.org/10.2134/agronj2008.0092Spain, http://agron.scijournals.org/cgi/reprint/100/6/1573.

Dinar, A., & Mody, J. (2004). Irrigation water management policies: Allocation and pricing principles and implementation experience. *Natural Resources Forum, 28*(2), 112–122. https://doi.org/10.1111/j.1477-8947.2004.00078.x.

Dolan, P., Hallsworth, M., Halpern, D., King, D., Metcalfe, R., & Vlaev, I. (2012). Influencing behaviour: The mindspace way. *Journal of Economic Psychology, 33*(1), 264–277. https://doi.org/10.1016/j.joep.2011.10.009.

FAO. (1993). *The state of food and agriculture: Water policies and agriculture*. FAO.

FAO. (2020). *The state of food and agriculture 2020: Overcoming water challenges in agriculture*. FAO.

Fereres, E., & Soriano, M. A. (2007). Deficit irrigation for reducing agricultural water use. *Journal of Experimental Botany, 58*(2), 147–159. https://doi.org/10.1093/jxb/erl165.

Fogg, B. (2009). A behavior model for persuasive design. In *ACM international conference proceeding series*, United States. 350. 10.1145/1541948.1541999..

Fogg, B. J. (2020). *Tiny habits: The small changes that change everything*. Harvest.

Georgantzis Garcia, D., Kipnis, E., Vasileiou, E., & Solomon, A. (2021). Consumption in the circular economy: Learning from our mistakes. *Sustainability, 13*(2), 601. https://doi.org/10.3390/su13020601.

Grafton, R. Q., Williams, J., Perry, C. J., Molle, F., Ringler, C., Steduto, P., Udall, B., Wheeler, S. A., Wang, Y., Garrick, D., & Allen, R. G. (2018). The paradox of irrigation efficiency. *Science (New York, N.Y.), 361*(6404), 748–750. https://doi.org/10.1126/science.aat9314.

Grothmann, T., & Patt, A. (2005). Adaptive capacity and human cognition: The process of individual adaptation to climate change. *Global Environmental Change, 15*(3), 199–213. https://doi.org/10.1016/j.gloenvcha.2005.01.002.

Hallsworth, M., & Kirkman, E. (2020). *Introducing behavioral insights*. MIT Press, 1–24. http://doi.org/10.7551/mitpress/12806.003.0004.

Hazneci, E., & Kızılaslan, H. (2017). Irrigation water use characteristics of farmers and their interaction with irrigation union in Bafra district of Samsun province, Turkey. *Anadolu Journal of Agricultural Sciences, 32*(1), 23. https://doi.org/10.7161/omuanajas.288816 23.

Jevons, W. S. (2018). The coal question. In *The economics of population: Key classic writings*(pp. 193–204). Taylor and Francis. https://www.taylorfrancis.com/books/9781351291514. https://doi.org/10.4324/9781351291521-27.

Kahneman, D. (2011). *Thinking, fast and slow*. FSG.

Kahneman, D., & Tversky, A. (1979). Prospect theory: An analysis of decision under risk. *Econometrica Journal of the Econometric Society, 47*(2), 263. https://doi.org/10.2307/1914185.

Kahneman, D., Knetsch, J. L., & Thaler, R. H. (1991). Anomalies: The endowment effect, loss aversion, and status quo bias. *Journal of Economic Perspectives, 5*(1), 193–206. https://doi.org/10.1257/jep.5.1.193.

Kebede, H., Fisher, D. K., Sui, R., & Reddy, K. N. (2014). Irrigation methods and scheduling in the delta region of mississippi: Current status and strategies to improve irrigation efficiency. *American Journal of Plant Sciences, 05*(20), 2917–2928. https://doi.org/10.4236/ajps.2014.520307.

Kizos, T., Marin-Guirao, J. I., Georgiadi, M. E., Dimoula, S., Karatsolis, E., Mpartzas, A., Mpelali, A., & Papaioannou, S. (2011). Survival strategies of farm households and multifunctional farms Greece. *Geographical Journal, 177*(4), 335–346. https://doi.org/10.1111/j.1475-4959.2011.00403.x.

Lawell, C. Y. C. L. (2016). The management of groundwater: Irrigation efficiency, policy, institutions, and externalities. *Annual Review of Resource Economics, 8*(1), 247–259. https://doi.org/10.1146/annurev-resource-100815-095425, http://arjournals.annualreviews.org/loi/resource.

Maréchal, J.-C. (2010). Editor's message: The sunk cost fallacy of deep drilling. *Hydrogeology Journal, 18*(2), 287–289. https://doi.org/10.1007/s10040-009-0515-2.

Moffitt, R., Buttenheim, A., & Beatty, A. (2023). *Behavioral economics: Policy impact and future directions* (pp. 1–246). National Academies Press. https://nap.nationalacademies.org/catalog/26874/behavioral-economics-policy-impact-and-future-directions. https://doi.org/10.17226/26874.

Molle, F., & Sanchis-Ibor, C. (2019). *Irrigation policies in the mediterranean: Trends and challenges* (pp. 279–313). Springer. 10.1007/978-3-030-03698-0_10..

Mullainathan, S., & Thaler, R. H. (2000). Behavioral economics. *SSRN Electronic Journal*. https://doi.org/10.2139/ssrn.245828.

O'Donoghue, T., & Rabin, M. (1999). Doing it now or later. *American Economic Review, 89*(1). https://doi.org/10.1257/aer.89.1.103.

Özerol, G., & Bressers, H. (2017). How do farmers align with the agri-environmental changes in irrigated agriculture? A case study from the harran plain, Turkey. *Irrigation and Drainage, 66*(1), 45–59. https://doi.org/10.1002/ird.2064.

Pakmehr, S., Yazdanpanah, M., & Baradaran, M. (2020). How collective efficacy makes a difference in responses to water shortage due to climate change in southwest Iran. *Land Use Policy, 99*, 104798. https://doi.org/10.1016/j.landusepol.2020.104798.

Palm-Forster, L. H., Ferraro, P. J., Janusch, N., Vossler, C. A., & Messer, K. D. (2019). Behavioral and experimental agri-environmental research: Methodological challenges, literature gaps, and recommendations. *Environmental and Resource Economics, 73*(3), 719–742. https://doi.org/10.1007/s10640-019-00342-x, www.wkap.nl/journalhome.htm/0924-6460.

Peake, A. S., Carberry, P. S., Raine, S. R., Gett, V., & Smith, R. J. (2016). An alternative approach to whole-farm deficit irrigation analysis: Evaluating the risk-efficiency of wheat irrigation strategies in sub-tropical Australia. *Agricultural Water Management, 169*, 61–76. https://doi.org/10.1016/j.agwat.2016.02.013.

Pereira, L. S. (2003). *Irrigation demand management to cope with drought and water scarcity*. Springer, 19–33. http://doi.org/10.1007/978-94-010-0129-8_2.

Perry, C., Steduto, P., & Karajeh, F. (2017). *Does improved irrigation technology save water? A review of the evidence*(p. 42). Regional Initiative on Water Scarcity for the Near East and North Africa.

Pfeiffer, L., & Lin, C. Y. C. (2014). Does efficient irrigation technology lead to reduced groundwater extraction? Empirical evidence. *Journal of Environmental Economics and Management, 67*(2), 189–208. https://doi.org/10.1016/j.jeem.2013.12.002.

Robbins, L (2007). *An essay on the nature and significance of economic science*. Ludwig von Mises Institute.

Rogers, D., Lamm, F., Alam, M., Trooien, T., Barnes, G. C. P., & Mankin, K. (1997). Efficiencies and water losses of irrigation systems. In *Irrigation Management Series*.

Salalı, E., Atış, E., & Günden, C. (2019). Su Kaynaklarının Korunmasında Yerel Tohum Çeşitlerinin Rolü Üzerine Çiftçi Görüşleri. *Tarım Ekonomisi Dergisi*. https://doi.org/10.24181/tarekoder.654006.

Sammis, T., Sharma, P., Shukla, M. K., Wang, J., & Miller, D. (2012). A water-balance drip-irrigation scheduling model. *Agricultural Water Management, 113*, 30–37. https://doi.org/10.1016/j.agwat.2012.06.012.

Scheierling, S. M., Young, R. A., & Cardon, G. E. (2006). Public subsidies for water-conserving irrigation investments: Hydrologic, agronomic, and economic assessment. *Water Resources Research, 42*(3). https://doi.org/10.1029/2004WR003809.

Simon, H. A. (1955). A Behavioral Model of Rational Choice. *The Quarterly Journal of Economics, 69*(1), 99–118. https://doi.org/10.2307/1884852.

Thaler, R. H., & Sunstein, C. R. (2008). *Nudge, improving decisions about health, wealth, and happiness*. Yale University Press.

Thivet, G., Fernandez, S. (2012). *Water demand management: The Mediterranean experience*. Global Water Partnership (GWP).

Tversky, A., & Kahneman, D. (1974). Judgment under uncertainty: Heuristics and biases. *Science (New York, N.Y.), 185*(4157), 1124–1131. https://doi.org/10.1126/science.185.4157.1124.

USAID, (2015). *Agricultural water management water and development strategy implementation brief*. USAID.

Venot, J.-P., Kuper, M., & Zwarteveen, M. (2017). *Drip irrigation for agriculture: Untold stories of efficiency, innovation and development*. Routledge, 1–386. https://doi.org/10.4324/9781315537146.

Wang, H. (2019). Irrigation efficiency and water withdrawal in US agriculture. *Water Policy, 21*(4), 768–786. https://doi.org/10.2166/wp.2019.175.

Ward, F. A., & Pulido-Velazquez, M. (2008). Water conservation in irrigation can increase water use. *Proceedings of the National Academy of Sciences of the United States of America, 105*(47), 18215–18220. https://doi.org/10.1073/pnas.0805554105, http://www.pnas.org/content/105/47/18215.full.pdf.

Whittlesey, N. K., & Huffaker, R. G. (1995). Water policy issues for the twenty-first century. *American Journal of Agricultural Economics,* 77(5), 1199–1203. https://doi.org/10.2307/1243347.

Wuepper, D., Bukchin-Peles, S., Just, D., & Zilberman, D. (2023). Behavioral agricultural economics. *Applied Economic Perspectives and Policy, 45*(4), 2094–2105. https://doi.org/10.1002/aepp.13343.

Yacoubi, S., Zayani, K., Zapata, N., Zairi, A., Slatni, A., Salvador, R., & Playán, E. (2010). Day and night time sprinkler irrigated tomato: Irrigation performance and crop yield. *Biosystems Engineering, 107*(1), 25–35. https://doi.org/10.1016/j.biosystemseng.2010.06.009.

Zilberman, D., & Schoengold, K. (2005). The use of pricing and markets for water allocation. *Canadian Water Resources Journal, 30*(1), 47–54. https://doi.org/10.4296/cwrj300147.

This page intentionally left blank

CHAPTER ELEVEN

The state's efforts for effective water storage management to enhance resilience against droughts: case studies from the Bursa District

Murat Can
State Hydraulic Works of Turkey, 1st District, Bursa, Türkiye

11.1 Introduction

Drought constitutes a severe hydrological anomaly that materializes when precipitation levels fall substantially below the long-term climatic norm, thereby disturbing the delicate equilibrium of the hydrological cycle. It is typically characterized by prolonged deficits in rainfall, which consequently impair soil moisture, reduce streamflow, and deplete groundwater reserves, often culminating in adverse socio-economic and ecological consequences. The World Meteorological Organization (WMO) (2022) has underscored that the past decade has marked the warmest period in recorded history, with 2022 alone registering a global mean temperature anomaly of approximately +1.15°C relative to pre-industrial levels (1850–1900). This unprecedented warming trajectory is anticipated to intensify in the coming decades, driven by persistent anthropogenic greenhouse gas emissions and inadequate mitigation measures.

The summer of 2022 vividly exemplified the accelerating impacts of climate change, as multiple regions worldwide experienced extreme heat waves and unprecedented drought conditions. Across Europe, China, Africa, and the United States, temperature thresholds were repeatedly shattered, triggering cascading hydrological stresses. In Europe, the continent grappled with its most severe drought event in the past five centuries, as evidenced by a confluence of depleted river flows, parched agricultural lands, and widespread forest fires. Simultaneously,

Drought Dynamics
DOI: https://doi.org/10.1016/B978-0-443-34205-9.00009-3
© 2026 Elsevier Inc. All rights are reserved, including those for text and data mining, AI training, and similar technologies.

the United States endured its driest summer in approximately 1200 years, highlighting the alarming recurrence of mega-droughts in North America. These extreme climatic episodes underscore the urgent need for integrative water resource management strategies and adaptive policy frameworks that can effectively mitigate the escalating frequency, intensity, and duration of drought phenomena under a warming climate.

The CDI, which integrates multiple drought-related variables—including precipitation anomalies, soil moisture deficits, and vegetation stress—provides a comprehensive depiction of the evolving hydrometeorological conditions across the region. According to this assessment, substantial precipitation shortfalls (classified under the "watch" category) and pronounced soil moisture depletion (categorized as a "warning" level) were observed, particularly in the central and western parts of Türkiye, including several agriculturally significant provinces (EDO, 2024). These findings signal heightened vulnerability to hydrological stress within the region.

In alignment with these international assessments, national-level analyzes corroborate the increasing prevalence of drought within Türkiye. Statistical evaluations and spatial analyzes conducted by the Turkish State Meteorological Service (MGM in Turkish acronyms) further emphasize this trend. Notably, the western regions—especially areas adjacent to the Marmara Sea—have been subjected to severe drought conditions, characterized by acute deficits in both rainfall and soil moisture reserves (MGM, 2024). Such climatic anomalies not only exacerbate agricultural water scarcity but also pose significant threats to regional ecosystems and socio-economic stability. Collectively, these assessments highlight the urgent necessity for robust drought monitoring systems, proactive adaptation strategies, and enhanced transboundary cooperation to address the escalating risks posed by climate variability in Türkiye and the broader Mediterranean basin.

An analysis of precipitation patterns during the recent drought period in Türkiye, examined at both regional and watershed scales, reveals a pronounced decline in rainfall across nearly all climatic zones of the country. This trend is clearly illustrated in the spatial precipitation distribution map published by the MGM, as shown in Fig. 11.1. The map demonstrates that precipitation levels have decreased markedly, with reductions ranging from 20% to 60% in several critical hydrological basins, most notably the Marmara, Menderes, and Susurluk river basins. Such a widespread and severe precipitation deficit not only signals an intensification of meteorological drought conditions but also portends far-reaching

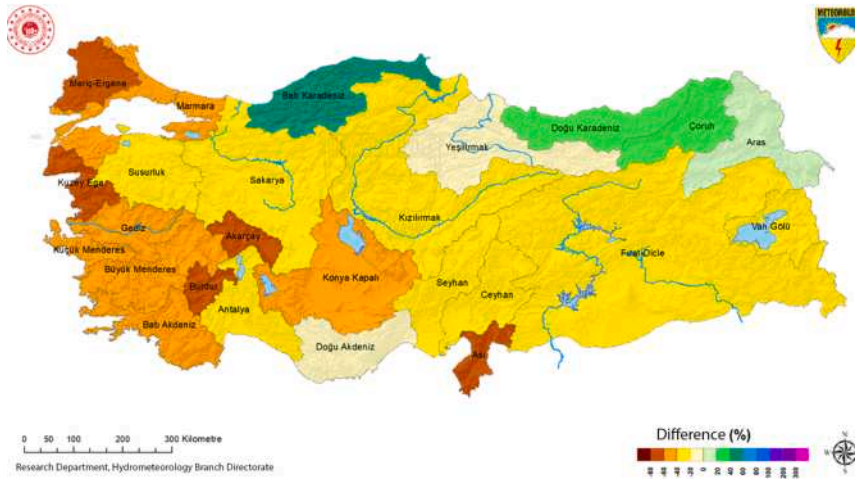


Figure 11.1 Comparison of Area Precipitation Norms by Watersheds for the Water Year (1 October 2024 to 30 November 2024).Map lines delineate study areas and do not necessarily depict accepted national boundaries.

hydrological consequences, particularly in regions that are heavily reliant on consistent rainfall for both agricultural and industrial purposes.

It is well documented in the scientific literature that drought extends far beyond its conventional meteorological, agricultural, and hydrological definitions, exerting profound and often irreversible socioeconomic and sociological repercussions. These multifaceted impacts have been increasingly magnified by the intensification of global climate change, which has led to heightened precipitation variability and extreme weather anomalies, particularly during the winter and spring seasons—periods that are pivotal for agricultural productivity, aquifer recharge, and ecosystem sustainability. The insufficiency of precipitation during these critical months severely disrupts crop phenology, diminishes agricultural yields, and jeopardizes food security, thereby placing considerable strain on rural livelihoods and exacerbating poverty in vulnerable communities. Furthermore, the continuous decline in annual rainfall volumes imposes escalating stress on both surface water bodies and groundwater reserves, threatening the long-term stability of urban and rural water supply networks.

The cascading effects of these hydrometeorological anomalies manifest across ecological, economic, and social domains. These include accelerated ecosystem degradation, loss of biodiversity, deterioration of soil quality, and the decline of agricultural economies, along with broader socio-political risks

associated with water scarcity. Given the severity of these interconnected challenges, the development and deployment of integrated water resource management (IWRM) frameworks, underpinned by rigorous scientific analysis, have become imperative. Such frameworks must incorporate high-resolution climate models, hydrological simulations, and socioeconomic vulnerability assessments to formulate adaptive policies that are both anticipatory and resilient to future climatic uncertainties. In recent years, the importance of effective risk management has grown markedly, as the frequency and intensity of both droughts and floods have increased worldwide. The persistence of such extreme hydrological events necessitates comprehensive risk analyzes and the implementation of proactive measures aimed at safeguarding human lives, protecting infrastructure, and preserving ecosystems (Krysanova et al., 2008). In Türkiye, significant institutional advancements have been made in the realm of water management to address these pressing challenges. The principal governmental agency responsible for the coordination and implementation of water-related policies is the General Directorate of State Hydraulic Works (*Devlet Su İşleri*, DSI), established in 1953. Operating through a decentralized structure composed of 26 regional directorates, the DSI is tasked with optimizing the protection and sustainable utilization of the nation's surface and groundwater resources.

Notably, the DSI's first regional office, the 1st Regional Directorate located in Bursa, has played a central role in managing water resources in the northwestern provinces of Bursa, Yalova, and Kocaeli. Since the early 2000s, this regional office has expanded its scope to encompass a range of initiatives, including flood mitigation, drought risk reduction, agricultural irrigation development, and the protection of water-dependent ecosystems (DSI, 2024). Its activities now encompass large-scale infrastructural projects, integrated watershed management plans, and the implementation of advanced monitoring systems to improve both water availability and quality. These institutional efforts underscore the critical importance of coordinated, science-based, and regionally tailored approaches to address the multifaceted risks posed by evolving climatic and hydrological regimes.

11.2 Applications and Practices

Droughts and floods, both categorized as hydrological risks, are widely recognized as manifestations of disruptions within the natural

hydrological cycle, often induced by climatic anomalies and anthropogenic pressures (Ward et al., 2020). In response to these increasingly frequent and severe events, a diverse array of water infrastructure solutions has been systematically developed and implemented by the DSI in Türkiye. Among the most prominent of these interventions are diversion weirs, flood diversion canals, and large-scale dam projects. Notably, dams serve as multipurpose hydraulic structures designed primarily to regulate river flows, mitigate flood hazards, store water for periods of scarcity, and ensure consistent water availability for domestic, agricultural, and industrial use (Lehner et al., 2011).

Given Türkiye's positioning within a predominantly semi-arid climatic zone, where seasonal rainfall variability and recurrent drought episodes pose significant threats to water security, the development of IWRM strategies has become indispensable. In this context, the DSI, as the principal governmental body charged with water governance, plays a pivotal role in optimizing the utilization, conservation, and equitable distribution of water resources nationwide. The agency adopts a methodologically robust, phased approach that systematically addresses both supply-side and demand-side water challenges.

- **At the core of DSI's methodology is an emphasis on land consolidation and irrigation efficiency enhancement**. This initial phase involves the reorganization of agricultural lands to improve irrigation effectiveness, reduce operational costs, and increase agricultural productivity. Through the implementation of advanced piping irrigation systems, DSI effectively minimizes water losses stemming from infiltration and surface evaporation, which are common in traditional open-channel irrigation methods.
- **Subsequently, DSI's technical strategy encompasses the comprehensive planning, design, construction, and operational management of water storage infrastructures**, ranging from large-scale surface reservoirs to localized underground cisterns and artificial ponds. These facilities are strategically developed to secure potable water supplies for urban centers and industrial complexes, while simultaneously providing critical reserves for agricultural irrigation during dry periods. This systematic storage approach ensures that water availability is maintained throughout hydrologically stressed seasons.
- **In parallel, DSI actively implements flood mitigation and land reclamation projects** aimed at protecting both residential settlements

and economically significant agricultural lands from the destructive impacts of floods. These measures include the construction of levees, embankments, flood bypass channels, and other hydraulic control structures designed to regulate peak flows and prevent inundation in vulnerable areas.

Over the past two decades, Türkiye has witnessed the accelerated development of such infrastructure, reflecting the government's intensified focus on bolstering national water security and climate resilience. Within this broader framework, the DSI 1st Regional Directorate—responsible for the northwestern provinces of Bursa, Yalova, and Kocaeli—has undertaken substantial investments in hydraulic infrastructure (Fig. 11.2). During this period, a total of 138 water-related facilities have been constructed in Bursa Province, alongside 26 in Kocaeli and 15 in Yalova. These projects encompass an integrated portfolio of dams, irrigation ponds, flood protection systems, and drinking water supply units, each tailored to address the specific hydrological and socioeconomic characteristics of their respective regions. Collectively, these efforts underscore the critical importance of methodical, regionally adapted, and technically rigorous water resource management strategies in fostering long-term resilience against hydrological extremes.

In this context, significant progress has been achieved in the province of Bursa over the past two decades through the systematic implementation of diverse water infrastructure projects led by the General Directorate of State Hydraulic Works (DSI). As depicted in Fig. 11.3,



Figure 11.2 The location map of the State Hydraulic Works (DSI) 1st Regional Directorate.Map lines delineate study areas and do not necessarily depict accepted national boundaries.

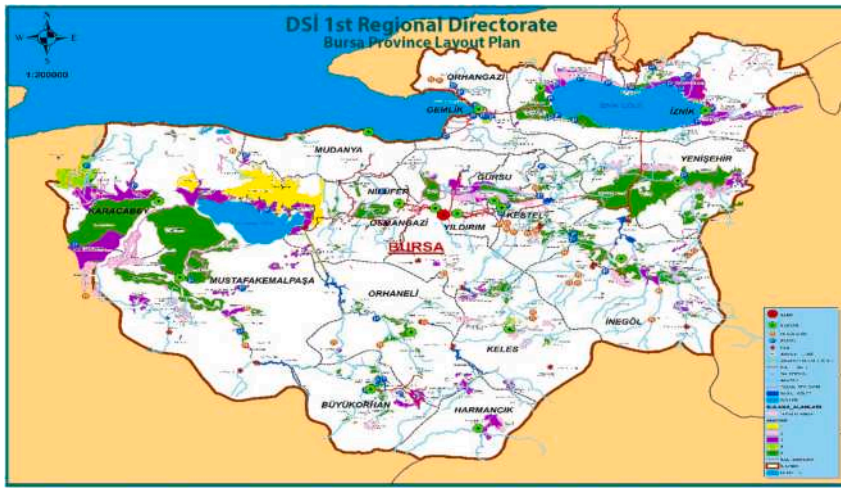


Figure 11.3 Investments within the Provincial Boundaries of Bursa by the General Directorate of State Hydraulic Works (DSI) 1st Regional Directorate.Map lines delineate study areas and do not necessarily depict accepted national boundaries.

these efforts have resulted in the construction of a comprehensive portfolio of hydraulic facilities, strategically designed to address regional water management challenges.

The major infrastructure developments completed in Bursa include:

- 3 drinking and utility water treatment facilities to ensure reliable potable water supplies,
- 24 large-scale dams for multipurpose water storage and flood regulation,
- 17 agricultural irrigation ponds for localized water retention,
- 9 underground storage structures to enhance groundwater recharge and augment water security during dry periods,
- 47 modern irrigation facilities equipped with high-efficiency systems,
- 5 land consolidation and integrated irrigation projects aimed at optimizing agricultural land use and improving irrigation efficiency,
- 21 flood protection and control infrastructures to safeguard residential and agricultural areas from hydrological hazards, and
- 12 hydroelectric power plants (HEPPs) contribute to the region's renewable energy portfolio.

Collectively, these projects have produced substantial hydrological, agricultural, and socioeconomic benefits:

- An annual provision of 90,980,000 m^3 of potable and utility water, supplying a population of approximately 2,349,488 residents.

- A total reservoir storage capacity of 520,720,000 m^3 was achieved through dam construction (Table 12.1), supplemented by an additional 8,370,000 m^3 from ponds and 8.60.000 m^3 from underground storage facilities.
- The opening of 568,410 decares (approximately 56,841 hectares) of agricultural land to modern irrigation, which has contributed to an annual increase of agricultural income estimated at 4,831,485,000 Turkish Lira.
- The successful completion of land consolidation initiatives covering 404,620 decares, significantly improved the efficiency of agricultural operations and facilitated large-scale irrigation schemes.
- The protection of 15 settlement areas and 47,403 decares of land from flood risks through targeted flood control measures.
- An annual hydroelectric energy generation capacity of approximately 660,000,000 kWh, enhancing the region's energy independence and contributing to the national renewable energy targets.

These outcomes not only reflect the technical and engineering success of the implemented projects but also underscore the broader socioeconomic transformations induced by IWRM strategies. The cumulative effects of these interventions have reinforced the resilience of the province of Bursa against hydrological extremes, strengthened local food and water security, and improved regional energy sustainability. Moreover, the strategic integration of water supply, irrigation, flood mitigation, and energy generation functions within a unified management framework demonstrates the effectiveness of multi-functional water infrastructure systems in semi-arid regions. Moving forward, such models provide critical insights for scaling up similar interventions in other regions facing compounded risks from climate change, water scarcity, and rapid urbanization.

In this regard, the total storage capacity of the 24 dams constructed is 520,740,000 m^3, providing an agricultural benefit of 280,950 decares. During this period, 17 reservoirs were built, with a total storage capacity of 8,365,000 m^3 (Table 11.1), contributing to agricultural irrigation across an area of 29,770 decares. As a result, the resilience against climate change and possible droughts has been improved to a great extent.

11.3 Further Applications and Investments

Between 2023 and 2024, the DSI 1st Regional Directorate successfully completed the construction of a total of 179 water-related

Table 11.1 Dams completed within the boundaries of Bursa province in the last 20 years.

No	Name of the dam	Height from the foundation (m)	Reservoir capacity (m^3)	The benefit derived (Decar)
1	Büyükorhan Kınık Pond	17,1	600,000	1890
2	Gemlik Hamidiye Pond	18	146,000	720
3	İnegöl Çavuşköy Pond	29	525,000	1410
4	İnegöl Olukman Tekke Pond	24,5	439,000	1640
5	İznik Derbent Pond	28,2	172,000	810
6	İznik Hisardere Pond	29,2	450,000	1800
7	Karacabey Bayramdere Pond	26	800,000	1920
8	Keles Sorgun Pond	26,5	525,000	1990
9	Kestel Çamlık Pond	20	383,000	2130
10	Kestel Nüzhetiye Pond	25,1	630,000	1090
11	Kestel Şevketiye Pond	20	490,000	4200
12	Nilüfer Güngören Pond	27	280,000	980
13	Yolçatı (Göbelye) Pond	22,80	645,000	1250
14	Orhaneli Göynükbelen Pond	27,50	738,000	1600
15	Orhaneli Söğüt Pond	21,6	283,000	890
16	Osmangazi Kızılkaya Pond	21	519,000	3300
17	Yenişehir Fethiye Pond	29	740,000	2150
TOTAL			**8,365,000**	**29,770**

infrastructure facilities across the provinces of Bursa, Kocaeli, and Yalova. These projects, realized through significant public investments, were meticulously planned and executed with the primary aim of enhancing regional water security and strengthening resilience against the adverse impacts of drought. The constructed facilities encompass a wide range of hydraulic structures including:

- **28 dams** designed for multipurpose water storage and flood mitigation,
- **21 irrigation ponds** serving as localized water reservoirs to support agricultural activities,
- **10 underground artificial recharge systems** aimed at augmenting groundwater reserves through managed aquifer recharge techniques, and
- **53 pressurized pipe irrigation networks** were developed to ensure efficient water distribution and minimize conveyance losses in agricultural fields. The remaining infrastructure includes various flood control installations and supplementary water management systems tailored to the unique hydrological characteristics of each province.

Notably, the cumulative storage capacity achieved by the construction of dams, ponds, and underground water storage facilities over the past two decades has been substantial, collectively amounting to **567,840,000 m^3** of water. This capacity has been distributed as follows:

- **537,630,000 m^3** in Bursa,
- **27,750,000 m^3** in Kocaeli, and
- **2,400,000 m^3** in Yalova.

Such a considerable increase in storage capacity has played a pivotal role in safeguarding these regions against the escalating risks of hydrological droughts and ensuring sustainable water availability for multiple sectors. By securing stable water reserves, these facilities have provided a critical buffer against seasonal rainfall fluctuations and long-term precipitation deficits, both of which have been exacerbated by the ongoing effects of climate change. Moreover, the parallel expansion of modern irrigation infrastructure has significantly improved agricultural productivity and water use efficiency across these regions. In total, 355,910 decares of agricultural land have been brought under irrigation through the implementation of pressurized pipe networks during the same period. The province-specific distribution of irrigated land demonstrates the central role of Bursa in the region's agricultural economy, with 320,720 decares in Bursa, followed by 40,180 decares in Kocaeli, and 5010 decares in Yalova. These outcomes not only reflect the technical achievements of DSI but also underscore the

Table 11.2 Summary of investments made by DSI 1st regional rirectorate in the last 20 years.

Province	Type	Reservoir capacity (m^3)	Irrigated land (da.)
Bursa	Dams	520,724,000	280,950
	Ponds	8,365,000	29,770
	Artificial recharge system storage	8,600,000	
SUBTOTAL		**537,689,000**	**310,720**
Kocaeli	Dams	12,530,000	7200
	Ponds	15,216,000	32,980
SUBTOTAL		**27,746,000**	**40,180**
Yalova	Dams	1,892,000	5010
	Artificial recharge system storage	500,000	–
SUBTOTAL		**2,392,000**	**5010**
DSI Bursa 1st Regional Directorate	Total of the benefit derived	567,827,000	355,910
TOTAL		**567,827,000**	**355,910**

strategic importance of IWRM in building regional resilience to drought. By systematically increasing storage capacity, improving irrigation efficiency, and reinforcing groundwater recharge, the DSI 1st Regional Directorate has laid a robust foundation for long-term water sustainability. Furthermore, these projects exemplify an adaptive management approach that prioritizes climate-resilient infrastructure, ensuring that local communities and key economic sectors are better equipped to withstand future hydrological stresses (Table 11.2).

11.4 Sum Up

The General Directorate of State Hydraulic Works was officially established on December 18, 1953, under Law No. 6200, and was subsequently organized across Türkiye in 1954. As a key public institution, DSI was endowed with comprehensive authority over the regulation, development, and utilization of the nation's water resources for their designated purposes, as mandated by its founding legislation. In this context, DSI has been entrusted with the planning, design, and

construction of critical water infrastructure, including facilities for irrigated agriculture, hydroelectric power generation, potable water supply, and flood protection. The institution's responsibilities also encompass the construction of multi-functional hydraulic structures, such as dams, ponds, and artificial storage systems, which serve both as protective barriers against floods and as reservoirs for strategic water storage (DSI, 2024).

Following its establishment, DSI was systematically decentralized through the formation of regional directorates, with the 1st Regional Directorate headquartered in Bursa—a region characterized by both agricultural richness and significant hydrological variability. Since its inception, the DSI 1st Regional Directorate has played a central role in enhancing regional water security. By 2023, it had achieved the conservation of approximately 111,500,000 m^3 of water through the construction of dams and ponds. However, particularly over the past two decades, the institution has markedly intensified its activities, leading to the conservation of an additional 567,840,000 m^3 of water through an expanded portfolio of water storage infrastructure. These strategic investments represent a critical step in reinforcing the region's resilience to recurrent drought events, especially considering Türkiye's geographical position within a semi-arid climatic zone prone to increasing water stress.

In parallel with water storage projects, DSI has implemented extensive irrigation modernization initiatives. Historically, open irrigation networks were developed on 723,510 decares of agricultural land; however, recognizing the inefficiencies associated with traditional systems—particularly losses due to infiltration and evaporation—the institution has shifted towards advanced pressurized pipe irrigation networks. As of 2023, a total of 355,910 decares of Class 1 agricultural land have been equipped with these modern irrigation systems, substantially reducing water loss and improving agricultural water use efficiency. Against the backdrop of accelerating global climate change—characterized by heightened precipitation variability, rising temperatures, and altered hydrological regimes—the DSI 1st Regional Directorate has strategically prioritized the conservation and efficient management of water resources in Bursa, Kocaeli, and Yalova. These efforts align directly with several key targets of the United Nations Sustainable Development Goals (SDGs), most notably:

- **SDG 6 (Clean Water and Sanitation):** Ensuring sustainable water management and universal access to clean water,
- **SDG 2 (Zero Hunger):** Supporting food security through irrigation development and sustainable agriculture,

- **SDG 13 (Climate Action):** Enhancing adaptive capacity to climate-related hazards and natural disasters, and
- **SDG 7 (Affordable and Clean Energy):** Promoting renewable energy through hydroelectric power development.

In particular, the region's water infrastructure initiatives serve as a cornerstone for climate adaptation strategies and are essential for building long-term hydrological resilience. As water scarcity intensifies, driven by both climatic and demographic pressures, Bursa's capacity to adapt hinges upon the continuous modernization of its water systems, guided by science-based policy interventions and IWRM frameworks.

In this respect, the role of the state—as exercised through DSI—remains indispensable in mobilizing the financial, technical, and institutional resources required to advance water security. Through its regional directorates, DSI not only addresses immediate drought mitigation needs but also lays the foundation for sustainable and equitable water governance in the decades ahead. As Bursa and the surrounding provinces continue to confront the twin challenges of urbanization and climate change, maintaining this momentum in water infrastructure development will be vital to securing a resilient and prosperous future for the region.

11.5 Future Projections

Given the escalating risks posed by groundwater depletion, reduced snowpacks, declining river flows, and heightened drought and wildfire threats, continuous investment in water resources remains essential for safeguarding Bursa's hydrological security. Recent efforts in water storage expansion, irrigation modernization, and resource conservation have shown promising results; however, sustained action is needed to address long-term climate vulnerabilities. The future applications should prioritize integrated water management approaches that incorporate advanced hydrological modeling, groundwater recharge strategies, and climate-resilient irrigation systems. Moreover, expanding monitoring networks and developing early warning mechanisms will be vital for adaptive planning. Strengthening collaborations between local authorities, research institutions, and stakeholders will be critical to ensure that Bursa remains both water-secure and climate-resilient in the decades ahead.

References

Devlet Su İşleri Genel Müdürlüğü (DSI). (2024). https://DSI.gov.tr/.

European Drought Observatory (EDO). (2024). https://edo.jrc.ec.europa.eu..

Krysanova, V., Buiteveld, H., Haase, D., Hattermann, F. F., van Niekerk, K., Roest, K., Martinez-Santos, P., & Schlüter, M. (2008). Practices and lessons learned in coping with climatic hazards at the river-basin scale: Floods and droughts. *Ecology and Society, 13*(2), 32 http://www.jstor.org/stable/26267974.

Lehner, B., Liermann, C. R., Revenga, C., Vörösmarty, C., Fekete, B., Crouzet, P., Döll, P., Endejan, M., Frenken, K., Magome, J., Nilsson, C., Robertson, J. C., Rödel, R., Sindorf, N., & Wisser, D. (2011). High-resolution mapping of the world's reservoirs and dams for sustainable river-flow management. *Frontiers in Ecology and the Environment, 9*(9), 494–502. https://doi.org/10.1890/100125.

Meteoroloji Genel Müdürlüğü (MGM). (2024). https://mgm.gov.tr/.

Ward, P. J., de Ruiter, M. C., Mård, J., Schröter, K., van Loon, A. F., Veldkamp, T., von Uexkull, N., Wanders, N., Aghakouchak, A., Arnbjerg-Nielsen, K., Capewell, L., Llasat, M. C., Day, R. J., Dewals, B. J., Di Baldassarre, G., Huning, L. S., Kreibich, H., Mazzoleni, M., Savelli, E., Teutschbein, C., & Wens, M. (2020). The need to integrate flood and drought disaster risk reduction strategies. *Water Securty, 11*, 100070. https://doi.org/10.1016/j.wasec.2020.100070.

World Meteorological Organisation (WMO). https://wmo.int/news/media-centre/eight-warmest-years-record-witness-upsurge-climate-change-impacts.

SECTION III

New trends in drought studies

This page intentionally left blank

CHAPTER TWELVE

Meteorological drought modeling using recurrent neural network and long short-term memory

Ali Danandeh Mehr[1], Hiba Alkubaisi[2], and Rifat Tur[3]
[1]Civil Engineering Department, Antalya Bilim University, Antalya, Türkiye,
[2]Electrical and Computer Engineering Program, Institute of Postgraduate Education, Antalya Bilim University, Antalya, Türkiye,
[3]Civil Engineering Department, Akdeniz University, Antalya, Türkiye

12.1 Introduction

Droughts are characterized by prolonged diminished precipitation (rainfall or snowfall). Global warming, which drives rising temperatures and reduced precipitation, has intensified the frequency of droughts across diverse regions. Recent studies highlight their adverse effects on critical sectors such as agriculture, water supply, ecosystems, public health, tourism, and food security (Maghrebi et al., 2020). To ensure sustainable water management and foster socioeconomic stability, effective drought monitoring and prediction are imperative (Soylu Pekpostalci et al., 2023). As a result, researchers have increasingly turned to advanced machine learning (ML) methods such as decision trees (DT), support vector regression (SVR), artificial neural networks (ANN), multivariate adaptive regression splines, M5Tree, recurrent neural networks (RNNs), genetic programming (GP), and long short-term memory (LSTM), for modeling and forecasting droughts (Alkubaisi et al., 2025). These ML frameworks are classified into three categories: time series analysis models, regression-based techniques, and classification approaches (Danandeh Mehr, 2021; Vidyarthi & Jain, 2020). For example, Danandeh Mehr (2021) applied decision DT, gradient boosting decision tree (GBT), and GP techniques for drought event classification in Türkiye. Their findings revealed that DT exhibited lower generalization skills, whereas GBT surpassed DT and GP.

Drought Dynamics
DOI: https://doi.org/10.1016/B978-0-443-34205-9.00020-2
© 2026 Elsevier Inc. All rights are reserved, including those for text and data mining, AI training, and similar technologies.

Several studies have reviewed applications of ML techniques in hydrological studies such as drought modeling and forecasting (Danandeh Mehr et al., 2018; Márquez-Grajales et al., 2024; Nandgude et al., 2023; Prodhan et al., 2022; Sundararajan et al., 2021). These studies have shown that the accuracy of ML models significantly differs depending on the local and temporal features of climate data, suggesting diverse performances in different regions. In addition, these studies have demonstrated that longer lead time forecasting may result in less accuracy, and traditional regression and ML techniques often struggle to precisely discern the underlying hydroclimatic phenomena. Therefore, hybrid ML models were suggested for more accurate solutions when standalone ML models are unable to model drought (Xu et al., 2022). However, the complexity of these hybrid models has been rarely discussed in the literature. For example, Vidyarthi and Jain (2020) utilized DT and ANN models to extract information from observed drought events in Bengal. They showed that DT-extracted rules may increase ANN's ability to model and forecast drought events. Mehr et al. (2022) showed that hybridizing random forest with GAs may result in more accurate drought models. In a more recent study, Achite et al. (2023) compared the efficiency of ML models, and suggested a hybrid adaptive neuro-fuzzy inference system optimized by the water cycle algorithm (WCA), for hydrological drought forecasting in Algeria. Further, some studies have reported that a hybridization strategy through data decomposition and integrating decomposed signals with ML techniques can increase prediction accuracy (Danandeh Mehr et al., 2023; Jamei et al., 2023).

Our review also demonstrates that forecasting drought is a complex undertaking due to the presence of extremely stochastic relationships among drought events and associated indicators. The current implementations of multilayer perception (MLP) in drought forecasting have shown that the existing studies have mostly focused on either structural optimization of the associated network via an external bioinspired optimization technique or hybridization through advanced signal processing techniques giving less attention to the complexity of the evolved models that made their application less possible by practitioners. RNNs and LSTMs are the most recent advancements in neural networks that have shown superior performance in the most recent hydrological studies (Waqas & Humphries, 2024). However, their efficiency for meteorological drought forecasting has not been explored yet. Therefore, in this study, we aimed to compare them for drought prediction. We have used the historical drought time

series with the pattern recognition feature of the RNN and LSTM model to predict the Standardized Precipitation Evapotranspiration Index (SPEI) as a drought index. To the best of our knowledge, this is the first study that compared these models for SPEI forecasting in Iraq.

12.2 Methods

Waqas and Humphries (2024) presented a critical review of the RNN and LSTM models. However, an overview of these methods is given here to secure the independence of this chapter.

12.2.1 Overview of recurrent neural network

RNNs are an advanced class of ANNs designed for processing sequential data by maintaining a memory of past inputs. Unlike traditional feedforward neural networks, RNNs have recurrent connections, i.e., memory through feedback loops, that allow information to persist, making them well-suited for tasks involving time series, natural language (text, speech) processing, and sequential decision-making. As shown in Fig. 12.1, at each timestep, the network processes an input (here X_{t-1}) and updates a hidden state (a vector representing past information, h_{t-2}). Then, the output at timestep t depends on both the current input x_t and the previous hidden state h_{t-1}.

Fig. 12.1 depicts a simple RNN, where the internal memory (h_t) is computed using Eq. (12.1):

$$h_t = f\,(W \cdot x_t + U \cdot h_t + b) \tag{12.1}$$

where $f(.)$ is the activation function (like Tanh), U and W are weights, b is the bias, and X is the input vector (here antecedent SPEI). Although they are suggested for time-sensitive applications, the main challenges for RNNs

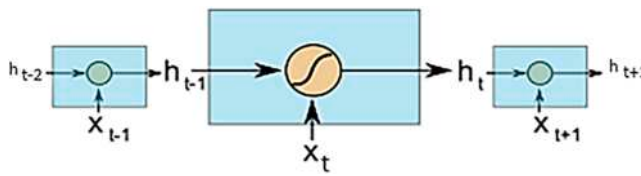


Figure 12.1 Simple recurrent neural network internal operation.

include difficulty in learning long-term dependencies. In addition, sequential processing limits parallelization (Kim, 2017).

12.2.2 Overview of long short-term memory

LSTMs (Hochreiter & Schmidhuber, 1997) are a popular type of RNN designed to overcome the vanishing gradient problem that often hampers traditional RNNs in modeling long-term dependencies. LSTMs are widely used in time series forecasting, natural language processing, and sequence-based tasks. Key features of LSTMs include:

- Memory Cells: LSTMs maintain a cell state, which serves as the network's memory, allowing information to persist over long sequences.
- Gates: LSTMs use a series of gates including forget gate (FG), input gate (IG), and output gate (OG), respectively for information discarding from the cell state, storing new information in the cell state, and controlling the output of the cell based on the cell state and the current input.
- Long-Term Dependency Handling: By explicitly controlling what to retain and discard, LSTMs excel at capturing long-term dependencies in sequential data.

As shown in Fig. 12.2, the architecture of an LSTM unit consists of: (1) an input layer that accepts sequential input data (e.g., time series data or text), (2) a hidden layer that contains the LSTM cells where computations involving the input, gates, and cell states occur, and (3) output layer that produces predictions or outputs for the task.

LSTMs remain one of the most powerful tools for sequence modeling, widely utilized in real-world applications and forming the basis for more advanced architectures like bidirectional LSTMs and sequence-to-sequence models. Handling long-term dependencies effectively mitigates vanishing

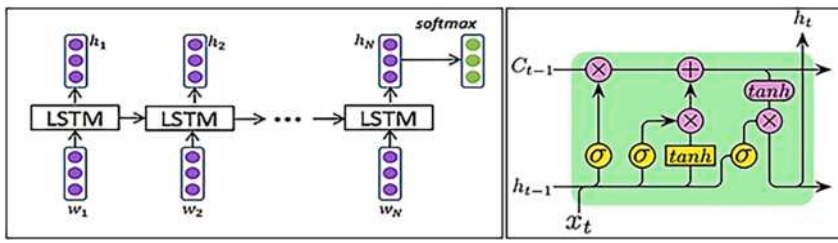


Figure 12.2 The long short-term memory structure and their unit.

gradient issues common in LSTM. The LSTM unit's update is expressed in Eq. (12.2) (Alkubaisi et al., 2025).

$$\begin{aligned} h^{((t))} = g_o^{(t)} f_h\left(s^{(t)}\right) \quad s^{(t-1)} = g_f^{(t)}.\, s^{(t-1)} + g_i^{(t)}.\, f_s\left(wh^{(t-1)}\right) \\ + uX^{(t)} + b) \quad g_i^{(t)} = sigmoid\left(w_i h^{(t-1)} + u_i X^{(t)}\right. \\ \left. + b_i\right) \quad g_f^{(t)} = sigmoid\left(w_f h^{(t-1)} + u_f X^{(t)} + b_f\right) \quad g_o^{(t)} \\ = sigmoid\left(w_o h^{(t-1)} + u_0 X^{(t)} + b_o\right) \end{aligned} \tag{12.2}$$

The activation functions of the system state and internal state are denoted as f_h and f_s, respectively. More details on the LSTM setup used in this study were given in Alkubaisi et al., 2025.

12.3 Drought data gathering for central Iraq

Drought indices are metrics used to quantify drought conditions like the Standardized Precipitation Index (SPI) (McKee et al., 1993), SPEI, or the Palmer Drought Severity Index (PDSI). Different indices measure various aspects of drought such as precipitation, soil moisture, or vegetation health. Several organizations like National Oceanic and Atmospheric Administration (NOAA), U.S. Department of Agriculture (USDA), and international bodies like the World Meteorological Organization (WMO), are involved in drought monitoring. Some reputed websites and platforms that provide drought indices, monitoring tools, and datasets include US Drought Monitor (droughtmonitor.unl.edu), NOAA's Climate Prediction Center (cpc.ncep.-noaa.gov), Global Drought Observatory (edo.jrc.ec.europa.eu/gdo), NASA's GRACE (Gravity Recovery and Climate Experiment; grace..jpl.nasa.gov), FAO's Agricultural Stress Index System (fao.org/giews/earthobservation), European Drought Observatory (edo.jrc.ec.europa.eu), and SPEI Global Drought Monitor (spei.csic.es). SPEI considers both precipitation and temperature to calculate meteorological conditions. In the *SPEI* computation, for the *i*-month, the difference D_i (water balance) between the precipitation P_i and potential evapotranspiration PET_i is considered as input (Lee et al., 2024).

$$D_i = P_i - PET_i \tag{12.3}$$

$$SPEI = \begin{cases} t - \dfrac{c_0 + c_1 t + c_2 t^2}{1 + d_1 t + d_2 t^2 + d_3 t^3}, \; t = \sqrt{2 \ln \Pr} \text{ for } Pr \le 0.5 \\ -\left(t - \dfrac{c_0 + c_1 t + c_2 t^2}{1 + d_1 t + d_2 t^2 + d_3 t^3}\right), \; t \\ \quad = \sqrt{2 \ln (1 - \Pr)} \text{ for } Pr > 0.5 \end{cases} \tag{12.4}$$

where $Pr = 1 - F(x)$ and represents the probability of exceeding a certain value of D. The values of the coefficients c and d are: $c_0 = 2.515517$, $c_1 = 0.802853$, $c_2 = 0.010328$, $d_1 = 1.432788$, $d_2 = 0.189269$, and $d_3 = 0.001308$ (Alkubaisi et al., 2025).

In this study, we extracted the SPEI time series with 6-month accumulation period from the SPEI Global Drought Monitor (GDM) website for four grid points (G1 to G4) located in central Iraq (Fig. 12.3). The data feature and LSTM-based drought forecasting using these data were presented by Alkubaisi et al. (2025). Other potential alternatives include (but are not limited to) National Centers for Environmental Information (https://www.ncei.noaa.gov/), Copernicus Climate Change Service (C3S)—ERA5 Reanalysis (https://climate.copernicus.eu/), and European Drought Observatory (edo.jrc.ec.europa.eu), however, these site coverage is limited only to Europe.

Fig. 12.3 shows that SPEI at all grid points exhibits significant fluctuations over time, suggesting a highly dynamic system oscillating between approximately −3 and 3, indicating standardized data. The SPEI patterns at G1 (blue) and G4 (cyan) seem to follow very similar trends,

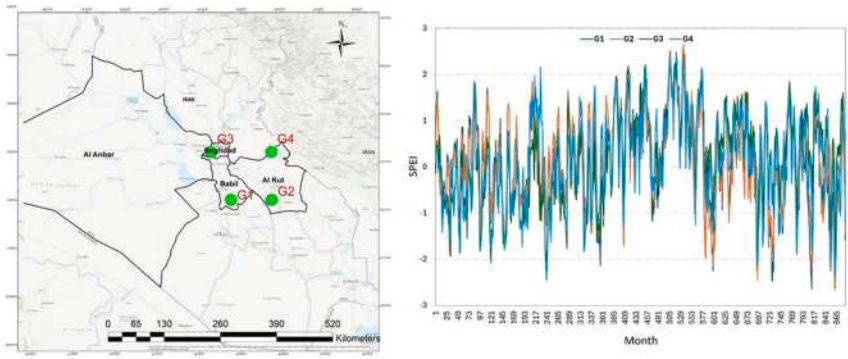


Figure 12.3 Map of the study area *(left)* and SPEI-6 time series *(right)* retrieved from global SPEI website. Map lines delineate study areas and do not necessarily depict accepted national boundaries.

implying a strong correlation between them. Further, G2 (orange) and G3 (green) also show similar SPEI movements but with slight deviations from G1 and G4. The mean arithmetic SPEI attained from these points was considered as the target SPEI for the study area.

12.4 Selection of the best predictors and model performance indices

As previously mentioned, this study adopts the same input sets as those proposed by Alkubaisi et al. (2025). This approach ensures a direct comparison between our developed RNN model, and the LSTM model presented for the same study area. The authors used mutual information (Eq. 12.5) and Pearson's correlation coefficient to detect the best predictors for $SPEI_t$ among its lags. In addition, root mean square error (*RMSE*) and Nash–Sutcliffe Efficiency (NSE) were used as the efficiency measures.

$$MI\left(SPEI_t,\ SPEI_{t+\alpha}\right) = \sum_{i,j} \rho\left(SPEI_t,\ SPEI_{t+\alpha}\right) \log\left(\frac{\rho\left(SPEI_t,\ SPEI_{t+\alpha}\right)}{\rho\left(SPEI_t\right),\ \rho\left(SPEI_{t+\alpha}\right)}\right) \tag{12.5}$$

where $\rho\left(SPEI_t\right)$ and $\rho\left(SPEI_{t+\alpha}\right)$ are the marginal probability distribution of $SPEI_t$ and, $SPEI_{t+\alpha}$ and $\rho\left(SPEI_t,\ SPEI_{t+\tau}\right)$ is the joint probability distribution function of $SPEI_t$ and $SPEI_{t+\alpha}$. The letter τ denotes lag time.

12.5 Results

12.5.1 Results of recurrent neural network

The results of the RNN (Table 12.1) models demonstrate the effectiveness of using different LSTM layer configurations for predicting the SPEI-6 drought index. Four projects were conducted, each with varying numbers of LSTM layers, from a single layer to four layers, to evaluate the models' predictive performance based on training and testing error metrics, specifically RMSE and NSE.

Fig. 12.4 depicts the forecasts of one-layer LSTM vs observed time series. The one-layer LSTM model achieved a Train RMSE of 0.3615 and a Test RMSE of 0.3752, with Train NSE of 0.8412 and Test NSE of 0.8131. This simple model performs well but leaves room for improvement.

Table 12.1 The structure of each recurrent neural network project.

Project	LSTM layers	Units per layer	Activation	Output layer
1	1	1st layer: 100 units	ReLU	Dense (1)
2	2	1st layer: 100 units2nd layer: 50 units	ReLU	Dense (1)
3	3	1st layer: 100 units2nd layer: 50 units 3rd layer: 50 units	ReLU	Dense (1)
4	4	1st layer: 100 units2nd layer: 50 units 3rd layer: 50 units4th layer: 50 units	ReLU	Dense (1)

LSTM, Long short-term memory.

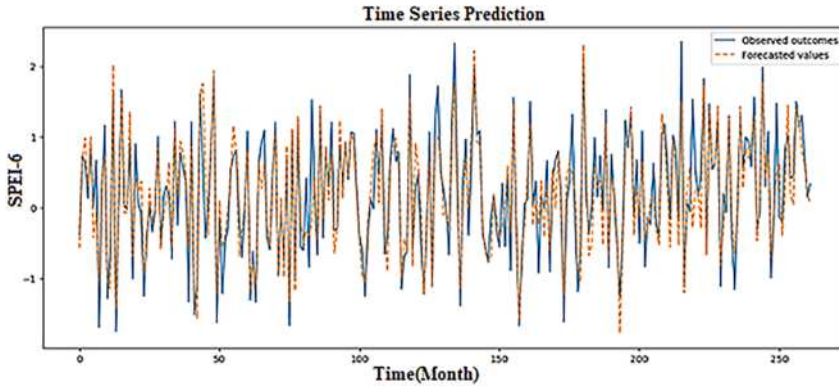


Figure 12.4 SPEI-6 time series of observed and forecasted values one-layer long short-term memory.

Adding a second LSTM layer improved the model's accuracy slightly, with a Train RMSE of 0.3578 and Test RMSE of 0.3723. The NSE values also improved to 0.8445 for training and 0.8160 for testing, indicating that an additional layer enhances the model's ability to capture patterns in the data.

Fig. 12.5 depicts the forecasts of three-layer LSTM vs observed time series. A three-layer LSTM model yielded the best Test RMSE of 0.3668, with a Train NSE of 0.8351 and Test NSE of 0.8214, suggesting that this architecture generalizes well on test data. However, the Train RMSE is slightly higher than in the two-layer model, possibly indicating slight overfitting.

Fig. 12.6 depicts the forecasts of one-layer LSTM vs observed time series. The four-layer LSTM model demonstrated similar performance to the two-layer model, with a Train RMSE of 0.3590 and Test RMSE of 0.3739. NSE values were also close, at 0.8434 for training and 0.8145 for testing, suggesting diminishing returns when further increasing model complexity.

The RNN model accuracy at training and testing periods was tabulated in Table 12.2. From these results, the three-layer model stands out as the

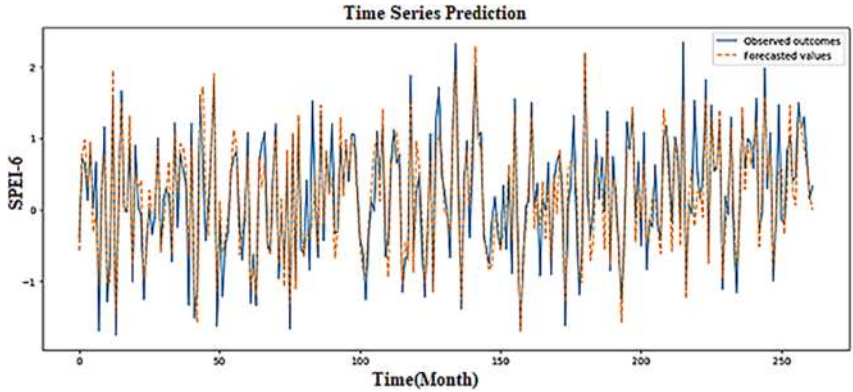


Figure 12.5 SPEI-6 time series of observed and forecasted values three-layer long short-term memory.

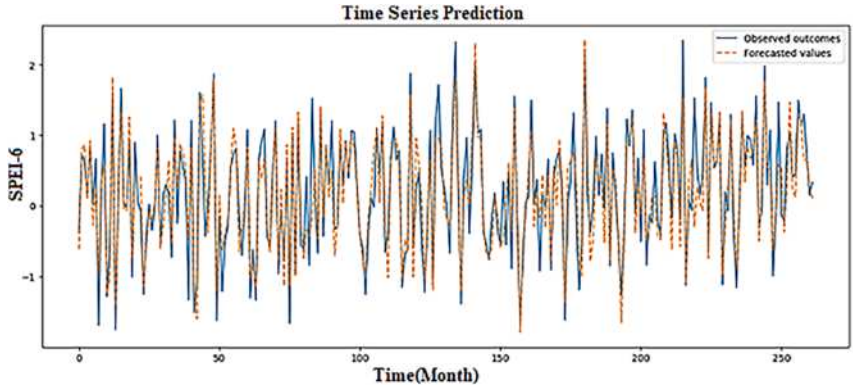


Figure 12.6 SPEI-6 time series of observed and forecasted values four-layer long short-term memory.

most accurate for test data, achieving the lowest Test RMSE of 0.3668 and the highest Test NSE of 0.8214. However, adding more than two LSTM layers provides only minor accuracy gains, indicating that an optimal balance of model complexity and performance is achieved with two to three LSTM layers for this specific dataset.

In summary, RNNs with two or three LSTM layers are optimal for SPEI-6 predictions, balancing accuracy and complexity. Future enhancements of the model could involve tuning layer sizes, activation functions, and dropout regularization.

12.5.2 Results of long short-term memory

According to Alkubaisi et al. (2025), the optimal LSTM model, configured with 50 units, achieved a training RMSE of 0.363 and a testing RMSE of 0.392, demonstrating its ability to effectively forecast SPEI-6 values for the study area. Additionally, the model acheived NSE values of 0.8427 for the training set and 0.7881 for the testing set, further confirming its predictive performance. Fig. 12.7 shows the time series of the best LSTM model during the testing period developed by Alkubaisi et al. (2025).

12.5.3 Recurrent neural network versus long short-term memory

The performance comparison between RNN models and LSTM models reveals some key differences in their capabilities for time series forecasting, particularly for predicting the SPEI-6 index. Both models utilized the same input features (SPEI-6 values at previous time steps), with each model incorporating similar configurations such as an output dense layer with a single unit and the Adam optimizer with mean squared error as the loss function.

Table 12.2 Recurrent neural network model's accuracy at training and testing periods.

Project	LSTM layers	Train RMSE	Test RMSE	Train NSE	Test NSE
1	1	0.3615	0.3752	0.8412	0.8131
2	2	0.3578	0.3723	0.8445	0.8160
3	3	0.3684	0.3668	0.8351	0.8214
4	4	0.3590	0.3739	0.8434	0.8145

LSTM, Long short-term memory; *NSE*, Nash–Sutcliffe Efficiency; *RMSE*, root mean square error.

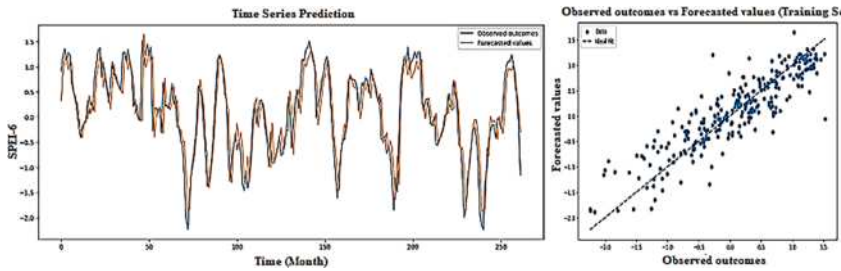


Figure 12.7 SPEI-6 time series of observed and forecasted values attained by long short-term memory.

The RNN models, with configurations of one to four LSTM layers, achieved solid performance, as indicated by RMSE values ranging from 0.3578 to 0.3752 on test data and NSE values ranging from 0.8131 to 0.8214. The three-layer RNN model achieved the best performance in the series, with a test RMSE of 0.3668 and a test NSE of 0.8214, suggesting an excellent fit for time series predictions. However, these models required more layers to achieve optimal results and, even then, did not outperform the LSTM model.

The LSTM model, optimized with 50 units in a single LSTM layer, attained a slightly higher test RMSE of 0.392 and a test NSE of 0.7881. While LSTM's performance was close, it showed slightly lower predictive accuracy on test data than the best RNN model with three layers. The primary advantage of LSTM, however, is its ability to capture long-term dependencies in the time series data more efficiently with fewer layers, due to its internal memory mechanism, which better retains information over long sequences. This suggests that while both architectures are viable for time series forecasting, RNNs may require deeper configurations, whereas LSTMs can provide comparable results with simpler architectures, albeit with minor trade-offs in accuracy in this specific case.

12.6 Conclusion

This study developed and evaluated both RNN and LSTM models for 1-month-ahead forecasting of the SPEI-6 index in Karbala, Iraq. Utilizing data from 1950 to 2024 sourced from GDM at four grid points nearest to the study area, the models were tuned through a trial-and-error approach to determine the optimal number of LSTM units and hidden layers. Results

showed that both RNN and LSTM models achieved acceptable accuracy, with NSE values greater than 0.78 in the testing dataset, indicating their ability to capture temporal drought patterns in the region.

Comparative analysis revealed that the three-layer RNN model delivered the best predictive accuracy, achieving a test RMSE of 0.3668 and a test NSE of 0.8214. While LSTM models are generally considered ideal for long-term dependencies, the RNN model, with fewer units but more layers, performed slightly better in this case. This suggests that simpler RNN architectures can be highly effective for shorter time series datasets, where the complexity of LSTM may not yield significant performance gains due to the limited training data length.

These findings highlight the potential of traditional RNNs for effective climatic time series forecasting, especially when data length is constrained, whereas the more complex LSTM may not always offer a distinct advantage. This underscores that model selection should consider both the data characteristics and the network architecture's depth and complexity. Future studies could explore the integration of hybrid architectures that combine the strengths of RNN and LSTM, alongside parameter optimization techniques and the inclusion of uncertainty quantification to further enhance model robustness. Additionally, extending the model to account for external meteorological and environmental variables may improve accuracy and applicability in diverse climatological settings.

AI disclosure

During the preparation of this work the author(s) used Chat GPT to improve English language. After using this tool/service, the author(s) reviewed and edited the content as needed and take(s) full responsibility for the content of the publication.

References

Achite, M., Gul, E., Elshaboury, N., Jehanzaib, M., Mohammadi, B., & Danandeh Mehr, A. (2023). An improved adaptive neuro-fuzzy inference system for hydrological drought prediction in Algeria. *Physics and Chemistry of the Earth, Parts A/B/C, 131*, 103451. https://doi.org/10.1016/j.pce.2023.103451.

Alkubaisi, H., Danandeh Mehr, A., Adarsh, S., & Khan, M. M. H. (2025). Drought modelling and forecasting using shallow and deep machine learning techniques. *Modeling Earth Systems and Environment, 11*(1). https://doi.org/10.1007/s40808-024-02268-w, https://www.springer.com/journal/40808.

Danandeh Mehr, A. (2021). Drought classification using gradient boosting decision tree. *Acta Geophysica, 69*(3), 909–918. https://doi.org/10.1007/s11600-021-00584-8.

Danandeh Mehr, A., Nourani, V., Kahya, E., Hrnjica, B., Sattar, A. M. A., & Yaseen, Z. M. (2018). Genetic programming in water resources engineering: A state-of-the-art review. *Journal of Hydrology, 566*, 643–667. https://doi.org/10.1016/j.jhydrol.2018.09.043, https://www.elsevier.com/inca/publications/store/5/0/3/3/4/3.

Danandeh Mehr, A., Reihanifar, M., Alee, M. M., Vazifehkhah Ghaffari, M. A., Safari, M. J. S., & Mohammadi, B. (2023). VMD-GP: A new evolutionary explicit model for meteorological drought prediction at ungauged catchments. *Water (Switzerland), 15*(15). https://doi.org/10.3390/w15152686, http://www.mdpi.com/journal/water.

Hochreiter, S., & Schmidhuber, J. (1997). Long short-term memory. *Neural Computation, 9*(8), 1735–1780. https://doi.org/10.1162/neco.1997.9.8.1735.

Jamei, M., Ahmadianfar, I., Karbasi, M., Malik, A., Kisi, O., & Yaseen, Z. M. (2023). Development of wavelet-based Kalman Online Sequential Extreme Learning Machine optimized with Boruta-Random Forest for drought index forecasting. *Engineering Applications of Artificial Intelligence, 117*, 105545. https://doi.org/10.1016/j.engappai.2022.105545.

Kim, K. (2017). Time-sensitive adaptation of regularization strength of recurrent neural networks for accurate learning. In *Proceedings—16th IEEE international conference on machine learning and applications* (pp. 194–198), ICMLA 2017, Institute of Electrical and Electronics Engineers Inc., South Korea. https://doi.org/10.1109/ICMLA.2017.00036.

Lee, S., Moriasi, D. N., Danandeh Mehr, A., & Mirchi, A. (2024). Sensitivity of standardized precipitation and evapotranspiration index (SPEI) to the choice of SPEI probability distribution and evapotranspiration method. *Journal of Hydrology: Regional Studies, 53*. https://doi.org/10.1016/j.ejrh.2024.101761, https://www.sciencedirect.com/science/journal/22145818.

Maghrebi, M., Noori, R., Bhattarai, R., Mundher Yaseen, Z., Tang, Q., Al-Ansari, N., Danandeh Mehr, A., Karbassi, A., Omidvar, J., Farnoush, H., Torabi Haghighi, A., Kløve, B., & Madani, K. (2020). Iran's agriculture in the anthropocene. *Earth's Future, 8*(9). https://doi.org/10.1029/2020ef001547.

Márquez-Grajales, A., Villegas-Vega, R., Salas-Martínez, F., Acosta-Mesa, H. G., & Mezura-Montes, E. (2024). Characterizing drought prediction with deep learning: A literature review. *MethodsX, 13*. https://doi.org/10.1016/j.mex.2024.102800, https://www.sciencedirect.com/science/journal/22150161.

McKee, T. B., Doesken, N. J., & Kleist, J. (1993). The relationship of drought frequency and duration to time scales. In *Proceedings of the 8th conference on applied climatology* (pp. 179–183). 17–22 January 1993, Anaheim, California.

Mehr, A. D., Haghighi, A. T., Jabarnejad, M., Safari, M. J. S., & Nourani, V. (2022). New evolutionary hybrid random forest model for SPEI forecasting. *Water, 14*, 755.

Nandgude, N., Singh, T. P., Nandgude, S., & Tiwari, M. (2023). Drought prediction: A comprehensive review of different drought prediction models and adopted technologies. *Sustainability, 15*(15), 11684. https://doi.org/10.3390/su151511684.

Prodhan, F. A., Zhang, J., Hasan, S. S., Pangali Sharma, T. P., & Mohana, H. P. (2022). A review of machine learning methods for drought hazard monitoring and forecasting: Current research trends, challenges, and future research directions. *Environmental Modelling and Software, 149*. http://doi.org/10.1016/j.envsoft.2022.105327, https://www.elsevier.com/inca/publications/store/4/2/2/9/2/1.

Soylu Pekpostalci, D., Tur, R., Danandeh Mehr, A., Vazifekhah Ghaffari, M. A., Dąbrowska, D., & Nourani, V. (2023). Drought monitoring and forecasting across Turkey: A contemporary review. *Sustainability, 15*(7), 6080. https://doi.org/10.3390/su15076080.

Sundararajan, K., Garg, L., Srinivasan, K., Bashir, A. K., Kaliappan, J., Ganapathy, G. P., Selvaraj, S. K., & Meena, T. (2021). A contemporary review on drought modeling using machine learning approaches. *CMES—Computer Modeling in Engineering and Sciences, 128*(2), 447–487. https://doi.org/10.32604/cmes.2021.015528, https://www.techscience.com/CMES/v128n2/43927.

Vidyarthi, V. K., & Jain, A. (2020). Knowledge extraction from trained ANN drought classification model. *Journal of Hydrology, 585*. https://doi.org/10.1016/j.jhydrol.2020.124804, https://www.elsevier.com/inca/publications/store/5/0/3/3/4/3.

Waqas, M., & Humphries, U. W. (2024). A critical review of RNN and LSTM variants in hydrological time series predictions. *MethodsX, 13*, 102946. https://doi.org/10.1016/j.mex.2024.102946.

Xu, D., Zhang, Q., Ding, Y., & Zhang, D. (2022). Application of a hybrid ARIMA-LSTM model based on the SPEI for drought forecasting. *Environmental Science and Pollution Research, 29*(3), 4128–4144. https://doi.org/10.1007/s11356-021-15325-z.

CHAPTER THIRTEEN

Data assimilation technologies

Samira Sadat Soltani
Institute of Bio- and Geosciences (IBG-3, Agrosphere), Forschungszentrum Jülich GmbH, Jülich, Germany

13.1 Introduction

Drought is one of the most frequent environmental disasters, with its occurrence expected to increase globally due to human-induced climate change (Dai, 2013; IPCC, 2012). Extreme weather events are predicted to become more severe, primarily caused by significant reductions in seasonal or annual precipitation (Mishra & Singh, 2010). The impacts of droughts extend beyond environmental degradation, threatening food security, water resource management, and even political stability (Dai, 2011; Mishra & Singh, 2010). Droughts result in billions of dollars in economic losses annually and account for approximately 20% of disaster-related damages (Cook et al., 2007). To effectively monitor and predict drought conditions, reliable instruments are essential (Luo & Wood, 2007). Accurate definitions and measurements of drought are crucial, with four primary categories identified: hydrological, agricultural, meteorological, and socioeconomic (Wilhite & Glantz, 1985). These categories are interconnected, as precipitation influences the hydrological system (Wilhite & Svoboda, 2000). Understanding the complex interactions between land-atmosphere processes and human activity is vital for assessing the broad impacts of drought on land surface conditions (Van Loon, 2015). Land Surface Models (LSMs), which combine river-routing systems and high-resolution atmospheric data, are essential tools for studying drought dynamics (Dirmeyer et al., 2006; Schellekens et al., 2017). They have evolved to support drought monitoring and forecasting by providing critical boundary conditions for atmospheric models (Balsamo et al., 2015). The use of Earth observations (EOs) provides long-term datasets that enhance LSM capabilities, offering comprehensive coverage of terrestrial hydrology, vegetation, and energy cycles (Lettenmaier et al., 2015).

Soil moisture (SM) is a critical variable in hydrological and climate modeling, serving as an early indicator of drought. Its sensitivity to changes

Drought Dynamics
DOI: https://doi.org/10.1016/B978-0-443-34205-9.00019-6
© 2026 Elsevier Inc. All rights are reserved, including those for text and data mining, AI training, and similar technologies.

in precipitation and evapotranspiration makes it essential for monitoring drought conditions. Monitoring SM is crucial for agricultural productivity and ecosystem health, especially in regions prone to prolonged dry spells. Remote sensing technologies, particularly satellite-based sensors, have significantly improved global SM monitoring. Instruments such as NASA's Soil Moisture Active Passive (SMAP), Soil Moisture and Ocean Salinity (SMOS), Sentinel-1, and the ESA Climate Change Initiative (CCI) provide real-time data on SM variability, enabling effective drought evaluation and prediction (Entekhabi et al., 2010). These advanced satellite missions offer complementary data that enhance our understanding of SM dynamics and contribute to more accurate drought assessments and forecasting. By incorporating satellite SM data into LSMs, we can enhance model accuracy and improve predictions of water availability and drought severity (Soltani, 2025).

Groundwater storage is also influenced by SM levels, with decreased SM during droughts directly affecting groundwater recharge rates (Rodell & Famiglietti, 2002). The GRACE satellites have been instrumental in tracking changes in groundwater storage across large spatial scales (Famiglietti et al., 2011; Soltani et al., 2020). By integrating GRACE data with hydrological models, we can obtain a more accurate depiction of groundwater dynamics and improve drought predictions. Combining GRACE data with other satellite measurements, such as SM, enhances our ability to monitor drought development and its effects on both surface and subsurface water systems (Famiglietti et al., 2011). Earth system data assimilation (DA) leverages real-time observations to enhance the accuracy of hydrologic forecasts (Kumar et al., 2014). By integrating current and historical observations with dynamic models, DA refines model state variables and parameters using the model's prognostic equations. This structured mathematical framework optimally combines observational data with model simulations, considering their respective uncertainties (Moradkhani, 2008). In forecasting applications, DA plays a crucial role in defining initial conditions from available observations, leading to more reliable predictions (Yan et al., 2017). Numerous studies have highlighted the benefits of assimilating remotely sensed data to enhance drought monitoring and forecasting (Kumar et al., 2014; Soltani et al., 2024; Yan et al., 2017).

In this chapter, we will assimilate SM data into a fully coupled surface–subsurface model, the PARallel FLOW (ParFlow)–Community Land Model (CLM) model, for a synthetic case study, while using GRACE

data for a real case study in Iran to illustrate the advantages of satellite remotely sensed DA. This dual approach aims to demonstrate how integrating high-resolution satellite observations with advanced modeling techniques can enhance the accuracy of hydrological forecasts and improve our understanding of drought dynamics. By leveraging synthetic SM data in modeling scenarios and real-world GRACE observations, we can gain valuable insights into SM variability and groundwater dynamics. Ultimately, this approach contributes to more effective drought monitoring and improved water resource management strategies. Additionally, we will discuss other remotely sensed data and their advantages for assimilation into hydrological models, providing a broader context for their application in drought monitoring. Throughout the chapter, we will explore various case studies, highlight the challenges and limitations associated with DA for drought, and offer insights into overcoming these obstacles.

13.2 Emerging data assimilation methods for drought monitoring

Kumar et al. (2014) demonstrated that short-term drought estimations can be greatly enhanced by including SM data. Optimal DA approaches are crucial for integrating observational data with model simulations (Abbaszadeh et al., 2019; Soltani et al., 2021). However, when used on complicated real-world systems, many of the assimilation algorithms now in use fail. The practice of adding high-frequency or real-time observational data to numerical models in order to correct model states and lower uncertainty is known as DA. The difficulties of drought prediction have led to the development of a number of creative methods. One of the most well-known is the Ensemble Kalman Filter (Evensen, 2003), which has been extensively utilized to combine data from meteorological stations, satellite-based remote sensing, and hydrological models to enhance drought forecasts (Soltani et al., 2021, 2024).

EnKF is ideal for dynamic systems like drought because it uses a statistical method that takes into consideration uncertainty in both model predictions and data. By eschewing constrictive assumptions on probability distributions and Gaussian errors in models and data, sequential Monte Carlo (SMC) techniques-especially those based on particle filters (PF), offer a more adaptable substitute. In nonlinear dynamic systems, these techniques

enable the propagation of complete probability distributions throughout time (Matgen et al., 2010; Moradkhani, 2008). The evolutionary PF was created by further improving the particle Filter-Markov chain Monte Carlo (PF-MCMC) approach using genetic algorithms, building on the developments of SMC. For high-dimensional systems, this method, which was first presented by Moradkhani et al. (2012), has shown increased accuracy in state and parameter estimation.

13.3 Data assimilation in agricultural drought monitoring

Root-zone SM is the basis for agricultural drought monitoring. Several methods, such as the SM percentile, SM anomaly, and standardized SM index, have been employed to measure the root-zone SM drought (Hao & AghaKouchak 2013; Luo & Wood 2007; Mao et al., 2015). While remotely sensed retrievals can offer previously unheard-of spatial and temporal resolution of SM, ground-based measurements of SM are only available at the point scale at a few sites in the United States. But because microwaves only reach the top few millimeters, they can only extract the moisture from the surface of the soil, not the root zone. Hydrologic model simulations may estimate long-term root-zone SM over a wide range of scales, but the findings may be biased due to inaccuracies in forcing data, parameters, and model physics shortcomings (DeChant & Moradkhani 2014; Parrish et al., 2012).

Incorporating satellite surface SM data into a dynamic hydrologic model to update the model states (root-zone SM storages) is a tenable method to enhance the root-zone SM estimation (Moradkhani 2008). The EnKF is currently used in most satellite SM DA research (Crow et al., 2008; Kumar et al., 2014; Reichle et al., 2008, 2002; Ryu et al., 2009; Soltani et al., 2024). The linear updating rule violates the conservation of mass, and the assumption of a Gaussian distribution of errors in the EnKF may not hold true for the highly nonlinear hydrologic models (DeChant & Moradkhani, 2012).

The cross-covariance between the root-zone and surface SM also affects how effective the EnKF is. When the satellite surface SM is absorbed, the EnKF is unable to efficiently update the root-zone SM due to the weak and extremely nonlinear connectivity between the surface and root-zone layers (Brocca et al., 2011; Massari et al., 2015). Alternatively, the PF approach

does not violate the conservation of mass and can relax the Gaussian assumption (Moradkhani et al., 2012). Additionally, the PF aims to achieve good performance for both the surface and root-zone layers simultaneously, independent of the cross-covariance between them.

Accordingly, the PF outperforms the EnKF technique in estimating root-zone SM (Yan et al., 2015). The root-zone SM estimates can be further enhanced using the recently established PF-MCMC (Moradkhani et al., 2012) approach, which combines PF with MCMC. According to Yan and Moradkhani (2016), the ability to monitor drought can be enhanced by improving the root-zone SM estimation by the use of PF-MCMC to assimilate satellite surface SM.

Furthermore, the root-zone SM uncertainty is not taken into account by the existing operational drought-monitoring system, which is a deterministic system (Mao et al., 2015; Sheffield et al., 2004; Wang et al., 2011). For agricultural drought monitoring, the DA framework allows for the explicit quantification of root-zone SM uncertainty inside an ensemble framework, resulting in an increasingly precise estimation of root-zone SM states.

13.4 Remote sensing in drought monitoring

Drought monitoring is based on drought indicators computed using hydro-meteorological variables. In general, the remotely sensed observations are not currently used for operational drought monitoring. One of the main limitations is the short length of the record (AghaKouchak et al., 2015; Lettenmaier et al., 2015). For instance, a decade of SM data from AMSR-E may not be sufficient to monitor drought. However, the remotely sensed observations still provide valuable information on the hydrologic variables at an unprecedented spatial and temporal resolution. For instance, the L-band SM from the SMAP mission provides immense opportunities to aid agricultural drought detection and improve early agricultural drought warning. In the meantime, current and future satellite missions offer opportunities to generate higher-quality and long-term data records by merging satellite observations with model simulations, the method which is referred to as DA data assimilation. In this chapter, the remotely sensed SM and GRACE data are used as an example to illustrate the agricultural drought-monitoring framework through DA. Fig. 13.1 presents the flowchart of the case studies conducted in this research.

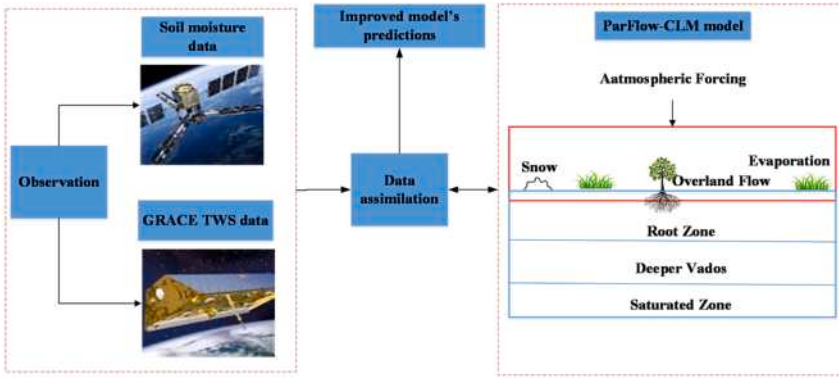


Figure 13.1 Methodology integrating soil moisture and Gravity Recovery and Climate Experiment (GRACE) terrestrial water storage (TWS) data via assimilation to enhance PARallel FLOW (ParFlow)–PARallel FLOW–Community Land Model (CLM) model predictions.

This flowchart outlines the methodology and processes followed in analyzing the impact of assimilating different data into a fully coupled surface–subsurface ParFlow–CLM model for drought monitoring.

13.4.1 Soil moisture

SM is a key hydrologic variable that significantly influences the global water cycle despite its small volume (McColl et al., 2017). Accurate SM estimation is vital for agricultural drought monitoring (Narasimhan & Srinivasan, 2005), vegetation growth (D'Odorico et al., 2007), and water resources management (Dobriyal et al., 2012). The ongoing climate change is causing more extreme weather (Huang et al., 2016; Samaniego et al., 2018; Schlaepfer et al., 2017), posing a significant risk of floods and droughts for agriculture. Prolonged and severe droughts have occurred in many areas of the globe (Mann & Gleick, 2015; Qiu, 2010; Spinoni et al., 2015), causing enormous socioeconomic losses, especially during the crop-growing season. Therefore, accurate water content monitoring is needed to estimate crop drought stress and water demand to provide early warning of agricultural drought in order to reduce crop production loss. SM is an important indicator of water content beneath the land surface and can be used to estimate agricultural drought conditions through observations or model simulations.

Satellite remote sensing provides the ability to monitor SM over a large spatial scale (Bolten et al., 2010; Wang & Qu, 2007; Ahmadalipour et al.,

2017; Soltani, 2022), which is practically and logistically unachievable from in-situ observation networks. The SM Active Passive (SMAP) mission, developed by NASA, measures global land surface SM fields derived from L-band radiances with a revisit frequency of 2–3 days (Entekhabi et al., 2010). Although in-situ sensors provide continuous SM measurements at multiple soil depths, they are only available at certain locations and are not suitable for large-scale studies. These networks are most often used for validation of satellite retrievals. Remotely sensed SM observations are achievable everywhere on the land surface, ideal for a wide range of large-scale hydroclimate applications (Abbaszadeh et al., 2019; Dong et al., 2019) such as drought monitoring (in particular, agricultural drought). A limitation of satellite data is its daily spatial coverage which is limited due to its revisit cycle. Another limitation of the satellite SM retrieval is its consideration of the surface layer (0–5 cm) only. Model simulations can provide spatiotemporal continuous estimations of SM. The SM simulations from LSMs and global hydrological models (GHMs) are widely used in water resources planning, drought monitoring, flood warning, and hydrological forecasts (Mujumdar & Nagesh Kumar, 2012; Srivastava et al., 2013; Xu et al., 2018; Xu et al., 2019b; Xu et al., 2019a; Yan et al., 2017).

Assimilating SM data into hydrological models is a crucial process for improving the accuracy and reliability of hydrological forecasts. Various DA techniques have been employed to incorporate SM observations into hydrological models. The EnKF is one of the most widely used methods, effectively combining model predictions with observational data to provide updated estimates of SM states (Reichle et al., 2002). The EnKF works by generating an ensemble of model states and updating these states based on the discrepancies between model forecasts and observations, accounting for the uncertainties inherent in both the model and the data. Another approach involves the use of PF, which can provide improved performance in nonlinear systems compared to traditional Kalman filtering methods. PFs utilize a set of particles to represent the probability distribution of model states and allow for more flexible representations of the uncertainty in model parameters and observations. These techniques are particularly useful in complex hydrological environments where traditional assumptions of Gaussian distributions may not hold (Moradkhani, 2008).

Assimilating SM data into hydrological models can lead to several significant benefits. First, improved forecast accuracy can be achieved by continuously updating model states with real-time SM observations, leading to more accurate predictions of streamflow, groundwater levels,

and drought conditions (Kumar et al., 2014). This enhancement is particularly beneficial for agricultural applications, where timely and precise forecasts can aid in irrigation planning and crop management. Second, accurate SM estimates are essential for monitoring agricultural drought. By assimilating SM data, models can provide early warning signs of drought conditions, allowing stakeholders to take proactive measures to mitigate potential crop losses (Dai, 2011).

However, challenges remain in the assimilation process. The spatial and temporal resolution of satellite SM products may not align with the scales needed for local hydrological modeling, potentially limiting the effectiveness of DA (McColl et al., 2017). Additionally, different hydrological models may represent SM dynamics in various ways, leading to uncertainties in model outputs that necessitate careful consideration of model selection and configuration (Soltani, 2025). Despite these challenges, the assimilation of SM data into hydrological models represents a promising approach that can enhance drought monitoring, improve water resource management, and increase the accuracy of hydrological forecasts.

For satellite SM assimilation, the majority of studies have used the EnKF algorithm (Kolassa et al., 2017; Reichle et al., 2019), while a few have utilized PF (Lu et al., 2017, 2019). The complexities of drought prediction have led to the development of innovative methods that leverage these DA techniques, ultimately contributing to more effective drought monitoring and improved water resource management strategies.

13.4.2 Application 1: assimilating soil moisture into PARallel FLOW–Community Land Model model

13.4.2.1 PARallel FLOW–Community Land Model model

The ParFlow-CLM model, is a comprehensive hydrological modeling framework that combines the advantages of the CLM and the ParFlow model. Because of this integration, it can accurately model the intricate relationships between subterranean water dynamics and land surface hydrology. According to Sulis et al. (2017), it is especially made to record the behavior of energy and water fluxes over wide geographic areas at high spatial resolutions. There are two main parts to the ParFlow-CLM model. The Richards equation, a crucial equation controlling water flow across three-dimensional variably saturated porous media, is solved by the

ParFlow model, which is the first part of the set (Ashby & Falgout, 1996; Kollet & Maxwell, 2006).

The Richards equation allows for the simulation of subsurface water transport by accounting for important variables including topography and soil characteristics. To effectively manage the complicated calculations required to simulate these complex processes, the ParFlow model makes use of parallel computing techniques and a finite difference approach (Kollet & Maxwell, 2006). Conversely, the goal of CLM (Oleson et al., 2004, 2008) is to depict processes on the land surface. Snow buildup and melt, vegetation dynamics, surface energy balance, and biogeochemistry are the topics covered in its modules. By interacting with the ParFlow subsurface component through flux exchanges, these modules allow for the effective simulation and integration of processes like heat transfer between the land surface and subsurface, evapotranspiration from vegetation, and water infiltration from the surface to the subsurface (Soltani et al., 2022).

13.4.2.2 Data

Fig. 13.2 provides some input data for the ParFlow-CLM model, including precipitation and soil configuration. It shows a sharp rainfall event around 110–120 hours, which influences infiltration and runoff. The soil profile consists of multiple layers extending to 100 m, impacting water movement and retention.

Fig. 13.3 presents additional input data for the ParFlow-CLM model, including slope in the x and y directions and initial pressure head. The top two maps represent terrain slopes in the x and y directions, with values ranging between −0.047 and 0.028, influencing surface and subsurface water flow. The bottom map shows the initial pressure head distribution, ranging from 65.80 to 98.18 m, which is crucial for defining initial groundwater conditions.

13.4.2.3 EnKF

The EnKF has been frequently employed in earlier publications due to its flexibility and ease of use in land surface models (Crow & Wood, 2003; Draper et al., 2012). Model state ensembles are built to estimate the error covariance matrix of the state variable. This enables the most efficient integration of observations and model predictions. The EnKF calculates the updated state ensemble at time step t, for the model-estimated state variable

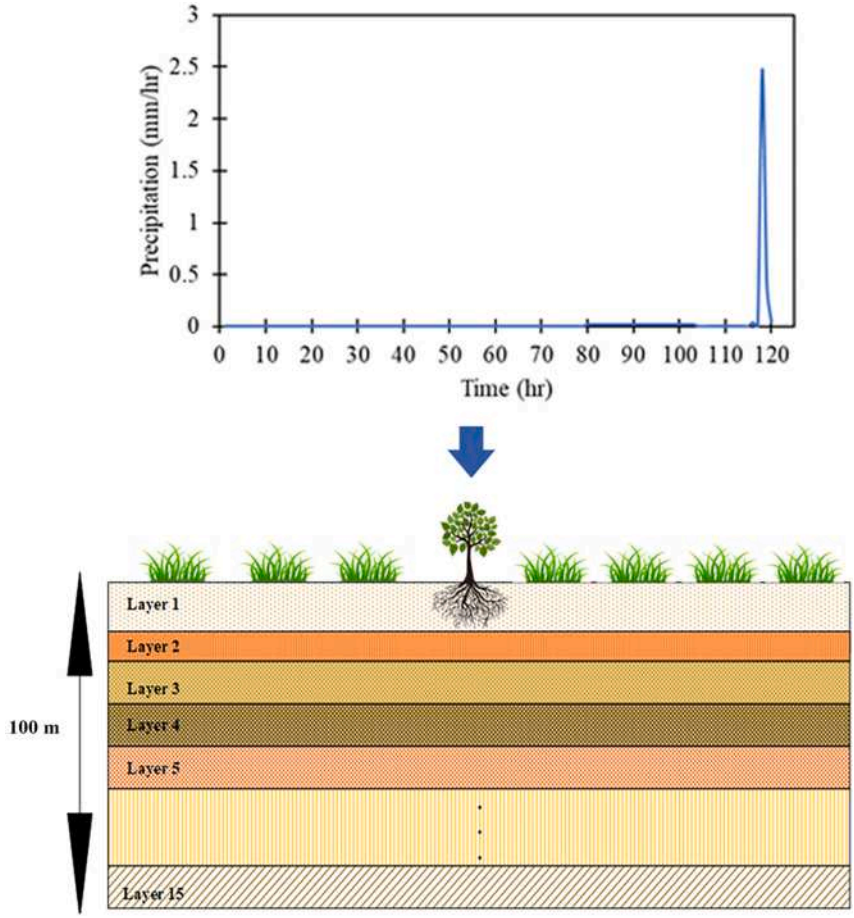


Figure 13.2 PARallel FLOW–Community Land Model input data: precipitation and soil composition.

X_t. This includes the saturation degree and pressure head of all grids for each ensemble member i. N is the number of ensembles.

$$X_t^{i+} = X_t^i + K_t[L_t - H_t X_t^i] \tag{13.1}$$

where the perturbed observation is L_t. Perturbed observation is SM and GRACE data for SM DA and GRACE DA, respectively. The Kalman gain K_t can be defined via:

$$K_t = P_t H_t^T [R_t + H_t P_t H_t^T]^{-1} \tag{13.2}$$

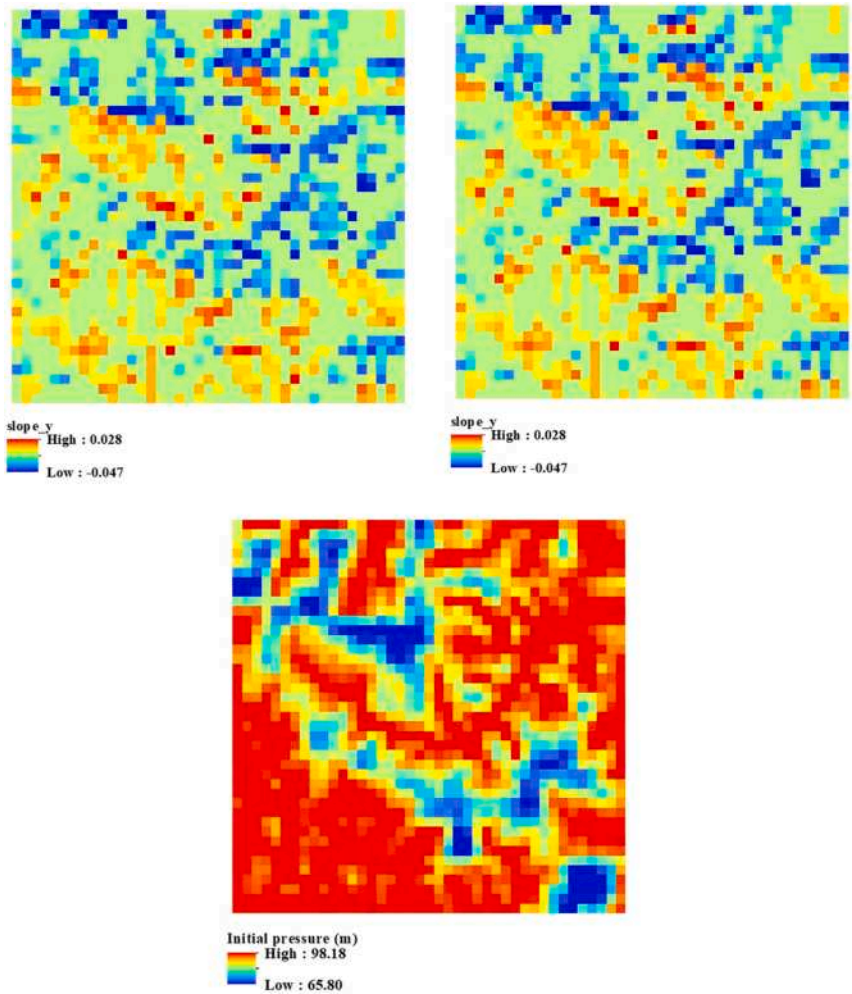


Figure 13.3 PARallel FLOW–Community Land Model input data: terrain slopes in the *x* and *y* directions and initial pressure head.

where R_t is the observation error matrix (a priori assigned as the expected observation error of the SM or GRACE TWS data), is the operator matrix that maps observations to model states at time t (transposed), and P_t is the error covariance matrix for the state variable related to model prediction, which is obtained from:

$$P_t = \sum (X_i - \overline{X})(X_i - \overline{X}^T/(N-1) \tag{13.3}$$

where, $\overline{x}$ is the ensemble mean that contains values for all of the grid cells. The number of ensemble members is given by N. Similarly, R_t is computed as:

$$R_t = \sum (L_i - \overline{L})(L_i - \overline{L})^T / (N - 1) \tag{13.4}$$

where L stores the perturbed observations and is the ensemble mean.

13.4.2.4 Evaluation assessment

To assess model performance in simulating hydrological variables, we use bias (*BIAS*), root mean square error (*RMSE*), and correlation coefficient (*R*). These metrics are calculated as follows:

$$BIAS = \frac{\Sigma \left(\hat{y}^t - y^i_{obs}\right)}{\Sigma y^i_{obs}} \tag{13.5}$$

$$RMSE = \frac{\sqrt{\Sigma \left(\hat{y}^t - y^i_{obs}\right)^2}}{n} \tag{13.6}$$

$$R = \frac{\Sigma^n_{t=1} (y^t_{obs} - \overline{y})(\hat{y}^t - \overline{\hat{y}^t})}{\sqrt{\Sigma^n_{t=1} (y^t_{obs} - \overline{y})^2 \Sigma^n_{t=1} (\hat{y}^t - \overline{\hat{y}^t})^2}} \tag{13.7}$$

where n is the total number of data points. y^t_{obs} is the observed data at time t, $\hat{y}^t$ is the predicted ensemble mean at time t, and $\overline{y}$ is the mean of the observed data.

13.4.2.5 Assimilating soil moisture into PARallel FLOW–Community Land Model model: results

Fig. 13.4 illustrates SM variations over a 120-hour period for three different spatial locations: (5, 5), (10, 10), and (30, 40). The green line represents the open loop SM simulation (SM-OL), the blue line represents the SM DA output (SM-DA), and the red line shows observed SM (SM-Observation).

Observation shows high variability, capturing real-world fluctuations in SM. The green SM-OL line, representing the open loop model without DA data assimilation, deviates more from the observations, indicating that it struggles to capture actual conditions. In contrast, the blue SM-DA line, which incorporates data assimilation, closely follows the observed values, demonstrating improved accuracy. Across all three locations, the data assimilation approach significantly enhances model performance, reducing

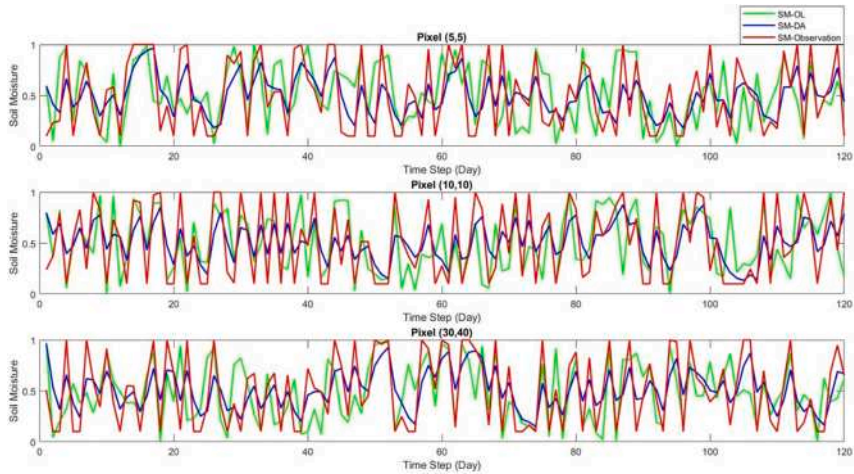


Figure 13.4 Simulated soil moisture variations from assimilating soil moisture data (SM DA) at three distinct spatial locations: (5, 5), (10, 10), and (30, 40). Observations (SM-Observation) and open loop (SM-OL) results are also included for comparison.

discrepancies between simulated and observed SM. This highlights the importance of integrating real-world data to improve hydrological model predictions.

Fig. 13.5 presents a spatial comparison of SM data over time using three different approaches: open loop simulation (SM-OL), data assimilation (SM-DA), and observed SM (SM-Observed).

From the comparison, we can see that SM-OL and SM-DA share similar spatial patterns with SM-Observed, but SM-DA appears to align more closely with observations, capturing finer spatial details and reducing discrepancies. Over time, the SM distribution evolves, and the SM-DA results show improved agreement with the observations compared to the open loop simulation. This highlights the effectiveness of DA in enhancing SM modeling accuracy.

Fig. 13.6 compares the RMSE and Bias between an open loop simulation and a DA approach over time. The top plot shows RMSE, where the open loop simulation (green) maintains a relatively high error (~0.32–0.35), while DA (blue) significantly reduces RMSE to around 0.2, indicating improved model accuracy. The bottom plot presents Bias, where the open loop results (green) fluctuate and remain negative, whereas the

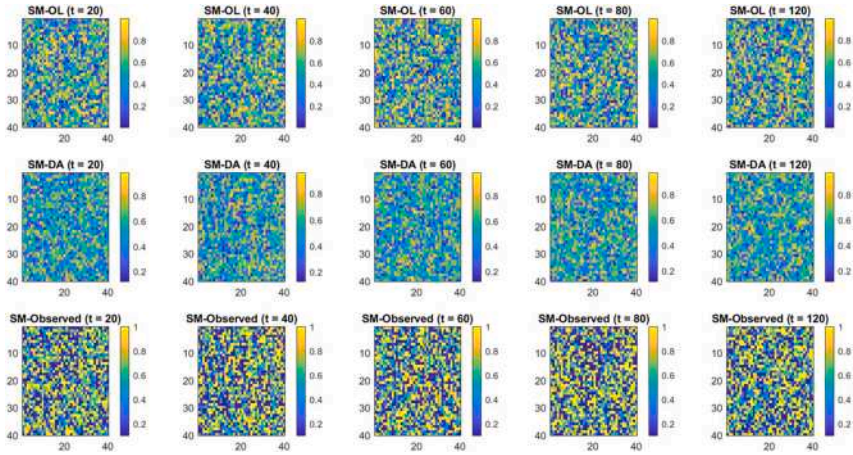


Figure 13.5 Spatially simulated soil moisture (SM) from SM DA at five time steps (20, 40, 60, 80, and 120 h), with observations and open loop results included for comparison.

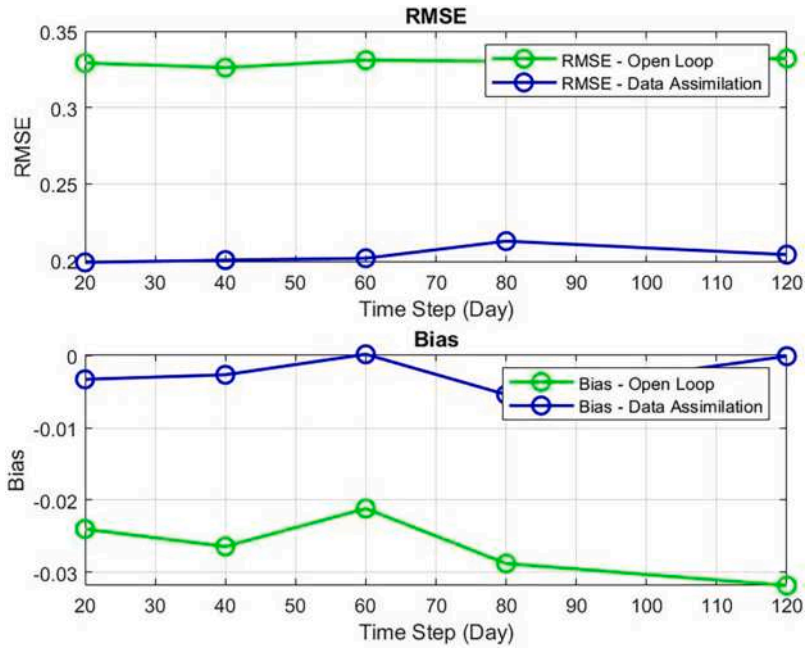


Figure 13.6 Root Mean Square Error (RMSE) and Bias of soil moisture estimates over time, comparing open loop *(green)* and data assimilation *(blue)* results.

data assimilation approach (blue) keeps the Bias close to zero, demonstrating reduced systematic errors.

13.4.3 Snow cover

Understanding the initial stages, severity, and consequences of drought requires regular monitoring of snow cover, especially in regions where snowmelt has a major impact on groundwater replenishment and river flow. The hydrological cycle, energy distribution, and balance of surface radiation all depend on snow cover (Kongoli et al., 2012). It is an essential source of SM for crops and serves as a natural water reservoir. Insufficient SM in the winter can cause agricultural drought, while a lack of winter snowpack can cause hydrological drought in the summer. Snow monitoring is therefore an essential component of managing water resources and a key instrument for predicting drought in different areas.

In order to provide comprehensive, real-time data on critical snowpack parameters, such as snow cover extent (SCE), snow water equivalent (SWE), snow depth (SD), and snow albedo (SA), remote sensing satellites have become indispensable (Kongoli et al., 2012). These measures are essential for improving drought forecasts and forecasting water availability during the snowmelt period. High-resolution data on SCE and albedo is provided by satellites equipped with optical sensors like NASA's Terra and Aqua satellites' MODIS (Moderate Resolution Imaging Spectroradiometer) (Hall et al., 2002). Snow cover is identified by optical measurements using the snow's low reflectivity in the middle infrared wavelengths and high reflection in the visible spectrum (Dozier et al., 2009; Lettenmaier et al., 2015). However, cloud cover may reduce the accuracy of these optical estimates, making them unsuitable for use in all types of weather. Passive microwave sensors, such SMAP (SM Active Passive) and AMSR-E (Advanced Microwave Scanning Radiometer-Earth Observing System), offer crucial data on SWE, which represents the water content in the snowpack, in order to overcome these difficulties (Lettenmaier et al., 2015). These microwave sensors are especially useful for winter monitoring in high-latitude regions since they are less vulnerable to cloud interference and can function in any weather (Romanov et al., 2000). In order to improve the accuracy of snow cover estimates, several researchers have created algorithms that incorporate data from both sensor types, despite their inferior spatial resolution when compared to optical sensors (Foster et al., 2011). Particularly in mountainous and high-latitude areas, active microwave sensors, like Synthetic Aperture Radar (SAR) aboard Sentinel-1 satellites, provide high-resolution observations of

snow depth and cover (Painter et al., 2009). Because SAR technology is not affected by sunshine or atmospheric conditions, it is a useful tool for tracking the dynamics of snowmelt in cloud-prone regions.

The accuracy of streamflow forecasts and drought assessments has significantly increased by the integration of satellite-derived snow data with the hydrological models. SNOwpack TELemetry (SNOTEL), an automated snow water equivalent monitoring system run by the U.S. Department of Agriculture (USDA) in Alaska and the Western United States, provides ground-based data for model validation (Molotch & Bales, 2006).

A key element of Drought Early Warning Systems (DEWS) is remote sensing data, particularly in regions where snowmelt is essential to supply water (Barnett et al., 2005). Water resource managers can anticipate future water shortages and send out early warnings for drought by tracking the amount and timing of snowmelt. Climate change has a direct impact on changes in snow cover volume and duration, according to long-term satellite measurements (Mote et al., 2005). By lowering seasonal water supply, snowpack reductions exacerbate drought conditions, especially in mid-latitude regions.

Nevertheless, despite these developments, there are still issues with incorporating snow cover data into functional drought forecasting systems. For precise monitoring, high-resolution data are required due to the considerable geographical variability of snow, particularly in mountainous areas (Gascoin et al., 2015). Furthermore, forecasts of snowpack depletion are made more difficult by the dynamic nature of snowmelt, which is impacted by temperature, precipitation, and solar radiation. Nonetheless, advancements in DA methods, which integrate data from remote sensing with hydrological and land surface models, improve the precision of drought forecasts and real-time snowpack monitoring (De Lannoy et al., 2012).

Improving snowmelt runoff estimates in the Sierra Nevada has been achieved with the integration of snow data from MODIS and microwave sensors (Dong et al., 2007). In addition to supporting drought monitoring, these DA techniques help water resource managers to make well-informed judgments on the contributions of snowmelt to total water availability. Even though snow-based drought indicators are still in their infancy because of the time and space lags between snowfall and its hydrological impact, continuous improvements in remote sensing and data integration present encouraging opportunities to improve drought monitoring and forecasting in snow-dominated areas.

13.4.4 Evapotranspiration

One of the main hydrological fluxes and an essential part of the hydrologic cycle is evapotranspiration (ET) (Sima et al., 2013). It has a major impact on crop output, irrigation water consumption, and agriculture. The ability of ground-based gauge observations of ET to record geographic fluctuations is constrained, much like that of precipitation. On the other hand, remotely sensed data provide useful instruments for large-scale ET estimation.

Actual and potential evapotranspiration (ET and PET) have been established and studied extensively for drought studies, leading to a variety of drought indicators that describe drought from different angles. These include the Palmer Drought Severity Index (PDSI) (Palmer, 1965), the Crop Water Stress Index (CWSI) (Jackson et al., 1981), the Supply-Demand Drought Index (SDDI) (Rind et al., 1990), the Reconnaissance Drought Index (RDI) (Tsakiris & Vangelis, 2005), the Evaporative Drought Index (EDI) (Yao et al., 2010), the Standardized Precipitation Evapotranspiration Index (SPEI) (Vicente-Serrano et al., 2010), the Evaporative Stress Index (ESI) (Anderson et al., 2011), the Drought Severity Index (DSI) (Mu et al., 2013), the Green Water Scarcity Index (GWSI) (Núñez et al., 2013), and the Green Water Stress Index (GrWSI). In order to evaluate drought conditions, these indices take ET into account. The MODIS is one of the most useful satellite tools for drought analysis with regard to ET. In order to track drought throughout the Contiguous United States (CONUS), Yao et al. (2010) developed the Evaporative Drought Index (EDI). Furthermore, Mu et al. (2007, 2011) created a technique that uses MOD16 products and an algorithm based on the Penman–Monteith equation to create a worldwide ET/PET dataset. They then developed the DSI, which takes vegetation state and ET/PET data into account (Mu et al., 2013).

Important factors affecting evapotranspiration include air temperature, radiation, and relative humidity (Yin et al., 2014). Therefore, in order to comprehend drought and ET, satellite missions that measure these variables are crucial. Land surface temperature (LST) is currently continuously measured globally by a number of remote-sensing platforms such as Terra/Aqua MODIS, Terra-Aster, NOAA-AVHRR, Meteosat-MVIRI, Landsat, and the ATSR series of instruments (Westermann et al., 2011). According to studies conducted in various locations, these LST products frequently provide precise values with a little amount of positive

bias (Sima et al., 2013). Radiation, another factor that influences ET, may be inferred from temperature data, and many studies have concentrated on predicting air temperature from satellite-derived land surface temperature observations (Benali et al., 2012). In order to improve model predictions of SM, latent heat flow, and ET itself, efforts to assimilate ET data have mostly concentrated on univariate techniques (Pan et al., 2008; Pipunic et al., 2008; Qin et al., 2008; Schuurmans et al., 2003). These developments help better drought prediction and management techniques by enhancing hydrological modeling. Zhang et al. (2016), for instance, showed how to successfully integrate satellite-derived ET data into the Variable Infiltration Capacity (VIC) model, resulting in more precise estimation of SM in the Southeast United States. Similarly, Liu and Chen (2024) improved the Noah land surface model's ability to simulate hydrological processes in a semiarid area by using ET estimations based on remote sensing. In addition to improving drought monitoring, these DA approaches help water resource managers make better decisions about water management and drought response plans. Effective drought mitigation efforts will be supported by additional improvements in the integration of ET data with hydrological models brought about by ongoing developments in remote sensing and modeling techniques.

13.4.5 Terrestrial water storage and groundwater

Since 2002, the GRACE mission has given monthly regional estimates of changes in terrestrial water storage (TWS), which includes water content on and below the ground surface (Reager & Famiglietti, 2009). Variations in surface water storage, SM storage, and groundwater storage are all included in changes in TWS. The two twin satellites that make up GRACE orbit the planet at a distance of roughly 220 km and a height of roughly 500 km. Researchers can identify TWS anomalies by accurately measuring the distance between these satellites, which is altered by variations in the Earth's gravity field. An extremely precise K-band microwave ranging technology is used to estimate the distance between satellites. The GRACE efficiently monitors changes in an area's gravity field, which are subsequently converted into TWS estimates (Rodell & Famiglietti, 2002). A useful tool for monitoring water availability is GRACE data (Velicogna et al., 2012). It has been used to evaluate the effects of water availability on vegetation development (Velicogna et al., 2012), investigate regional climate variability

and drought (Chen et al., 2013; Zhang et al., 2015), and integrate into land surface models (Reager et al., 2015). Many researchers have created methods for calculating various hydrological variables using GRACE data. For example, Rodell et al. (2004) used GRACE data to estimate basin-scale ET devised a method to estimate basin discharge using GRACE data. Despite its benefits, GRACE has drawbacks that can make it unsuitable for regional drought evaluations. For example, it provides data at a spatial resolution of more than 150,000 km^2 per grid. Furthermore, the GRACE TWS timeseries only has data spanning roughly 14 years, which might not be enough for evaluating dryness from a climatological view. In order to overcome these obstacles, scientists have employed statistical approaches, including Artificial Neural Networks, to downscale GRACE TWS data to smaller spatial resolutions (Zaitchik et al., 2008) and to extend and reconstruct TWS data for prior years (Zhang et al., 2015). Investigating the effects of drought and calculating the quantity of precipitation needed for drought recovery are made possible by the information provided by GRACE TWS data.

TWS has been found to be a useful drought indicator in a number of studies, especially when using data from the GRACE twin satellites (Houborg et al., 2012; Soltani, 2025). By recording the complete vertical integration of surface and subsurface water compartments, these measurements offer a thorough understanding of water storage. Particularly in the Murray-Darling Basin (MDB), the GRACE data have been extensively utilized to examine patterns of water distribution and evaluate the effects of climate variability (Awange et al., 2011; Brown & Tregoning, 2010; Forootan et al., 2014; Soltani et al., 2022).

Numerous studies have shown how to use the GRACE data in hydrological models to enhance water resource management and drought monitoring. For example, Banerjee and Kumar (2019) improved groundwater level projections in California's Central Valley by including GRACE-derived TWS estimations into the VIC model. The model's ability to accurately simulate hydrological dynamics under various climatic situations was enhanced by this assimilation. Soltani et al. (2024) were the first to assimilate GRACE TWS data into the ParFlow-CLM hydrological model to improve groundwater storage over a case study in Iran. They have assimilated both GRACE and SMOS data in different assimilation scenarios using only SOMS data, only GRACE TWS data, and using both data simultaneously.

13.4.6 Application 2: assimilating Gravity Recovery and Climate Experiment terrestrial water storage data into PARallel FLOW–Community Land Model model

13.4.6.1 Case study description

The case study area includes portions of the Persian Gulf and the Sea of Oman basins, as well as many large subbasins in Iran's western and southwestern areas. This area includes the Karun, Jarahi, and Karkheh subbasins, which together encompass a large area of 158,000 km^2. This territory accounts for around 10% of Iran's total land area. This case study is located in the west of Iran, between [29°N and 35°N] and [46°E and 53°E], and includes key cities like Ahvaz, Khorramshahr, Shahr-e Kord, Kermanshah, and Yasuj (Fig. 13.7). The height in the mountainous regions ranges from above 4000 m above sea level (mASL) to zero mASL along the Persian Gulf coast (Fig. 13.7).

Due to the influence of the complex topography and the passage of mid-latitude storms that originate in the Mediterranean Sea region, precipitation varies seasonally and spatially (Kiany et al., 2020). The average annual precipitation in the research area is between 100 mm in the southwest plains and over 900 mm in some of the eastern mountainous regions (Raziei et al., 2012). The average summer and winter temperatures are 48°C and 4°C, respectively. The 1.3 × 10^6 ha deserts in this zone,

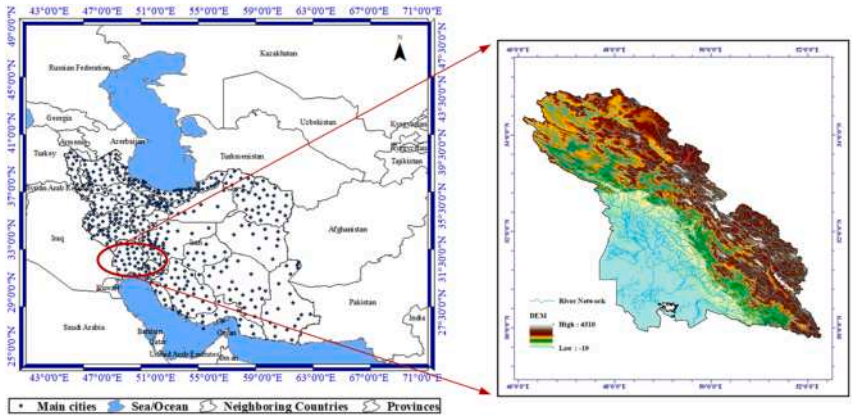


Figure 13.7 Study area location, highlighting the selected region within a broader geographic context *(left)* and its detailed Digital Elevation Model (DEM) with river networks *(right)*. Map lines delineate study areas and do not necessarily depict accepted national boundaries.

which make up about 8% of the basin's total area, are mostly found in the arid and hyperarid climatic zones in the south and southwest (Ardebili & Khademalrasoul, 2018). The major rivers that flow through this basin are the Jarahi, Karkheh, Karun, Zohreh, and Dez. Together, they provide 34 $\times$ 10^9 m^3 of water, or around 33% of the nation's total water resources. Agricultural use accounted for 83% of water consumption in Zohreh-Jarahi, 88% in Karun, and 89% in Karkheh (Rahmani et al., 2021). According to Ardebili and Khademalrasoul (2018), this basin serves as a hub for the development of crops and trees that are fed by the five major rivers and flourish in the southwestern plains that are appropriate for agriculture. Among the most significant crops cultivated in these basins are rice, wheat, barley, cotton, corn, sugarcane, and summer crops.

13.4.6.2 Land surface data and atmospheric forcing

Topography, land cover, soil properties, and canopy physiological parameters are examples of static variables that are included in the land surface input data. A Digital Elevation Model (DEM) with a resolution of 1 km was created using the Global Multiresolution Terrain Elevation Data 2010 (Danielson et al., 2010) (Fig. 13.7). Additionally, the land-use classification from the Moderate Resolution Imaging Spectroradiometer (MODIS) satellite (Friedl et al., 2002) was utilized and transformed into Plant Functional Types (PFT). Using the FAO/UNESCO Digital Soil Map of the World (Batjes, 1997), which contains 19 different soil classes based on Schaap and Leij's (1998) pedotransfer functions, the percentage of soil and clay was calculated ito incorporate the soil properties. The values suggested by Asante et al. (2008) based on the link between roughness and landcover type are utilized for Manning's coefficient. The atmospheric forcing of the coupled ParFlow model with CLM is derived from GLDAS-Noah Land Surface Model L4 V2.1 data (https://disc.gsfc.nasa.gov/datasets/GLDAS_NOAH025_3H_2.1). This data include barometric pressure, wind speed, precipitation, specific humidity, downward shortwave and longwave radiations, and air temperature near the surface. Due to the temporal resolution of the GLDAS data, this has a geographic resolution of 0.25° and a temporal resolution of 3 hours. The data utilization spans from 2015 to 2020. Table 13.1 contains the input data list. To have an equivalent cell size and 0.25° resolution, all of the model inputs listed in were re-projected. The model was used in this investigation for a total thickness of 300 m over

Table 13.1 List of PARallel FLOW–Community Land Model input data.

		Resolution: spatial/temporal	Data source	Download link or reference
Input data	Atmospheric forcing	0.25°/3-hourly	GLDAS_NOAH	https://disc.gsfc.nasa.gov/datasets/GLDAS_NOAH025_3H_2.1
	Plant Functional Type	500 m/Yearly	MODIS satellite (land-use classification)	https://lpdaac.usgs.gov/products/mcd12q1v006/
	Soil Texture Data, Sand and Clay Percentage	-	FAO/UNESCO Digital Soil Map of the World	Batjes (1997)
	DEM	1 km	Global Multiresolution Terrain Elevation Data 2010	https://earthexplorer.usgs.gov/
	Manning's coefficient	-	Relationship between landcover type and manning's coefficient	Asante et al. (2008)

DEM, Digital Elevation Model; *MODIS*, Moderate Resolution Imaging Spectroradiometer.

100 model layers ($nz = 100$) of varying thickness. The horizontal resolution of the model's implementation was 0.25°. The x-direction of this grid has 28 cells ($nx = 28$), whereas the y-direction has 24 cells ($ny = 24$).

13.4.6.3 Gravity Recovery and Climate Experiment terrestrial water storage data

The Center for Space Research (CSR) at the University of Texas at Austin provided GRACE data release 05 (RL05) (Bettadpur, 2012). The monthly spherical harmonic coefficients (SHC) up to degree and order 96 are included in this release. The following formula is used to determine the GRACE-derived TWS and its uncertainty over the case study: First, the value obtained from the satellite laser range (Cheng & Tapley, 2004) is used in place of the C20 term, and Swenson and Wahr (2006) degree 1 coefficients (SHC) are restored. Second, to create the SHC variations, the monthly product is subtracted from the mean for the period from March 2015 to June 2017. Then, to reduce the high-frequency noise, the SHC variations are subjected to restriping (Swenson & Wahr, 2006) using a 300-km radius Gaussian smoothing filters. Third, the TWS variation is calculated from the filtered SHC fluctuations using the procedure described by Wahr et al. (1998). The approach uses a forward model constructed solely from GRACE data to repeatedly search for the genuine TWS. Prior to the assimilation process, the absolute TWS is produced by adding the ParFlow-CLM estimates of TWS temporal mean value (March 2015–June 2017) to the GRACE-derived TWS in order to be compatible with the model estimate (Zaitchik et al., 2008).

13.4.6.4 Groundwater data

The Iran Water Resources Management Company (IWRMC) provides in-situ groundwater level data for observation of wells spread throughout the case study area (http://www.wrm.ir). The conversion of volumetric groundwater change values from IWRMC to equivalent water height depends critically on the size of each aquifer. To guarantee a valid comparison, this conversion procedure is essential. An area-averaged time record of groundwater changes for every aquifer is then used to assess the findings. In particular, the aquifer's average assimilation results are compared to the modified in-situ groundwater time series, which have been adjusted for seasonal variations, well characteristics, or calibration factors to correct for biases or inaccuracies in the original measurements. This comparison sheds light on how well the modifications made to the in-situ groundwater time series matched the average assimilation results for the aquifer.

13.4.6.5 Methodology

Filter algorithm parameters, observation files, and instructions for creating an ensemble of model runs are required as input for the DA framework (Fig. 13.8). During preprocessing, ensembles of input data were acquired, and the error information of TWS data was determined using GRACE level 2. Postprocessing entails comparing the output of ParFlow-CLM with separate data sets. As seen in Fig. 13.8, we cross-validated the modeling results with in-situ groundwater measurements.

13.4.6.6 Assimilating GRACE TWS data into ParFlow-CLM model: results

Fig. 13.9 compares the correlation performance and groundwater storage fluctuation between an open loop simulation and GRACE data assimilation (GRACE-DA). Variations in groundwater storage over time, from March 2015 to May 2017, are depicted in the top plot. The observed in-situ data trend is generally followed by the GRACE-DA and open loop simulations; however, GRACE-DA seems to be in greater agreement with the in-situ measurements. The correlation coefficient (R) for GRACE-DA and open loop is shown in the bottom plot. With a better R-value of 0.82 than the open loop simulation's 0.77, GRACE-DA shows that model performance improves with DA. In comparison to the open loop simulation, these findings generally imply that incorporating GRACE data improves the precision of groundwater storage forecasts, resulting in a higher correlation with observed in-situ observations.

Fig. 13.10 shows the spatial distribution of bias in temporally averaged groundwater level variations (cm) from open loop simulations, GRACE DA, and in-situ measurements. Bias represents the difference between modeled or satellite-derived groundwater levels and actual ground-based observations. This comparison highlights the advantage of assimilating GRACE satellite data to improve groundwater estimates by reducing uncertainties and providing a more accurate representation of groundwater storage changes.

13.5 Conclusions and future perspectives

Although DA technologies for drought prediction have made promising advances, there are still a number of challenges to their

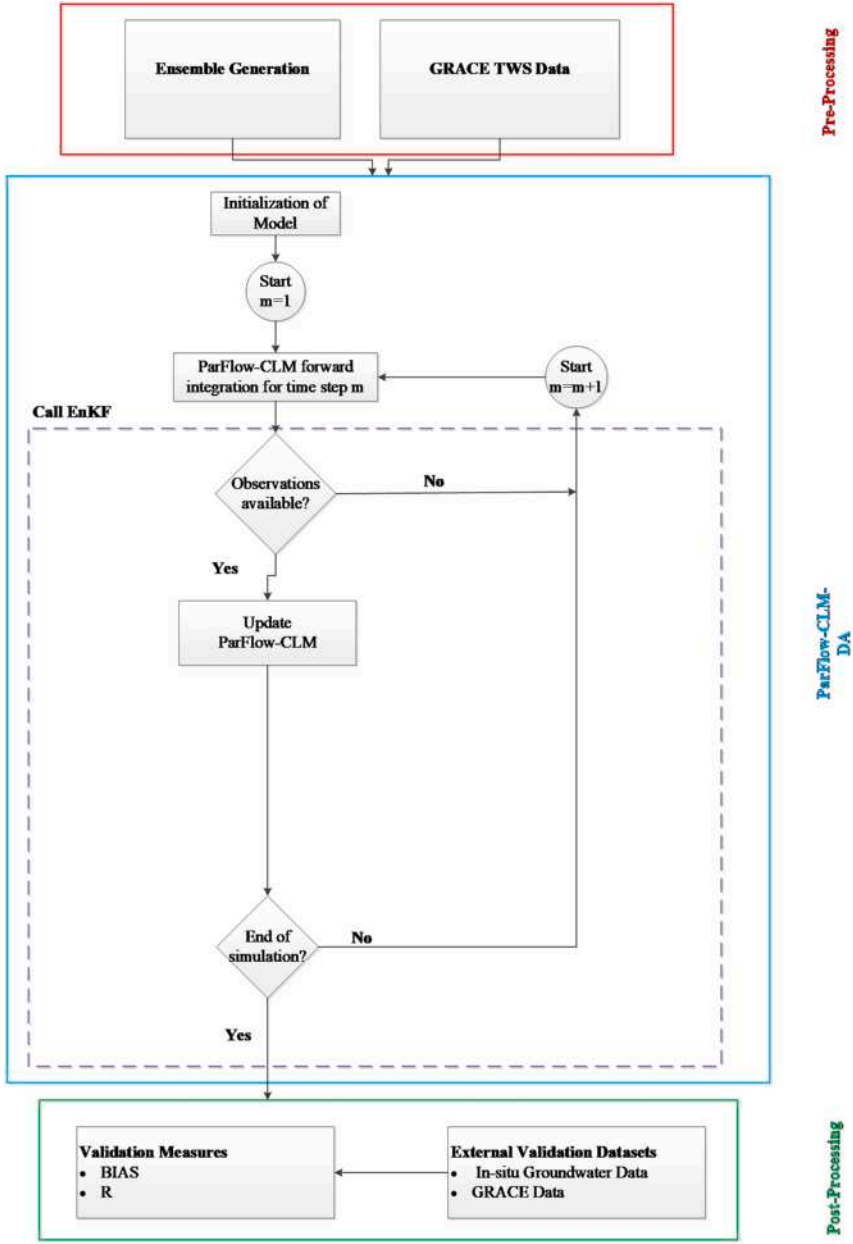


Figure 13.8 Data assimilation (DA) framework including per-processing, filter algorithm and postprocessing. Modified from Soltani, S., Sadat, B., Ataie-Ashtiani, A., Bitar, Simmons, A., Younes, M., & Fahs (2024). Assimilating multivariate remote sensing data into a fully coupled subsurface-land surface hydrological model. *Journal of Hydrology, 641*.

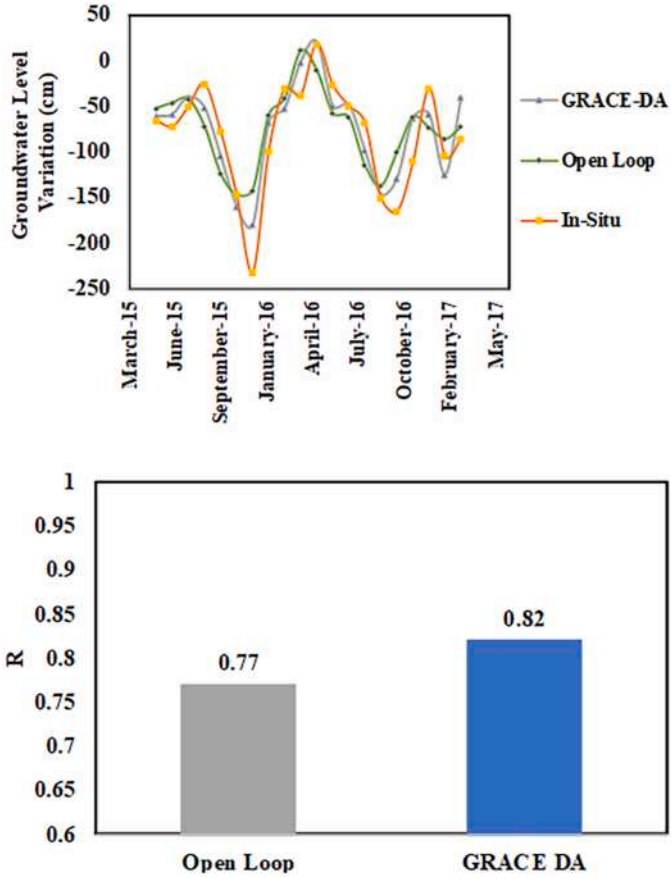


Figure 13.9 Simulated groundwater level variations from Gravity Recovery and Climate Experiment (GRACE) data assimilation (DA) over the case study, including in-situ and open loop results for comparison. The correlation coefficient (*R*) between in-situ and simulated groundwater level variations from GRACE DA and the open loop model is also presented.

widespread use. The quality and accessibility of observational data are one major obstacle. For instance, remote sensing products, while valuable, sometimes come with inherent mistakes due to air conditions, sensor limits, and spatial resolution constraints. Assimilating low-quality or sparse data into hydrological models might introduce more uncertainties, which can decrease the credibility of drought forecasts (McCabe et al., 2017). Strong quality control procedures and mistake correction methods must be integrated into DA systems to solve this problem.

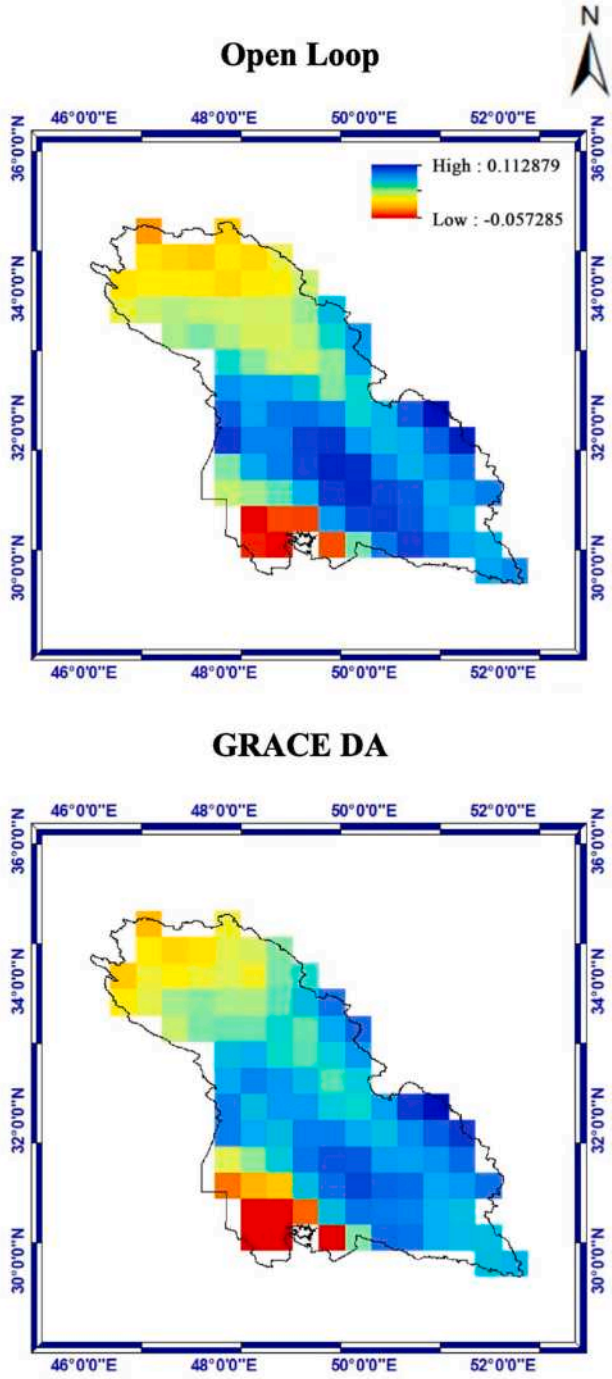


Figure 13.10 Bias between temporally averaged groundwater level variations (cm) obtained using open loop, Gravity Recovery and Climate Experiment (GRACE) data assimilation (DA) and in-situ groundwater level measurements. Map lines delineate study areas and do not necessarily depict accepted national boundaries.

The complicated nature of climate and hydrological models presents another difficulty. A number of variables, such as soil characteristics, ET, precipitation patterns, and human activities like irrigation, can affect the complicated phenomenon of drought. Incorporating all of these aspects into a single predictive model can be computationally expensive and requires advanced DA approaches that can handle high-dimensional data. Furthermore, the efficacy of DA approaches depends extensively on the model's capacity to effectively describe the system dynamics. The assimilation procedure might not result in appreciable improvements in predictions if the model is imprecise or oversimplified (Soltani et al., 2020). Another major problem is the data's spatiotemporal resolution (Soltani, 2025). It can be challenging to smoothly incorporate disparate data sources into a coherent model since they frequently function at different temporal and spatial scales. For instance, while ground-based weather stations give high temporal resolution but restricted spatial coverage, satellite observations may offer worldwide coverage at low spatial resolution. For DA researchers, balancing these disparate data sources and making sure they work with the hydrological model is still a challenge.

Lastly, assimilating data in real-time poses a major operational problem. Operational forecasting systems might not always have the effective computational resources needed to integrate vast volumes of real-time data. As droughts evolve over time, the absorption process needs to be adjusted often to take into account the system's changing condition. This ongoing integration necessitates high-frequency data inputs, quick processing, and an adaptive system that can react in real time to changing circumstances. Through the improvement of DA frameworks, machine learning (ML) has become a potent tool for bettering drought monitoring and prediction. The EnKF and variational approaches are two examples of traditional DA techniques that rely on statistical and model physics assumptions that might not adequately reflect nonlinearities in hydrological systems. By discovering complex correlations between observed and modeled variables, ML techniques in particular, deep learning and hybrid modeling approaches can be helpful in closing this gap. Recent research has demonstrated that by detecting spatial-temporal patterns that traditional approaches can miss, neural networks, support vector machines, and random forests can enhance the assimilation of SM and groundwater data (Shen, 2018). To improve drought assessments and groundwater modeling, for example, ML-based downscaling of GRACE-derived terrestrial water storage has proven effective.

Adaptive error correction and enhanced uncertainty quantification in drought forecasting are also made possible by combining ML with DA. In order to improve the accuracy of estimations of SM, evapotranspiration, and groundwater, hybrid approaches that integrate physical models with ML algorithms can dynamically modify model outputs based on real-time observations (Fang et al., 2017). Furthermore, precipitation datasets used in drought modeling have been subjected to ML-driven bias correction techniques, which have improved the datasets' dependability for hydrological forecasts (Chadalawada et al., 2020). It is expected that ML would become increasingly more important in enhancing the effectiveness and precision of frameworks for assimilation of drought data as processing power and high-resolution remote sensing data increase.

References

Abbaszadeh, P., Moradkhani, H., & Zhan, X. (2019). Downscaling SMAP radiometer soil moisture Over the CONUS using an ensemble learning method. *Water Resources Research, 55*(1), 324–344. https://doi.org/10.1029/2018wr023354.

AghaKouchak, A., Farahmand, A., Melton, F. S., Teixeira, J., Anderson, M. C., Wardlow, B. D., & Hain, C. R. (2015). Remote sensing of drought: Progress, challenges and opportunities. *Reviews of Geophysics, 53*(2), 452–480. https://doi.org/10.1002/2014rg000456.

Ahmadalipour, A., Moradkhani, H., Yan, H., & Zarekarizi, M. (2017). *Remote sensing of drought: Vegetation, soil moisture, and data assimilation*. Springer International Publishing Switzerland..

Anderson, M. C., Hain, C., Wardlow, B., Pimstein, A., Mecikalski, J. R., & Kustas, W. P. (2011). Evaluation of drought indices based on thermal remote sensing of evapotranspiration over the continental United States. *Journal of Climate, 24*(8), 2025–2044. https://doi.org/10.1175/2010jcli3812.1.

Ardebili, S., & Khademalrasoul, S. (2018). An analysis of liquid-biofuel production potential from agricultural residues and animal fat (Case study: Khuzestan Province). *Journal of Cleaner Production, 204*.

Asante, K. O., Artan, G. A., Pervez, C., Bandaragoda, J. P., & Verdin, J. P. (2008). *Technical manual for the geospatial stream flow model(Geosfm)*. U. S. Geological Survey.

Ashby, S. F., & Falgout, R. D. (1996). A parallel multigrid preconditioned conjugate gradient algorithm for groundwater flow simulations. *Nuclear Science and Engineering, 124*(1), 145–159. https://doi.org/10.13182/NSE96-A24230, http://www.new.ans.org/pubs/journals/nse/.

Awange, J. L., Fleming, K. M., Featherstone, W. E., Heck, B., & Anjasmara, I. (2011). On the suitability of the 4× 4 Grace mascon solutions for remote sensing Australian hydrology. *Remote Sensing of Environment, 115*.

Balsamo, G., Albergel, C., Beljaars, A., Boussetta, S., Brun, E., Cloke, H., Dee, D., Dutra, E., Muñoz-Sabater, J., Pappenberger, F., de Rosnay, P., Stockdale, T., & Vitart, F. (2015). ERA-Interim/Land: A global land surface reanalysis data set. *Hydrology and Earth System Sciences, 19*(1), 389–407. https://doi.org/10.5194/hess-19-389-2015.

Banerjee, C., & Kumar, D. N. (2019). *Integration of GRACE data for improvement of hydrological models*. Springer Science and Business Media LLC, 1–22. http://doi.org/10.1007/978-3-030-02197-9_1.

Barnett, T. P., Adam, J. C., & Lettenmaier, D. P. (2005). Potential impacts of a warming climate on water availability in snow-dominated regions. *Nature, 438*(7066), 303–309. https://doi.org/10.1038/nature04141.

Batjes, N. H. (1997). A world dataset of derived soil properties by FAO–UNESCO soil unit for global modelling. *Soil Use and Management, 13*(1), 9–16. https://doi.org/10.1111/j.1475-2743.1997.tb00550.x.

Benali, A., Carvalho, A. C., Nunes, J. P., Carvalhais, N., & Santos, A. (2012). Estimating air surface temperature in Portugal using MODIS LST data. *Remote Sensing of Environment, 124*, 108–121. https://doi.org/10.1016/j.rse.2012.04.024.

Bettadpur, S. (2012). *Level-2 gravity field product user handbook*. GRACE, 327–734.

Bolten, J. D., Crow, W. T., Zhan, X., Jackson, T. J., & Reynolds, C. A. (2010). Evaluating the utility of remotely sensed soil moisture retrievals for operational agricultural drought monitoring. *IEEE Journal of Selected Topics in Applied Earth Observations and Remote Sensing, 3*(1), 57–66. https://doi.org/10.1109/jstars.2009.2037163.

Brocca, L., Moramarco, T., Melone, F., Wagner, W., Hasenauer, S., & Hahn, S. (2011). Assimilation of surface-and root-zone ascat soil moisture products into rainfall–runoff modeling. *IEEE Transactions on Geoscience and Remote Sensing, 50*.

Brown, N. J., & Tregoning, P. (2010). Quantifying GRACE data contamination effects on hydrological analysis in the Murray-Darling Basin, southeast Australia. *Australian Journal of Earth Sciences, 57*(3), 329–335. https://doi.org/10.1080/08120091003619241.

Chadalawada, J., Herath, H. M. V. V., & Babovic, V. (2020). Hydrologically informed machine learning for rainfall-runoff modeling: A genetic programming-based toolkit for automatic model induction. *Water Resources Research, 56*(4). https://doi.org/10.1029/2019WR026933, http://agupubs.onlinelibrary.wiley.com/hub/journal/10.1002/(ISSN)1944-7973/.

Chen, Y., Velicogna, I., Famiglietti, J. S., & Randerson, J. T. (2013). Satellite observations of terrestrial water storage provide early warning information about drought and fire season severity in the Amazon. *Journal of Geophysical Research: Biogeosciences, 118*(2), 495–504. https://doi.org/10.1002/jgrg.20046.

Cheng, M., & Tapley, B. D. (2004). Variations in the Earth's oblateness during the past 28 years. *Journal of Geophysical Research: Solid Earth, 109*(B9). https://doi.org/10.1029/2004jb003028.

Cook, E. R., Seager, R., Cane, M. A., & Stahle, D. W. (2007). North American drought: Reconstructions, causes, and consequences. *Earth-Science Reviews, 81*(1–2), 93–134. https://doi.org/10.1016/j.earscirev.2006.12.002.

Crow, W., Kustas, W., & Prueger, J. (2008). Monitoring root-zone soil moisture through the assimilation of a thermal remote sensing-based soil moisture proxy into a water balance model. *Remote Sensing of Environment, 112*(4), 1268–1281. https://doi.org/10.1016/j.rse.2006.11.033.

Crow, W. T., & Wood, E. F. (2003). The assimilation of remotely sensed soil brightness temperature imagery into a land surface model using Ensemble Kalman filtering: A case study based on ESTAR measurements during SGP97. *Advances in Water Resources, 26*(2), 137–149. https://doi.org/10.1016/s0309-1708(02)00088-x.

Dai, A. (2011). Drought under global warming: A review. *Wiley Interdisciplinary Reviews: Climate Change, 2*(1), 45–65. https://doi.org/10.1002/wcc.81, http://onlinelibrary.wiley.com/journal/10.1002/(ISSN)1757-7799.

Dai, A. (2013). Increasing drought under global warming in observations and models. *Nature Climate Change, 3*(1), 52–58. https://doi.org/10.1038/nclimate1633.

Danielson, J. J., & Gesch, D. B. (2010). *Global multi-resolution terrain elevation data*. US Geological Survey.

DeChant, C. M., & Moradkhani, H. (2012). Examining the effectiveness and robustness of sequential data assimilation methods for quantification of uncertainty in hydrologic forecasting. *Water Resources Research, 48*(4). https://doi.org/10.1029/2011wr011011.

DeChant, C. M., & Moradkhani, H. (2014). Hydrologic prediction and uncertainty quantification. In *Handbook of engineering hydrology: Modeling, climate change, and variability*. CRC Press, 387–414. https://doi.org/10.1201/b16683, http://www.tandfebooks.com/doi/book/10.1201/b16683.

De Lannoy, J. M. G., Reichle, R. H., Arsenault, K. R., Houser, P. R., Kumar, S., Verhoest, N. E. C., & Pauwels, V. (2012). Multiscale assimilation of advanced microwave scanning radiometer–EOS snow water equivalent and moderate resolution imaging spectroradiometer snow cover fraction observations in Northern Colorado. *Water Resources Research, 48*.

Dirmeyer, P. A., Gao, X., Zhao, M., Guo, Z., Oki, T., & Hanasaki, N. (2006). GSWP-2: Multimodel analysis and implications for our perception of the land surface. *Bulletin of the American Meteorological Society, 87*(10), 1381–1398. https://doi.org/10.1175/bams-87-10-1381.

Dobriyal, P., Qureshi, A., Badola, R., & Hussain, S. A. (2012). A review of the methods available for estimating soil moisture and its implications for water resource management. *Journal of Hydrology, 458-459*, 110–117. https://doi.org/10.1016/j.jhydrol.2012.06.021.

D'Odorico, P., Caylor, K., Okin, G. S., & Scanlon, T. M. (2007). On soil moisture-vegetation feedbacks and their possible effects on the dynamics of dryland ecosystems. *Journal of Geophysical Research: Biogeosciences, 112*(4). https://doi.org/10.1029/2006JG000379, http://onlinelibrary.wiley.com/journal/10.1002/(ISSN)2169-8961.

Dong, J., Crow, W., Reichle, R., Liu, Q., Lei, F., & Cosh, M. H. (2019). A global assessment of added value in the SMAP Level 4 soil moisture product relative to its baseline land surface model. *Geophysical Research Letters, 46*(12), 6604–6613. https://doi.org/10.1029/2019gl083398.

Dong, J., Walker, J. P., Houser, P. R., & Sun, C. (2007). Scanning multichannel microwave radiometer snow water equivalent assimilation. *Journal of Geophysical Research: Atmospheres, 112*(D7). https://doi.org/10.1029/2006jd007209.

Dozier, J., Green, R. O., Nolin, A. W., & Painter, T. H. (2009). Interpretation of snow properties from imaging spectrometry. *Remote Sensing of Environment, 113*(1), S25. https://doi.org/10.1016/j.rse.2007.07.029.

Draper, C. S., Reichle, R. H., De Lannoy, G. J. M., & Liu, Q. (2012). Assimilation of passive and active microwave soil moisture retrievals. *Geophysical Research Letters, 39*(4). https://doi.org/10.1029/2011GL050655, http://onlinelibrary.wiley.com/journal/10.1002/(ISSN)1944-8007/issues?year=2012.

Entekhabi, D., Njoku, E. G., O'Neill, P. E., Kellogg, K. H., Crow, W. T., Edelstein, W. N., Entin, J. K., Goodman, S. D., Jackson, T. J., Johnson, J., Kimball, J., Piepmeier, J. R., Koster, R. D., Martin, N., McDonald, K. C., Moghaddam, M., Moran, S., Reichle, R., Shi, J. C., ... Van Zyl, J. (2010). The soil moisture active passive (SMAP) mission. In: *Proceedings of the IEEE, 98*(5), 704–716. https://doi.org/10.1109/jproc.2010.2043918.

Evensen, G. (2003). The ensemble Kalman filter: Theoretical formulation and practical implementation. *Ocean Dynamics, 53*(4), 343–367. https://doi.org/10.1007/s10236-003-0036-9.

Famiglietti, J. S., Lo, M., Ho, S. L., Bethune, J., Anderson, K. J., Syed, T. H., Swenson, S. C., de Linage, C. R., & Rodell, M. (2011). Satellites measure recent rates of groundwater depletion in California's Central Valley. *Geophysical Research Letters, 38*(3). https://doi.org/10.1029/2010gl046442.

Fang, K., Shen, C., Kifer, D., & Yang, X. (2017). Prolongation of SMAP to spatiotemporally seamless coverage of continental U.S. using a deep learning neural network. *Geophysical Research Letters, 44*(21). https://doi.org/10.1002/2017gl075619.

Forootan, E., Rietbroek, R., Kusche, J., Sharifi, M. A., Awange, J. L., Schmidt, M., Omondi, P., & Famiglietti, J. (2014). Separation of large scale water storage patterns over Iran using GRACE, altimetry and hydrological data. *Remote Sensing of Environment, 140*, 580–595. https://doi.org/10.1016/j.rse.2013.09.025.

Foster, J. L., Hall, D. K., Eylander, J. B., Riggs, G. A., Nghiem, S. V., Tedesco, M., Kim, E., Montesano, P. M., Kelly, R. E. J., Casey, K. A., & Choudhury, B. (2011). A blended global snow product using visible, passive microwave and scatterometer satellite data. *International Journal of Remote Sensing, 32*(5), 1371–1395. https://doi.org/10.1080/01431160903548013.

Friedl, M. A., McIver, D. K., Hodges, J. C. F., Zhang, X. Y., Muchoney, D., Strahler, A. H., Woodcock, C. E., Gopal, S., Schneider, A., Cooper, A., Baccini, A., Gao, F., & Schaaf, C. (2002). Global land cover mapping from MODIS: Algorithms and early results. *Remote Sensing of Environment, 83*(1–2), 287–302. https://doi.org/10.1016/s0034-4257(02)00078-0.

Gascoin, S., Hagolle, O., Huc, M., Jarlan, L., Dejoux, J.-F., Szczypta, C., Marti, R., & Sánchez, R. (2015). A snow cover climatology for the Pyrenees from MODIS snow products. *Hydrology and Earth System Sciences, 19*(5), 2337–2351. https://doi.org/10.5194/hess-19-2337-2015.

Hall, D. K., Riggs, G. A., Salomonson, V. V., DiGirolamo, N. E., & Bayr, K. J. (2002). MODIS snow-cover products. *Remote Sensing of Environment, 83*(1–2), 181–194. https://doi.org/10.1016/s0034-4257(02)00095-0.

Hao, Z., & AghaKouchak, A. (2013). Multivariate standardized drought index: A parametric multi-index model. *Advances in Water Resources, 57*, 12–18. https://doi.org/10.1016/j.advwatres.2013.03.009.

Houborg, R., Rodell, M., Li, B., Reichle, R., & Zaitchik, B. F. (2012). Drought indicators based on model-assimilated Gravity Recovery and Climate Experiment (GRACE) terrestrial water storage observations. *Water Resources Research, 48*(7). https://doi.org/10.1029/2011wr011291.

Huang, J., Yu, H., Guan, X., Wang, G., & Guo, R. (2016). Accelerated dryland expansion under climate change. *Nature Climate Change, 6*(2), 166–171. https://doi.org/10.1038/nclimate2837.

IPCC (2012). *Managing the risks of extreme events and disasters to advance climate change adaptation*. Cambridge University Press.

Jackson, R. D., Idso, S. B., Reginato, R. J., & Pinter, P. J. (1981). Canopy temperature as a crop water stress indicator. *Water Resources Research, 17*(4), 1133–1138. https://doi.org/10.1029/WR017i004p01133.

Kiany, M. S. K., Masoodian, S. A., Balling, R. C., Jr, & Montazeri, M. (2020). Evaluation of the Trmm 3b42 product for extreme precipitation analysis over Southwestern Iran. *Advances in Space Research, 66*.

Kolassa, J., Reichle, R., Liu, Q., Cosh, M., Bosch, D., Caldwell, T., Colliander, A., Holifield Collins, C., Jackson, T., Livingston, S., Moghaddam, M., & Starks, P. (2017). Data assimilation to extract soil moisture information from SMAP observations. *Remote Sensing, 9*(11), 1179. https://doi.org/10.3390/rs9111179.

Kollet, S. J., & Maxwell, R. M. (2006). Integrated surface-groundwater flow modeling: A free-surface overland flow boundary condition in a parallel groundwater flow model. *Advances in Water Resources, 29*(7), 945–958. https://doi.org/10.1016/j.advwatres.2005.08.006.

Kongoli, C., Romanov, P., & Ferraro, R. (2012). Snow cover monitoring from remote-sensing satellites: Possibilities for drought assessment. In Publications, agencies and staff

of the U.S. Department of Commerce (No. 554). U.S. Department of Commerce. http://digitalcommons.unl.edu/usdeptcommercepub/554

Kumar, S. V., Peters-Lidard, C. D., Mocko, D., Reichle, R., Liu, Y., Arsenault, K. R., Xia, Y., Ek, M., Riggs, G., Livneh, B., & Cosh, M. (2014). Assimilation of remotely sensed soil moisture and snow depth retrievals for drought estimation. *Journal of Hydrometeorology, 15*(6), 2446–2469. https://doi.org/10.1175/jhm-d-13-0132.1.

Lettenmaier, D. P., Alsdorf, D., Dozier, J., Huffman, G. J., Pan, M., & Wood, E. F. (2015). Inroads of remote sensing into hydrologic science during the WRR era. *Water Resources Research, 51*(9), 7309–7342. https://doi.org/10.1002/2015wr017616.

Liu, C., & Chen, Y. D. (2024). Impacts of vegetation dynamics on hydrological simulations under drought conditions in a humid river basin in Southern China. *Ecohydrology, 17*(3). https://doi.org/10.1002/eco.2630.

Lu, Y., Dong, J., & Steele-Dunne, S. C. (2019). Impact of soil moisture data resolution on soil moisture and surface heat flux estimates through data assimilation: A case study in the southern great plains. *Journal of Hydrometeorology, 20*(4), 715–730. https://doi.org/10.1175/jhm-d-18-0234.1.

Lu, Y., Steele-Dunne, S. C., Farhadi, L., & van de Giesen, N. (2017). Mapping surface heat fluxes by assimilating SMAP soil moisture and GOES land surface temperature data. *Water Resources Research, 53*(12), 10858–10877. https://doi.org/10.1002/2017wr021415.

Luo, L., & Wood, E. F. (2007). Monitoring and predicting the 2007 U.S. drought. *Geophysical Research Letters, 34*(22). https://doi.org/10.1029/2007gl031673.

Mann, M. E., & Gleick, P. H. (2015). Climate change and California drought in the 21st century. *Proceedings of the National Academy of Sciences, 112*(13), 3858–3859. https://doi.org/10.1073/pnas.1503667112.

Mao, Y., Nijssen, B., & Lettenmaier, D. P. (2015). Is climate change implicated in the 2013–2014 California drought? A hydrologic perspective. *Geophysical Research Letters, 42*(8), 2805–2813. https://doi.org/10.1002/2015gl063456.

Massari, C., Brocca, L., Tarpanelli, A., & Moramarco, T. (2015). Data assimilation of satellite soil moisture into rainfall-runoff modelling: A complex recipe? *Remote Sensing, 7*(9), 11403–11433. https://doi.org/10.3390/rs70911403.

Matgen, P., Montanari, M., Hostache, R., Pfister, L., Hoffmann, L., Plaza, D., Pauwels, V. R. N., De Lannoy, G. J. M., De Keyser, R., & Savenije, H. H. G. (2010). Towards the sequential assimilation of SAR-derived water stages into hydraulic models using the Particle Filter: Proof of concept. *Hydrology and Earth System Sciences, 14*(9), 1773–1785. https://doi.org/10.5194/hess-14-1773-2010, http://www.hydrol-earth-syst-sci.net/volumes_and_issues.html.

McCabe, M. F., Rodell, M., Alsdorf, D. E., Miralles, D. G., Uijlenhoet, R., Wagner, W., Lucieer, A., Houborg, R., Verhoest, N. E. C., Franz, T. E., Shi, J., Gao, H., & Wood, E. F. (2017). The future of Earth observation in hydrology. *Hydrology and Earth System Sciences, 21*(7), 3879–3914. https://doi.org/10.5194/hess-21-3879-2017.

McColl, K. A., Alemohammad, S. H., Akbar, R., Konings, A. G., Yueh, S., & Entekhabi, D. (2017). The global distribution and dynamics of surface soil moisture. *Nature Geoscience, 10*(2), 100–104. https://doi.org/10.1038/ngeo2868.

Mishra, A. K., & Singh, V. P. (2010). A review of drought concepts. *Journal of Hydrology, 391*(1–2), 202–216. https://doi.org/10.1016/j.jhydrol.2010.07.012.

Molotch, N. P., & Bales, R. C. (2006). Comparison of ground-based and airborne snow surface albedo parameterizations in an alpine watershed: Impact on snowpack mass balance. *Water Resources Research, 42*(5). https://doi.org/10.1029/2005WR004522.

Moradkhani, H. (2008). Hydrologic remote sensing and land surface data assimilation. *Sensors, 8*(5), 2986–3004. https://doi.org/10.3390/s8052986.

Moradkhani, H., DeChant, C. M., & Sorooshian, S. (2012). Evolution of ensemble data assimilation for uncertainty quantification using the particle filter-Markov chain Monte Carlo method. *Water Resources Research, 48*(12). https://doi.org/10.1029/2012wr012144.

Mote, P. W., Hamlet, A. F., Clark, M. P., & Lettenmaier, D. P. (2005). Declining mountain snowpack in western north america★. *Bulletin of the American Meteorological Society, 86*(1), 39–50. https://doi.org/10.1175/bams-86-1-39.9756968551.

Mu, Q., Heinsch, F. A., Zhao, M., & Running, S. W. (2007). Development of a global evapotranspiration algorithm based on MODIS and global meteorology data. *Remote Sensing of Environment, 111*(4), 519–536. https://doi.org/10.1016/j.rse.2007.04.015.

Mu, Q., Zhao, M., Kimball, J. S., McDowell, N. G., & Running, S. W. (2013). A remotely sensed global terrestrial drought severity index. *Bulletin of the American Meteorological Society, 94*(1), 83–98. https://doi.org/10.1175/bams-d-11-00213.1.

Mu, Q., Zhao, M., & Running, S. W. (2011). Improvements to a MODIS global terrestrial evapotranspiration algorithm. *Remote Sensing of Environment, 115*(8), 1781–1800. https://doi.org/10.1016/j.rse.2011.02.019.

Mujumdar, P. P., & Nagesh Kumar, D. (2012). *Floods in a changing climate: Hydrologic modeling*. Cambridge University Press.

Narasimhan, B., & Srinivasan, R. (2005). Development and evaluation of soil moisture Deficit Index (SMDI) and Evapotranspiration Deficit Index (ETDI) for agricultural drought monitoring. *Agricultural and Forest Meteorology, 133*(1-4), 69–88. https://doi.org/10.1016/j.agrformet.2005.07.012.

Núñez, M., Pfister, S., Antón, A., Muñoz, P., Hellweg, S., Koehler, A., & Rieradevall, J. (2013). Assessing the environmental impact of water consumption by energy crops grown in Spain. *Journal of Industrial Ecology, 17*(1), 90–102. https://doi.org/10.1111/j.1530-9290.2011.00449.x.

Oleson, K. W., Niu, G.-Y., Yang, Z.-L., Lawrence, D. M., Thornton, P. E., Lawrence, P. J., Stöckli, R., Dickinson, R. E., Bonan, G. B., Levis, S., Dai, A., & Qian, T. (2008). Improvements to the community land model and their impact on the hydrological cycle. *Journal of Geophysical Research: Biogeosciences, 113*(G1). https://doi.org/10.1029/2007jg000563.

Oleson, K., Dai, Y., Bonan, B., Bosilovichm, M., Dickinson, R., Dirmeyer, P., Hoffman, F., Houser, P., Levis, S., Niu, G.Y. and Thornton, P., 2004. Technical description of the community land model (CLM).

Painter, T. H., Rittger, K., McKenzie, C., Slaughter, P., Davis, R. E., & Dozier, J. (2009). Retrieval of subpixel snow covered area, grain size, and albedo from MODIS. *Remote Sensing of Environment, 113*(4), 868–879. https://doi.org/10.1016/j.rse.2009.01.001.

Palmer, W. C. (1965). *Meteorological drought* (pp. 1–58). US Weather Bureau, Research Paper No. 45.

Pan, M., Wood, E. F., Wójcik, R., & McCabe, M. F. (2008). Estimation of regional terrestrial water cycle using multi-sensor remote sensing observations and data assimilation. *Remote Sensing of Environment, 112*(4), 1282–1294. https://doi.org/10.1016/j.rse.2007.02.039.

Parrish, M. A., Moradkhani, H., & DeChant, C. M. (2012). Toward reduction of model uncertainty: Integration of Bayesian model averaging and data assimilation. *Water Resources Research, 48*(3). https://doi.org/10.1029/2011wr011116.

Pipunic, R., Walker, J., & Western, A. (2008). Assimilation of remotely sensed data for improved latent and sensible heat flux prediction: A comparative synthetic study. *Remote Sensing of Environment, 112*(4), 1295–1305. https://doi.org/10.1016/j.rse.2007.02.038.

Qin, C., Jia, Y., Su, Z., Zhou, Z., Qiu, Y., & Suhui, S. (2008). Integrating remote sensing information into a distributed hydrological model for improving water budget

predictions in large-scale basins through data assimilation. *Sensors, 8*(7), 4441–4465. https://doi.org/10.3390/s8074441.

Qiu, J. (2010). China drought highlights future climate threats. *Nature, 465*(7295), 142–143. https://doi.org/10.1038/465142a.

Rahmani, A., Jalili, A., Dargahian, F., Lotfi Nasab, S., Razavi Zade, S., Zandifar, S., & Saeedifar, Z. (2021). Investigation of water management in Karun, Karkheh, and Zohreh-Jarahi basins and its relationship with dust in Khuzestan. *Iran Nature, 6*.

Raziei, T., Mofidi, A., Santos, J. A., & Bordi, I. (2012). Spatial patterns and regimes of daily precipitation in Iran in relation to large-scale atmospheric circulation. *International Journal of Climatology, 32*(8), 1226–1237. https://doi.org/10.1002/joc.2347.

Reager, J. T., & Famiglietti, J. S. (2009). Global terrestrial water storage capacity and flood potential using GRACE. *Geophysical Research Letters, 36*(23). https://doi.org/10.1029/2009gl040826.

Reager, J., Thomas, A., Sproles, E., Rodell, M., Beaudoing, H., Li, B., & Famiglietti, J. (2015). Assimilation of GRACE terrestrial water storage observations into a land surface model for the assessment of regional flood potential. *Remote Sensing,* 7(11), 14663–14679. https://doi.org/10.3390/rs71114663.

Reichle, R. H., Crow, W. T., & Keppenne, C. L. (2008). An adaptive ensemble Kalman filter for soil moisture data assimilation. *Water Resources Research, 44*(3). https://doi.org/10.1029/2007wr006357.

Reichle, R. H., Liu, Q., Koster, R. D., Crow, W. T., De Lannoy, G. J. M., Kimball, J. S., Ardizzone, J. V., Bosch, D., Colliander, A., Cosh, M., Kolassa, J., Mahanama, S. P., Prueger, J., Starks, P., & Walker, J. P. (2019). Version 4 of the SMAP Level-4 soil moisture algorithm and data product. *Journal of Advances in Modeling Earth Systems, 11*(10), 3106–3130. https://doi.org/10.1029/2019ms001729.

Reichle, R. H., McLaughlin, D. B., & Entekhabi, D. (2002). Hydrologic Data assimilation with the ensemble Kalman filter. *Monthly Weather Review, 130*(1), 103–114 doi: 10.1175/1520-0493(2002)130 < 0103:hdawte > 2.0.co;2.

Rind, D., Goldberg, R., Hansen, J., Rosenzweig, C., & Ruedy, R. (1990). Potential evapotranspiration and the likelihood of future drought. *Journal of Geophysical Research: Atmospheres, 95*(D7), 9983–10004. https://doi.org/10.1029/jd095id07p09983.

Rodell, M., & Famiglietti, J. S. (2002). The potential for satellite-based monitoring of groundwater storage changes using GRACE: The high plains aquifer, Central US. *Journal of Hydrology, 263*(1–4), 245–256. https://doi.org/10.1016/s0022-1694(02)00060-4.

Rodell, M., Famiglietti, J. S., Chen, J., Seneviratne, S. I., Viterbo, P., Holl, S., & Wilson, C. R. (2004). Basin scale estimates of evapotranspiration using GRACE and other observations. *Geophysical Research Letters, 31*(20). https://doi.org/10.1029/2004GL020873.

Romanov, P., Gutman, G., & Csiszar, I. (2000). Automated monitoring of snow cover over North America with multispectral satellite data. *Journal of Applied Meteorology, 39*(11), 1866–1880. https://doi.org/10.1175/1520-0450(2000)039<1866:amosco>2.0.co;2.

Ryu, D., Crow, W. T., Zhan, X., & Jackson, T. J. (2009). Correcting unintended perturbation biases in hydrologic data assimilation. *Journal of Hydrometeorology, 10*(3), 734–750. https://doi.org/10.1175/2008jhm1038.1.

Samaniego, L., Thober, S., Kumar, R., Wanders, N., Rakovec, O., Pan, M., Zink, M., Sheffield, J., Wood, E. F., & Marx, A. (2018). Anthropogenic warming exacerbates European soil moisture droughts. *Nature Climate Change, 8*(5), 421–426. https://doi.org/10.1038/s41558-018-0138-5.

Schaap, M. G., & Leij, F. J. (1998). Database-related accuracy and uncertainty of pedotransfer functions. *Soil Science, 163*(10), 765–779. https://doi.org/10.1097/00010694-199810000-00001.

Schellekens, J., Dutra, E., Martínez-de la Torre, A., Balsamo, G., van Dijk, A., Weiland, F. S., Minvielle, M., Calvet, J.-C., Decharme, B., Eisner, S., Fink, G., Flörke, M., Peßenteiner, S., van Beek, R., Polcher, J., Beck, H., Orth, R., Calton, B., Burke, S., ... Weedon, G. P. (2017). A global water resources ensemble of hydrological models: The eartH2Observe Tier-1 dataset. *Earth System Science Data, 9*(2), 389–413. https://doi.org/10.5194/essd-9-389-2017.

Schlaepfer, D. R., Bradford, J. B., Lauenroth, W. K., Munson, S. M., Tietjen, B., Hall, S. A., Wilson, S. D., Duniway, M. C., Jia, G., Pyke, D. A., Lkhagva, A., & Jamiyansharav, K. (2017). Climate change reduces extent of temperate drylands and intensifies drought in deep soils. *Nature Communications, 8*(1). https://doi.org/10.1038/ncomms14196.

Schuurmans, J. M., Troch, P. A., Veldhuizen, A. A., Bastiaanssen, W. G. M., & Bierkens, M. F. P. (2003). Assimilation of remotely sensed latent heat flux in a distributed hydrological model. *Advances in Water Resources, 26*(2), 151–159. https://doi.org/10.1016/s0309-1708(02)00089-1.

Sheffield, J., Goteti, G., Wen, F., & Wood, E. F. (2004). A simulated soil moisture based drought analysis for the United States. *Journal of Geophysical Research: Atmospheres, 109*(D24). https://doi.org/10.1029/2004jd005182.

Shen, C. (2018). A transdisciplinary review of deep learning research and its relevance for water resources scientists. *Water Resources Research, 54*(11), 8558–8593.

Sima, S., Ahmadalipour, A., & Tajrishy, M. (2013). Mapping surface temperature in a hyper-saline lake and investigating the effect of temperature distribution on the lake evaporation. *Remote Sensing of Environment, 136*, 374–385. https://doi.org/10.1016/j.rse.2013.05.014.

Soltani, S. S. (2025). Assimilating grace data into a hydrological model. In *Remote sensing for geophysicists*. CRC Press.

Soltani, S., Sadat, B., Ataie-Ashtiani, A., Bitar, Simmons, A., Younes, M., & Fahs (2024). Assimilating multivariate remote sensing data into a fully coupled subsurface-land surface hydrological model. *Journal of Hydrology, 641*.

Soltani, S. S., Ataie-Ashtiani, B., Danesh-Yazdi, M., & Simmons, C. T. (2020). A probabilistic framework for water budget estimation in low runoff regions: A case study of the central Basin of Iran. *Journal of Hydrology, 586*, 124898. https://doi.org/10.1016/j.jhydrol.2020.124898.

Soltani, S. S., Ataie-Ashtiani, B., & Simmons, C. T. (2021). Review of assimilating GRACE terrestrial water storage data into hydrological models: Advances, challenges and opportunities. *Earth-Science Reviews, 213*, 103487. https://doi.org/10.1016/j.earscirev.2020.103487.

Soltani, S. S., Fahs, M., Bitar, A. A., & Ataie-Ashtiani, B. (2022). Improvement of soil moisture and groundwater level estimations using a scale-consistent river parameterization for the coupled ParFlow-CLM hydrological model: A case study of the Upper Rhine Basin. *Journal of Hydrology, 610*, 127991. https://doi.org/10.1016/j.jhydrol.2022.127991.

Spinoni, J., Naumann, G., Vogt, J. V., & Barbosa, P. (2015). The biggest drought events in Europe from 1950 to 2012. *Journal of Hydrology: Regional Studies, 3*, 509–524. https://doi.org/10.1016/j.ejrh.2015.01.001.

Srivastava, P. K., Han, D., Rico-Ramirez, M. A., Al-Shrafany, D., & Islam, T. (2013). Data fusion techniques for improving soil moisture deficit using SMOS satellite and WRF-NOAH land surface model. *Water Resources Management, 27*(15). https://doi.org/10.1007/s11269-013-0452-7.

Sulis, M., Williams, J. L., Shrestha, P., Diederich, M., Simmer, C., Kollet, S. J., & Maxwell, R. M. (2017). Coupling groundwater, vegetation, and atmospheric processes: A comparison of two integrated models. *Journal of Hydrometeorology, 18*(5), 1489–1511. https://doi.org/10.1175/jhm-d-16-0159.1.

Swenson, S., & Wahr, J. (2006). Post-processing removal of correlated errors in GRACE data. *Geophysical Research Letters, 33*(8). https://doi.org/10.1029/2005GL025285.

Tsakiris, G., & Vangelis (2005). Establishing a drought index incorporating evapotranspiration. *European Water, 9*, 3–11.

Van Loon, A. F. (2015). Hydrological drought explained. *Wiley Interdisciplinary Reviews: Water, 2*(4), 359–392.

Velicogna, I., Tong, J., Zhang, T., & Kimball, J. S. (2012). Increasing subsurface water storage in discontinuous permafrost areas of the Lena River basin, Eurasia, detected from GRACE. *Geophysical Research Letters, 39*(9). https://doi.org/10.1029/2012gl051623.

Vicente-Serrano, S. M., Beguería, S., & López-Moreno, J. I. (2010). A multiscalar drought index sensitive to global warming: The standardized precipitation evapotranspiration index. *Journal of Climate, 23*(7), 1696–1718. https://doi.org/10.1175/2009jcli2909.1.

Wahr, J., Molenaar, M., & Bryan, F. (1998). Time variability of the Earth's gravity field: Hydrological and oceanic effects and their possible detection using GRACE. *Journal of Geophysical Research: Solid Earth, 103*(B12), 30205–30229.

Wang, A., Lettenmaier, D. P., & Sheffield, J. (2011). Soil moisture drought in China, 1950–2006. *Journal of Climate, 24*(13), 3257–3271. https://doi.org/10.1175/2011jcli3733.1.

Wang, L., & Qu, J. J. (2007). NMDI: A normalized multi-band drought index for monitoring soil and vegetation moisture with satellite remote sensing. *Geophysical Research Letters, 34*(20). https://doi.org/10.1029/2007GL031021.

Westermann, S., Langer, M., & Boike, J. (2011). Spatial and temporal variations of summer surface temperatures of high-arctic tundra on Svalbard—Implications for MODIS LST based permafrost monitoring. *Remote Sensing of Environment, 115*(3), 908–922. https://doi.org/10.1016/j.rse.2010.11.018.

Wilhite, D. A., & Glantz, M. H. (1985). Understanding: The drought phenomenon: The role of definitions. *Water International, 10*(3), 111–120. https://doi.org/10.1080/02508068508686328.

Wilhite, D. A., & Svoboda, M. D. (2000). *Drought early warning systems in the context of drought preparedness and mitigation* (pp. 1–21). WMO.

Xu, L., Chen, N., & Zhang, X. (2019b). Global drought trends under 1.5 and 2 °C warming. *International Journal of Climatology, 39*(4), 2375–2385. https://doi.org/10.1002/joc.5958.

Xu, L., Chen, N., Zhang, X., & Chen, Z. (2018). An evaluation of statistical, NMME and hybrid models for drought prediction in China. *Journal of Hydrology, 566*, 235–249. https://doi.org/10.1016/j.jhydrol.2018.09.020.

Xu, L., Chen, N., Zhang, X., Chen, Z., Hu, C., & Wang, C. (2019a). Improving the North American multi-model ensemble (NMME) precipitation forecasts at local areas using wavelet and machine learning. *Climate Dynamics, 53*(1–2), 601–615. https://doi.org/10.1007/s00382-018-04605-z.

Yan, H., DeChant, C. M., & Moradkhani, H. (2015). Improving soil moisture profile prediction with the particle filter-Markov chain Monte Carlo Method. *IEEE Transactions on Geoscience and Remote Sensing, 53*(11), 6134–6147. https://doi.org/10.1109/TGRS.2015.2432067.

Yan, H., & Moradkhani, H. (2016). Combined assimilation of streamflow and satellite soil moisture with the particle filter and geostatistical modeling. *Advances in Water Resources, 94*, 364–378. https://doi.org/10.1016/j.advwatres.2016.06.002.

Yan, H., Moradkhani, H., & Zarekarizi, M. (2017). A probabilistic drought forecasting framework: A combined dynamical and statistical approach. *Journal of Hydrology, 548*, 291–304. https://doi.org/10.1016/j.jhydrol.2017.03.004.

Yao, Y., Liang, S., Qin, Q., & Wang, K. (2010). Monitoring drought over the conterminous united states using MODIS and NCEP reanalysis-2 data. *Journal of Applied Meteorology and Climatology, 49*(8), 1665–1680. https://doi.org/10.1175/2010jamc2328.1.

Yin, D., Roderick, M. L., Leech, G., Sun, F., & Huang, Y. (2014). The contribution of reduction in evaporative cooling to higher surface air temperatures during drought. *Geophysical Research Letters, 41*(22), 7891–7897. https://doi.org/10.1002/2014gl062039.

Zaitchik, B. F., Rodell, M., & Reichle, R. H. (2008). Assimilation of GRACE terrestrial water storage data into a land surface model: Results for the Mississippi river basin. *Journal of Hydrometeorology, 9*(3), 535–548. https://doi.org/10.1175/2007jhm951.1.

Zhang, J., Mu, Q., & Huang, J. (2016). Assessing the remotely sensed drought severity index for agricultural drought monitoring and impact analysis in North China. *Ecological Indicators, 63*, 296–309. https://doi.org/10.1016/j.ecolind.2015.11.062.

Zhang, Z., Chao, B. F., Chen, J., & Wilson, C. R. (2015). Terrestrial water storage anomalies of Yangtze River Basin droughts observed by GRACE and connections with ENSO. *Global and Planetary Change, 126*, 35–45. https://doi.org/10.1016/j.gloplacha.2015.01.002.

Soltani, S. (2022). Assimilating remote sensing information into a distributed hydrological model for improving water budget predictions [Doctoral dissertation, Université de Strasbourg; Sharif University of Technology]. HAL Open Science. https://theses.hal.science/tel-04194915

SECTION IV

Case studies

This page intentionally left blank

CHAPTER FOURTEEN

Models (linear, nonlinear, machine learning)

Babak Mohammadi
Hydrology Research Unit, Swedish Meteorological and Hydrological Institute, Norrköping, Sweden

14.1 Introduction

Drought is one of the most destructive natural hazards affecting human societies and ecosystems worldwide, with far-reaching implications for water resources management, agricultural productivity, and socioeconomic stability (Akbari et al., 2021; Yang et al., 2023; Yu et al., 2020). This slow-onset phenomenon has become increasingly frequent and severe due to climate change, causing significant disruptions to water supply systems, reducing crop yields, and triggering cascading effects across various sectors of the economy. The complex nature of drought, characterized by its temporal and spatial variability, makes it particularly challenging to forecast and manage effectively (Brunner et al., 2021; Kiem et al., 2016). Understanding drought dynamics through robust analytical approaches and modeling techniques is therefore important for developing early warning systems, implementing adaptation strategies, and enhancing resilience in water-stressed regions (Haro-Monteagudo et al., 2017; Rubio-Martín et al., 2020). This is especially relevant in regions where water resources play a vital role in supporting both human activities and environmental sustainability, necessitating accurate drought assessment and prediction methodologies to inform decision-making processes and policy development.

Streamflow Drought Index (SDI) has emerged as a metric for quantifying and monitoring hydrological drought conditions, enabling effective monitoring of water resources and drought severity (Hong et al., 2015; Jahangir & Yarahmadi, 2020; Nalbantis & Tsakiris, 2009). This standardized index effectively captures the temporal variations in streamflow patterns, making it particularly valuable for water resource managers, policymakers, and stakeholders in making informed decisions about water

Drought Dynamics
DOI: https://doi.org/10.1016/B978-0-443-34205-9.00010-X
© 2026 Elsevier Inc. All rights are reserved, including those for text and data mining, AI training, and similar technologies.

allocation and drought mitigation strategies. The ability to accurately predict SDI values holds significant importance for proactive drought management, as it enables authorities to anticipate potential water shortages and implement appropriate measures before severe impacts occur. Furthermore, in regions where streamflow monitoring stations are limited or data collection is challenging, the capacity to estimate SDI values using data from neighboring stations becomes particularly valuable, offering a practical solution for extending drought monitoring coverage and improving regional water resource management strategies. Drought prediction via the neighboring stations approach enhances the spatial resolution of drought monitoring networks and provides a cost-effective method for maintaining continuous drought surveillance, which has been considered by previous studies on Standardized Precipitation Index (SPI) prediction (Mehr et al., 2020; Mohammadi, 2023).

Linear and nonlinear models have proven to be valuable tools in forecasting hydrological and environmental variables, due to their interpretability and computational efficiency (Ahani et al., 2017; Masselot et al., 2016; Ouali et al., 2017). Linear models assume a linear relationship between input and target variables, offering significant practical advantages in real-world applications due to their straightforward implementation and interpretation (Clarke, 1973; Diskin, 1970; Makhoul, 1975). Unlike linear models, nonlinear approaches, particularly polynomial regression, can account for the intricate interactions between various hydrological variables and their surrounding environments (Lall et al., 2006; Shah et al., 2021). These models are particularly valuable when the relationship between the input and target data exhibits clear nonlinear patterns (Kravtsov et al., 2005). The flexibility of nonlinear regression (NLR) models in capturing these complex relationships often results in improved prediction accuracy compared to linear regression (LR) approaches, especially for hydrological modeling in regions with diverse topography or varying climatological conditions that influence streamflow patterns.

Machine learning (ML) models have revolutionized hydrological forecasting and drought prediction by offering sophisticated approaches to capture complex, nonlinear relationships in the environmental systems (Achite et al., 2023; Wang et al., 2022). In the context of drought index estimation, ML models can effectively represent the relationships between drought conditions at different stations, accounting for varying degrees of influence that neighboring stations may have on the target location (Mehr et al., 2020; Mohammadi, 2023). Random Forest (RF) and M5 tree (M5)

models, as ML models, have demonstrated acceptable performance in drought estimation in different regions (Elbeltagi et al., 2022; Mokhtar et al., 2021; Shamshirband et al., 2020; Yaseen et al., 2021) due to their ability to handle complex interactions between variables, and maintain robust performance across diverse climate conditions. The inherent ensemble approach of RF allows for a comprehensive evaluation of the relative significance of different stations in regional drought patterns, while M5 models offer the additional advantage of producing rules that can enhance understanding of drought propagation mechanisms. Furthermore, these ML approaches have shown superior adaptability to various environmental conditions and demonstrated robust performance in handling complex relationships between hydrological and meteorological variables (Bahmani et al., 2020; Bhattacharya & Solomatine, 2005; Schoppa et al., 2020; Wang et al., 2019), making them particularly valuable for drought prediction.

The primary objective of this study is to evaluate comprehensive modeling approaches for estimating SDI values using data from neighboring stations in Sweden, with a specific focus on the Heåkra station. This research aims to compare the performance of traditional statistical methods, including LR and NLR models, with advanced ML techniques such as RF and M5 models in predicting both 3-month (SDI-3) and 6-month (SDI-6) drought indices. Through rigorous analysis of nine streamflow stations across Sweden, this study seeks to establish reliable methodologies for drought estimation in locations where direct measurements might be limited or temporarily unavailable. Additionally, this research endeavors to contribute to the broader understanding of drought dynamics and enhance drought prediction capacity.

14.2 Materials and methods

14.2.1 Case study and data used

The present study focuses on nine streamflow stations located across Sweden (shown in Fig. 14.1): Heåkra, Bröddebacken, Ellinge, Hålabäck, Klippan, Möckeln, Simlångsen, Svedala, and Vombsjön. The streamflow data used in this study were obtained from the Swedish Meteorological and Hydrological Institute (SMHI). A single modeling scenario was adopted across all techniques (LR, NLR, RF, M5). The Heåkra station served as the target for SDI estimation, while SDI values from the eight neighboring

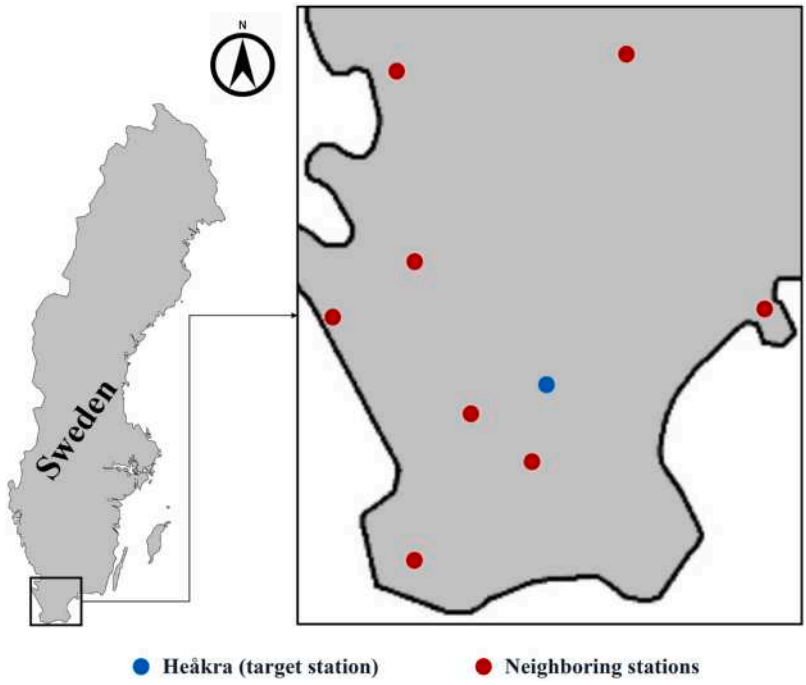


Figure 14.1 Schematic map of the study area indicating the approximate location of the target and neighboring streamflow stations.

stations (Bröddebacken, Ellinge, Hålabäck, Klippan, Möckeln, Simlången, Svedala, and Vombsjön) were used as predictor inputs. This approach assumes that spatial dependencies between streamflow stations can effectively characterize regional drought dynamics at the target location. Streamflow data from August 1973 to December 2021 was used in this study. The dataset was randomly partitioned, with 80% allocated for model training and 20% reserved for testing.

14.2.2 Streamflow drought index

The SDI was employed in this study to quantify hydrological drought conditions across the selected stations. The SDI calculation follows the methodology proposed by Nalbantis and Tsakiris (2009), which transforms streamflow volumes into standardized values that enable drought severity assessment and comparison across different locations and time scales. For a given station, let $Q_{i,j}$ be the streamflow volume for the ith hydrological year and jth month, where $i = 1, 2, \ldots, N$ years, and $j = 1, 2, \ldots, 12$ months.

The cumulative streamflow volume ($V_{i,k}$) for each reference period k (e.g., 3-month time window) is calculated as (Nalbantis and Tsakiris, 2009):

$$V_{i,k} = \sum_{j=1}^{3k} Q_{i,j} \tag{14.1}$$

where the summation is calculated for each reference period (k) over the respective months. The SDI value for the ith hydrological year and kth reference period is then computed as:

$$SDI_{i,k} = \frac{V_{i,k} - \overline{V_k}}{s_k} \tag{14.2}$$

where $\overline{V_k}$ is the mean of cumulative streamflow volumes for reference period k, and s_k is the standard deviation of cumulative streamflow volumes for reference period k.

In this study, both SDI-3 and SDI-6 time scales were analyzed to capture different aspects of drought development and persistence. According to the SDI classification scheme, drought conditions are categorized as (Nalbantis & Tsakiris, 2009): nondrought (SDI ≥ 0.0), mild drought (−1.0 ≤ SDI < 0.0), moderate drought (−1.5 ≤ SDI < −1.0), severe drought (−2.0 ≤ SDI < −1.5), and extreme drought (SDI < −2.0). Time series of observed SDI-3 and SDI-6 for Heåkra station are shown in Fig. 14.2.

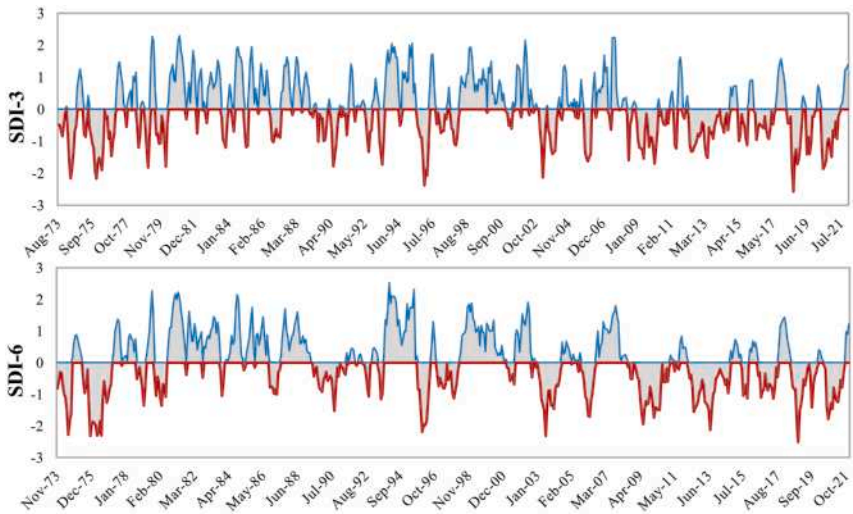


Figure 14.2 Time series of observed SDI-3 and SDI-6 for Heåkra station.

14.2.3 Models

14.2.3.1 Linear regression

LR modeling was implemented to establish relationships between the SDI values at the target station (Heåkra) and SDI values at other (neighboring) stations. The LR model can be expressed mathematically as:

$$SDI_{Heåkra} = \beta_0 + \beta_1 SDI_1 + \beta_2 SDI_2 + .+\beta_n SDI_n + \varepsilon \quad (14.3)$$

where $SDI_{Heåkra}$ is the SDI value at Heåkra station, SDI_1 through SDI_2 are the SDI values from the n predictor (other) stations, β_0 is the intercept term, β_1 through β_n are the regression coefficients corresponding to each predictor station, and ε is the error term.

14.2.3.2 Nonlinear regression

To account for potential nonlinear relationships between SDI values at different stations, a polynomial regression model was implemented. This approach extends the LR framework by incorporating higher-order terms of the predictor variables, allowing for more flexible modeling of complex relationships (Kravtsov et al., 2005; Ostertagová, 2012; Wilkinson & Rogers, 1973). In this study, a second-degree polynomial regression was employed to capture potential curvilinear relationships (15.4). For each predictor station, both first-order and second-order terms were included in the model, allowing for the detection of both linear and quadratic relationships. This approach allows for a more flexible representation of the relationship between stations while maintaining interpretability through the polynomial structure.

$$SDI_{Heåkra} = \beta_0 + \sum_{i=1}^{n} \left(\beta_{1,i}\ SDI_i + \beta_{2,i}\ SDI_i^2\right) \quad (14.4)$$

where $SDI_{Heåkra}$ is the SDI value at Heåkra station, n is the number of neighboring stations (eight stations in this study), β_0 is intercept term, SDI_i is the SDI value at the neighbor station (ith station), $\beta_{1,i}$ is the linear coefficient for the ith station, and $\beta_{2,i}$ is the quadratic coefficient for the ith station.

14.2.3.3 Machine learning models

This study employed two ML approaches (namely RF and M5 models) to estimate SDI-3 and SDI-6 in Heåkra station. The RF model (Breiman, 2001) was implemented using the "randomForest" package in R (Breiman et al., 2018), utilizing an ensemble learning approach that combines multiple decision trees to improve prediction accuracy. The model was configured with 500 trees

($n$tree = 500) to ensure robust predictions while maintaining computational efficiency. Each decision tree in the forest was constructed using a bootstrap sample of the training data, with random feature selection at each split point. The M5 model (Quinlan, 1992, 1993) was implemented using the "Cubist" package in R (Kuhn et al., 2024). The model was configured with 10 committees to enhance prediction accuracy through ensemble learning. The M5 algorithm constructs a decision tree where the splitting criteria are chosen to minimize the standard deviation of class values that reach each node, and regression-based models are fitted at the terminal nodes.

14.2.4 Evaluation metrics

To assess the performance of the applied models, four widely-used statistical metrics were employed: mean absolute error (MAE), root mean square error (RMSE), ratio of RMSE to the standard deviation of the observations (RSR), and coefficient of determination (R^2). These metrics can be calculated from Eqs. (14.5–14.8) and they provide complementary information about model accuracy, error magnitude, and prediction reliability.

$$MAE = \frac{\sum_{i=1}^{n} | SDI_{o,i} - SDI_{e,i} |}{n} \tag{14.5}$$

$$RMSE = \sqrt{\frac{\sum_{i=1}^{n} (SDI_{o,i} - SDI_{e,i})^2}{n}} \tag{14.6}$$

$$RSR = \frac{RMSE}{STD_o} \tag{14.7}$$

$$R^2 = 1 - \frac{\sum_{i=1}^{n} (SDI_{o,i} - SDI_{e,i})^2}{\sum_{i=1}^{n} (SDI_{o,i} - \overline{SDI}_o)^2} \tag{14.8}$$

where $SDI_{o,i}$ and $SDI_{e,i}$ are the ith observed and estimated SDI values, respectively, and $\overline{SDI}_o$ is the mean of observed SDI values. In addition, the variable "n" is the total number of observed values, and STD_o is the standard deviation of observed SDI.

14.3 Results and discussion

Table 14.1 lists the performance evaluation of the four models (LR, NLR, RF, and M5) for SDI-3 estimation across both training and testing

Table 14.1 Performance of linear regression (LR), nonlinear regression (NLR), random forest (RF), and M5 tree (M5) models for SDI-3 estimation during training and testing phases.

Phase	Metrics	LR	NLR	RF	M5
Train	*MAE*	0.28	0.25	0.12	0.25
	RMSE	0.37	0.32	0.15	0.32
	RSR	0.39	0.33	0.16	0.33
	R^2	0.85	0.89	0.98	0.89
Test	*MAE*	0.33	0.29	0.29	0.28
	RMSE	0.43	0.37	0.36	0.36
	RSR	0.45	0.38	0.38	0.38
	R^2	0.80	0.85	0.87	0.86

phases. During the training phase, the RF model demonstrated superior performance with notably lower error metrics ($MAE = 0.12$, $RMSE = 0.15$, $RSR = 0.16$) and the highest R^2 value (0.98) compared to other models. The LR model showed relatively higher error metrics ($MAE = 0.28$, $RMSE = 0.37$, $RSR = 0.39$) and the lowest R^2 value (0.85) among all models during training, while both NLR and M5 models exhibited identical performance metrics ($MAE = 0.25$, $RMSE = 0.32$, $RSR = 0.33$, $R^2 = 0.89$), suggesting similar capability in capturing the relationships between predictor and target stations during the training period.

The testing phase results reveal a different pattern, with all models showing comparable performance and reduced differences in their error metrics. The M5 model demonstrated slightly better performance with the lowest *MAE* (0.28), while both RF and NLR models showed almost similar error metrics ($MAE = 0.29$). The LR model maintained relatively higher error values ($MAE = 0.33$, $RMSE = 0.43$, $RSR = 0.45$) and the lowest R^2 (0.80) during testing, indicating less optimal performance compared to other models. Notably, the RF model's performance metrics in the testing phase ($R^2 = 0.87$) showed a more substantial decrease from its training phase performance ($R^2 = 0.98$) compared to other models. The consistent performance of the M5 model across both phases, with minimal degradation in accuracy metrics between training and testing, suggests it may be the most robust choice for practical applications in SDI-3 estimation.

The scatter plots comparing observed and estimated SDI-3 values across all four models (shown in Fig. 14.3) reveal distinct patterns in prediction accuracy and model behavior. The LR model shows the most dispersed

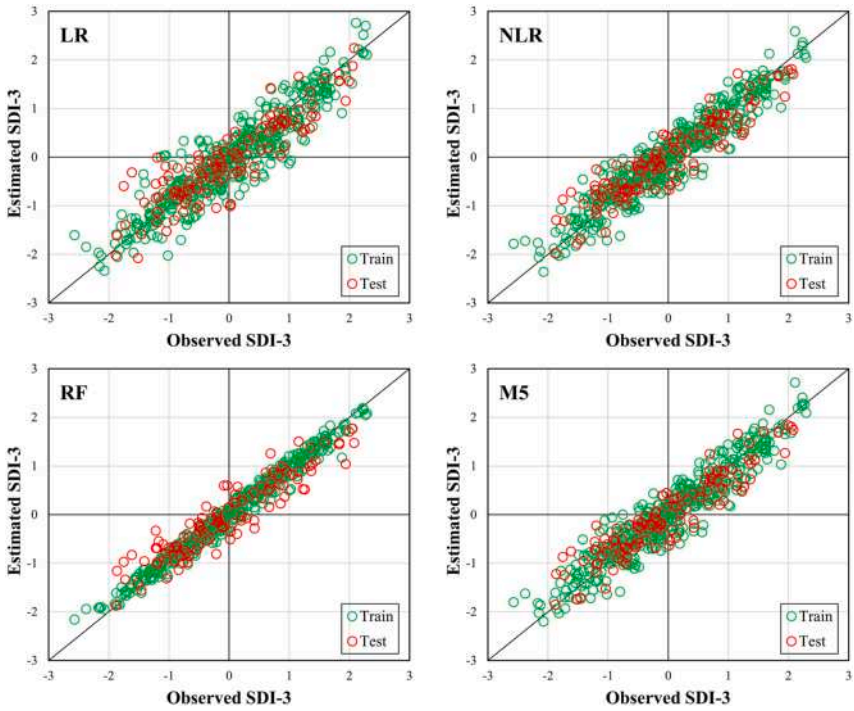


Figure 14.3 Scatter plots of observed SDI-3 and estimated SDI-3 by linear regression (LR), nonlinear regression (NLR), random forest (RF), and M5 tree (M5) models during training and testing phases.

pattern around the 1:1 line, indicating relatively lower prediction accuracy compared to other models. The NLR model demonstrates improved clustering around the 1:1 line compared to the LR model. However, some scatter is still evident at the extremes, suggesting challenges in capturing more severe drought or wet conditions. Both the RF and M5 models exhibit notably tighter clustering patterns around the 1:1 line across the entire range of SDI-3 values, with the RF model showing particularly strong performance in the training phase, as evidenced by the close alignment of points with the diagonal line. The M5 model demonstrates the most consistent performance between training and testing phases, with similar scatter patterns for both green and red points, indicating robust generalization capability. Both LR and NLR models show comparable patterns between training and testing phases, though with greater overall scatter than the ML models.

Table 14.2 lists employed models' performances for SDI-6 estimation during the training and testing phases. The comparative analysis of model performance for SDI-6 estimation reveals distinct patterns across the training phase, with the RF model demonstrating exceptional performance compared to other approaches. During training, the RF model achieved notably lower error metrics ($MAE = 0.12$, $RMSE = 0.16$, $RSR = 0.16$) and the highest R^2 value (0.98). The M5 model showed the second-best performance during training ($MAE = 0.22$, $RMSE = 0.29$, $RSR = 0.30$, $R^2 = 0.91$), while the NLR model ($MAE = 0.26$, $RMSE = 0.32$, $RSR = 0.33$, $R^2 = 0.89$) and LR model ($MAE = 0.29$, $RMSE = 0.40$, $RSR = 0.40$, $R^2 = 0.87$) demonstrated progressively higher error metrics and lower R^2 values during the training period (compared with other models).

The testing phase results present a notably different pattern, with the M5 model emerging as the top performer across all evaluation metrics ($MAE = 0.23$, $RMSE = 0.31$, $RSR = 0.33$, $R^2 = 0.89$). This (almost) consistent performance between training and testing phases suggests robust generalization capability of the M5 model for SDI-6 estimation. Both RF and NLR models showed almost similar performance during testing ($MAE = 0.27$), while the LR model maintained relatively higher error metrics ($MAE = 0.32$, $RMSE = 0.42$, $RSR = 0.44$). The M5 model's superior performance during testing, coupled with its consistent accuracy across both phases, suggests it may be the most reliable choice for practical applications in SDI-6 estimation.

The scatter plots for SDI-6 estimation across the four modeling approaches are shown in Fig. 14.4. The LR model exhibits the widest

Table 14.2 Performance of linear regression (LR), nonlinear regression (NLR), random forest (RF), and M5 tree (M5) models for SDI-6 estimation during training and testing phases.

Phase	Metrics	LR	NLR	RF	M5
Train	*MAE*	0.29	0.26	0.12	0.22
	RMSE	0.40	0.32	0.16	0.29
	RSR	0.40	0.33	0.16	0.30
	R^2	0.87	0.89	0.98	0.91
Test	*MAE*	0.32	0.27	0.27	0.23
	RMSE	0.42	0.35	0.33	0.31
	RSR	0.44	0.37	0.35	0.33
	R^2	0.86	0.87	0.88	0.89

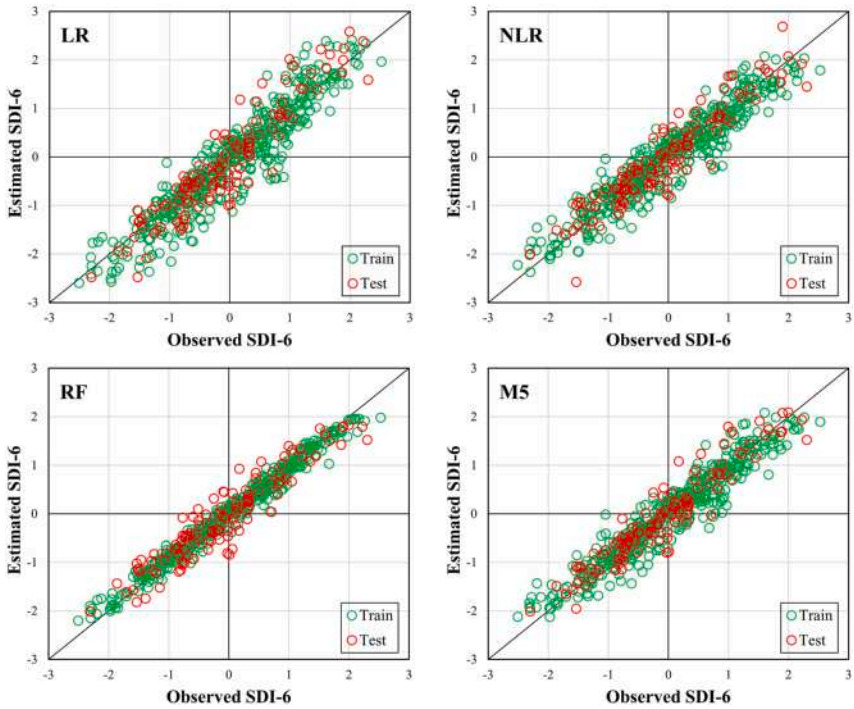


Figure 14.4 Scatter plots of observed SDI-6 and estimated SDI-6 by linear regression (LR), nonlinear regression (NLR), random forest (RF), and M5 tree (M5) models during training and testing phases.

dispersion around the 1:1 line, while the NLR model shows improved performance compared to the linear model. However, it displays some notable outliers. The RF model demonstrates good performance across both training and testing phases, with points closely aligned with the 1:1 line. The M5 model shows similarly strong performance, with tight clustering around the diagonal line and minimal deviation between training and testing phases.

The Taylor diagram (Fig. 14.5) effectively visualizes the statistical relationships between observed and estimated SDI-3 values across all four modeling approaches during the entire data period (train and test together). The RF model demonstrates superior performance, positioned closest to the "observed" point on the diagram, indicating the highest correlation and lowest standard deviation difference with observed values. The M5 and NLR models show almost similar performance patterns, positioned slightly

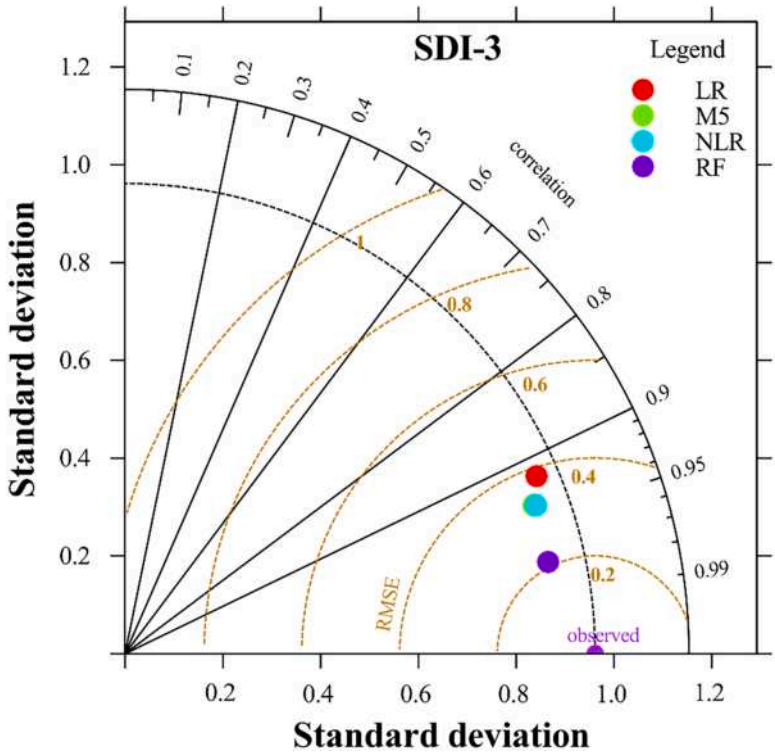


Figure 14.5 Taylor diagram comparing observed SDI-3 and estimated SDI-3 by linear regression (LR), nonlinear regression (NLR), random forest (RF), and M5 tree (M5) models for the entire study duration.

farther from the observed reference point, while the LR model exhibits the greatest distance from the observed point, suggesting relatively lower performance in terms of both correlation and standard deviation representation. All models maintain reasonable correlation coefficients, with standard deviations ranging between 0.8 and 1.0, indicating generally good performance in capturing the variability of SDI-3 patterns despite their different mathematical approaches.

The Taylor diagram for SDI-6 estimation shown in Fig. 14.6 reveals distinct performance characteristics among the four modeling approaches during the entire data period (train and test together). The RF model exhibits the strongest performance, positioned nearest to the observed reference point with the highest correlation and closest standard deviation match to the observed data. The M5 and NLR models demonstrate similar

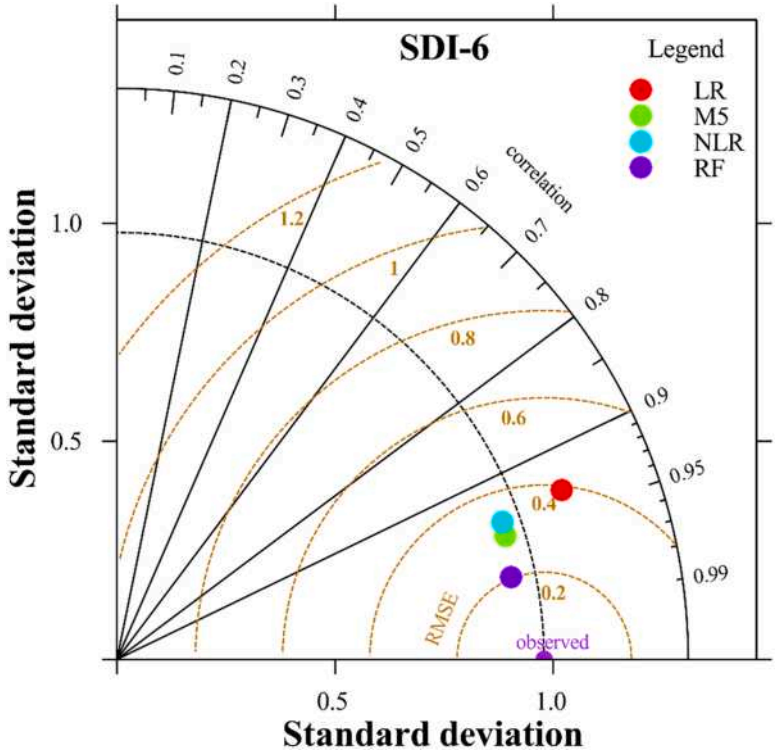


Figure 14.6 Taylor diagram comparing observed SDI-6 and estimated SDI-6 byby linearlinear regression (LR), nonlinear regression (NLR), random forest (RF), and M5 tree (M5) models for the entire study duration.

statistical characteristics, clustering relatively close to each other on the diagram, though positioned slightly farther from the observed point than the RF model. The LR model shows the greatest deviation from the observed reference, with a higher standard deviation and lower correlation compared to other models, indicating a relatively less accurate representation of SDI-6 patterns.

The LR model, while providing a baseline for comparison, demonstrated relatively higher error metrics and lower correlation coefficients across both SDI-3 and SDI-6 predictions (compared to other models). This performance limitation suggests that the LR approach may not adequately capture the complex, nonlinear relationships inherent in drought propagation processes. The NLR model showed modest improvements over the LR approach, indicating that incorporating polynomial terms helps better

represent the underlying relationships between neighboring stations' drought indices.

The RF model exhibited exceptional performance during the training phase for both SDI-3 and SDI-6 predictions, achieving the highest R^2 values (0.98) and lowest error metrics among all models. This superior training performance can be attributed to the model's ensemble approach and ability to capture complex, nonlinear relationships without assuming a specific functional form. However, a difference between training and testing performance in the RF model was observed. The M5 model emerged as the most robust approach, demonstrating consistent performance across both training and testing phases for SDI-3 and SDI-6 predictions. The model's ability to maintain stable performance metrics, particularly in testing (R^2 =0.86 for SDI-3 and 0.89 for SDI-6), indicates strong generalization capability and reliability in operational settings. The superior performance of RF and M5 models can be partially attributed to their ability to capture nonlinear spatial dependencies between the target station (Heåkra) and neighboring stations. Traditional regression-based models (LR/NLR) failed to fully leverage these relationships, whereas ML approaches (RF and M5) effectively quantified complex interactions between stations, resulting in more accurate drought forecasting in this study.

Future research in this domain could benefit from several enhancements and extensions. First, exploring the application of deep learning approaches, particularly recurrent neural networks, could enhance the capture of temporal dependencies in drought propagation. Second, extending the analysis to include climate change scenarios and their potential impact on model performance would be valuable for long-term drought management planning. Additionally, developing hybrid modeling approaches that combine the strengths of different methods could potentially improve prediction accuracy while maintaining model robustness.

14.4 Conclusions

This study presents a comprehensive analysis of drought prediction capabilities using four distinct modeling approaches, namely LR, NLR, RF, and M5 models to estimate SDI values at multiple time scales. The comparative analysis of these models for both SDI-3 and SDI-6 estimation

at the Heåkra station in Sweden, using data from eight neighboring stations, reveals several important findings regarding their relative performance and practical applicability. The ML models, particularly RF and M5, demonstrated superior performance compared to traditional regression approaches across both time scales. During the training phase, the RF model achieved exceptional accuracy with R^2 values of 0.98 for both SDI-3 and SDI-6 predictions, along with the lowest error metrics among all models. However, the testing phase results revealed that the M5 model exhibited more consistent performance between training and testing periods, suggesting better generalization capability. This was particularly evident in SDI-6 predictions, where the M5 model maintained robust performance metrics ($R^2 = 0.89$) and showed the lowest error values ($MAE = 0.23$, $RMSE = 0.31$) during testing. The NLR model showed modest improvement over the LR approach, though both models demonstrated limitations in predicting extreme drought events. The Taylor diagram analysis further confirmed these findings, with the RF and M5 models positioned closer to the observed reference point, indicating better correlation and standard deviation representation. The study's results suggest that while all models demonstrate reasonable capability in drought prediction, the M5 model offers the most balanced performance between accuracy and generalization, making it particularly suitable for operational drought monitoring and prediction applications.

AI disclosure

During the preparation of this work the author used Claude 3.7 Sonnet (developed by Anthropic) in order to improve readability and language of the manuscript. All content was thoroughly reviewed, verified, and edited by the author to ensure scientific accuracy. After using this tool/service, the author reviewed and edited the content as needed and takes full responsibility for the content of the publication.

References

Achite, M., Katipoğlu, O., Jehanzaib, M., Elshaboury, N., Kartal, V., & Ali, S. (2023). Hydrological drought prediction based on hybrid extreme learning machine: Wadi Mina Basin Case Study, Algeria. *Atmosphere, 14*, 1447. https://doi.org/10.3390/atmos14091447.

Ahani, A., Shourian, M., & Rad, P. (2017). Performance assessment of the linear, nonlinear and nonparametric data driven models in river flow forecasting. *Water Resources Management, 32*, 383–399. https://doi.org/10.1007/s11269-017-1792-5.

Akbari, M., Alamdarlo, N., & Mosavi, S. (2021). Economic effects of changing the quality and quantity of water in drought conditions, case study: Qazvin, Iran. *International Journal of Environmental Science and Technology*. https://doi.org/10.1007/s13762-021-03406-y.

Bahmani, R., Solgi, A., & Ouarda, T. B. (2020). Groundwater level simulation using gene expression programming and M5 model tree combined with wavelet transform. *Hydrological Sciences Journal, 65*(8), 1430–1442. https://doi.org/10.1080/02626667.2020.1749762.

Bhattacharya, B., & Solomatine, D. P. (2005). Neural networks and M5 model trees in modelling water level–discharge relationship. *Neurocomputing, 63*, 381–396. https://doi.org/10.1016/j.neucom.2004.04.016.

Breiman, L. (2001). Random forests. *Machine Learning, 45*, 5–32.

Breiman, L., Cutler, A., Liaw, A., & Wiener, M. (2018). *Package 'randomforest'*. University of California, Berkeley. https://cran.r-project.org/package=randomForest.

Brunner, M., Slater, L., Tallaksen, L., & Clark, M. (2021). Challenges in modeling and predicting floods and droughts: A review. *Wiley Interdisciplinary Reviews: Water, 8*. https://doi.org/10.1002/wat2.1520.

Clarke, R. T. (1973). A review of some mathematical models used in hydrology, with observations on their calibration and use. *Journal of Hydrology, 19*(1), 1–20. https://doi.org/10.1016/0022-1694(73)90089-9.

Diskin, M. H. (1970). Definition and uses of the linear regression model. *Water Resources Research, 6*(6), 1668–1673. https://doi.org/10.1029/WR006i006p01668.

Elbeltagi, A., AlThobiani, F., Kamruzzaman, M., Shaid, S., Roy, D., Deb, L., Islam, M., Kundu, P., & Rahman, M. (2022). Estimating the standardized precipitation evapotranspiration index using data-driven techniques: A regional study of Bangladesh. *Water, 14*. https://doi.org/10.3390/w14111764.

Haro-Monteagudo, D., Solera, A., & Andréu, J. (2017). Drought early warning based on optimal risk forecasts in regulated river systems: Application to the Jucar River Basin (Spain). *Journal of Hydrology, 544*, 36–45. https://doi.org/10.1016/J.JHYDROL.2016.11.022.

Hong, X., Guo, S., Zhou, Y., & Xiong, L. (2015). Uncertainties in assessing hydrological drought using streamflow drought index for the upper Yangtze River basin. *Stochastic Environmental Research and Risk Assessment, 29*, 1235–1247. https://doi.org/10.1007/s00477-014-0949-5.

Jahangir, M., & Yarahmadi, Y. (2020). Hydrological drought analyzing and monitoring by using Streamflow Drought Index (SDI) (case study: Lorestan, Iran). *Arabian Journal of Geosciences, 13*, 1–12. https://doi.org/10.1007/s12517-020-5059-8.

Kiem, A., Johnson, F., Westra, S., Dijk, A., Evans, J., O'Donnell, A., Rouillard, A., Barr, C., Tyler, J., Thyer, M., Jakob, D., Woldemeskel, F., Sivakumar, B., & Mehrotra, R. (2016). Natural hazards in Australia: droughts. *Climatic Change, 139*, 37–54. https://doi.org/10.1007/s10584-016-1798-7.

Kravtsov, S., Kondrashov, D., & Ghil, M. (2005). Multilevel regression modeling of nonlinear processes: Derivation and applications to climatic variability. *Journal of Climate, 18*, 4404–4424. https://doi.org/10.1175/JCLI3544.1.

Kuhn, M., Weston, S., Keefer, C., Coulter, N., & Quinlan, R. (2024). Package 'Cubist'. Rule- and Instance-Based Regression Modeling. https://cran.r-project.org/web/packages/Cubist/index.html. (Accessed 3 January 2025)..

Lall, U., Moon, Y., Kwon, H., & Bosworth, K. (2006). Locally weighted polynomial regression: Parameter choice and application to forecasts of the Great Salt Lake. *Water Resources Research, 42*. https://doi.org/10.1029/2004WR003782.

Makhoul, J. (1975). Linear prediction: A tutorial review. In: *Proceedings of the IEEE, 63*(4), 561–580. https://doi.org/10.1109/PROC.1975.9792.

Masselot, P., Dabo-Niang, S., Chebana, F., & Ouarda, T. (2016). Streamflow forecasting using functional regression. *Journal of Hydrology, 538*, 754–766. https://doi.org/10.1016/j.jhydrol.2016.04.048.

Mehr, A. D., Vaheddoost, B., & Mohammadi, B. (2020). ENN-SA: A novel neuro-annealing model for multi-station drought prediction. *Computers & Geosciences, 145*, 104622. https://doi.org/10.1016/j.cageo.2020.104622.

Mohammadi, B. (2023). Modeling various drought time scales via a merged artificial neural network with a firefly algorithm. *Hydrology, 10*(3), 58. https://doi.org/10.3390/hydrology10030058.

Mokhtar, A., Jalali, M., He, H., Al-Ansari, N., Elbeltagi, A., Alsafadi, K., Abdo, H., Sammen, S., Gyasi-Agyei, Y., & Rodrigo-Comino, J. (2021). Estimation of SPEi meteorological drought using machine learning algorithms. *IEEE Access, 9*, 65503–65523. https://doi.org/10.1109/ACCESS.2021.3074305.

Nalbantis, I., & Tsakiris, G. (2009). Assessment of hydrological drought revisited. *Water Resources Management, 23*, 881–897. https://doi.org/10.1007/s11269-008-9305-1.

Ostertagová, E. (2012). Modelling using polynomial regression. *Procedia Engineering, 48*, 500–506. https://doi.org/10.1016/j.proeng.2012.09.545.

Ouali, D., Chebana, F., & Ouarda, T. (2017). Fully nonlinear statistical and machine-learning approaches for hydrological frequency estimation at ungauged sites. *Journal of Advances in Modeling Earth Systems, 9*, 1292–1306. https://doi.org/10.1002/2016MS000830.

Quinlan, J. R. (1992). Learning with continuous classes. In *5th Australian joint conference on artificial intelligence* (Vol. 92, pp. 343–348)..

Quinlan, J. R. (1993). Combining instance-based and model-based learning. In *Proceedings of the tenth international conference on machine learning* (pp. 236–243)..

Rubio-Martín, A., Pulido-Velazquez, M., Macian-Sorribes, H., & García-Prats, A. (2020). System dynamics modeling for supporting drought-oriented management of the Jucar river system, Spain. *Water, 12*. https://doi.org/10.3390/w12051407.

Schoppa, L., Disse, M., & Bachmair, S. (2020). Evaluating the performance of random forest for large-scale flood discharge simulation. *Journal of Hydrology, 590*, 125531. https://doi.org/10.1016/j.jhydrol.2020.125531.

Shah, V., Jagupilla, S., Vaccari, D., & Gebler, D. (2021). Non-linear visualization and importance ratio analysis of multivariate polynomial regression ecological models based on river hydromorphology and water quality. *Water, 13*. https://doi.org/10.3390/w13192708.

Shamshirband, S., Hashemi, S., Salimi, H., Samadianfard, S., Asadi, E., Shadkani, S., Kargar, K., Mosavi, A., Nabipour, N., & Chau, K. (2020). Predicting standardized streamflow index for hydrological drought using machine learning models. *Engineering Applications of Computational Fluid Mechanics, 14*, 339–350. https://doi.org/10.1080/19942060.2020.1715844.

Wang, G., Zhang, Q., Band, S., Dehghani, M., Chau, K., Tho, Q., Zhu, S., Samadianfard, S., & Mosavi, A. (2022). Monthly and seasonal hydrological drought forecasting using multiple extreme learning machine models. *Engineering Applications of Computational Fluid Mechanics, 16*, 1364–1381. https://doi.org/10.1080/19942060.2022.2089732.

Wang, S., Lian, J., Peng, Y., Hu, B., & Chen, H. (2019). Generalized reference evapotranspiration models with limited climatic data based on random forest and gene expression programming in Guangxi, China. *Agricultural Water Management, 221*, 220–230. https://doi.org/10.1016/j.agwat.2019.03.027.

Wilkinson, G. N., & Rogers, C. E. (1973). Symbolic description of factorial models for analysis of variance. *Journal of the Royal Statistical Society Series C: Applied Statistics, 22*(3), 392–399.

Yang, X., Liao, X., Di, D., & Shi, W. (2023). A review of drought disturbance on socioeconomic development. *Water, 15*. https://doi.org/10.3390/w15223912.

Yaseen, Z., Ali, M., Sharafati, A., Al-Ansari, N., & Shahid, S. (2021). Forecasting standardized precipitation index using data intelligence models: Regional investigation of Bangladesh. *Scientific Reports, 11*. https://doi.org/10.1038/s41598-021-82977-9.

Yu, L., Gao, X., & Zhao, X. (2020). Global synthesis of the impact of droughts on crops' water-use efficiency (WUE): Towards both high WUE and productivity. *Agricultural Systems, 177*, 102723. https://doi.org/10.1016/j.agsy.2019.102723.

CHAPTER FIFTEEN

Climate and drought (climate variability, climate changes, future droughts)

Mohammad Jamali, and Saeid Eslamian
Department of Water Science and Engineering, College of Agriculture, Isfahan University of Technology, Isfahan, Iran

15.1 Introduction

Climate and weather are two distinct yet interconnected meteorological concepts that are often confused. Weather is the state of the atmosphere at a specific place and time. It includes factors like temperature, humidity, precipitation, wind, and air pressure. The weather can be unpredictable and can change quickly. Climate, on the other hand, refers to the long-term average weather conditions of a region. It represents the typical weather pattern of a place over many years. Climate, which is the long-term average weather conditions of a specific region includes temperature, precipitation, humidity, wind speed, atmospheric pressure, and solar radiation (Qian, 2017).

Climate is crucial for a multitude of reasons, impacting everything from agriculture and ecosystems to human health and economies. Climate directly influences crop growth, livestock health, and agricultural productivity. Climate change, characterized by extreme fluctuations in temperature and rainfall, jeopardizes food security and can lead to famine and humanitarian crises (Jamali & Eslamian, 2024; Jamali et al., 2025). Understanding climate patterns helps farmers plan their planting and harvesting seasons. Climate patterns determine water availability, influencing water scarcity or flooding. Climate change can alter rainfall patterns, leading to droughts or excessive rainfall (Dore, 2005). Effective water resource management relies on accurate climate information. Climate change can lead to increased heat waves, causing heatstroke and other health issues (Marx et al., 2021). Changes in temperature and humidity can affect the spread of diseases. Extreme weather events like floods and storms can lead

Drought Dynamics
DOI: https://doi.org/10.1016/B978-0-443-34205-9.00012-3
© 2026 Elsevier Inc. All rights are reserved, including those for text and data mining, AI training, and similar technologies.

to injuries and fatalities. Climate change disrupts ecosystems by altering temperature, precipitation, and ocean acidity. This can lead to species extinction, loss of biodiversity, and damage to natural habitats. Understanding climate patterns helps in conservation efforts and ecosystem management. Climate change can also affect industries like agriculture, tourism, and insurance. Extreme weather events can cause significant economic losses. Climate-related disasters can displace people and disrupt livelihoods. Climate information is crucial for designing and building infrastructure that can withstand extreme weather events. Urban planning and coastal development need to consider future climate scenarios. Infrastructure projects must be resilient to climate-related risks (Jamali et al., 2022).

Drought and climate are two interconnected phenomena that significantly influence each other (Cook et al., 2018). Droughts, a common occurrence in climate patterns, are often defined by a lack of rainfall. However, this simplistic view overlooks the complex nature of droughts and their varied impacts (Coles & Eslamian, 2017). Dictionaries provide various definitions of drought including "persistent dry weather," "severe dryness due to lack of rain," and "a prolonged period of low precipitation" (Mcleod & Hanks, 1982; Ostler, 1969). Drought is generally defined as an extended period with significantly below-average precipitation, resulting in water shortages that impact agriculture, industry, and ecosystems. This dry period can be short-term (like a season) or long-term (several years) and severe enough to compromise the water supply needed for normal activities (Schneider, 2011). Drought severity is influenced by a combination of natural factors like reduced rainfall and increased evaporation, as well as human activities such as over-extraction of water, land-use change, and poor water management. Human actions often worsen the impacts of drought, prolonging dry periods and expanding affected areas (Aghakouchak et al., 2021; Handmer et al., 2012).

A clear understanding of climate allows us to effectively plan and manage for various weather phenomena. In this context, two key terms are often used interchangeably but have distinct meanings: climate variables and climate change. Climate variables are factors that describe the weather conditions in a specific area. These include temperature, precipitation, humidity, wind, air pressure, and solar radiation. These variables are constantly changing, and these natural fluctuations are known as climate variability. Climate change, on the other hand, is a long-term process involving significant changes in the statistical distribution of weather

patterns over periods of time. While natural factors such as volcanic activity or solar cycles can influence climate, in recent decades, human activities and greenhouse gas emissions have become the primary drivers of climate change (Werndl, 2016).

Drought, a prominent consequence of climate change, manifests as a significant decrease in rainfall and an increase in evaporation (Wilhite & Glantz, 1985). This phenomenon can occur not only in the short term but also over extended periods, with negative consequences for human life, the environment, and the economy. From reduced agricultural and livestock production to water crises, forced migration, and even social conflicts, droughts have a wide range of adverse effects (Mishra & Singh, 2010). Given the harmful consequences of drought, accurate and timely prediction of this event is of paramount importance. A thorough understanding of a region's climatic characteristics, identification of patterns in climate change, and comprehension of the relationship between climatic variables, climate change, and drought are the first steps towards predicting and better managing droughts. With accurate predictions, preventive measures can be implemented to mitigate the resulting damages.

This chapter delves into the intricate relationship between drought and climate variability and climate change. With a forward-looking perspective, it aims to address how climate change will influence the occurrence and severity of future droughts. Initially, fundamental concepts such as climate variability, climate change, and drought are precisely defined, and their complex interconnections are elucidated. Subsequently, various drought types and commonly employed indices for their quantification and monitoring are introduced. Furthermore, future climate change scenarios and their potential impacts on regional precipitation and temperature patterns are explored. Advanced methodologies for forecasting future droughts are also presented and evaluated. Additionally, this chapter highlights key findings from prominent research studies on drought and climate change. The overarching objective of this investigation is to provide a comprehensive overview of the current and future state of droughts, while offering potential strategies for their effective management.

15.2 Climate variability

Climate variability refers to the natural fluctuations in the Earth's climate system and its climatic elements over time. Climatic elements

include temperature, humidity, precipitation, air pressure, wind, solar radiation, and cloudiness. These elements are constantly changing. Weather forecasting involves measuring and analyzing climatic variables to predict future weather conditions. By understanding rainfall and evaporation data, better water resource management can be achieved. Climatic variables are also crucial in agriculture. Furthermore, climatic variables play a significant role in the production of renewable energy such as solar and wind energy.

Numerous studies have been conducted by researchers to investigate the variability of climatic elements (Mote et al., 2013; Nicholson, 2019). Jamali et al. (2022) conducted a comprehensive analysis to examine the spatiotemporal trends in precipitation characteristics and rising temperatures over time in Iran, using data from 1951 to 2019. Temporal trends in precipitation and temperature were examined using the nonparametric Mann–Kendall test and quantile regression analysis. The results showed limited evidence of a similar increase in maximum 3-hour and 24-hour precipitation at higher temperatures, leading to an increase in annual precipitation. In fact, most stations across Iran exhibited trends consistent with drying and decreasing precipitation at higher temperatures. Overall, most regions in Iran showed a negative trend in annual precipitation, with a decrease ranging from -2.64 to -0.44 mm for each degree Celsius increase in temperature. Additionally, the study revealed that with increasing elevation, the intensity of precipitation changes shifted from autumn to winter, although these effects were not statistically significant at the national level (Jamali et al., 2022). Da Silva (2004) investigated the climatic variables in northeastern Brazil. By analyzing time series of eight climatic variables across annual and dry/wet seasons, the study aimed to identify diverse climatic patterns in the region. Results from the Mann–Kendall test indicated that most variables exhibited a significant increasing trend (at the 95% or 99% confidence level). However, relative humidity and precipitation showed a decreasing trend. These findings suggest that many of the studied stations are undergoing a process of environmental drying. In other words, the results of this research indicate that historical climatic changes in northeastern Brazil, particularly in semiarid and coastal areas, have been associated with increasing temperatures and decreasing precipitation (Da Silva, 2004).

Recent studies at continental and global scales have demonstrated clear evidence of climate variability and its widespread impacts. For instance, Intergovernmental Panel on Climate Change (IPCC) reports (IPCC, 2021) highlight consistent global trends in increasing surface temperatures,

changing precipitation patterns, and more frequent extreme weather events. Hartmann et al. (2013) analyzed global surface temperature records and found a significant warming trend since the mid-20th century, strongly linked to both natural variability and anthropogenic influences. On a continental scale, Seneviratne et al. (2012) reported an increase in the frequency and intensity of heat waves across Europe and North America. Similarly, Trenberth et al., (2014) emphasized the role of ocean–atmosphere interactions in driving large-scale climate variability, with widespread consequences for water resources, agriculture, and ecosystems globally. These findings underscore the importance of considering global and continental-scale processes in climate variability studies.

Understanding climate variables is essential for predicting and managing their impacts on both the society and environment. By better understanding these fluctuations, we can take the necessary actions to adapt to climate change and mitigate its effects.

In addition, large-scale climate variability is often influenced by major atmospheric and oceanic circulation patterns known as climatic indices. Notable among these are the El Niño–Southern Oscillation (ENSO), the North Atlantic Oscillation (NAO), the Arctic Oscillation (AO), the Indian Ocean Dipole (IOD), and the Madden–Julian Oscillation (MJO). These indices play a critical role in modulating regional and global climate patterns including changes in precipitation and temperature. For instance, ENSO is known to cause significant interannual variations in rainfall over many parts of the World, including Iran, while NAO and AO affect weather conditions in Europe and parts of Asia (Cheng et al., 2024; Domeisen et al., 2019; Islam et al., 2018; Lyon, 2004). Incorporating these indices into climate variability studies enhances our understanding of the underlying drivers of climatic trends.

15.3 Climate change

The Earth's atmosphere, composed of various gases, absorbs, scatters, and reflects different wavelengths of sunlight, regulating phenomena such as atmospheric temperature. Among these gases, greenhouse gases—including water vapor, carbon dioxide, methane, and halocarbons—play a crucial role in controlling the Earth's surface temperature. Sunlight, primarily composed of shortwave radiation, passes through these gases and reaches the Earth's surface. Upon heating, the Earth emits long-wave

infrared radiation, which is absorbed by greenhouse gases, causing them to warm up. This process contributes to the increase in the Earth's surface temperature (Leavesley, 1994). The excessive use of fossil fuels and the expansion of industrial activities to meet the growing demands of the global population have led to an increase in greenhouse gas concentrations, disrupting the Earth's energy balance. This imbalance results in significant changes in long-term average weather patterns, a phenomenon known as climate change. Climate change is one of the most pressing and complex challenges facing the World today. Climate change affects various climate variables such as temperature, precipitation, evaporation, transpiration, and humidity. It leads to an increase in global average temperature, decreased precipitation in arid regions, and rising sea levels due to the melting of polar ice caps (Arnell, 1999).

Climate change and global warming are among the most pressing environmental issues of our time. Researchers have extensively documented changes in global weather patterns. Many regions are experiencing decreased precipitation, reduced surface water flow, and disruptions in agricultural productivity. To mitigate the impacts of climate change, a deeper understanding of these issues is crucial (Brekke, 2009). Climate change significantly impacts various water resources and uses. Understanding and analyzing these impacts often requires years of research. Since 1950, the frequency of heat waves has increased, leading to more hot nights. Additionally, due to declining rainfall and increased evaporation caused by rising temperatures, the number of regions experiencing droughts has grown. Conversely, the frequency of days with heavy rainfall, resulting in floods, has also increased. Although the annual frequency of tropical storms and hurricanes fluctuates, evidence indicates that their intensity and duration have been on the rise since the 1970s (Gellens & Roulin, 1998; Jamali, Gohari, & Akhavan Saraf, 2024; Osborne et al., 2013; Roudier et al., 2011).

Climate change has also impacted other aspects of human life. Climate change has had a detrimental impact on agriculture, reducing crop yields and increasing water demand (Fischer & Van Velthuizen, 1996; Fischer et al., 2007; You et al., 2009). Increasing levels of atmospheric carbon dioxide can affect agricultural productivity, water use efficiency of crops, and expand agricultural potential in higher latitudes. However, the realization of these potential benefits is uncertain due to changes in temperature, precipitation, evaporation, radiation, and the increased prevalence of pests, diseases, and weeds. Consequently, long-term shifts

in climate patterns and agricultural potential can have profound implications for land use and the ability of future generations to secure adequate food and agricultural products (Mason, 2004; Tokarska et al., 2020). According to the IPCC in 2013, climate change will have negative impacts on water resources in dry and semiarid countries of Asia. Iran, with its arid climate, is no exception. Projections indicate that changes in temperature, soil moisture, and river runoff will have significant impacts of climate change in this region (Tokarska et al., 2020).

As water resources dwindle in arid regions, water demand and efforts to compensate for reduced access to surface water will increase (Jamali & Eslamian, 2024). This is because reduced water availability leads to decreased economic benefits, resulting in social conflicts, accelerated environmental degradation, and threats to societal survival. Accurate assessments of future climates are indispensable for planning effective strategies to address climate change.

15.4 Climate change models and scenarios

Given the available evidence, scientists have a high degree of certainty that greenhouse gas concentrations in the Earth's atmosphere are increasing, leading to global warming. However, the exact impacts of this warming on regional climates are still uncertain. Therefore, instead of making precise predictions about future conditions, climate scientists use climate scenarios. Climate scenarios provide potential future climate conditions based on climate models and available data. Atmosphere–ocean general circulation models (AOGCMs) are essential tools for understanding and quantifying the impacts of climate change on meteorological variables (O'neill et al., 2016). These models simulate future changes in meteorological parameters by considering numerous factors such as carbon dioxide, aerosols, and vegetation, and by applying physical laws and mathematical relationships. AOGCMs are complex models that simulate the atmosphere, ocean, land surface, ice sheets, and biosphere, coupling them together to represent the Earth's climate system. These models use three-dimensional grids to represent the Earth, and the number of vertical layers in the ocean is greater than in the atmosphere due to the ocean's greater complexity (Gudmundsson et al., 2012). AOGCMs have been continuously improved in IPCC assessment reports, leading to increased accuracy in simulating climate change. Despite the sophistication

of climate models, the inherent complexity of the climate system and necessary simplifications in the models introduce uncertainties into the results. Given the crucial role of AOGCMs in climate change research, assessing their accuracy is of great importance. By comparing and ranking these models based on their accuracy, more accurate and reliable results can be obtained in future climate projections (Tebaldi et al., 2021).

Various AOGCMs have been assessed and presented by the IPCC in several phases to predict the future climate of the World. From 1991 to 2007, the IPCC initiated a project to standardize the use of AOGCM outputs and produced four assessment reports. The IPCC has released several assessment reports since its inception including the First Assessment Report (FAR) in 1990, the Second Assessment Report (SAR) in 1996, the Third Assessment Report (TAR) in 2001, and the Fourth Assessment Report (AR4) in 2007. In 2008, the World Meteorological Organization's Climate Research Program established the coupled model intercomparison project (CMIP) to create a collection of climate models from international climate modeling centers. In 2011, the first results from the coupled model intercomparison project phase 5 (CMIP5) became publicly available. CMIP5 models utilized representative concentration pathways (RCPs), which are emission scenarios based on radiative forcing levels up to 2100. These scenarios represent different pathways of future greenhouse gas changes and provide estimates of atmospheric greenhouse gas concentrations. While the spatial resolution of the models improved significantly in the fifth and sixth assessment reports compared to earlier phases—with CMIP5 models generally ranging from approximately 1° to 2.5°, and selected high-resolution CMIP6 models reaching up to ~0.5°—some limitations still existed.

In this regard, the IPCC began its sixth assessment cycle in 2016 to prepare the Sixth Assessment Report (AR6). This report is being prepared by three working groups: mitigation of climate change, the physical science basis, and impacts, adaptation, and vulnerability. Thirty-three research centers worldwide are collaborating with the IPCC to develop various models for the AR6. The result of this collaboration has been the creation of 58 models to predict the future climate of the World. These models are expected to be completed by 2022, and the final IPCC report on this topic is also expected by this date. However, outputs from some of these models have been gradually made available to the public through various databases (Tebaldi et al., 2021).

Table 15.1 presents 10 CMIP6 models with complete historical and future data. Daily and monthly data are available for each model from 1850

Table 15.1 Characteristics of coupled model intercomparison project phase 6 models.

No.	Model name	Developing country	Research center	Spatial resolution
1	BCC-CSM2-MR	China	Beijing Climate Center, China Meteorological Administration	1.12° × 1.12°
2	CESM2	USA	Community Earth System Model Contributors	1.25° × 0.94°
3	CNRM-CM6-1	France	Centre National de Recherches Météorologiques Scientifique (CNRM)	1.4° × 1.4°
4	CanESM5	Canada	Canadian Centre for Climate Modeling and Analysis-Canada	2.81° × 2.78°
5	MIROC6	Japan	National Institute for Environmental Studies, The University of Tokyo	1.4° × 1.4°
6	MRI-ESM2-0	Japan	Meteorological Research Institute	1.12° × 1.12°
7	IPSL-CM6A-LR	France	Institute Pierre-Simon Laplace	2.5° × 1.26°
8	GISS-E2-1-G	USA	NASA Goddard Institute for Space Studies	2.5° × 2°
9	HadGEM3-GC31-LL	UK	Meteorological Office Hadley Centre	1.88° × 1.25°
10	NESM3	China	Nanjing University of Information and Technology (NUIST)	1° × 1.3°

to 2014. To extract future climate projections, different emission scenarios are used. RCPs represent various socioeconomic pathways and greenhouse gas emission levels. They consider factors such as economic development, population growth, and technological advancements.

The four primary emission scenarios used in CMIP6 models are:

- Shared socioeconomic pathways (SSP)1–2.6: A low greenhouse gas emissions scenario leading to a moderate warming level.
- SSP2–4.5: An intermediate greenhouse gas emissions scenario leading to a moderate warming level.
- SSP3–7.0: A high greenhouse gas emissions scenario leading to a high warming level.
- SSP5–8.5: A very high greenhouse gas emissions scenario leading to a very high warming level.

These scenarios represent a range of potential future climate conditions, from optimistic to pessimistic. More details about these models are provided in Table 15.2.

15.5 Drought

Drought, a severe natural hazard, has drawn the attention of scientists from diverse fields including climatology, hydrology, agriculture, and biology. This phenomenon is not confined to arid or semiarid regions; it can occur in areas with significant rainfall as well. In essence, drought refers to a prolonged period of deficient precipitation resulting in a water shortage. Numerous factors contribute to the occurrence and severity of droughts, such as temperature patterns, precipitation intensity and distribution, relative humidity, wind speed, and changes in vegetation cover. Unlike arid conditions, which are a permanent feature of certain regions, droughts are temporary events. They can have devastating impacts on society, the

Table 15.2 Specifications of the release scenarios of the sixth intergovernmental panel on climate change report.

Scenario name	Radiative forcing category	Radiative forcing (W/m^2)
SSP5–8.5	Very high	8.5
SSP3–7.0	High	7.0
SSP2–4.5	Intermediate	4.5
SSP1–2.6	Low	2.6

environment, and the economy. Heat waves are often confused with droughts, but they are distinct phenomena. While heat waves are characterized by short-term periods of abnormally high temperatures, droughts are long-term events associated with decreased water availability. The combination of heat waves and droughts can exacerbate negative impacts, leading to severe crises (Chang & Wallace, 1987; Mishra & Singh, 2010).

The increasing global demand for water, driven by population growth and expanding agricultural, energy, and industrial sectors, has led to water scarcity in many regions. This problem is exacerbated by climate change and water pollution. There has been a notable rise in the occurrence of severe floods and droughts in recent times. The intervals between these extreme events appear to be shortening in certain areas. This trend has been noted by researchers such as Aswathanarayana (2001) and Jamali et al. (2022).

Droughts can have far-reaching consequences, affecting both surface and groundwater resources. Degraded water quality, reduced water supply, crop failures, diminished rangeland productivity, disrupted riparian ecosystems, decreased power generation, and curtailed recreational activities are just some of the impacts. Additionally, droughts can alter hydrologic regimes, leading to changes in lake chemistry as sediment, organic matter, and nutrients are less readily transported to surface waters (Webster et al., 1996).

Droughts have far-reaching consequences, affecting various sectors of society and causing significant economic and social damage. In fact, droughts have been identified as one of the most devastating natural disasters of the 20th century (Bruce, 1994). Over the past few decades, large-scale droughts have become increasingly prevalent, impacting extensive areas in Europe, Africa, Asia, Australia, South America, Central America, and North America (Le Comte, 1994). As a result, there has been growing global concern about the significant costs associated with these events (Downing & Bakker, 2016).

The past two decades have seen a substantial increase in the frequency and severity of droughts in the United States, making them one of the most economically damaging natural disasters (Cook et al., 2007). Similarly, European regions have experienced worsening drought conditions, with an average annual economic impact of €5.3 billion since 1991 (Stein et al., 2016). Furthermore, the 2003 European drought alone caused at least €8.7 billion economic damage. In Asia, rising temperatures, increased frequency of El Niño events, and reduced rainfall have led to water stress

and declining agricultural yields, particularly for rice, maize, and wheat (Bates, 2008). A devastating multi-year drought ravaged Central and Southwest Asia from 1999 to 2000, impacting a population of up to 60 million (Agrawala et al., 2001). Countries like Iran, Afghanistan, Pakistan, Tajikistan, Uzbekistan, and Turkmenistan were particularly hard-hit. India, another vulnerable region, has faced drought conditions at least once every three years in the past five decades. Also, droughts have caused significant damage in both Australia and Africa.

15.6 Future of drought and forecasting techniques

Drought is one of the most complex and devastating natural hazards, whose frequency, intensity, and spatial extent are projected to increase significantly under ongoing climate change. Unlike sudden-onset hazards such as floods or earthquakes, droughts evolve gradually and can persist for months or years, often causing widespread socioeconomic and environmental impacts. As the planet warms, changes in atmospheric circulation patterns, reduced snowpack, increased evapotranspiration, and alterations in precipitation regimes are leading to the intensification of drought conditions in many parts of the World. Therefore understanding the future trajectory of droughts and developing accurate forecasting systems have become priorities in global water resources management and climate adaptation strategies (Toreti et al., 2024; Zhou et al., 2025).

Climate change is reshaping the global hydrological cycle in ways that profoundly affect drought dynamics. Warmer temperatures increase atmospheric demand for moisture, accelerating evapotranspiration rates and reducing soil moisture availability. Additionally, changes in precipitation—whether in quantity, intensity, or temporal distribution—can lead to more prolonged and severe droughts, especially in regions already vulnerable due to aridity or water scarcity. According to the IPCC AR6, many mid-latitude and subtropical regions are likely to experience an increase in agricultural and ecological drought due to reduced precipitation and soil moisture deficits. In this context, anticipating future drought patterns is essential not only for disaster risk reduction but also for ensuring food security, energy production, and sustainable ecosystem management (Cook et al., 2020; Seneviratne et al., 2010).

Forecasting droughts involves predicting their occurrence in terms of timing, duration, magnitude, and spatial extent (Aghakouchak et al., 2022).

Effective drought forecasts allow policymakers, farmers, water utilities, and disaster managers to implement timely mitigation measures, allocate resources efficiently, and minimize losses. However, drought prediction is inherently challenging due to the interplay of multiple climatic, hydrologic, and anthropogenic variables (Brunner et al., 2021). Furthermore, the diversity of drought types—meteorological, agricultural, hydrological, and socioeconomic—adds layers of complexity to the forecasting task.

15.6.1 Overview of drought forecasting methods

Over the past decades, numerous models and techniques have been developed for forecasting droughts, ranging from traditional statistical approaches to advanced machine learning (ML) and hybrid models. Each methodology brings distinct advantages and limitations, and their selection depends on the target region, available data, temporal scale, and type of drought.

Statistical methods represent the earliest attempts at drought forecasting and remain widely used due to their interpretability and low computational cost (Fernández-Manso et al., 2011; Han et al., 2013).

- Linear and multiple regression models: These models estimate drought indicators (e.g., SPI, SPEI) based on relationships with predictors such as rainfall, temperature, and streamflow (Meng et al., 2017; Stagge et al., 2015).
- Time-series models (AR, MA, ARIMA): Mossad and Alazba (2015) employed ARIMA models for long-term drought forecasting using the SPEI index in hyper-arid climates. Their results demonstrated reliable performance for long-term indices (e.g., SPEI-24), although prediction accuracy declined for short-term scales. Karthika and Thirunavukkarasu (2017) applied ARIMA to forecast short-term meteorological drought in the Lower Thirumanimuthar Sub-basin of India, achieving reasonable accuracy for 1- to 3-year lead times.
- Markov chain models: These probabilistic models estimate the transition probabilities between different drought states over time (Junfei & Yang, 2012; Rahmat et al., 2017). Sun et al. (2017) compared first- and second-order Markov chain models using SPEI and SRI indices, concluding that first-order models offered adequate performance in capturing the joint behavior of precipitation and runoff anomalies.

With the increasing availability of large-scale hydroclimatic data and advancements in computational power, artificial intelligence (AI) and ML

models have gained significant traction in drought forecasting (Marj & Meijerink, 2011).

- Artificial neural networks (ANNs): Kousari et al., (2017) applied ANNs to predict SPI values in Fars Province, Iran, across lead times ranging from 3–24 months. The study found that although ANNs performed well for short-term forecasts, their accuracy decreased with longer lead times. Optimization techniques were also suggested to enhance ANN performance.
- Support vector machines (SVMs), decision trees, and random forests: These models have been used in various contexts to capture nonlinear relationships between climate variables and drought indices.
- Hybrid AI models: Ozger et al. (2021) combined wavelet transforms with fuzzy logic (W-FL) and ANNs (W-ANN) to forecast the Palmer Drought Severity Index (PDSI) in Texas. Their results demonstrated that the W-FL model outperformed W-ANN in long-term drought prediction, highlighting the potential of hybrid models.
- Other ML approaches: Recent studies (e.g., Belayneh et al., 2016; Prodhan et al., 2022) have applied ensemble learning, long short-term memory (LSTM) networks, and convolutional neural networks (CNNs) for drought forecasting at various temporal and spatial scales.

Dynamic system models, which incorporate feedback loops and state transitions over time, have been proposed as tools to model the complex behavior of droughts. Bowden et al. (2016) and Dehghani et al. (2017) developed dynamic system frameworks that integrate climatic, hydrological, and land-use data to simulate and predict drought evolution. Fung et al. (2019) suggested that combining dynamic models with real-time monitoring systems can enhance situational awareness and forecasting reliability.

15.6.2 Factors affecting forecast accuracy

Accurate drought forecasting hinges on several critical elements (Alawsi et al., 2022; Tyagi et al., 2022):

- Input data quality and selection: Datasets must be accurate, complete, and relevant. Using appropriate temporal scales (e.g., monthly vs. seasonal) and indices (e.g., SPI, SPEI, PDSI) is essential for reliable results.
- Forecast lead time: There is often a trade-off between forecast horizon and accuracy. Short-term forecasts are generally more accurate, whereas long-term forecasts offer strategic value but involve greater uncertainty.

- Preprocessing techniques: Normalization, noise reduction, dimensionality reduction (e.g., PCA), and feature selection methods improve the stability and performance of ML models.
- Model complexity and interpretability: While complex models like deep learning offer higher accuracy, they often lack transparency. Therefore model selection should balance accuracy with interpretability based on the end-user's needs.

15.6.3 Integration of real-time data, big data, and adaptive forecasting systems

The increasing complexity of drought events under changing climatic conditions has driven a paradigm shift in drought forecasting—from isolated models toward integrated, adaptive, and real-time systems. This transformation is enabled by recent advancements in big data analytics, cloud computing, remote sensing, and Internet of Things (IoT) technologies, which collectively enhance both the accuracy and timeliness of drought monitoring and prediction (Tao et al., 2024). Real-time data acquisition is at the core of this evolution. High-resolution satellite platforms such as MODIS (Moderate Resolution Imaging Spectroradiometer), TRMM (Tropical Rainfall Measuring Mission), and SMAP (Soil Moisture Active Passive) now provide near-continuous observations of key hydrometeorological variables including precipitation, land surface temperature, vegetation indices, and soil moisture. When combined with data from ground-based weather stations, stream gauges, and soil sensors, these inputs allow for dynamic and responsive drought monitoring across various spatial and temporal scales (Prodhan et al., 2021; Xu et al., 2023). Big data platforms further enable the integration of vast and heterogeneous datasets encompassing climate records, hydrological flows, agricultural outputs, land-use maps, and socioeconomic indicators. The fusion of these diverse data sources provides a more holistic view of drought impacts and enhances situational awareness for decision-makers. Additionally, the application of ML and AI techniques to these multi-dimensional datasets allows for the detection of early warning signals, pattern recognition, and predictive modeling with improved accuracy. Beyond monitoring and forecasting, smart drought management systems can also attribute observed impacts to specific drought phases—distinguishing, for instance, between direct effects such as crop failure and indirect consequences like market price surges or water use restrictions.

This capability is essential for designing targeted mitigation strategies and for conducting post-event assessments. Building on these technological foundations, researchers and institutions are now moving toward the development of adaptive drought early warning systems (DEWS). These systems are designed to not only forecast droughts with greater precision but also to evolve and adjust based on feedback, new data, and changing environmental conditions. Key features of modern DEWS include:

- Multi-source data integration, incorporating climate, hydrology, soil characteristics, vegetation conditions, and socioeconomic variables to generate comprehensive drought profiles;
- Multi-model ensemble forecasting, which leverages the strengths of statistical, ML, and hybrid models to reduce uncertainty and improve robustness;
- Real-time data assimilation, enabling continuous model updates and more accurate near-future projections;
- Risk-based communication and visualization tools, which translate complex forecasts into actionable insights for stakeholders such as farmers, water managers, and policymakers.

By combining the predictive capabilities of advanced algorithms with the responsiveness of real-time systems and the flexibility of adaptive management, such integrated frameworks hold tremendous potential for proactive drought risk reduction. They support better preparedness, facilitate early intervention, and ultimately enhance the resilience of communities and ecosystems in the face of increasing drought frequency and severity (Hanadé Houmma et al., 2022).

Ultimately, as climate variability and the frequency of extreme events continue to intensify, accurate drought forecasting becomes increasingly vital for sustainable water resource management, agricultural resilience, and disaster preparedness. While traditional statistical models still offer valuable insights, recent advancements in ML, hybrid modeling approaches, and real-time monitoring systems have marked a significant shift in the landscape of drought prediction. The future of drought forecasting lies in integrated, data-driven, and adaptive frameworks that harness the complementary strengths of diverse methodologies to deliver timely, reliable, and actionable information. These innovations will play a critical role in enhancing the resilience of societies and ecosystems in the face of one of the most persistent and complex climate-related hazards of our time.

15.7 Conclusion

Climate plays a fundamental role in regulating environmental systems, influencing precipitation, temperature, humidity, wind, and solar radiation. These variables collectively shape water availability, ecosystem stability, agricultural productivity, and socioeconomic well-being. Among the various climate-induced hazards, drought stands out as one of the most pervasive and complex, resulting from prolonged periods of precipitation deficit, often exacerbated by high temperatures and increased evapotranspiration. It is important to distinguish between climate variability and climate change, as both have distinct implications for drought occurrence. Climate variability refers to the natural fluctuations in climate patterns over short to medium time scales—such as seasonal shifts, El Niño-Southern Oscillation (ENSO), or multi-year drought cycles—which can temporarily alter precipitation and temperature regimes. In contrast, climate change denotes long-term alterations in average climatic conditions, largely driven by anthropogenic factors such as greenhouse gas emissions, land-use change, and industrialization. While variability causes episodic drought events, climate change can increase the baseline risk, leading to more frequent, prolonged, and spatially extensive droughts. These changing dynamics emphasize the need for advanced and adaptive drought monitoring and forecasting systems. As future projections indicate a rise in the severity and frequency of droughts—particularly in already water-stressed regions—there is a growing urgency to strengthen both mitigation and adaptation strategies. Accurate forecasting based on an understanding of both climate variability and long-term climate change is vital for early warning, risk reduction, and sustainable resource management. To minimize the adverse impacts of droughts, a multi-faceted approach is required. This includes improving early warning systems, enhancing real-time data collection, promoting water-efficient practices, developing drought-resilient crops, and investing in robust climate adaptation frameworks. Moreover, long-term efforts to mitigate climate change—especially by reducing greenhouse gas emissions—are essential to curb the intensification of drought patterns. In summary, understanding and addressing both the short-term fluctuations of climate variability and the long-term trends of climate change is essential for enhancing drought resilience. An integrated approach that blends scientific forecasting, policy planning, and community-level action will be key to confronting the escalating challenges of drought under a changing climate.

References

Aghakouchak, A., Mirchi, A., Madani, K., Di Baldassarre, G., Nazemi, A., Alborzi, A., Anjileli, H., Azarderakhsh, M., Chiang, F., Hassanzadeh, E., Huning, L. S., Mallakpour, I., Martinez, A., Mazdiyasni, O., Moftakhari, H., Norouzi, H., Sadegh, M., Sadeqi, D., Van Loon, A. F., & Wanders, N. (2021). Anthropogenic drought: Definition, challenges, and opportunities. *Reviews of Geophysics, 59* e2019RG000683.

Aghakouchak, A., Pan, B., Mazdiyasni, O., Sadegh, M., Jiwa, S., Zhang, W., Love, C. A., Madadgar, S., Papalexiou, S. M., Davis, S. J., Hsu, K., & Sorooshian, S. (2022). Status and prospects for drought forecasting: Opportunities in artificial intelligence and hybrid physical–statistical forecasting. *Philosophical Transactions of the Royal Society A: Mathematical, Physical and Engineering Sciences, 380*, 20210288.

Agrawala, S., Barlow, M., Cullen, H., & Lyon, B. (2001). The drought and humanitarian crisis in central and southwest Asia: A climate perspective.

Alawsi, M. A., Zubaidi, S. L., Al-Bdairi, N. S. S., Al-Ansari, N., & Hashim, K. (2022). Drought forecasting: A review and assessment of the hybrid techniques and data pre-processing. *Hydrology, 9*(7), 115.

Arnell, N. W. (1999). Climate change and global water resources. *Global Environmental Change, 9*, S31–S49.

Aswathanarayana, U. (2001). *Water resources management and the environment*. CRC Press.

Bates, B. (2008). Climate change and water: Technical paper VI. http://www.ipcc.ch/pdf/technical-papers/climate-change-water-en.pdf.

Belayneh, A., Adamowski, J., Khalil, B., & Quilty, J. (2016). Coupling machine learning methods with wavelet transforms and the bootstrap and boosting ensemble approaches for drought prediction. *Atmospheric Research, 172–173*, 37–47.

Bowden, J. H., Talgo, K. D., Spero, T. L., & Nolte, C. G. (2016). Assessing the added value of dynamical downscaling using the standardized precipitation index. *Advances in Meteorology, 2016*, 8432064.

Brekke, L. D. (2009). *Climate change and water resources management: A federal perspective*. Diane Publishing.

Bruce, J. P. (1994). Natural disaster reduction and global change. *Bulletin of the American Meteorological Society, 75*, 1831–1835.

Brunner, M. I., Slater, L., Tallaksen, L. M., & Clark, M. (2021). Challenges in modeling and predicting floods and droughts: A review. *WIREs Water, 8*, e1520.

Chang, F.-C., & Wallace, J. M. (1987). Meteorological conditions during heat waves and droughts in the united states great plains. *Monthly Weather Review, 115*, 1253–1269.

Cheng, X., Chen, S., Chen, W., Wu, R., Yang, R., Hu, P., Chen, & Aru, H. (2024). Selective influence of the Arctic Oscillation on the Indian Ocean Dipole and El Niño-Southern Oscillation. *Climate Dynamics, 62*(5), 3783–3798.

Coles, N. A., & Eslamian, S. (2017). *Definition of drought. Handbook of drought and water scarcity*. CRC Press.

Cook, B. I., Mankin, J. S., & Anchukaitis, K. J. (2018). Climate change and drought: From past to future. *Current Climate Change Reports, 4*, 164–179.

Cook, B. I., Mankin, J. S., Marvel, K., Williams, A. P., Smerdon, J. E., & Anchukaitis, K. J. (2020). Twenty-first century drought projections in the CMIP6 forcing scenarios. *Earth's Future, 8*(6) e2019EF001461.

Cook, E. R., Seager, R., Cane, M. A., & Stahle, D. W. (2007). North American drought: Reconstructions, causes, and consequences. *Earth-Science Reviews, 81*, 93–134.

Da Silva, V. D. P. R. (2004). On climate variability in Northeast of Brazil. *Journal of Arid Environments, 58*, 575–596.

Dehghani, M., Saghafian, B., Rivaz, F., & Khodadadi, A. (2017). Evaluation of dynamic regression and artificial neural networks models for real-time hydrological drought forecasting. *Arabian Journal of Geosciences, 10*, 266.

Domeisen, D. I., Garfinkel, C. I., & Butler, A. H. (2019). The teleconnection of El Niño Southern Oscillation to the stratosphere. *Reviews of Geophysics, 57*(1), 5–47.

Dore, M. H. I. (2005). Climate change and changes in global precipitation patterns: What do we know? *Environment International, 31*, 1167–1181.

Downing, T. E., & Bakker, K. (2016). Drought discourse and vulnerability. *Droughts,* 631–648.

Fernández-Manso, A., Quintano, C., & Fernández-Manso, O. (2011). Forecast of NDVI in coniferous areas using temporal ARIMA analysis and climatic data at a regional scale. *International Journal of Remote Sensing, 32*, 1595–1617.

Fischer, G., Tubiello, F. N., Van Velthuizen, H., & Wiberg, D. A. (2007). Climate change impacts on irrigation water requirements: Effects of mitigation, 1990–2080. *Technological Forecasting and Social Change, 74*, 1083–1107.

Fischer, G., & Van Velthuizen, H. T. (1996). *Climate change and global agricultural potential project: A case of Kenya*. Laxenburg, Austria: International Institute for Applied Systems Analysis (IIASA).

Fung, K. F., Huang, Y. F., Koo, C. H., & Soh, Y. W. (2019). Drought forecasting: A review of modelling approaches 2007–2017. *Journal of Water and Climate Change, 11*, 771–799.

Gellens, D., & Roulin, E. (1998). Streamflow response of Belgian catchments to IPCC climate change scenarios. *Journal of Hydrology, 210*, 242–258.

Gudmundsson, L., Bremnes, J. B., Haugen, J. E., & Engen-Skaugen, T. (2012). Technical Note: Downscaling RCM precipitation to the station scale using statistical transformations – A comparison of methods. *Hydrology and Earth System Sciences, 16*, 3383–3390.

Han, P., Wang, P., Tian, M., Zhang, S., Liu, J., & Zhu, D. (2013). Application of the ARIMA models in drought forecasting using the standardized precipitation index. In D. Li, & Y. Chen (Eds.). *Computer and computing technologies in agriculture VI, 2013* (pp. 352–358). Springer Berlin Heidelberg.

Hanadé Houmma, I., El Mansouri, L., Gadal, S., Garba, M., & Hadria, R. (2022). Modelling agricultural drought: A review of latest advances in big data technologies. *Geomatics, Natural Hazards and Risk, 13*(1), 2737–2776.

Handmer, J., Honda, Y., Kundzewicz, Z. W., Arnell, N., Benito, G., Hatfield, J., Mohamed, I. F., Peduzzi, P., Wu, S., & Sherstyukov, B. (2012). Changes in impacts of climate extremes: Human systems and ecosystems. In *Managing the risks of extreme events and disasters to advance climate change adaptation special report of the intergovernmental panel on climate change*. Cambridge University Press, 231–290.

Hartmann, D. L., Klein Tank, A. M. G., Rusticucci, M., Alexander, L. V., Brönnimann, S., Charabi, Y., & Zhai, P. (2013). Observations: Atmosphere and surface. In T. Stocker, D. Qin, G.-K. Plattner, M. Tignor, S. Allen, J. Boschung, A. Nauels, Y. Xia, V. Bex, & P. Midgley (Eds.). *Climate change 2013: The physical science basis. Contribution of working group I to the fifth assessment report of the intergovernmental panel on climate change* (pp. 159–254). United Kingdom and New York, NY, USA: Cambridge University Press.

IPCC. (2021). Climate change 2021: The physical science basis. In *Contribution of working group I to the sixth assessment report (AR6) of the intergovernmental panel on climate change*.

Islam, M. A., Chan, A., Ashfold, M. J., Ooi, C. G., & Azari, M. (2018). Effects of El-Niño, Indian Ocean Dipole, and Madden-Julian Oscillation on surface air temperature and rainfall anomalies over Southeast Asia in 2015. *Atmosphere, 9*(9), 352.

Jamali, M., & Eslamian, S. (2024). Climate adaptation and water–environment–energy nexus. In *Handbook of Climate Change Impacts on River Basin Management*. CRC Press.

Jamali, M., Gohari, A., & Akhavan Saraf, G. (2024). Spatiotemporal evaluation of temperature and precipitation extremes indices over Iran under the influence of climate change. *Water and Irrigation Management*.
Jamali, M., Gohari, A., Motamedi, A., & Haghighi, A. T. (2022). Spatiotemporal changes in air temperature and precipitation extremes over Iran. *Water [Online],* 14.
Jamali, M., Yazdian, H., Bahman, G., & Eslamian, S. (2025). Water agriculture nexus a system dynamics approach for the next three decades. *Scientific Reports, 15*(1), 5946.
Junfei, C., & Yang, Y. (2012). SPI-based regional drought prediction using weighted markov chain model. *Research Journal of Applied Sciences, Engineering and Technology, 4*, 4293–4298.
Karthika, M., & Thirunavukkarasu, V. (2017). Forecasting of meteorological drought using ARIMA model. *Indian Journal of Agricultural Research, 51*, 103–111.
Kousari, M. R., Hosseini, M. E., Ahani, H., & Hakimelahi, H. (2017). Introducing an operational method to forecast long-term regional drought based on the application of artificial intelligence capabilities. *Theoretical and Applied Climatology, 127*, 361–380.
Le Comte, D. (1994). Highlights around the world. *Weatherwise, 47*, 23–26.
Leavesley, G. H. (1994). Modeling the effects of climate change on water resources—A review. *Climatic Change, 28*, 159–177.
Lyon, B. (2004). The strength of El Niño and the spatial extent of tropical drought. *Geophysical Research Letters, 31*.
Marj, A. F., & Meijerink, A. M. J. (2011). Agricultural drought forecasting using satellite images, climate indices and artificial neural network. *International Journal of Remote Sensing, 32*, 9707–9719.
Marx, W., Haunschild, R., & Bornmann, L. (2021). Heat waves: A hot topic in climate change research. *Theoretical and Applied Climatology, 146*, 781–800.
Mason, S. J. (2004). Simulating climate over Western North America using stochastic weather generators. *Climatic Change, 62*, 155–187.
Mcleod, W. T., & Hanks, P. (1982). *The New Collins concise dictionary of the English language*. Collins.
Meng, L., Ford, T., & Guo, Y. (2017). Logistic regression analysis of drought persistence in East China. *International Journal of Climatology, 37*, 1444–1455.
Mishra, A. K., & Singh, V. P. (2010). A review of drought concepts. *Journal of Hydrology, 391*, 202–216.
Mossad, A., & Alazba, A. A. (2015). Drought forecasting using stochastic models in a hyper-arid climate. *Atmosphere [Online], 6*.
Mote, P. W., Abatzoglou, J. T., & Kunkel, K. E. (2013). Climate. In M. M. Dalton, P. W. Mote, & A. K. Snover (Eds.). *Climate change in the northwest: Implications for our landscapes, waters, and communities*. Island Press/Center for Resource Economics.
Nicholson, S. E. (2019). A review of climate dynamics and climate variability in Eastern Africa. *Limnology, Climatology and paleoclimatology of the East African lakes,* 25–56.
O'neill, B. C., Tebaldi, C., Van Vuuren, D. P., Eyring, V., Friedlingstein, P., Hurtt, G., Knutti, R., Kriegler, E., Lamarque, J. F., Lowe, J., Meehl, G. A., Moss, R., Riahi, K., & Sanderson, B. M. (2016). The scenario model intercomparison project (ScenarioMIP) for CMIP6. *Geoscientific Model Development, 9*, 3461–3482.
Osborne, T., Rose, G., & Wheeler, T. (2013). Variation in the global-scale impacts of climate change on crop productivity due to climate model uncertainty and adaptation. *Agricultural and Forest Meteorology, 170*, 183–194.
Ostler, G. (1969). *The little oxford dictionary (LOD)*. Clarendon Press.
Ozger, M., Mishra, A. K., & Singh, V. P. (2021). Estimating palmer drought severity index using a wavelet fuzzy logic model based on meteorological variables. *International Journal of Climatology, 31*, 2021–2032.

Prodhan, F. A., Zhang, J., Hasan, S. S., Pangali Sharma, T. P., & Mohana, H. P. (2022). A review of machine learning methods for drought hazard monitoring and forecasting: Current research trends, challenges, and future research directions. *Environmental Modelling & Software, 149*, 105327.

Prodhan, F. A., Zhang, J., Yao, F., Shi, L., Pangali Sharma, T. P., Zhang, D., & Mohana, H. P. (2021). Deep learning for monitoring agricultural drought in South Asia using remote sensing data. *Remote sensing, 13*(9), 1715.

Qian, W. (2017). *Weather and climate. Temporal climatology and anomalous weather analysis.*. Springer.

Rahmat, S. N., Jayasuriya, N., & Bhuiyan, M. A. (2017). Short-term droughts forecast using Markov chain model in Victoria, Australia. *Theoretical and Applied Climatology, 129*, 445–457.

Roudier, P., Sultan, B., Quirion, P., & Berg, A. (2011). The impact of future climate change on West African crop yields: What does the recent literature say? *Global Environmental Change, 21*, 1073–1083.

Schneider, S. H. (2011). *Encyclopedia of climate and weather*. Oxford University Press.

Seneviratne, S. I., Corti, T., Davin, E. L., Hirschi, M., Jaeger, E. B., Lehner, I., & Teuling, A. J. (2010). Investigating soil moisture–climate interactions in a changing climate: A review. *Earth-Science Reviews, 99*(3–4), 125–161.

Seneviratne, S., Nicholls, N., Easterling, D., Goodess, C., Kanae, S., Kossin, J., Zwiers, F. W., et al. (2012). Changes in climate extremes and their impacts on the natural physical environment. In *Managing the Risks of Extreme Events and Disasters to Advance Climate Change Adaptation*. Cambridge University Press.

Stagge, J. H., Kohn, I., Tallaksen, L. M., & Stahl, K. (2015). Modeling drought impact occurrence based on meteorological drought indices in Europe. *Journal of Hydrology, 530*, 37–50.

Stein, U., Özerol, G., Tröltzsch, J., Landgrebe, R., Szendrenyi, A., & Vidaurre, R. (2016). European drought and water scarcity policies. In *Governance for drought resilience: Land and water drought management in Europe*. SpringerOpen, 17–43.

Sun, P., Zhang, Q., Singh, V. P., Xiao, M., & Zhang, X. (2017). Transitional variations and risk of hydro-meteorological droughts in the Tarim River basin, China. *Stochastic Environmental Research and Risk Assessment, 31*, 1515–1526.

Tao, Y., Tian, B., Adhikari, B. R., Zuo, Q., Luo, X., & Di, B. (2024). A review of cutting-edge sensor technologies for improved flood monitoring and damage assessment. *Sensors, 24*(21), 7090.

Tebaldi, C., Debeire, K., Eyring, V., Fischer, E., Fyfe, J., Friedlingstein, P., Knutti, R., Lowe, J., O'neill, B., Sanderson, B., Vuuren, V. A. N., Riahi, D., Meinshausen, K., Nicholls, M., Tokarska, Z., Hurtt, K. B., Kriegler, G., Lamarque, E., Meehl, J. F., ... Ziehn, T. (2021). Climate model projections from the scenario model intercomparison project (ScenarioMIP) of CMIP6. *Earth System Dynamics, 12*, 253–293.

Tokarska, K. B., Stolpe, M. B., Sippel, S., Fischer, E. M., Smith, C. J., Lehner, F., & Knutti, R. (2020). Past warming trend constrains future warming in CMIP6 models. *Science Advances, 6*, eaaz9549.

Toreti, A., Tsagai, D., Maurer, T., Cremonese, E., Rossi, L., Werth, M., & Wemens, S. E. (2024). *World drought atlas*. Publications Office of the European Union.

Trenberth, K. E., Fasullo, J. T., & Shepherd, T. G. (2014). Attribution of climate extreme events. *Nature climate change, 5*(8), 725–730.

Tyagi, S., Zhang, X., Saraswat, D., Sahany, S., Mishra, S. K., & Niyogi, D. (2022). Flash drought: Review of concept, prediction and the potential for machine learning, deep learning methods. *Earth's Future, 10*(11) e2022EF002723.

Webster, K. E., Kratz, T. K., Bowser, C. J., Magnuson, J. J., & Rose, W. J. (1996). The influence of landscape position on lake chemical responses to drought in northern Wisconsin. *Limnology and Oceanography, 41*, 977–984.

Werndl, C. (2016). On defining climate and climate change. *The British Journal for the Philosophy of Science, 67*, 337–364.

Wilhite, D. A., & Glantz, M. H. (1985). Understanding: The drought phenomenon: The role of definitions. *Water International, 10*, 111–120.

Xu, Z., Sun, H., Zhang, T., Xu, H., Wu, D., & Gao, J. (2023). Evaluating established deep learning methods in constructing integrated remote sensing drought index: A case study in China. *Agricultural Water Management, 286*, 108405.

You, L., Rosegrant, M. W., Wood, S., & Sun, D. (2009). Impact of growing season temperature on wheat productivity in China. *Agricultural and Forest Meteorology, 149*, 1009–1014.

Zhou, C., Wang, G., Jiang, H., Li, S., Shi, X., Hu, Y., & Cabral, P. (2025). Spatio-temporal patterns of compound dry-hot extremes in China. *Atmospheric Research, 314*, 107795.

CHAPTER SIXTEEN

A regional case study of investigation of the meteorological drought trend using the SPI index and the Mann–Kendall test

Saeid Eslamian[1], **and Yaser Sabzevari**[1,2]
[1]Department of Water Science and Engineering, College of Agriculture, Isfahan University of Technology, Isfahan, Iran
[2]Institute of Hydrology, Slovak Academy of Sciences, Bratislava, Slovakia

16.1 Introduction

The importance of water has increased in recent years,mainly due to the growing population, global warming, overexploitation of environmental resources, and decrease in rainfall compared to the past. The reduction of precipitation and extreme fluctuations of precipitation are the factors that have aggravated the water scarcit in recent times. The phenomenon of drought is a critical natural disaster defined as the deficiency of precipitation over an extended period (Mahmoudi et al., 2015). Drought can be separated into different types according to the studied parameters: meteorological, Agricultural, hydrological, and socioeconomic droughts (Delpla et al., 2009; Tigkas et al., 2016). Meteorological drought is the first to occur, often preceding other types of droughts.Meteorological drought initially leads to agricultural droughts with a time delay in one place and then to hydrological droughts (Mahmoudi et al., 2015). One of the basic steps in drought and drought studies is determining the indicators based on which the strength and length of drought can be evaluated. The Standard Precipitation Index (SPI) is useful and confirmed by World Meteorological Organization (WMO) as an indicator for studying drought (Ellis et al., 2010; Hao & Singh, 2013; Mishra & Singh, 2010).

Drought Dynamics
DOI: https://doi.org/10.1016/B978-0-443-34205-9.00014-7
© 2026 Elsevier Inc. All rights are reserved, including those for text and data mining, AI training, and similar technologies.

Analyzing the spatial and transient changes of the dry season can be compelling in giving way to better arrangements for administration and natural planning. There are different strategies for looking at spatial changes, among which the Mann–Kendall (MK) drift examination test, which could be a nonnonparametric-parametric test, can be considered for evaluating drought conditions. In this field, numerous inquiries have been conducted in numerous nations, which are specified below. A dry season could is charactorized by lack of precipitation for longer duration that reduced soil dampness and diminished surface water. From a climatological point of view, a region is considered to be experiencing dry season whenever the precipitation received during a specific period falls below the long-term average for that same period. In spite of the fact that a few human components straightforwardly influence the creation of dry seasons, the main cause is the lack of precipitation. Climate change models anticipate more recurrence and concentrated summer dry spells due to increase in temperature. Groundwater is a critical component of the hydrological cycle and could be a crucial asset for nature, particularly wetlands and coastal biological systems, and for water capacity, particularly drinking water. Groundwater recharge depends on a few factors, particularly summer precipitation. Perceptions appear less groundwater energize due to climate change and more extraction. It is additionally anticipated that the groundwater levels will diminish.

Since less sustenance happens due to shortened growing season and the decrease of water storage in the form of snow, while the increase in winter precipitation essentially increases the groundwater supply and soil moisture conditions, which suggests accelerated infilteration of surface runoff into the groundwater. Considers appears that the effect of groundwater supply on hotter climates in precipitous regions is moderately less and depends on the type of arrive utilize.

Drought is a usual and recurrent climatic phenomenon. This phenomenon is likely to occur in all parts of the World. Although its characteristics are completely variable and distinct from one point to another. It is very difficult to provide a single definition for drought, because different definitions of the phenomenon of drought can be provided depending on climatic differences, existing needs and systems, and strategies adopted in different places. For example, drought in Libya occurs, when the annual rainfall is less than 180 mm, while supposedly in Switzerland, drought refers to a period when it does not rain for only six days. The basis of this definition is the climatic characteristics of each region, which are the

determining factors for the definition of drought. It is also possible to express a drought, based on the needs in a region. For example, in different rainfed crops, the amount of water needed by each crop is different from one another, and therefore, the absence of rainfall in a period of one month may mean drought for rice cultivation. Further, drought also refers to the lack of sufficient rainfall during a period of time and that causes a lack of water for some activities, some groups, or parts of the environment. In any case, with any approach and any definition of drought, the fact that drought is only a physical and climatic phenomenon is completely unreal and unscientific.

Drought is a period in which the lack of rain causes severe damage to agricultural products and a decrease in production. The conceptual definition of drought can also be useful and effective in formulating policies to deal with drought. For example, a law can be formulated that if the rainfall decreases to a certain extent, people can use the benefits of drought insurance. This point can be called a critical danger point. The points above this point are called the normal risk zone. Of course, determining the critical point requires detailed research in various fields of meteorology, hydrology, agriculture, herbal medicine, etc. Compilation of these laws will clarify the support policies of the governments in the field of dealing with the drought crisis and its consequences. The accurate definition of the critical point and its correct recognition by farmers and other interested groups will minimize the amount of arguments and conflicts during drought.

As mentioned, drought can be examined and studied from different perspectives and aspects. In each of these areas and fields, specific characteristics are considered. Basically, in different sources, they examine and analyze drought from the following four perspectives:

Meteorological drought is usually expressed based on the amount and degree of dryness and the duration of dryness (compared to the normal amount of precipitation). In this aspect of drought, what should be considered are the characteristics and differences of the climate, which cause a great difference in the amount of precipitation in different areas. For example, in some regions of the World where rainfall usually occurs throughout the year (tropical and subtropical humid regions), drought is considered as rainfall less than the specified amount during several consecutive days. While this definition cannot be reliable in low rainfall areas and the average annual, seasonal, or monthly rainfall should be considered as most appropriate criterion.

Agricultural drought links different aspects of climatic drought or hydrological drought to agricultural impacts. In this definition, more attention and focus is on the lack of rainfall, the difference between actual evaporation and transpiration, and potential evaporation and transpiration, the lack of soil moisture, the level of groundwater, or reservoirs. The water required by plants depends entirely on the prevailing climatic conditions of the region, the biological characteristics of the desired plant, the growth stage, and the physical and biological characteristics of the soil. The threshold of agricultural drought should be defined and determined in such a way that the amount of water required by different plants in different periods of growth from the seed stage to full maturity can be provided. The lack of surface soil moisture during planting may prevent germination or at least delay the growth and germination of the plant, and ultimately lead to a decrease in plant density per unit area and a decrease in production. But if the surface soil moisture is sufficient during early growth and the subsurface soil moisture is low, it will not affect the final yield of the plant, provided that this decrease in subsurface soil moisture during the plant growth period is compensated by irrigation or by rainfall.

Hydrological drought should be examined along with the effects of reduced rainfall (including snowfall). Hydrological droughts usually do not coincide with climatic and agricultural droughts and occur with a delay compared to them, because a longer time is needed before this decrease in precipitation can manifest itself in the components of the hydrological system such as a decrease in soil moisture, river water flow, or water level. Therefore, the role and impact of hydrological drought in different economic and social sectors are completely different from each other. For example, a decrease in rainfall can cause a rapid decrease in soil moisture, which can be easily seen and understood by agricultural experts and officials in the first place. However, the officials of electric power plants or the environment may find out these effects with a delay of several months. Moreover, flowing water or water stored in hydrological systems such as rivers and reservoirs have many users and multi-purpose uses such as flood control, irrigation, shipping, health and drinking, fishing and wildlife, and therefore the consequences and intensity ofthe effects are multifaceted and vary across sectors and time scales. It makes the hydrological drought more and more complicated, and when the drought occurs, the competition over the use of water resources causes conflicts between water users.

Hydrological systems are the link connecting different regions, and the lack of precipitation in one region may also affect regions outside its range.

For example, the lack of rainfall in the upstream areas of the watershed will put the whole area at risk of drought. The recent multi-year drought in the east of the country, due to the drought in the upstream areas of the Hirmand watershed in Afghanistan, which led to the water cut and the drying up of the Hirmand river, is a clear example of these effects. In addition, land use changes in the upstream of the watershed will affect the hydrological characteristics of the watershed, such as permeability and the amount of runoff production, and will first cause floods and finally drought in the downstream.

Therefore, land use changes are one of the factors that, despite the absence of noticeable changes in the parameters affecting climatic drought, may intensify the severity of water shortage and hydrological drought in the region. Another effective factor in aggravating drought is the excessive exploitation of groundwater. The intensification of the use of groundwater to raise the cultivated area has put additional pressure on the groundwater resources, and this increasing pressure causes a drastic drop in the groundwater table. In drought years when the use of these resources doubles, the drop in the level of groundwater tables reaches a critical state. Degradation of lands caused by excessive grazing and inappropriate methods of agriculture and irrigation, and their subsequent water and wind erosion intensifies the effects of drought.

Irrigation efficiency can also be another factor affecting drought. In Iran, the maximum irrigation efficiency is 35%, which means that about twice the water that is used is wasted. The drinking water consumption pattern also aggravates the effects of drought. For example, the per capita water consumption of Tehran's citizens is about 239 L, while this figure is about 120 L in Western European countries. In both cases, increasing pressure is placed on water resources, and the effects of drought are aggravated in other sectors.

The order and sequence of the effects of different droughts can help to distinguish and recognize each type of drought. Usually, when a drought occurs, the agricultural sector will be the first sector to feel the effects of the drought due to its deep dependence on soil moisture. The amount of soil water will decrease quickly and under the influence of the drought period. If the drought continues, other people who use different water sources will also be affected. Groups of people who use surface and groundwater sources will be the last group to address this issue. Of course, the amount of these effects depends directly on the length of the drought period, certainly, longer drought periods will have more destructive effects.

When the climatic drought ends and the rainfall returns to normal conditions, it is time to restore the conditions of the surface and subsurface waters, which have been greatly decreased under drought conditions.

The definitions of socioeconomic drought are related to some economic goods that carry the climatic, hydrological, and agricultural elements of drought. This type of drought is completely different from previous kinds of droughts. Because this type of drought depends on the time and place of the source and demand process. Economic properties such as water, legumes, fodder, fish, and aquatic animals, and electric power depend on weather conditions. Due to natural climatic changes, the supply of water needed by people will fluctuate in different years.

Therefore, socioeconomic drought happens when the amount of demand for an economic commodity dependent on water exceeds the amount of its supply, which has decreased under the influence of reduced rainfall.

This phenomenon is more complex than other natural disasters and affects more parts of the society, and causes damage as much as floods and storms. The degree of weakness of human societies to the phenomenon of drought is strongly influenced by factors such as population growth, demographic changes, statistical characteristics, the level of development and level of technology, the trend and pattern of water consumption, government policies, social behaviors, and the level of environmental awareness. These factors are always changing, and therefore, according to these changes, the level of vulnerability may increase or decrease.

Worldwide heating is added imperative reason for water deficiency. When our discuss temperature gets hotter, the water in streams and lakes dissipates more quickly. As a result, individuals who depend on these water sources for drinking water suffer from the effects of global warming. This issue also influences neighborhood water sources.

Illegal dumping of garbage is another important reason for water shortage. Most industries dump their business waste into nearby rivers and lakes because it is an easy and cheap way to dispose of waste, but illegal dumping of waste leads to serious water pollution. Therefore, people who rely on these water sources for water supply, face a severe water shortage.

Usual tragedies such as tsunamis and floods may also cause severe water scarcities for limited residents because, in the such events, local water sources may be completely destroyed and become seriously polluted. As a result, after flooding, the local rivers are no longer appropriate for providing drinking water sources.

Ahmadebrahimpour et al. (2019) studied the effect of climate change on dry spells within the Lake Urmia basin. They analyzed dry spell occasions from 2011 to 2100 utilizing the standardized precipitation record (SPI) and the standardized precipitation evapotranspiration record (SPEI), comparing them with information from 1976 to 2005. Utilizing precipitation and temperature information from the CanESM2 demonstrated beneath the distinctive representative concentration pathway (RCP) scenarios, they found that dry season recurrence and duration are anticipated to extend, particularly under the cynical RCP 8.5 scenario. The SPEI, which considers both precipitation and potential evapotranspiration, has been demonstrated to be more viable than the SPI in surveying dry season in a changing climate.

Alizade Govarchin Ghale et al. (2018) explored the water budget of Lake Urmia and the seriousness of the dry season in Lake Urmia from 1985 to 2010. They displayed a modern theory to evaluate the human and climatic impacts of Lake Urmia's diminish. Their perceptions appeared that human impacts and exercises can be much more important than climatic impacts. Human impacts and climatic components respectively influence 80% and 20% of Lake Urmia's drying. Their examination revealed that in spite of the fact that it was already accepted that the groundwater yield from Lake Urmia is immaterial, the results of this study indicate the presence of noteworthy spillage of groundwater leakage from Lake Urmia. Major changes within the lessening of the water level of Lake Urmia have been observed since 1998. Therefore, the primary step within the reclamation of Lake Urmia can be a survey of surface water administration and the misuse of dams and groundwater resources. The following step is to examine and classify rural item developed within the locale in terms of water utilization and educate the nearby individuals about legitimate water system strategies. Yarahmadi and Rostamizad (2019) investigated and analyzed hydrological droughts in the northern Lake Urmia, especially the Darian Chai River over 31 years, using the threshold level method with NIZOWKA 2003 software, the characteristics of hydrological droughts include time of occurrence, duration, and intensity. They have calculated the minimum discharge observed during the drought event. Frequency analysis based on partial series and by fitting different distribution functions has been done to investigate the probability of occurrence of drought events as well as their intensity and duration. The results showed that 38 hydrological dry periods occurred in this river, and more than 60% had a duration of more than 200 days. In terms of time distribution, about 71 %

(27 occurrences) of dry spells have started in spring. The largest drought event was 577 days, and the second largest drought period, with a duration of 365 days, occurred with a delay of 2 months. The deficit of surface flow caused by dry periods in this river equals 117 million cm^3. Abou Zaki et al. (2020) in their research analyzed the consequences of alterations in land use and the incidence of meteorological and hydrological droughts through the use of groundwater information sourced from 30 shafts, the SPI, and the river flow drought index (SDI). The data and variations in the wetland were assessed utilizing the normalized difference water index (NDWI) values and the reduction in water mass in the basin with gravity recovery and data from the weather trial (GRACE). The outcomes of the study revealed that hydrological droughts escalated after the implementation of large irrigation projects in the Zayandeh Roud basin. The depletion of groundwater and drought in the river were shown to be related to human activities. Byzedi et al. (2014) performed an analysis of river flow during a drought using the cut level method (at a 70% level) with daily flow in 54 places in the southwestern Iran. The research findings indicated that the area of the watershed was the greatest important factor that had a high correlation with the amount of drought deficiency.

McKee et al. (1993) presented a rainfall index for drought monitoring and used this index for drought monitoring in the state of Colorado. Mishra and Desai (2005) investigated the spatio-temporal drought of the Kansabati river plain of India using SPI and a geographical information system, and the results showed that a severe drought happened in 1980. Rahman and Lateh (2016) studied the meteorological drought in Bangladesh. The results showed that the north, northwest, west, southwest, and vital regions were the greatest drought regions of the country in order of occurrence and severity. Suryabhagavan (2017) analyzed climate change based on (GIS) and drought characteristics by SPI index in Ethiopia from 1983–2012, the results showed that among the major droughts, the droughts of 1984–1985 was reported as a severe drought in Wollo, also the longest drought period during 1983–2012 was spent in Borena region in southern Ethiopia.

Abuzar et al., (2019) assessed drought risk with satellite remote sensing and geographic methods in the Khushab region of Pakistan and also used SPI values to control meteorological drought. The obtained outcomes show that 21.30% of the region has moderate drought, and the severity of drought in the southern Khoshab region is more than the northern region. Aladaileh et al. (2019) investigated the spatial and temporal changes of

drought in Jordan using the MK test and the kriging interpolation method. The outcomes presented that based on the MK test, there was a decreasing trend for all stations except Madaba, and meteorological drought also occurred. Shahian et al. (2009) investigated the drought situation in Fars province by using the precipitation index and GIS. The result showed that the southern and eastern regions and part of the western and central regions have witnessed more droughts than other parts of the province, and most of the droughts have been mild drought.

Tatina et al. (2010) studied the drought in Gilan province, Iran, in a 30-year statistical period. The outcomes presented that the drought occurred in a varied and relatively regular cycle in the region, as well as the spatial and temporal pattern of the drought after monitoring. It indicates the occurrence of continuous and intermittent droughts in the study area, which creates critical conditions for natural and human resources. Khosravani et al. (2013) by studying the statistics of six weather stations in Khuzestan province, Iran, with a statistical period of 25 years in an annual time scale, showed that the lowest value and the highest value (SPI) are related to the city of Ahvaz. Hejazi Zadeh et al. (2014) examined the drought in Kerman-Iran and used the MK test to investigate changes in its trend. The outcomes presented that the trend of variations in spring rainfall in Kerman province is significant, and also the spring season is changing towards dry periods.

16.2 Case study

In this section, a sample study is given to investigate the regional meteorological drought variations in the western Iran. The need to deal with the various effects of drought makes it essential to know the past situation of different regions in terms of drought. Therefore, the aim of the current research is to monitor the annual meteorological drought and investigate its 21-year changes at the level of Lorestan province.

Lorestan area, with a zone of 28064 km, is located between 46°51' to 50°3' East of the longitude and 32'34°22' North of latitude within the western Iran. Its stature from ocean level shifts from the most elevated point with a height of 4050 m to the lowest point within the south of the territory with a height of 500 m above sea level. The capital of this territory is Khorramabad city. Fig. 16.1 illustrates the borders of the Lorestan area and the area of the selected stations.

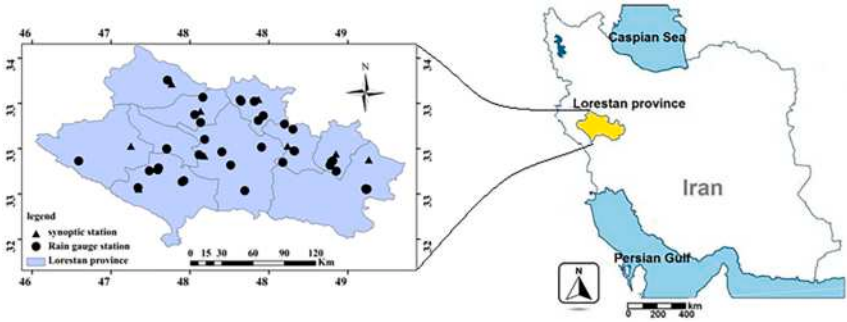


Figure 16.1 Location of Lorestan and the study stations. Note: Map lines delineate study areas and do not necessarily depict accepted national boundaries.

In this research, to monitor the annual meteorological drought in Lorestan province, 21 years of precipitation data (1998–2018) related to 9 synoptic stations and 23 rain gauge stations in the province were used. The region of Lorestan province was obtained. The MKtest was used to check the trend of annual changes. Table. 16.1 shows the characteristics of the nine meteorological stations studied in this research in Lorestan province.

16.2.1 Standardized precipitation index

The SPI was developed by McKee et al. (1993) to monitor drought conditions in Colorado. McKee and colleagues set up a classification system to control dryness and wetness at stations, and the obtained SPI values show diverse strengths of drought in the area. Another feature is that, based on this method, the drought threshold can be determined for each time period. Therefore, in adding to the harshness of the drought, its duration can also be determined based on this index. The SPI is based on the chance of rainfall for each time period. This index is designed to minimize the lack of rainfall in multiple time periods (Rostamian, et al., 2013). These different time scales express the special effects of drought on access to different water resources.

$$SPI = \frac{X_i - \overline{X}}{S_X} \tag{16.1}$$

where X_i is rainfall/month, $\bar{x}$ is mean rainfall on a time scale, and S_X is the standard deviation of rainfall on a time scale.

Table. 16.2 is proposed to classify the SPI method.

Table 16.1 Characteristics of weather stations in Lorestan province.

Station type	Average annual rainfall (m)	Height (m)	Latitude	longitude	Station code	Station name
Synoptic	409.6	1872	´27 °33	´25 °49	1	Azna
Synoptic	444.1	1567	´49 °33	´15 °48	2	Selseleh
Synoptic	387.7	2022	´24 °33	´42 °49	3	Aligudarz
Synoptic	456.2	1629	´35 °33	´45 °48	4	Boroujerd
Synoptic	358.8	713	´09 °33	´43 °47	5	Poldokhtar
Synoptic	499	1148	´26 °33	´17 °45	6	Khorramabad
Synoptic	627.1	1527	´29 °33	´04 °49	7	Dorud
Synoptic	365.8	1198	´31 °33	´39 °47	8	Koohdasht
Synoptic	465.8	1860	´03 °34	´00 °48	9	Noorabad

Table 16.2 Classification scale of SPI values.

Extremely wet	Very wet	Medium wet	Almost normal	Medium dry	Very dry	Extremely dry	class
2 <	99.1 t 5.1	49.1 to 1	99.0 to 99.0-	49.1- to 1-	-1.99 to -1.49	2- >	SPI values

16.2.2 Mann–Kendall test

Untill now, distinctive strategies have been planned to consider the drift of time arrangements, which are for the most part partitioned into three categories: graphical, parametric and nonparametric strategies. Nonparametric tests are not sensitive to the design of information conveyance and can be utilized in case the data are not typical (Sabzevari & Eslamian, 2022). Their conveyance is arbitrary, so utilizing parametric strategies such as Pearson's strategy to decide the slope in this information is troublesome and the outcome will not be exceptionally precise, so the nonparametric MK test for this reason has been utilized (Sabzevari et al., 2025).

The MK test is utilized to check for the presence or absence of patterns over time for separate time series. This test is founded on non-parametric direct relapse rationale. The outcome of this test indicates whether there's a

critical growth or diminish within the level of certainty within the variable time arrangement drift or not. Utilizing the non-parametric MK test isn't sensitive to the normality of the data. The MK test was created by Kendall (1975). The utilization of this strategy was prescribed by the WMO (Stasik et al., 2016). One of the qualities of the MK strategy is that it is appropriate for time series that don't follow a particular distribution. In this study, the exceed expectations of computer program was utilized to determine the trend using by MK test.

The strategy is utilized to look at the stream of information. In this strategy, the *S*measurement for the *g*th month and the *k*th station is calculated as follows:

$$\mathrm{S_{gk}} = \sum_{i}^{n-1} \sum_{j=t+1}^{n-1} \mathrm{sgn}(\mathrm{Xjgk} - \mathrm{Xigk}),\ \forall \le \mathrm{i} < \mathrm{j} \le \mathrm{n} \tag{16.2}$$

where *n* is the number of arrangement information and *sgnθ* is the work of the sign and *θ* is the distinction between the two observations in each of the examined factors in several a long time *i* and *j*, which is characterized as follows:

$$\mathrm{Sgn}(\theta) = \begin{cases} 1\ if\theta > 0 \\ 0\ if\theta = 0 \\ -1\ if\theta < 0 \end{cases} \tag{16.3}$$

Mann and Kendall presented that when $n \le 10$ is 10, the *S* statistic is spread virtually uniformly and has a mean of 0, and the resulting standard deviation:

$$(\sigma_{gg})\mathrm{k} = \frac{[n(n-1)(2n+5) - \sum d(d-1)(2d+5)]}{18} \tag{16.4}$$

where *d* is the same amount of information within the time arrangement. In this strategy, S_{gk} is normalized as follows:

$$S'_{gk} = S_{gk} - sgn\left(S_{gk}\right) \tag{16.5}$$

at that point, the standardized test measurement or *Z*, which contains a standard ordinary deviation with a cruel of zero and a standard deviation of 1, is obtained as follows:

$$Z_{gk} = \frac{S'_{gk}}{(\sigma_{gg})} \tag{16.6}$$

Suspicion zero (need of slant at noteworthiness level ∝) is acknowledged as long as $-Z_{1+a/2} < Z_{gk} < Z_{1+a/2}$, something else rejected (Ansari et al., 2016).

16.2.2.1 Improved Mann–Kendall test

In case the first-order autocorrelation constant within the information customary is noteworthy, the autocorrelation effect is removed from the information arrangement by pre-whitening. To deny, to begin with, the unused information arrangement with regard to the slant of the slant line, β, is calculated as follows:

$$X'_i = X_i - (\beta \times i) \tag{16.7}$$

where β is the inclination of the drift line. At that point, the modern arrangement is obtained as follows:

$$\gamma'_{\mathrm{I}} = X'_{\mathrm{I}} - r_1 \times X'_{\mathrm{i}-1} \tag{16.8}$$

where r_1 is the first-order autocorrelation coefficient. By re-adding the slant sentence ($\beta \times_i$) to the later information arrangement, the following arrangement is obtained:

$$\gamma_i = \gamma'_i - (\beta \times i) \tag{16.9}$$

In case the esteem of Z is more prominent than $\hat{A} \pm 1.96$, the information incorporates a slant and the null hypothesis is rejected; otherwise, something else it has no slant.

where Z is the standard typical conveyance measurement and can take diverse values in a 2-domain test depending on the certainty levels tested. The esteem of Z measurement for 95% and 99% certainty levels is considered break even with 1.96 and 2.58, respectively.

16.3 Results and discussion

To investigate the drought in the province, the graph of the drought changes of the synoptic stations of each city is presented as a representative of the existing stations in each city. Drought assessment in 21 years in Lorestan Province graphs indicate that based on the

classification scale of values (SPI), Aligoudarz city was very dry in 1999 and 2008, and in 2017 it was moderately wet and in 2000 it was moderately dry and the rest of the year has had a normal condition. According to the graph of changes in the drought trend in Poldokhtar, in 2000, there was a positive jump compared to 2001, and it went from moderately dry to normal. Also, in 2012, the situation was very dry, and in 2013, the situation was normal. While in the years 2007 and 2008, the mutation happened in a negative way, so that in the year 2008, a very dry situation occurred. A severe drought occurred in Koohdasht city in 2008, and droughts occurred in 1999, 2008, 2012, and 2015; in contrast to the drought in 2016, it was wet. Khorramabad city was very dry in 1999, 2008, 2011, and 2012, and very wet in 2016 and 2007. According to the SPI, the city of Selseleh was extremely wet in 2010 and 2016. Dorud city was in a very dry state in 1999, and moderate drought occurred in 2000, 2008, 2012, and 2018. In 2016, the city of Boroujerd was in a very humid state, and in 2012 it was relatively dry. According to the SPI index, Azna city experienced a very dry drought in 2008 and 2012, and a very wet drought in 2004, and Noorabad city was extremely wet in 2016, and drought did not occur in this city during this statistical period.

The MK test was applied to investigate the variations in annual drought in Lorestan province over a 21-year statistical period, and the results are shown in Table. 16.3. Based to Table. 16.3, at the probability level of 95%, the value of the SPI index of Selseleh has increased, and this increase is significant, which indicates the decreasing trend of drought, and in other words, the increase of drought in the city of Selseleh. The 21-year change trend of the SPI index value in the rest of the cities has no significance. However, in Azna, Boroujerd, Durod, and Koohdasht station, there was a decreasing trend, and in fact the general trend was towards drought. On the other hand, there has been an increasing trend in Aligoudarz, Noorabad, Poldokhtar, and Khorramabad stations, which shows that the general trend has been to get worse in these stations.

Table. 16.4 contains the number of different categories of drought for the selected stations of Lorestan province, which shows the general drought situation of the station in the studied period. According to this table, Khorramabad station, as the capital of the province, had 13 normal years, 3 relatively dry years, 3 very dry years, and 2 very wet years. According to this table, the driest station can be introduced as Koohdasht station, because it has had one very dry year, three very dry years, and two relatively dry years. On the other hand, Noorabad station is introduced as the wettest

Table 16.3 Drought trend values.

City	Azna	Boroujerd	Dorud	Selseleh	Khorramabad	Koohdasht	Poldokhtar	Noorabad	Aligudarz
Z value	393.0-	514.0-	212.0-	146.2	212.0	302.0-	514.0	363.0	632.1

Table 16.4 The number of different categories of drought for the selected stations in the 21-year mode period.

Station	Ultra wet	Very wet	Relatively moist	Normal	Relatively dry	Very dry	Ultra dry
Khorramabad	0	2	0	13	3	3	0
Koohdasht	0	0	1	14	2	3	1
Noorabad	1	2	3	15	0	0	0
Selseleh	0	1	0	17	2	1	0
Poldokhtar	0	0	1	16	1	3	0
Dorud	0	1	1	14	4	0	1
Boroujerd	0	1	3	16	1	0	0
Aligudarz	0	1	3	12	3	2	0
Azna	0	1	0	15	3	2	0

station because it has had one extra wet year, two very wet years, and three relatively wet years.

16.4 Conclusion

In this research, the climatic condition of Lorestan province during a statistical period of 21 years is investigated using the SPI. The outcomes show that based on the scale of classification of SPI, the cities of Dorud in 1999 and Koohdasht in 2008 were extremely dry, and Selseleh in 2010 and 2016, and Noorabad city were extremely wet in 2016. By examining the trend of drought using the MK test, it is found that the city of Selseleh has a positive and significant trend at the probability level of 95, while the rest of the cities do not have a significant trend. By examining the time series of the SPI index of different stations, the year 2012 is chosen as the representative of dry years, the year 2016 as the representative of wet years, and the year 2018 as the representative of normal years. In general, the driest station is Koohdasht, and the wettest station is Noorabad. Based on the outcomes of this research and the amount of different droughts in diverse parts of the Lorestan, to contract with the properties of this phenomenon, correct and appropriate preparation of water resources and coverage of crops, particularly in Koohdasht city, which is added to other regions of the Lorestan with drought has been faced, it is proposed.

References

Abou Zaki, N., Torabi Haghighi, A., Rossi, P. M., Tourian, M. J., Bakhshaee, A., & Kløve, B. (2020). Evaluating impacts of irrigation and drought on river, groundwater and a terminal wetland in the Zayanderud Basin, Iran. *Water, 12*(5), 1302. https://doi.org/10.3390/w12051302.

Abuzar, M. K., Shafiq, M., Mahmood, S. A., Irfan, M., Khalil, T., Khubaib, N., & Shaista, S. (2019). Drought risk assessment in the Khushab region of Pakistan using satellite remote sensing and geospatial methods. *International Journal of Economic and Environmental Geology, 10*(1), 48–56.

Ahmadebrahimpour, E., Aminnejad, B., & Khalili, K. (2019). Assessing future drought conditions under a changing climate: A case study of the Lake Urmia basin in Iran. *Water Supply, 19*(6), 1851–1861. https://doi.org/10.2166/ws.2019.062.

Aladaileh, H., Al Qinna, M., Karoly, B., Al-Karablieh, E., & Rakonczai, J. (2019). An investigation into the spatial and temporal variability of the meteorological drought in Jordan. *Climate, 7*(6), 82. https://doi.org/10.3390/cli7060082.

Alizade Govarchin Ghale, Y., Altunkaynak, A., & Unal, A. (2018). Investigation anthropogenic impacts and climate factors on drying up of Urmia Lake using water

budget and drought analysis. *Water Resources Management, 32*(1), 325–337. https://doi.org/10.1007/s11269-017-1812-5.

Byzedi, M., Saghafian, B., Mohammadi, K., & Siosemarde, M. (2014). Regional analysis of streamflow drought: A case study in southwestern Iran. *Environmental Earth Sciences, 71*(6), 2955–2972. https://doi.org/10.1007/s12665-013-2674-7, https://link.springer.com/journal/12665.

Delpla, I., Jung, A.-V., Baures, E., Clement, M., & Thomas, O. (2009). Impacts of climate change on surface water quality in relation to drinking water production. *Environment International, 35*(8), 1225–1233. https://doi.org/10.1016/j.envint.2009.07.001.

Ellis, A. W., Goodrich, G. B., & Garfin, G. M. (2010). A hydroclimatic index for examining patterns of drought in the Colorado River Basin. *International Journal of Climatology: A Journal of the Royal Meteorological Society, 30*(2), 236–255.

Hao, Z., & Singh, V. P. (2013). Entropy-based method for bivariate drought analysis. *Journal of Hydrologic Engineering, 18*(7), 780–786. https://doi.org/10.1061/(asce)he.1943-5584.0000621.

Hejazi Zadeh, Z., Nasserzadeh, Hatemif, M. H., & Rezaei, D. (2014). Application of statistical methods and drought profiles in analyzing precipitation fluctuations. Case Study: Kerman Station. *Geographic Study of Arid Regions. 17* Issue.

Kendall, M. G. (1975). *Rank Correlation Methods* (4th Edition). London: Charles Griffin.

Khosravani, Z., Parsamehr, A., Mohammadi, B., Farsi, Z. (2013). Drought investigation of Khuzestan province using SPI and PNPI index. In The 6th national *conference on watershed management and management of water and soil resources of the country*. (In Farsi).

Mahmoudi, P., Tavosi, T., & Shahuzai, A. (2015). Drought and its impact on the quality of surface water resources in Sistan and Baluchistan province (In Farsi). *Journal of Water Research in Agriculture, 29*(1), 21–35.

McKee, T. B., Doesken, N. J., & Kleist, J. (1993). The relationship of drought frequency and duration to time scales. *In Proceedings of the 8th Conference on Applied Climatology, 17*(22), 179–183.

Mishra, A. K., & Desai, V. R. (2005). Spatial and temporal drought analysis in the Kansabati river basin, India. *International Journal of River Basin Management, 3*(1), 31–41. https://doi.org/10.1080/15715124.2005.9635243.

Mishra, A. K., & Singh, V. P. (2010). A review of drought concepts. *Journal of Hydrology, 391*(1–2), 202–216. https://doi.org/10.1016/j.jhydrol.2010.07.012.

Rahman, M. R., & Lateh, H. (2016). Meteorological drought in Bangladesh: Assessing, analysing and hazard mapping using SPI, GIS and monthly rainfall data. *Environmental Earth Sciences, 75*(12). https://doi.org/10.1007/s12665-016-5829-5, http://www.springerlink.com/content/121380/.

Rostamian, R., Eslamian, S., & Farzaneh, M. R. (2013). Application of standardised precipitation index for predicting meteorological drought intensity in Beheshtabad watershed, central Iran. *International Journal of Hydrology Science and Technology, 3*(1), 63–76. https://doi.org/10.1504/IJHST.2013.05523 Iran: Inderscience Publishers.

Sabzevari, Y., & Eslamian, S. (2022). Predicting the effect of temperature changes on reference evapotranspiration by means of time series modeling (case study: Khorramabad Basin). *Irrigation Science and Engineering, 45*(2), 125–138.

Sabzevari, Y., Eslamian, S., Pamula, A. S. P., & Bazrkar, M. H. (2025). Drought Trend Analysis Using Standardized Precipitation Evapotranspiration Index in Cold-Climate Regions. *Atmosphere, 16*(4), 482.

Shahian, R., Jame, A. A., Arianfar, R., Haghighat, M., & Dehghan, H. (2009). Assessment of the drought crisis threshold of in the fars provice of using the standard precipitation

index and the geographic information system. *Water Engineering Journal, 2*(4), 33–42 In Farsi.

Suryabhagavan, K. V. (2017). GIS-based climate variability and drought characterization in Ethiopia over three decades. *Weather and Climate Extremes, 15*, 11–23. https://doi.org/10.1016/j.wace.2016.11.005.

Tatina, M., Roshani, M., & Bigdeli, A. (2010). MOnitoring and zoning of drought in Guilan province. *Journal of Geographical Landscape, 5*(11), 35–56 in Farsi.

Tigkas, D., Vangelis, H., & Tsakiris, G. (2016). Introducing a modified reconnaissance drought index (RDIe) incorporating effective precipitation. *Procedia Engineering, 162*, 332–339.

Yarahmadi, J., & Rostamizad, G. (2019). The analysis of the hydrological droughts in the northern part of lake Urmia. *Hydrogeomorphology, 6*, 79–100.

This page intentionally left blank

CHAPTER SEVENTEEN

Spatiotemporal analysis of temperature rise impact on snow drought in Erzurum, Türkiye

Egemen Aras, Muhammet Savas, Babak Vaheddoost, and Damla Yılmaz Çelik
Department of Civil Engineering, Bursa Technical University, Bursa, Türkiye

17.1 Introduction

Recent studies highlight that widespread droughts pose significant threats to global water resources and continuously affect the meteorological, agricultural, hydrological, ecological, and socioeconomical equilibrium (Mishra & Singh, 2010; Yihdego et al., 2019). Droughts, as a long-term and unpredictable phenomenon, exacerbate these issues and, if left unmitigated, can result in severe consequences. But, activities such as afforestation/reforestation, soil moisture conservation, watershed management, and sustainable groundwater allocation can help mitigate drought effects (Karavitis, Tsesmelis, et al., 2014; Lin et al., 2015).

The complexity of droughts lies in the uncertainty surrounding their onset and cessation, their accumulation and escalation, their varied temporal impacts, and their economic ramifications (Brunner et al., 2021; Panu & Sharma, 2002; Salvador et al., 2020). Global warming, driven by climate change, exacerbates the duration, severity, and magnitude of droughts, disrupting natural equilibria and increasing socioeconomic costs. This is largely due to the increase in greenhouse gas emissions, primarily carbon dioxide and methane, resulting from the uncontrolled consumption of fossil fuels (Tramblay et al., 2020; Vicente-Serrano et al., 2020).

The United Nations World Bank Group High-Level Water Panel report projects that by 2030, up to 700 million people may be displaced due to water scarcity, with half of the World's population experiencing

Drought Dynamics
DOI: https://doi.org/10.1016/B978-0-443-34205-9.00022-6
© 2026 Elsevier Inc. All rights are reserved, including those for text and data mining, AI training, and similar technologies.

water scarcity by 2050 (United Nations High-Level Panel On Water Outcome Document, 2018). In this regard, the rapid increase in the average global temperatures, unprecedented in historical records, is attributed to anthropogenic activities, particularly the consumption of fossil fuels. This leads to higher concentrations of greenhouse gases, which trap additional heat in the Earth's lower atmosphere, thereby intensifying global warming.

Snow cover responds to variation in temperature and precipitation rates, serving as a water resource that remains beyond human control (Winkler et al., 2021). In essence, the snow drought can be defined as a deficit in snowfall, and is the outcome of precipitation falling as raindrops instead of snowflakes due to rising temperature and changes in the behavior of the atmospheric layers (Reich et al., 2018). Broader climatic trends leading to warmer conditions have been shown to result in increased rainfall and decreased snowfall, eventually leading to reduced snowpack and/or snow drought conditions. This simply means that the rainfall records in the region may show some degree of inclination whilst the snowfall is on the decline. This issue is particularly problematic in regions where hydrology relies on snow reserves or where there are significant disparities in precipitation between dry and wet periods. In many regions of the World, water resources such as rivers, lakes, and groundwater reserves primarily depend on the amount of precipitation. But, in cold climates, where precipitation falls as snow, water is stored in the snowpack and subsequently contributes to increased runoff in spring and early summer as it melts with rising temperatures. Regions that receive most of their precipitation in the form of snow, face a number of challenges when snow droughts occur, e.g., interruption in ecosystem, incline in reservoir levels, water resources degradation, and reduction in winter tourism demand (Dierauer et al., 2019; Staudinger et al., 2014). For instance, in the context of a changing climate, mountainous water resources are gaining increasing importance. These resources primarily rely on snowmelt, which constitutes a significant portion of total runoff (base flow) and contributes substantially to groundwater recharge. In hydrological studies, snow cover is usually characterized by snow water equivalent (SWE) rate (Jonas et al., 2009; Yuan et al., 2023). Yet, the snow drought issues have been reported as the warming winter climate reduces snow cover, causing snowmelt during winter and decreasing snowmelt in spring. Additionally, the anticipated increased variation in climate patterns could result in greater fluctuations in snow cover. The lack of snowmelt in return, can heighten the probability

of droughts in spring and early summer, and eventually affect the critical growth periods of plants and crops. Snow drought measures are often dependent on the severity of the drought events, usually expressed in terms of duration, magnitude, and intensity of indices used for this aim.

In Türkiye's high-altitude regions, winter precipitation predominantly falls as snow. The snow cover persists for nearly half the year, particularly in the mountainous and elevated areas of Erzurum province in the Eastern Anatolia region. This region serves as the primary source of the Euphrates River, which holds significant historical and socioeconomic importance for contemporary Iraq, Syria, and Türkiye. In recent years, widespread drought events have been frequently observed, attributed to rising air temperatures. However, this claim remains largely anecdotal and is primarily based on local narratives. Although many studies addressed drought in Türkiye, only a few studies conducted some related analysis regarding the snow (Gulsever, 2006; Keskin & Kanat, 2018; Oruc, 2021; Basak, 2017). As a notable contribution to its field, (Aslan, 2020) utilized data records from the Van (1980–2018), Tatvan (1980–2015), Ercis (1980–2011), and Ahlat (1988–2011) meteorological stations to analyze snow drought in the region. The study determined that snow drought is primarily driven by increasing winter temperatures and/or a lack of precipitation. Furthermore, the highest average severity, probability, and risk values of snow droughts were associated with warm snow droughts. These warm snow droughts occur when rising winter temperatures cause precipitation to fall as rain or sleet instead of snow. An analysis of the seasonal temperature values in the basin over several years (1980–2018) reveals an increasing trend in all seasons including winter. Consequently, the prevalence of warm snow droughts in the basin is an anticipated outcome.

In this context, the main aim of this study is to monitor the historical precipitation and snowfall deficit in the region. To achieve this, the so-called standardized precipitation index (SPI), standardized precipitation evaporation index (SPEI), and the standardized snow precipitation index (SSPI) with 1-, 3-, and 12-months moving average periods are used in the analysis. Afterward, the characteristics of the historical droughts are investigated with the help of generated maps using the interpolated projection for severity (S), duration (D), and intensity (I) droughts. The study is expected to serve as the initial benchmark for snow drought analysis in the region, paving the way for similar studies and applications.

17.2 Materials and methods

17.2.1 Study area and data

In this study, drought analysis is performed for the Erzurum district at the upstream of the Euphrates River, located roughly at 39°N latitude, 41°E longitude, in Türkiye. Analysis are conducted with the help of monthly precipitation, temperature, and snow records at six meteorological stations during the 1976–2021 period (45 years). The locations of the observation stations are shown in Fig. 17.1, while the details are given in Table 17.1

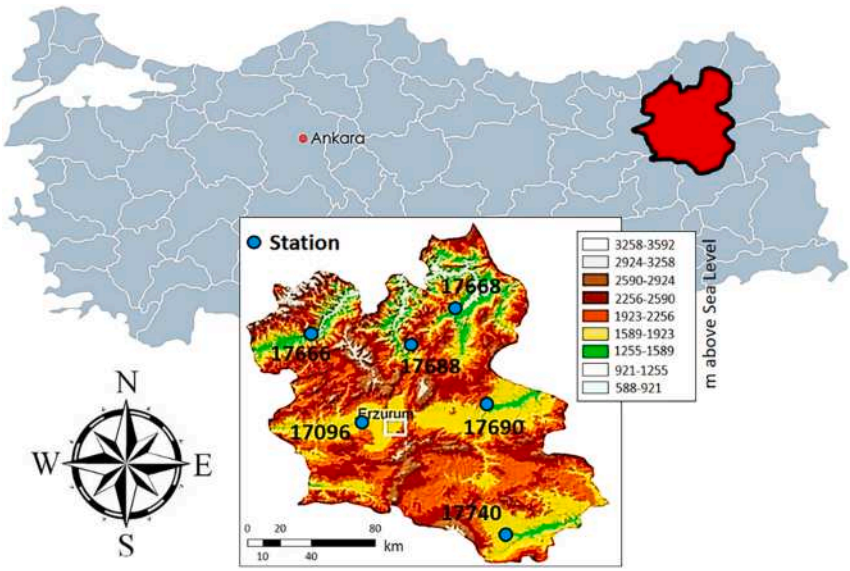


Figure 17.1 Study area and location of the selected stations. Map lines delineate study areas and do not necessarily depict accepted national boundaries.

Table 17.1 Information on observation stations in Erzurum province (Source: Meteorology Genel Mudurlugu MGM, 2023).

No	Station Code	Station Name	ICAO	Latitude	Longitude	Altitude
1	17096	Erzurum Airport	LTCE	39.95	41.18	1758 m
2	17666	Ispir	ISPR	40.48	40.99	1217 m
3	17668	Oltu	OLTU	40.54	41.99	1300 m
4	17688	Tortum	TORT	40.30	41.54	1580 m
5	17690	Horasan	HRSN	40.04	42.17	1550 m
6	17740	Hinis	HINS	39.36	41.69	1716 m

Accordingly, the monthly total precipitation (mm), monthly average temperature (°C), snow cover depth (mm), and snow equivalent water depth (mm) recorded at the observation stations are acquired from the 12th Region Erzurum Representative Office of the General Directorate of Meteorology.

In Erzurum, approximately 58% of the land is designated for agricultural use, covering 474,813 ha. However, the region's susceptibility to drought poses significant challenges to those farmlands. Droughts can significantly deplete soil moisture levels and diminish crop yields, thereby exacerbating the existing constraints on land suitability. For instance, in the Ispir district, where merely 0.9% of the land exhibits high suitability for agriculture owing to its steep terrain, the ramifications of drought are notably deleterious to agricultural productivity and sustainability within this locale (Karavitis, Chortaria, et al., 2014; Kaymaz et al., 2022). As detailed in Fig. 17.1 and Table 17.1, the selected stations are scattered around the district and have a good coverage over the study area. Based on this preliminary information, the Erzurum Airport and Ispir station, respectively, have the highest and the lowest altitudes among the selected stations. Accordingly, the double mass curve is used to test for the homogeneity of the data and check if the conducted analysis is relevant. Then, to investigate the drought patterns in the region, the SPI, SPEI, and SSPI drought indices are used, which are detailed in the following section.

17.3 Drought indices

17.3.1 Standardized precipitation index

The SPI is a method applied in the determination of the meteorological droughts at monthly, seasonal, annual, and multi-annual scales. Developed by McKee et al., 1993 and recommended for further application by the World Meteorological Organization (WMO), the *SPI* index is calculated as

$$SPI = \frac{X_i - X_{ort}}{\sigma} \tag{17.1}$$

where *Xi* is the precipitation (mm) of month *i*th, *Xort* is the long-term average precipitation, and σ is the standard deviation of the same data records. Afterward, the SPI values can be evaluated based on the predefined boundary limits, which are well documented in the statement of the art (Yihdego et al., 2019; Danandeh & Vaheddoost, 2020). It is noteworthy

that in application, the probability distribution function of the precipitation data at various time frames is expected to follow a Gamma distribution (Savas & Vaheddoost, 2023), whilst there exist studies which preferred other types of probability distribution fits instead.

17.3.2 Standardized precipitation evapotranspiration index

The SPEI was developed by Vicente-Serrano et al., 2010, based on similar principles of SPI. Precipitation and temperature data are used as inputs to assess the drought condition. Hence, the SPEI is capable of encompassing the impacts that may arise beyond global warming, particularly those associated with temperature variations (Akgunduz et al., 2017). It can be calculated as

$$D_i = P_i - PET_i \tag{17.2}$$

while Pi is the amount of precipitation (mm) in the ith month, and PET_i is the potential evapotranspiration at the same period. This difference, D_i, is the water deficit or surplus, while the PET can be obtained as: (1)a monthly temperature index, determined according to the average temperature of each month,

$$i = \left(\frac{t}{5}\right)^{1.514} \tag{17.3}$$

where t is the average monthly temperature (°C) and i is the monthly temperature index.

(2) The temperature index for each month is summed up to obtain the annual temperature index,

$$I = \sum_{k=1}^{12} i \tag{17.4}$$

where I is the annual temperature index. Using the calculated monthly and annual temperature indices, the potential evapotranspiration (i.e., monthly PET) is calculated,

$$PET = 16\star\left(\frac{10t}{I}\right)^{a} \tag{17.5}$$

and

$$a = (0.0000000675I^3) - (0.000077I^2) + (0.01792I) + 0.49239 \tag{17.6}$$

where t is the average monthly temperature (°C), I is the annual temperature index, and a is the coefficient for further assessment.

17.3.3 Standardized snow precipitation index

The SSPI is computed analogously to the SPI, utilizing daily records of snow water equivalent (SWE). The values derived from the SSPI mostly fall within the range of -3 to 3. To compute this index, the *SWE* must first be determined. Various methodologies exist for calculating *SWE*, one of which involves utilizing snow depth data. A robust relationship exists between snow water equivalent, snow density, and snow depth that can be calculated as follows:

$$\rho_b = 60.1 H_s^{0.89} + 237 \tag{17.7}$$

$$SWE = (\rho_b + 237) H_s \tag{17.8}$$

where ρ_b and *SWE* are respectively the density of the snow cover on the surface and snow water equivalent, and H_s is the snow height (mm). It is noteworthy that the snow density and SWE can also be determined from snow depth at each station (Jonas et al., 2009).

The SWE values are calculated using a ready-to-use package named "*nixmass*" (https://cran.r-project.org/web/packages/nixmass/index.html) designed for the R-Studio environment. Using daily snow depth data as input, the SWE was calculated through the process-based "*delta.snow*" and empirical regression models. These models incorporate the relationships between snow density and various field parameters (Winkler et al., 2021). The SWE data rarely follow a normal distribution, and therefore, a Gamma distribution fit is preferred in most of the monthly, seasonal, annual, and multi-annual analysis. As a result, the SSPI is calculated by dividing the difference of the daily SWE from the long-run mean by the long-term standard deviation as

$$SSPI = \frac{SWE_i - SWE_{ort}}{SWE_{std}} \tag{17.9}$$

where *SWEi* is the snow water equivalent in month i, SWE_{ort} is the long-run average snow water equivalent, and SWE_{std} is the long-term standard deviation (Bazrkar & Chu, 2021).

The selection of the SSPI for estimating snow drought is motivated by its capacity to utilize remote sensing technology, deliver quantitative estimates of snow water equivalent, cover extensive spatial scales, facilitate comparative analyzes, and aid operational decision-making across various

sectors impacted by snow drought (Gottlieb & Mankin, 2022). Finally, the drought indices obtained for the study region, including the SPI, the SPEI, and the SSPI, are evaluated based on the criteria outlined in Table 17.2.

17.3.4 Duration, severity, and intensity of indices

Negative values of SPI, SPEI, and SSPI are considered deficits, while the positive values are considered periods of surplus in the allocated variable. Therefore, a threshold value should be defined to quantify the length of the drought period and the magnitude of drought severity. In this respect, the drought D can be defined as a period of continuous negative values in either SPI, SPEI, or SSPI reads (i.e., ≤-1). This can also be introduced as the length of the period initiated with a negative value of SPI, SPEI, and SSPI records and ends when they turn positive. Drought severity (S), on the other hand, can be expressed as the sum of either SPI, SPEI, or SSPI values over the allocated time period as,

$$S = -\sum_{i=1}^{D} SPI,\ SPEI,\ or SSPI \tag{17.10}$$

where S and D respectively are the drought severity and duration for SPI, SPEI, or SSPI indices.

Finally, the intensity of the drought (I) represents the maximum reads of the alocated index with respect to the allocated time frame (Mishra & Singh, 2010).

After the determination of the SPI, SPEI, and SSPI for the selected stations, the Kriging method is used to obtain D, S, and I maps associated with 1-, 3-, and 12-months moving average drought indices. One-month

Table 17.2 Category classification of drought indices.

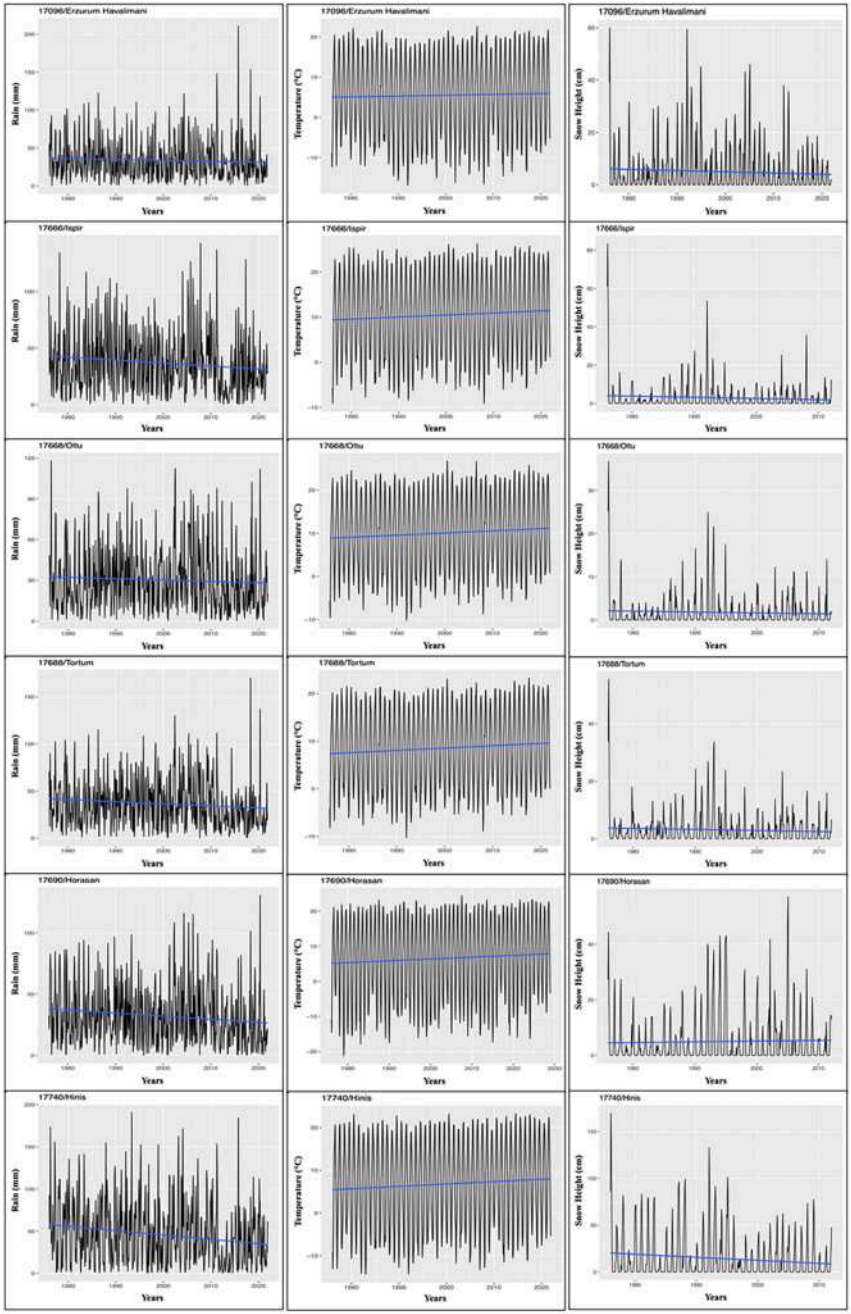
SPI–SPEI–SSPI	Situation
≥2.00	Excessive humidity
1.50–1.99	Very moist
1.00–1.49	Medium humid
0.50–0.99	Slightly moist
-0.49 to -0.49	Normal
-0.99 to -0.50	Slightly arid
-1.49 to -1.00	Medium arid
-1.99 to -1.50	Severe drought
≤-2.00	Extreme drought

periods are used to assess the short-term drought events, which are useful in understanding sudden water shortages and short-term rainfall deficiencies. These short-term droughts can affect the water requirements of crops and irrigation needs. Critical to the agriculture sector, this information helps farmers and water managers make instant decisions. The 3-month periods are usually used to determine seasonal droughts. This helps to understand whether precipitation is below the normal rate in a given season. Seasonal changes affect sectors such as agriculture and hydrology. Drought analysis during this period is important for crop planning, water reservoir management, and the regulation of economic activities. The 12-month periods, on the other hand, are used to analyze the long-term drought trends and persistence. This is critical for understanding annual rainfall totals and long-term water scarcity. Long-term drought can have lasting impacts on water reservoirs, groundwater levels, and ecosystem health. This analysis is essential for water management planning, environmental protection, and sustainability strategies.

Analyzing droughts across varying temporal scales allows a comprehensive understanding of the diverse types and impacts of drought. This approach addresses the multifaceted dimensions and consequences of drought without being confined to a single time frame. Short, medium, and long-term analyzes furnish decision-makers in various sectors with information pertinent to their specific needs and timescales, thereby facilitating more informed and timely decisions. Furthermore, monitoring droughts over different time periods enhances the effectiveness of early warning systems, enabling societies and economies to better prepare for drought events. In this respect, the 1-, 3-, and 12-month periods are widely utilized in drought-related studies and are considered to provide crucial insights into the historical droughts of a region.

17.4 Results

The annual precipitation records in six meteorological observation stations were found to follow a slightly decreasing trend at all stations. This decreasing trend is more pronounced in the southern and eastern regions of the study area. In terms of precipitation, strong differences were observed in the south compared to other regions. On the other hand, due to the strong seasonality with a continental climate, large differences between monthly precipitation amounts were determined (Fig. 17.2).



Şekil Hata! Belgede belirtilen stilde metne rastlanmadı..**1** : Erzurum ili 6 istasyona ait Yağış-Sıcaklık-Kar Yükseklik değişimi.

Figure 17.2 Precipitation–temperature–snow height records at selected stations.

Examining the annual variations in average temperatures reveals an increasing trend in temperature values across the entire region. This rise is evident at all observation stations. With the exception of the 17096/Erzurum Airport station situated at the center of the study area, monthly mean temperatures exceeded 20°C at all other stations, reaching their peak values during the summer months. During winter, while monthly average temperatures drops below 0°C in the eastern and southern parts, stations in the west and north experience temperatures above 0°C as early as March (Fig. 17.2). When considering the annual changes in average snow height, a declining trend is observed across all stations. Seasonal analysis indicates that the highest average snow heights are recorded in winter and fall. Although snow height data are collected at the regional observation stations during spring, no snow height data were recorded at the 17666/Ispir station in May. The annual variation in SWE data corresponds closely with the trends in snow depth data. Precipitation in the southern and eastern parts of the region primarily falls as snow, whereas it transitions to rain in the western and northern parts. Notably, at the 17740/Hinis station located in the southern part of the region, the decreasing trend in SWE is particularly pronounced.

At the 17690/Horasan observation station, the slight increase in snow height data, coupled with the decrease in SWE data, suggests a significant rise in regional temperatures. This rise leads to increased evaporation, with water vapor mixing into the air (Fig. 17.2). Prior to calculating the drought indices, the long-term annual precipitation data for all stations were analyzed using double mass curves. The analysis yielded an R^2 value of 0.99 across all stations, indicating that the trend in precipitation amounts is statistically significant at the 99% confidence level.

Analyzing the SPI time series reveals that arid and humid periods become increasingly pronounced over time. The findings indicate the presence of mild, moderate, severe, and occasionally extreme drought conditions across all stations. Table 17.1 provides detailed information on the drought *D*, *S*, and *I* associated with SPI-1, SPI-3, and SPI-12, respectively, for the respective stations. Notably, the percentage of severe drought months has increased in most regions over the observation period. The longest drought period, lasting 35 months, was recorded at station 17740 based on SPI-12 values. The most severe drought, with an SPI-12 value of -109.51, was also observed at station 17740. Fig. 17.3 presents the SPI projection map derived from the preliminary analysis. The highest drought magnitude, with a value of -5.20, was detected in the SPI-3 analysis at station 17666 in

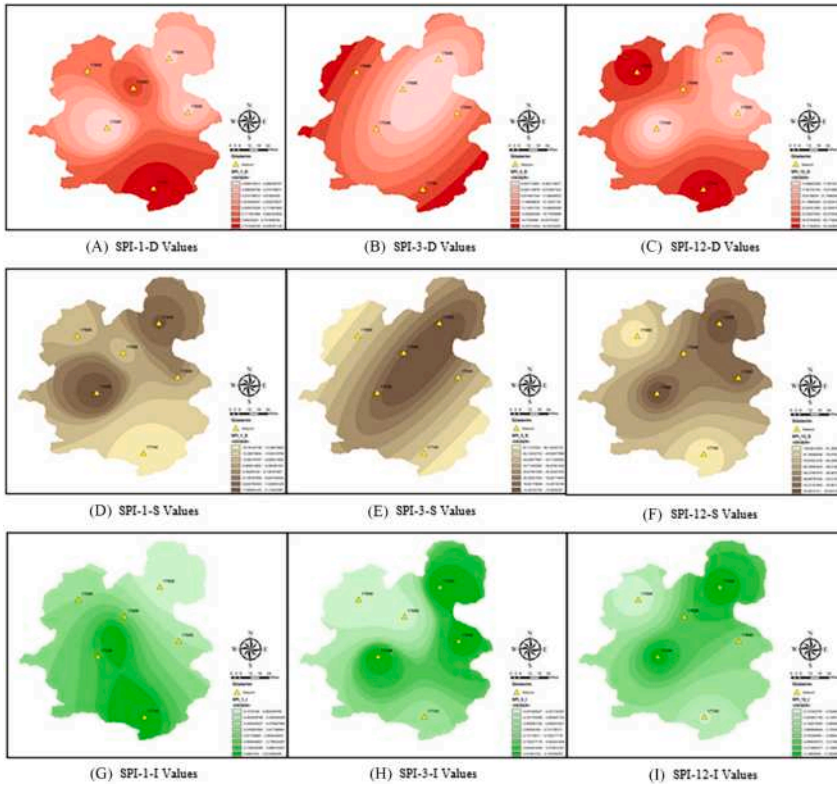


Figure 17.3 Details regarding the severity (*S*), duration (*D*), and intensity (*I*) for standardized precipitation index-1 (SPI-1), SPI-3, and SPI-12. Map lines delineate study areas and do not necessarily depict accepted national boundaries.

2021 (Table 17.3). Additionally, the map analysis of SPI results across all stations revealed consistent findings in terms of drought classification, duration, intensity, and maximum drought intensity. The stations experiencing the most severe drought were Ispir and Hini, while Erzurum Airport station recorded the least drought severity.

When analyzing the variations in SPEI, it becomes evident that arid and humid periods have become increasingly pronounced over time. Mild, moderate, severe, and some extreme droughts were observed at all stations. Table 17.4 provides a detailed account of drought *D*, *S*, and *I* associated with SPEI-1, SPEI-3, and SPEI-12. The data indicate that drought frequencies have increased in recent years across all stations in the study region. The longest drought period, lasting 45 months, was recorded at

Table 17.3 Drought summary of standardized precipitation index (SPI) analysis.

Station	Time Scale	Length		Intensity		Magnitude	
		Year	*D*	Year	*S*	Year	*I*
17096	SPI-1	2021	3	2021	-5.13	1990	-3.72
	SPI-3	2013–2014	10	2013	-15.55	2004	-3.23
	SPI-12	2013–2014	14	2013–2014	-26.89	2014	-2.99
17666	SPI-1	2013	5	2013	-10.25	2021	-4.06
	SPI-3	2012–2014	19	2012–2014	-49.38	2021	-5.20
	SPI-12	2012–2014	33	2012–2014	-103.58	2013	-5.14
17668	SPI-1	2011–2012	4	2011–2012	-7.30	2015	-5.02
	SPI-3	1978	8	2017	-13.68	2021	-3.12
	SPI-12	2013–2014	18	2017–2018	-27.71	2014	-2.75
17688	SPI-1	2013–2014	6	2013–2014	-10.29	2007	-3.84
	SPI-3	2011–2012	8	2021	-14.37	2021	-4.76
	SPI-12	2013–2015	23	2013–2015	-47.06	2014	-3.49
17690	SPI-1	2017	4	2017	-9.21	1995	-4.29
	SPI-3	2017–2018	11	2017–2018	-23.56	2020	-3.34
	SPI-12	2017–2018	17	2017–2018	-38.93	2018	-3.74
17740	SPI-1	2011–2012	9	2011–2012	-18.76	2000	-3.62
	SPI-3	2011–2013	20	2011–2013	-49.12	2012	-3.90
	SPI-12	2012–2015	35	2012–2015	-109.51	2013	-4.59

D: Number of dry months; *S*: Total value of drought severity; and *I*: Maximum drought value. No permission required.

station 17688 based on SPEI-12 values. The most severe drought, with an SPEI-12 value of -74.11, was observed at station 17666. Additionally, the highest drought magnitude was detected in the SPEI-1 analysis at station 17688 in 2021, with a value of -2.99. Fig. 17.4 illustrates the SPEI results on the map, revealing that evaluations of drought classifications, duration, intensity, and maximum drought intensity yielded almost similar results. The most severe drought conditions were observed at the Ispir and Hinis stations, while the Erzurum Airport station experienced the least drought severity.

Analyzing the variations in SSPI reveals that arid and humid periods have become increasingly pronounced over time. Table 17.5 details the drought *D*, *S*, and *I* associated with SSPI-1, SSPI-3, and SSPI-12. The data indicate the presence of mild, moderate, severe, and some extreme drought conditions across all stations. The frequency of droughts has increased in recent years across the research region. The longest drought period, lasting

Table 17.4 Drought summary of standard precipitation evapotranspiration index (SPEI) analysis.

Station	Time Scale	Length		Intensity		Magnitude	
		Year	*D*	Year	*S*	Year	*I*
17096	SPEI-1	2021	4	2021	-6.96	2006	-2.39
	SPEI-3	2019–2020	8	2019–2020	-10.72	2017	-2.45
	SPEI-12	2013–2014	18	2013–2014	-26.98	2021	-2.16
17666	SPEI-1	2021	4	2021	-8.29	2021	-2.63
	SPEI-3	2012–2014	28	2012–2014	-47.45	2021	-2.34
	SPEI-12	2012–2015	43	2012–2015	-74.11	2014	-2.24
17668	SPEI-1	2017	4	2017	-6.52	2018	-2.19
	SPEI-3	2020–2021	10	2020–2021	-18.10	2021	-2.70
	SPEI-12	2013–2014	18	2017–2018	-25.08	2021	-2.43
17688	SPEI-1	2013–2014	6	2013–2014	-9.52	2021	-2.99
	SPEI-3	2019–2020	8	2013–2014	-11.96	2021	-2.70
	SPEI-12	2012–2015	45	2012–2015	-64.10	2021	-2.15
17690	SPEI-1	2017	5	2017	-7.62	2010	-2.57
	SPEI-3	2017–2018	12	2017–2018	-19.23	2021	-2.33
	SPEI-12	2017–2018	19	2017–2018	-30.54	2018	-2.19
17740	SPEI-1	2012–2013	7	2012–2013	-9.75	2015	-2.27
	SPEI-3	2011–2012	9	2013–2014	-14.02	2015	-2.36
	SPEI-12	2012–2015	35	2012–2015	-60.83	2013	-2.04

D: Number of dry months; *S*: Total value of drought severity; and *I*: Maximum drought value.

24 months, was recorded at station 17668 based on SSPI-12 values. The most severe drought, with an SSPI-12 value of -32.31, was observed at station 17690. Additionally, the highest drought magnitude was detected in the SSPI-1 analysis at station 17096 in 1983, with a value of -3.52. Fig. 17.5 presents the SSPI values on the map, showing that evaluations of drought classifications, duration, intensity, and maximum drought intensity yielded almost identical results. The most severe drought conditions were recorded at the Ispir and Hinis stations, whereas the 17096/Erzurum Airport station experienced the least drought severity.

17.5 Discussion

Given the significance of snow reserves in the Erzurum region of Türkiye, we examined historical snow droughts using the SSPI alongside

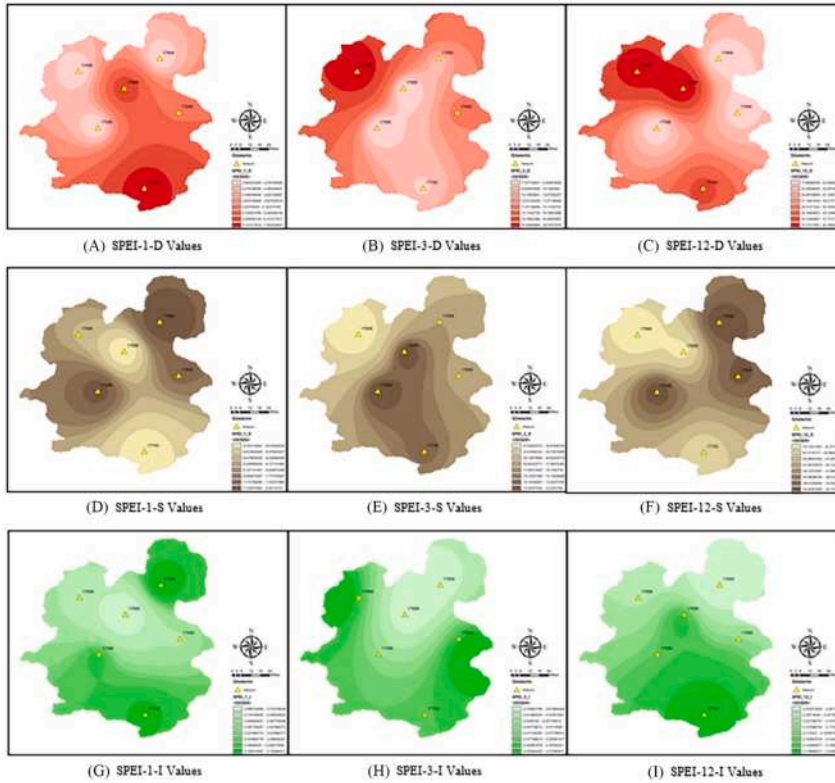


Figure 17.4 Details regarding the severity (*S*), duration (*D*), and intensity (*I*) for standard precipitation evapotranspiration index-1 (SPEI-1), SPEI-3, and SPEI-12. Map lines delineate study areas and do not necessarily depict accepted national boundaries.

the well-known SPI and SPEI indices. Comparing drought duration obtained with a one-month time period revealed consistent drought events in the southern and southeastern parts of Erzurum across all indices (SPI, SPEI, and SSPI). The longest drought duration was recorded at Hinis station, followed by Tortum and Horasan stations.

When comparing drought intensities, the Hinis station exhibited the highest drought intensity according to the SPI index. However, when considering the SPEI index, which accounts for temperature, the Tortum station showed an equivalent drought impact. The SSPI index, calculated using snow water equivalent, indicated a significant snow drought effect

Table 17.5 Drought summary of the standardized snow precipitation index (SSPI) analysis.

Station	Time Scale	Length		Intensity		Magnitude	
		Year	*D*	Year	*S*	Year	*I*
17096	SSPI-1	1996	3	1977	-3.91	1977	-2.34
	SSPI-3	1984	5	1984	-7.89	1983	-2.86
	SSPI-12	1984	12	1983	-23.44	1983	-3.52
17666	SSPI-1	1983–1984	2	1983–1984	-2.50	1984	-1.43
	SSPI-3	1983–1984	3	1983–1984	-5.21	1984	-2.13
	SSPI-12	1982–1983	11	1979	-15.47	1979	-1.78
17668	SSPI-1	1999	2	1999	-3.33	1999	-2.01
	SSPI-3	2012	3	2012	-5.70	2012	-2.12
	SSPI-12	2009–2011	24	2009–2011	-29.98	2012	-2.24
17688	SSPI-1	1978–1979	4	1978–1979	-4.89	1997	-2.55
	SSPI-3	1978–1979	6	1978–1979	-8.37	2010	-2.15
	SSPI-12	2009–2011	14	2009–2011	-16.68	1979	-1.91
17690	SSPI-1	1983–1984	4	1983–1984	-6.86	1997	-2.84
	SSPI-3	1984	5	1984	-8.27	1997	-2.44
	SSPI-12	2010–2011	23	2010–2011	-32.31	2011	-2.06
17740	SSPI-1	1997	4	1997	-5.74	2010	-2.51
	SSPI-3	2010–2011	4	2010–2011	-6.25	2010	-2.54
	SSPI-12	2010–2011	13	2010–2011	-16.41	2011	-1.69

D: Number of dry months; *S*: Total value of drought severity; and *I*: Maximum drought value. No permission required.

around Horasan station. The highest drought values depended on both magnitude and severity.

Analyzing the time-dependent changes over three-month periods showed that drought was prevalent around Ispir station in the northwest according to the SPI and SPEI indices. In contrast, the SSPI index indicated the longest snow drought duration at Tortum station in the central part of the research region and surrounding stations. Drought severity exhibited a similar distribution relative to drought magnitude. Erzurum Airport, Tortum, and Horasan stations, located centrally in the research region, experienced the highest snow drought intensity.

While the SPI and SPEI indices showed similar characteristics, the SSPI index presented different results. Comparing drought duration over a 12-month period, the SPI and SPEI indices recorded the most significant drought events at Ispir station in the northwest and Hinis

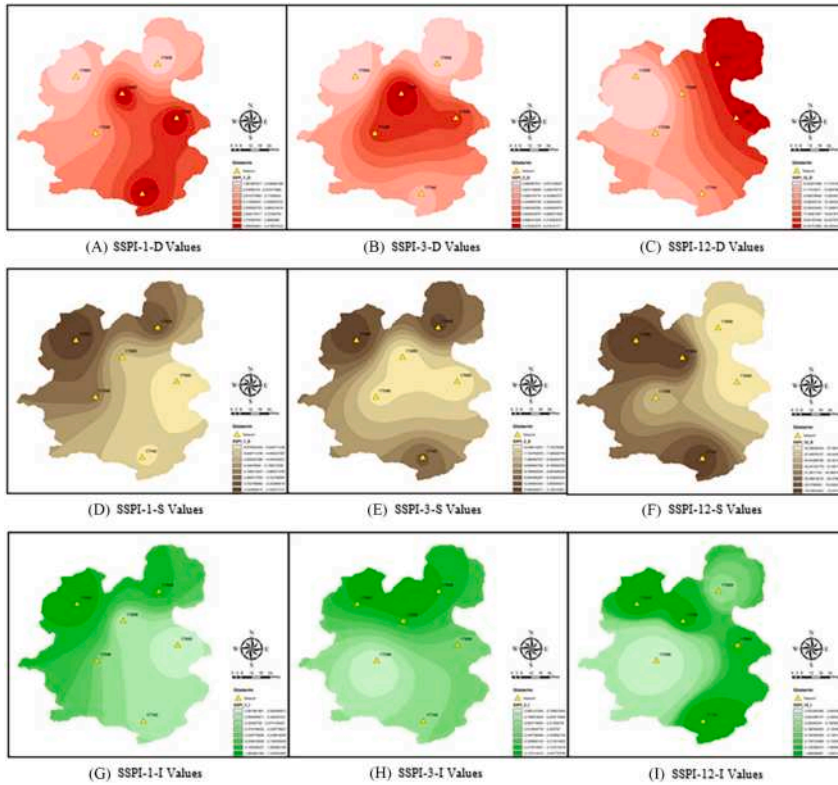


Figure 17.5 Details regarding the *severity (S), duration (D), and intensity (I)* for standardized snow precipitation index-1 (SSPI-1), SSPI-3, and SSPI-12. Map lines delineate study areas and do not necessarily depict accepted national boundaries.

station in the south. The SSPI index, however, indicated the longest snow drought duration in the eastern parts of the Oltu and Horasan stations. Drought intensities were similar to drought magnitudes, with the highest snow drought value observed at Erzurum Airport station, centrally located in the study region, and increasing towards the east.

Finally, comparing drought periods of different lengths across SPI, SPEI, and SSPI indices, the 1-month period values showed the most similarity, while the 3-month and 12-month period values exhibited less similarity. This discrepancy arises because the SPEI analysis incorporates evaporation using temperature data, and the SSPI index accounts for regional climate factors influenced by snow data.

The analysis suggests that rising temperatures, likely driven by climate change (Akyurek et al., 2011; Kuslu & Barik, 2024) are causing precipitation in the region to fall more as rain rather than snow. This shift impacts river hydrology patterns and the discharge/recharge dynamics of aquifers in the region.

17.6 Conclusions

This study investigates droughts related to precipitation and snowfall records in the Erzurum district of eastern Anatolia. We utilized time series data on precipitation, temperature, and snow depth from six meteorological stations to compute SPI, SPEI, and SSPI drought indices based on 1-, 3-, and 12-month moving averages. By analyzing drought duration, severity, and intensity, we generated drought maps, revealing a decreasing trend in snowfall across the region.

Examining annual temperature changes from 1976 to 2021, we observed a significant increase in average temperatures across all stations. This upward trend is expected to persist, exacerbating the region's climatic variations. In terms of precipitation, the southern and eastern areas primarily experience snowfall, while the western and northern regions receive more rain. Analyzing annual changes in snow height and snow water equivalent, a decreasing trend was evident at all observation stations. Severe drought conditions have been prevalent in the region since 2000 across all time periods analyzed. Increasing temperatures and decreasing precipitation, especially in mountainous areas, have led to snow droughts, characterized by reduced snow cover and rainfall replacing snowfall. These findings highlight the ongoing drought issues in Erzurum province, driven by climatic changes.

To address future drought challenges, spatial analysis studies should be conducted, considering potential climatic variations. This approach will aid in developing strategies to mitigate the impacts of drought on the region.

Authorship contribution statement

Muhammet Savas: Conceptualization, Methodology, and Writing-original draft. **Egemen Aras:** Data curation, Validation, Writing–review, and Editing. **Babak Vaheddoost:** Investigation, Writing–review, and Editing. **Damla Yılmaz Çelik**: Investigation, writing–review, and Editing.

Data availability

Data will be made available on request.

Declaration of competing interest

The authors declare that they have no known competing financial interests or personal relationships that could have appeared to influence the work reported in this paper.

Acknowledgments

We would like to thank Erzurum 12th Regional Meteorological Directorate for their continuous support for the provision of meteorological data.

Statements and declarations

The authors declare that no funds, grants, or other support were received during the preparation of this manuscript.

Artificial intelligence disclosure

During the preparation of this work the author(s) used chatgpt in order to paraphrasing. After using this tool/service, the author(s) reviewed and edited the content as needed and take(s) full responsibility for the content of the publication.

References

Akgunduz, A., Arabaci, H., Camalan, H., Cetin, G., & Coskun, M. (2017). Turkey-wide drought change and trend projections according to SPEI index IV. In: Turkey Climate Change Congress 5–7 July, Istanbul, Turkey, 2017.

Akyurek, Z., Surer, S., & Beser, Ö. (2011). Investigation of the snow-cover dynamics in the Upper Euphrates Basin of Turkey using remotely sensed snow-cover products and hydrometeorological data. *Hydrological Processes, 25*(23), 3637–3648. https://doi.org/10.1002/hyp.8090.

Aslan. (2020). Exploration of snow drought in Van Lake Basin (Doctoral dissertation).

Basak. (2017). Drought analysis and estimation of the drought index using artificial neural networks of five provinces In the lower Euthrat Basin..

Bazrkar, M. H., & Chu, X. (2021). Ensemble stationary-based support vector regression for drought prediction under changing climate. *Journal of Hydrology, 603*, 127059. https://doi.org/10.1016/j.jhydrol.2021.127059.

Brunner, M. I., Slater, L., Tallaksen, L. M., & Clark, M. (2021). Challenges in modeling and predicting floods and droughts: A review. *Wiley Interdisciplinary Reviews: Water, 8*(3). https://doi.org/10.1002/wat2.1520, http://wires.wiley.com/WileyCDA/WiresJournal/wisId-WAT2.html.

Danandeh, M. A., & Vaheddoost, B. (2020). Identification of the trends associated with the SPI and SPEI indices across Ankara, Turkey. *Theoretical and Applied Climatology, 139*, 1531–1542.

Dierauer, J. R., Allen, D. M., & Whitfield, P. H. (2019). Snow drought risk and susceptibility in the Western United states and Southwestern Canada. *Water Resources Research, 55*(4), 3076–3091. https://doi.org/10.1029/2018WR023229, http://agupubs.onlinelibrary.wiley.com/hub/journal/10.1002/(ISSN)1944-7973/.

Gottlieb, A. R., & Mankin, J. S. (2022). Observing, measuring, and assessing the consequences of snow drought. *Bulletin of the American Meteorological Society, 103*(4),

E1041. https://doi.org/10.1175/BAMS-D-20-0243.1, https://journals.ametsoc.org/view/journals/bams/103/4/BAMS-D-20-0243.1.xml.

Gulsever. (2006). *Temperature-precipitation and drought analysis in the Tigris basin*. Doctoral dissertation, Dicle University, Diyarbakır,Türkiye.

Jonas, T., Marty, C., & Magnusson, J. (2009). Estimating the snow water equivalent from snow depth measurements in the Swiss Alps. *Journal of Hydrology, 378*(1–2), 161–167. https://doi.org/10.1016/j.jhydrol.2009.09.021.

Karavitis, C. A., Tsesmelis, D. E., Skondras, N. A., Stamatakos, D., Alexandris, S., Fassouli, V., Vasilakou, C. G., Oikonomou, P. D., Gregorič, G., Grigg, N. S., & Vlachos, E. C. (2014). Linking drought characteristics to impacts on a spatial and temporal scale. *Water Policy, 16*(6), 1172–1197. https://doi.org/10.2166/wp.2014.205, http://www.iwaponline.com/wp/01606/1172/016061172.pdf.

Karavitis, C. A., Chortaria, C., Alexandris, S., Athanasopoulos, G., & Karavitis, G. A. (2014). Drought and climate change impacts on an agriculture watershed: A case study. *Desalination and Water Treatment, 52*(10-12), 1900–1913.

Kaymaz, Ç. K., Birinci, S., & Kızılkan, Y. (2022). Sustainable development goals assessment of Erzurum province with SWOT-AHP analysis. *Environment, Development and Sustainability, 24*(3), 2986–3012. https://doi.org/10.1007/s10668-021-01584-w.

Keskin, A., & Kanat, Z. (2018). Studies on climate change in the world and the current situation in Turkey (In Turkish). *Atatürk University Journal Of Agricultural Faculty, 49*(1).

Kuslu, Y., & Barik, K. (2024). Examining the climate change phenomenon using temperature and precipitation observations: The case of Erzurum. In *The water, climate, and food nexus: Linkages, challenges and emerging solutions*. Turkey: Springer International Publishing, 149–166. https://link.springer.com/book/10.1007/978-3-031-50962-9.

Lin, W., Wen, C., Wen, Z., & Gang, H. (2015). Drought in Southwest China: A review. *Atmospheric and Oceanic Science Letters, 8*(6), 339–344. https://doi.org/10.3878/AOSL20150043, http://www.keaipublishing.com/en/journals/atmospheric-and-oceanic-science-letters/.

McKee, T. B., Doesken, N. J., & Kleist, J. (1993). The relationship of drought frequency and duration to time scales. In: *Proceedings of the 8th conference on applied climatology* (pp. 179–183) Anaheim, 17–22 January 1993.

Meteorology Genel Mudurlugu (MGM) (2023). 12th regional directorate-Erzurum, Turkiye. www.erzurum.mgm.gov.tr.

Mishra, A. K., & Singh, V. P. (2010). A review of drought concepts. *Journal of Hydrology, 391*(1-2), 202–216. https://doi.org/10.1016/j.jhydrol.2010.07.012.

Oruc, S. (2021). Visual and statistical inference of hourly and sub-hourly extreme rainfall trends Central Anatolia, Turkey case. *Acta Geophys, 69*, 199–216. https://doi.org/10.1007/s11600-020-00512-2.

Panu, U. S., & Sharma, T. C. (2002). Challenges in drought research: Some perspectives and future directions. *Hydrological Sciences Journal, 47*(sup1), S19. https://doi.org/10.1080/02626660209493019.

Reich, K. D., Berg, N., Walton, D.B., Schwartz, M. Sun, F., Huang, X., & Hall, A.(2018). *Climate change in the Sierra Nevada: California's water future*. UCLA Center for Climate Science.

Salvador, C., Nieto, R., Linares, C., Díaz, J., & Gimeno, L. (2020). Effects of droughts on health: Diagnosis, repercussion, and adaptation in vulnerable regions under climate change. Challenges for future research. *Science of The Total Environment, 703*, 134912. https://doi.org/10.1016/j.scitotenv.2019.134912.

Savas, M.A., & Vaheddoost, B. (2023). Drought analysis of Erzurum province using SPI Index. In: Cukurova 10th International Scientific Researches Conference (pp. 173–182) April 2–4, Adana, TURKEY.

Staudinger, M., Stahl, K., & Seibert, J. (2014). A drought index accounting for snow. *Water Resources Research, 50*(10), 7861–7872. https://doi.org/10.1002/2013wr015143.

Tramblay, Y., Koutroulis, A., Samaniego, L., Vicente-Serrano, S. M., Volaire, F., Boone, A., Le Page, M., Llasat, M. C., Albergel, C., Burak, S., Cailleret, M., Kalin, K. C., Davi, H., Dupuy, J.-L., Greve, P., Grillakis, M., Hanich, L., Jarlan, L., Martin-StPaul, N., ... Polcher, J. (2020). Challenges for drought assessment in the Mediterranean region under future climate scenarios. *Earth-Science Reviews, 210*, 103348. https://doi.org/10.1016/j.earscirev.2020.103348.

United Nations. (2018). High level panel on water outcome document.

Vicente-Serrano, S. M., Beguería, S., & López-Moreno, J. I. (2010). A multiscalar drought index sensitive to global warming: The standardized precipitation evapotranspiration index. *Journal of Climate, 23*(7), 1696–1718. https://doi.org/10.1175/2009JCLI2909.1Spain, http://journals.ametsoc.org/doi/pdf/10.1175/2009JCLI2909.1.

Vicente-Serrano, S. M., Quiring, S. M., Peña-Gallardo, M., Yuan, S., & Domínguez-Castro, F. (2020). A review of environmental droughts: Increased risk under global warming? *Earth-Science Reviews, 201*, 102953. https://doi.org/10.1016/j.earscirev.2019.102953.

Winkler, M., Schellander, H., & Gruber, S. (2021). Snow water equivalents exclusively from snow depths and their temporal changes: The Δsnow model. *Hydrology and Earth System Sciences, 25*(3), 1165–1187. https://doi.org/10.5194/hess-25-1165-2021.

Yihdego, Y., Vaheddoost, B., & Al-Weshah, R. A. (2019). Drought indices and indicators revisited. *Arabian Journal of Geosciences, 12*(3). https://doi.org/10.1007/s12517-019-4237-z, http://www.springer.com/geosciences/journal/12517?cm_mmc=AD-_-enews-_-PSE1892-_-0.

Yuan, X., Wang, Y., Ji, P., Wu, P., Sheffield, J., & Otkin, J. A. (2023). A global transition to flash droughts under climate change. *Science (New York, N.Y.), 380*(6641), 187–191. https://doi.org/10.1126/science.abn6301, https://www.science.org/doi/pdf/10.1126/science.abn6301.

This page intentionally left blank

CHAPTER EIGHTEEN

A CMIP6-based frequency analysis of the extreme precipitation events in Virginia, USA

Sura Dhiyaa Hussein, and Mustafa Nuri Balov
Department of Civil Engineering, Istanbul Gelişim University, Istanbul, Türkiye

18.1 Introduction

Global warming and climate variability have increased the uncertainty of extreme hydrological events worldwide (Christensen & Christensen, 2004; Papalexiou & Montanari, 2019; Shen et al., 2022; Shiu et al., 2012). The change in the global hydrological cycle is the most consistent and widespread indicator of climate change in the 21st century (Allen & Ingram, 2002; Madakumbura et al., 2019; Trenberth et al., 2003; Trenberth, 2011). As a result, precipitation regimes have changed significantly, which has been even observed in terms of both intensity and frequency variation of precipitation events (Giorgi et al., 2011; Madakumbura et al., 2019; Trenberth et al., 2003). There is a large literature investigating the contribution of human activities to global warming (e.g., IPCC, 2013a, 2013b; Ring et al., 2012). Rising temperatures and the increased water-holding capacity of the atmosphere accelerate the global water cycle (Huntington, 2006; Trenberth, 2011) and cause more intense and frequent precipitation events (Alfieri et al., 2015; Min et al., 2011). This is especially recorded in both high latitudes and tropical regions, as well as in the winter seasons of the northern mid-latitudes (Seneviratne et al., 2012). Global warming has triggered the intensification of such extreme precipitation events in the tropics by changing the water vapor content, moisture supply, and circulation patterns of the atmosphere (Shen et al., 2022; Ullah et al., 2020). According to the Sixth Assessment Report of the Climate Change Monitoring Group (IPCC-AR6), climate change has altered the frequency and intensity of precipitation events and

Drought Dynamics
DOI: https://doi.org/10.1016/B978-0-443-34205-9.00017-2
© 2026 Elsevier Inc. All rights are reserved, including those for text and data mining, AI training, and similar technologies.

has produced serious consequences (IPCC, 2021). It has been found that changes in future extreme precipitation events will be more pronounced in India, Southeast Asia, Indonesia, Central and Southern Africa, and South America. Extreme precipitation events are one of the indicators of climate change (IPCC, 2013a, 2013b). Evidence confirms that the average temperature of global land areas has continued to increase, especially in recent years (Cheng et al., 2019). Furthermore, the intensity of precipitation has been observed to vary significantly over time. Changes in temperature and precipitation are expected to trigger a series of climate extremes (Duan et al., 2021; Kodinariya & Makwana, 2013). Heat waves and droughts have increased, and floods have become more frequent, especially in urban areas (Guptha et al., 2021; Nandi & Swain, 2023; Patel et al., 2022; Sahoo et al., 2022; Swain et al. 2022a, 2022b, 2022c, 2022d). The impact of extreme and frequent rainfall events resulting from climate change has been found to be more significant in urban areas because these areas are centers of human activities (Ali & Mishra, 2018; Mishra et al., 2015; Rosenzweig et al., 2010). Some recent studies have shown a strong relationship between increasing precipitation extremes and global warming (Berg et al., 2013; Fischer & Knutti, 2016; Ghosh et al., 2012; Hennessy et al., 1997; Kharin et al., 2013; Mishra et al., 2012; Zhou et al., 2018). Namely, it is stated that as a result of the increase in global mean surface temperature, the moisture-holding capacity of the atmosphere has increased, and as a result, the hydrological cycle has intensified (Jacob & Hagemann, 2007; Sharma & Mujumdar, 2019). The Intergovernmental Panel on Climate Change (IPCC), in its special report on global warming (SR15; IPCC, 2018), estimated that the global mean temperature has increased by approximately 1.08°C since the beginning of the industrial revolution. At the same time, changes in the frequency and intensity of various weather and climate extremes have been observed in many regions around the World (e.g., Alexander et al., 2006; Coumou & Rahmstorf, 2012; Donat et al., 2013; Fischer & Knutti, 2014; Kim et al., 2016; Li et al., 2017; Min et al., 2011; Zhang et al., 2011; Kharin et al., 2018; Zwiers et al., 2011; Lorenz et al., 2019). This is also documented in the IPCC special report Managing Extreme Event Risks for Adaptation to Climate Change Adaptation (SREX; Seneviratne et al., 2012).

Over the past two decades, the frequency and intensity of extreme precipitation events have increased globally (Camici et al., 2014; Karl & Knight, 1998; Osborn et al., 2000; Roy & Balling, 2004; Solomon et al., 2007; Maurer et al., 2002; Mukherjee et al., 2018). Changes in

precipitation are a phenomenon that has serious impacts on human society and has been the subject of research in many scientific fields such as hydrology, agriculture, and environmental sciences (Zhao et al., 2018). Therefore, it is an undeniable fact that the intensification of climate change affects the development and survival of humanity globally (Feng & Hu, 2014). Different economic sectors, such as fisheries, industry, livestock, agriculture, and health, have been affected by changes in temperature and precipitation. Therefore, future precipitation and temperature assessments will help to increase the capacity to plan for climate-related impacts (Wang et al., 2018). Extreme rainfall can lead to serious consequences such as flooding, loss of water quality, disease, and damage to property and agriculture (Chamani et al., 2018; de Paola et al., 2014; Tarhule, 2005). The 2021 Global State of the climate report published by the World Meteorological Organization (WMO) stated that rainfall extremes have caused many deaths and major economic losses in the last 50 years for 1970–2019 (World Meteorological Organization (WMO), 2021). During this period, the number of deaths reported due to floods was recorded as more than 59000, and due to drought was more than 650000 (World Meteorological Organization (WMO), 2021). Understanding current and future rainfall extremes is vital to quantify and manage risks to lives and livelihoods. The characteristics of extreme rainfall can be examined using various indicators such as the frequency of wet days or percentile-based indices representing moderate extremes occurring on an annual basis. It can also be studied by looking at rare extremes that recur over several years or more (Wang et al., 2013). Warming-induced changes in precipitation extremes are characterized by changes in two properties, frequency and intensity, and occur in four possible forms: more frequent and more intense events, more frequent and less intense events, less frequent and more intense events, or less frequent and less intense precipitation events (Madakumbura et al., 2019). General circulation models (GCMs) are widely used in climate studies, and their ability to simulate representative historical climate statistics has been demonstrated (Agel & Barlow, 2020; Zhan et al., 2020). Moreover, GCMs are critical tools widely used in predicting average and extreme climate events (Akinsanola et al., 2021; Knutti et al., 2008; Stouffer et al., 2017; Zhu & Yang, 2020). Based on both the GCMs and expert team on climate change detection and indicators (ETCCDI) indices, researchers have projected an overall increase in extreme precipitation events on a global scale (Chen et al., 2020; Wehner, 2020). Global warming is expected to continue in the future,

which includes ongoing changes in weather and climate extremes (e.g., IPCC SR15)

The primary aim of this chapter is to investigate the effects of climate change on future extreme precipitation events. In this context, the frequency of extreme precipitation was analyzed by using climate models–called general circulation models (GCMs)–developed by various organizations. The objectives of the study are specifically stated as follows:

- To download and analyze the daily precipitation values measured between 1985–2014 for four meteorological stations in Virginia, United States.
- To interpolate the simulations of five different climate models (GCM) between 1985–2014 (the reference period) on the stations.
- To obtain (download) climate projections under SSP2–4.5 and SSP5–8.5 emission scenarios for the periods 2015–2040, 2041–2070, and 2071–2100.
- Reducing the effects of uncertainty in the GCMs' outputs by using the linear scaling bias correction method.
- Frequency analysis of extreme precipitation by using annual maxima (AM) and peaks-over-threshold (POT) methods for different return periods.

18.2 Study area and data collection

The daily precipitation values measured between 1985–2014 of four meteorological stations located in Virginia, United States, were used in this study. The locations of these stations are shown in Fig. 18.1. Historical trends of climate change in Virginia show significant changes in temperature and precipitation patterns over the past century. According to the Virginia Council on Environmental Quality (VDEQ), average temperatures in the state have increased by about 1.5 °F (about 8.3°C) since the beginning of the 20th century, with further temperature increases observed since the 1970s (Virginia Department of Environmental Quality (VDEQ), 2021). Virginia is experiencing changes in precipitation patterns due to temperature increases. Although average annual precipitation is relatively stable, an increase in the number of earthquakes and severe climate events has been detected (Virginia Department of Environmental Quality (VDEQ), 2021). Coastal areas are particularly unsafe due to sea level rise,

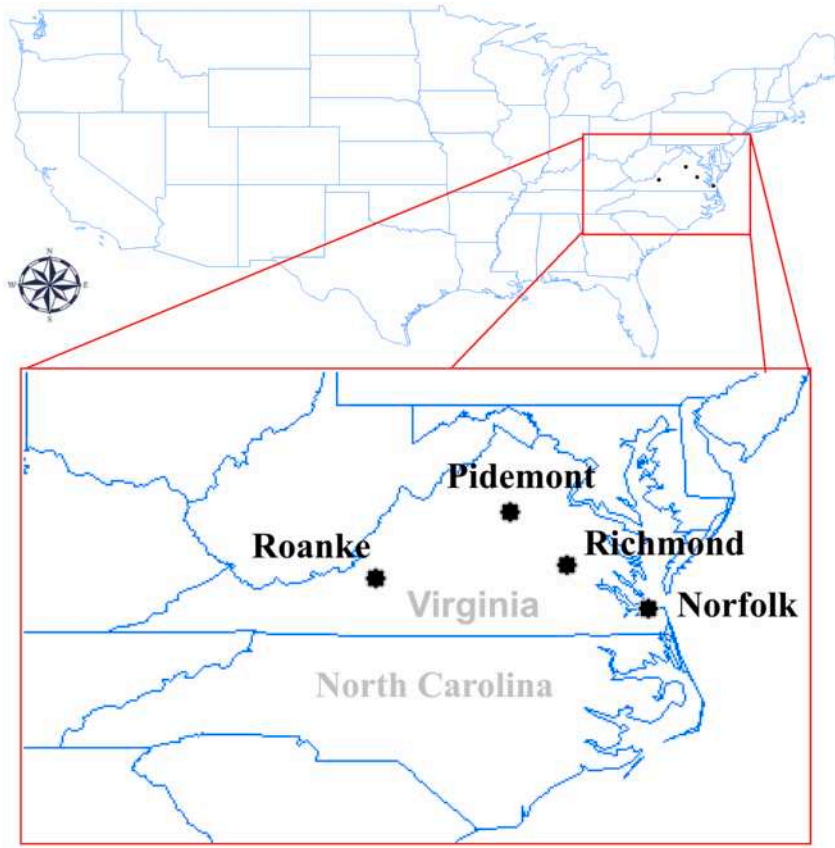


Figure 18.1 The study area and the location of the stations. Map lines delineate study areas and do not necessarily depict accepted national boundaries.

Table 18.1 Meteorological stations.

No.	Stations	Coordinates	COOPID	Altitude (m)
1	Pidemont	39,48141° N, 79,04813° W	446712	157–159
2	Roanke	37,27068° N, 79,94491° W	447285	339–350
3	Norfolk	36,84388° N, 76,28607° W	446139	3.3–7.3
4	Richmond	37,54057° N, 77,43338° W	447201	50–50.7

which poses threats to infrastructure, organizations, and communities (Virginia Department of Environmental Quality (VDEQ), 2021).

The information of the meteorological stations whose data were used in this study is summarized in Table 18.1. These precipitation data were downloaded hourly from the National oceanic and atmospheric administration (NOAA) website (https://www.ncei.noaa.gov/cdo-web/search) and converted into daily totals.

18.2.1 General circulation model

In this study, to take a closer look at the future of the intensity and recurrence of extreme precipitation events in the Virginia region, the outputs of five GCMs under the SSP2–4.5 and SSP5–8.5 scenarios were used (Table 18.2). These outputs were divided into two parts: the reference period 1985–2014 and the following period 2015–2100. Future period assessments were made in three periods: 2015–2040, 2041–2070, and 2071–2100. GCM data were downloaded from https://www.climate4impact.eu/c4i-frontend/.

18.3 Methodology

18.3.1 Double-mass curve

The double-mass curve is used to check the consistency of precipitation data obtained from the stations. The measured data of four different meteorological stations were used in this study. In this way, the double-mass curve was used to determine whether these data were consistent with each other and to correct them if they were not consistent. In order to plot

Table 18.2 The list of general circulation models (GCMs) used in this study.

Model	Country	Resolution (lon, lat)	Reference
BCC-CSM2-MR	China	$1.1^{0} \times 1.1^{0}$	Wu et al. (2021)
CMCC-ESM2	Italy	$1.3^{0} \times 0.9^{0}$	Lovato et al. (2022)
GFDL-ESM4	USA	$1^{0} \times 1^{0}$	Horowitz et al. (2018)
HadGEM3-GC31-LL	UK	$1.9^{0} \times 1.3^{0}$	
MPI-ESM-1–2-LR	Germany	$1.9^{0} \times 1.9^{0}$	Gutjahr et al. (2019)

this curve, the cumulative annual precipitation of the stations to control is plotted on the x-axis, and the cumulative annual precipitation obtained from the average of other stations is plotted on the y-axis. The consistency of the data is decided according to the possible changes in the slope of the plotted curve. For example, curves that continue with an approximately constant slope are an indicator of the consistency of the data. In case of a change in the slope, the data can be made consistent by recalculating the slope of the curve. For this, the data before the change are multiplied by a coefficient K = (slope after the change/slope before the change).

18.3.2 Bias correction

In practice, there are some biases between the model values and the observed data. In hydrological studies, it is mandatory to use appropriate correction methods to minimize the effects of uncertainty before using the outputs of global circulation models (Chen et al., 2013). In many studies, a number of bias correction methods, such as alpha variability, linear scaling, etc., have been used. These methods can be classified as statistical and distribution-based methods (Prasanna, 2018; Räty et al., 2014; Teutschbein and Seibert, 2012; Tschöke et al., 2017). Teutschbein and Seibert (2012) compared various correction methods to be used in hydrological studies based on the impacts of climate change. The researchers found that all methods can improve their performance based on the correction of average climate parameters (precipitation and temperature), while for other statistical variables, these methods should be used with caution. In the extreme value and frequency analysis, the main variables are the maximum and extreme monthly or annual precipitation events. In this study, the linear scaling method is used for correction. The following formula is used in the linear scaling method:

$$P_{\text{corr}}(d) = P_{\text{raw}}(d) \times \left[\frac{\mu_{\text{m,obs.,d}}}{\mu_{m,raw.,d}} \right] \tag{18.1}$$

where $P_{\text{corr}}(d)$ is the adjusted daily precipitation value of the model in the reference and/or future periods, $P_{\text{raw}}(d)$ is the model output, and $\mu_{m,\text{obs,d}}$ and $\mu_{m,\text{raw,d}}$ are the monthly mean precipitation values obtained from daily observations and GCM's in the reference period.

18.3.3 Frequency analysis

18.3.3.1 Annual maxima

One of the most widely used methods for extreme value analysis is the AM method (e.g., Coles, 2001). In this method, the maximum values of an equal divided time block (usually 1 year) are selected. This new time series, which is independent, consistent, and uniformly distributed, is assumed to fit well with the generalized extreme value distribution (GEVD) (Wi et al., 2016). Since the number of samples is limited in this approach, GEVD may be more useful (Shao et al., 2015). For a given time series containing annual maximum values such as $x_1, x_2, ., x_n$, the cumulative distribution function (CDF) of the GEVD can be written as follows depending on variables such as mean, μ, scale factor, σ, and shape parameter, k (Jahanbaksh Asl et al., 2013):

$$F(x) = \exp\left(-\left[-\left\{1 - k\left(\frac{x-\mu}{\sigma}\right)\right\}^{1/k}\right]\right) \tag{18.2}$$

Accordingly, the probability of occurrence of a value with a T-year recurrence period (Zp) is calculated as:

$$Zp = \mu - \frac{\sigma}{k}\left[1 - \left(-\log\left(1 - \frac{1}{T}\right)\right)^{-k}\right] \tag{18.3}$$

Rainfall intensity for different return periods (2, 5, 10, 20, 50, 100, and 500 years) can be obtained from the inverse CDF.

18.3.3.2 Peaks-over-threshold

In this study, another method used to determine both the magnitude and frequency of extreme precipitation events is the POT method. These values are assumed to be uniform, independent, and consistent (Kyselý et al., 2010). According to Coles (2001) and Sugahara et al. (2009), such values can be approximately fitted to the generalized pareto distribution (GPD) introduced by Balkema and de Haan (1974), and Pickands III (1975). This method has been widely used by researchers in various disciplines such as finance (Gilli & Këllezi, 2006), earthquake analysis (Pisarenko & Sornette, 2003), climatology, and hydrology studies (Paxian et al., 2015; Varga et al., 2016; Yilmaz et al., 2014). In GPD theory, the cumulative distribution function can be expressed by the space parameter (threshold) u, the measurement factor σ, and the shape factor γ as:

$$F(x) = 1 - \left\{1 + \frac{\gamma}{\sigma}(x - u)\right\}^{-\frac{1}{\gamma}} \gamma \neq 0 \tag{18.4}$$

$$F(x) = 1 - \exp\left(-\frac{x - u}{\sigma}\right)\gamma = 0 \tag{18.5}$$

where $x \in [u, \infty)$ for $\gamma \geq 0$ and $x \in [u, u - \sigma / \gamma]$ for $\gamma < 0$ (Um et al., 2010).

The accuracy of the fit was examined using graphical (probability-probability (P-P) and quantile-quantile (Q-Q) curves) and statistical (Kolmogorov-Smirnov (KS)) tests. For the P-P plot, empirical and theoretical cumulative distribution function (CDF) values are used as x and y axes. For the Q-Q plot, the x-axis is set with the observed data values and the y-axis with the fitted distribution quantiles. The goodness of fit can be interpreted from the distribution of data points around the perfect fit line with a slope of 45 degrees.

The most important part of this method is determining a threshold value. The magnitude of the threshold value can lead to changes in the variance of the estimated parameters. For example, a high threshold value can result in a low number of high-level statistics and higher variance of the estimated parameters, and a low threshold value results in lower variance of the estimated parameters (Um et al., 2010).

Among different selection methods, such as choosing a high percentage, such as 95% (e.g., Gu et al., 2017; Yilmaz, 2015), a number of studies (Burn et al., 2016; Jahanbaksh Asl et al., 2013; Yilmaz et al., 2014) have suggested the mean residual life plot (MRLP) method (Lehner et al., 2008) as a most useful tool to determine the most appropriate threshold during climate extremes. In MRLP, the average of the differences between extreme values and threshold values should be plotted with respect to different threshold values. The position of the points can be calculated as:

$$\left\{\left(u, \frac{1}{nu}\sum_{i=1}^{nu}(x(i) - u)\right) : u < X\max\right\} \tag{18.6}$$

where $x(1),.,x(nu)$ are the observed data exceeding the u limit. According to Coles (2001), the linearity of the line around the selected threshold and satisfactory fit of GPD can be useful criteria for determining the optimum threshold. On the other hand, Yilmaz et al. (2014) suggested that the number of extremes per block can be useful, from 1.65 to 3.0. Finally, consecutive values are removed from the data series for the independence

of the series. After determining the threshold and constructing the partial series of extreme precipitation, the precipitation intensity can be calculated from the inverse cumulative distribution function for 2, 5, 10, 20, 50, 100, and 500 year recurrence periods.

18.3.3.3 Kolmogorov-Smirnov test

The KS test, an alternative to the X^2 goodness-of-fit tests, was first proposed by Kolmogorov in 1933. It was later developed by Smirnov in 1939. The KS goodness-of-fit test is used in many applications to test normality in climate research. The test is based on the maximum difference between the empirical and hypothetical cumulative distribution. The KS test is based on the empirical distribution function especially the empirical cumulative distribution function (ECDF). In the KS test (a non-parametric test), for a random variable X and a sample series $\{x_1, x_2, x_3,.., x_n\}$, the empirical CDF of x can be calculated as:

$$F(\mathrm{X}) = \frac{1}{n}\sum_{i=1}^{n} \mathrm{I}\left(Xi \le X\right) \tag{18.7}$$

The condition I is taken as 1 for true and 0 for false (Salarpour et al., 2012). The KS ($D+$ and $D-$) statistical test values for two CDFs, such as F_x and F_y are calculated as (Salarpour et al., 2012):

$$D + = \max\left(F_x\left(X\right) - F_y\left(X\right)\right) \tag{18.8}$$

$$D - = \max\left(F_y\left(X\right) - F_x\left(X\right)\right) \tag{18.9}$$

18.4 Results and discussions

In this study, daily data measured between 1985 and 2014 at five precipitation measurement stations in Virginia were used to analyze precipitation intensity. These data were subjected to consistency testing before being used for analysis. Fig. 18.2 presents the double-mass curves of the stations. As can be seen in the figure, the curves of all stations have approximately constant slopes except for small deviations, which can lead to conclude the consistency of the used data.

For frequency analyzes, the outputs of five climate models, namely BCC-CSM2-MR (China), CMCC-ESM2 (Italy), GFDL-ESM4 (America), HadGEM3-GC31-LL (England), and MPI-ESM1–2-LR

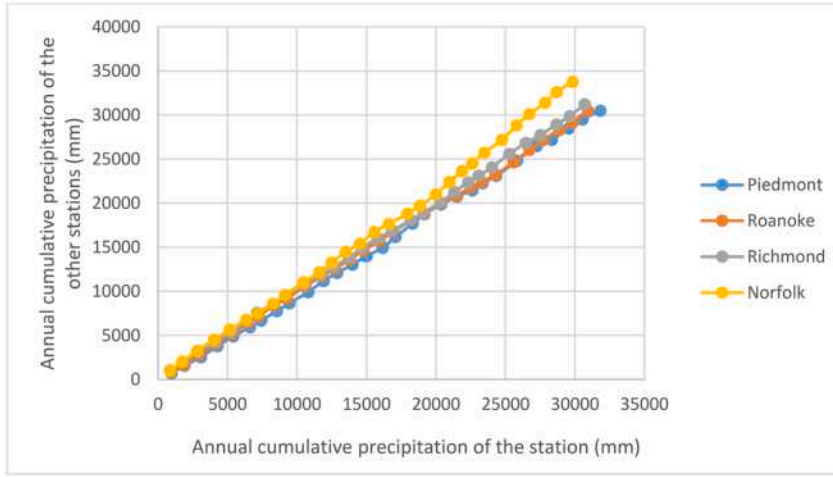


Figure 18.2 The double-mass curve for the study stations.

(Germany), obtained with two emission scenarios (SSP2–4.5 and SSP5–8.5) were used. These outputs were corrected by comparing the simulations in the reference period with the measured data. The linear scaling method was applied for correction. Analyzes were made in four periods as 1985–2014 (reference and future periods), 2015–2040 (near future), 2041–2070 (medium term future), and 2071–2100 (far future).

Daily maximum precipitation intensity values obtained for the stations from AM and POT are summarized in Tables 18.3 and 18.4 and for the periods 2015–2040, 2041–2070, and 2071–2100, respectively. In the tables, precipitation intensities are obtained from the observation data at the stations for a 100-year return period, the reference period, and future projections of the models for the SSP2–4.5 and SSP5–8.5 emission scenarios. In addition, the difference in precipitation intensities calculated for the future period compared to the reference period is shown in the tables as percentages (values in parentheses).

The values of differences vary from model to model and station to station. Considering the ensemble mean of GCMs, the maximum daily rainfall intensity is projected to decrease for all stations under SSP2–4.5 scenario whereas, decrease for Piedmont and Roanoke stations and increase for Norfolk and Richmond stations based on the frequency analysis by using AM under SSP 5–8.5 scenario during the near future (2015–2040).

Table 18.3 The values of maximum daily rainfall intensity with 100-year return period during the near future (2015–2040).

Model	Dataset	AM				POT			
		Pidemont	Roanoke	Norfolk	Richmond	Pidemont	Roanoke	Norfolk	Richmond
	Obs.	158.87	198.8	264.28	174.41	139	165	228.2	148.4
BCC-CSM2-MR	Ref.	75.56	200.5	241.93	293.32	61.77	176	217.7	230.8
	SSP2–4.5	59.31	197.3	231.5	304	59.18	187	196.2	257
		(-21.51)	(-1.6)	(-4.31)	(3.64)	(-4.19)	(6.25)	(-9.88)	(11.35)
	SSP5–8.5	71.74	177.9	329.7	366	60.63	165	241.2	270.5
		(-5.06)	(-11.27)	(36.28)	(24.78)	(-1.85)	(-6.25)	(10.79)	(17.2)
CMCC-ESM2	Ref.	64.79	149.1	172.93	180.14	50.24	149	156.8	164.3
	SSP2–4.5	55.16	210.8	175.6	189	49.36	174	147.9	169.9
		(-14.86)	(41.38)	(1.54)	(4.92)	(-1.75)	(16.78)	(-5.68)	(3.41)
	SSP5–8.5	52.87	198.3	167.3	176	52.34	169	173.3	178.6
		(-18.4)	(33)	(-3.26)	(-2.3)	(4.18)	(13.42)	(10.52)	(8.7)
GFDL-ESM4	Ref.	66.19	181.6	209.97	210.46	54.9	149	184.3	172.9
	SSP2–4.5	43.82	116.1	170	162	40.3	113	151.1	148.9
		(-33.8)	(-36.07)	(-19.04)	(-23.03)	(-26.59)	(-24.16)	(-18.01)	(-13.88)

	SSP5–8.5	58.57	142.1	189.1	228	50.47	131	173.4	202.2
		(-11.51)	(-21.75)	(-9.94)	(8.33)	(-8.07)	(-12.08)	(-5.91)	(16.95)
HadGEM3-GC31-LL	Ref.	51.97	195	409.74	254.33	42.21	133	234.5	170.2
	SSP2–4.5	47.25	177.1	271.6	174	48.58	154	229.9	141.9
		(-9.08)	(-9.18)	(-33.71)	(-31.58)	(15.09)	(15.79)	(-1.96)	(-16.63)
	SSP5–8.5	66.9	200.9	450.3	293	52.44	161	286.8	201.4
		(28.73)	(3.03)	(9.9)	(15.2)	(24.24)	(21.05)	(22.3)	(18.33)
MPI-ESM1–2-LR	Ref.	63.57	186.8	237.58	237.81	54.33	154	198.2	197.3
	SSP2–4.5	78.3	195.8	249	263	57.37	155	219.8	199.1
		(23.17)	(4.82)	(4.81)	(10.59)	(5.6)	(0.65)	(10.9)	(0.91)
	SSP5–8.5	70.23	183.9	274.1	228	60.31	160	221	214.8
		(10.48)	(-1.55)	(15.37)	(-4.13)	(11.01)	(3.9)	(11.5)	(8.87)
Ensemble mean	Ref.	64.42	183	254	235	52.7	152	198.3	187.1
	SSP2–4.5	56.77	179	220	219	51	156	189	183.4
		(-11.88)	(-2.19)	(-13.39)	(-6.81)	(-3.23)	(2.63)	(-4.69)	(-1.98)
	SSP5–8.5	64.06	181	282	258	55.2	157	219.1	213.5
		(-0.56)	(-1.09)	(11.02)	(9.79)	(4.74)	(3.29)	(10.49)	(14.11)

Table 18.4 The values of maximum daily rainfall intensity with 100-year return period during the mid-term future (2041–2070).

Model	Dataset	AM				POT			
		Pidemont	Roanoke	Norfolk	Richmond	Pidemont	Roanoke	Norfolk	Richmond
	Obs.	158.9	198.82	264.28	174.41	139	165	228.2	148.4
BCC-CSM2-MR	Ref.	75.56	200.53	241.93	293.32	61.77	176	217.7	230.8
	SSP2–4.5	87.46	244.2	244.2	243	77.25	243	233.2	271.1
		(15.75)	(21.78)	(0.94)	(-17.16)	(25.06)	(38.07)	(7.12)	(17.46)
	SSP5–8.5	92.94	215.5	385	401	75.58	191	297.5	317
		(23)	(7.47)	(59.14)	(36.71)	(22.36)	(8.52)	(36.66)	(37.35)
CMCC-ESM2	Ref.	64.79	149.07	172.93	180.14	50.24	149	156.8	164.3
	SSP2–4.5	64.42	150.2	138.6	155	46.02	134	143.6	152.6
		(-0.57)	(0.76)	(-19.85)	(-13.96)	(-8.4)	(-10.07)	(-8.42)	(-7.12)
	SSP5–8.5	57.88	163.4	294.2	289	52.63	160	203.3	219.9
		(-10.67)	(9.61)	(70.13)	(60.43)	(4.76)	(7.38)	(29.66)	(33.84)
GFDL-ESM4	Ref.	66.19	181.55	209.97	210.46	54.9	149	184.3	172.9
	SSP2–4.5	60.91	117.94	203.4	204	48.08	118	164.3	165
		(-7.98)	(-35.04)	(-3.13)	(-3.07)	(-12.42)	(-20.81)	(-10.85)	(-4.57)
	SSP5–8.5	58.64	149.6	212.3	192	52.24	135	181.4	177.4

		(-11.41)	(-17.6)	(1.11)	(-8.77)	(-4.85)	(-9.4)	(-1.57)	(2.6)
HadGEM3-GC31-LL	Ref.	51.97	194.99	409.74	254.33	42.21	133	234.5	170.2
	SSP2–4.5	55.8	139.3	444.6	284	47.46	145	353.2	249
		(7.37)	(-28.56)	(8.51)	(11.67)	(12.44)	(9.02)	(50.62)	(46.3)
	SSP5–8.5	62.26	189.1	290.8	290	54.1	150	266.7	234.9
		(19.8)	(-3.02)	(-29.03)	(14.03)	(28.17)	(12.78)	(13.73)	(38.01)
MPI-ESM1–2-LR	Ref.	63.57	186.82	237.58	237.81	54.33	154	198.2	197.3
	SSP2–4.5	73.03	225.03	262.7	259	59.45	184	253.8	235.6
		(14.88)	(20.45)	(10.57)	(8.91)	(9.42)	(19.48)	(28.05)	(19.41)
	SSP5–8.5	62.07	160.7	244	217	58.14	155	231.9	221.1
		(-2.36)	(-13.98)	(2.7)	(-8.75)	(7.01)	(0.65)	(17)	(12.06)
Ensemble mean	Ref.	64.42	183	254	235	52.7	152	198.3	187.1
	SSP2–4.5	68.32	175	259	229	55.6	165	229.6	214.6
		(6.05)	(-4.37)	(1.97)	(-2.55)	(5.5)	(8.55)	(15.78)	(14.7)
	SSP5–8.5	66.76	176	285	278	58.5	158	236.2	234.1
		(3.63)	(-3.83)	(12.2)	(18.3)	(11.01)	(3.95)	(19.11)	(25.12)

The results which are obtained by using the POT method, show a different manner, where, it is projected that the maximum 24-hour rainfall intensity will decrease under SSP2–4.5 and increase under SSP5–8.5 scenarios for all stations except Roanoke, under SSP2–4.5 which an increase is projected.

On the other hand, for the mid-term future (2041–2070), taking the ensemble mean of the model into account, an increase in daily maximum rainfall intensities for all stations under both scenarios, with some exceptions, such as a decrease in Roanoke station under both scenarios and for Richmond under the SSP2–4.5 scenario. However, by the end of the century (2071–2100), compared to the reference period (1985–2014), a more significant increase was projected, where, an increase of 45% in daily maximum rainfall for Richmond station is expected (Table 18.5). Additionally, in most of the cases, the results were found to be parallel for

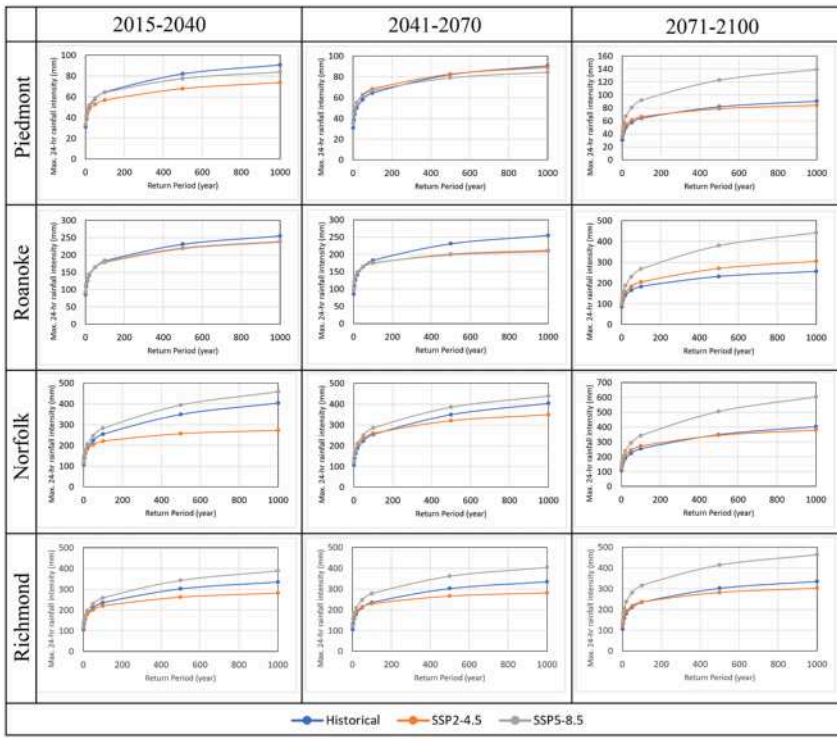


Figure 18.3 The results of frequency analysis by using annual maxima (AM) approach.

Piedmont and Roanoke stations and Norfolk and Richmond stations. This condition can be explained by considering the distance from the shoreline.

The effects of applying different emission scenarios are well pictured in Fig. 18.3, where the results of frequency analysis by using the AM approach are presented for each station under both scenarios for all time periods, together with the reference period. The same conditions can be considered for the POT approach. In the figure, especially for the late future, the remarkable difference between the values for SSP5–8.5 and SSP2–4.5 can be interpreted. During the late future, due to the structure of the scenarios, the maximum daily rainfall intensities are projected to be close to the values of the reference period under the SSP2–4.5 scenario and increase significantly under the SSP5–8.5 scenario by the end of the current century.

18.5 Conclusion

In this study, frequency analyzes based on annual maximum and threshold exceeding peaks methods between 1985–2013 were conducted with data observed from five meteorological stations in Virginia. In addition, in order to investigate the effects of climate change, the outputs of BCC-CSM2-MR, CMCC-ESM2, GFDL-ESM4, HadGEM3-GC31-LL, and MPI-ESM1–2-LR global circulation models were examined under SSP2–4.5 and SSP8.5 emission scenarios. In addition, the outputs of these models were corrected with the linear scaling method.

The results show that by the end of the current century, the comparison of the outputs with the observed data in terms of precipitation shows that both the frequency and intensity of extreme precipitation events will increase under both scenarios; however, the results were not found to be the same for all stations. In addition, it was found that the storms calculated with the annual maximum method were larger than those calculated with the POT method.

Under the SSP5–8.5 scenario, the increase in 24-hour precipitation intensity compared to SSP2–4.5 was found to be greater than the observed data, with the opposite being true in some regions. For different sections of the study, deviations between the projection and observed values were corrected by selecting the appropriate method. Extreme precipitation events in Virginia were examined in terms of trends in extreme

Table 18.5 The values of maximum daily rainfall intensity with 100-year return period during the mid-term future (2071–2100).

Model	Dataset	AM				POT			
		Pidemont	Roanoke	Norfolk	Richmond	Pidemont	Roanoke	Norfolk	Richmond
	Obs.	158.9	198.82	264.28	174.41	139	165	228.2	148.4
BCC-CSM2-MR	Ref.	75.56	200.53	241.93	293.32	61.77	176	217.7	230.8
	SSP2–4.5	97.49	324.7	304	322	82.75	244	263.5	311.7
		(29.02)	(61.92)	(25.66)	(9.78)	(33.96)	(38.64)	(21.04)	(35.05)
	SSP5–8.5	110.2	354.8	319.9	305	98.84	269	308	316.5
		(45.84)	(76.93)	(32.23)	(3.98)	(60.01)	(52.84)	(41.48)	(37.13)
CMCC-ESM2	Ref.	64.79	149.07	172.93	180.14	50.24	149	156.8	164.3
	SSP2–4.5	64.42	149.9	211.9	185	52.83	145	180.3	178.5
		(-0.57)	(0.56)	(22.54)	(2.7)	(5.16)	(-2.68)	(14.99)	(8.64)
	SSP5–8.5	98.72	308.9	387	330	70.71	217	253	248.8
		(52.37)	(107.22)	(123.79)	(83.19)	(40.74)	(45.64)	(61.35)	(51.43)
GFDL-ESM4	Ref.	66.19	181.55	209.97	210.46	54.9	149	184.3	172.9
	SSP2–4.5	47.43	121.7	209.1	197	42.13	117	179.3	180.2
		(-28.34)	(-32.97)	(-0.41)	(-6.4)	(-23.26)	(-21.48)	(-2.71)	(4.22)
	SSP5–8.5	66.22	153.4	204.1	247	56.35	129	191.7	214.6

		(0.05)	(-15.51)	(-2.8)	(17.36)	(2.64)	(-13.42)	(4.02)	(24.12)
HadGEM3-GC31-LL	Ref.	51.97	194.99	409.74	254.33	42.21	133	234.5	170.2
	SSP2–4.5	70.67	276.1	426.4	262	61.36	200	299.7	192.6
		(35.98)	(41.6)	(4.07)	(3.02)	(45.37)	(50.38)	(27.8)	(13.16)
	SSP5–8.5	99.3	285.6	474.8	404	75.28	219	348.8	324.9
		(91.07)	(46.47)	(15.88)	(58.85)	(78.35)	(64.66)	(48.74)	(90.89)
MPI-ESM1–2-LR	Ref.	63.57	186.82	237.58	237.81	54.33	154	198.2	197.3
	SSP2–4.5	52.51	155.1	208.4	215	50.79	144	196	212.8
		(-17.4)	(-16.98)	(-12.28)	(-9.59)	(-6.52)	(-6.49)	(-1.11)	(7.86)
	SSP5–8.5	84.49	231.2	325.4	294	75.62	195	275.6	255.5
		(32.91)	(23.76)	(36.96)	(23.63)	(39.19)	(26.62)	(39.05)	(29.5)
Ensemble mean	Ref.	64.42	183	254	235	52.7	152	198.3	187.1
	SSP2–4.5	66.5	205	272	236	58	170	223.8	215.2
		(3.23)	(12.02)	(7.09)	(0.43)	(10.06)	(11.84)	(12.86)	(15.02)
	SSP5–8.5	91.79	267	342	316	75.4	206	275.4	272.1
		(42.49)	(45.9)	(34.65)	(34.47)	(43.07)	(35.53)	(38.88)	(45.43)

precipitation indices and frequency analyzes of maximum daily precipitation intensity.

This study showed that as a result of the increase in precipitation in the coming years (2041–2070 and 2071–2100), the precipitation amount will be greater than the years 2015–2040. The study also revealed that the duration and frequency will increase in the forthcoming years, and this increase will be more pronounced for all stations under the SSP5–8.5 scenario.

Therefore, the following points are suggested for the future:

- The increase in the frequency and magnitude of extreme precipitation events makes it important to revise the infrastructures, especially in urban areas.
- Considering the fact that the precipitation pattern will change, it may be beneficial to remove excess water for later use.
- Emergency plans should be created and prepared in case of flooding.
- It is important to protect the environment, preserve natural areas, and implement environmental projects.
- It is necessary to encourage the use of green architecture to control water flow.

References

Agel, L., & Barlow, M. (2020). How Well Do CMIP6 historical runs match observed northeast U.S. precipitation and extreme precipitation–related circulation? *Journal of Climate, 33*(22), 9835–9848. https://doi.org/10.1175/jcli-d-19-1025.1.

Akinsanola, A. A., Ongoma, V., & Kooperman, G. J. (2021). Evaluation of CMIP6 models in simulating the statistics of extreme precipitation over Eastern Africa. *Atmospheric Research, 254*. https://doi.org/10.1016/j.atmosres.2021.105509, http://www.elsevier.com/inca/publications/store/5/0/3/3/2/3/index.htt.

Alexander, L. V., Zhang, X., Peterson, T. C., Caesar, J., Gleason, B., Klein Tank, A. M. G., Haylock, M., Collins, D., Trewin, B., Rahimzadeh, F., Tagipour, A., Rupa Kumar, K., Revadekar, J., Griffiths, G., Vincent, L., Stephenson, D. B., Burn, J., Aguilar, E., Brunet, M., Taylor, M., New, M., Zhai, P., Rusticucci, M., & Vazquez-Aguirre, J. L. (2006). Global observed changes in daily climate extremes of temperature and precipitation. *Journal of Geophysical Research: Atmospheres, 111*(D5). https://doi.org/10.1029/2005jd006290.

Alfieri, L., Burek, P., Feyen, L., & Forzieri, G. (2015). Global warming increases the frequency of river floods in Europe. *Hydrology and Earth System Sciences, 19*(5), 2247–2260. https://doi.org/10.5194/hess-19-2247-2015.

Ali, H., & Mishra, V. (2018). Increase in subdaily precipitation extremes in India under 1.5 and 2.0 °C warming worlds. *Geophysical Research Letters, 45*(14), 6972–6982. https://doi.org/10.1029/2018GL078689, http://agupubs.onlinelibrary.wiley.com/hub/journal/10.1002/(ISSN)1944-8007/.

Allen, M. R., & Ingram, W. J. (2002). Constraints on future changes in climate and the hydrologic cycle. *Nature, 419*(6903), 224–232. https://doi.org/10.1038/nature01092.

Balkema, A. A., & de Haan, L. (1974). Residual life time at great age. *The Annals of Probability, 2*(5). https://doi.org/10.1214/aop/1176996548.

Berg, P., Moseley, C., & Haerter, J. O. (2013). Strong increase in convective precipitation in response to higher temperatures. *Nature Geoscience, 6*(3), 181–185. https://doi.org/10.1038/ngeo1731.

Burn, D. H., Whitfield, P. H., & Sharif, M. (2016). Identification of changes in floods and flood regimes in Canada using a peaks over threshold approach. *Hydrological Processes, 30*(18), 3303–3314. https://doi.org/10.1002/hyp.10861, http://onlinelibrary.wiley.com/journal/10.1002/(ISSN)1099-1085.

Camici, S., Brocca, L., Melone, F., & Moramarco, T. (2014). Impact of climate change on flood frequency using different climate models and downscaling approaches. *Journal of Hydrologic Engineering, 19*(8). https://doi.org/10.1061/(asce)he.1943-5584.0000959.

Chamani, R., Monkam, D., & Yepdo Djomou, Z. (2018). Return times and return levels of July–September extreme rainfall over the major climatic sub-regions in Sahel. *Atmospheric Research, 212*, 77–90. https://doi.org/10.1016/j.atmosres.2018.04.026, http://www.elsevier.com/inca/publications/store/5/0/3/3/2/3/index.htt.

Chen, J., Brissette, F. P., Chaumont, D., & Braun, M. (2013). Finding appropriate bias correction methods in downscaling precipitation for hydrologic impact studies over North America. *Water Resources Research, 49*(7), 4187–4205. https://doi.org/10.1002/wrcr.20331, http://agupubs.onlinelibrary.wiley.com/hub/journal/10.1002/(ISSN)1944-7973/.

Chen, H., Sun, J., Lin, W., & Xu, H. (2020). Comparison of CMIP6 and CMIP5 models in simulating climate extremes. *Science Bulletin, 65*(17), 1415–1418. https://doi.org/10.1016/j.scib.2020.05.015.

Cheng, T. F., Lu, M., & Dai, L. (2019). The zonal oscillation and the driving mechanisms of the extreme western North Pacific subtropical high and its impacts on East Asian summer precipitation. *Journal of Climate, 32*(10), 3025–3050. https://doi.org/10.1175/JCLI-D-18-0076.1, https://journals.ametsoc.org/doi/pdf/10.1175/JCLI-D-18-0076.1.

Christensen, O. B., & Christensen, J. H. (2004). Intensification of extreme European summer precipitation in a warmer climate. *Global and Planetary Change, 44*(1-4), 107–117. https://doi.org/10.1016/j.gloplacha.2004.06.013.

Coles, S. (2001). *An introduction to statistical modeling of extreme values*. Springer-Verlag. http://doi.org/10.1007/978-1-4471-3675-0.

Coumou, D., & Rahmstorf, S. (2012). A decade of weather extremes. *Nature Climate Change, 2*(7), 491–496. https://doi.org/10.1038/nclimate1452.

de Paola, F., Giugni, M., Topa, M. E., & Bucchignani, E. (2014). Intensity-Duration-Frequency (IDF) rainfall curves, for data series and climate projection in African cities. *SpringerPlus, 3*(1), 1–18. https://doi.org/10.1186/2193-1801-3-133, http://www.springerplus.com/archive.

Donat, M. G., Alexander, L. V., Yang, H., Durre, I., Vose, R., Dunn, R. J. H., Willett, K. M., Aguilar, E., Brunet, M., Caesar, J., Hewitson, B., Jack, C., Klein Tank, A. M. G., Kruger, A. C., Marengo, J., Peterson, T. C., Renom, M., Oria Rojas, C., Rusticucci, M., Salinger, J., Elrayah, A. S., Sekele, S. S., Srivastava, A. K., Trewin, B., Villarroel, C., Vincent, L. A., Zhai, P., Zhang, X., & Kitching, S. (2013). Updated analyses of temperature and precipitation extreme indices since the beginning of the twentieth century: The HadEX2 dataset. *Journal of Geophysical Research: Atmospheres, 118*(5), 2098–2118. https://doi.org/10.1002/jgrd.50150.

Duan, R., Huang, G., Li, Y., Zhou, X., Ren, J., & Tian, C. (2021). Stepwise clustering future meteorological drought projection and multi-level factorial analysis under climate change: A case study of the Pearl River Basin, China. *Environmental Research, 196*, 110368. https://doi.org/10.1016/j.envres.2020.110368.

Feng, J., & Hu, D. (2014). How much does heat content of the western tropical Pacific Ocean modulate the South China Sea summer monsoon onset in the last four decades? *Journal of Geophysical Research: Oceans, 119*(7), 4029–4044. https://doi.org/10.1002/2013jc009683.

Fischer, E. M., & Knutti, R. (2014). Detection of spatially aggregated changes in temperature and precipitation extremes. *Geophysical Research Letters, 41*(2), 547–554. https://doi.org/10.1002/2013gl058499.

Fischer, E. M., & Knutti, R. (2016). Observed heavy precipitation increase confirms theory and early models. *Nature Climate Change, 6*(11), 986–991. https://doi.org/10.1038/nclimate3110.

Ghosh, S., Das, D., Kao, S. C., & Ganguly, A. R. (2012). Lack of uniform trends but increasing spatial variability in observed Indian rainfall extremes. *Nature Climate Change, 2*(2), 86–91. https://doi.org/10.1038/nclimate1327.

Gilli, M., & Këllezi, E. (2006). An application of extreme value theory for measuring financial risk. *Computational Economics, 27*(2-3), 207–228. https://doi.org/10.1007/s10614-006-9025-7.

Giorgi, F., Im, E.-S., Coppola, E., Diffenbaugh, N. S., Gao, X. J., Mariotti, L., & Shi, Y. (2011). Higher Hydroclimatic Intensity with Global Warming. *Journal of Climate, 24*(20), 5309–5324. https://doi.org/10.1175/2011jcli3979.1.

Gu, X., Zhang, Q., Singh, V. P., & Shi, P. (2017). Nonstationarity in timing of extreme precipitation across China and impact of tropical cyclones. *Global and Planetary Change, 149*, 153–165. https://doi.org/10.1016/j.gloplacha.2016.12.019, http://www.sciencedirect.com/science/journal/09218181.

Guptha, G. C., Swain, S., Al-Ansari, N., Taloor, A. K., & Dayal, D. (2021). Evaluation of an urban drainage system and its resilience using remote sensing and GIS. *Remote Sensing Applications: Society and Environment, 23*. https://doi.org/10.1016/j.rsase.2021.100601, http://www.journals.elsevier.com/remote-sensing-applications-society-and-environment/.

Gutjahr, O., Putrasahan, D., Lohmann, K., Jungclaus, J. H., Von Storch, J. S., Brüggemann, N., Haak, H., & Stössel, A. (2019). Max planck institute earth system model (MPI-ESM1.2) for the high-resolution model intercomparison project (HighResMIP). *Geoscientific Model Development, 12*(7), 3241–3281. https://doi.org/10.5194/gmd-12-3241-2019, http://www.geosci-model-dev.net/volumes_and_issues.html.

Hennessy, K. J., Gregory, J. M., & Mitchell, J. F. B. (1997). Changes in daily precipitation under enhanced greenhouse conditions. *Climate Dynamics, 13*(9), 667–680. https://doi.org/10.1007/s003820050189.

Horowitz, L. W., Naik, V., Sentman, L., Paulot, F., Blanton, C., McHugh, C., Radhakrishnan, A., Rand, K., Vahlenkamp, H., Zadeh, N. T., Wilson, C., Ginoux, P., He, J., John, J. G., Lin, M., Paynter, D. J., Ploshay, J., Zhang, A., & Zeng, Y. (2018). NOAA-GFDL GFDL-ESM4 model output prepared for CMIP6 AerChemMIP. *Earth System Grid Federation*. https://doi.org/10.22033/ESGF/CMIP6.1404.

Huntington, T. G. (2006). Evidence for intensification of the global water cycle: Review and synthesis. *Journal of Hydrology, 319*(1-4), 83–95. https://doi.org/10.1016/j.jhydrol.2005.07.003, http://www.elsevier.com/inca/publications/store/5/0/3/3/4/3.

Pickands III, J. (1975). Statistical inference using extreme order statistics. *The Annals of Statistics, 3*(1). https://doi.org/10.1214/aos/1176343003.

IPCC (2013a). Climate change 2013: The Physical science basis summary for policymakers (pp. 3–29). Cambridge University Press, Cambridge University Press.

IPCC (2013b). Climate Change 2013: The physical sciences basis. Cambridge University Press.

IPCC (2021). Climate Change 2021: The physical science basis contribution of working group i to the sixth assessment report of the intergovernmental panel on climate change. Cambridge University Press..

IPCC (2018). GlobalWarming of 1.58. Cambridge University Press.

Jacob, D., & Hagemann S. (2007). Intensification of the hydrological cycle—an important signal of climate change 170–173.

Jahanbaksh Asl, S., Khorshiddoust, A. M., Dinpashoh, Y., & Sarafrouzeh, F. (2013). Frequency analysis of climate extreme events in Zanjan, Iran. *Stochastic Environmental Research and Risk Assessment, 27*(7), 1637–1650. https://doi.org/10.1007/s00477-013-0701-6.

Karl, T. R., & Knight, R. W. (1998). Secular trends of precipitation amount, frequency, and intensity in the United States. 2 *Bulletin of the American Meteorological Society, 79*, 231–241. 2 http://ams.allenpress.com.

Kharin, V. V., Flato, G. M., Zhang, X., Gillett, N. P., Zwiers, F., & Anderson, K. J. (2018). Risks from climate extremes change differently from 1.5 C to 2.0 C depending on rarity. *Earth's Future, 6*(5), 704–715.

Kharin, V. V., Zwiers, F. W., Zhang, X., & Wehner, M. (2013). Changes in temperature and precipitation extremes in the CMIP5 ensemble. *Climatic Change, 119*(2), 345–357. https://doi.org/10.1007/s10584-013-0705-8.

Kim, Y. H., Min, S. K., Zhang, X., Zwiers, F., Alexander, L. V., Donat, M. G., & Tung, Y. S. (2016). Attribution of extreme temperature changes during 1951–2010. *Climate Dynamics, 46*(5-6), 1769–1782. https://doi.org/10.1007/s00382-015-2674-2, http://link.springer.de/link/service/journals/00382/index.htm.

Knutti, R., Allen, M. R., Friedlingstein, P., Gregory, J. M., Hegerl, G. C., Meehl, G. A., Meinshausen, M., Murphy, J. M., Plattner, G. K., Raper, S. C. B., Stocker, T. F., Stott, P. A., Teng, H., & Wigley, T. M. L. (2008). A review of uncertainties in global temperature projections over the twenty-first century. *Journal of Climate, 21*(11), 2651–2663. https://doi.org/10.1175/2007JCLI2119.1Switzerland, http://ams.allenpress.com/archive/1520-0442/21/11/pdf/i1520-0442-21-11-2651.pdf.

Kodinariya, T. M., & Makwana, P. R. (2013). Review on determining number of Cluster in K-Means Clustering, 1.

Kyselý, J., Picek, J., & Beranová, R. (2010). Estimating extremes in climate change simulations using the peaks-over-threshold method with a non-stationary threshold. *Global and Planetary Change, 72*(1-2), 55–68. https://doi.org/10.1016/j.gloplacha.2010.03.006.

Lehner, B., Verdin, K., & Jarvis, A. (2008). New global hydrography derived from spaceborne elevation data. *EOS (Rome, Italy), 89*(10), 93–94. https://doi.org/10.1029/2008EO100001.

Li, C., Zhang, X., Zwiers, F., Fang, Y., & Michalak, A. M. (2017). Recent very hot summers in northern hemispheric land areas measured by wet bulb globe temperature will be the norm within 20 years. *Earth's Future, 5*(12), 1203–1216. https://doi.org/10.1002/2017EF000639, http://onlinelibrary.wiley.com/journal/10.1002/(ISSN)2328-4277.

Lorenz, R., Stalhandske, Z., & Fischer, E. M. (2019). Detection of a climate change signal in extreme heat, heat stress, and cold in europe from observations. *Geophysical Research Letters, 46*(14), 8363–8374. https://doi.org/10.1029/2019GL082062, http://agupubs.onlinelibrary.wiley.com/hub/journal/10.1002/(ISSN)1944-8007/.

Lovato, T., Peano, D., Butenschön, M., Materia, S., Iovino, D., Scoccimarro, E., Fogli, P. G., Cherchi, A., Bellucci, A., Gualdi, S., Masina, S., & Navarra, A. (2022). CMIP6 simulations with the CMCC earth system model (CMCC-ESM2). *Journal of Advances in Modeling Earth Systems, 14*(3). https://doi.org/10.1029/2021ms002814.

Madakumbura, G. D., Kim, H., Utsumi, N., Shiogama, H., Fischer, E. M., Seland, Ø., Scinocca, J. F., Mitchell, D. M., Hirabayashi, Y., & Oki, T. (2019). Event-to-event intensification of the hydrologic cycle from 1.5 °C to a 2 °C warmer world. *Scientific Reports, 9*(1). https://doi.org/10.1038/s41598-019-39936-2, https://www.nature.com/srep/index.html.

Min, S. K., Zhang, X., Zwiers, F. W., & Hegerl, G. C. (2011). Human contribution to more-intense precipitation extremes. *Nature, 470*(7334), 378–381. https://doi.org/10.1038/nature09763, http://www.nature.com/nature/index.html.

Mishra, V., Ganguly, A. R., Nijssen, B., & Lettenmaier, D. P. (2015). Changes in observed climate extremes in global urban areas. *Environmental Research Letters, 10*(2). https://doi.org/10.1088/1748-9326/10/2/024005, http://iopscience.iop.org/1748-9326/10/2/024005/pdf/1748-9326_10_2_024005.pdf.

Mishra, V., Wallace, J. M., & Lettenmaier, D. P. (2012). Relationship between hourly extreme precipitation and local air temperature in the United States. *Geophysical Research Letters, 39*(16). https://doi.org/10.1029/2012GL052790, http://onlinelibrary.wiley.com/journal/10.1002/(ISSN)1944-8007/issues?year=2012.

Mukherjee, S., Aadhar, S., Stone, D., & Mishra, V. (2018). Increase in extreme precipitation events under anthropogenic warming in India. *Weather and Climate Extremes, 20*, 45–53. https://doi.org/10.1016/j.wace.2018.03.005, http://www.journals.elsevier.com/weather-and-climate-extremes/.

Nandi, S., & Swain, S. (2023). Analysis of heatwave characteristics under climate change over three highly populated cities of South India: A CMIP6-based assessment. *Environmental Science and Pollution Research, 30*(44), 99013–99025. https://doi.org/10.1007/s11356-022-22398-x, https://www.springer.com/journal/11356.

Osborn, T. J., Hulme, M., Jones, P. D., & Basnett, T. A. (2000). Observed trends in the daily intensity of United Kingdom precipitation. *International Journal of Climatology, 20*(4), 347–364. https://doi.org/10.1002/(SICI)1097-0088(20000330)20:4<347::AID-JOC475>3.0.CO;2-C.

Papalexiou, S. M., & Montanari, A. (2019). Global and regional increase of precipitation extremes under global warming. *Water Resources Research, 55*(6), 4901–4914. https://doi.org/10.1029/2018WR024067, http://agupubs.onlinelibrary.wiley.com/hub/journal/10.1002/(ISSN)1944-7973/.

Patel, P., Thakur, P. K., Aggarwal, S. P., Garg, V., Dhote, P. R., Nikam, B. R., Swain, S., & Al-Ansari, N. (2022). Revisiting 2013 Uttarakhand flash floods through hydrological evaluation of precipitation data sources and morphometric prioritization. *Geomatics, Natural Hazards and Risk, 13*(1), 646–666. https://doi.org/10.1080/19475705.2022.2038696, http://www.tandfonline.com/toc/tgnh20/current.

Paxian, A., Hertig, E., Seubert, S., Vogt, G., Jacobeit, J., & Paeth, H. (2015). Present-day and future mediterranean precipitation extremes assessed by different statistical approaches. *Climate Dynamics, 44*(3-4), 845–860. https://doi.org/10.1007/s00382-014-2428-6.

Pisarenko, V. F., & Sornette, D. (2003). Characterization of the frequency of extreme earthquake events by the generalized pareto distribution. *Pure and Applied Geophysics, 160*(12), 2343–2364. https://doi.org/10.1007/s00024-003-2397-x.

Prasanna, V. (2018). Statistical bias correction method applied on CMIP5 datasets over the Indian region during the summer monsoon season for climate change applications. *Theoretical and Applied Climatology, 131*(1-2), 471–488. https://doi.org/10.1007/s00704-016-1974-8.

Räty, O., Räisänen, J., & Ylhäisi, J. S. (2014). Evaluation of delta change and bias correction methods for future daily precipitation: Intermodel cross-validation using ENSEMBLES simulations. *Climate Dynamics, 42*(9-10), 2287–2303. https://doi.org/

10.1007/s00382-014-2130-8, http://link.springer.de/link/service/journals/00382/index.htm.

Ring, M. J., Lindner, D., F. Cross, E., & E. Schlesinger, M. (2012). Causes of the global warming observed since the 19th century. *Atmospheric and Climate Sciences, 02*(04), 401–415. https://doi.org/10.4236/acs.2012.24035.

Rosenzweig, C., Solecki, W., Hammer, S. A., & Mehrotra, S. (2010). Cities lead the way in climate-change action. *Nature, 467*(7318), 909–911. https://doi.org/10.1038/467909a.

Roy, S. S., & Balling, R. C. (2004). Trends in extreme daily precipitation indices in India. *International Journal of Climatology, 24*(4), 457–466. https://doi.org/10.1002/joc.995.

Sahoo, S., Majumder, A., Swain, S., Gareema, Pateriya, B., & Al-Ansari, N. (2022). Analysis of decadal land use changes and its impacts on urban heat island (UHI) using remote sensing-based approach: Asmart city perspective. *Sustainability, 14*(19), 11892. https://doi.org/10.3390/su141911892.

Salarpour, M., Yusop, Z., & Yusof, F. (2012). Modeling the distributions of flood characteristics for a tropical river basin. *Journal of Environmental Science and Technology, 5*(6), 419.

Seneviratne, S. I., Nicholls, N., Easterling, D., Goodess, C. M., Kanae, S., Kossin, J., Luo, Y., Marengo, J., Mc Innes, K., Rahimi, M., Reichstein, M., Sorteberg, A., Vera, C., Zhang, X., Rusticucci, M., Semenov, V., Alexander, L. V., Allen, S., Benito, G., Cavazos, T., Clague, J., Conway, D., Della-Marta, P. M., Gerber, M., Gong, S., Goswami, B. N., Hemer, M., Huggel, C., Van den Hurk, B., Kharin, V. V., Kitoh, A., Klein Tank, A. M. G., Li, G., Mason, S., Mc Guire, W., Van Oldenborgh, G. J., Orlowsky, B., Smith, S., Thiaw, W., Velegrakis, A., Yiou, P., Zhang, T., Zhou, T., & Zwiers, F. W. (2012). Changes in climate extremes and their impacts on the natural physical environment. In *Managing the risks of extreme events and disasters to advance climate change adaptation: special report of the intergovernmental panel on climate change*. Switzerland: Cambridge University Press, 109–230. http://doi.org/10.1017/CBO9781139177245, http://doi.org/10.1017/CBO9781139177245.006.

Shao, Y., Wu, J., Ye, J., & Liu, Y. (2015). Frequency analysis and its spatiotemporal characteristics of precipitation extreme events in China during 1951–2010. *Theoretical and Applied Climatology, 121*(3-4), 775–787. https://doi.org/10.1007/s00704-015-1481-3, http://link.springer.de/link/service/journals/00704/.

Sharma, S., & Mujumdar, P. P. (2019). On the relationship of daily rainfall extremes and local mean temperature. *Journal of Hydrology, 572*, 179–191. https://doi.org/10.1016/j.jhydrol.2019.02.048.

Shen, L., Wen, J., & Zhang, Y. (2022). Changes in population exposure to extreme precipitation in the Yangtze River Delta. *Climate Services, 27*. https://doi.org/10.1016/j.cliser.2022.100317.

Shiu, C. J., Liu, S. C., Fu, C., Dai, A., & Sun, Y. (2012). How much do precipitation extremes change in a warming climate? *Geophysical Research Letters, 39*(17). https://doi.org/10.1029/2012GL052762, http://onlinelibrary.wiley.com/journal/10.1002/(ISSN)1944-8007/issues?year=2012.

Solomon, S., Qin, D., Manning, M., Chen, Z., Marquis, M., Averyt, K. B., Tignor, M., & Miller H. L.(2007). IPCC, Climate Change 2007: The physical science basis contribution of working group I to the fourth assessment report of the intergovernmental panel on climate change (pp. 98–101).

Stouffer, R. J., Eyring, V., Meehl, G. A., Bony, S., Senior, C., Stevens, B., & Taylor, K. E. (2017). CMIP5 Scientific Gaps and Recommendations for CMIP6. *Bulletin of the American Meteorological Society, 98*(1), 95–105. https://doi.org/10.1175/bams-d-15-00013.1.

Sugahara, S., da Rocha, R. P., & Silveira, R. (2009). Non-stationary frequency analysis of extreme daily rainfall in Sao Paulo, Brazil. *International Journal of Climatology, 29*(9),

1339–1349. https://doi.org/10.1002/joc.1760Brazil, http://www3.interscience.wiley.com/cgi-bin/fulltext/121542918/PDFSTART.

Swain, S., Mishra, S. K., Pandey, A., Dayal, D., & Srivastava, P. K. (2022d). Appraisal of historical trends in maximum and minimum temperature using multiple non-parametric techniques over the agriculture-dominated Narmada Basin, India. *Environmental Monitoring and Assessment, 194*(12). https://doi.org/10.1007/s10661-022-10534-6, https://www.springer.com/journal/10661.

Swain, S., Mishra, S. K., Pandey, A., & Dayal, D. (2022a). Assessment of drought trends and variabilities over the agriculture-dominated Marathwada Region, India. *Environmental Monitoring and Assessment, 194*(12). https://doi.org/10.1007/s10661-022-10532-8, https://www.springer.com/journal/10661.

Swain, S., Mishra, S. K., Pandey, A., & Dayal, D. (2022b). Spatiotemporal assessment of precipitation variability, seasonality, and extreme characteristics over a Himalayan catchment. *Theoretical and Applied Climatology, 147*(1-2), 817–833. https://doi.org/10.1007/s00704-021-03861-0, https://rd.springer.com/journal/volumesAndIssues/704.

Swain, S., Mishra, S. K., & Pandey, A. (2022). Assessing spatiotemporal variation in drought characteristics and their dependence on timescales over Vidarbha Region, India. *Geocarto International, 37*(27), 17971–17993. https://doi.org/10.1080/10106049.2022.2136260, http://www.tandfonline.com/toc/tgei20/current.

Tarhule, A. (2005). Damaging rainfall and flooding: The other sahel hazards. *Climatic Change, 72*(3), 355–377. https://doi.org/10.1007/s10584-005-6792-4.

Teutschbein, C., & Seibert, J. (2012). Bias correction of regional climate model simulations for hydrological climate-change impact studies: Review and evaluation of different methods. *Journal of Hydrology, 456-457*, 12–29. https://doi.org/10.1016/j.jhydrol.2012.05.052.

Trenberth, K. E. (2011). Changes in precipitation with climate change. *Climate Research, 47*(1-2), 123–138. https://doi.org/10.3354/cr00953, http://www.int-res.com/articles/cr_oa/c047p123.pdf.

Trenberth, K. E., Dai, A., Rasmussen, R. M., & Parsons, D. B. (2003). The changing character of precipitation. *Bulletin of the American Meteorological Society, 84*(9), 1161–1205. https://doi.org/10.1175/BAMS-84-9-1205.

Tschöke, G. V., Kruk, N. S., de Queiroz, P. I. B., Chou, S. C., & de Sousa Junior, W. C. (2017). Comparison of two bias correction methods for precipitation simulated with a regional climate model. *Theoretical and Applied Climatology, 127*(3–4), 841–852. https://doi.org/10.1007/s00704-015-1671-z, http://link.springer.de/link/service/journals/00704/.

Ullah, S., You, Q., Zhang, Y., Bhatti, A. S., Ullah, W., Hagan, D. F. T., Ali, A., Ali, G., Jan, M. A., Khan, S. N., & Ali, A. (2020). Evaluation of CMIP5 models and projected changes in temperatures over South Asia under global warming of 1.5 oC, 2 oC, and 3 oC. *Atmospheric Research, 246*, 105122. https://doi.org/10.1016/j.atmosres.2020.105122.

Um, M. J., Cho, W., & Heo, J. H. (2010). A comparative study of the adaptive choice of thresholds in extreme hydrologic events. *Stochastic Environmental Research and Risk Assessment, 24*(5), 611–623. https://doi.org/10.1007/s00477-009-0348-5.

Varga, L., Rakonczai, P., & Zempléni, A. (2016). Applications of threshold models and the weighted bootstrap for Hungarian precipitation data. *Theoretical and Applied Climatology, 124*(3-4), 641–652. https://doi.org/10.1007/s00704-015-1438-6, http://link.springer.de/link/service/journals/00704/.

Virginia Department of Environmental Quality (VDEQ). (2021). *Virginia's Greenhouse Gas Inventory: 1990-2019*. Virginia Department of Environmental Quality.

Wang, X. L., Trewin, B., Feng, Y., & Jones, D. (2013). Historical changes in Australian temperature extremes as inferred from extreme value distribution analysis. *Geophysical*

Research Letters, 40(3), 573–578. https://doi.org/10.1002/grl.50132, http://onlinelibrary.wiley.com/journal/10.1002/(ISSN)1944-8007/issues?year=2012.

Wang, Z., Zhong, R., Lai, C., Zeng, Z., Lian, Y., & Bai, X. (2018). Climate change enhances the severity and variability of drought in the Pearl River Basin in South China in the 21st century. *Agricultural and Forest Meteorology, 249*, 149–162. https://doi.org/10.1016/j.agrformet.2017.12.077.

Wehner, M. F. (2020). Characterization of long period return values of extreme daily temperature and precipitation in the CMIP6 models: Part 2, projections of future change. *Weather and Climate Extremes, 30*, 100284. https://doi.org/10.1016/j.wace.2020.100284.

Wi, S., Valdés, J. B., Steinschneider, S., & Kim, T. W. (2016). Non-stationary frequency analysis of extreme precipitation in South Korea using peaks-over-threshold and annual maxima. *Stochastic Environmental Research and Risk Assessment, 30*(2), 583–606. https://doi.org/10.1007/s00477-015-1180-8, http://link.springer-ny.com/link/service/journals/00477/index.htm.

Wu, T., Yu, R., Lu, Y., Jie, W., Fang, Y., Zhang, J., Zhang, L., Xin, X., Li, L., Wang, Z., Liu, Y., Zhang, F., Wu, F., Chu, M., Li, J., Li, W., Zhang, Y., Shi, X., Zhou, W., Yao, J., Liu, X., Zhao, H., Yan, J., Wei, M., Xue, W., Huang, A., Zhang, Y., Zhang, Y., Shu, Q., & Hu, A. (2021). BCC-CSM2-HR: A high-resolution version of the Beijing Climate Center Climate System Model. *Geoscientific Model Development, 14*(5), 2977–3006. https://doi.org/10.5194/gmd-14-2977-2021.

Yilmaz, A. G., Hossain, I., & Perera, B. J. C. (2014). Effect of climate change and variability on extreme rainfall intensity–frequency–duration relationships: A case study of Melbourne. *Hydrology and Earth System Sciences, 18*(10), 4065–4076. https://doi.org/10.5194/hess-18-4065-2014.

Yilmaz, A. G. (2015). The effects of climate change on historical and future extreme rainfall in Antalya, Turkey. *Hydrological Sciences Journal, 60*(12), 2148–2162. https://doi.org/10.1080/02626667.2014.945455.

Zhan, W., He, X., Sheffield, J., & Wood, E. F. (2020). Projected seasonal changes in large-scale global precipitation and temperature extremes based on the CMIP5 ensemble. *Journal of Climate, 33*(13), 5651–5671. https://doi.org/10.1175/jcli-d-19-0311.1.

Zhang, X., Alexander, L., Hegerl, G. C., Jones, P., Tank, A. K., Peterson, T. C., Trewin, B., & Zwiers, F. W. (2011). Indices for monitoring changes in extremes based on daily temperature and precipitation data. *Wiley Interdisciplinary Reviews: Climate Change, 2*(6), 851–870. https://doi.org/10.1002/wcc.147, http://onlinelibrary.wiley.com/journal/10.1002/(ISSN)1757-7799.

Zhao, N., Yue, T., Li, H., Zhang, L., Yin, X., & Liu, Y. (2018). Spatio-temporal changes in precipitation over Beijing-Tianjin-Hebei region, China. *Atmospheric Research, 202*, 156–168. https://doi.org/10.1016/j.atmosres.2017.11.029, http://www.elsevier.com/inca/publications/store/5/0/3/3/2/3/index.htt.

Zhou, X., Huang, G., Wang, X., & Cheng, G. (2018). Future changes in precipitation extremes over Canada: Driving factors and inherent mechanism. *Journal of Geophysical Research: Atmospheres, 123*(11), 5783–5803. https://doi.org/10.1029/2017jd027735.

Zhu, Y. Y., & Yang, S. (2020). Evaluation of CMIP6 for historical temperature and precipitation over the Tibetan Plateau and its comparison with CMIP5. *Advances in Climate Change Research, 11*(3), 239–251. https://doi.org/10.1016/j.accre.2020.08.001, http://www.sciencedirect.com/science/journal/aip/16749278.

Zwiers, F. W., Zhang, X., & Feng, Y. (2011). Anthropogenic influence on long return period daily temperature extremes at regional scales. *Journal of Climate, 24*(3), 881–892. https://doi.org/10.1175/2010JCLI3908.1Canada, http://journals.ametsoc.org/doi/pdf/10.1175/2010JCLI3908.1.

World Meteorological Organization (WMO). (2021). *WMO atlas of mortality and economic losses from weather, climate and water extremes (1970–2019) (WMO-No. 1267)*. Geneva, Switzerland. [2022-10-14]. https://library.wmo.int/index.php?lvl=notice_display&id=21930#.Y0uvcnbP2Uk.

Maurer, E.P., Wood, A.W., Adam, J.C., Lettenmaier, D.P., & Nijssen, B. (2002). A long-term hydrologically based dataset of land surface fluxes and states for the conterminous United States. *Journal of Climate*, *15*(22), 3237-3251. https://doi.org/10.1175/1520-0442(2002)015 < 3237:althbd > 2.0.co;2.

CHAPTER NINETEEN

Integrated modeling, prediction, and analysis of climate drought and groundwater quality: a comprehensive study of 609 sites in Iran

Soroosh Sharifi[1], **and Saeed Azimi**[2]
[1]Civil Engineering Department, University of Birmingham, Birmingham, United Kingdom
[2]Civil Engineering Department, Iran University of Science and Technology, Tehran, Iran

19.1 Introduction

A fundamental requirement for sustainable water resource planning is the accurate prediction of water availability for agricultural, industrial, and urban applications. This is particularly crucial in arid and semiarid regions, where the contribution of permanent surface water flows to groundwater recharge is minimal. In such regions, precipitation plays a significant role in either replenishing water reserves or, conversely, in exacerbating drought conditions that lead to a decline in groundwater quality (Nasrabadi and Bidabadi). Drought events alter water availability, leading to resource shortages that impact various sectors of society, particularly those reliant on groundwater. Therefore, predicting the hydrological behavior of each region over different timeframes is essential for effective planning and sustainable resource management through reliable methodologies.

Among natural disasters, drought has a profound impact on multiple aspects of human life and the environment (Jalalkamali et al., 2015). Over the past few decades, artificial intelligence (AI) techniques have been increasingly recognized as effective tools for forecasting natural phenomena. However, predicting the occurrence of spatial drought events, and specifically in this study, forecasting the likelihood of negative changes in the drinking water quality index of groundwater resources, remains a

Drought Dynamics
DOI: https://doi.org/10.1016/B978-0-443-34205-9.00015-9
© 2026 Elsevier Inc. All rights are reserved, including those for text and data mining, AI training, and similar technologies.

complex challenge. It is nearly impossible to predict these changes with full certainty based solely on empirical relationships between various environmental parameters and variables. Similarly, water resource management is highly dependent on an accurate understanding of the future status of water availability in a given region, which is crucial for urban and agricultural planning (Eberhard & Hamawand, 2017). Groundwater levels are undergoing rapid fluctuations, necessitating the continuous identification of new sources to meet the demand (Bajc et al., 2017). Given that groundwater reservoirs serve multiple purposes—including drinking water supply, irrigation, and industrial use—predicting variations in water quality parameters is essential for implementing appropriate management interventions. Such predictions should ideally be conducted on at least an annual basis to support informed decision-making and ensure resource sustainability (Mosaferi et al., 2014).

Drought is defined as a prolonged period of water scarcity, affecting one or more components of the hydrological cycle such as precipitation, river discharge, or groundwater recharge. It occurs when the available water in a given system is insufficient to meet the biological, economical, and social demands over an extended period (Tabari et al., 2013). Despite the absence of a universally accepted definition of drought, the phenomenon can still be assessed using climate indicators. These indicators provide a quantitative basis for identifying the onset and termination of droughts, as well as for determining their severity (Tsakiris et al., 2007). Currently, the most widely used method for analyzing drought events is based on precipitation data, which serves as a key determinant of different drought types (Brekhovskikh et al., 2009). In scientific literature, the most extensive research on drought assessment focuses on climate droughts, largely due to the comprehensive availability of rainfall data and its strong correlation with other drought-related factors (Ferral et al., 2017). A quantitative assessment of drought requires a well-defined index capable of precisely distinguishing between wet and dry periods, thereby ensuring accurate monitoring and management (Da Silva, 2004).

This study is structured into three main components:

1. **Prediction of groundwater quality decline:** This section investigates the probability of declining groundwater quality in relation to drought occurrences (i.e., reductions in aquifer water levels) using artificial neural networks (ANNs) and fuzzy clustering methods. The primary objective is to generate a spatial distribution map depicting the likelihood of negative changes in groundwater quality indices due to

drought. To achieve this, it was first necessary to use digitized observational data to evaluate the potential drinking water quality across Iranian plains, employing geographic information systems (GIS) in accordance with Schuler and World Health Organization (WHO) standards. Using the analytical hierarchy process (AHP) method, groundwater quality indices were analyzed over a ten-year interval. The optimal zoning model was identified by comparing standard errors, and a rasterized layer was extracted to assess groundwater quality potential. Five key parameters—total hardness (TH), total dissolved solids (TDS), sodium (Na), chloride (Cl), and sulfate (SO4)—were used to calculate groundwater quality potential. Additionally, to compute the groundwater resource index (GRI), standard drought classes were established for all 11,383 wells across Iranian aquifers. A continuous GRI index layer was then generated using the geostatistical tool, with the most suitable zoning method selected based on the comparison of samples recorded between 1994 and 2023 (Azimi et al., 2019).

2. **Association analysis of climate drought and groundwater quality decline:** The second component of this study involves an association analysis between climate drought and groundwater quality degradation using Gaussian process classification (GPC) and back-propagation (BP) artificial neural networks. This methodology aims to establish a decision-making framework for minimizing uncertainty in water resource management calculations, particularly for optimizing groundwater management strategies. The calculations are based on historical rainfall data and aquifer water levels recorded across Iran between 2013 and 2023. The dataset includes maximum synoptic station readings and groundwater observation well measurements. Groundwater levels from 609 study plains in Iran were used to predict drought conditions over the test period spanning 2023 to 2027. The artificial intelligence methods were implemented within a Python coding environment to compute annual precipitation rates. The accuracy of the predictions was validated through statistical analyzes of rasterized zoning map cells. By examining the correlation between groundwater quality deterioration in Iranian aquifers and periods of groundwater drought, the study validates its findings through an analysis of climate drought effects using the standardized precipitation index (SPI) and the GRI (Azimi et al., 2020).
3. **Predictive modeling of future drought impacts on groundwater quality:** The third part of this study extends the previous analyzes by

developing a predictive model that estimates future drought impacts on groundwater quality. Again, utilizing GPC and BP artificial neural networks, this segment aims to refine decision-making processes and reduce uncertainties in groundwater management. The analysis leverages historical rainfall and aquifer water level data collected between 2013 and 2023 from Iran's synoptic stations and groundwater observation wells. Groundwater levels across the 609 study plains are utilized to project drought conditions from 2023 to 2027, employing Python-based AI modeling. The results are further validated through a statistical summary of rasterized zoning map cells. At the conclusion of this study, it is anticipated that high-risk aquifers, along with specific Iranian regions most susceptible to severe drought stress, will be identified with minimal overall error. The study's predictions are confirmed through an analysis of climate drought effects using the SPI and their correlation with observed groundwater drought occurrences based on the GRI (Azimi et al., 2018).

By integrating AI techniques with geospatial analysis, this study aims to enhance predictive accuracy in groundwater management and improve methodologies for assessing climate-induced groundwater quality deterioration. The findings will provide policymakers and water resource managers with critical insights for formulating adaptive strategies to mitigate the adverse effects of climate change on groundwater resources.

19.2 Background

Over the years, extensive research has been conducted on the application of ANNs in predicting groundwater levels and assessing water quality. Daliakopoulos et al. (2005) employed various ANN structures to forecast groundwater levels, concluding that the Levenberg-Marquardt model demonstrated superior predictive accuracy. Similarly, Lallahem et al. (2005) utilized ANNs to estimate the time required to determine groundwater levels in a piezometer, and identify the multilayer perceptron network as the most efficient model with minimal latency.

Chandramouli et al. (2007) explored optimal training iterations for backpropagation neural networks (BPNN), revealing that excessive or insufficient training could lead to inaccurate predictions. Mishra and Singh (2009) developed a model to analyze the impact of climate on severity-area-frequency (SAF) curves for annual droughts in the Kansabati river,

India. Their study employed a Bayesian neural network (BNN) for downscaling general circulation model (GCM) predictions under uncertainty, indicating a significant increase in severe drought probabilities between 2001 and 2050 compared to historical data.

In the field of water quality assessment, Sakizadeh (2016) applied ANNs to predict the WQI from 2006 to 2013. Banerjee et al. (2011) introduced an artificial neural skeleton model for forecasting groundwater salinity, while Hosseini-Moghari et al. (2015) employed a fuzzy water quality index (FWQI) to evaluate groundwater quality. Additionally, Shamsuddin et al. (2017) demonstrated that ANNs could accurately predict groundwater levels one day in advance, accounting for river–aquifer interactions near the Langat river.

Nourani (2017) implemented emotional ANN (EANN) models to simulate daily rainfall-runoff processes, reporting improvements of up to 13% in training accuracy and 34% in predictive performance compared to traditional feedforward neural networks (FFNNs). Ahmad et al. (2017) developed a dynamic ANN model for estimating water quality indicators in the Perak river basin, achieving high accuracy with R-squared values of 90% and 93% and mean squared error (MSE) reductions of 17% and 11.5%, respectively.

Qaderi and Babanejad (2017) applied ANN techniques to predict groundwater quality and assess the economic costs of drinking water treatment over a 13-year period in Ilam, Iran. Their findings showed that an ANN model trained using the Levenberg-Marquardt algorithm significantly reduced daily treatment costs. Charulatha et al. (2017) explored regression and ANN models for assessing groundwater pollutants, particularly nitrite ion concentrations, demonstrating high efficiency in prediction. Sahoo et al., 2017 proposed Bayesian and entropy-based methods for water quality evaluation, concluding that the WQI improved during dry periods due to reduction in pollutant concentration.

Overall, these studies underscore the effectiveness of AI, particularly ANNs, in predicting groundwater level variations and assessing water quality. By leveraging machine learning techniques, researchers have been able to enhance forecasting accuracy, optimize resource management, and develop robust decision-making frameworks for mitigating drought impacts and ensuring sustainable water supplies.

19.3 Materials and methods

19.3.1 Study area

This study focuses on the geographical extent of Iran, spanning between 25° to 40° North latitude and 44° to 64° East longitude. The research encompasses 609 plains across the country, covering approximately 567,828 km^2. Iran exhibits diverse climatic conditions, ranging from arid and semiarid regions in the central and southern parts to humid areas in the northern regions. This variation, along with distinct geological structures and aquifer characteristics, poses significant challenges in groundwater resource management. Iranian aquifers are categorized as semi-confined or unconfined systems, with their hydrological responses influenced by both natural and anthropogenic factors. The western regions, characterized by high population densities, experience direct human impact on groundwater resources, while the eastern and central parts primarily rely on surface water interactions for aquifer recharge. Fig. 19.1 represents the spatial distribution of Iran's aquifers and plains.

19.3.2 Methodological approach

The research employs AI-based modeling techniques to assess groundwater quality deterioration and its association with climate-induced drought. The study integrates the radial basis function neural network (RBFNN), probabilistic neural network (PNN), and fuzzy logic clustering (FLC) to predict groundwater quality trends. Additionally, the ArcSDM extension within a GIS environment and the GeoXplore software were utilized for spatial analysis and data processing.

19.3.2.1 Fuzzy clustering approach

Clustering a set of components by a learning system based on their characteristic vector is a powerful tool for gaining knowledge based on observations stored in data files (Milligan, 1996). Given a collection of vector properties, in a self-organization process, they are converted into classes with similar values of properties, with a process of divisive or down-to-top clustering. A class can also be set up under a supervised training process in which any input vector is labeled and parameters are processed until the output is learned for each input vector, consistent with the target output.

Suppose a set of property vectors (Q) $\{x(q)$: $q = 1,\ldots,Q\}$ which is converted to clusters $\{Ck$: $k=1,\ldots,K\}$. For the kth cluster, C_k is a sample

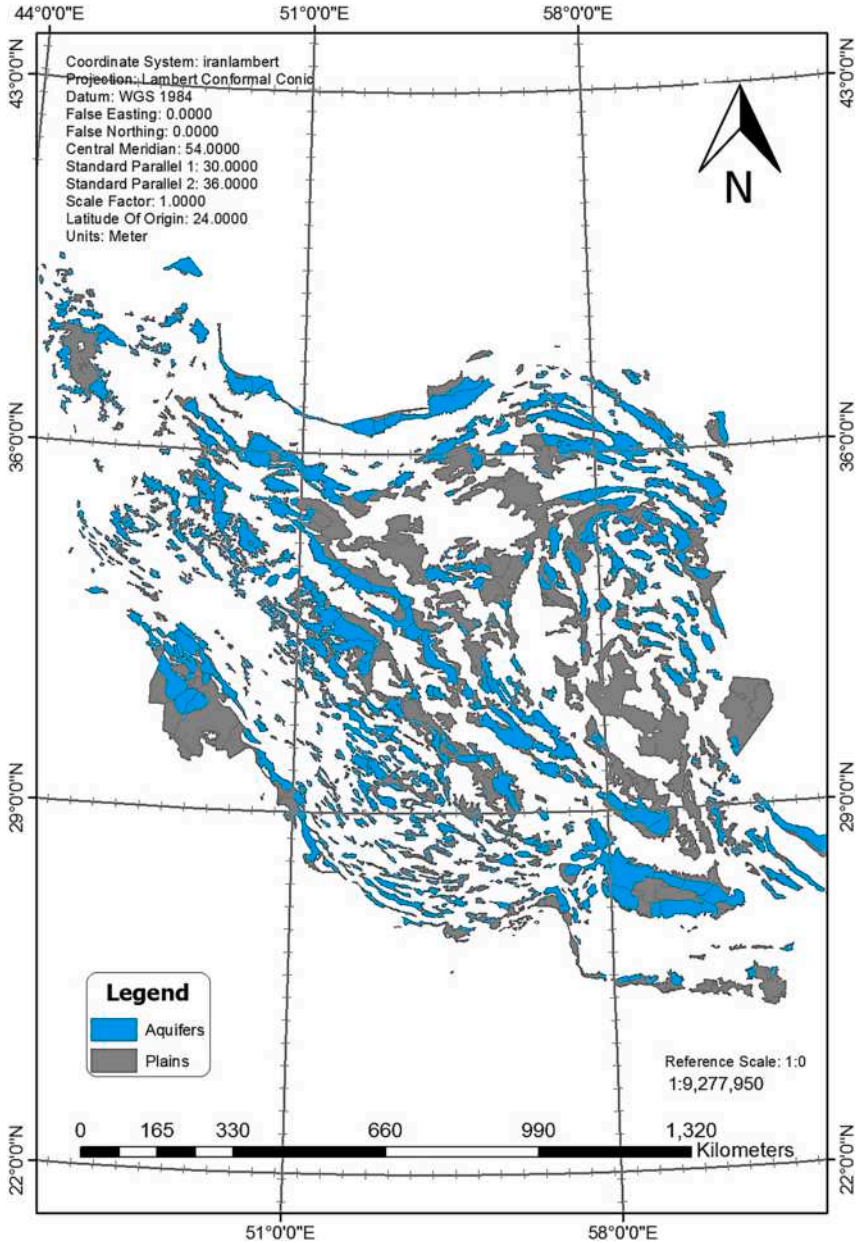


Figure 19.1 Location of study area including the aquifers and plains of Iran. Map lines delineate study areas and do not necessarily depict accepted national boundaries.

determined by $C(k)$. The dimensional of the component vector $x(q)=(x1(q),\ldots,xN(q))$ and the centers $c(k)=(c1(k),\ldots,cN(k))$ equals to N. The feature vectors are standardized in an independent way in each section, and so the vectors are in the N-dimensional cube [0,1] N.

19.3.2.2 Validation of cluster selection

Hub-shaped vectors do not have a uniform distribution of cluster structure (Milligan & Hirtle, 2003). But if sets of vectors fall into multiple subsets; these subsets are compressed around their distribution centers, then they are in a strong clustering structure. It will be accepted that such clustering is organized and properly disassociated. The measurement of cluster validity provides the value of clustering superiority (Pal & Bezdek, 1995). Some general measures for cluster validity are partition coefficients (PCs), classification entropy (CEs), and proportional exponent (PE). Uniform distribution functional (UDF) is another criterion pointed out by. UDF is in fact a product of compactness and separation. The relative compression-separation coefficient for a larger number of K is defined in (19.1).

$$\nu = \frac{\frac{1}{K}\sum_{K=1}^{K}\sigma_k^2}{D_{\min}^2}; \sigma_k^2 \sum_{q=1}^{Q} W_{kq} \,||\, x^{(q)} - c^{(k)} \,||^2, \; k = 1, \ldots, K \quad (19.1)$$

where D_{min} is least distance between the samples (center of the cluster) and is the fuzzy variance of the weight of the Kth cluster. The larger D_{min} means a lower cross-reference. Each is smaller for compact clusters. Consequently, the lower value of ν means more compression and separation. In measuring the Xie-Beni fuzzy validity, only the members of each cluster are changed instead of all Q samples for each cluster. It is also mutually, so a larger value of K represents a better clustering, and K is a measure of the Xie-Beni cluster's validity.

19.3.2.3 Fuzzy clustering

The weighted fuzzy expected value (WFEV) is defined as a set of real values of $X1, \ldots, Xp$ as a sample value representing a comprehensive representation of medium or intermediate categories (Schneider & Craig, 1992). This is done exponentially with the use of two-sided reduction and dip, but in this calculation, instead of the tangent, the shape of the Gaussian function is used in Eq. (19.2). The reason is that a membership function is a conventional fuzzy set for the "near-center" variable. After calculating the arithmetic mean of a set of real values, $X1, \ldots, Xp$ is used as the value of the primary center, so that to obtain a new value using Picard iteration.

$$\mu^{(r+1)} = \sum_{p=1}^{P} \alpha_p^{(r)} X_p, \qquad (\sigma^2)^{(r+1)} = \sum_{p=1}^{P} \alpha_p^{(r)} (X_p - \mu^{(r)})^2 \tag{19.2}$$

$$\alpha_p^{(r)} = \exp\left(\frac{-(X_p - \mu^{(r)})^2}{(2\sigma^2)^{(r)}}\right) \Big/ \left(\sum_{m=1}^{P} \exp\left(\frac{-(X_p - \mu^{(r)})^2}{(2\sigma^2)^{(r)}}\right)\right) \tag{19.3}$$

The value means the modified convergence process with the fuzzy expectation value. In spatial computing tools, these outcomes are also used as an expanded and more efficient approach.

19.3.2.4 Radial basis function artificial neural networks

A popular type of artificial neural network can be introduced as a radial basis function (RBF). RBF networks, which are the most used ones, require a greater number of nerve units, but their superiority lies in shorter design time than standard backpropagation networks. These networks have a remarkable performance when training vectors are very large.

RBF networks require a lot of neurons to train, and in the same way, the performance of these networks is best done by using a large number of training vectors. In these networks, unlike the common training networks, the entire input space is not equally responsive. First, the center of the input space is calculated, and then the inputs that are close enough to the center are analyzed. As a result, these networks respond locally to inputs. RBF networks have two layers, the first layer is a radial basis type, and the output layer is linear (Fig. 19.2). The training process is also conducted here using competitive learning methods (K-Means clustering).

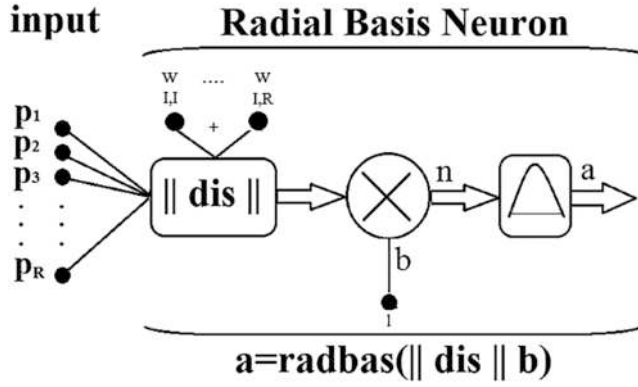


Figure 19.2 A radial basis function with input *R*.

The input of the radial nerve unit is different from that of the perception unit. For this input unit, the radial transfer function is the distance vector of the weight vector W and the input vector p, which is multiplied by the base b. The transfer function of radial base nerve unit is given by (19.4). This function has been illustrated in Fig. 19.3.

$$\text{radbas}(n) = e^{(-n^2)} \tag{19.4}$$

Given a zero input, this function has its maximum value of 1. In this way, as the distance between W and p decreases, the output of the radial transfer function increases. Therefore, the radial basis nerve unit acts as a recognition identifier for W and p. This means that when W and p are identical, the radial transfer function produces output 1.

19.3.2.5 Radial base network architecture

The radial base networks are composed of two layers. The architecture of these types of networks is shown in Fig. 19.4. The hidden and output layers have $s1$ and $s2$ nerve units, respectively.

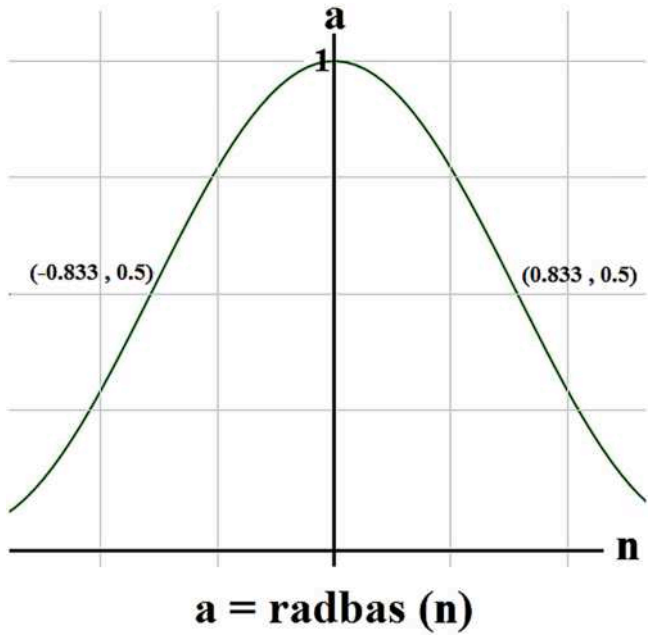


Figure 19.3 Nerve transfer unit of radial basis function.

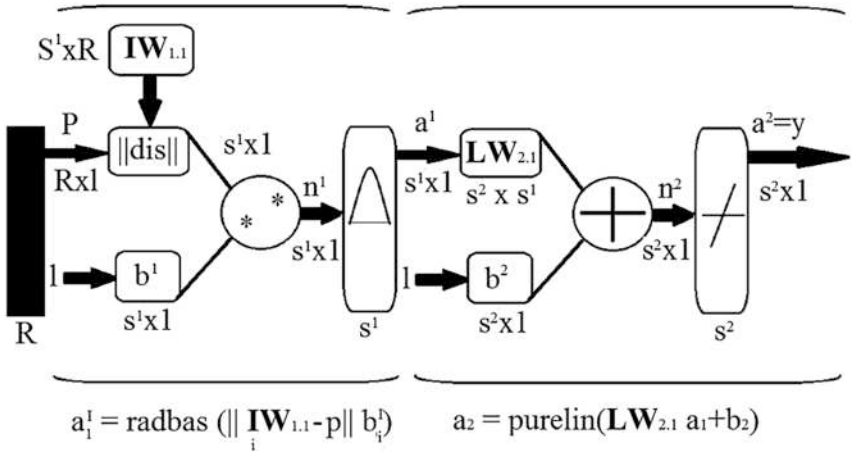


Figure 19.4 Radial basis function network architecture.

The operator, receives the input vector and the vector of weights *IW*1,1 and generates a vector with element *s*1. Then the output and the vector *b*1 are combined with each other (multiplication of elements to elements) and the output of this layer is generated. Thus, the output of the hidden layer is the distance of the input vector from the corresponding weights. If the inputs are spaced in large weights, the output of the radial transfer function is a value close to zero. This small amount will have very little effect on the output of the linear layer (second layer), and vice versa. If the input vector is close to the weights, the output of the radial function will be 1, and thus the second-wave weights will show more effect on the network.

RBFs were initiated in 1964 as the source potential functions (Looney, 1997). As mentioned before, the architecture and training algorithm for RBFNNs are simple, and they expand the learning network more quickly than a multilayer perceptron (MLP). Unlike MLPs, the algorithm for interpretation can be computed when it is described as a fuzzy rule-based system. According to Pao et al. (1994), by using RBFs and random vector functional-link network (RVFLNs), a more general and powerful application of the RBFLN method was used in this study.

Fig. 19.5 illustrates RBF on the vector *x*. An RBF with a center vector in *v* is generally defined in the *N*th dimension of the property vectors (*x*) as follows.

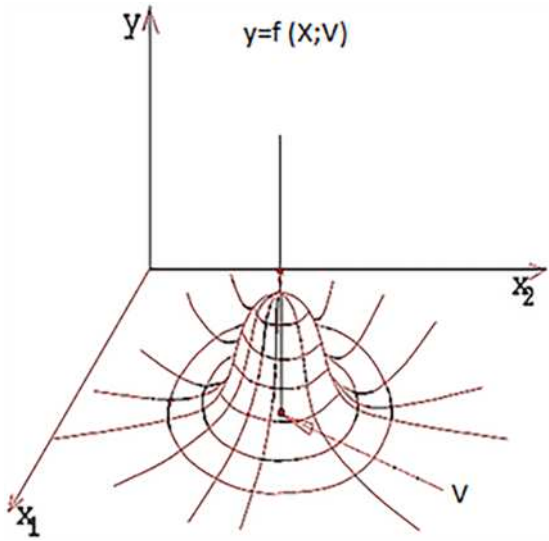


Figure 19.5 A radial basis function defining cluster center.

$$f = (x;\ v,\ \sigma) = \exp\left[-\frac{||\ x - v\ ||^2}{2\sigma^2}\right] \tag{19.5}$$

Expansion parameter (σ) indicates that all points are equally spaced from the function V, and have the functionality equal to y. The number of M of these radial-based functions can be accumulated in the center of M, so that a circle of radius σ_m covers an expected bounded area in the property space. In the spatial model, V is considered as the sample or center of a cluster with radius σ.

19.3.2.6 Radial basis functional-link neural networks neural networks

Radial basis functional-link nets (RBFLN), as shown in Fig. 19.6, include an input layer of N nodes, a hidden layer with M nerve units, and an output layer of J nerve units. The property vector (X) feeds the input layer. The corresponding output from the Mth nerve unit of the hidden layers and the jth node is the output layer for the qth input of the sample vector $x(q)$ as follows:

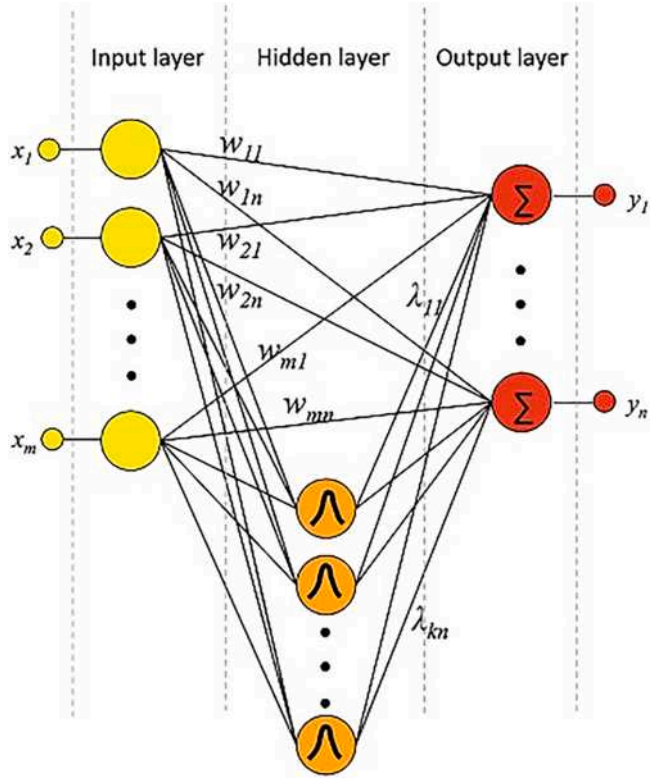


Figure 19.6 Schematic structure of radial basis functional-link nets artificial neural network (Sahoo et al., 2017).

$$\gamma_m^q = \exp\left[-\frac{||X^q - V^m||^2}{2\sigma_m^2}\right], \quad Z_j^q = \left(\frac{1}{M}\right)\left[\sum_{m=1}^{M} u_{mj}\gamma_m^q + b_j\right] \tag{19.6}$$

where $m = 1, \ldots, M$, and $j = 1, \ldots, J$. The u_{mj} weight is the output of the layers of the hidden layers to the final layer.

19.3.2.7 Probabilistic neural network

PNN is a kind of neural network that estimates the probability that a sample will be assigned to a class. In fact, there is a kind of network that estimates probability density functions. This particular type of ANN provides a general solution to the problem of clustering using the probabilities obtained on the basis of the Bayesian decision theory. These networks are of radial base nets, and their functionalities are based on the

performance of radial nets. These networks are made up of two layers. However, the second layer in these networks, unlike other networks, is of a competitive type and target the outputs in the form of vectors with values between 0 and 1. Given a network input, the distance between the input and the other inputs is computed, and a vector is generated in which the elements indicate the closeness of the input vector to the training set. Correspondingly, for other inputs, this operation is repeated (Fig. 19.7). Finally, the total calculated distances are transmitted in the form of a probability vector to the output layer, which is obtained by the corresponding functions of the network output values (Demuth & Beale, 2009).

The specialized assistance layer of a 3-unit network has been used as an example for evaluation of quality classes for the qualitative potential index in the study area. Using the class number conversion tool, three categories, including "favorable", "permissions", and "nonpermissive", were created. The classes "acceptable", "inappropriate", and "bad" are equivalent to "favorable", "good" is equivalent to "nonpermissive", and the "temporarily drinkable" is equivalent to "permissive". Nonpermissive areas are actually areas in which the probability of negative (unfavorable) classes is low, so that the expected target class is not observed. Permissive areas are those in which the present characteristics express the properties associated with this type of target recognition (poor grades of the qualitative index). Favorable areas are also areas in which processes associated with the formation of an undesirable type of class can occur.

The assistance layer expresses the expert opinion about the class or probability of occurrence of a target phenomenon. According to the drinking water quality index, the assistance layer corresponds to the

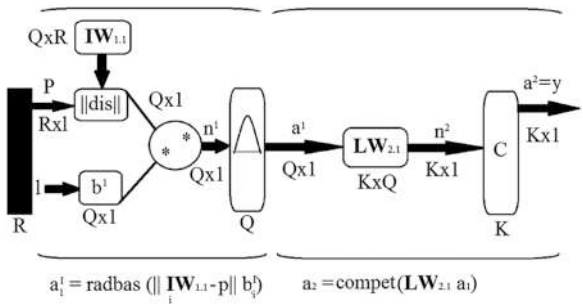


Figure 19.7 Architecture of a probabilistic neural network.

calculation of the aquifer quality assessment. This layer represents the average water quality potential in the period between 2013 and 2023 and is obtained in the GIS environment.

19.4 Results and discussion

In this section, we provide the results of ANN and fuzzy clustering methods using the ArcSDM extension and fuzzy logic tool in a GIS environment (GeoXplore program). The probability of occurrence of negative annual changes in different classes of drinking water quality is estimated using RBFLN, PNN, and fuzzy FUC methods. In this way, the spatial distribution map of the probability of negative changes in the quality index of groundwater resources was obtained. The calculations were based on the extraction of the water quality potential layer using a geographical information system and according to the Schuler and WHO standards.

In the output layers, the probability of quality change in the annual period is expressed in the form of fuzzy membership. Moreover, a sensitivity analysis is conducted for the detection of qualitative changes, with the help of the evidence layers according to the raster class mapping. The analysis was performed using the GRI index and the five parameters of the Schuler standard (TH, TDS, Cl, Na, and SO4). The reason for the selection of the 10-year computational period of this evidence, from 2013 to 2023, is to produce results with the same distribution of available data as possible and close to the effects of the final drought calculation in 2023 with the forecast approach.

The raster layer of the groundwater quality potential index is selected as the criterion for determining and locating the class points. Afterward, the values of this layer were changed into three classes to determine the location of the two "occurrence" and "nonoccurrence" points. That is, based on the same three classifications, this diagnosis takes place. Finally, the layer has been used to determine the membership severity of each of these two classes. With the criterion of the index of potential, the quality of groundwater resources was nominated into three classes, "favorable", "permissions", and "nonpermissive". Afterward, the location of the occurrence and nonoccurrence points is determined. For this purpose, the automatic combination of the fuzzy operators was used to determine the membership value of the layer's points.

The prediction of the occurrence of a qualitative class called as "temporarily drinkable" resulted in the production of spatial distribution figures. Figs. 19.8 and 19.9 are derived using the PNN and RBFLN neural network methods, both of which yield computational results that are more similar to each other than those obtained by fuzzy logic. As previously mentioned, RBFLN and PNN methods have a more accurate and faster computing capability than the FUC method (as shown in Fig. 19.10), and thus they have higher credibility.

The value of the productivity index of the classifier is about 96.1%, which indicates a high level of accuracy. In addition, the area under the CAPP curve (54.23%) confirmed the randomness of class production in the process of ANN. Dispersion representation of higher membership indicates that the altered conditions in a large part of the country's aquifers are related to the lowest water quality and the highest droughts. The least uncertainty of the PNN's output was obtained for the 7th class. The outcomes indicate that in the southeast aquifers, south of Fars province, areas of the central parts of the country, and in particular the major parts of the Khorasan aquifers, are on the verge of a crisis. In addition, the aquifers in these areas are similar to drought stress and are in a very poor condition. In other words, with the repetition of the drought of underground water, the probability of a decrease in the quality of water in areas where the highest drought was occurring has a higher membership rate. At the same time, the RBFLN method clearly shows the difference between the responses of drought situations to probabilistic tensions. Thus, relatively fewer regions are considered as vulnerable parts of the crisis, but there is no significant difference in the output obtained by RBFLN compared to the PNN method.

To confirm the recent discussion, by converting the calculated values of each method to the vector points and then receiving the output in the spreadsheet environment, the value of the detection coefficient was obtained by the regression model. This value showed the highest correlation of about 74% between the two methods of RBFLN and PNN, and then 72% between the PNN and FUC methods, and finally 39% between the RBFLN and FUC methods. The reason behind the similarity of the results of these two superior methods is based on their "radial base" structure. Particularly, the areas where the occurrence of drought can clearly affect the negative change in the quality of underground drinking water, the range from the southwest to the northeast of the 609 study areas, is more consistent with the results of the FUC and

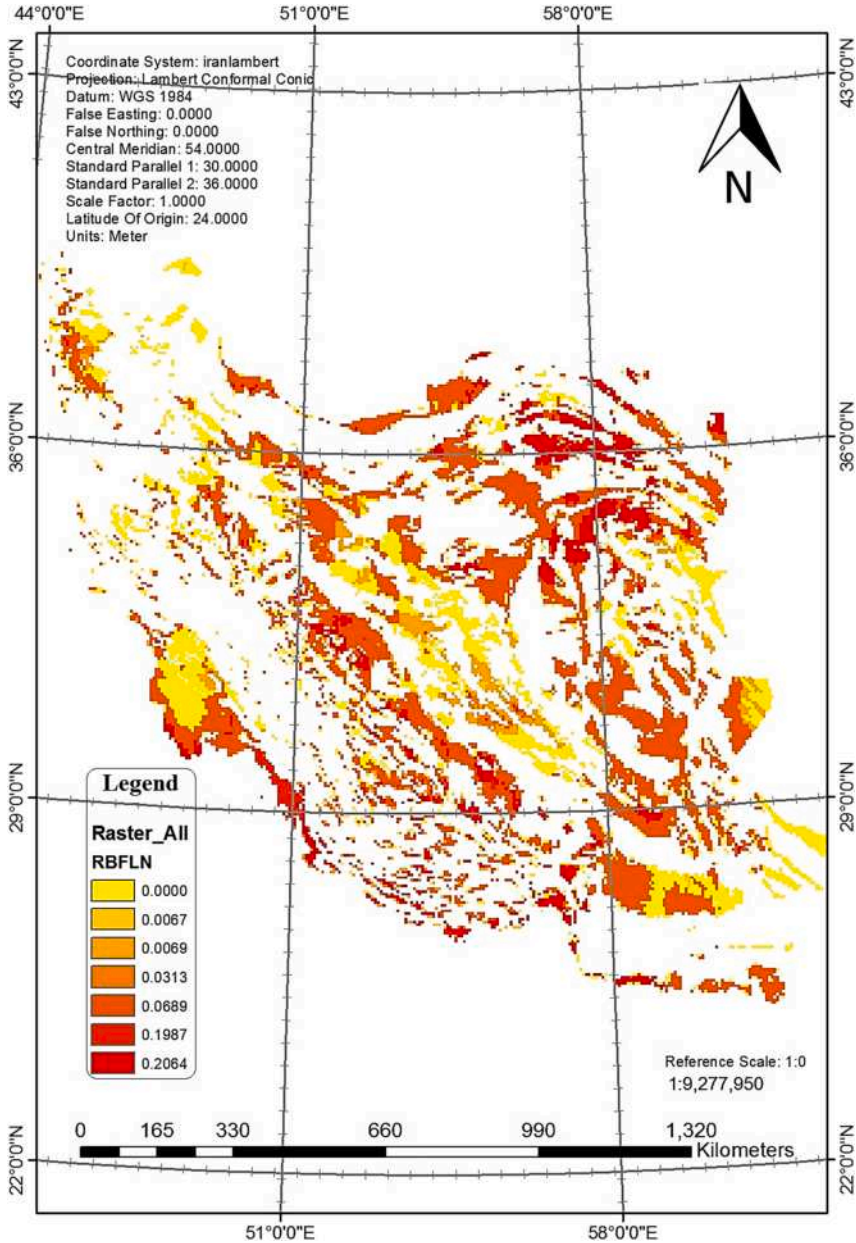


Figure 19.8 Prediction layer of the reduction in drinking water quality in the probabilistic neural network method. Map lines delineate study areas and do not necessarily depict accepted national boundaries.

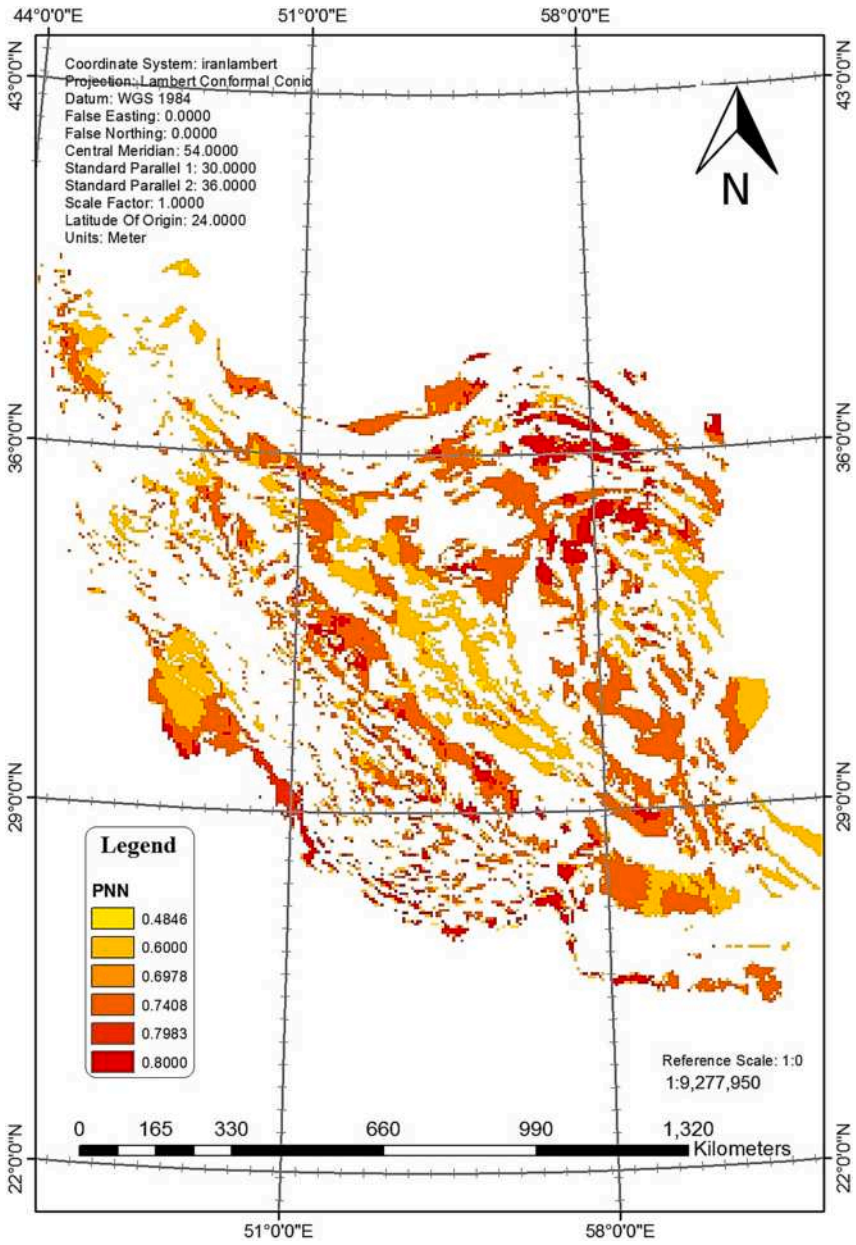


Figure 19.9 Prediction layer of the reduction in drinking water quality in the radial basis functional-link nets method. Map lines delineate study areas and do not necessarily depict accepted national boundaries.

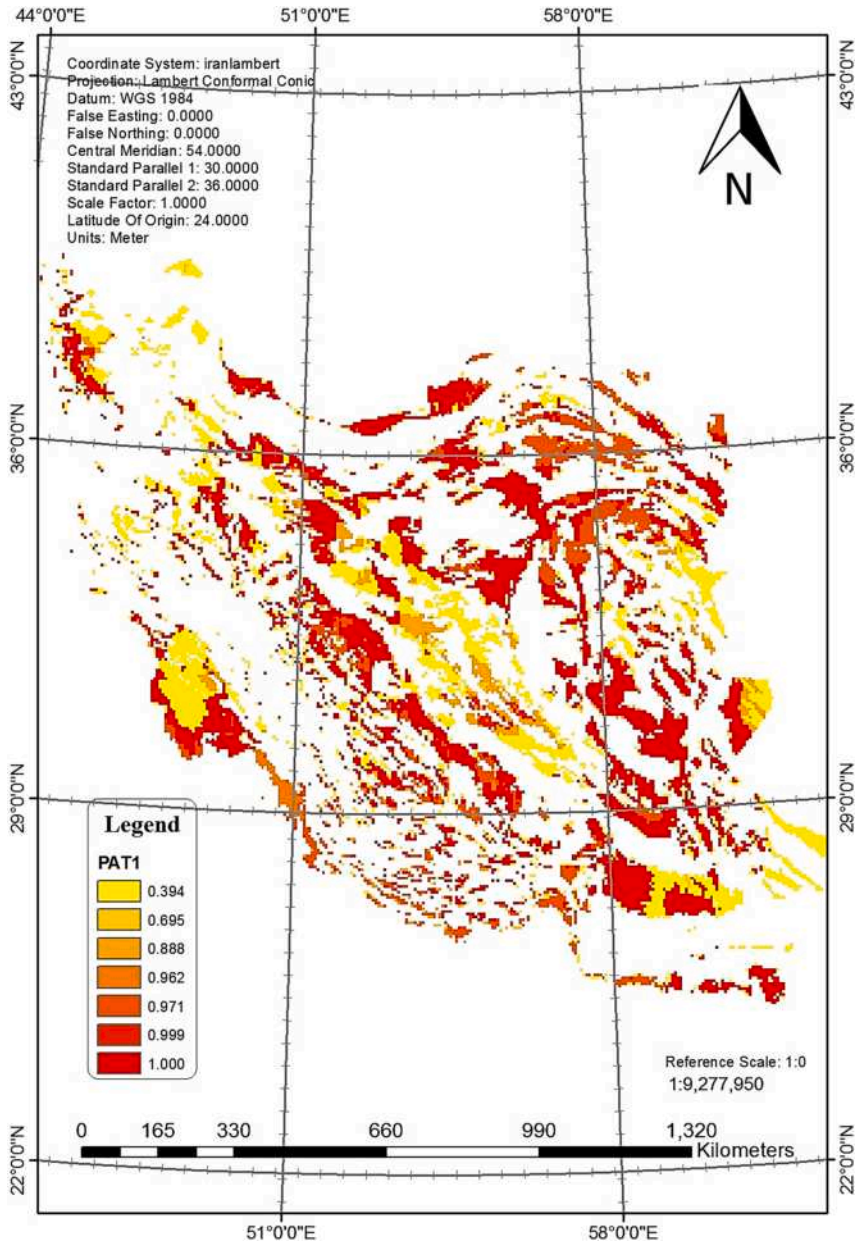


Figure 19.10 The prediction layer for quality reduction of groundwater drinking water by the FUC method. Map lines delineate study areas and do not necessarily depict accepted national boundaries.

RBFLN methods. It can be concluded that in both PNN and RBFLN methods, despite the same initial weight in the selection of six control layers, the most significant relationship between the quality class and the occurrence of drought was found. Therefore, in aquifers that pass through the quality threshold, it is expected to repeat the changes with less progress, while the aquifers in the "bad" class of the Schuler standard are most sensitive; however, they necessarily did not get the highest membership value of the prediction. This means that in some of the country's aquifers, the water quality status is not relatively poor. However, the quantitative changes in the depth of water in these aquifers, based on the results of the prediction of ANN, indicate that the conditions for the future are considered critical.

In order to compare three methods, the standardization of the spreadsheet environment was used. The output value of this function is depicted in Fig. 19.11. The graphs of these figures visually confirm the negative decline in drinking water quality in the three classes 1, 4, and 7, in all three computational methods. However, for classes 6, 5, 2, and 3, the results of the PNN and RBFLN methods are more similar in terms of the relative risk of water quality loss. Thus, 63.67% of the study areas (359640 km^2) are subjected to severe deterioration in drinking water quality.

In order to predict the annual precipitation rate in the year 2023, there is a need to provide the format of the input layer digits. This step was performed using the Python code of the artificial post-propagation network, according to the aforementioned descriptions in the research theory section. In order to

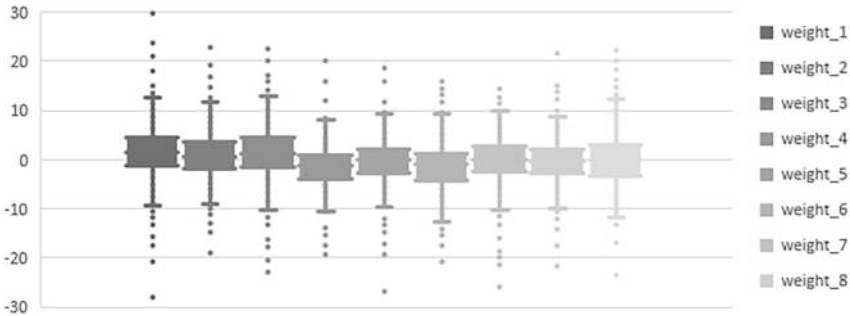


Figure 19.11 A box plot graph showing the distribution of weight values across 8 different categories labeled weight1 through weight8. The plot displays median, quartiles and outliers for each category.

provide the maximum level of statistical relationships in the input layer column, each time series in 374 synoptic stations of the country was divided into 12 rows and 9 columns. In each data section, the cumulative rainfall data was used as output, and for each element of output, nine successive rainfall variables were used. Also, one of the requirements for using postpropagation neural network code is to supply input variables in the normal structure and in the range of 0 to 1. By implementing an algorithm for the training dataset, an optimal relationship was obtained. Finally, for all 362 synoptic stations in the country, normalized tables are obtained for educational examples. In each run of the post-propagation artificial neural network model, a randomised weighing order has been used. The output of this command was normalized using 1000 training repetitions and the allocation of new and corrective weights with a value of 0.862 and equal to 3,780,300 mm per year for the average of all stations. Similarly, the random weight is generated for all 362 synoptic stations as illustrated in Fig. 19.12. Cultivars can show the trend of changes to the artificial neural network model. In Fig. 19.3, the maximum range of variations in weight No. 1 and the lowest in weight No. 6. The Box and whisker chart shows that the average weight variations are around 0 and the range of variations in all cases is approximately the same and at the same time has been symmetric for the positive and negative range. This can put the output guess around an average.

As a result of the implementation of training and extracting the solution for the final matrix, as specified in Fig. 19.12, each of the points in the standard normal space range 0 to 1 specifies a predicted digit that corresponds to the values for all synoptic stations in 2017. The dispersed points, which are arranged in ascending order of the plain area of the

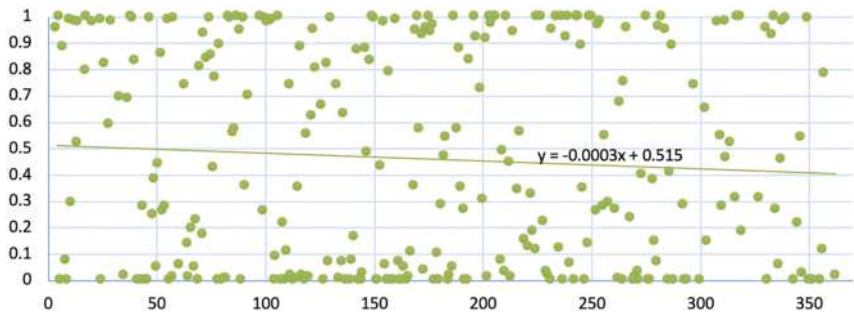


Figure 19.12 Distributed spotted points of normal cultivars precipitation forecast in 362 synoptic stations.

country, indicate that the accumulation and multiplication of more than half of the predicted values on the right side of the graph (wide plains) is known to be less than the mean long term. Meanwhile, with a negative slope of close to zero, the variables predicted a relatively straight regression line. This suggests a repeat of the relative increase in drought in 2023 for the eastern and southeastern parts of the country, which generally have a larger share of the vast plains.

The predicted precipitation levels, before the precipitation change in millimeters per year, are roughly equal to the long-term average and, of course, with a relative decline for vast plains. However, the process of change is not necessarily linear and varies from one station to another. This change, after the extraction of the SPI drought indicator, is derived from the standard normal transformations based on the sigmoid function. According to the results of the model, the range of drought to areas in the country that were located in near normal conditions in 2019 has increased at the time of forecasting. After the development of the SPI model in the spreadsheet environment, the average of the annual aggregated rainfall drought index for all stations and in all computational years.

With the purpose of describing the spatial distribution of the SPI index around the study area for all stations, the production of interpolation maps required the analysis and processing of raw data. In this way, firstly, through a survey tool for non-random processes in data, this value was obtained in a set of three-dimensional diagrams. Fig. 19.13 shows the existence of a non-randomized second-order trend in the direction of north to south and east to west in the initial mean data of the SPI index in the long term.

Given the initial assumptions in the Kriging method, the normalization of data is a fundamental condition. In this study, Minitab software is used to analyze the statistical distribution of data. According to the results of the analysis, the outcomes have confirmed the distribution of abnormalities in all years. Fig. 19.14 shows the unpredictable statistical distribution of the average SPI index data in a long-term interval.

The main factors of creating interlayer layers have been recognized using the GeoStatistical tool. Accordingly, the continuous levels of the static Markov chain of these indexes were developed for 10 years interval. The choice of optimal method was based on a comparison between the produced samples during the range from 1994 to 2015. The results of this experiment are presented in Table 19.1. For this purpose, two distinct methods of inverse distance weighting (IDW) with three potentials 1, 2, and 3 were used. In addition, using the GPI method with degrees 1, 2, and

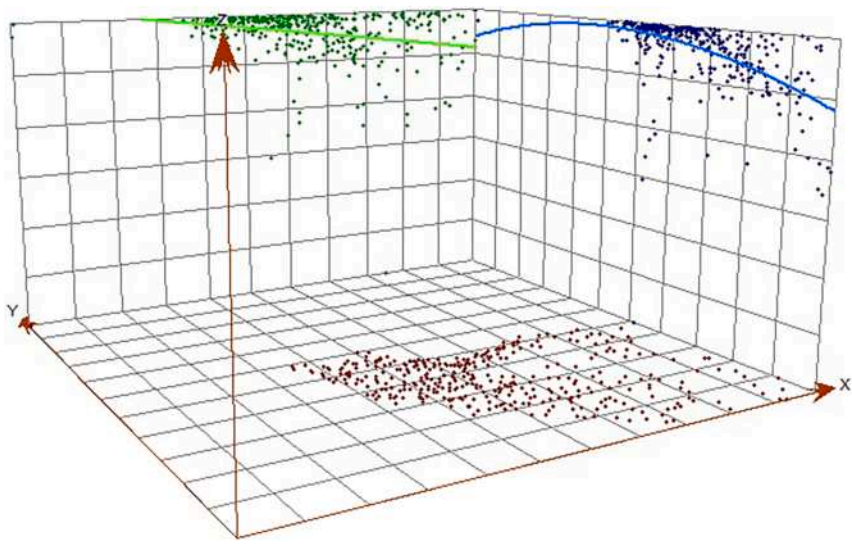


Figure 19.13 Trend in the average in interval 1994–2023.

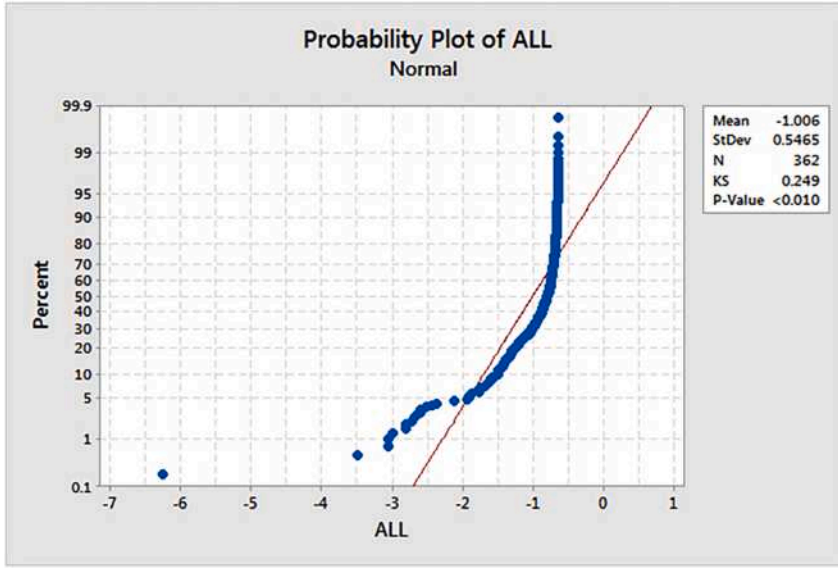


Figure 19.14 Distribution of abnormal mean data in interval 1994–2023.

Table 19.1 Comparison of errors between different methods for the production of continuous interpolation.

Error index	**Type of interpolation method**						
	Kriging					EBK	
Ordinary	Simple				Universal		
	Stable	J-Bessel	Gaussian	Spherical			
Mean	0.005	0.002-	0.003-	0.002-	0.002-	0.005	0.002
RMS	0.499	0.496	0.495	0.496	0.496	0.586	0.514
MS	0.012	0.005-	0.007-	0.005-	0.005-	0.005-	0.003
RMSS	1.120	1.021	1.017	1.021	1.016	1.210	1.059
ASE	0.444	0.485	0.486	0.485	0.488	0.512	0.481

Error index	**Type of interpolation method**						
	IDW			GPI			RBF
	Power one	Power two	Power three	First grade	second grade	third grade	
Mean	0.005-	0.013-	0.012-	0.001	0.001-	0.000	0.001-
RMS	0.518	0.541	0.559	0.507	0.498	0.496	0.519

3, the RBF method, and the Ordinary and Universal Kriging, as well as Simple Kriging with four stable, J-Bessel, Gaussian, and spherical functions, were continuously mapped.

In the Empirical Bayesian Kriging method, using 100 repetitions of the Semivariogram, a continuous layer was generated, which in comparison to the entire samples, ultimately reduced the estimation errors. More specifically, the mean error was reduced to 0.00198, the root mean square error (RMSE) to 0.514, the standardised error to 0.003, the standardised square root error to 1.059, and finally the standard mean error to 0.481. The error was due to the simple Kriging method selection with the Stable function as the final approach. In Fig. 19.15, result of the conditional code for the calculation of the SPI Index classification model is provided. In these figures, a class of color scheme was also used. Accordingly, visual comparisons between the variations of the raster cells are provided.

Based on continuous maps, it can be concluded that meteorological droughts have been repeated from the beginning of the study period for a large area in the southeast of the country, and in particular in Sistan and Baluchestan province.

Though, drought investigation in the central, eastern, and southeastern parts of the country can be more important due to longer and more severe occurrences and also due to special regional conditions. For example, the magnitude of droughts can lead to the loss of surface water resources, which itself feeds on groundwater reservoirs and reservoirs. Also, the severity of resource dependence in the eastern and southeastern parts of the country is much higher due to the small amount of precipitation and the short rainy season. Investigating the changes in the SPI Meteorological Drought Index indicates that the trend towards higher grade classes has increased in most of the country, as the severity of the drought in the final years of the study period. In recent maps, with the increase of the numerical value of the class number, the status of the changes indicated a shortage in rainfall observations, and as a result of the increased drought.

According to GRI drought prediction maps, the least drought is expected in the central parts of the country. However, changes in the drought class are clearly observed in all regions without any correlation with a particular location. The wetness class in 2023 and in the five years of its forecast was limited to the central and western areas. In 2027 (Fig. 19.16), the occurrence of groundwater droughts in many parts of the country is predicted for aquifer water levels. The observed trend over the next four years is also very similar to the initial two years. Indeed, the

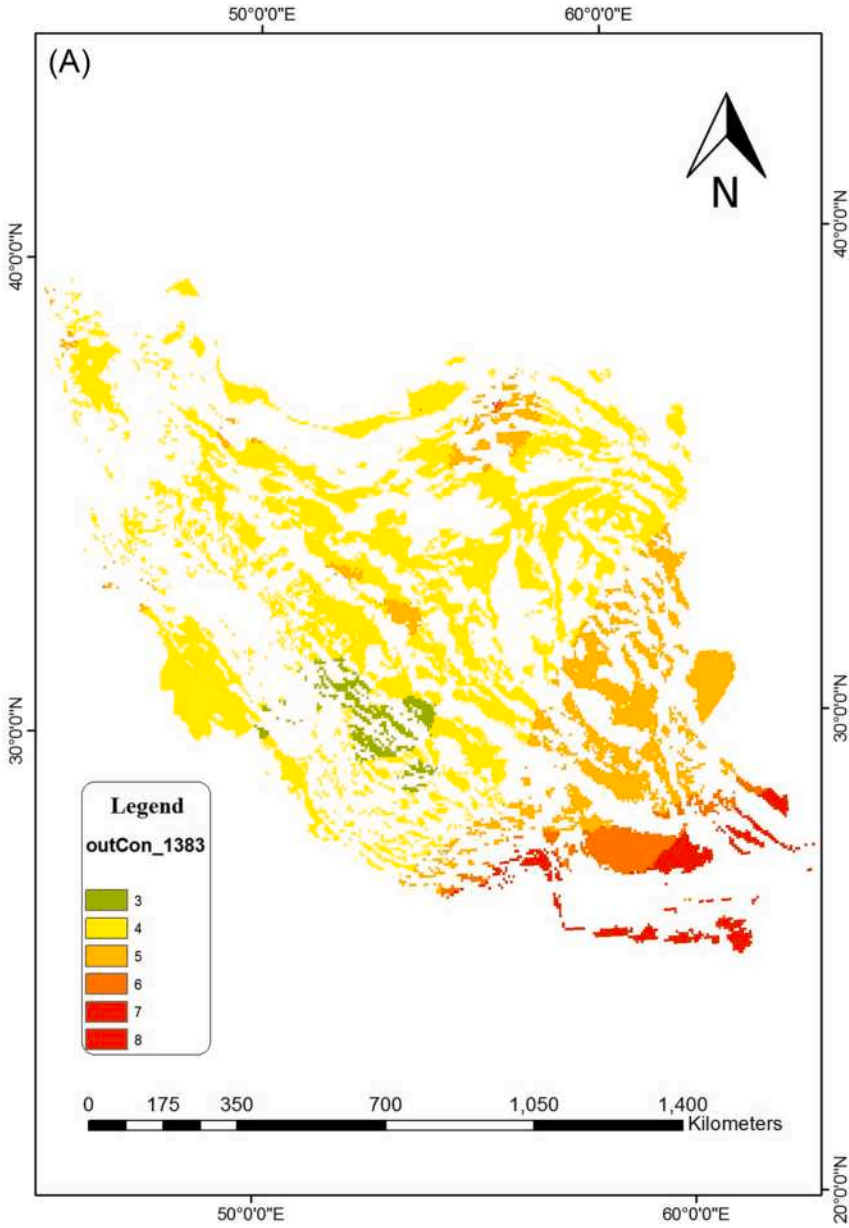


Figure 19.15 SPI calculations in the years 2012–2021. Map lines delineate study areas and do not necessarily depict accepted national boundaries.

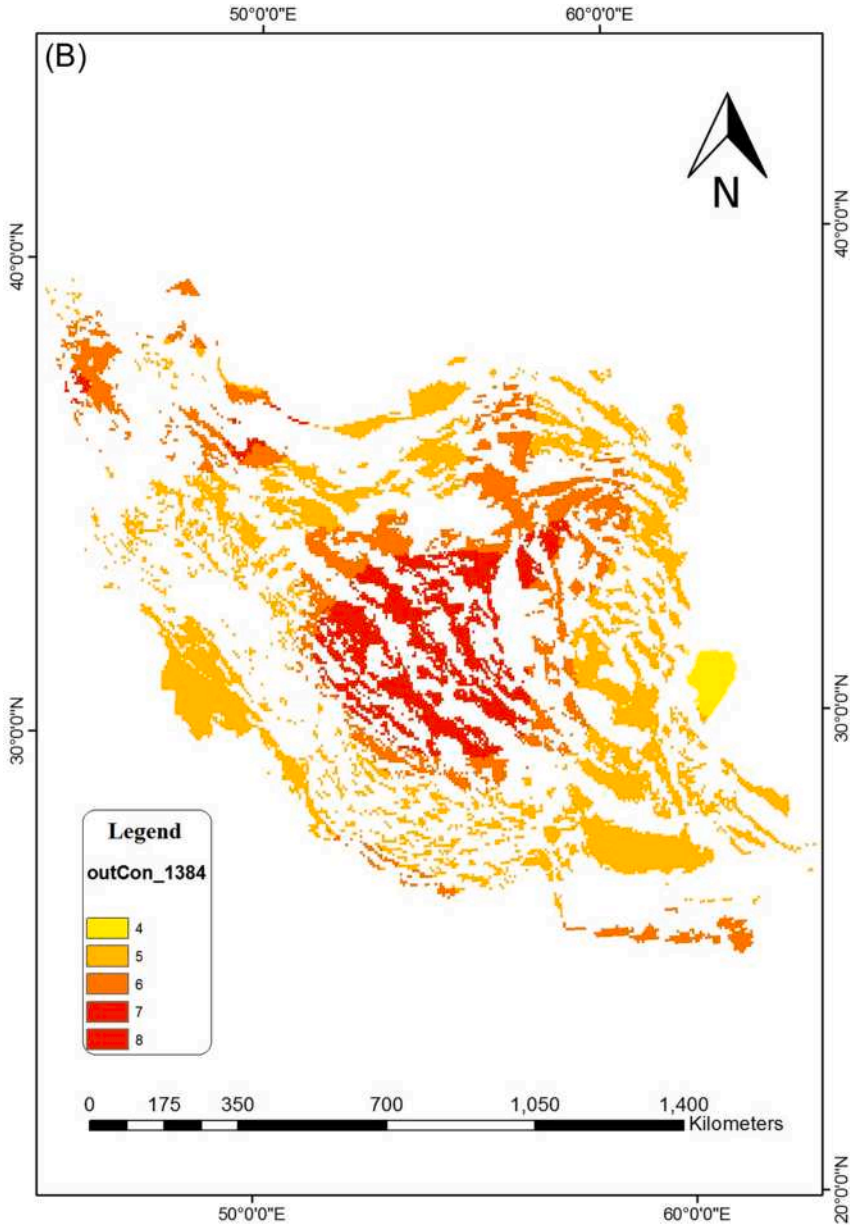


Figure 19.15 (*continued*)

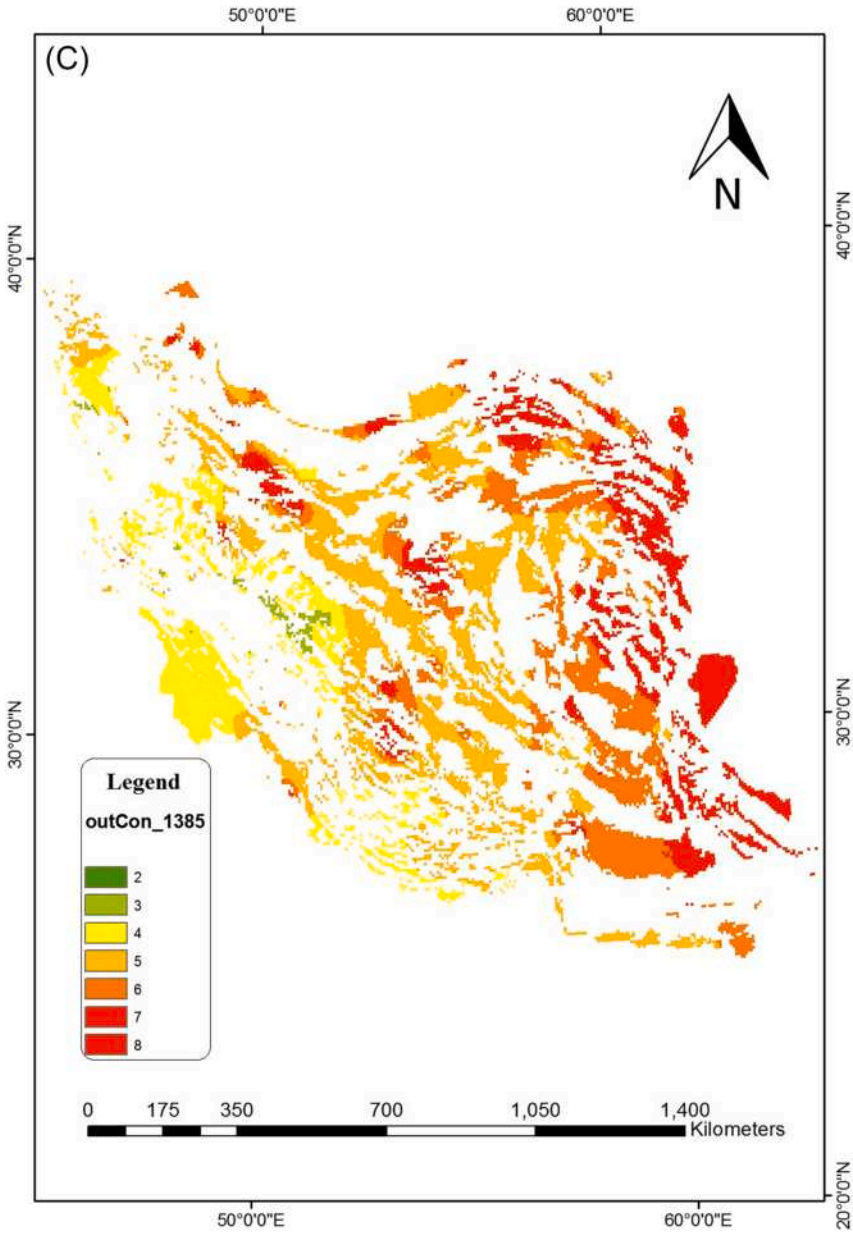


Figure 19.15 (*continued*)

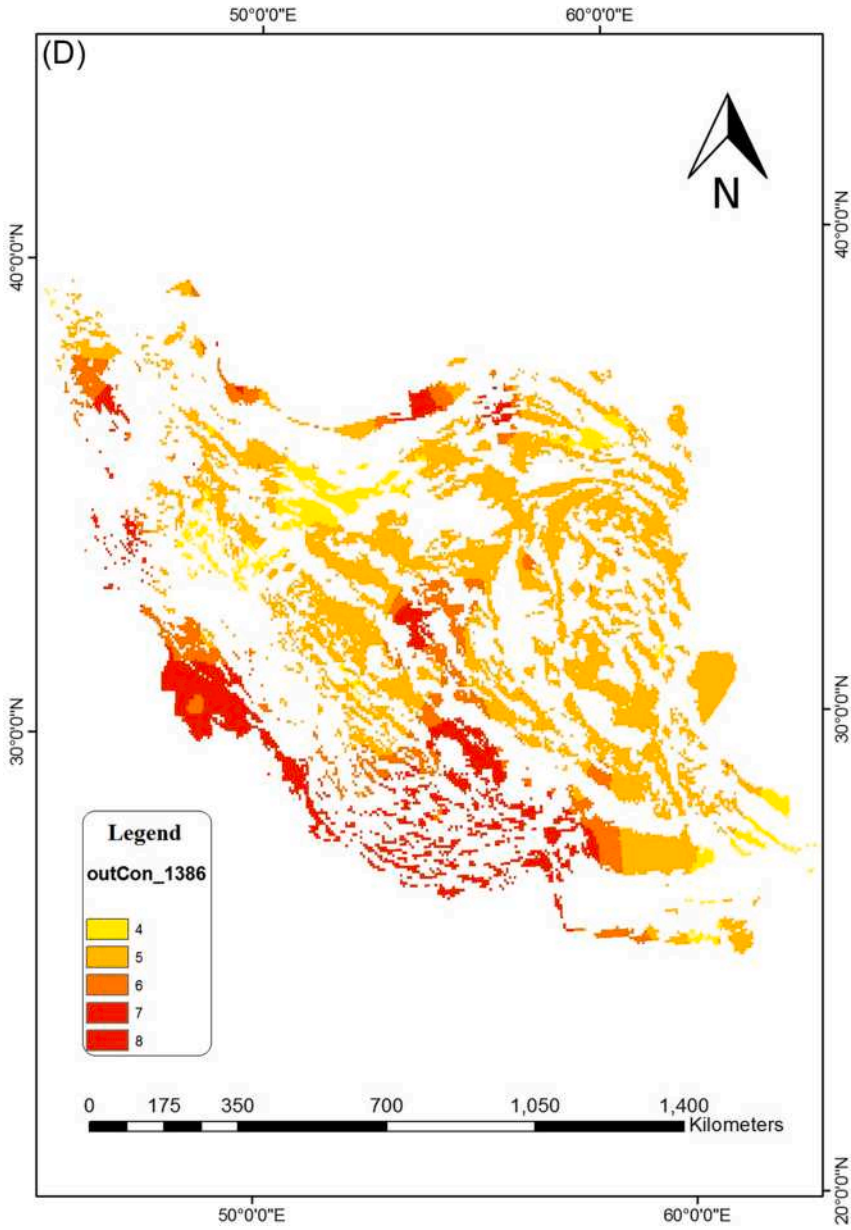


Figure 19.15 (*continued*)

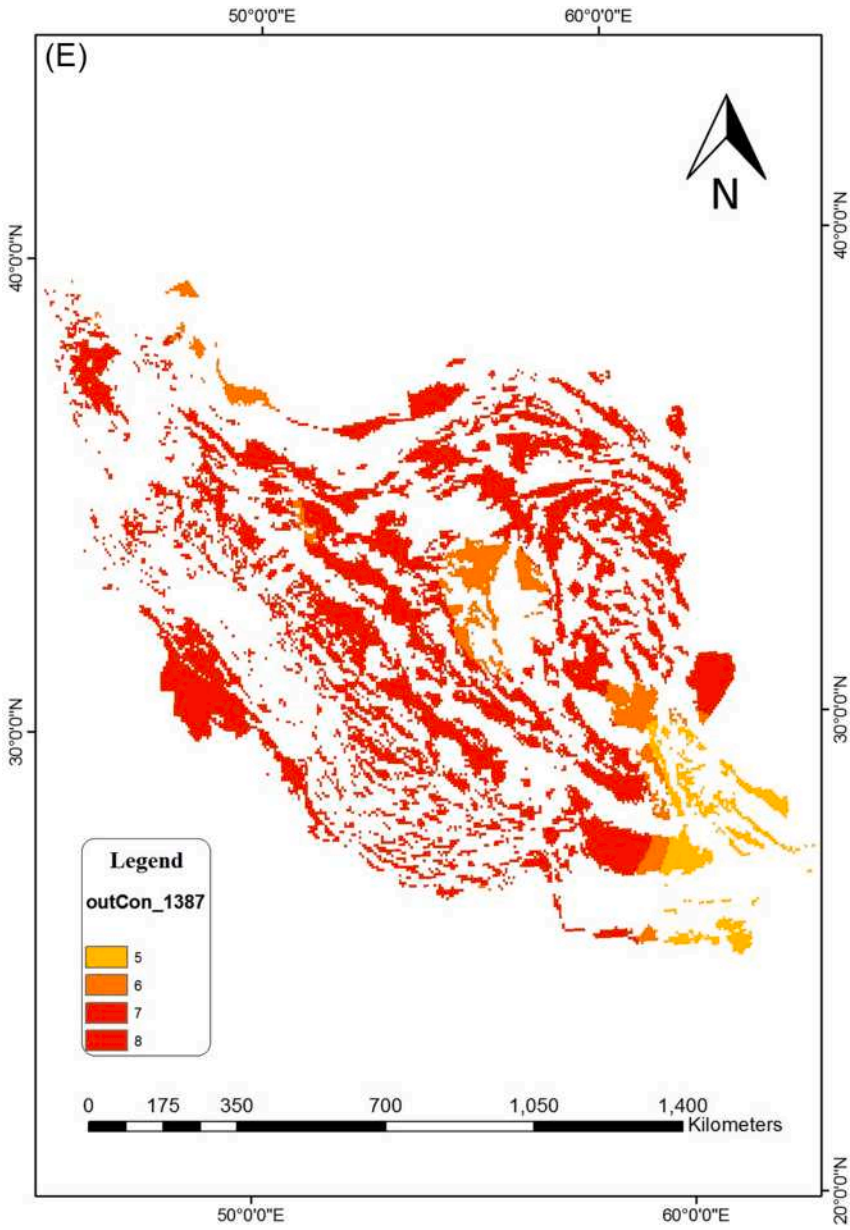


Figure 19.15 (*continued*)

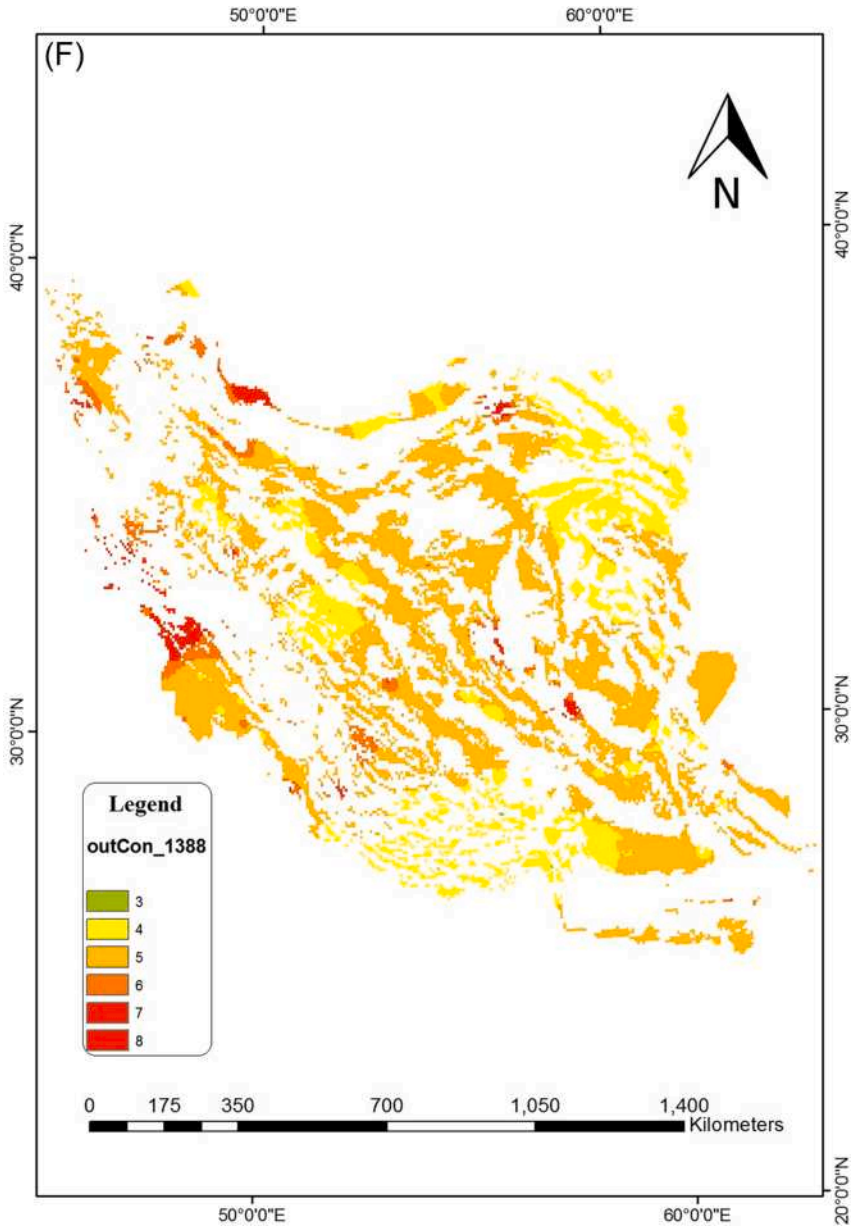


Figure 19.15 (*continued*)

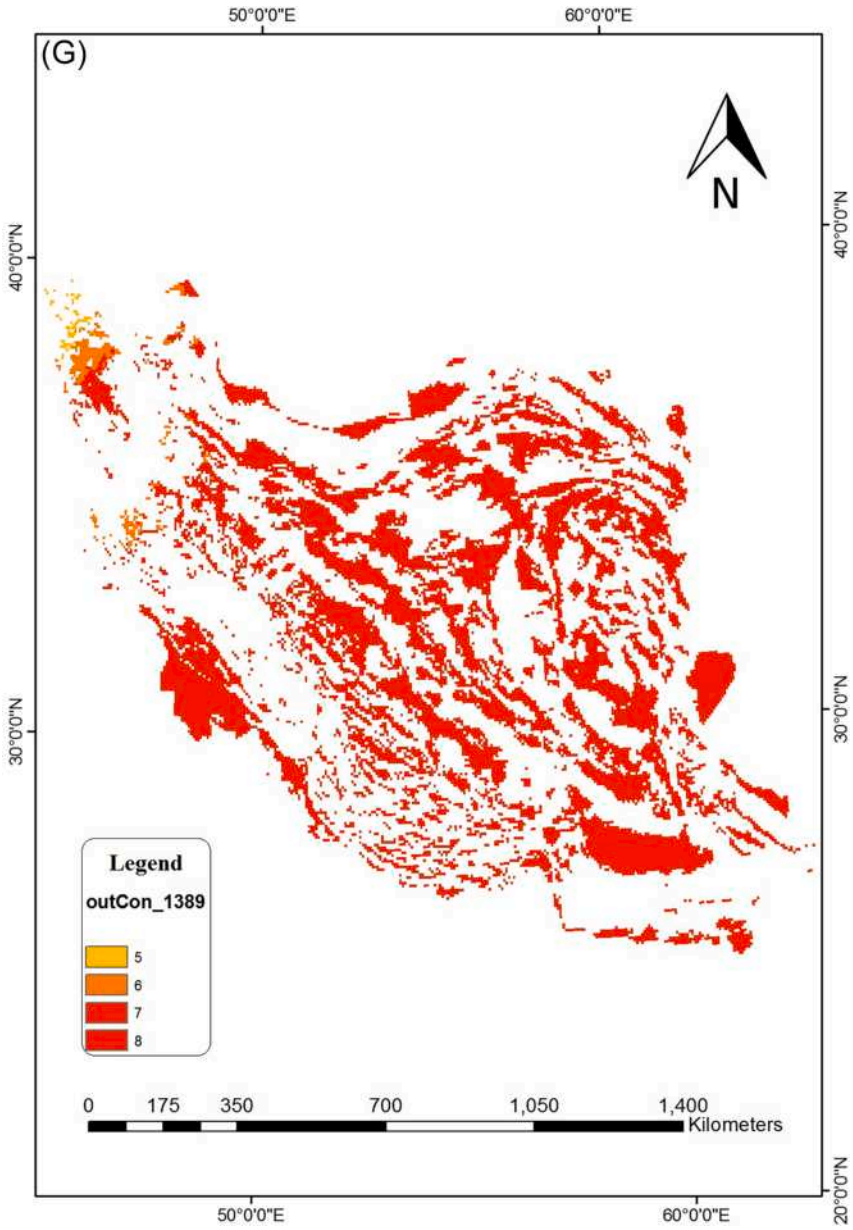


Figure 19.15 (*continued*)

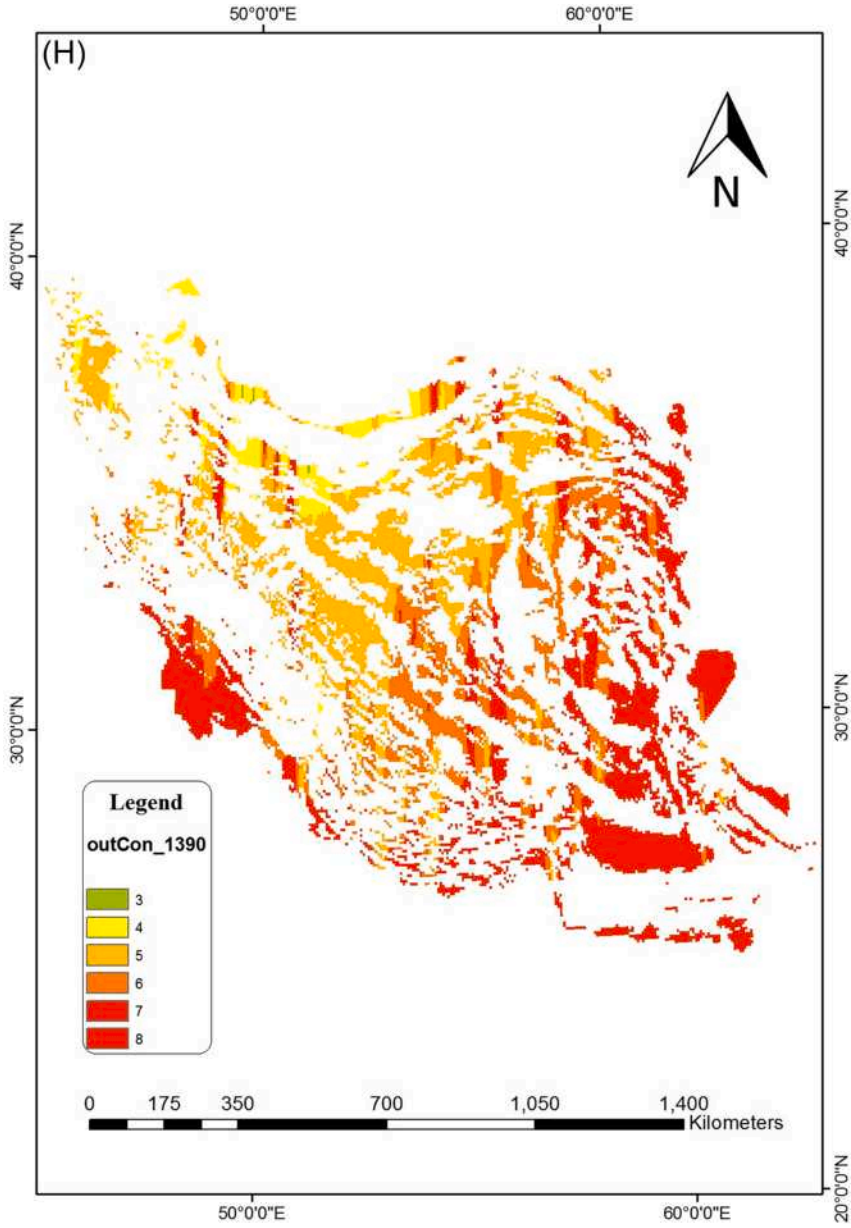


Figure 19.15 (*continued*)

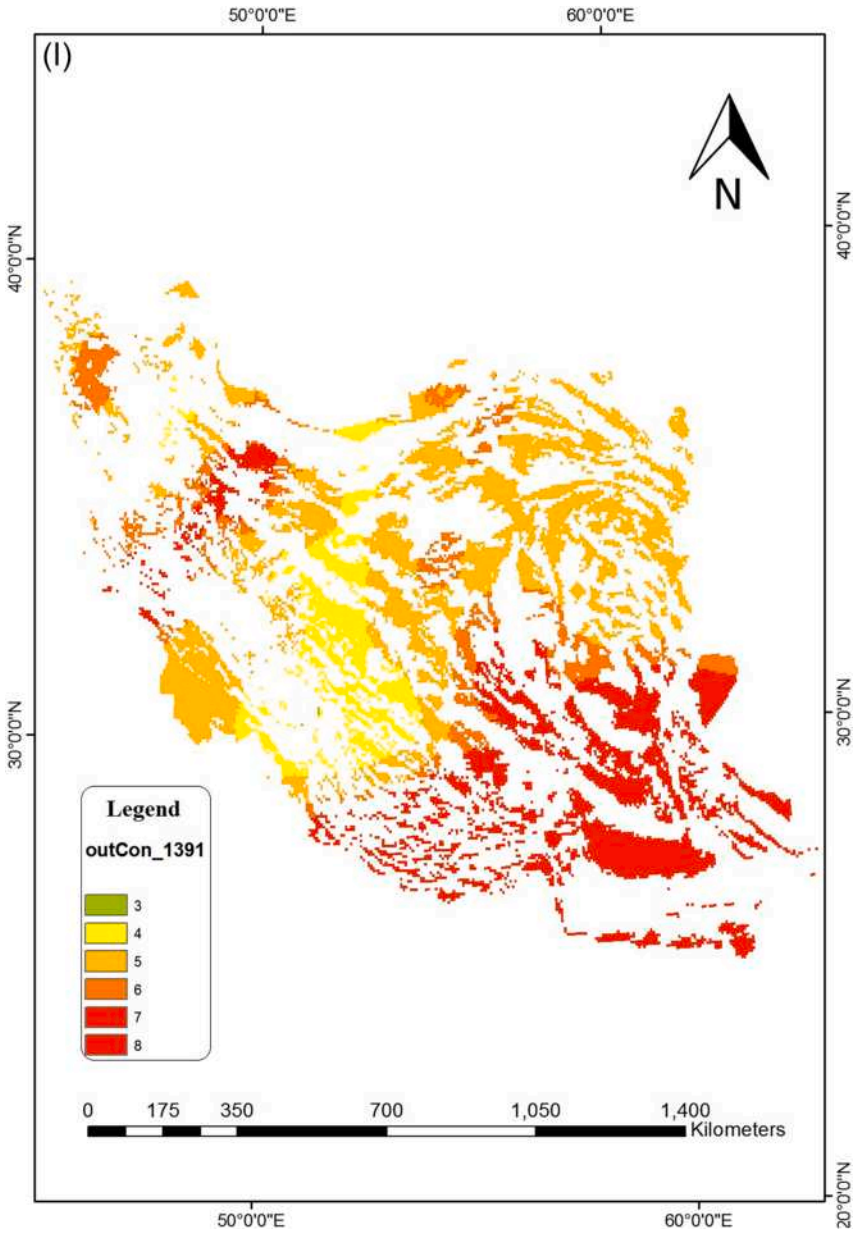


Figure 19.15 (*continued*)

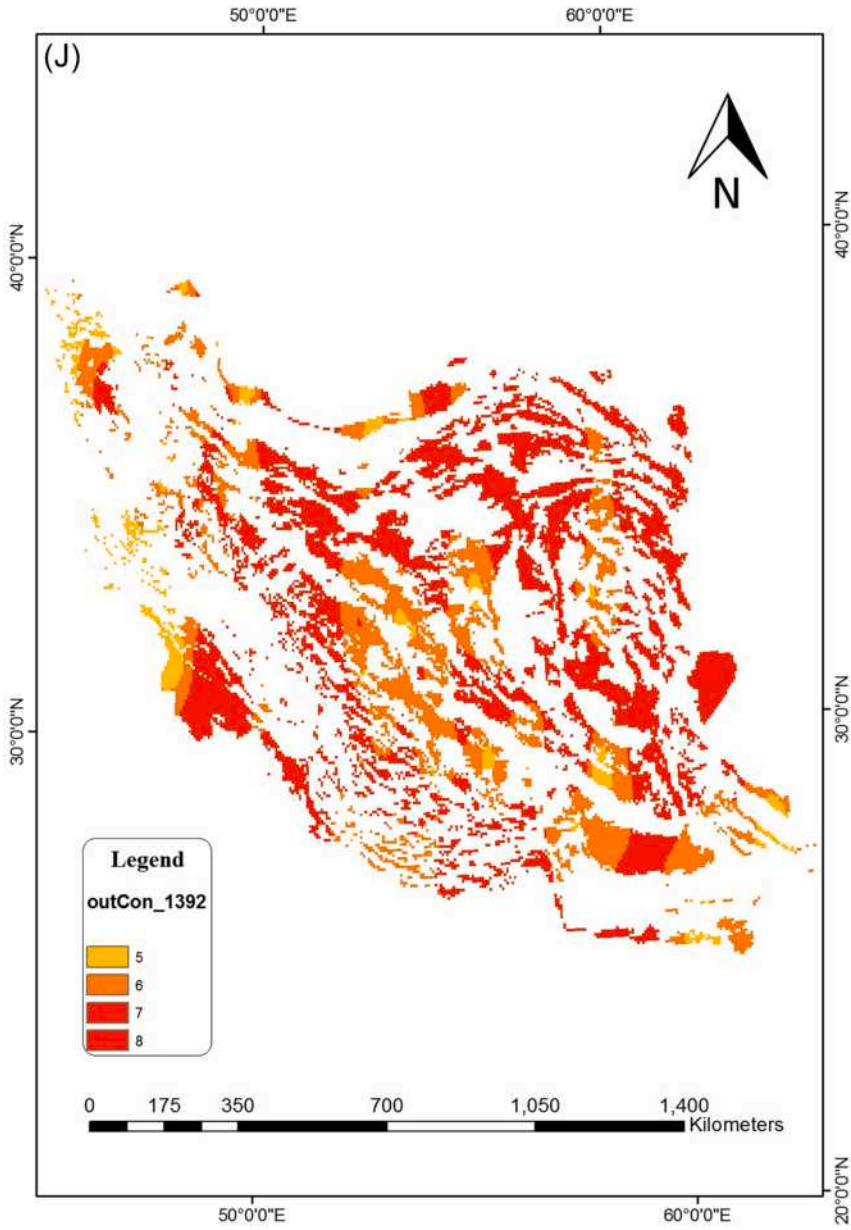


Figure 19.15 (*continued*)

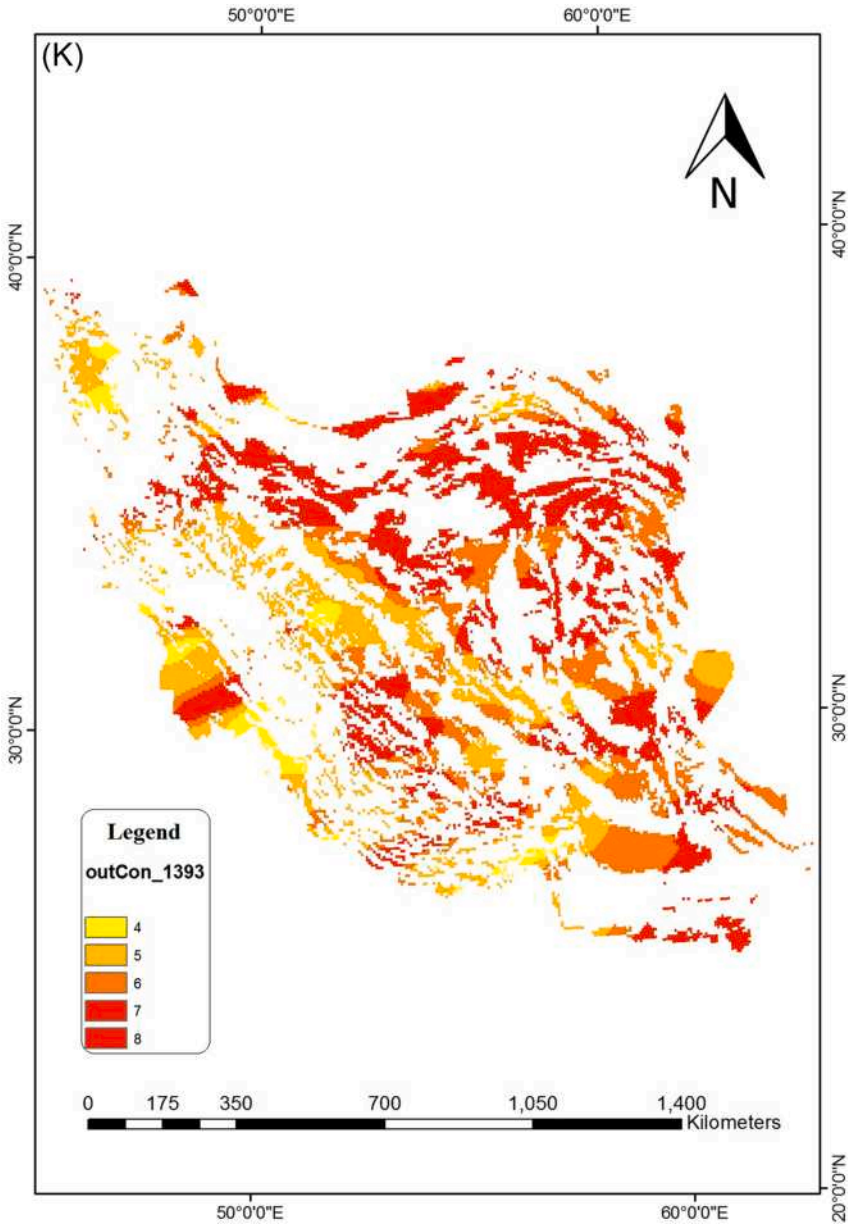


Figure 19.15 (*continued*)

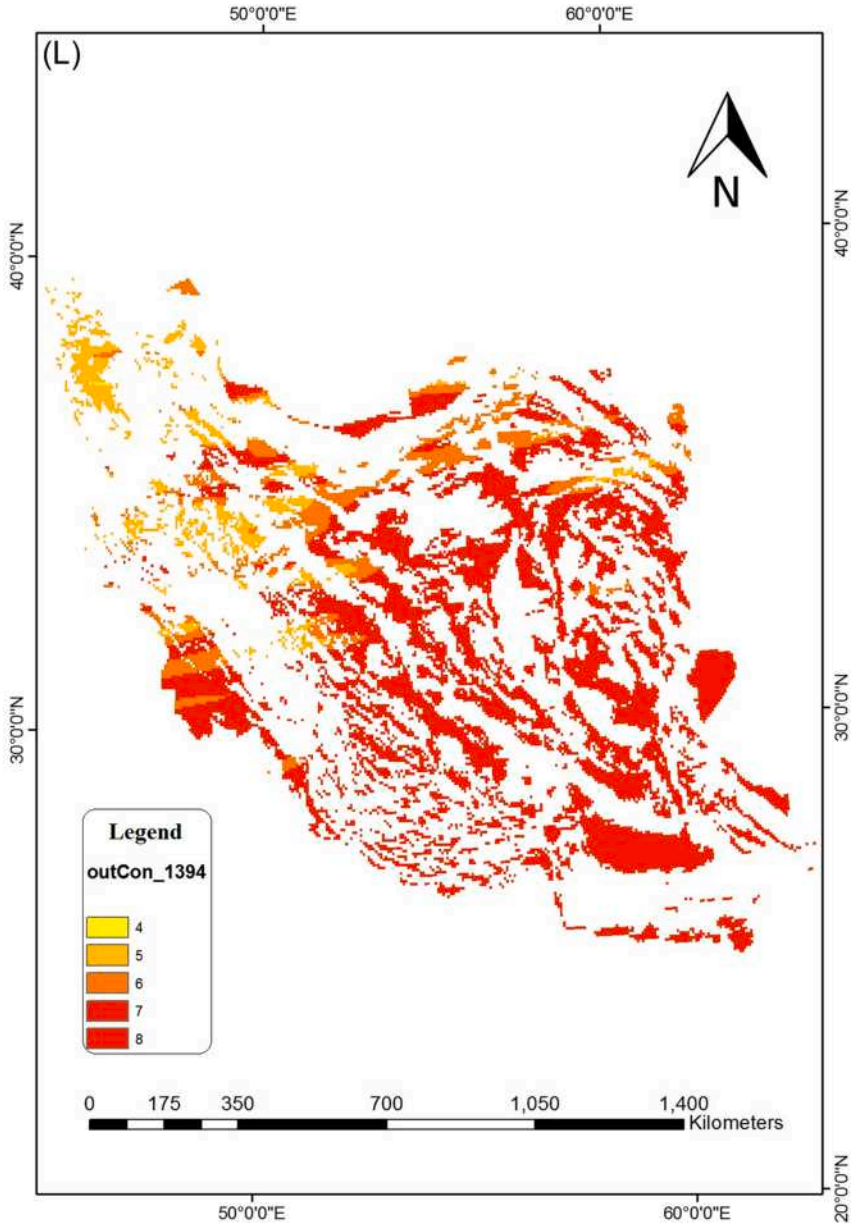


Figure 19.15 (*continued*)

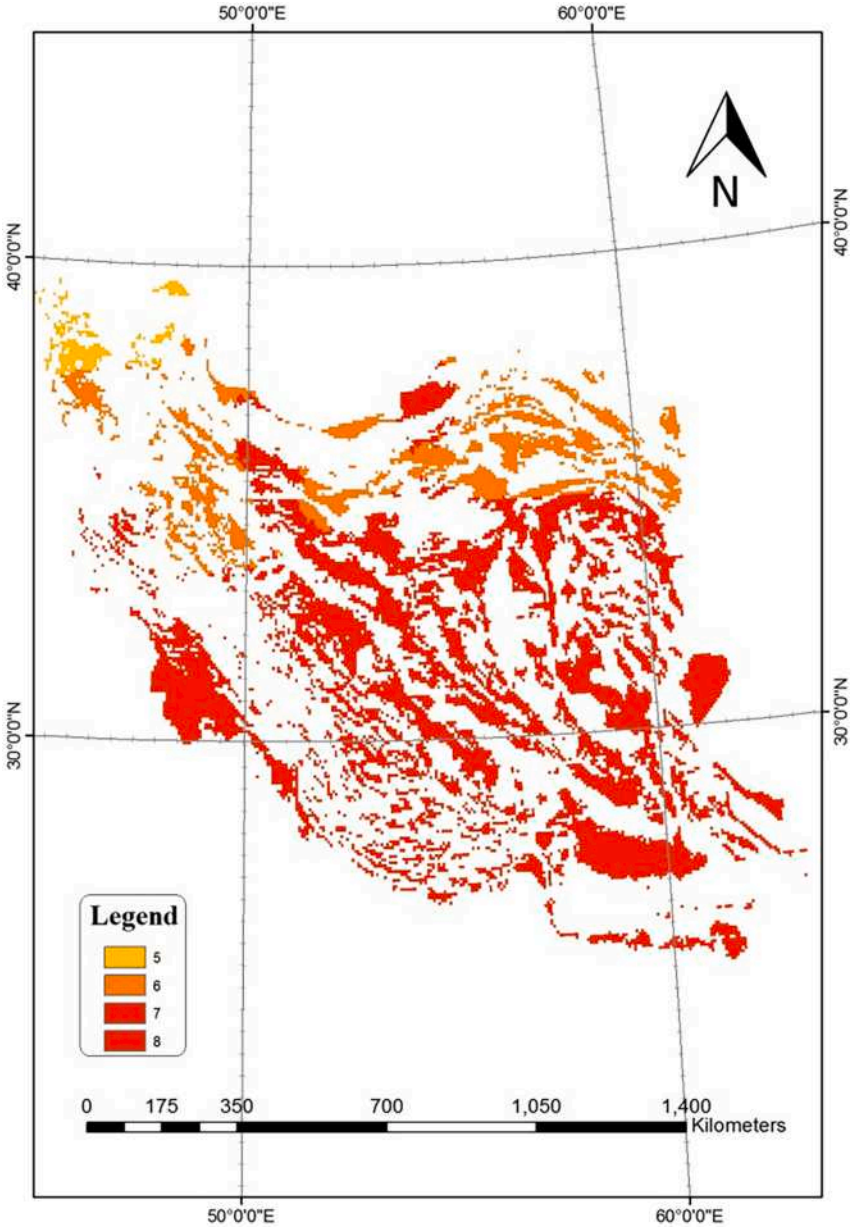


Figure 19.16 Standardized precipitation index, year 2027. Map lines delineate study areas and do not necessarily depict accepted national boundaries.

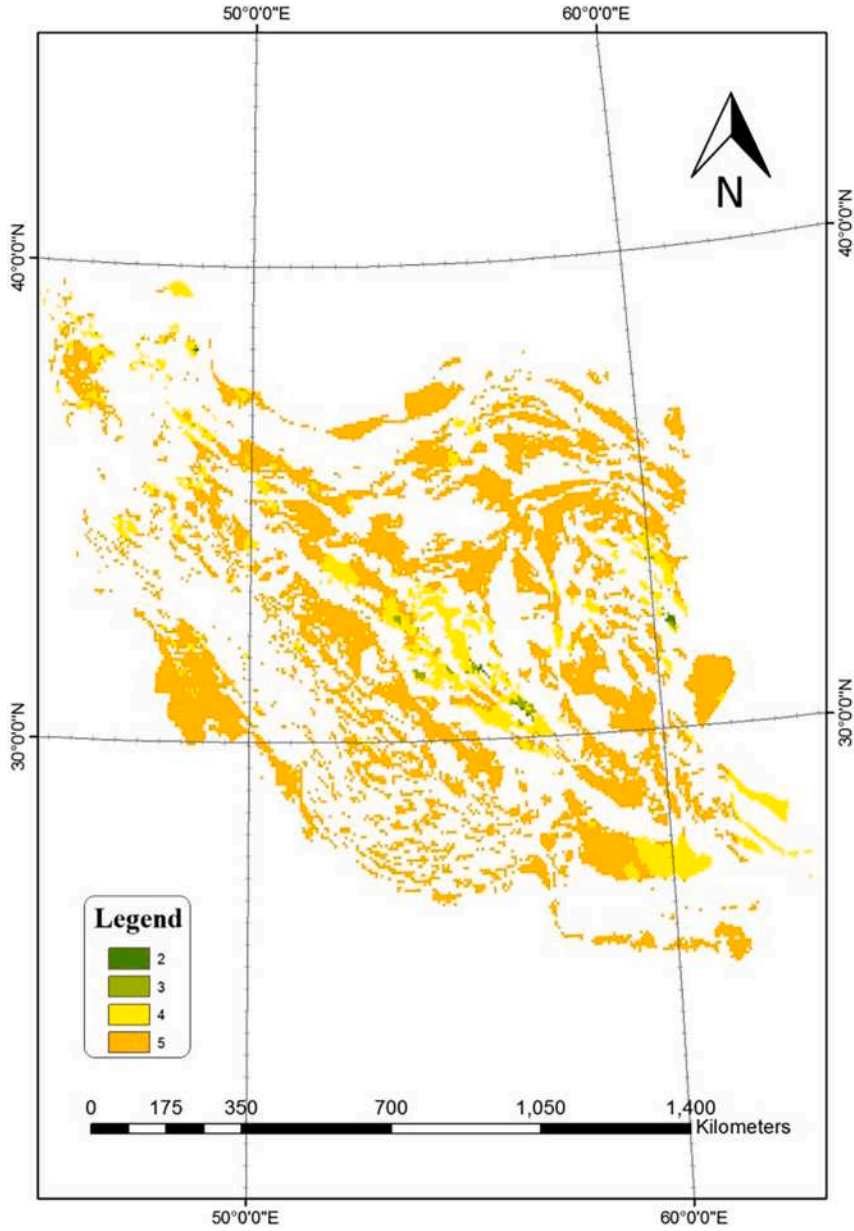


Figure 19.17 Groundwater resource index, year 2027. Map lines delineate study areas and do not necessarily depict accepted national boundaries.

trend of increasing and decreasing relative droughts of water levels in aquifers is predicted in the form of a sinusoidal function during each two-year period. However, in all periods, the two central parts of the country and the middle regions of the eastern coast, in the south of Khorasan province, will still be protected from drought. This can be attributed to the absence of specific aquifers in these areas, as well as to the difference in the nature and structure of the aquifer in relation to mountainous regions. In the western regions of Iran, the rate of exploitation of underground water is much higher than the eastern regions and especially the central parts of the country due to the development of the agricultural sector and the high population density.

In short, it can be concluded that despite the unchanged conditions of exploitation and according to the prediction maps of the GRI index, the severity of drought is reduced compared to the observation period. The reason for reducing the occurrence of droughts in the forecast period is the repetition of a randomized process. In other words, from 2023 to 2027, a large portion of groundwater aquifers is projected to fall short of meeting regional water demands. Thus, in practice, with the change in water harvesting resources for agriculture, this phenomenon will intensify and relative droughts will also decrease (Fig. 19.17).

The scarcity of groundwater happens when aquifers, as an important source of supplying water, are affected by long-term drought. Given the importance of this issue, in this chapter, intelligent forecasting models were proposed to predict the negative annual changes in the groundwater quality in larger area of Iran. The calculation was performed using GIS tools in accordance with Schuler's standard and WHO guidelines. In addition, the continuous layer of the GRI was obtained through the GeoStatistical tool. The results of ANN, PNN, and fuzzy logic clustering methods were compared.

According to the obtained result, the productivity index of the classifier with a 98.8% level of accuracy of the calculation process, as well as the level of 50% under the cumulative probability curve, confirmed the randomness of class production in the result of the ANN. The results of the GRI indices showed that the drought occurrence will increase from 2.8% during the first 10 years to 72.4% in the second 10 years, and in the same way, the normal grade of wetlands decreased from 88.2% to 29.1%. In aquifers that have violated the quality threshold values, the repetition of variations is expected to be lower in progress, while the "aquifers" belong to the "bad" class (regarding Schuler standard) are most susceptible. The findings

showed that the central regions and parts of northern Khorasan provinces, as well as a wide range of Fars province, and generally the southern regions of Iran, experienced severe drought conditions. Based on the evaluation of drought maps between 1994 and 2023, it can be stated that about 66% of the study areas are subjected to severe deterioration in drinking water quality. The results of the lowest available water quality and the highest drought using ANNs show that the qualitative stress conditions in a large part of the country's aquifers are in unfavorable conditions. This means that the possibility of dropping groundwater quality due to its cause, the occurrence of drought, is contemporary in many aquifers in the country.

Due to the large extent of the study area (609 plains of the country), the irregular distribution of the observation data (acquisition points), as well as the missing data points, the distribution of the uncertainty and the accuracy of the results have been partly decreased. Therefore, due to the vulnerability of the country's aquifers and the need for integrated water resources management to make decisions at the lowest cost, it is necessary to develop and improve data collection methods and to change these methods from a traditional form to an online one. It is suggested that in order to more accurately analyze the calculations with shorter steps, we will develop methods for rebuilding incomplete data with the least error. In order to develop the present research, the future research topics are suggested as follows:

- Modeling uncertainty analysis using numerical computational methods.
- The extension of the method of predicting groundwater quality loss by analyzing the groundwater level changes in long-term periods.

Based on the results of SPI in the second period, the "mild drought" indicator has a more rapid trend than the "near normal" drought. Due to these changes, the southern and eastern parts of the country, as well as certain parts of the northeast of the country during the period from 2013 to 2023, have been classified into two classes as "severe drought" and "very severe drought". Also, an examination of the first observation period indicates that the plains of Sistan and Baluchestan province in the southeast of the country have been facing a much longer period of drought. The average SPI index for the period 1994 to 2023 in Rudbar Jiroft Plain, Hamoon Jazmourian, Dahang Chigi, Chah Hashim, Bazman Sedghal, Iranshahr Bampur, Meshkatan, and the Southern Plains of Sistan and Baluchestan provinces face severe and very severe droughts. With the exception of the central parts of Khorasan, it is possible to calculate the total area of the eastern, southeast, and southern regions of the country, along

with the areas near Qazvin plain in the northwest of the country, for the long range in the absolute drought class.

19.5 Conclusions

This study highlights the significant impact of climate-induced drought on groundwater quality and availability in Iran's 609 study areas. By integrating artificial intelligence techniques, including ANNs, fuzzy clustering, and GPC, the research successfully modeled and predicted groundwater quality degradation in response to drought stress. The findings emphasize the urgent need for improved groundwater management strategies to mitigate the effects of prolonged drought periods.

The key findings of this study are as follows:

- Drought has a severe impact on groundwater quality and availability.
- The most affected regions are in the southern and central plains of Iran, where groundwater resources are highly vulnerable.
- Prolonged drought periods accelerate groundwater depletion and lead to increased water quality deterioration.
- Predictive analysis indicates worsening groundwater conditions from 2023 to 2027.
- A significant portion of groundwater reservoirs is projected to become unable to meet water demands.
- Despite a predicted reduction in drought severity compared to past observations, groundwater stress is expected to persist.
- Changes in water harvesting for agriculture are likely to intensify the depletion of groundwater reserves and reduce drinking water quality.
- AI and statistical modeling validated the effect of climate drought on groundwater.
- The GPC method confirmed the link between SPI-based climate drought and GRI-based groundwater drought.
- Statistical analyzes of rasterized zoning maps reinforced the prediction results, highlighting areas at greatest risk.
- The AI-driven SPI drought index prediction suggests that the most severe future droughts will affect the southern and middle plains of Iran.
- Groundwater extraction pressures are driven by multiple factors.
- Population growth and increased agricultural activity near aquifers contribute to higher groundwater exploitation.

- Reduced surface water reserves have led to a greater reliance on underground water resources.
- The return of irrigation water to aquifers has negatively impacted drinking water quality, increasing contamination risks.
- Future research should focus on improving prediction accuracy and water management strategies.
- Enhancing uncertainty modeling using numerical computational methods to reduce forecasting errors.
- Expanding the scope of groundwater quality predictions by analyzing long-term fluctuations in aquifer levels.
- Further investigating the mechanisms driving climate drought effects on groundwater depletion and resource vulnerability.

Future research should focus on improving prediction accuracy and water management strategies. Enhancing uncertainty modeling using numerical computational methods will help refine forecasting techniques. Additionally, expanding the scope of groundwater quality predictions by analyzing long-term fluctuations in aquifer levels is crucial for understanding patterns of resource depletion. Further studies should also investigate the mechanisms driving climate drought effects on groundwater vulnerability, enabling more effective mitigation and adaptation strategies.

References

Azimi, S., Azhdary Moghaddam, M., & Hashemi Monfared, S. A. (2019). Prediction of annual drinking water quality reduction based on Groundwater Resource Index (GRI) using artificial neural network and fuzzy clustering. *Journal of Contaminant Hydrology, 220*, 6–17.

Azimi, S., Azhdary Moghaddam, M., & Hashemi Monfared, S. A. (2020). Modeling the short term forecast of rainfall using artificial intelligence and its effects on the SPI drought index. *Water Resources Management, 34*, 1369–1405.

Azimi, S., Azhdary Moghaddam, M., & Hashemi Monfared, S. A. (2018). Large-scale association analysis of climate drought and decline in groundwater quality using gaussian process classification (Case Study: 609 Study Area of Iran). *Journal of Environmental Health Science and Engineering,* 1–17.

Ahmad, Z., et al. (2017). Improving water quality index prediction in Perak River basin Malaysia through a combination of multiple neural networks. *International Journal of River Basin Management, 15*(1), 79–87.

Bajc, A. F., et al. (2017). Evaluating the groundwater resource potential of the Dundas buried bedrock valley, southwestern Ontario: An integrated geological and hydrogeological case study. *Canadian Journal of Earth Sciences,* (999), 1–18.

Banerjee, P., et al. (2011). Artificial neural network model as a potential alternative for groundwater salinity forecasting. *Journal of Hydrology, 398*(3), 212–220.

Brekhovskikh, V., Volkova, Z., & Lomova, D. (2009). Assessment of water quality in the rivers of northernEuropean Russia by using oxygen demand indices. *Russian Meteorology and Hydrology, 34*, 321–330.

Chandramouli, V., Lingireddy, S., & Brion, G. (2007). Robust training termination criterion for back-propagation ANNs applicable to small data sets. *Journal of Computing in Civil Engineering, 21*(1), 39–46.
Charulatha, G., et al. (2017). Evaluation of ground water quality contaminants using linear regression and artificial neural network models. *Arabian Journal of Geosciences, 10*(6), 1–9.
Da Silva, V. D. P. R. (2004). On climate variability in Northeast of Brazil. *Journal of Arid Environments, 58*, 575–596.
Daliakopoulos, I. N., Coulibaly, P., & Tsanis, I. K. (2005). Groundwater level forecasting using artificial neural networks. *Journal of Hydrology, 309*(1), 229–240.
Demuth, H., & Beale, M. (2009). *Matlab neural network toolbox user's guide version 6*. The MathWorks Inc.
Eberhard, F., & Hamawand, I. (2017). Selective electrodialysis for copper removal from brackish water and coal seam gas water. *International Journal of Environmental Research, 11*(1), 1–11.
Ferral, A., Solis, V., Frery, A., Orueta, A., Bernasconi, I., Bresciano, J., & Scavuzzo, C. M. (2017). Spatio-temporal changes in water quality in an eutrophic lake with artificial aeration. *Journal of Water and Land Development, 35*, 27–40.
Hosseini-Moghari, S.-M., Ebrahimi, K., & Azarnivand, A. (2015). Groundwater quality assessment with respect to fuzzy water quality index (FWQI): An application of expert systems in environmental monitoring. *Environmental Earth Sciences, 74*(10), 7229.
Jalalkamali, A., Moradi, M., & Moradi, N. (2015). Application of several artificial intelligence models and ARIMAX model for forecasting drought using the Standardized Precipitation Index. *International Journal of Environmental Science and Technology, 12*, 1201–1210.
Lallahem, S., et al. (2005). On the use of neural networks to evaluate groundwater levels in fractured media. *Journal of Hydrology, 307*(1), 92–111.
Looney, C. G. (1997). *Pattern recognition using neural networks: Theory and algorithms for engineers and scientists*. Oxford University Press, Inc.
Milligan, G. W., & Hirtle, S. C. (2003). Clustering and classification methods. *Handbook of psychology*.
Milligan, G. W. (1996). Clustering validation: Results and implications for applied analyses. In *Clustering and classification*. World Scientific.
Mishra, A., & Singh, V. P. (2009). Analysis of drought severity-area-frequency curves using a general circulation model and scenario uncertainty. *Journal of Geophysical Research: Atmospheres, 114*(D6).
Mosaferi, M., et al. (2014). Quality modeling of drinking groundwater using GIS in rural communities, northwest of Iran. *Journal of Environmental Health Science and Engineering, 12*(1), 99.
Nourani, V. (2017). An Emotional ANN (EANN) approach to modeling rainfall-runoff process. *Journal of Hydrology, 544*, 267–277.
Pal, N. R., & Bezdek, J. C. (1995). On cluster validity for the fuzzy c-means model. *IEEE Transactions on Fuzzy Systems, 3*, 370–379.
Pao, Y.-H., Park, G.-H., & Sobajic, D. J. (1994). Learning and generalization characteristics of the random vector functional-link net. *Neurocomputing, 6*, 163–180.
Qaderi, F., & Babanejad, E. (2017). Prediction of the groundwater remediation costs for drinking use based on quality of water resource, using artificial neural network. *Journal of Cleaner Production*.
Sahoo, M. M., et al. (2017). Evaluation of water quality with application of Bayes' rule and entropy weight method. *European Journal of Environmental and Civil Engineering, 21*(6), 730–752.
Sakizadeh, M. (2016). Artificial intelligence for the prediction of water quality index in groundwater systems. *Modeling Earth Systems and Environment, 2*(1), 8.

Schneider, M., & Craig, M. (1992). On the use of fuzzy sets in histogram equalization. *Fuzzy Sets and Systems, 45*, 271–278.
Shamsuddin, M. K. N., et al. (2017). Forecasting of groundwater level using artificial neural network by incorporating river recharge and river bank infiltration. In *MATEC Web of Conferences*. EDP Sciences.
Tabari, H., Nikbakht, J., & Talaee, P. H. (2013). Hydrological drought assessment in Northwestern Iran based on streamflow drought index (SDI). *Water Resources Management, 27*, 137–151.
Tsakiris, G., Pangalou, D., & Vangelis, H. (2007). Regional drought assessment based on the Reconnaissance Drought Index (RDI). *Water Resources Management, 21*, 821–833.

Further reading

Edwards, D. C. (1997). *Characteristics of 20th century drought in the United States at multiple time scales*. Air Force Inst Of Tech Wright-Patterson Afb Oh.
Kang, F., et al. (2015). System probabilistic stability analysis of soil slopes using Gaussian process regression with Latin hypercube sampling. *Computers and Geotechnics, 63*, 13–25.
Lecun, Y., Bengio, Y., & Hinton, G. (2015). Deep learning. *Nature, 521*, 436–444.
Li, Y., et al. (2009b). The improved training algorithm of back propagation neural network with self-adaptive learning rate. In Computational intelligence and natural computing, CINC'09. International Conference on. 2009. IEEE.
Li, Y., Fu, Y., Li, H., & Zhang, S.-W. (2009a). The improved training algorithm of back propagation neural network with self-adaptive learning rate. In Computational Intelligenceand Natural Computing, CINC'09 (pp. 73–76). International Conference on, 2009. IEEE.
Nasrabadi, T., & Bidabadi, N.S. (n.d). *Evaluating the spatial distribution of quantitative risk and hazard level of arsenic exposure in groundwater, case study of Qorveh County*, Kurdistan Iran.
Pal, M., & Deswal, S. (2010). Modelling pile capacity using Gaussian process regression. *Computers and Geotechnics, 37*(7), 942–947.
Rasmussen, C. E., & Nickisch, H. (2010). Gaussian processes for machine learning (GPML) toolbox. *Journal of Machine Learning Research, 11*(Nov), 3011–3015.
Schmidhuber, J. (2015a). Deep learning in neural networks: An overview. *Neural Networks, 61*, 85–117.
Schmidhuber, J. (2015b). Deep learning in neural networks: An overview. *Neural Networks, 61*, 85–117.
Xie, X. L., & Beni, G. (1991). A validity measure for fuzzy clustering. *IEEE Transactions on Pattern Analysis and Machine Intelligence, 13*, 841–847.
Zhang, G., Patuwo, B. E., & Y. Hu, M. (1998b). Forecasting with artificial neural networks The state of the art. *International Journal of Forecasting, 14*(1), 35–62.
Zhang, G., Patuwo, B. E., & Hu, M. Y. (1998a). Forecasting with artificial neural networks: The state of the art. *International Journal of Forecasting, 14*, 35–62.

This page intentionally left blank

CHAPTER TWENTY

Historical fluctuations of water storage in response to drought: a study of Iran

Behnam Khorrami
Department of Remote Sensing and GIS, University of Tabriz, Tabriz, Iran

20.1 Introduction

The availability of water, whether on the Earth's surface or beneath it, is crucial for supporting both human and wildlife populations, in addition to promoting economic and agricultural development. This significance is particularly highlighted in contexts where climate change and increasing population demand greater access to water resources to satisfy essential needs (Khorrami & Gunduz, 2019). Water storage is a critical component of the hydrological cycle and plays a vital role in sustaining ecosystems, agriculture, and human livelihoods. However, water storage is highly vulnerable to climate variability, particularly in regions that experience frequent and severe droughts (Khorrami, 2023). Understanding the fluctuations of water storage in response to drought events is crucial for water resource management and policymaking.

One of the most effective ways to assess the large-scale variations in water storage is through the terrestrial water storage (TWS) variations. The aggregate of water held in glaciers, snowpacks, and surface water bodies (including lakes, reservoirs, and wetlands), as well as the moisture found in soils, vegetation canopies, and underground aquifers, is referred to as TWS (Rodell & Famiglietti, 2001). The multifaceted nature of TWS and its critical role compel researchers to gather precise information on its fluctuations across different spatial and temporal scales, thereby facilitating the effective oversight and management of water resources.

The establishment of the gravity recovery and climate experiment (GRACE) satellite mission has constituted a breakthrough in the remote sensing of hydrology, specifically targeting the global assessment of fluctuations in TWS (Tapley et al., 2004). The GRACE and GRACE

Drought Dynamics
DOI: https://doi.org/10.1016/B978-0-443-34205-9.00016-0
© 2026 Elsevier Inc. All rights reserved, including those for text and data mining, AI training, and similar technologies.

follow-on (GRACE-FO) missions have provided us with global observations of TWS variations, and their data have so far been extensively used by many researchers to monitor hydroclimatic events and variations of TWS and other water cycle components at local, regional, and global domains (Ali et al., 2024; Ali, Khorrami, Jehanzaib, Tariq, Ajmal, Arshad, Shafeeque, Dilawar, Basit, Zhang, Sadri, Niaz, Jamil, Khan 2023; Forootan et al., 2014; Khorrami & Arik, & Gunduz, 2021; Khorrami & Gunduz, 2021; Khorrami & Gündüz, 2023; Khorrami, Ali, Abadi, et al., 2023; Tariq et al., 2023). Both natural and human-induced factors play a significant role in the spatiotemporal dynamics of hydroclimatic parameters, consequently impacting the distribution of water storage (Khorrami, Ali, et al., 2023).

Iran, a country characterized by arid and semiarid climatic conditions, has faced recurrent drought events over the past decades, significantly impacting water resources (Madani, 2014). The water resources of Iran are experiencing significant strain due to factors such as population growth and dry periods, along with their associated consequences. The burgeoning population has directly heightened the demand for fresh water in urban areas. Indirectly, this demographic shift has led to an increased requirement for agricultural land and the expansion of irrigation systems (Ardakani, 2009). The interplay between limited freshwater availability, swift population growth, and the climate change impacts significantly heightens the country's vulnerability to future climate-related impacts. During the past few years, there has been a marked rise in the volume of research concerning climate change in Iran, which has denoted a significant warming trend in the country over the last half-century (Modarres et al., 2016). The consecutive droughts that occurred in the region, have significantly affected the water resources in Iran (Khaki & Hoteit, 2021). It is documented that Iran is experiencing recurrent droughts of different severities every 2.5 years (Khorrami et al., 2018; Zarch et al., 2011).

This study aims to analyze historical fluctuations in water storage across different climate regions of Iran in response to drought events by utilizing GRACE-derived TWS. By examining the temporal and spatial variations of TWS concerning drought indices, this research seeks to enhance our understanding of the hydrological response to drought in Iran and provide insights for sustainable water resource management.

20.2 Study area

Iran, encompassing an area of approximately 1.6 million km^2, is situated between the latitudinal coordinates of 24° 16'N and 40°N, as well as the longitudinal coordinates of 44°E to 64° 16'E (Fig. 20.1). The country is divided into six different zones according to its diverse climatic conditions (Najafi & Alizadeh, 2023). Table 20.1 illustrates these climate zones with the statistics on their area coverage, mean annual precipitation (MAP), and mean annual evapotranspiration (MAET) values. Around 80% of the country is classified as having an arid to semiarid climate (Table 20.1), featuring intensely hot summers, especially in the central and southern coastal regions. The MAP of the country ranges between 18 mm (in Zone VI) and 951 mm (in Zone III). The scarcity of water in

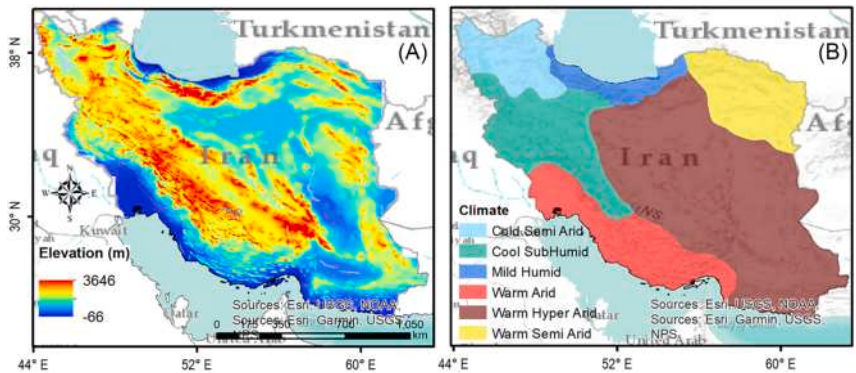


Figure 20.1 (A) Geographic location of Iran and (B) climate zones of Iran (Najafi & Alizadeh, 2023). Map lines delineate study areas and do not necessarily depict accepted national boundaries.

Table 20.1 Statistics of the climate zones of Iran.

Climate zones	Climate type	Area (%)	MAP (mm)	MAET (mm)
Zone I	Cold and semiarid	7.48	434	413
Zone II	Cool and sub-humid	14.69	411	310
Zone III	Mild and humid	4.16	951	345
Zone IV	Warm and semiarid	11.36	234	168
Zone V	Warm and arid	13.92	226	211
Zone VI	Warm and yperarid	48.38	118	139

the region has brought about an unequal distribution of this water resource across Iran, resulting in environmental issues. A considerable portion of the country is situated within the arid zones (Fig. 20.1), highlighting the chronic insufficiency of water resources to meet the diverse demands for municipal, recreational, and industrial activities; for irrigation and aquaculture in agricultural contexts; as well as for non-consumptive applications, primarily in energy production and transportation.

20.3 Data preparation and analysis

This study used different remote sensing data as well as model outputs to evaluate the variations of TWS and their associations with drought across different climate zones of Iran from 2002 to 2024. The following gives details on the datasets applied in the analysis.

20.4 GRACE and GRACE-FO data

The GRACE stands as an innovative remote sensing endeavor operated by the National Aeronautics and Space Administration (NASA) alongside the German Space Agency (DLR). This mission features the deployment of two satellites that operate in close formation to collect comprehensive data on the Earth's gravitational field (Tapley et al., 2019). The initiative was launched with the first satellite pair in March 2002. The GRACE-1 satellite effectively monitored the gravity field for a total of 16 years, with its mission concluding in June 2017. After an 11-month interval, the subsequent mission commenced with the launch of the GRACE-Follow On (GRACE-FO) satellite in May 2018. The present analysis employs TWS data from the latest mascon products of GRACE and GRACE-FO (CSR, JPL, and GSFC) to investigate the dynamics of water storage in Iran over the timeframe from April 2002 to April 2024.

20.5 Standardized precipitation index

Standardized precipitation index (SPI) is a commonly used drought index, and it has multi-time scale characteristics (McKee et al., 1993). Drought conditions are evaluated through the analysis of total precipitation levels. In this study, the SPI data were received from the National

Oceanic and Atmospheric Administration's (NOAA) Climate Prediction Center (CPC) (https://www.drought.gov/data-maps-tools/global-gridded-standardized-precipitation-index-spi-cmorph-daily).

20.6 Wetness percentile index

Scientists at NASA's Goddard Space Flight Center generate weekly metrics to assess drought conditions related to groundwater and soil moisture. These metrics are derived from TWS information collected by the GRACE-FO satellite and are further refined by incorporating supplementary observational data through a sophisticated numerical model that simulates the dynamics of water and energy at the land surface (Li et al., 2019). Water storage fluctuations, which encompass medium- to long-term meteorological patterns, serve as a valuable indicator of drought intensity and persistence, presenting a more concrete assessment than that provided by a precipitation index (Li et al., 2019). This dataset includes three key indicators of drought: groundwater storage percentile, root zone soil moisture percentile, and surface soil moisture percentile. For this research, the ensemble mean of these indicators was employed to formulate a drought indicator known as the wetness percentile index (WPI).

20.7 Reconstruction of the missing GRACE /GRACE-FO data

The intermittent absence of TWS data from the GRACE satellite, in conjunction with a continuous 11-month break between the GRACE and GRACE-FO missions, complicates the effective oversight of water resources. Thus, it is vital to enhance the dataset by incorporating the missing months. In this investigation, the months lacking data from the GRACE and GRACE-FO missions were reconstructed through the application of the Seasonal Trend decomposition using the Loess (STL) approach, as suggested by Khorrami (2023). The integration of the STLas a comprehensive filtering strategy for the disaggregation of time series datasets supports the precise representation and articulation of the authentic TWS characteristics observed by the GRACE, which incorporates both natural and anthropogenic elements. Thus, it proficiently compensates for the deficiencies in the global TWS dataset (Khorrami, Ali, Sahin, et al., 2023;

Ali, Khorrami, Jehanzaib, Tariq, Ajmal, Arshad, Shafeeque, Dilawar, Basit, Zhang, Sadri, Niaz, Jamil, Khan 2023). The STL initially breaks down the time series data into its constituent parts (Eq. (20.1)). Subsequently, it fills the missing data by incorporating the mean seasonal and residual values, in addition to the trend component specific to the missing month (Eq. (20.2))

$$TWS = Trend_t + Seasonal_t + Residual_t \tag{20.1}$$

$$TWS_t = y\,(Trend_t) + \overline{Seasonal_t + Residual_t} \tag{20.2}$$

where $Trend_t + Seasonal_t + Residual_t$ at time t is the trend, seasonal, and residual of TWS time series, respectively.

In the course of this study, a total of 33 missing data points from the GRACE and GRACE-FO missions were observed, which accounted for 22 months of mission interruptions—20 of which were linked to the GRACE mission and 2 to the GRACE-FO mission. In addition, there were 11 months of gaps that arose during the transitional period between the two missions. The STL technique was applied to fill these gaps, resulting in a unified dataset that facilitated the analysis.

20.8 Seasonality assessment

The concept of seasonality encapsulates the fluctuations that occur throughout the year. In this study, standard deviation was employed as a method to assess and illustrate the seasonal fluctuations of TWS annually (Wasko et al., 2020). Standard deviation is a fundamental measure of statistical dispersion utilized in probability statistics. It is calculated as the square root of the average of the squared differences between each data point and the mean of the dataset. This measure is essential for quantifying the variability present within a dataset. An elevated standard deviation indicates a heightened degree of variability within a specific year, suggesting a more significant seasonal influence. Conversely, a diminished standard deviation reflects a lesser degree of seasonal variability.

20.9 Trend analysis

The Mann-Kendall (MK) trend test, formulated and refined by Kendall (1975), was utilized to discern trends in the time series data.

This non-parametric statistical method does not impose any distributional assumptions on the input variables, as indicated by Alhaji et al. (2018). Thus, it is a prevalent choice for trend analysis in hydrometeorological time series. The MK trend test is performed through the application of specific mathematical equations.

$$S = \sum_{i=1}^{SS-1} \sum_{j=i+1}^{SS} \operatorname{sgn}(x_i - x_j) \ldots forj > I \tag{20.3}$$

$$V(S) = \frac{SS(SS-1)(2SS+5) - \sum_{m=1}^{SS} ti(m-1)(2m+5)m}{18} \tag{20.4}$$

$$Z = \begin{cases} \frac{S-1}{\sqrt{V(S)}} S > 0 \\ 0 S = 0 \\ \frac{S+1}{\sqrt{V(S)}} S < 0 \end{cases} \tag{20.5}$$

where SS is the sample size, x_i and x_j are the sequential data in the time series, $V(S)$ is the variance of S, t_i is the number of ties of length m, and Z is the standardized S (Blain, 2013).

Within the framework of the MK test, the null hypothesis (H_0) maintains that there is no discernible trend in the time series, a claim that can be assessed in alignment with the Z value. Therefore, the H_0 can be rejected if $|Z| > Z_{1-(\alpha/2)}$. In this scenario, the rejection of H_0 is seen as favorable, leading to the conclusion that the trend within the time series is significant. The trend's direction is determined by the Z value, where a positive Z indicates an upward trend and a negative Z suggests a downward trend (Gocic & Trajkovic, 2013). In this analysis, the significance of each time series trend was examined at a significance level (α) of 0.05.

20.10 Results and discussion

20.10.1 Fluctuations of water storage

The assessment of water storage fluctuations involved the use of TWS from the GRACE. A time series graph was generated to illustrate the long-term trends of TWS across different climate zones of Iran (Fig. 20.2). The results demonstrate a wax and wane pattern over all the zones from 2002 to 2008.

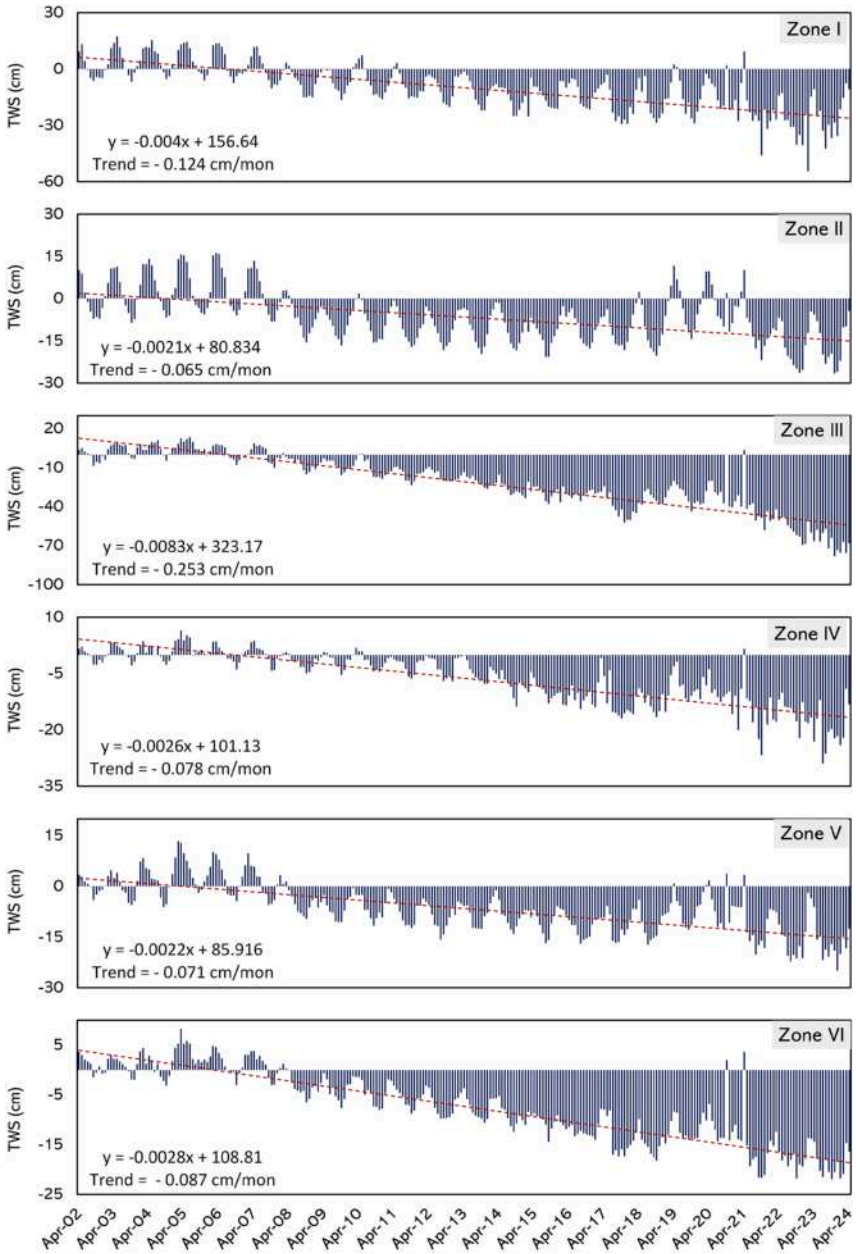


Figure 20.2 Fluctuations of terrestrial water storage (TWS) across climate zones of Iran.

The variations in water storage show a diminishing pattern from 2008 onwards. The statistical results demonstrate that over all the climate zones of Iran, the overall trend of TWS is significantly decreasing. The maximum and minimum trend is observed over Zone III and Zone II, with monthly diminishing water storage of − 0.253 cm and − 0.065 cm, respectively.

The overall evaluation of the trends indicates that the country has experienced a severe loss of water storage, as also reported by Khaki and Hoteit (2021). During the study period, Iran has lost about − 17.84 km^3/yr of its water storage, which is equivalent to − 392.48 km^3 of total storage loss for the last 22 years. The alarming status of water storage variations in Iran was also documented from 2002 to 2015 (Bozorg-Haddad et al., 2020). The zonal evaluation of TWS loss is given in Table 20.2. The trend analysis reveals that Zone III is the most critical climate zone of the country with the mean zonal water storage loss of about − 3.04 cm per year. The maximum storage loss considering the area of each zone has occurred in Zone VI with a total water storage depletion of − 183.15 km^3.

20.11 Seasonal dynamics of water storage

Fig. 20.3 portrays the temporal seasonal cycle of the TWS for the whole study period (April 2002 − April 2024) across the climate zones of Iran. The country-wise values suggest that the TWS shows decreasing values throughout all the seasons over the region. The maximum and minimum storage depletion values for the TWS occur in July (− 11.84 cm), and January (− 3.90 cm), respectively. The zonal seasonal variations of TWS indicate decreasing water storage throughout all the seasons for all the climate

Table 20.2 Zonal fluctuations of terrestrial water storage (TWS).

Climate zone	TWS trend			*P*-value	Trend test (α = 0.05)
	cm/yr	km^3/yr	**Total loss** (km^3)		
Zone I	− 1.49	− 1.83	− 40.36	0.000	*Descending trend
Zone II	− 0.78	− 1.89	− 41.56	0.000	*Descending trend
Zone III	− 3.04	− 2.08	− 45.78	0.000	*Descending trend
Zone IV	− 0.94	− 1.75	− 38.55	0.000	*Descending trend
Zone V	− 0.85	− 1.96	− 43.02	0.000	*Descending trend
Zone VI	− 1.04	− 8.33	− 183.15	0.000	*Descending trend

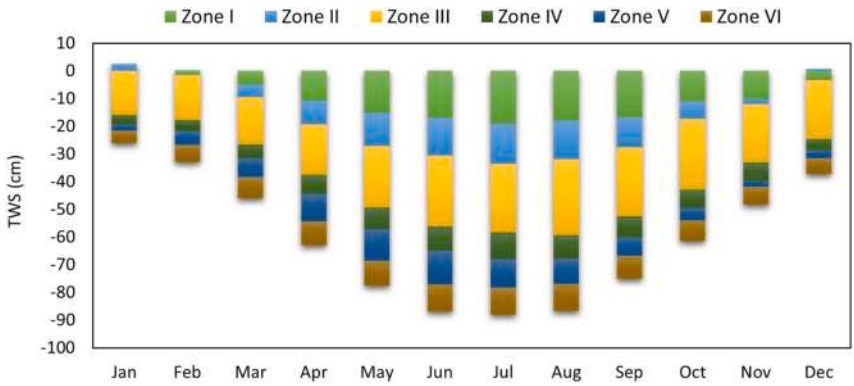


Figure 20.3 Seasonal dynamics of TWS across climate zones of Iran (2002–2024).

zones, excluding the TWS variations in January over Zone I and Zone II with positive variation values of 0.02 cm and 2.59 cm, respectively. Different seasonality is seen over the climate zones of the country. The most severe depletion of the climate zones occurs between June and August. The results show that for Zone I, Zone II, and Zone IV the most storage loss happens in July with the TWS values of − 19.09cm, − 14.36cm, and − 09.80cm respectively. For Zone V and Zone VI, on the other hand, the most storage loss takes place in June with the TWS values of − 12.01 cm and − 09.88 cm, respectively. The most critical seasonality is seen over Zone III in August, with the maximum storage loss of − 27.39 cm.

The seasonality of TWS (Fig. 20.4) demonstrates the spatial patterns of the seasonal cycle for TWS, over the country. According to the result, TWS shows that the most seasonal impacts are observed over northern Iran in Zone III, reaching up to 32 cm.

20.12 Variations of standardized precipitation index

To show the drought status in Iran, the SPI data were used, and the corresponding temporal scales (SPI-01, SPI-03, SPI-06, SPI-09, SPI-12) were extracted (Fig. 20.5). To select the most suitable time scale of SPI for the analysis, the associations between TWS and SPIs were examined, and it was found that with the temporal correlation of 0.43, the SPI-12 had the most powerful interaction with TWS over Iran. The correlation between the TWS and SPI-01, SPI-03, SPI-06, and SPI-09 was − 0.03,

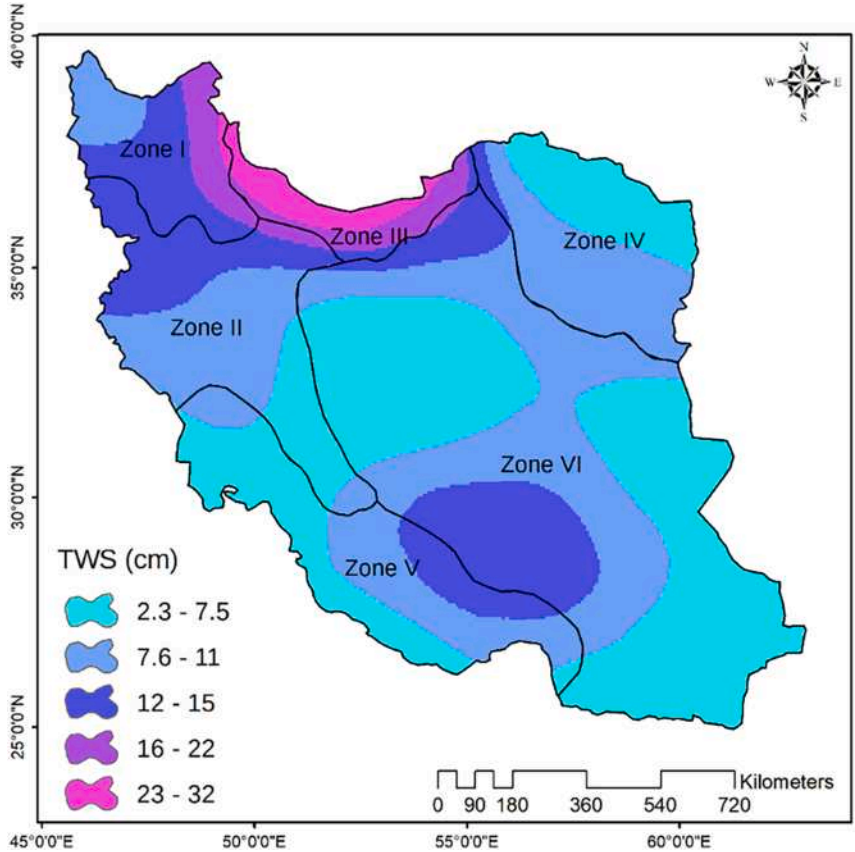


Figure 20.4 Spatial patterns of seasonality of terrestrial water storage (TWS) across Iran. Map lines delineate study areas and do not necessarily depict accepted national boundaries.

0.02, 0.17, and 0.32, respectively. As a result, SPI-12 was used in the analysis.

The variations of SPI suggest different stages of dry conditions in Iran. It can be inferred that the country has gone through dryness in 2008–2009, 2018, and 2021. According to the literature, mega-droughts in 1998–2001 and 2007–2008 have impacted the Middle East region (Barlow et al., 2016). The footprints of the 2007–2008 mega-drought are seen in the variations of SPI over Iran. Severe drought incidents during the years between 2000 and 2020, were identified and reported in Iran (Hameed et al., 2018; Lashkari et al., 2021).

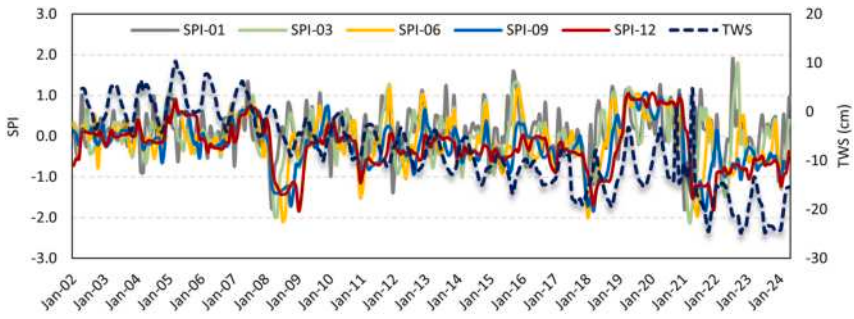


Figure 20.5 Temporal variations of standardized precipitation index (SPI) over Iran (2002–2024).

20.13 Associations between water storage variations and drought indices

To draw a temporal analogy between the TWS variations and SPI over different zones of the study, the zonal mean values were graphed (Fig. 20.6). The statistical results show low to moderate zonal associations between TWS and SPI in Zone I (0.36), Zone II (0.47), Zone III (0.40), Zone IV (0.36), Zone V (0.27), and Zone VI (0.31). The weakness seen in the associations between SPI and TWS can be ascribed to the nature of these two parameters. The TWS shows variations of the total water storage, which reflects the interactions between different hydrological fluxes including precipitation, evapotranspiration, and surface and subsurface factors as well. The SPI, on the other hand, discloses dry and wet events only based on the deviations of precipitation; thus, it does not directly capture subsurface water storage variations. Therefore, SPI correlates better with surface and near-surface hydrological components. Another influential parameter is the hydroclimatic and geological characteristics of the region of interest. The relationship between the SPI and TWS is notably weak in arid and semiarid regions, primarily due to their slow rates of infiltration and reliance on deeper groundwater supplies (Chen et al., 2016). In contrast, regions with high humidity, which experience significant surface runoff and possess shallow soil moisture reserves, tend to exhibit stronger SPI–TWS correlations. This phenomenon is also reflected in the relationships observed across different climate zones in the study. The most robust correlations are observed in the humid Zones II and III, while the more arid zones demonstrate weaker relationships.

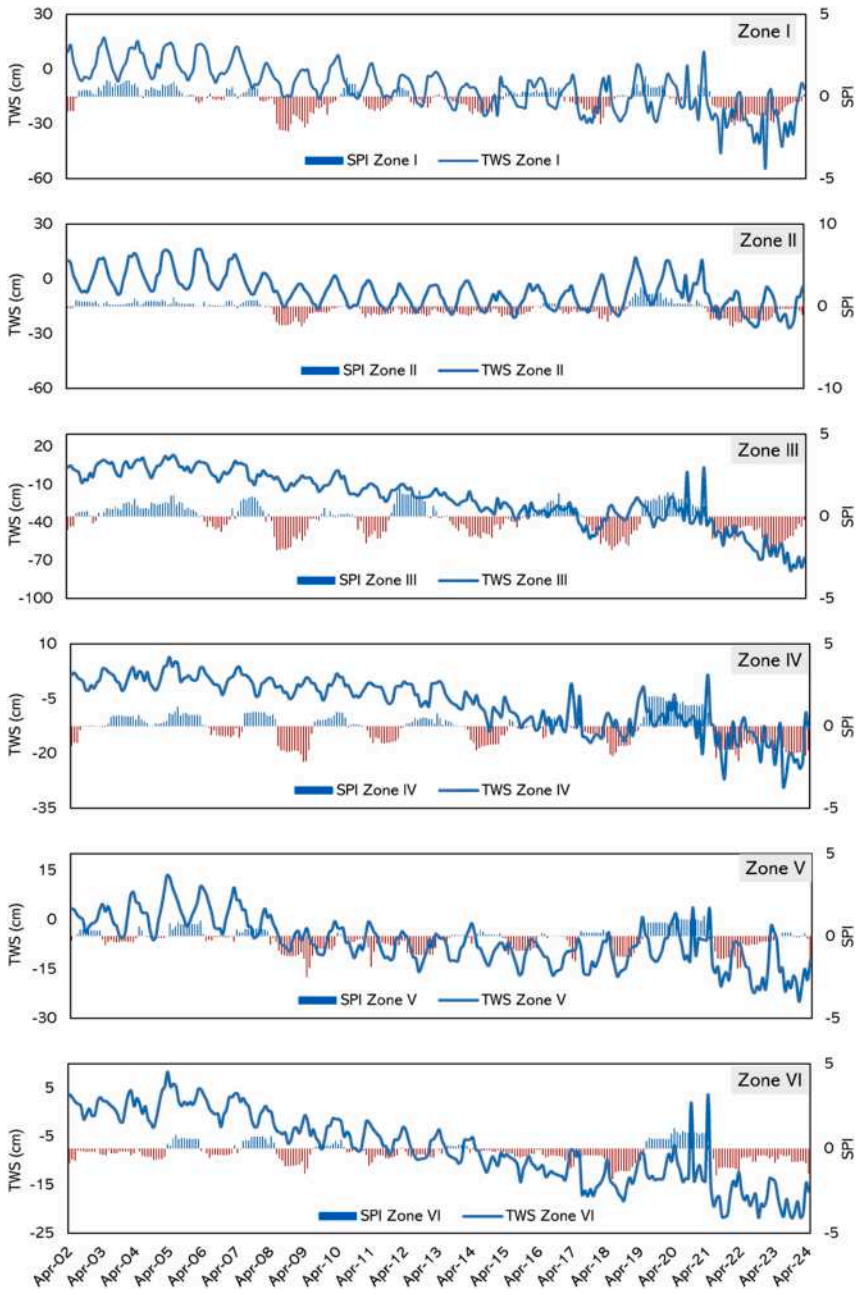


Figure 20.6 Associations between terrestrial water storage (TWS) and standardized precipitation index (SPI).

Furthermore, the weaker correlation between SPI and TWS can be linked to the dependency of SPI on timescales. Our analysis indicates that as the time scale of SPI increases, the correlations become more pronounced. This finding is supported by Zhong et al. (2020), who suggest that longer accumulation periods enhance SPI correlations with TWS, as prolonged precipitation deficits significantly influence deeper storage elements. It is believed that with even longer periods of SPI, for instance, SPI-24 to SPI-36, even stronger correlations for the TWS-SPI variations can be achieved. In this study, because of the limited global SPI timescales (limited to the used timescales in this study), longer periods of SPI were not available to use.

To better investigate the interactions between SPI and TWS, the associations were assessed from the viewpoint of the trend analysis results (Fig. 20.7). The analysis shows that SPI, similar to TWS, is significantly decreasing across all the climate zones of the study, suggesting that drying condition leads to reduced water storage or at least exacerbate the diminishing water storage over the study areas. illustrates the multiyear trend maps of TWS and SPI in Iran.

The temporal variations in WPI (Fig. 20.8) reveal that the wetness of the region is decreasing from 2003 to 2024, which is in a high consistency with what the TWS variations suggest. The correlation between TWS and WPI across Zone I, Zone II, Zone III, Zone IV, Zone V, and Zone VI is

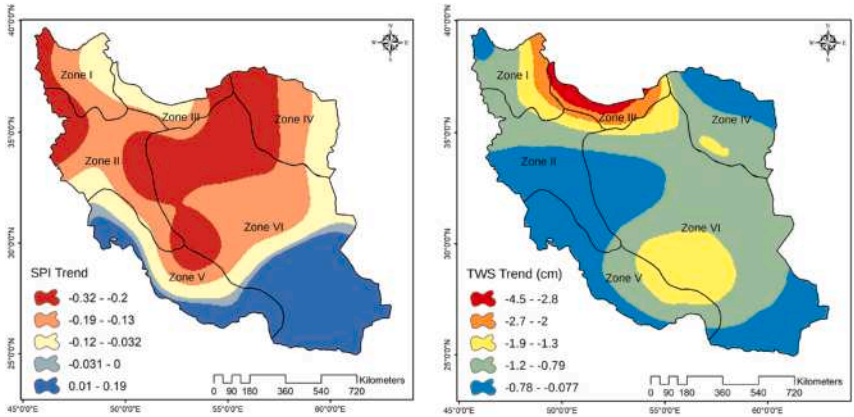


Figure 20.7 Multiyear trend map of terrestrial water storage (TWS) and standardized precipitation index (SPI). Map lines delineate study areas and do not necessarily depict accepted national boundaries.

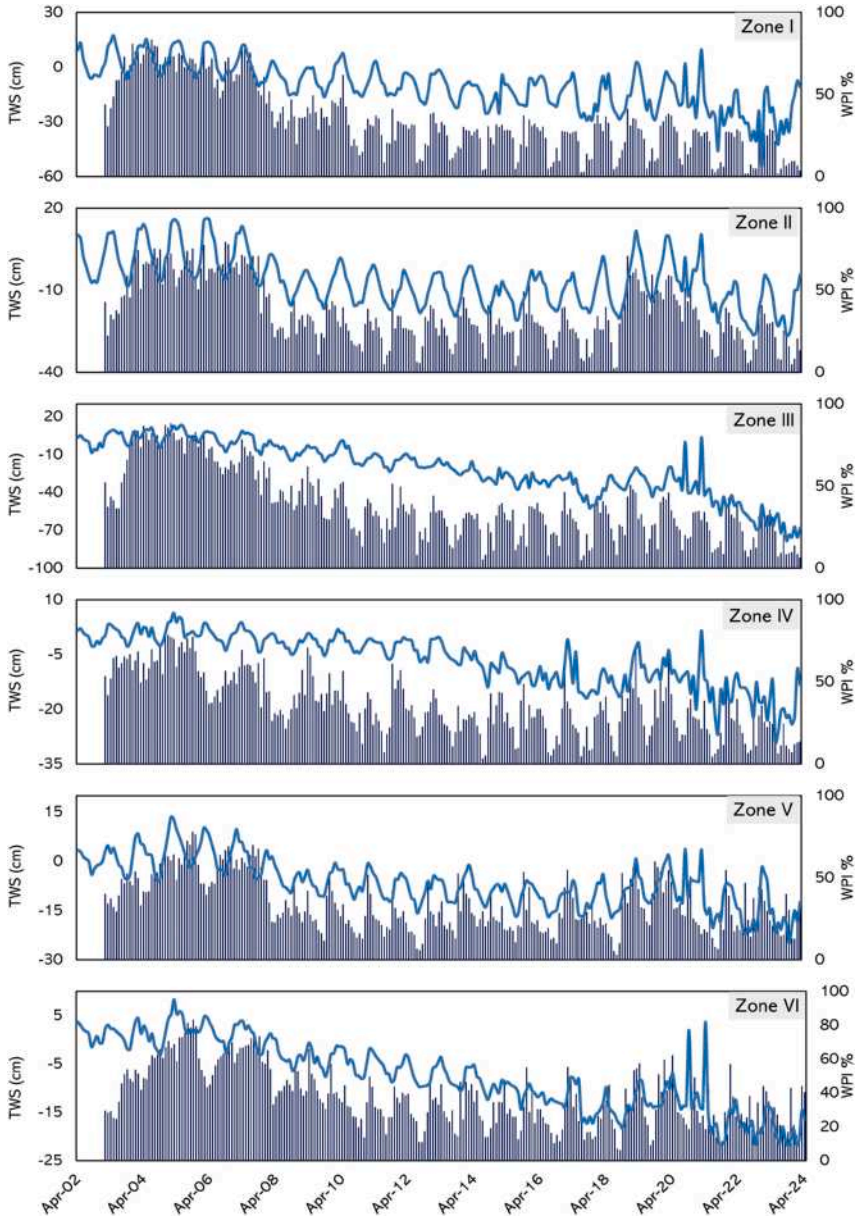


Figure 20.8 Associations between wetness percentile index (WPI) and terrestrial water storage (TWS).

0.76, 0.67, 0.74, 0.67, 0.63, and 0.67, respectively. WPI is in good consistency with the GRACE-observed TWS. This can be ascribed to different parameters. First, the two parameters are of an interlinked nature. The WPI is produced using the TWS values to better reveal the dry and wet hydrological conditions and ensure that wetness conditions remain closely aligned with the water storage variations (Tangdamrongsub et al., 2020). The second issue is the impacts of the climate and the interactions between surface and subsurface water. Over humid and semihumid regions where groundwater and soil moisture are strongly coupled, higher correlations are seen between TWS and WPI (Maxwell & Condon, 2016). Under arid climate conditions, where groundwater is the dominant component of the TWS, WPI captures long-term trends in TWS depletion and recovery cycles (Rodell et al., 2015). In Iran, a great proportion of water requirement is met through the extraction of groundwater from aquifers due to the limited water provided by precipitation (Joodaki et al., 2014). Another parameter influencing the associations between TWS and WPI is the snow and surface water storage. In snow-dominated regions, seasonal snow accumulation and melt cycles drive TWS and WPI in parallel, leading to strong correlations (Richey et al., 2015).

20.14 Conclusion

This study investigated the spatiotemporal variability of water storage and its associations with drought indices over different climate zones of Iran during the GRACE era from 2002 to 2024. The main findings are as follows:

1. Water storage in Iran is shrinking swiftly with an annual trend of − 17.84 km^3 resulting in the total storage depletion of − 392.48 km^3 during the last 22 years.
2. Zone III is the most critical climate zone of the country with a water storage loss of about− 3.04 cm per year. While the maximum storage loss considering the area of each zone has occurred in Zone VI.
3. Iran has gone through dryness mainly in three periods: 2008–2009, 2018, and 2021.
4. From 2008 onwards, a sharp, continuous declining trend in water storage across all the climate zones of the country has been observed.

The results of this study are essential for the understanding of the dynamics of water storage and droughts in Iran. The zonal analysis

according to the dominant climate of each one can significantly improve our understanding of the interactions of droughts and water storage variations, which further underlines the impacts of drought on water dynamics.

References

Alhaji, U. U., Yusuf, A. S., Edet, C. O., Oche, C. O., & Agbo, E. P. (2018). Trend analysis of temperature in gombe state using mann kendall trend test. *Journal of Scientific Research and Reports, 20*(3), 1–9. https://doi.org/10.9734/jsrr/2018/42029.

Ali, S., Khorrami, B., Jehanzaib, M., Tariq, A., Ajmal, M., Arshad, A., Shafeeque, M., Dilawar, A., Basit, I., Zhang, L., Sadri, S., Niaz, M. A., Jamil, A., & Khan, S. N. (2023). Spatial downscaling of GRACE data based on XG boost model for improved understanding of hydrological droughts in the indus basin irrigation system (IBIS). *Remote Sensing, 15*(4), 873. https://doi.org/10.3390/rs15040873.

Ali, S., Ran, J., Luan, Y., Khorrami, B., Xiao, Y., & Tangdamrongsub, N. (2024). The GWR model-based regional downscaling of GRACE/GRACE-FO derived groundwater storage to investigate local-scale variations in the North China Plain. *Science of The Total Environment, 908*, 168239. https://doi.org/10.1016/j.scitotenv.2023.168239.

Ardakani, R. (2009). Overview of water management in Iran. In *Proceeding of regional center on urban water management*.

Barlow, M., Zaitchik, B., Paz, S., Black, E., Evans, J., & Hoell, A. (2016). A review of drought in the middle East and Southwest Asia. *Journal of Climate, 29*(23), 8547–8574. https://doi.org/10.1175/jcli-d-13-00692.1.

Blain, G. C. (2013). The modified Mann-Kendall test: on the performance of three variance correction approaches. *Bragantia, 72*(4), 416–425. https://doi.org/10.1590/brag.2013.045.

Bozorg-Haddad, O., Zolghadr-Asli, B., Sarzaeim, P., Aboutalebi, M., Chu, X., & Loáiciga, H. A. (2020). Evaluation of water shortage crisis in the Middle East and possible remedies. *Journal of Water Supply: Research and Technology—AQUA. 69*(1), 85–98. https://watermark.silverchair.com/jws0690085.pdf https://doi.org/10.2166/aqua.2019.049, https://watermark.silverchair.com/jws0690085.pdf.

Chen, J., Famigliett, J. S., Scanlon, B. R., & Rodell, M. (2016). Groundwater storage changes: Present status from GRACE observations. *Surveys in Geophysics, 37*(2), 397–417. https://doi.org/10.1007/s10712-015-9332-4, http://www.wkap.nl/journalhome.htm/0169-3298.

Forootan, E., Rietbroek, R., Kusche, J., Sharifi, M. A., Awange, J. L., Schmidt, M., Omondi, P., & Famiglietti, J. (2014). Separation of large scale water storage patterns over Iran using GRACE, altimetry and hydrological data. *Remote Sensing of Environment, 140*, 580–595. https://doi.org/10.1016/j.rse.2013.09.025.

Gocic, M., & Trajkovic, S. (2013). Analysis of changes in meteorological variables using Mann-Kendall and Sen's slope estimator statistical tests in Serbia. *Global and Planetary Change, 100*, 172–182. https://doi.org/10.1016/j.gloplacha.2012.10.014.

Hameed, M., Ahmadalipour, A., & Moradkhani, H. (2018). Apprehensive drought characteristics over Iraq: Results of a multidecadal spatiotemporal assessment. *Geosciences, 8*(2), 58. https://doi.org/10.3390/geosciences8020058.

Joodaki, G., Wahr, J., & Swenson, S. (2014). Estimating the human contribution to groundwater depletion in the Middle East, from GRACE data, land surface models, and well observations. *Water Resources Research, 50*(3), 2679–2692. https://doi.org/10.1002/2013wr014633.

Kendall, M. G. (1975). *Rank correlation methods*..

Khaki, M., & Hoteit, I. (2021). Monitoring water storage decline over the Middle East. *Journal of Hydrology, 603*, 127166. https://doi.org/10.1016/j.jhydrol.2021.127166.

Khorrami, B., Ali, S., Sahin, O. G., & Gunduz, O. (2023). Model-coupled GRACE-based analysis of hydrological dynamics of drying Lake Urmia and its basin. *Hydrological Processes, 37*(5), 10991085. http://onlinelibrary.wiley.com/journal/10.1002/(ISSN)1099-1085 https://doi.org/10.1002/hyp.14893, http://onlinelibrary.wiley.com/journal/10.1002/(ISSN)1099-1085.

Khorrami, B., Ali, S., Abadi, L. H., & Jehanzaib, M. (2023). Spatio-temporal variations in characteristics of terrestrial water storage and associated drought over different geographic regions of Türkiye. *Earth Science Informatics, 16*(1), 717–731. https://www.springer.com/journal/12145 https://doi.org/10.1007/s12145-022-00907-3, https://www.springer.com/journal/12145.

Khorrami, B. (2023). Satellite-based investigation of water stress at the basin scale: An integrated analysis of downscaled GRACE estimates and remotely sensed data. *Journal of Hydroinformatics, 25*(4), 1501–1512. https://doi.org/10.2166/hydro.2023.062.

Khorrami, B., Ali, S., & Gündüz, O. (2023). An appraisal of the local-scale spatio-temporal variations of drought based on the integrated GRACE / GRACE-FO observations and fine-resolution FLDAS model. *Hydrological Processes, 37*(11). https://doi.org/10.1002/hyp.15034.

Khorrami, B., Arik, F., & Gunduz, O. (2021). Land deformation and sinkhole occurrence in response to the fluctuations of groundwater storage: An integrated assessment of GRACE gravity measurements, ICESat/ICESat-2 altimetry data, and hydrologic models. *GIScience & Remote Sensing, 58*(8), 1518–1542. https://doi.org/10.1080/15481603.2021.2000349.

Khorrami, B., & Gunduz, O. (2021). Evaluation of the temporal variations of groundwater storage and its interactions with climatic variables using GRACE data and hydrological models: A study from Turkey. *Hydrological Processes, 35*(3). https://doi.org/10.1002/hyp.14076.

Khorrami, B., & Gunduz, O. (2019). Analyses of meteorological drought and its impacts on groundwater fluctuations, a case Study: Marand plain (Iran). *Pamukkale University Journal of Engineering Sciences, 25*(6), 711–717. https://doi.org/10.5505/pajes.2019.63600.

Khorrami, B., & Gündüz, O. (2023). Remote sensing-based monitoring and evaluation of the basin-wise dynamics of terrestrial water and groundwater storage fluctuations. *Environmental Monitoring and Assessment, 195*(7). https://doi.org/10.1007/s10661-023-11480-7.

Khorrami, B., Valizadeh Kamran, K., & Roostaei, S. (2018). Assessment of groundwater-level susceptibility to degradation based on analytical network process (ANP). *International Journal of Environment and Geoinformatics, 5*(3), 314–324. https://doi.org/10.30897/ijegeo.451067.

Lashkari, A., Irannezhad, M., Zare, H., & Labzovskii, L. (2021). Assessing long-term spatio-temporal variability in humidity and drought in Iran using Pedj Drought Index (PDI). *Journal of Arid Environments, 185*, 104336. https://doi.org/10.1016/j.jaridenv.2020.104336.

Li, B., Rodell, M., Kumar, S., Beaudoing, H. K., Getirana, A., Zaitchik, B. F., de Goncalves, L. G., Cossetin, C., Bhanja, S., Mukherjee, A., Tian, S., Tangdamrongsub, N., Long, D., Nanteza, J., Lee, J., Policelli, F., Goni, I. B., Daira, D., Bila, M., de Lannoy, G., Mocko, D., Steele-Dunne, S. C., Save, H., & Bettadpur, S. (2019). Global GRACE data assimilation for groundwater and drought monitoring: Advances and challenges. *Water Resources Research, 55*(9), 7564–7586. http://agupubs.onlinelibrary.wiley.com/hub/journal/10.1002/(ISSN)1944-7973/ https://doi.org/10.1029/2018WR024618, http://agupubs.onlinelibrary.wiley.com/hub/journal/10.1002/(ISSN)1944-7973/.

Madani, K. (2014). Water management in Iran: What is causing the looming crisis? *Journal of Environmental Studies and Sciences, 4*(4), 315–328. https://doi.org/10.1007/s13412-014-0182-z.

Maxwell, R. M., & Condon, L. E. (2016). Connections between groundwater flow and transpiration partitioning. *Science, 353*(6297), 377–380. http://science.sciencemag.org/content/sci/353/6297/377.full.pdf https://doi.org/10.1126/science.aaf7891, http://science.sciencemag.org/content/sci/353/6297/377.full.pdf.

McKee, T. B., Doesken, N. J., & Kleist, J. (1993). The relationship of drought frequency and duration to time scales. In *Proceedings of the 8th conference on applied climatology, Anaheim, 17–22 January 1993*179–183.

Modarres, R., Sarhadi, A., & Burn, D. H. (2016). Changes of extreme drought and flood events in Iran. *Global and Planetary Change, 144*, 67–81. http://www.sciencedirect.com/science/journal/09218181 https://doi.org/10.1016/j.gloplacha.2016.07.008, http://www.sciencedirect.com/science/journal/09218181.

Najafi, M. S., & Alizadeh, O. (2023). Climate zones in Iran. *Meteorological Applications, 30*(5), 14698080. http://onlinelibrary.wiley.com/journal/10.1002/(ISSN)1469-8080 https://doi.org/10.1002/met.2147, http://onlinelibrary.wiley.com/journal/10.1002/(ISSN)1469-8080.

Richey, A. S., Thomas, B. F., Lo, M. H., Reager, J. T., Famiglietti, J. S., Voss, K., Swenson, S., & Rodell, M. (2015). Quantifying renewable groundwater stress with GRACE. *Water Resources Research, 51*(7), 5217–5237. http://onlinelibrary.wiley.com/journal/10.1002/(ISSN)1944-7973 https://doi.org/10.1002/2015WR017349, http://onlinelibrary.wiley.com/journal/10.1002/(ISSN)1944-7973.

Rodell, M., Beaudoing, H. K., L'Ecuyer, T. S., Olson, W. S., Famiglietti, J. S., Houser, P. R., Adler, R., Bosilovich, M. G., Clayson, C. A., Chambers, D., Clark, E., Fetzer, E. J., Gao, X., Gu, G., Hilburn, K., Huffman, G. J., Lettenmaier, D. P., Liu, W. T., Robertson, F. R., Schlosser, C. A., Sheffield, J., & Wood, E. F. (2015). The observed state of the water cycle in the early twenty-first century. *Journal of Climate, 28*(21), 8289–8318. https://doi.org/10.1175/jcli-d-14-00555.1.

Rodell, M., & Famiglietti, J. S. (2001). An analysis of terrestrial water storage variations in Illinois with implications for the gravity recovery and climate experiment (GRACE). *Water Resources Research, 37*(5), 1327–1339. https://doi.org/10.1029/2000wr900306.

Tangdamrongsub, N., Ditmar, P., Ran, J., & Klees, R. (2020). Improvement of hydrological signals from GRACE gravity fields by means of proper filtering and leakage reduction. *Water Resources Research, 56*(9).

Tapley, B. D., Watkins, M. M., Flechtner, F., Reigber, C., Bettadpur, S., Rodell, M., Sasgen, I., Famiglietti, J. S., Landerer, F. W., Chambers, D. P., Reager, J. T., Gardner, A. S., Save, H., Ivins, E. R., Swenson, S. C., Boening, C., Dahle, C., Wiese, D. N., Dobslaw, H., Tamisiea, M. E., & Velicogna, I. (2019). Contributions of GRACE to understanding climate change. *Nature Climate Change, 9*(5), 358–369. http://www.nature.com/nclimate/index.html https://doi.org/10.1038/s41558-019-0456-2, http://www.nature.com/nclimate/index.html.

Tapley, B. D., Bettadpur, S., Ries, J. C., Thompson, P. F., & Watkins, M. M. (2004). GRACE measurements of mass variability in the Earth system. *Science (New York, N.Y.), 305*(5683), 503–505. https://doi.org/10.1126/science.1099192.

Tariq, A., Ali, S., Basit, I., Jamil, A., Farmonov, N., Khorrami, B., Khan, M. M., Sadri, S., Baloch, M. Y. J., Islam, F., Junaid, M. B., & Hatamleh, W. A. (2023). Terrestrial and groundwater storage characteristics and their quantification in the Chitral (Pakistan) and Kabul (Afghanistan) river basins using GRACE/GRACE-FO satellite data. *Groundwater for Sustainable Development, 23*, 100990. https://doi.org/10.1016/j.gsd.2023.100990.

Wasko, C., Nathan, R., & Peel, M. C. (2020). Trends in global flood and streamflow timing based on local water year. *Water Resources Research, 56*(8). http://agupubs.

onlinelibrary.wiley.com/hub/journal/10.1002/(ISSN)1944-7973/ https://doi.org/10.1029/2020WR027233, http://agupubs.onlinelibrary.wiley.com/hub/journal/10.1002/(ISSN)1944-7973/.

Zarch, M. A. A., Malekinezhad, H., Mobin, M. H., Dastorani, M. T., & Kousari, M. R. (2011). Drought monitoring by reconnaissance drought index (RDI) in Iran. *Water Resources Management, 25*(13), 3485–3504. https://doi.org/10.1007/s11269-011-9867-1.

Zhong, Y., Zhong, M., Mao, Y., & Ji, B. (2020). Evaluation of evapotranspiration for exorheic catchments of china during the GRACE Era: From a water balance perspective. *Remote Sensing, 12*(3), 511. https://doi.org/10.3390/rs12030511.

Index

Note: Page numbers followed by "*f*" and "*t*" refer to figures and tables, respectively.

A

Ability, 261–262
Accountability, 228–230
Adaptability, 228–230
Adaptation appraisal, 262–263
Adaptive Neuro-Fuzzy Inference System (ANFIS) model, 299–300
Adequate funding, 244
Afghanistan, Kabul river basin in, 140–142, 142*f*, 143*t*
Aggregate Drought Index (ADI), 45–54
Agricultural drought, 16–17, 150, 293
  data assimilation-based monitoring, 322–323
Agricultural drought index, 55, 56*t*, 152
Agricultural Reference Index for Drought (ARID), 55–56
Agricultural water demand management (AWDM), 254
Agricultural water management (AWM), 253–254
American Psychological Association (APA), 212
AMSR-E, 333–334
Anahita, 161
Analytical hierarchy process (AHP) method, 470–471
Annual maxima (AM), 444, 448
Anxiety, 211
Architectural features, of buildings, 172–176, 175*f*
ArcSDM extension, 483
Arctic Oscillation (AO), 381
Arid and semiarid regions, 134
Aridity, 16
Aridity Anomaly Index (AAI), 56–57, 57*t*
Aridity Index (AI), 56–57, 58*t*
  De Martonne Aridity Index, 60, 61*t*
  Palfai Aridity Index, 75–76, 76*t*
Artificial intelligence (AI) techniques, 469–470
Artificial neural network (ANN), 69–70, 390, 470–471
Atmosphere–ocean general circulation models (AOGCMs), 383–384
Atmospheric Sciences, 33–34
Autonomous factors, 232–233

B

Backpropagation (BP), 471
Backpropagation neural networks (BPNN), 472–473
Bayesian decision theory, 481–482
Bayesian neural network (BNN), 472–473
Behavioral insights approach, 263–267
Behaviors, 260
Benefit of Governance in Drought Adaptation (DROP) project, 226
Bias-correction, 116, 117*t*, 447
Bibliometric analysis, 17–28
  citation analysis, 20–22, 21*f*, 22*t*
  drought-related research, trends of, 20, 20*f*
  leading journals and citation analysis, 25–26, 26*t*
  productive countries and international collaborations, 22–25, 23*f*, 23*t*
Big data analytics, 391–392
Blue cluster keywords, 31
BNKR Arquitectura, 199–200
Boolean operators, 26–27
Borujerdi house, 175
Buildings, architectural features of, 172–176, 175*f*
Bursa province (case study)
  dams completed within the boundaries of, 282*t*
  investments within provincial boundaries, 280*f*
  Regional Directorate in, 285

C

Capability, 228–230
CDD, 121
Cellar, 173–175
Center for Space Research (CSR), 341
China-Z Index (CZI), 8–9, 57–58, 59*t*
Choice architecture, 264–265
Chronic stress, economic uncertainty and, 209–210
Citation analysis, 20–21, 21*f*, 22*t*
Citation Topics Meso, 28–29
Classification entropy (CEs), 476
Clayton copula, 74–75
Climate, 377, 393–394
Climate change, 377–379, 381–383, 399–400, 419
  mental health and, 206
  models and scenarios, 383–386, 385*t*, 386*t*
Climate Change Initiative (CCI), 319–320
Climate information, 377–378
Climate patterns, 377–378
Climate Prediction Center (CPC), 518–519
Climate variability, 378–381, 441–442
Climate variables, 378–379
Climatically appropriate for existing conditions (CAFEC), 78
Climatic architecture, 163–165, 164*f*, 201–202
Co-authorship network map, 24, 24*f*
Coefficient of determination (R^2), 365
Cognitive and emotional coping strategies, 215–216
Cognitive restructuring, 215–216
Collaboration among stakeholders, 236–237
Combined Drought Indicator (CDI) map, 274, 274*f*
Community participation, 235–236
Copernicus Climate Change Service (C3S), 310
Coping mechanisms, 215
  cognitive and emotional coping strategies, 215–216
  policies and educational programs, 216–217
Copula functions, 291–292
Coupled Model Intercomparison Project (CMIP), 109–110, 384, 385*t*
Crop Science, 28–29
Crop Water Stress Index (CWSI), 58–60, 335
"Cubist" package, 364–365
Cultivars, 488–489
Cumulative distribution function (CDF), 448
CWD, 121

D

Data assimilation (DA), 320
  in agricultural drought monitoring, 322–323
  for drought monitoring, 321–322
  GRACE data assimilation (GRACE-DA), 342, 344*f*, 345*f*
Data gathering, for central Iraq, 309–311, 310*f*
Data preparation and analysis, 518
Decile Index (DI), 81, 82*t*
Deciles, 7*t*, 8–11
Deep learning (DL), 27–28
Degree of likelihood, 116, 116*t*
Demand management, 253–254
De Martonne Aridity Index (I_{DM}), 60, 61*t*
Dependent factors, 232–233, 246
Depression, 210
Depthscraper, 199, 200*f*
Deviation of EP (DEP), 64–65
Digital Elevation Model (DEM), 338*f*, 339–341
Discrepancy measure (DM), 11, 137, 146*t*
Discrepancy Precipitation Index (DPI), 10–11, 137, 144
  Kabul river basin, 142, 143*t*
  Mauritania, Trarza region of, 140, 140*f*, 143*t*, 145*t*
  Somalia, Putland region of, 139*t*
  Turkey, Aegean region of, 145*t*
Double-mass curve, 423, 446–447
DrinC software, 123
Drip irrigation, 255–256
Drought, 118, 386–388, 470
  assessment methods, 4–11
  characterization of, 42–44
  definition of, 3–4, 15, 42–44, 225, 378

and forecasting techniques, 388–392
governance and risk management, 225–226
history of, 161–162
impacts of, 119
parameters affecting the occurrence of, 293*f*
psychological effects of, 207–212
severity, intensity, and duration, 293–294
types of, 16–17, 17*f*, 43*f*, 119, 150, 292–293
Drought Area Index (DAI), 60–61, 61*t*
Drought assessment, 135
Drought coping mechanisms, 215
cognitive and emotional coping strategies, 215–216
policies and educational programs, 216–217
Drought damage, 69
Drought Early Warning Systems (DEWS), 334, 391–392
Drought Frequency Index (DFI), 61–62
Drought indicators, 44
Drought indices, 41, 119–120
category classification of, 426*t*
overview of, 46*t*
taxonomy, 44
Drought management, 135
Drought prediction, methods and indices for, 33–35, 34*f*
Drought propagation, 154
Drought-related research
datasets used in, 31–33, 32*t*
distribution of, 26–28
journals on, 26*t*
trending topics and emerging themes in, 28–31, 28*t*, 29*t*, 30*f*
trends of, 20, 20*f*
WoS categories and corresponding topics in, 29*t*
Drought Severity Index (DSI), 62–64, 64*t*, 335
D-score values, 8*t*
drought classification according to, 137, 137*t*
Duration, of drought, 293–294

E

Earthquakes, 3
Earth's atmosphere, 381–382
Earthscrapers, 196–201
Earth-sheltered structures, 183–184
Eco-anxiety, 212–213
definition of, 212
drought-induced
economic anxieties and social collapse, 214–215
future anxiety and uncertainty, 214
mitigation strategies, 215
Ecological grief, 207–208
Educational programs, 216–217
Effective drought governance, 243–246
challenges and barriers to, 243–245
framework for, 228–230, 229*f*
Effective Drought Index (EDI), 64–65, 65*t*, 296
Effective precipitation, 64–65
deviation of, 64–65
El Niño–Southern Oscillation (ENSO), 381, 393–394
Emission scenarios, 112–115
Representative Concentration Pathways, 112–113
Shared Socioeconomic Pathways, 113–115
Emotional ANN (EANN) models, 473
Emotional support, 216
Empirical Bayesian Kriging method, 493
Empirical cumulative distribution function (ECDF), 450
Empirical regression models, 425
Ensemble Kalman filter (EnKF), 321, 325, 327–330
Environmental Sciences and Agronomy, 28–29
ERA5 Reanalysis, 310
European Drought Observatory (EDO), 274, 309–310
Evaluation metrics, 365
Evaporation, 177–179
Evaporative Drought Index (EDI), 335
Evaporative Stress Index (ESI), 65–66, 66*t*, 335

Evapotranspiration, 335–336
Evapotranspiration Deficit Index (ETDI), 66–67, 67*t*
Expansion parameter, 480
Expert Team on Climate Change Detection and Index (ETCCDI), 120, 121*t*, 442–444
Extreme climatic events, 109–110, 118
  types of, 118
Extreme persistent function (EPF), 61–62
Extreme rainfall indices, 120–122
  applications of, 122
Extreme weather events, 319

F

Facilitator, 262
Fairness, 228–230
Farm and Ranch Stress Assistance Network, 216–217
Feedforward neural networks (FFNNs), 473
Financial constraints, 244
Financial incentives, 257
Fogg Behavior Model (FBM), 261–262
Food and Agriculture Organization (FAO), 155
Forecasting, 389–390
  AI and ML models, 389–390
  factors affecting, 390–391
  real-time data, big data, and adaptive forecasting systems, 391–392
  statistical methods, 389
Four-layer LSTM, 313, 313*f*
Frank copula, 74–75
Frequency analysis, 448–450
  annual maxima, 448
  peaks-over-threshold, 448–450
Fuzzy clustering, 470–471, 474–477
Fuzzy index, 298
Fuzzy logic, 299–300, 484
Fuzzy logic clustering (FLC), 474
Fuzzy water quality index (FWQI), 473

G

Gamma distribution, 423–424
Gamma PDF distribution, 89–90
Gamma-SPI (SPI-G), 5–7, 135–136, 144, 146*t*, 152
  Kabul river basin, 143*t*
  Mauritania, Trarza region of, 145*t*
  at Putland region of Somalia, 139*t*
  Turkey, Aegean region of, 145*t*
Garden pits, 181
Gates, 308
Gaussian function, 476–477
Gaussian process classification (GPC), 471
General circulation model (GCM), 109–112, 125, 444, 446, 472–473
  case study, 122–123, 123*f*, 124*t*
  downscaling, 115
  uncertainty issue, 116
General Directorate of State Hydraulic Works (DSI), 276–277
  applications and practices, 277–281
  investments, 281–284, 284*t*
  investments made by, 284*t*
  Regional Directorate.Map, 279*f*
Generalized extreme value distribution (GEVD), 448
Generalized extreme values (GEVs), 291–292
Generalized pareto distribution (GPD), 448–449
Geographical analysis, 35
Geographic information systems (GIS), 470–471
GeoXplore, 474, 483
Glazed ceiling, 199–200
GLDAS, 339–341
Global climate models (GCMs), 442–444
Global Drought Observatory, 309–310
Global Risk Report, 205
Global warming, 164–165, 305, 382, 419, 441–442
Governance Assessment Tool (GAT), 226
Governance, drought, 226, 245
  collaboration among stakeholders, 236–237
  effective, 243–244
    challenges and barriers to, 243–245
    framework for, 228–230, 229*f*

factors influencing, 233, 239*t*
climatic and meteorological factors, 233–234
economic factors, 234
environmental factors, 235
institutional factors, 236
social factors, 235–236
technological factors, 234
legal regulations, 238
mitigation planning and crisis management, 237–238
preparedness planning and risk management, 237
GRACE data assimilation (GRACE-DA), 342, 344*f*, 345*f*
GRACE-Follow On (GRACE-FO) data, 518
GRACE mission, 320, 515–516, 518
terrestrial water storage (TWS), 336–342
Green cluster keywords, 30
Green Water Scarcity Index (GWSI), 335
Green Water Stress Index (GrWSI), 335
Groundwater quality potential index, 483
Groundwater Resource Index (GRI), 67–68
drought severity based on, 69*t*
groundwater detention reservoir calculation algorithm for, 68*f*
Groundwater storage, 320, 336–337
Gumbel copula, 74–75

H

Heåkra station, 361–362, 363*f*
Heat-related health problems, 207
Heat waves, 207–208, 386–387
High-Level Meeting on National Drought Policy (HMNDP), 4, 155
Hot and arid climate, 165–193
Hybrid AI models, 390
Hybrid Drought Index (HDI), 69–70, 70*t*
Hydroelectric power plants (HEPPs), 280
Hydrological drought, 16–17, 26–27, 150, 152–153, 293
Hydrological events, 118
Hydro-thermal Coefficient of Selyaninov (HTC), 70–71, 71*t*

I

Inclusiveness, 228–230
India Meteorological Department (IMD), 56–57
Indian Ocean Dipole (IOD), 381
Influence–dependence analysis, 246
Influential factors, 232–233, 246
Integrated drought index (IDI), 299
Integrated water resource management (IWRM) frameworks, 276–277
Intensity, of drought, 293–294
Intergovernmental Panel on Climate Change (IPCC), 109–110, 212, 380–381, 441–442
Inverse distance weighting (IDW), 490–493
Iranian traditional house, orientation of, 169–171, 173*f*
Iran Water Resources Management Company (IWRMC), 341
Irrigation methods, 255–256
Irrigation scheduling, 256

J

Jevon's Paradox, 257–258

K

Kabul river basin (KRB), 140
DPI and SPI-G, 143*t*
meteorological stations, 142*f*
Kandovan village homes, 182*f*
K-band microwave ranging technology, 336–337
Keetch-Byram Drought Index (KBDI), 71–72, 72*t*
Khorasan aquifers, 484
Kolmogorov-Smirnov (KS) test, 450
Kriging method, 490

L

Landsat, 335–336
Land surface models (LSMs), 319
Land surface temperature (LST), 72–73, 335–336
Legal regulations, 238
Legitimacy, 228–230
Level of confidence, 116, 116*t*

Levenberg-Marquardt algorithm, 473
Linear and multiple regression models, 389
Linear regression model, 360, 364–372, 366*t*, 368*t*
Linear scaling method, 447, 450–451
Linguistic variable scale, 231*t*
Linkage factors, 232–233, 246
Log-normal standardized precipitation index, 5
Log-SPI, 152
Long short-term memory (LSTM) model, 308–309
  four-layer, 313, 313*f*
  one-layer, 311, 312*f*
  vs. recurrent neural network, 314–315
  results of, 314, 315*f*
  structure and their unit, 308*f*
  three-layer, 312, 313*f*
Loss of identity, 207–208
LSTM. *See* Long short-term memory (LSTM) model

M

Machine learning (ML), 27–28, 305, 360–361, 364–365
Madden–Julian Oscillation (MJO), 381
Maladaptive responses, 263–264
Malqaf, 176–177, 177*f*
Mann–Kendall (MK) test, 380, 399–400, 520–521
Markov chain models, 389
Matmata's subterranean habitats, 184, 185*f*
Mauritania, Trarza region of, 140
  DPI and SPI-G, 140, 145*t*
  meteorological stations, 140*f*
Mean absolute error (MAE), 365
Mean annual evapotranspiration (MAET), 517–518
Mean annual precipitation (MAP), 517–518
Mean effective precipitation (MEP), 64–65
Mean residual life plot (MRLP) method, 449–450
Mean squared error (MSE), 473
Memory cells, 308
Mental health disorders, 208–209
Meteorological drought, 16–17, 119, 150, 292
Meteorological Drought Map, 275*f*
Meteorological events, 118
Meteorology, 33–34
Meteosat-MVIRI, 335–336
Meymand underground settlement, 181–182, 183*f*, 184*f*
MICMAC method, 227, 230–233, 231*f*
  classification of factors using, 238–243, 239*t*, 240*f*, 241*t*
  influence-dependence chart, 232*f*, 242*f*
Microclimate, 163–164
Microwave Integrated Drought Index (MIDI), 72–73, 74*t*
Microwave sensors, 333–334
Mild drought indicator, 509–510
Mindfulness, 216
Mindfulness-based interventions, 216
MINDSPACE Framework, 264–265
Minitab software, 490
Model of Private Proactive Adaptation to Climate Change (MPPACC), 262–263
Moderate Resolution Imaging Spectroradiometer (MODIS), 30, 335, 339–341, 391–392
Modern architecture, 171–172
Motivation, 261–262
M5 tree model, 364–365, 366*t*, 367*f*, 368*t*
Multilayer perceptron (MLP), 306–307, 479
Multivariate Standardized Drought Index (MSDI), 73–74, 75*t*, 296–297, 297*f*

N

NASA's GRACE, 309–310
Nash–Sutcliffe Efficiency (NSE), 311
National Aeronautics and Space Administration (NASA), 518
National Centers for Environmental Information, 310
National Meteorological Center of China (NMCC), 8–9
National Oceanic and Atmospheric Administration (NOAA), 446, 518–519
Near-infrared spectral reflectance (NIR), 295

Neuro-fuzzy models, 299–300
Nighttime irrigation, 256
Nissar, 173–175
NOAA-AVHRR, 335–336
NOAA's Climate Prediction Center, 309–310
Nonconsumed water, 254–255
Nonconsumptive water, on-farm, 255–256
Nonlinear regression (NLR) models, 360, 364–372, 366*t*, 368*t*
Nonnonparametric-parametric test, 399–400
Non-parametric statistical method, 520–521
Normalized Difference Vegetation Index (NDVI), 30, 42, 295
Normal-standardized precipitation index (SPI-N), 5
North Atlantic Oscillation (NAO), 381
Nudges, 264–265
Null hypothesis, 521

O

Oceanography, 33–34
Office of Foreign Disaster Assistance (OFDA), 134
One-layer LSTM, 311, 312*f*
On-farm irrigation efficiency, 254–255
On-farm nonconsumptive water, 255–256
Operational forecasting systems, 346

P

Palfai Aridity Index (PAI), 75–76, 76*t*
Palmer Drought Severity Index (PDSI), 76–79, 79*t*, 295
Palmer Hydrological Drought Index (PHDI), 79, 80*t*
PARallel FLOW–Community Land Model, 320–321, 324*f*, 326–327
  GRACE terrestrial water storage data assimilation into, 338–342, 343*f*
  soil moisture assimilation into, 326–332, 328*f*, 329*f*, 331*f*
ParFlow model, 326–327
Partition coefficients (PCs), 476
Peaks-over-threshold (POT) methods, 444, 448–450
Percent of normal (PN), 6*t*, 7
Percent of Normal Index (PNI), 80, 81*t*
Percent of Normal Precipitation Index (PNPI), 296
Perlucor ceiling, 201
Perpendicular Drought Index (PDI), 80–81, 82*f*
Picard iteration, 476–477
Policy recommendations, 247–248
Polynomial regression, 364
Posttraumatic stress disorder (PTSD), 211–212
Potential evapotranspiration (PET), 9, 55–56, 76–77, 98–99
Potential loss (PL), 76–77
Potential recharge (PR), 76–77
Potential runoff (PRO), 76–77
PRCPTOT, 120
Precipitation, 44
  effective, 64–65
  mean effective, 64–65
Precipitation amount, 150
Precipitation Condition Index (PCI), 72–73
Precipitation index, 519
Preparedness planning, 237
Probabilistic neural network (PNN), 474, 481–483
  architecture of, 482*f*
Probability density functions (PDFs), 42
Process-based accumulated drought index, 298
Proportional exponent (PE), 476
Protection Motivation Theory (PMT), 262–263
Psychological effects, 207
  anxiety, 211
  depression, 210
  ecological grief and loss of identity, 207–208
  economic uncertainty and chronic stress, 209–210
  mental health disorders, 208–209
  posttraumatic stress disorder, 211–212
Psychosocial support, 215
Public awareness campaigns, 248

Public education and awareness campaigns, 244–245
Python code, 488–489

Q

Qanat, 173–175, 186–190
  interconnected network of, 194*f*
  with its components, 189*f*
  plan and schematic section of, 188*f*
Quantile regression, 380

R

Radial base network architecture, 478–480, 479*f*
Radial basis functional-link nets (RBFLN), 480–481
Radial basis functional-link neural networks, 480–481
Radial basis function artificial neural networks, 477–478
Radial basis function neural network (RBFNN), 474
Radial transfer function, 479
Radiation, 335–336
Rainfall Anomaly Index (RAI), 83, 83*t*
Rainfall Drought Index (RAI), 299–300
Random forest (RF), 364–365, 366*t*, 368*t*
Random vector functional-link network (RVFLNs), 479
Reconnaissance Drought Index (RDI), 9–10, 83–84, 84*t*, 335
Recurrent neural network (RNN) model, 307, 312*t*
  accuracy at training and testing periods, 313–314, 314*t*
  internal operation, 307*f*
  vs. long short-term memory, 314–315
Regional Streamflow Deficiency Index (RSDI), 84–85
Remote sensing, 323–324, 324*f*
  evapotranspiration, 335–336
  snow cover, 333–334
  soil moisture, 324–326
  terrestrial water storage and groundwater, 336–337
Representative Concentration Pathways (RCPs), 112–113, 384
Resilience, 228–230
Restrictive policies, 259
Richards equation, 326–327
Risk appraisal, 262–263, 266–267
Risk management, 225–226
  preparedness planning and, 237
RMSE-observations standard deviation ratio (RSR), 365
Root mean square error (RMSE), 311, 330, 365, 493
  of soil moisture, 332*f*
Root-zone SM, 322
R95P, 121
R99P, 121
Run theory, 293–294, 294*f*
RX1Day, 121–122
RX5Day, 121–122

S

Satellite remote sensing, 324–325
Scaled Drought Condition Index (SDCI), 85, 86*t*
Scatter plots, 366–369, 367*f*, 369*f*
Seasonality assessment, 520
Self-calibrated Palmer Drought Severity Index (sc-PDSI), 297–298
Semiarid region, 134
Sensitivity analysis, 483
Sentinel-1, 319–320, 333–334
Sequential Monte Carlo (SMC) techniques, 321–322
Severity-area-frequency (SAF), 472–473
Severity, drought, 293–294
Shared Socioeconomic Pathways (SSPs), 113–115
  SSP1, 113
  SSP2, 113–114
  SSP3, 114
  SSP4, 114
  SSP5, 114–115
Short-period meteorological events, 149–150
Shovadan, 190–193
  interconnected network of, 194*f*
  parts of, 191*f*
  section and spatial organization of, 191*f*
  underground space of, 192*f*
  ventilation of, 193*f*

Signal, 262
SM. *See* Soil moisture (SM)
Snow cover, remote sensing, 333–334
SNOwpack TELemetry (SNOTEL), 334
Snow water equivalent (SWE) rate, 420–421, 425
Social capital, 235–236
Socioeconomical equilibrium, 419
Socioeconomic drought, 16–17, 43, 150, 293
Soil moisture (SM), 152, 319–320
  PARallel FLOW-Community Land Model, 326–332, 328*f*, 329*f*, 331*f*
  remote sensing, 324–326
  root mean square error of, 332*f*
Soil Moisture Active Passive (SMAP), 319–320, 324–325, 333–334, 391–392
Soil Moisture and Ocean Salinity (SMOS), 319–320
Soil Moisture Anomaly Index (SMAI), 151*t*, 152
Soil Moisture Deficit Index (SMDI), 85–86, 87*t*
Soil Moisture Saturation Index (SMSI), 72–73
Soil Water Deficit Index (SWDI), 86–87, 88*t*
Somalia, droughts in, 134–135
  Puntland region of, 138, 138*f*, 139*t*
SOS Children's Village, 194–196, 196*f*, 197*f*
  ground-floor plan of, 195*f*
Spark, 262
Spatial orientation, sunlight, 169–172, 170*f*, 173*f*
SPEI Global Drought Monitor, 309–310
Spherical harmonic coefficients (SHC), 341
SPI. *See* Standard Precipitation Index (SPI)
SPI-G. *See* Gamma-SPI (SPI-G)
Sprinkler irrigation, 255–256
Stakeholder engagement, 228–230, 245
Standardized Anomaly Index (SAI), 87–88, 88*t*
Standardized evapotranspiration index (SEI), 295
Standardized Palmer Drought Index (SPDI), 299
Standardized Precipitation Evapotranspiration Index (SPEI), 9, 21–22, 88–89, 90*t*, 297–298, 306–307, 335, 421, 424, 432*t*
Standardized Precipitation Index (SPI), 4–7, 11, 30, 89–91, 92*t*, 151–152, 151*t*, 421, 423–427, 518–519
  drought classification, 6*t*
  drought summary of, 431*t*
  gamma-, 5–7
  log-normal, 5
  normal-, 5
  temporal variations of, 526*f*
  variations of, 524–525
Standardized Runoff Index (SRI), 91–92, 93*t*
Standardized Snow Precipitation Index (SSPI), 421, 425–426
Standardized Soil Moisture Index (SSI), 295
Standardized Streamflow Index (SSI), 92–93, 94*t*
Standardized Water-level Index (SWI), 93–94, 94*t*
Standard Precipitation Index (SPI), 135–136, 294, 399
  based drought classification, 136*t*
  Kabul river basin, 142, 143*t*
  Mauritania, Trarza region of, 140, 140*f*, 145*t*
  at Putland region of Somalia, 139*t*
  Turkey, Aegean region of, 145*t*
State Hydraulic Works. *See* General Directorate of State Hydraulic Works
Streamflow Drought Index (SDI), 95, 96*t*, 152–153, 153*t*, 359–360, 362–363
  estimation during training and testing phases, 366*t*, 368*t*
  linear regression models, 364
  machine learning models, 364–365
  nonlinear regression models, 364
Subterranean building, designing methods, 182*f*, 183–184
Supply-Demand Drought Index (SDDI), 335

Support vector machines (SVMs), 390
Surface SM, 322–323
Surface Water Supply Index (SWSI), 95–96, 96*t*
Sustainable Development Goals (SDGs), 29–30, 285–286
Sustainable financing mechanisms, 247
Sustainable water resource planning, 469
Swedish Meteorological and Hydrological Institute (SMHI), 361–362
Synthetic Aperture Radar (SAR), 333–334

T

Taylor diagram, 369–370, 370*f*, 371*f*, 372–373
Temperature Condition Index (TCI), 72–73
Temperature Vegetation Drought Index (TVDI), 97–98, 97*f*
Terra/Aqua MODIS, 335–336
Terra-Aster, 335–336
Terrestrial water storage (TWS), GRACE-derived, 336–342
Theory of Rational Choice, 260
Thermal events, 118
Thornthwaite Moisture Index (TMI), 98–99, 100*t*
Three-layer LSTM, 312, 313*f*
T.I.B.I index, 298
Time-series models, 389
Total dissolved solids (TDS), 470–471
Total Storage Deficit Index (TSDI), 99–100, 101*t*
Total water storage (TWS), 515–516, 519–520, 522*f*
  zonal fluctuations of, 523*t*
Traditional architecture, 162, 201
  contemporary design inspired by, 193–201
  in hot and arid climate, 165–193
Transboundary droughts, 248
Transparency, 228–230
Trend analysis, water storage, 520–521
Trigger, 261–262
Tropical Rainfall Measuring Mission (TRMM), 391–392
Turkey, Aegean region of, 142–144
  DPI and SPI-G, 145*t*
  meteorological stations, 144*f*
Turkey Climate Change Report, 208–209

U

Uncertainty, 209–210
Underground architecture, 179–193, 202
  Kandovan village homes, 182*f*
  Matmata's subterranean habitats, 185*f*
  Meymand underground settlement, 183*f*, 184*f*
  Qanat, 186–190
  Shovadan, 190–193
Underground constant temperature, 198*f*
Underground urbanism, 196–197
Uniform distribution functional (UDF), 476
United Nations Convention to Combat Desertification (UNCCD), 155
UN-Water Activity Information System, 146
Urban fabric, characteristics of, 167–168, 167*f*
Urban structure
  of Tunis, 168*f*
  of Yazd, 169*f*
Urban underground, 196–197
US Drought Monitor, 309–310

V

Validation of cluster selection, 476
Variable Infiltration Capacity (VIC) model, 335–336
Vegetation Temperature Condition Index (VTCI), 100–101, 102*t*
Virginia Council on Environmental Quality (VDEQ), 444–446
VOSviewer software, 17–18

W

Water, 161, 253–254
Water Balance Derived Drought Index (WBDDI), 101–102, 102*t*
Water cycle algorithm (WCA), 305–306
Water scarcity, 208, 233

Water storage, 515
  associations between water storage variations and drought indices, 526–530
  data preparation and analysis, 518
  fluctuations of, 521–523
  GRACE and GRACE-FO data, 518
  reconstruction of missing GRACE /GRACE-FO data, 519–520
  seasonal dynamics of, 523–524
  seasonality assessment, 520
  Standardized Precipitation Index, 518–519
  study area, 517–518
  trend analysis, 520–521
Water stress (WS), 66–67
Water use behavior, 262–263
Water use efficiency, 256
Web of Science (WoS) database, 18–19, 28*t*
Weighted fuzzy expected value (WFEV), 476–477
Wetness Percentile Index (WPI), 519
Wind catcher, 176–179, 180*f*
  multidirectional, 179*f*
  unidirectional, 178*f*
World Health Organization (WHO), 470–471
World Meteorological Organization (WMO), 89–90, 273, 399, 423–424, 442–444

X

Xeriscape, 190

Y

Yazd, Iran
  traditional house in, 174*f*
  urban structure of, 169*f*
Yellow cluster keyword, 31

Drought Dynamics

Modeling and Assessment to Confront a Changing Climate

Drought Dynamics: Modeling and Assessment to Confront a Changing Climate synthesizes the latest research findings and practical insights from leading experts in the field. It provides the knowledge and tools necessary to understand the causes and impacts of drought, predict its occurrence, and implement practical measures to mitigate its effects.

The book begins with an in-depth review of fundamental drought theory followed by a closer examination of related aspects like social behavior, food security, health, climate, architecture, and education. Next is a close look at geography information systems (GIS), data mining techniques, predictive models, decision support systems (DSS), and drought indices. The chapters then explore drought management along with community resilience, adaptation, practice, policy, and the economy. New trends in drought studies are presented including the latest practical technologies and the use of artificial intelligence (AI). Lastly, a series of detailed case studies offers practical insights on data assessment, modeling, experimental studies, and climate change.

The editors and contributing authors offer this resource to help build resilience and sustainability in the face of one of the most pressing environmental challenges of our time.

Key Features

- Advances drought dynamic understanding as well as climate change adaptation strategies via interdisciplinary perspectives
- Examines recent revolutionary approaches for drought modeling to give readers insight about progress in the field
- Illustrates the implementation of different approaches for drought analysis techniques through a variety of case studies
- Recommends practical and actionable adaptation strategies to enhance resilience in dealing with climate change-induced droughts

About the Editors

Dr. Mir Jafar Sadegh Safari is a hydrologist and associate professor at Yaşar University, and currently a research associate at Toronto Metropolitan University. His comprehensive research portfolio centers on water resources, hydrological modeling, environmental systems, and hydraulics. His interdisciplinary work integrates AI, GIS, and hydrological modeling for sustainable water management. His endeavors transcend conventional approaches by innovating adaptive and integrated techniques to address the challenges posed by climate change variability and uncertainties.

Dr. Babak Vaheddoost serves as an associate professor at Bursa Technical University, Türkiye. His work reflects a sustained scholarly commitment to hydrological sciences, particularly through the application of sophisticated data analysis and mining approaches to both linear and nonlinear systems, examined across temporal and spectral domains. His research activities encompass a wide array of topics, including groundwater–surface water interactions, drought and flood characterization, water-energy budget, climate change implications, water quality assessment, and flow dynamics.

ISBN 978-0-443-34205-9

9 780443 342059

ELSEVIER shop.elsevier.com